

INTRODUCTION TO ELASTICITY

David Roylance
Department of Materials Science and Engineering
Massachusetts Institute of Technology
Cambridge, MA 02139

January 21, 2000

Introduction

This module outlines the basic mechanics of *elastic* response — a physical phenomenon that materials often (but do not always) exhibit. An *elastic* material is one that deforms immediately upon loading, maintains a constant deformation as long as the load is held constant, and returns immediately to its original undeformed shape when the load is removed. This module will also introduce two essential concepts in Mechanics of Materials: *stress* and *strain*.

Tensile strength and tensile stress

Perhaps the most natural test of a material's mechanical properties is the *tension test*, in which a strip or cylinder of the material, having length L and cross-sectional area A , is anchored at one end and subjected to an axial load P — a load acting along the specimen's long axis — at the other. (See Fig. 1). As the load is increased gradually, the axial deflection δ of the loaded end will increase also. Eventually the test specimen breaks or does something else catastrophic, often fracturing suddenly into two or more pieces. (Materials can fail mechanically in many different ways; for instance, recall how blackboard chalk, a piece of fresh wood, and Silly Putty break.) As engineers, we naturally want to understand such matters as how δ is related to P , and what ultimate fracture load we might expect in a specimen of different size than the original one. As materials technologists, we wish to understand how these relationships are influenced by the constitution and microstructure of the material.

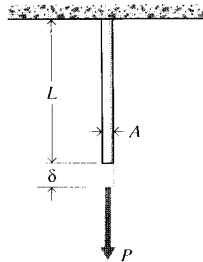


Figure 1: The tension test.

One of the pivotal historical developments in our understanding of material mechanical properties was the realization that the strength of a uniaxially loaded specimen is related to the

magnitude of its *cross-sectional area*. This notion is reasonable when one considers the strength to arise from the number of chemical bonds connecting one cross section with the one adjacent to it as depicted in Fig. 2, where each bond is visualized as a spring with a certain stiffness and strength. Obviously, the number of such bonds will increase proportionally with the section’s area¹. The axial strength of a piece of blackboard chalk will therefore increase as the *square* of its diameter. In contrast, increasing the *length* of the chalk will not make it stronger (in fact it will likely become weaker, since the longer specimen will be statistically more likely to contain a strength-reducing flaw.)

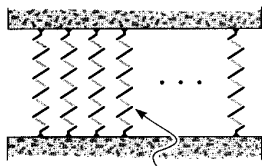


Figure 2: Interplanar bonds (surface density approximately 10^{19} m^{-2}).

Galileo (1564–1642)² is said to have used this observation to note that giants, should they exist, would be very fragile creatures. Their strength would be greater than ours, since the cross-sectional areas of their skeletal and muscular systems would be larger by a factor related to the square of their height (denoted L in the famous DaVinci sketch shown in Fig. 3). But their *weight*, and thus the loads they must sustain, would increase as their volume, that is by the *cube* of their height. A simple fall would probably do them great damage. Conversely, the “proportionate” strength of the famous arachnid mentioned weekly in the *SpiderMan* comic strip is mostly just this same size effect. There’s nothing magical about the muscular strength of insects, but the ratio of L^2 to L^3 works in their favor when strength per body weight is reckoned. This cautions us that simple scaling of a previously proven design is not a safe design procedure. A jumbo jet is not just a small plane scaled up; if this were done the load-bearing components would be too small in cross-sectional area to support the much greater loads they would be called upon to resist.

When reporting the strength of materials loaded in tension, it is customary to account for this effect of area by dividing the breaking load by the cross-sectional area:

$$\boxed{\sigma_f = \frac{P_f}{A_0}} \quad (1)$$

where σ_f is the *ultimate tensile stress*, often abbreviated as UTS, P_f is the load at fracture, and A_0 is the original cross-sectional area. (Some materials exhibit substantial reductions in cross-sectional area as they are stretched, and using the original rather than final area gives the so-call *engineering* strength.) The units of stress are obviously load per unit area, N/m^2 (also

¹The surface density of bonds N_S can be computed from the material’s density ρ , atomic weight W_a and Avogadro’s number N_A as $N_S = (\rho N_A / W_a)^{2/3}$. Illustrating for the case of iron (Fe):

$$N_S = \left(\frac{7.86 \frac{\text{g}}{\text{cm}^3} \cdot 6.023 \times 10^{23} \frac{\text{atoms}}{\text{mol}}}{55.85 \frac{\text{g}}{\text{mol}}} \right)^{\frac{2}{3}} = 1.9 \times 10^{15} \frac{\text{atoms}}{\text{cm}^2}$$

$N_S \approx 10^{15} \frac{\text{atom}}{\text{cm}^2}$ is true for many materials.

²Galileo, *Two New Sciences*, English translation by H. Crew and A. de Salvio, The Macmillan Co., New York, 1933. Also see S.P. Timoshenko, *History of Strength of Materials*, McGraw-Hill, New York, 1953.

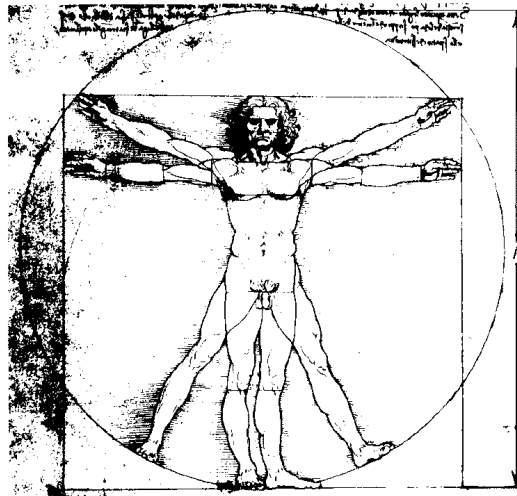


Figure 3: Strength scales with L^2 , but weight scales with L^3 .

called Pascals, or Pa) in the SI system and lb/in² (or psi) in units still used commonly in the United States.

Example 1

In many design problems, the loads to be applied to the structure are known at the outset, and we wish to compute how much material will be needed to support them. As a very simple case, let's say we wish to use a steel rod, circular in cross-sectional shape as shown in Fig. 4, to support a load of 10,000 lb. What should the rod diameter be?

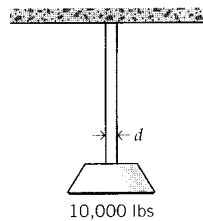


Figure 4: Steel rod supporting a 10,000 lb weight.

Directly from Eqn. 1, the area A_0 that will be just on the verge of fracture at a given load P_f is

$$A_0 = \frac{P_f}{\sigma_f}$$

All we need do is look up the value of σ_f for the material, and substitute it along with the value of 10,000 lb for P_f , and the problem is solved.

A number of materials properties are listed in the *Materials Properties* module, where we find the UTS of carbon steel to be 1200 MPa. We also note that these properties vary widely for given materials depending on their composition and processing, so the 1200 MPa value is only a preliminary design estimate. In light of that uncertainty, and many other potential ones, it is common to include a “factor of safety” in the design. Selection of an appropriate factor is an often-difficult choice, especially in cases where weight or cost restrictions place a great penalty on using excess material. But in this case steel is

relatively inexpensive and we don't have any special weight limitations, so we'll use a conservative 50% safety factor and assume the ultimate tensile strength is $1200/2 = 600$ MPa.

We now have only to adjust the units before solving for area. Engineers must be very comfortable with units conversions, especially given the mix of SI and older traditional units used today. Eventually, we'll likely be ordering steel rod using inches rather than meters, so we'll convert the MPa to psi rather than convert the pounds to Newtons. Also using $A = \pi d^2/4$ to compute the diameter rather than the area, we have

$$d = \sqrt{\frac{4A}{\pi}} = \sqrt{\frac{4P_f}{\pi\sigma_f}} = \left[\frac{4 \times 10000(\text{lb})}{\pi \times 600 \times 10^6 (\text{N/m}^2) \times 1.449 \times 10^{-4} \left(\frac{\text{lb/in}^2}{\text{N/m}^2} \right)} \right]^{\frac{1}{2}} = 0.38 \text{ in}$$

We probably wouldn't order rod of exactly 0.38 in, as that would be an oddball size and thus too expensive. But $3/8''$ (0.375 in) would likely be a standard size, and would be acceptable in light of our conservative safety factor.

If the specimen is loaded by an axial force P less than the breaking load P_f , the *tensile stress* is defined by analogy with Eqn. 1 as

$$\boxed{\sigma = \frac{P}{A_0}} \quad (2)$$

The tensile stress, the force per unit area acting on a plane transverse to the applied load, is a fundamental measure of the internal forces within the material. Much of Mechanics of Materials is concerned with elaborating this concept to include higher orders of dimensionality, working out methods of determining the stress for various geometries and loading conditions, and predicting what the material's response to the stress will be.

Example 2

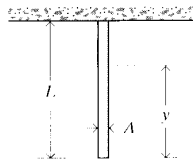


Figure 5: Circular rod suspended from the top and bearing its own weight.

Many engineering applications, notably aerospace vehicles, require materials that are both strong and lightweight. One measure of this combination of properties is provided by computing how long a rod of the material can be that when suspended from its top will break under its own weight (see Fig. 5). Here the stress is not uniform along the rod: the material at the very top bears the weight of the entire rod, but that at the bottom carries no load at all.

To compute the stress as a function of position, let y denote the distance from the bottom of the rod and let the weight density of the material, for instance in N/m^3 , be denoted by γ . (The weight density is related to the mass density ρ [kg/m^3] by $\gamma = \rho g$, where $g = 9.8 \text{ m/s}^2$ is the acceleration due to gravity.) The weight supported by the cross-section at y is just the weight density γ times the volume of material V below y :

$$W(y) = \gamma V = \gamma A y$$

The tensile stress is then given as a function of y by Eqn. 2 as

$$\sigma(y) = \frac{W(y)}{A} = \gamma y$$

Note that the area cancels, leaving only the material density γ as a design variable.

The length of rod that is just on the verge of breaking under its own weight can now be found by letting $y = L$ (the highest stress occurs at the top), setting $\sigma(L) = \sigma_f$, and solving for L :

$$\sigma_f = \gamma L \Rightarrow L = \frac{\sigma_f}{\gamma}$$

In the case of steel, we find the mass density ρ in Appendix A to be $7.85 \times 10^3(\text{kg/m}^3)$; then

$$L = \frac{\sigma_f}{\rho g} = \frac{1200 \times 10^6(\text{N/m}^2)}{7.85 \times 10^3(\text{kg/m}^3) \times 9.8(\text{m/s}^2)} = 15.6 \text{ km}$$

This would be a long rod indeed; the purpose of such a calculation is not so much to design superlong rods as to provide a vivid way of comparing materials (see Prob. 4).

Stiffness

It is important to distinguish *stiffness*, which is a measure of the *load* needed to induce a given *deformation* in the material, from the *strength*, which usually refers to the material's resistance to failure by fracture or excessive deformation. The stiffness is usually measured by applying relatively small loads, well short of fracture, and measuring the resulting deformation. Since the deformations in most materials are very small for these loading conditions, the experimental problem is largely one of measuring small changes in length accurately.

Hooke³ made a number of such measurements on long wires under various loads, and observed that to a good approximation the load P and its resulting deformation δ were related linearly as long as the loads were sufficiently small. This relation, generally known as *Hooke's Law*, can be written algebraically as

$$\boxed{P = k\delta} \tag{3}$$

where k is a constant of proportionality called the *stiffness* and having units of lb/in or N/m. The stiffness as defined by k is not a function of the material alone, but is also influenced by the specimen shape. A wire gives much more deflection for a given load if coiled up like a watch spring, for instance.

A useful way to adjust the stiffness so as to be a purely materials property is to normalize the load by the cross-sectional area; i.e. to use the tensile stress rather than the load. Further, the deformation δ can be normalized by noting that an applied load stretches all parts of the wire uniformly, so that a reasonable measure of "stretching" is the deformation per unit length:

$$\boxed{\epsilon = \frac{\delta}{L_0}} \tag{4}$$

³Robert Hooke (1635–1703) was a contemporary and rival of Isaac Newton. Hooke was a great pioneer in mechanics, but competing with Newton isn't easy.

Here L_0 is the original length and ϵ is a dimensionless measure of stretching called the *strain*. Using these more general measures of load per unit area and displacement per unit length⁴, Hooke's Law becomes:

$$\frac{P}{A_0} = E \frac{\delta}{L_0} \quad (5)$$

or

$$\boxed{\sigma = E\epsilon} \quad (6)$$

The constant of proportionality E , called *Young's modulus*⁵ or the *modulus of elasticity*, is one of the most important mechanical descriptors of a material. It has the same units as stress, Pa or psi. As shown in Fig. 6, Hooke's law can refer to either of Eqns. 3 or 6.

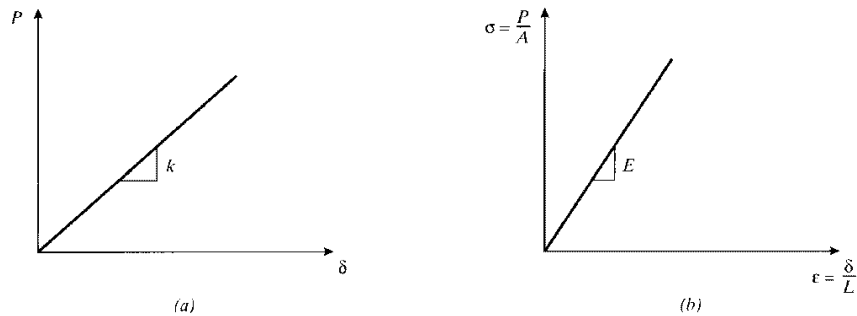


Figure 6: Hooke's law in terms of (a) load-displacement and (b) stress-strain.

The Hookean stiffness k is now recognizable as being related to the Young's modulus E and the specimen geometry as

$$k = \frac{AE}{L} \quad (7)$$

where here the 0 subscript is dropped from the area A ; it will be assumed from here on (unless stated otherwise) that the change in area during loading can be neglected. Another useful relation is obtained by solving Eqn. 5 for the deflection in terms of the applied load as

$$\boxed{\delta = \frac{PL}{AE}} \quad (8)$$

Note that the stress $\sigma = P/A$ developed in a tensile specimen subjected to a fixed load is independent of the material properties, while the deflection depends on the material property E . Hence the stress σ in a tensile specimen at a given load is the same whether it's made of steel or polyethylene, but the strain ϵ would be different: the polyethylene will exhibit much larger strain and deformation, since its modulus is two orders of magnitude less than steel's.

⁴It was apparently the Swiss mathematician Jakob Bernoulli (1655-1705) who first realized the correctness of this form, published in the final paper of his life.

⁵After the English physicist Thomas Young (1773-1829), who also made notable contributions to the understanding of the interference of light as well as being a noted physician and Egyptologist.

Example 3

In Example 1, we found that a steel rod 0.38'' in diameter would safely bear a load of 10,000 lb. Now let's assume we have been given a second design goal, namely that the geometry requires that we use a rod 15 ft in length but that the loaded end cannot be allowed to deflect downward more than 0.3'' when the load is applied. Replacing A in Eqn. 8 by $\pi d^2/4$ and solving for d , the diameter for a given δ is

$$d = 2\sqrt{\frac{PL}{\pi\delta E}}$$

From Appendix A, the modulus of carbon steel is 210 GPa; using this along with the given load, length, and deflection, the required diameter is

$$d = 2\sqrt{\frac{10^4(\text{lb}) \times 15(\text{ft}) \times 12(\text{in}/\text{ft})}{\pi \times 0.3(\text{in}) \times 210 \times 10^9(\text{N}/\text{m}^2) \times 1.449 \times 10^{-4} \left(\frac{\text{lb}/\text{in}^2}{\text{N}/\text{m}^2}\right)}} = 0.5 \text{ in}$$

This diameter is larger than the 0.38'' computed earlier; therefore a larger rod must be used if the deflection as well as the strength goals are to be met. Clearly, using the larger rod makes the tensile stress in the material less and thus lowers the likelihood of fracture. This is an example of a *stiffness-critical* design, in which deflection rather than fracture is the governing constraint. As it happens, many structures throughout the modern era have been designed for stiffness rather than strength, and thus wound up being "overdesigned" with respect to fracture. This has undoubtedly lessened the incidence of fracture-related catastrophes, which will be addressed in the modules on fracture.

Example 4

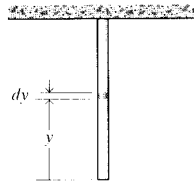


Figure 7: Deformation of a column under its own weight.

When very long columns are suspended from the top, as in a cable hanging down the hole of an oil well, the deflection due to the weight of the material itself can be important. The solution for the total deflection is a minor extension of Eqn. 8, in that now we must consider the increasing weight borne by each cross section as the distance from the bottom of the cable increases. As shown in Fig. 7, the total elongation of a column of length L , cross-sectional area A , and weight density γ due to its own weight can be found by considering the incremental deformation $d\delta$ of a slice dy a distance y from the bottom. The weight borne by this slice is γAy , so

$$d\delta = \frac{(\gamma Ay) dy}{AE}$$

$$\delta = \int_0^L d\delta = \frac{\gamma}{E} \frac{y^2}{2} \Big|_0^L = \frac{\gamma L^2}{2E}$$

Note that δ is independent of the area A , so that finding a fatter cable won't help to reduce the deformation; the critical parameter is the *specific modulus* E/γ . Since the total weight is $W = \gamma AL$, the result can also be written

$$\delta = \frac{WL}{2AE}$$

The deformation is the same as in a bar being pulled with a tensile force equal to half its weight; this is just the average force experienced by cross sections along the column.

In Example 2, we computed the length of a steel rod that would be just on the verge of breaking under its own weight if suspended from its top; we obtained $L = 15.6\text{km}$. Were such a rod to be constructed, our analysis predicts the deformation at the bottom would be

$$\delta = \frac{\gamma L^2}{2E} = \frac{7.85 \times 10^3(\text{kg/m}^3) \times 9.8(\text{m/s}^2) \times [15.6 \times 10^3(\text{m})]^2}{2 \times 210 \times 10^9(\text{N/m}^2)} = 44.6 \text{ m}$$

However, this analysis assumes Hooke's law holds over the entire range of stresses from zero to fracture. This is not true for many materials, including carbon steel, and later modules will address materials response at high stresses.

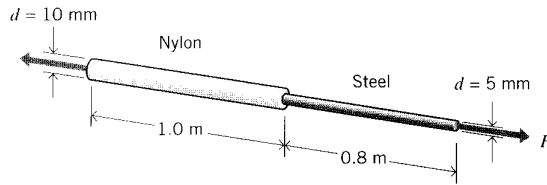
A material that obeys Hooke's Law (Eqn. 6) is called *Hookean*. Such a material is *elastic* according to the description of elasticity given in the introduction (immediate response, full recovery), and it is also *linear* in its relation between stress and strain (or equivalently, force and deformation). Therefore a Hookean material is *linear elastic*, and materials engineers use these descriptors interchangeably. It is important to keep in mind that not all elastic materials are linear (rubber is elastic but nonlinear), and not all linear materials are elastic (viscoelastic materials can be linear in the mathematical sense, but do not respond immediately and are thus not elastic).

The linear proportionality between stress and strain given by Hooke's law is not nearly as general as, say, Einstein's general theory of relativity, or even Newton's law of gravitation. It's really just an approximation that is observed to be reasonably valid for many materials as long the applied stresses are not too large. As the stresses are increased, eventually more complicated material response will be observed. Some of these effects will be outlined in the *Module on Stress-Strain Curves*, which introduces the experimental measurement of the strain response of materials over a range of stresses up to and including fracture.

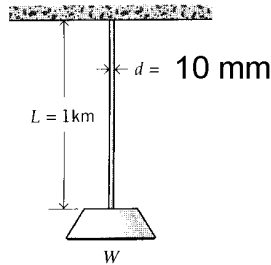
If we were to push on the specimen rather than pulling on it, the loading would be described as *compressive* rather than tensile. In the range of relatively low loads, Hooke's law holds for this case as well. By convention, compressive stresses and strains are negative, so the expression $\sigma = E\epsilon$ holds for both tension and compression.

Problems

1. Determine the stress and total deformation of an aluminum wire, 30 m long and 5 mm in diameter, subjected to an axial load of 250 N.
2. Two rods, one of nylon and one of steel, are rigidly connected as shown. Determine the stresses and axial deformations when an axial load of $F = 1 \text{ kN}$ is applied.
3. A steel cable 10 mm in diameter and 1 km long bears a load in addition to its own weight of $W = 150 \text{ N}$. Find the total elongation of the cable.
4. Using the numerical values given in the *Module on Material Properties*, rank the given materials in terms of the length of rod that will just barely support its own weight.
5. Plot the maximum self-supporting rod lengths of the materials in Prob. 4 versus the cost (per unit cross-sectional area) of the rod.



Prob. 2

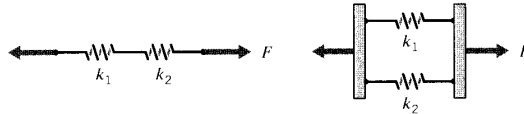


Prob. 3

6. Show that the effective stiffnesses of two springs connected in (a) series and (b) parallel is

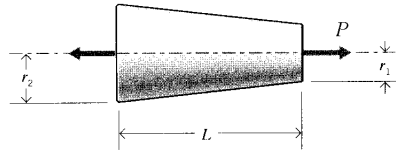
$$(a) \text{ series : } \frac{1}{k_{eff}} = \frac{1}{k_1} + \frac{1}{k_2} \quad (b) \text{ parallel : } k_{eff} = k_1 + k_2$$

(Note that these are the reverse of the relations for the effective electrical resistance of two resistors connected in series and parallel, which use the same symbols.)

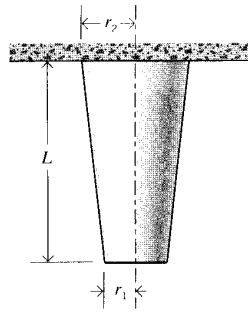


Prob. 6

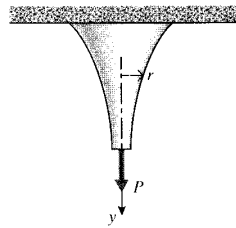
7. A tapered column of modulus E and mass density ρ varies linearly from a radius of r_1 to r_2 in a length L . Find the total deformation caused by an axial load P .
8. A tapered column of modulus E and mass density ρ varies linearly from a radius of r_1 to r_2 in a length L , and is hanging from its broad end. Find the total deformation due to the weight of the bar.
9. A rod of circular cross section hangs under the influence of its own weight, and also has an axial load P suspended from its free end. Determine the shape of the bar, i.e. the function $r(y)$ such that the axial stress is constant along the bar's length.
10. A bolt with 20 threads per inch passes through a sleeve, and a nut is threaded over the bolt as shown. The nut is then tightened one half turn beyond finger tightness; find the stresses in the bolt and the sleeve. All materials are steel, the cross-sectional area of the bolt is 0.5 in^2 , and the area of the sleeve is 0.4 in^2 .



Prob. 7



Prob. 8



Prob. 9



Prob. 10

ATOMISTIC BASIS OF ELASTICITY

David Roylance
Department of Materials Science and Engineering
Massachusetts Institute of Technology
Cambridge, MA 02139

January 27, 2000

Introduction

The *Introduction to Elastic Response* Module introduced two very important material properties, the ultimate tensile strength σ_f and the Young's modulus E . To the effective mechanical designer, these aren't just numerical parameters that are looked up in tables and plugged into equations. The very nature of the material is reflected in these properties, and designers who try to function without a sense of how the material really works are very apt to run into trouble. Whenever practical in these modules, we'll make an effort to put the material's mechanical properties in context with its processing and microstructure. This module will describe how for most engineering materials the modulus is controlled by the atomic bond energy function.

For most materials, the amount of stretching experienced by a tensile specimen under a small fixed load is controlled in a relatively simple way by the tightness of the chemical bonds at the atomic level, and this makes it possible to relate stiffness to the chemical architecture of the material. This is in contrast to more complicated mechanical properties such as fracture, which are controlled by a diverse combination of microscopic as well as molecular aspects of the material's internal structure and surface. Further, the stiffness of some materials — notably rubber — arises not from bond stiffness but from disordering or entropic factors. Some principal aspects of these atomistic views of elastic response are outlined in the sections to follow.

Energetic effects

Chemical bonding between atoms can be viewed as arising from the electrostatic attraction between regions of positive and negative electronic charge. Materials can be classified based on the nature of these electrostatic forces, the three principal classes being

1. *Ionic materials*, such as NaCl, in which an electron is transferred from the less electronegative element (Na) to the more electronegative (Cl). The ions therefore differ by one electronic charge and are thus attracted to one another. Further, the two ions feel an attraction not only to each other but also to other oppositely charged ions in their vicinity; they also feel a repulsion from nearby ions of the same charge. Some ions may gain or lose more than one electron.
2. *Metallic materials*, such as iron and copper, in which one or more loosely bound outer electrons are released into a common pool which then acts to bind the positively charged atomic cores.

3. Covalent materials, such as diamond and polyethylene, in which atomic orbitals overlap to form a region of increased electronic charge to which both nuclei are attracted. This bond is directional, with each of the nuclear partners in the bond feeling an attraction to the negative region between them but not to any of the other atoms nearby.

In the case of ionic bonding, Coulomb's law of electrostatic attraction can be used to develop simple but effective relations for the bond stiffness. For ions of equal charge e the attractive force f_{attr} can be written:

$$f_{attr} = \frac{Ce^2}{r^2} \quad (1)$$

Here C is a conversion factor; For e in Coulombs, $C = 8.988 \times 10^9 \text{ N-m}^2/\text{Coul}^2$. For singly ionized atoms, $e = 1.602 \times 10^{-19} \text{ Coul}$ is the charge on an electron. The *energy* associated with the Coulombic attraction is obtained by integrating the force, which shows that the bond energy varies inversely with the separation distance:

$$U_{attr} = \int f_{attr} dr = \frac{-Ce^2}{r} \quad (2)$$

where the energy of atoms at infinite separation is taken as zero.

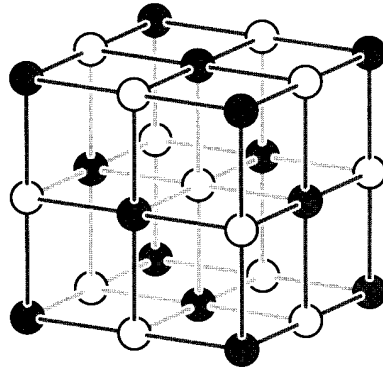


Figure 1: The interpenetrating cubic NaCl lattice.

If the material's atoms are arranged as a perfect crystal, it is possible to compute the electrostatic binding energy field in considerable detail. In the interpenetrating cubic lattice of the ionic NaCl structure shown in Fig. 1, for instance, each ion feels attraction to oppositely charged neighbors and repulsion from equally charged ones. A particular sodium atom is surrounded by 6 Cl^- ions at a distance r , 12 Na^+ ions at a distance $r\sqrt{2}$, 8 Cl^- ions at a distance $r\sqrt{3}$, etc. The total electronic field sensed by the first sodium ion is then:

$$\begin{aligned} U_{attr} &= -\frac{Ce^2}{r} \left(\frac{6}{\sqrt{1}} - \frac{12}{\sqrt{2}} + \frac{8}{\sqrt{3}} - \frac{6}{\sqrt{4}} + \frac{24}{\sqrt{5}} - \dots \right) \\ &= \frac{-ACe^2}{r} \end{aligned} \quad (3)$$

where $A = 1.747558 \dots$ is the result of the previous series, called the *Madelung constant*¹. Note that it is not sufficient to consider only nearest-neighbor attractions in computing the bonding energy; in fact the second term in the series is larger in magnitude than the first. The specific value for the Madelung constant is determined by the crystal structure, being 1.763 for CsCl and 1.638 for cubic ZnS.

At close separation distances, the attractive electrostatic force is balanced by mutual repulsion forces that arise from interactions between overlapping electron shells of neighboring ions; this force varies much more strongly with the distance, and can be written:

$$U_{rep} = \frac{B}{r^n} \quad (4)$$

Compressibility experiments have determined the exponent n to be 7.8 for the NaCl lattice, so this is a much steeper function than U_{attr} .

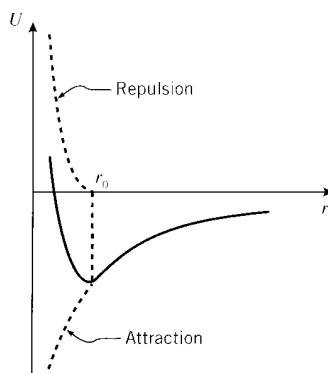


Figure 2: The bond energy function.

As shown in Fig. 2, the total binding energy of one ion due to the presence of all others is then the sum of the attractive and repulsive components:

$$U = -\frac{ACe^2}{r} + \frac{B}{r^n} \quad (5)$$

Note that the curve is *anharmonic* (not shaped like a sine curve), being more flattened out at larger separation distances. The system will adopt a configuration near the position of lowest energy, computed by locating the position of zero slope in the energy function:

$$\begin{aligned} (f)_{r=r_0} &= \left(\frac{dU}{dr} \right)_{r=r_0} = \left(\frac{ACe^2}{r^2} - \frac{nB}{r^{n+1}} \right)_{r=r_0} = 0 \\ r_0 &= \left(\frac{nB}{ACe^2} \right)^{\frac{1}{n-1}} \end{aligned} \quad (6)$$

The range for n is generally 5–12, increasing as the number of outer-shell electrons that cause the repulsive force.

¹C. Kittel, *Introduction to Solid State Physics*, John Wiley & Sons, New York, 1966. The Madelung series does not converge smoothly, and this text includes some approaches to computing the sum.

Example 1

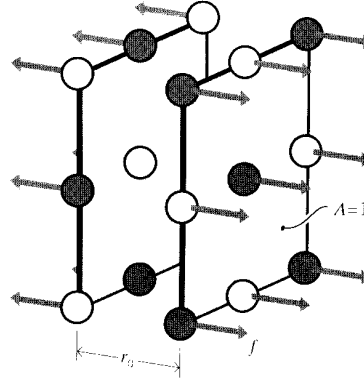


Figure 3: Simple tension applied to crystal face.

In practice the n and B parameters in Eqn. 5 are determined from experimental measurements, for instance by using a combination of X-ray diffraction to measure r_0 and elastic modulus to infer the slope of the $U(r)$ curve. As an illustration of this process, picture a tensile stress σ applied to a unit area of crystal ($A = 1$) as shown in Fig. 3, in a direction perpendicular to the crystal cell face. (The $[100]$ direction on the (100) face, using crystallographic notation².) The total force on this unit area is numerically equal to the stress: $F = \sigma A = \sigma$.

If the interionic separation is r_0 , there will be $1/r_0^2$ ions on the unit area, each being pulled by a force f . Since the total force F is just f times the number of ions, the stress can then be written

$$\sigma = F = f \frac{1}{r_0^2}$$

When the separation between two adjacent ions is increased by an amount δ , the strain is $\epsilon = \delta/r_0$. The differential strain corresponding to a differential displacement is then

$$d\epsilon = \frac{dr}{r_0}$$

The elastic modulus E is now the ratio of stress to strain, in the limit as the strain approaches zero:

$$E = \left. \frac{d\sigma}{d\epsilon} \right|_{\epsilon \rightarrow 0} = \left. \frac{1}{r_0} \frac{df}{dr} \right|_{r \rightarrow r_0} = \frac{1}{r_0} \frac{d}{dr} \left(\frac{ACe^2}{r^2} - \frac{nB}{r^{n+1}} \right) \Big|_{r \rightarrow r_0}$$

Using $B = ACe^2 r_0^{n-1}/n$ from Eqn. 6 and simplifying,

$$E = \frac{(n-1)ACe^2}{r_0^4}$$

Note the very strong dependence of E on r_0 , which in turn reflects the tightness of the bond. If E and r_0 are known experimentally, n can be determined. For NaCl, $E = 3 \times 10^{10}$ N/m²; using this along with the X-ray diffraction value of $r_0 = 2.82 \times 10^{-10}$ m, we find $n = 1.47$.

Using simple tension in this calculation is not really appropriate, because when a material is stretched in one direction, it will *contract* in the transverse directions. This is the *Poisson effect*, which will be treated in a later module. Our tension-only example does not consider the transverse contraction, and the resulting value of n is too low. A better but slightly more complicated approach is to use hydrostatic

²See the *Module on Crystallographic Notation* for a review of this nomenclature.

compression, which moves all the ions closer to one another. Problem 3 outlines this procedure, which yields values of n in the range of 5–12 as mentioned earlier.

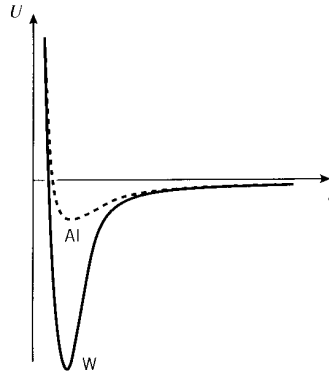


Figure 4: Bond energy functions for aluminum and tungsten.

The stiffnesses of metallic and covalent systems will be calculated differently than the method used above for ionic crystals, but the concept of electrostatic attraction applies to these non-ionic systems as well. As a result, bond energy functions of a qualitatively similar nature result from all these materials. In general, the “tightness” of the bond, and hence the elastic modulus E , is related to the curvature of the bond energy function. Steeper bond functions will also be deeper as a rule, so that within similar classes of materials the modulus tends to correlate with the energy needed to rupture the bonds, for instance by melting. Materials such as tungsten that fill many bonding and few antibonding orbitals have very deep bonding functions³, with correspondingly high stiffnesses and melting temperatures, as illustrated in Fig. 4. This correlation is obvious in Table 1, which lists the values of modulus for a number of metals, along with the values of melting temperature T_m and melting energy ΔH .

Table 1: Modulus and bond strengths for transition metals.

Material	E GPa (Mpsi)	T_m °C	ΔH kJ/mol	α_L $\times 10^{-6}, ^\circ\text{C}^{-1}$
Pb	14 (2)	327	5.4	29
Al	69 (10)	660	10.5	22
Cu	117 (17)	1084	13.5	17
Fe	207 (30)	1538	15.3	12
W	407 (59)	3410	32	4.2

The system will generally have sufficient thermal energy to reside at a level somewhat above the minimum in the bond energy function, and will oscillate between the two positions labeled A and B in Fig. 5, with an average position near r_0 . This simple idealization provides a rationale for why materials expand when the temperature is raised. As the internal energy is increased by the

³A detailed analysis of the cohesive energies of materials is an important topic in solid state physics; see for example F. Seitz, *The Modern Theory of Solids*, McGraw-Hill, 1940.

addition of heat, the system oscillates between the positions labeled A' and B' with an average separation distance r'_0 . Since the curve is anharmonic, the average separation distance is now greater than before, so the material has expanded or stretched. To a reasonable approximation, the relative thermal expansion $\Delta L/L$ is often related linearly to the temperature rise ΔT , and we can write:

$$\boxed{\frac{\Delta L}{L} = \epsilon_T = \alpha_L \Delta T} \quad (7)$$

where ϵ_T is a *thermal strain* and the constant of proportionality α_L is the *coefficient of linear thermal expansion*. The expansion coefficient α_L will tend to correlate with the depth of the energy curve, as is seen in Table 1.

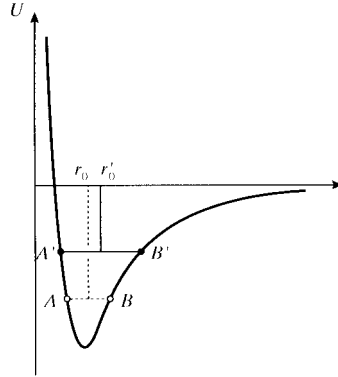


Figure 5: Anharmonicity of the bond energy function.

Example 2

A steel bar of length L and cross-sectional area A is fitted snugly between rigid supports as shown in Fig. 6. We wish to find the compressive stress in the bar when the temperature is raised by an amount ΔT .

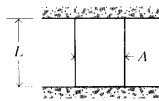


Figure 6: Bar between rigid supports.

If the bar were free to expand, it would increase in length by an amount given by Eqn. 7. Clearly, the rigid supports have to push on the bar – i.e. put in into compression – to suppress this expansion. The magnitude of this thermally induced compressive stress could be found by imagining the material free to expand, then solving $\sigma = E\epsilon_T$ for the stress needed to “push the material back” to its unstrained state. Equivalently, we could simply set the sum of a thermally induced strain and a mechanical strain ϵ_σ to zero:

$$\epsilon = \epsilon_\sigma + \epsilon_T = \frac{\sigma}{E} + \alpha_L \Delta T = 0$$

$$\sigma = -\alpha_L E \Delta T$$

The minus sign in this result reminds us that a negative (compressive) stress is induced by a positive temperature change (temperature rises.)

Example 3

A glass container of stiffness E and thermal expansion coefficient α_L is removed from a hot oven and plunged suddenly into cold water. We know from experience that this “thermal shock” could fracture the glass, and we’d like to see what materials parameters control this phenomenon. The analysis is very similar to that of the previous example.

In the time period just after the cold-water immersion, before significant heat transfer by conduction can take place, the outer surfaces of the glass will be at the temperature of the cold water while the interior is still at the temperature of the oven. The outer surfaces will try to contract, but are kept from doing so by the still-hot interior; this causes a tensile stress to develop on the surface. As before, the stress can be found by setting the total strain to zero:

$$\epsilon = \epsilon_\sigma + \epsilon_T = \frac{\sigma}{E} + \alpha_L \Delta T = 0$$

$$\sigma = -\alpha_L E \Delta T$$

Here the temperature change ΔT is negative if the glass is going from hot to cold, so the stress is positive (tensile). If the glass is not to fracture by thermal shock, this stress must be less than the ultimate tensile strength σ_f ; hence the maximum allowable temperature difference is

$$-\Delta T_{max} = \frac{\sigma_f}{\alpha_L E}$$

To maximize the resistance to thermal shock, the glass should have as low a value of $\alpha_L E$ as possible. “Pyrex” glass was developed specifically for improved thermal shock resistance by using boron rather than soda and lime as process modifiers; this yields a much reduced value of α_L .

Material properties for a number of important structural materials are listed in the *Module on Material Properties*. When the column holding Young’s Modulus is plotted against the column containing the Thermal Expansion Coefficients (using log-log coordinates), the graph shown in Fig. 7 is obtained. Here we see again the general inverse relationship between stiffness and thermal expansion, and the distinctive nature of polymers is apparent as well.

Not all types of materials can be described by these simple bond-energy concepts: *intra*-molecular polymer covalent bonds have energies entirely comparable with ionic or metallic bonds, but most common polymers have substantially lower moduli than most metals or ceramics. This is due to the *inter*molecular bonding in polymers being due to secondary bonds which are much weaker than the strong intramolecular covalent bonds. Polymers can also have substantial entropic contributions to their stiffness, as will be described below, and these effects do not necessarily correlate with bond energy functions.

Entropic effects

The internal energy as given by the function $U(r)$ is sufficient to determine the atomic positions in many engineering materials; the material “wants” to minimize its internal energy, and it does this by optimizing the balance of attractive and repulsive electrostatic bonding forces.

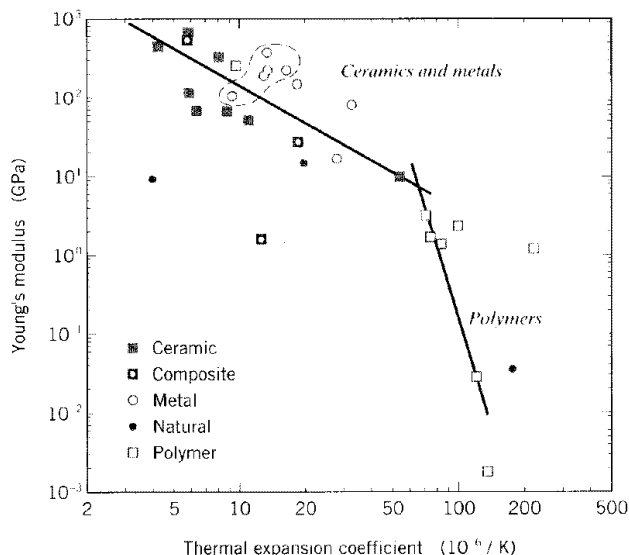


Figure 7: Correlation of stiffness and thermal expansion for materials of various types.

But when the absolute temperature is greater than approximately two-thirds of the melting temperature, there can be sufficient molecular mobility that entropic or disordering effects must be considered as well. This is often the case for polymers even at room temperature, due to their weak intermolecular bonding.

When the temperature is high enough, polymer molecules can be viewed as an interpenetrating mass of (extremely long) wriggling worms, constantly changing their positions by rotation about carbon-carbon single bonds. This wriggling does not require straining the bond lengths or angles, and large changes in position are possible with no change in internal bonding energy.

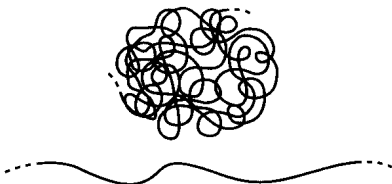


Figure 8: Conformational change in polymers.

The shape, or “conformation” of a polymer molecule can range from a fully extended chain to a randomly coiled sphere (see Fig. 8). Statistically, the coiled shape is much more likely than the extended one, simply because there are so many ways the chain can be coiled and only one way it can be fully extended. In thermodynamic terms, the entropy of the coiled conformation is very high (many possible “microstates”), and the entropy of the extended conformation is very low (only one possible microstate). If the chain is extended and then released, there will be more wriggling motions tending to the most probable state than to even more highly stretched states; the material would therefore shrink back to its unstretched and highest-entropy state. Equivalently, a person holding the material in the stretched state would feel a tensile force as the material tries to unstretch and is prevented from doing so. These effects are due to entropic

factors, and not internal bond energy.

It is possible for materials to exhibit both internal energy and entropic elasticity. Energy effects dominate in most materials, but rubber is much more dependent on entropic effects. An *ideal rubber* is one in which the response is completely entropic, with the internal energy changes being negligible.

When we stretch a rubber band, the molecules in its interior become extended because they are *crosslinked* by chemical or physical junctions as shown in Fig. 9. Without these links, the molecules could simply slide past one another with little or no uncoiling. “Silly Putty ” is an example of uncrosslinked polymer, and its lack of junction connections cause it to be a viscous fluid rather than a useful elastomer that can bear sustained loads without continuing flow. The crosslinks provide a means by which one molecule can pull on another, and thus establish load transfer within the materials. They also have the effect of limiting how far the rubber can be stretched before breaking, since the extent of the entropic uncoiling is limited by how far the material can extend before pulling up tight against the network of junction points. We will see below that the stiffness of a rubber can be controlled directly by adjusting the crosslink density, and this is an example of process-structure-property control in materials.

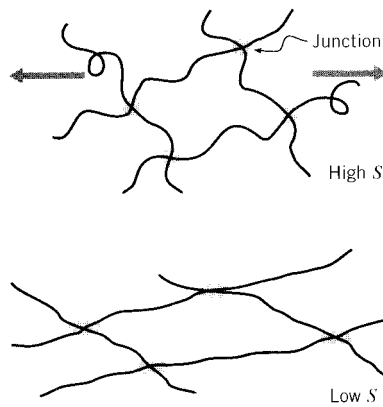


Figure 9: Stretching of crosslinked or entangled polymers.

As the temperature is raised, the Brownian-type wriggling of the polymer is intensified, so that the material seeks more vigorously to assume its random high-entropy state. This means that the force needed to hold a rubber band at fixed elongation *increases* with increasing temperature. Similarly, if the band is stretched by hanging a fixed weight on it, the band will *shrink* as the temperature is raised. In some thermodynamic formalisms it is convenient to model this behavior by letting the coefficient of thermal expansion be a variable parameter, with the ability to become negative for sufficiently large tensile strains. This is a little tricky, however; for instance, the stretched rubber band will contract only along its long axis when the temperature is raised, and will become thicker in the transverse directions. The coefficient of thermal expansion would have to be made not only stretch-dependent but also dependent on direction (“anisotropic”).

Example 4

An interesting demonstration of the unusual thermal response of stretched rubber bands involves replacing the spokes of a bicycle wheel with stretched rubber bands as seen in Fig. 10, then mounting

the wheel so that a heat lamp shines on the bands to the right or left of the hub. As the bands warm up, they contract. This pulls the rim closer to the hub, causing the wheel to become unbalanced. It will then rotate under gravity, causing the warmed bands to move out from under the heat lamp and be replaced other bands. The process continues, and the wheel rotates in a direction opposite to what would be expected were the spokes to expand rather than contract on heating.

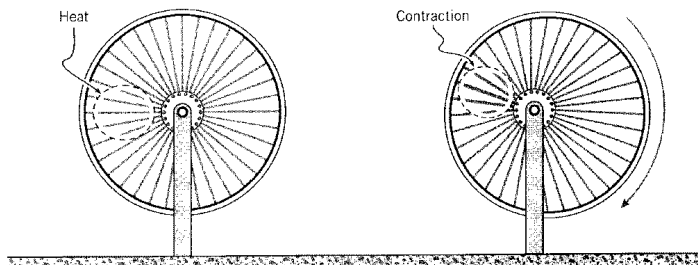


Figure 10: A bicycle wheel with entropic spokes.

The bicycle-wheel trick produces a rather weak response, and it is easy to stop the wheel with only a light touch of the finger. However, the same idea, using very highly stretched urethane bands and employing superheated geothermal steam as a heat source, becomes a viable route for generating mechanical energy.

It is worthwhile to study the response of rubbery materials in some depth, partly because this provides a broader view of the elasticity of materials. But this isn't a purely academic goal. Rubbery materials are being used in increasingly demanding mechanical applications (in addition to tires, which is a very demanding application itself). Elastomeric bearings, vibration-control supports, and biomedical prostheses are but a few examples. We will outline what is known as the "kinetic theory of rubber elasticity," which treats the entropic effect using concepts of statistical thermodynamics. This theory stands as one of the very most successful atomistic theories of mechanical response. It leads to a result of satisfying accuracy without the need for adjustable parameters or other fudge factors.

When pressure-volume changes are not significant, the competition between internal energy and entropy can be expressed by the Helmholtz free energy $A = U - TS$, where T is the temperature and S is the entropy. The system will move toward configurations of lowest free energy, which it can do either by reducing its internal energy or by increasing its entropy. Note that the influence of the entropic term increases explicitly with increasing temperature. With certain thermodynamic limitations in mind (see Prob. 5), the mechanical work $dW = F dL$ done by a force F acting through a differential displacement dL will produce an increase in free energy given by

$$F dL = dW = dU - T dS \quad (8)$$

or

$$F = \frac{dW}{dL} = \left(\frac{\partial U}{\partial L} \right)_{T,V} - T \left(\frac{\partial S}{\partial L} \right)_{T,V} \quad (9)$$

For an ideal rubber, the energy change dU is negligible, so the force is related directly to the temperature and the change in entropy dS produced by the force. To determine the force-deformation relationship, we obviously need to consider how S changes with deformation.

We begin by writing an expression for the conformation, or shape, of the segment of polymer molecule between junction points as a statistical probability distribution. Here the length of the *segment* is the important molecular parameter, not the length of the entire molecule. In the simple form of this theory, which turns out to work quite well, each covalently bonded segment is idealized as a freely-jointed sequence of n rigid links each having length a .

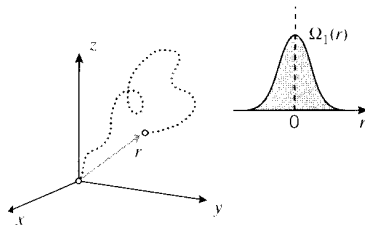


Figure 11: Random-walk model of polymer conformation

A reasonable model for the end-to-end distance of a randomly wriggling segment is that of a “random walk” Gaussian distribution treated in elementary statistics. One end of the chain is visualized at the origin of an xyz coordinate system as shown in Fig. 11, and each successive link in the chain is attached with a random orientation relative to the previous link. (An elaboration of the theory would constrain the orientation so as to maintain the 109° covalent bonding angle.) The probability $\Omega_1(r)$ that the other end of the chain is at a position $r = (x^2 + y^2 + z^2)^{1/2}$ can be shown to be

$$\Omega_1(r) = \frac{\beta^3}{\sqrt{\pi}} \exp(-\beta^2 r^2) = \frac{\beta^3}{\sqrt{\pi}} \exp \left[-\beta^2 (x^2 + y^2 + z^2) \right]$$

The parameter β is a scale factor related to the number of units n in the polymer segment and the bond length a ; specifically it turns out that $\beta = \sqrt{3/2n}/a$. This is the “bell-shaped curve” well known to seasoned test-takers. The most probable end-to-end distance is seen to be zero, which is expected because the chain will end up a given distance to the left (or up, or back) of the origin exactly as often as it ends up the same distance to the right.

When the molecule is now stretched or otherwise deformed, the relative positions of the two ends are changed. Deformation in elastomers is usually described in terms of *extension ratios*, which are the ratios of stretched to original dimensions, L/L_0 . Stretches in the x , y , and z directions are denoted by λ_x , λ_y , and λ_z respectively. The deformation is assumed to be *affine*, i.e. the end-to-end distances of each molecular segment increase by these same ratios. Hence if we continue to view one end of the chain at the origin the other end will have moved to $x_2 = \lambda_x x$, $y_2 = \lambda_y y$, $z_2 = \lambda_z z$. The configurational probability of a segment being found in this stretched state is then

$$\Omega_2 = \frac{\beta^3}{\sqrt{\pi}} \exp \left[-\beta^2 (\lambda_x^2 x^2 + \lambda_y^2 y^2 + \lambda_z^2 z^2) \right]$$

The relative change in probabilities between the perturbed and unperturbed states can now be written as

$$\ln \frac{\Omega_2}{\Omega_1} = -\beta^2 \left[(\lambda_x^2 - 1) x^2 + (\lambda_y^2 - 1) y^2 + (\lambda_z^2 - 1) z^2 \right]$$

Several strategies have been used in the literature to simplify this expression. One simple approach is to let the initial position of the segment end x, y, z be such that $x^2 = y^2 = z^2 = \overline{r_0^2}/3$, where $\overline{r_0^2}$ is the initial mean square end-to-end distance of the segment. (This is not zero, since when squares are taken the negative values no longer cancel the positive ones.) It can also be shown (see Prob. 8) that the distance $\overline{r_0^2}$ is related to the number of bonds n in the segment and the bond length a by $\overline{r_0^2} = na^2$. Making these substitutions and simplifying, we have

$$\ln \frac{\Omega_2}{\Omega_1} = -\frac{1}{2} (\lambda_x^2 + \lambda_y^2 + \lambda_z^2 - 3) \quad (10)$$

As is taught in subjects in statistical thermodynamics, changes in configurational probability are related to corresponding changes in thermodynamic entropy by the “Boltzman relation” as

$$\Delta S = k \ln \frac{\Omega_2}{\Omega_1}$$

where $k = 1.38 \times 10^{-23}$ J/K is Boltzman’s constant. Substituting Eqn. 10 in this relation:

$$\Delta S = -\frac{k}{2} (\lambda_x^2 + \lambda_y^2 + \lambda_z^2 - 3)$$

This is the entropy change for one segment. If there are N chain segments per unit volume, the total entropy change per unit volume ΔS_V is just N times this quantity:

$$\Delta S_V = -\frac{Nk}{2} (\lambda_x^2 + \lambda_y^2 + \lambda_z^2 - 3) \quad (11)$$

The associated work (per unit volume) required to change the entropy by this amount is

$$\boxed{\Delta W_V = -T\Delta S_V = +\frac{NkT}{2} (\lambda_x^2 + \lambda_y^2 + \lambda_z^2 - 3)} \quad (12)$$

The quantity ΔW_V is therefore the strain energy per unit volume contained in an ideal rubber stretched by $\lambda_x, \lambda_y, \lambda_z$.

Example 5

Recent research by Prof. Christine Ortiz has demonstrated that the elasticity of individual polymer chains can be measured using a variety of high-resolution force spectroscopy techniques, such as atomic force microscopy (AFM). At low to moderate extensions, most polymer chains behave as ideal, entropic, random coils; i.e. molecular rubber bands. This is shown in Fig. 12, which displays AFM data (retraction force, F_{chain} , versus chain end-to-end separation distance) for stretching and uncoiling of single polystyrene chains of different lengths. By fitting experimental data with theoretical polymer physics models of freely-jointed chains (red lines in Fig. 12) or worm-like chains, we can estimate the “statistical segment length” or local chain stiffness and use this parameter as a probe of chemical structure and local environmental effects (e.g. electrostatic interactions, solvent quality, etc.). In addition, force spectroscopy can be used to measure noncovalent, physisorption forces of single polymer chains on surfaces and covalent bond strength (chain “fracture”).

To illustrate the use of Eqn. 12 for a simple but useful case, consider a rubber band, initially of length L_0 which is stretched to a new length L . Hence $\lambda = \lambda_x = L/L_0$. To a very good approximation, rubbery materials maintain a constant volume during deformation, and this lets us compute the transverse contractions λ_y and λ_z which accompany the stretch λ_x . An

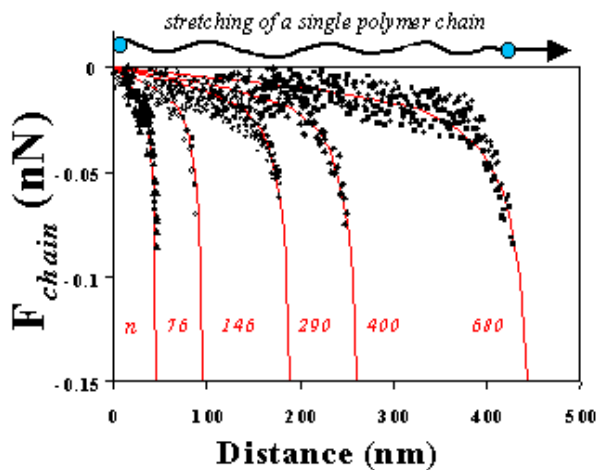


Figure 12: Experimental measurements from numerous force spectroscopy (AFM) experiments of force-elongation response of single polystyrene segments in toluene, compared to the freely-jointed chain model. The statistical segment length is 0.68, and n = number of molecular units in the segment.

expression for the change ΔV in a cubical volume of initial dimensions a_0, b_0, c_0 which is stretched to new dimensions a, b, c is

$$\Delta V = abc - a_0b_0c_0 = (a_0\lambda_x)(b_0\lambda_y)(c_0\lambda_z) - a_0b_0c_0 = a_0b_0c_0(\lambda_x\lambda_y\lambda_z - 1)$$

Setting this to zero gives

$$\lambda_x\lambda_y\lambda_z = 1 \quad (13)$$

Hence the contractions in the y and z directions are

$$\lambda_y^2 = \lambda_z^2 = \frac{1}{\lambda}$$

Using this in Eqn. 12, the force F needed to induce the deformation can be found by differentiating the total strain energy according to Eqn. 9:

$$F = \frac{dW}{dL} = \frac{d(V \Delta W_V)}{L_0 d\lambda} = A_0 \frac{NkT}{2} \left(2\lambda - \frac{2}{\lambda^2} \right)$$

Here $A_0 = V/L_0$ is the original area. Dividing by A_0 to obtain the engineering stress:

$$\boxed{\sigma = NkT \left(\lambda - \frac{1}{\lambda^2} \right)} \quad (14)$$

Clearly, the parameter NkT is related to the stiffness of the rubber, as it gives the stress σ needed to induce a given extension λ . It can be shown (see Prob. 10) that the initial modulus — the slope of the stress-strain curve at the origin — is controlled by the temperature and the crosslink density according to $E = 3NkT$.

Crosslinking in rubber is usually done in the “vulcanizing” process invented by Charles Goodyear in 1839. In this process sulfur abstracts reactive hydrogens adjacent to the double

bonds in the rubber molecule, and forms permanent bridges between adjacent molecules. When crosslinking is done by using approximately 5% sulfur, a conventional rubber is obtained. When the sulfur is increased to $\approx 30\text{--}50\%$, a hard and brittle material named ebonite (or simply “hard rubber”) is produced instead.

The volume density of chain segments N is also the density of junction points. This quantity is related to the specimen density ρ and the molecular weight between crosslinks M_c as $M_c = \rho N_A / N$, where N is the number of crosslinks per unit volume and $N_A = 6.023 \times 10^{23}$ is Avogadro’s Number. When N is expressed in terms of moles per unit volume, we have simply $M_c = \rho / N$ and the quantity NkT in Eqn. 14 is replaced by NRT , where $R = kN_A = 8.314$ J/mol-°K is the Gas Constant.

Example 6

The Young’s modulus of a rubber is measured at $E = 3.5$ MPa for a temperature of $T = 300$ °K. The molar crosslink density is then

$$N = \frac{E}{3RT} = \frac{3.5 \times 10^6 \text{ N/m}^2}{3 \times 8.314 \frac{\text{N}\cdot\text{m}}{\text{mol}\cdot\text{K}} \times 300 \text{ K}} = 468 \text{ mol/m}^3$$

The molecular weight per segment is

$$M_c = \frac{\rho}{N} = \frac{1100 \text{ kg/m}^3}{468 \text{ mol/m}^3} = 2350 \text{ gm/mol}$$

Example 7

A person with more entrepreneurial zeal than caution wishes to start a bungee-jumping company, and naturally wants to know how far the bungee cord will stretch; the clients sometimes complain if the cord fails to stop them before they reach the asphalt. It’s probably easiest to obtain a first estimate from an energy point of view: say the unstretched length of the cord is L_0 , and that this is also the distance the jumper free-falls before the cord begins to stretch. Just as the cord begins to stretch, the the jumper has lost an amount of potential energy wL_0 , where w is the jumper’s weight. The jumper’s velocity at this time could then be calculated from $(mv^2)/2 = wL_0$ if desired, where $m = w/g$ is the jumper’s mass and g is the acceleration of gravity. When the jumper’s velocity has been brought to zero by the cord (assuming the cord doesn’t break first, and the ground doesn’t intervene), this energy will now reside as entropic strain energy within the cord. Using Eqn. 12, we can equate the initial and final energies to obtain

$$wL_0 = \frac{A_0 L_0 \cdot NRT}{2} \left(\lambda^2 + \frac{2}{\lambda} - 3 \right)$$

Here $A_0 L_0$ is the total volume of the cord; the entropic energy per unit volume ΔW_V must be multiplied by the volume to give total energy. Dividing out the initial length L_0 and using $E = 3NRT$, this result can be written in the dimensionless form

$$\frac{w}{A_0 E} = \frac{1}{6} \left(\lambda^2 + \frac{2}{\lambda} - 3 \right)$$

The closed-form solution for λ is messy, but the variable $w/A_0 E$ can easily be plotted versus λ (see Fig. 13.) Note that the length L_0 has canceled from the result, although it is still present implicitly in the extension ratio $\lambda = L/L_0$.

Taking a typical design case for illustration, say the desired extension ratio is taken at $\lambda = 3$ for a rubber cord of initial modulus $E = 100$ psi; this stops the jumper safely above the pavement and is verified

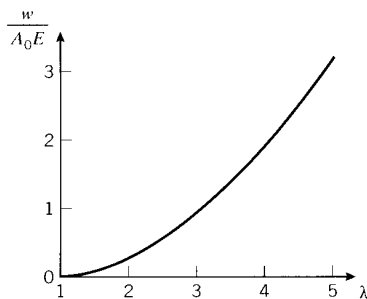


Figure 13: Dimensionless weight versus cord extension.

to be well below the breaking extension of the cord. The value of the parameter w/AE corresponding to $\lambda = 3$ is read from the graph to be 1.11. For a jumper weight of 150 lb, this corresponds to $A = 1.35 \text{ in}^2$, or a cord diameter of 1.31 in.

If ever there was a strong case for field testing, this is it. An analysis such as this is nothing more than a crude starting point, and many tests such as drops with sandbags are obviously called for. Even then, the insurance costs would likely be very substantial.

Note that the stress-strain response for rubber elasticity is nonlinear, and that the stiffness as given by the stress needed to produce a given deformation is predicted to increase with increasing temperature. This is in accord with the concept of more vigorous wriggling with a statistical bias toward the more disordered state. The rubber elasticity equation works well at lower extensions, but tends to deviate from experimental values at high extensions where the segment configurations become nongaussian.

Deviations from Eqn. 14 can also occur due to crystallization at high elongations. (Rubbers are normally noncrystalline, and in fact polymers such as polyethylene that crystallize readily are not elastomeric due to the rigidity imparted by the crystallites.) However, the decreased entropy that accompanies stretching in rubber increases the crystalline melting temperature according to the well-known thermodynamic relation

$$T_m = \frac{\Delta U}{\Delta S} \quad (15)$$

where ΔU and ΔS are the change in internal energy and entropy on crystallization. The quantity ΔS is reduced if stretching has already lowered the entropy, so the crystallization temperature rises. If it rises above room temperature, the rubber develops crystallites that stiffen it considerably and cause further deviation from the rubber elasticity equation. (Since the crystallization is exothermic, the material will also increase in temperature; this can often be sensed by stretching a rubber band and then touching it to the lips.) Strain-induced crystallization also helps inhibit crack growth, and the excellent abrasion resistance of natural rubber is related to the ease with which it crystallizes upon stretching.

Problems

1. Justify the first two terms of the Madelung series given in Eqn. 3.
2. Using Eqn. 6 to write the parameter B in terms of the equilibrium interionic distance r_0 , show that the binding energy of an ionic crystal, per bond pair, can be written as

$$U = -\frac{(n-1)ACe^2}{nr_0}$$

where A is the Madelung constant, C is the appropriate units conversion factor, and e is the ionic charge.

3. Measurements of bulk compressibility are valuable for probing the bond energy function, because unlike simple tension, hydrostatic pressure causes the interionic distance to decrease uniformly. The *modulus of compressibility* K of a solid is the ratio of the pressure p needed to induce a relative change in volume dV/V :

$$K = -\frac{dp}{(dV)/V}$$

The minus sign is needed because positive pressures induce reduced volumes (volume change negative).

- (a) Use the relation $dU = pdV$ for the energy associated with pressure acting through a small volume change to show

$$\frac{K}{V_0} = \left(\frac{d^2U}{dV^2} \right)_{V=V_0}$$

where V_0 is the crystal volume at the equilibrium interionic spacing $r = a_0$.

- (b) The volume of an ionic crystal containing N negative and N positive ions can be written as $V = cNr^3$ where c is a constant dependent on the type of lattice (2 for NaCl). Use this to obtain the relation

$$\frac{K}{V_0} = \left(\frac{d^2U}{dV^2} \right)_{V=V_0} = \frac{1}{9c^2N^2r^2} \cdot \frac{d}{dr} \left(\frac{1}{r^2} \frac{dU}{dr} \right)$$

- (c) Carry out the indicated differentiation of the expression for binding energy to obtain the expression

$$\frac{K}{V_0} = \frac{K}{cNr_0^3} = \frac{N}{9c^2Nr_0^2} \left[\frac{-4ACe}{r_0^5} + \frac{n(n+3)B}{r_0^{n+4}} \right]$$

Then using the expression $B = ACe^2r_0^{n-1}/n$, obtain the formula for n in terms of compressibility:

$$n = 1 + \frac{9cr_0^4K}{ACe^2}$$

4. Complete the spreadsheet below, filling in the values for repulsion exponent n and lattice energy U .

type	r_0 (pm)	K (GPa)	A	n	U (kJ/mol)	U_{expt}
LiF	201.4	6.710e+01	1.750			-1014
NaCl	282.0	2.400e+01	1.750			-764
KBr	329.8	1.480e+01	1.750			-663

The column labeled U_{expt} lists experimentally obtained values of the lattice energy.

5. Given the definition of Helmholtz free energy:

$$A = U - TS$$

along with the first and second laws of thermodynamics:

$$dU = dQ + dW$$

$$dQ = TdS$$

where U is the internal energy, T is the temperature, S is the entropy, Q is the heat and W is the mechanical work, show that the force F required to hold the ends of a tensile specimen a length L apart is related to the Helmholtz energy as

$$F = \left(\frac{\partial A}{\partial L} \right)_{T,V}$$

6. Show that the temperature dependence of the force needed to hold a tensile specimen at fixed length as the temperature is changed (neglecting thermal expansion effects) is related to the dependence of the entropy on extension as

$$\left(\frac{\partial F}{\partial T} \right)_L = - \left(\frac{\partial S}{\partial L} \right)_T$$

7. (a) Show that if an ideal rubber ($dU = 0$) of mass M and specific heat c is extended adiabatically, its temperature will change according to the relation

$$\frac{\partial T}{\partial L} = \frac{-T}{Mc} \left(\frac{\partial S}{\partial L} \right)$$

i.e. if the entropy is reduced upon extension, the temperature will rise. This is known as the *thermoelastic effect*.

- (b) Use this expression to obtain the temperature change dT in terms of an increase $d\lambda$ in the extension ratio as

$$dT = \frac{\sigma}{\rho c} d\lambda$$

where σ is the engineering stress (load divided by original area) and ρ is the mass density.

8. Show that the end-to-end distance r_0 of a chain composed of n freely-jointed links of length a is given by $r_0 = na^2$.

9. Evaluate the temperature rise in a rubber specimen of $\rho = 1100 \text{ kg/m}^3$, $c = 2 \text{ kJ/kg}\cdot\text{K}$, $NkT = 500 \text{ kPa}$, subjected to an axial extension $\lambda = 4$.
10. Show that the initial engineering modulus of a rubber whose stress-strain curve is given by Eqn. 14 is $E = 3NRT$.
11. Calculate the Young's modulus of a rubber of density 1100 gm/mol and whose inter-crosslink segments have a molecular weight of 2500 gm/mol . The temperature is 25°C .
12. Show that in the case of biaxial extension (λ_x and λ_y prescribed), the x -direction stress based on the original cross-sectional dimensions is

$$\sigma_x = NkT \left(\lambda_x - \frac{1}{\lambda_x^3 \lambda_y^2} \right)$$

and based on the deformed dimensions

$${}^t\sigma_x = NkT \left(\lambda_x^2 - \frac{1}{\lambda_x^2 \lambda_y^2} \right)$$

where the t subscript indicates a "true" or current stress.

13. Estimate the initial elastic modulus E , at a temperature of 20°C , of an elastomer having a molecular weight of $7,500 \text{ gm/mol}$ between crosslinks and a density of 1.0 gm/cm^3 . What is the percentage change in the modulus if the temperature is raised to 40°C ?
14. Consider a line on a rubber sheet, originally oriented at an angle ϕ_0 from the vertical. When the sheet is stretched in the vertical direction by an amount $\lambda_y = \lambda$, the line rotates to a new inclination angle ϕ' . Show that

$$\tan \phi' = \frac{1}{\lambda^{3/2}} \tan \phi_0$$

15. Before stretching, the molecular segments in a rubber sheet are assumed to be distributed uniformly over all directions, so the the fraction of segments $f(\phi)$ oriented in a particular range of angles $d\phi$ is

$$f(\phi) = \frac{dA}{A} = \frac{2\pi r^2 \sin \phi d\phi}{2\pi r}$$

The *Herrman orientation parameter* is defined in terms of the mean orientation as

$$f = \frac{1}{2} (3 \langle \cos^2 \phi' \rangle - 1), \quad \langle \cos^2 \phi' \rangle = \int_0^{\pi/2} \cos^2 \phi' f(\phi) d\phi$$

Using the result of the previous problem, plot the orientation function f as a function of the extension ratio λ .

INTRODUCTION TO COMPOSITE MATERIALS

David Roylance
Department of Materials Science and Engineering
Massachusetts Institute of Technology
Cambridge, MA 02139

March 24, 2000

Introduction

This module introduces basic concepts of stiffness and strength underlying the mechanics of fiber-reinforced advanced composite materials. This aspect of composite materials technology is sometimes terms “micromechanics,” because it deals with the relations between macroscopic engineering properties and the microscopic distribution of the material’s constituents, namely the volume fraction of fiber. This module will deal primarily with unidirectionally-reinforced continuous-fiber composites, and with properties measured along and transverse to the fiber direction.

Materials

The term *composite* could mean almost anything if taken at face value, since all materials are composed of dissimilar subunits if examined at close enough detail. But in modern materials engineering, the term *usually* refers to a “matrix” material that is reinforced with fibers. For instance, the term “FRP” (for Fiber Reinforced Plastic) usually indicates a thermosetting polyester matrix containing glass fibers, and this particular composite has the lion’s share of today’s commercial market. Figure 1 shows a laminate fabricated by “crossplying” unidirectionally-reinforced layers in a 0° - 90° stacking sequence.

Many composites used today are at the leading edge of materials technology, with performance and costs appropriate to ultrademanding applications such as spacecraft. But heterogeneous materials combining the best aspects of dissimilar constituents have been used by nature for millions of years. Ancient society, imitating nature, used this approach as well: the Book of Exodus speaks of using straw to reinforce mud in brickmaking, without which the bricks would have almost no strength.

As seen in Table 1¹, the fibers used in modern composites have strengths and stiffnesses far above those of traditional bulk materials. The high strengths of the glass fibers are due to processing that avoids the internal or surface flaws which normally weaken glass, and the strength and stiffness of the polymeric aramid fiber is a consequence of the nearly perfect alignment of the molecular chains with the fiber axis.

¹F.P. Gerstle, “Composites,” *Encyclopedia of Polymer Science and Engineering*, Wiley, New York, 1991. Here E is Young’s modulus, σ_b is breaking stress, ϵ_b is breaking strain, and ρ is density.

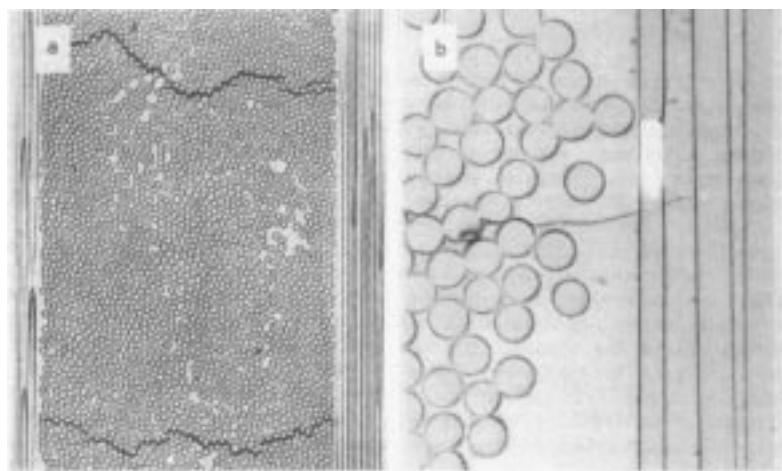


Figure 1: A crossplied FRP laminate, showing nonuniform fiber packing and microcracking (from Harris, 1986).

Table 1: Properties of Composite Reinforcing Fibers.

Material	E (GPa)	σ_b (GPa)	ϵ_b (%)	ρ (Mg/m ³)	E/ρ (MJ/kg)	σ_b/ρ (MJ/kg)	cost (\$/kg)
E-glass	72.4	2.4	2.6	2.54	28.5	0.95	1.1
S-glass	85.5	4.5	2.0	2.49	34.3	1.8	22–33
aramid	124	3.6	2.3	1.45	86	2.5	22–33
boron	400	3.5	1.0	2.45	163	1.43	330–440
HS graphite	253	4.5	1.1	1.80	140	2.5	66–110
HM graphite	520	2.4	0.6	1.85	281	1.3	220–660

Of course, these materials are not generally usable as fibers alone, and typically they are impregnated by a matrix material that acts to transfer loads to the fibers, and also to protect the fibers from abrasion and environmental attack. The matrix dilutes the properties to some degree, but even so very high specific (weight-adjusted) properties are available from these materials. Metal and glass are available as matrix materials, but these are currently very expensive and largely restricted to R&D laboratories. Polymers are much more commonly used, with unsaturated styrene-hardened polyesters having the majority of low-to-medium performance applications and epoxy or more sophisticated thermosets having the higher end of the market. Thermoplastic matrix composites are increasingly attractive materials, with processing difficulties being perhaps their principal limitation.

Stiffness

The fibers may be oriented randomly within the material, but it is also possible to arrange for them to be oriented preferentially in the direction expected to have the highest stresses. Such a material is said to be *anisotropic* (different properties in different directions), and control of the anisotropy is an important means of optimizing the material for specific applications. At a microscopic level, the properties of these composites are determined by the orientation and

distribution of the fibers, as well as by the properties of the fiber and matrix materials. The topic known as composite *micromechanics* is concerned with developing estimates of the overall material properties from these parameters.

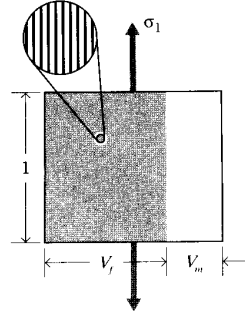


Figure 2: Loading parallel to the fibers.

Consider a typical region of material of unit dimensions, containing a volume fraction V_f of fibers all oriented in a single direction. The matrix volume fraction is then $V_m = 1 - V_f$. This region can be idealized as shown in Fig. 2 by gathering all the fibers together, leaving the matrix to occupy the remaining volume — this is sometimes called the “slab model.” If a stress σ_1 is applied along the fiber direction, the fiber and matrix phases act in *parallel* to support the load. In these parallel connections the strains in each phase must be the same, so the strain ϵ_1 in the fiber direction can be written as:

$$\epsilon_f = \epsilon_m = \epsilon_1$$

The forces in each phase must add to balance the total load on the material. Since the forces in each phase are the phase stresses times the area (here numerically equal to the volume fraction), we have

$$\sigma_1 = \sigma_f V_f + \sigma_m V_m = E_f \epsilon_1 V_f + E_m \epsilon_1 V_m$$

The stiffness in the fiber direction is found by dividing by the strain:

$$E_1 = \frac{\sigma_1}{\epsilon_1} = V_f E_f + V_m E_m \quad (1)$$

This relation is known as a *rule of mixtures* prediction of the overall modulus in terms of the moduli of the constituent phases and their volume fractions.

If the stress is applied in the direction transverse to the fibers as depicted in Fig. 3, the slab model can be applied with the fiber and matrix materials acting *in series*. In this case the stress in the fiber and matrix are equal (an idealization), but the deflections add to give the overall transverse deflection. In this case it can be shown (see Prob. 5)

$$\frac{1}{E_2} = \frac{V_f}{E_f} + \frac{V_m}{E_m} \quad (2)$$

Figure 4 shows the functional form of the parallel (Eqn. 1) and series (Eqn. 2) predictions for the fiber- and transverse-direction moduli.

The prediction of transverse modulus given by the series slab model (Eqn. 2) is considered unreliable, in spite of its occasional agreement with experiment. Among other deficiencies the

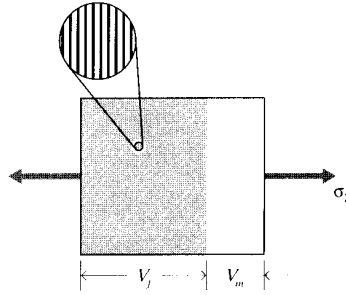


Figure 3: Loading perpendicular to the fibers.

assumption of uniform matrix strain being untenable; both analytical and experimental studies have shown substantial nonuniformity in the matrix strain. Figure 5 shows the photoelastic fringes in the matrix caused by the perturbing effect of the stiffer fibers. (A more complete description of these photoelasticity can be found in the *Module on Experimental Strain Analysis*, but this figure can be interpreted simply by noting that closely-spaced photoelastic fringes are indicative of large strain gradients.

In more complicated composites, for instance those with fibers in more than one direction or those having particulate or other nonfibrous reinforcements, Eqn. 1 provides an *upper bound* to the composite modulus, while Eqn. 2 is a *lower bound* (see Fig. 4). Most practical cases will be somewhere between these two values, and the search for reasonable models for these intermediate cases has occupied considerable attention in the composites research community. Perhaps the most popular model is an empirical one known as the *Halpin-Tsai* equation², which can be written in the form:

$$E = \frac{E_m[E_f + \xi(V_f E_f + V_m E_m)]}{V_f E_m + V_m E_f + \xi E_m} \quad (3)$$

Here ξ is an adjustable parameter that results in series coupling for $\xi = 0$ and parallel averaging for very large ξ .

Strength

Rule of mixtures estimates for strength proceed along lines similar to those for stiffness. For instance, consider a unidirectionally reinforced composite that is strained up to the value at which the fibers begin to break. Denoting this value ϵ_{fb} , the stress transmitted by the composite is given by multiplying the stiffness (Eqn. 1):

$$\sigma_b = \epsilon_{fb} E_1 = V_f \sigma_{fb} + (1 - V_f) \sigma^*$$

The stress σ^* is the stress in the matrix, which is given by $\epsilon_{fb} E_m$. This relation is linear in V_f , rising from σ^* to the fiber breaking strength $\sigma_{fb} = E_f \epsilon_{fb}$. However, this relation is not realistic at low fiber concentration, since the breaking strain of the matrix ϵ_{mb} is usually substantially greater than ϵ_{fb} . If the matrix had *no* fibers in it, it would fail at a stress $\sigma_{mb} = E_m \epsilon_{mb}$. If the fibers were considered to carry no load at all, having broken at $\epsilon = \epsilon_{fb}$ and leaving the matrix

²c.f. J.C.. Halpin and J.L. Kardos, *Polymer Engineering and Science*, Vol. 16, May 1976, pp. 344–352.

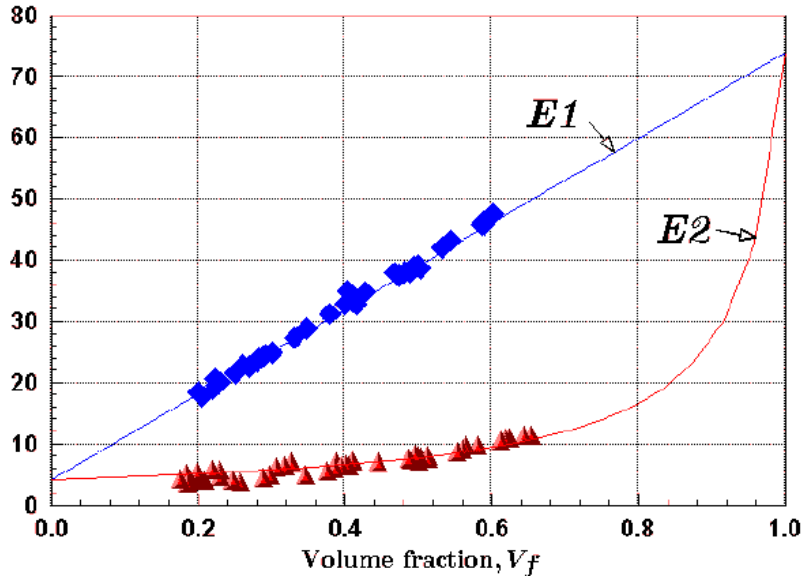


Figure 4: Rule-of-mixtures predictions for longitudinal (E_1) and transverse (E_2) modulus, for glass-polyester composite ($E_f = 73.7$ MPa, $E_m = 4$ GPa). Experimental data taken from Hull (1996).

to carry the remaining load, the strength of the composite would fall off with fiber fraction according to

$$\sigma_b = (1 - V_f)\sigma_{mb}$$

Since the breaking strength actually observed in the composite is the greater of these two expressions, there will be a range of fiber fraction in which the composite is *weakened* by the addition of fibers. These relations are depicted in Fig. 6.

References

1. Ashton, J.E., J.C. Halpin and P.H. Petit, *Primer on Composite Materials: Analysis*, Technomic Press, Westport, CT, 1969.
2. , Harris, B., *Engineering Composite Materials*, The Institute of Metals, London, 1986.
3. Hull, D. and T.W. Clyne, *An Introduction to Composites Materials*, Cambridge University Press, 1996.
4. Jones, R.M., *Mechanics of Composite Materials*, McGraw-Hill, New York, 1975.
5. Powell, P.C, *Engineering with Polymers*, Chapman and Hall, London, 1983.
6. Roylance, D., *Mechanics of Materials*, Wiley & Sons, New York, 1996.

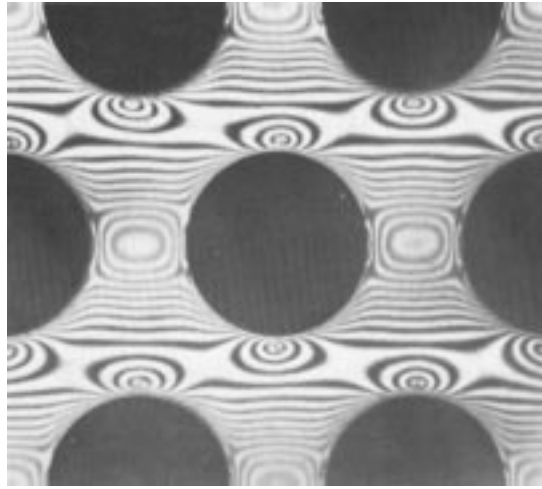


Figure 5: Photoelastic (isochromatic) fringes in a composite model subjected to transverse tension (from Hull, 1996).

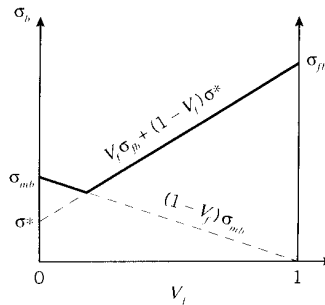


Figure 6: Strength of unidirectional composite in fiber direction.

Problems

1. Compute the longitudinal and transverse stiffness (E_1, E_2) of an S-glass epoxy lamina for a fiber volume fraction $V_f = 0.7$, using the fiber properties from Table 1, and matrix properties from the *Module on Materials Properties*.
2. Plot the longitudinal stiffness E_1 of an E-glass/nylon unidirectionally-reinforced composite, as a function of the volume fraction V_f .
3. Plot the longitudinal tensile strength of a E-glass/epoxy unidirectionally-reinforced composite, as a function of the volume fraction V_f .
4. What is the maximum fiber volume fraction V_f that could be obtained in a unidirectionally reinforced with optimal fiber packing?
5. Using the slab model and assuming uniform strain in the matrix, show the transverse modulus of a unidirectionally-reinforced composite to be

$$\frac{1}{E_2} = \frac{V_f}{E_f} + \frac{V_m}{E_m}$$

or in terms of compliances

$$C_2 = C_f V_f + C_m V_m$$

STRESS-STRAIN CURVES

David Roylance
Department of Materials Science and Engineering
Massachusetts Institute of Technology
Cambridge, MA 02139

August 23, 2001

Introduction

Stress-strain curves are an extremely important graphical measure of a material's mechanical properties, and all students of Mechanics of Materials will encounter them often. However, they are not without some subtlety, especially in the case of ductile materials that can undergo substantial geometrical change during testing. This module will provide an introductory discussion of several points needed to interpret these curves, and in doing so will also provide a preliminary overview of several aspects of a material's mechanical properties. However, this module will not attempt to survey the broad range of stress-strain curves exhibited by modern engineering materials (the atlas by Boyer cited in the References section can be consulted for this). Several of the topics mentioned here — especially yield and fracture — will appear with more detail in later modules.

“Engineering” Stress-Strain Curves

Perhaps the most important test of a material's mechanical response is the tensile test¹, in which one end of a rod or wire specimen is clamped in a loading frame and the other subjected to a controlled displacement δ (see Fig. 1). A transducer connected in series with the specimen provides an electronic reading of the load $P(\delta)$ corresponding to the displacement. Alternatively, modern servo-controlled testing machines permit using load rather than displacement as the controlled variable, in which case the displacement $\delta(P)$ would be monitored as a function of load.

The engineering measures of stress and strain, denoted in this module as σ_e and ϵ_e respectively, are determined from the measured the load and deflection using the original specimen cross-sectional area A_0 and length L_0 as

$$\sigma_e = \frac{P}{A_0}, \quad \epsilon_e = \frac{\delta}{L_0} \quad (1)$$

When the stress σ_e is plotted against the strain ϵ_e , an *engineering stress-strain curve* such as that shown in Fig. 2 is obtained.

¹Stress-strain testing, as well as almost all experimental procedures in mechanics of materials, is detailed by standards-setting organizations, notably the American Society for Testing and Materials (ASTM). Tensile testing of metals is prescribed by ASTM Test E8, plastics by ASTM D638, and composite materials by ASTM D3039.

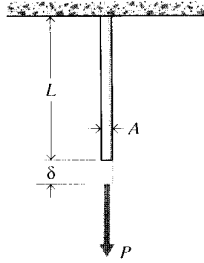


Figure 1: The tension test.

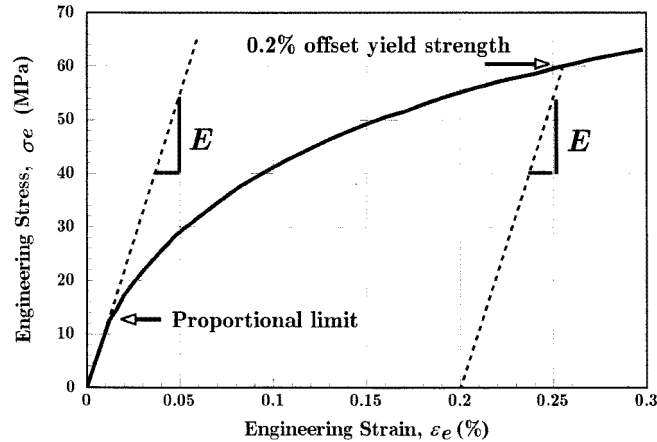


Figure 2: Low-strain region of the engineering stress-strain curve for annealed polycrystalline copper; this curve is typical of that of many ductile metals.

In the early (low strain) portion of the curve, many materials obey Hooke’s law to a reasonable approximation, so that stress is proportional to strain with the constant of proportionality being the modulus of elasticity or Young’s modulus, denoted E :

$$\sigma_e = E\epsilon_e \quad (2)$$

As strain is increased, many materials eventually deviate from this linear proportionality, the point of departure being termed the proportional limit. This nonlinearity is usually associated with stress-induced “plastic” flow in the specimen. Here the material is undergoing a rearrangement of its internal molecular or microscopic structure, in which atoms are being moved to new equilibrium positions. This plasticity requires a mechanism for molecular mobility, which in crystalline materials can arise from dislocation motion (discussed further in a later module.) Materials lacking this mobility, for instance by having internal microstructures that block dislocation motion, are usually brittle rather than ductile. The stress-strain curve for brittle materials are typically linear over their full range of strain, eventually terminating in fracture without appreciable plastic flow.

Note in Fig. 2 that the stress needed to increase the strain beyond the proportional limit in a ductile material continues to rise beyond the proportional limit; the material requires an ever-increasing stress to continue straining, a mechanism termed *strain hardening*.

These microstructural rearrangements associated with plastic flow are usually not reversed

when the load is removed, so the proportional limit is often the same as or at least close to the materials’s elastic limit. Elasticity is the property of complete and immediate recovery from an imposed displacement on release of the load, and the elastic limit is the value of stress at which the material experiences a permanent residual strain that is not lost on unloading. The residual strain induced by a given stress can be determined by drawing an unloading line from the highest point reached on the $\sigma_e - \epsilon_e$ curve at that stress back to the strain axis, drawn with a slope equal to that of the initial elastic loading line. This is done because the material unloads elastically, there being no force driving the molecular structure back to its original position.

A closely related term is the yield stress, denoted σ_Y in these modules; this is the stress needed to induce plastic deformation in the specimen. Since it is often difficult to pinpoint the exact stress at which plastic deformation begins, the yield stress is often taken to be the stress needed to induce a specified amount of permanent strain, typically 0.2%. The construction used to find this “offset yield stress” is shown in Fig. 2, in which a line of slope E is drawn from the strain axis at $\epsilon_e = 0.2\%$; this is the unloading line that would result in the specified permanent strain. The stress at the point of intersection with the $\sigma_e - \epsilon_e$ curve is the offset yield stress.

Figure 3 shows the engineering stress-strain curve for copper with an enlarged scale, now showing strains from zero up to specimen fracture. Here it appears that the rate of strain hardening² diminishes up to a point labeled UTS, for Ultimate Tensile Strength (denoted σ_f in these modules). Beyond that point, the material appears to strain soften, so that each increment of additional strain requires a smaller stress.

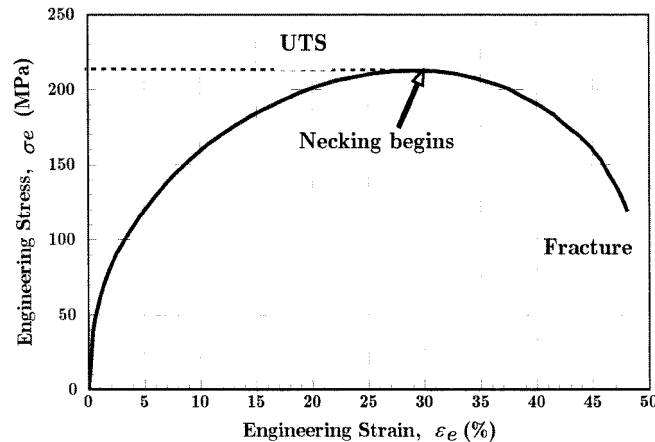


Figure 3: Full engineering stress-strain curve for annealed polycrystalline copper.

The apparent change from strain hardening to strain softening is an artifact of the plotting procedure, however, as is the maximum observed in the curve at the UTS. Beyond the yield point, molecular flow causes a substantial reduction in the specimen cross-sectional area A , so the true stress $\sigma_t = P/A$ actually borne by the material is larger than the engineering stress computed from the original cross-sectional area ($\sigma_e = P/A_0$). The load must equal the true stress times the actual area ($P = \sigma_t A$), and as long as strain hardening can increase σ_t enough to compensate for the reduced area A , the load and therefore the engineering stress will continue to rise as the strain increases. Eventually, however, the decrease in area due to flow becomes larger than the increase in true stress due to strain hardening, and the load begins to fall. This

²The strain hardening rate is the slope of the stress-strain curve, also called the *tangent modulus*.

is a geometrical effect, and if the true stress rather than the engineering stress were plotted no maximum would be observed in the curve.

At the UTS the differential of the load P is zero, giving an analytical relation between the true stress and the area at necking:

$$P = \sigma_t A \rightarrow dP = 0 = \sigma_t dA + A d\sigma_t \rightarrow -\frac{dA}{A} = \frac{d\sigma_t}{\sigma_t} \quad (3)$$

The last expression states that the load and therefore the engineering stress will reach a maximum as a function of strain when the fractional decrease in area becomes equal to the fractional increase in true stress.

Even though the UTS is perhaps the materials property most commonly reported in tensile tests, it is not a direct measure of the material due to the influence of geometry as discussed above, and should be used with caution. The yield stress σ_Y is usually preferred to the UTS in designing with ductile metals, although the UTS is a valid design criterion for brittle materials that do not exhibit these flow-induced reductions in cross-sectional area.

The true stress is not quite uniform throughout the specimen, and there will always be some location - perhaps a nick or some other defect at the surface - where the local stress is maximum. Once the maximum in the engineering curve has been reached, the localized flow at this site cannot be compensated by further strain hardening, so the area there is reduced further. This increases the local stress even more, which accelerates the flow further. This localized and increasing flow soon leads to a “neck” in the gage length of the specimen such as that seen in Fig. 4.



Figure 4: Necking in a tensile specimen.

Until the neck forms, the deformation is essentially uniform throughout the specimen, but after necking all subsequent deformation takes place in the neck. The neck becomes smaller and smaller, local true stress increasing all the time, until the specimen fails. This will be the failure mode for most ductile metals. As the neck shrinks, the nonuniform geometry there alters the uniaxial stress state to a complex one involving shear components as well as normal stresses. The specimen often fails finally with a “cup and cone” geometry as seen in Fig. 5, in which the outer regions fail in shear and the interior in tension. When the specimen fractures, the engineering strain at break — denoted ϵ_f — will include the deformation in the necked region and the unnecked region together. Since the true strain in the neck is larger than that in the unnecked material, the value of ϵ_f will depend on the fraction of the gage length that has necked. Therefore, ϵ_f is a function of the specimen geometry as well as the material, and thus is only a

crude measure of material ductility.



Figure 5: Cup-and-cone fracture in a ductile metal.

Figure 6 shows the engineering stress-strain curve for a semicrystalline thermoplastic. The response of this material is similar to that of copper seen in Fig. 3, in that it shows a proportional limit followed by a maximum in the curve at which necking takes place. (It is common to term this maximum as the yield stress in plastics, although plastic flow has actually begun at earlier strains.)

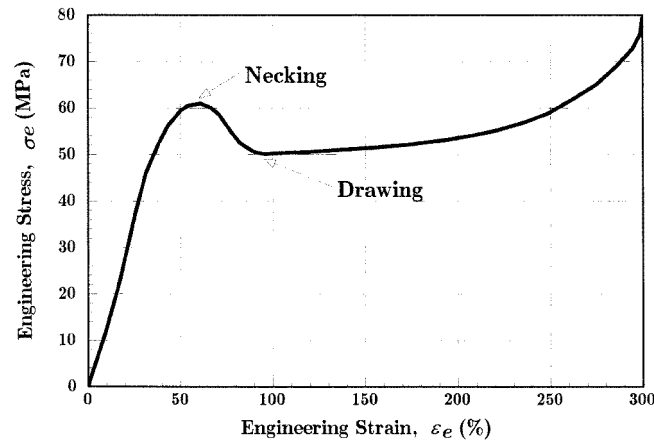


Figure 6: Stress-strain curve for polyamide (nylon) thermoplastic.

The polymer, however, differs dramatically from copper in that the neck does not continue shrinking until the specimen fails. Rather, the material in the neck stretches only to a “natural draw ratio” which is a function of temperature and specimen processing, beyond which the material in the neck stops stretching and new material at the neck shoulders necks down. The neck then propagates until it spans the full gage length of the specimen, a process called *drawing*. This process can be observed without the need for a testing machine, by stretching a polyethylene “six-pack holder,” as seen in Fig. 7.

Not all polymers are able to sustain this drawing process. As will be discussed in the next section, it occurs when the necking process produces a strengthened microstructure whose breaking load is greater than that needed to induce necking in the untransformed material just outside the neck.



Figure 7: Necking and drawing in a 6-pack holder.

“True” Stress-Strain Curves

As discussed in the previous section, the engineering stress-strain curve must be interpreted with caution beyond the elastic limit, since the specimen dimensions experience substantial change from their original values. Using the true stress $\sigma_t = P/A$ rather than the engineering stress $\sigma_e = P/A_0$ can give a more direct measure of the material’s response in the plastic flow range. A measure of strain often used in conjunction with the true stress takes the increment of strain to be the incremental increase in displacement dL divided by the current length L :

$$d\epsilon_t = \frac{dL}{L} \rightarrow \epsilon_t = \int_{L_0}^L \frac{1}{L} dL = \ln \frac{L}{L_0} \quad (4)$$

This is called the “true” or “logarithmic” strain.

During yield and the plastic-flow regime following yield, the material flows with negligible change in volume; increases in length are offset by decreases in cross-sectional area. Prior to necking, when the strain is still uniform along the specimen length, this volume constraint can be written:

$$dV = 0 \rightarrow AL = A_0L_0 \rightarrow \frac{L}{L_0} = \frac{A}{A_0} \quad (5)$$

The ratio L/L_0 is the *extension ratio*, denoted as λ . Using these relations, it is easy to develop relations between true and engineering measures of tensile stress and strain (see Prob. 2):

$$\sigma_t = \sigma_e (1 + \epsilon_e) = \sigma_e \lambda, \quad \epsilon_t = \ln(1 + \epsilon_e) = \ln \lambda \quad (6)$$

These equations can be used to derive the true stress-strain curve from the engineering curve, up to the strain at which necking begins. Figure 8 is a replot of Fig. 3, with the true stress-strain curve computed by this procedure added for comparison.

Beyond necking, the strain is nonuniform in the gage length and to compute the true stress-strain curve for greater engineering strains would not be meaningful. However, a complete true stress-strain curve could be drawn if the neck area were monitored throughout the tensile test, since for logarithmic strain we have

$$\frac{L}{L_0} = \frac{A}{A_0} \rightarrow \epsilon_t = \ln \frac{L}{L_0} = \ln \frac{A}{A_0} \quad (7)$$

Ductile metals often have true stress-strain relations that can be described by a simple power-law relation of the form:

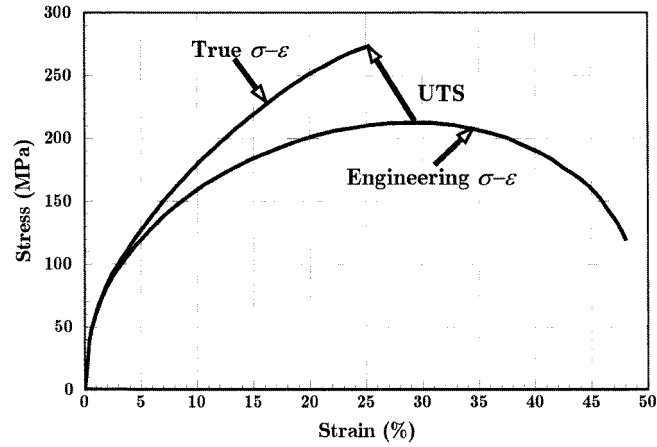


Figure 8: Comparison of engineering and true stress-strain curves for copper. An arrow indicates the position on the “true” curve of the UTS on the engineering curve.

$$\sigma_t = A\epsilon_t^n \rightarrow \log \sigma_t = \log A + n \log \epsilon_t \quad (8)$$

Figure 9 is a log-log plot of the true stress-strain data³ for copper from Fig. 8 that demonstrates this relation. Here the parameter $n = 0.474$ is called the *strain hardening parameter*, useful as a measure of the resistance to necking. Ductile metals at room temperature usually exhibit values of n from 0.02 to 0.5.

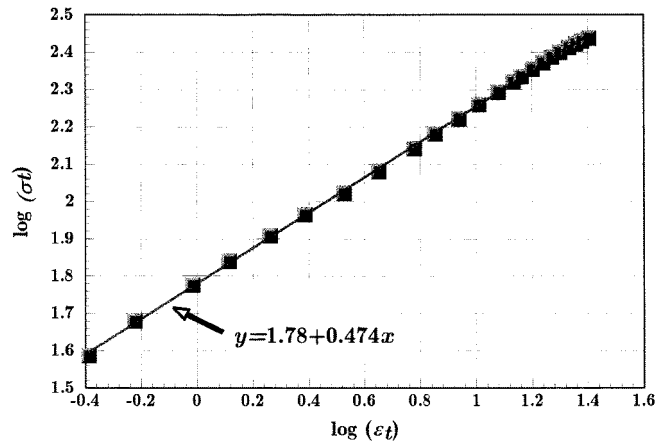


Figure 9: Power-law representation of the plastic stress-strain relation for copper.

A graphical method known as the “Considère construction” uses a form of the true stress-strain curve to quantify the differences in necking and drawing from material to material. This method replots the tensile stress-strain curve with true stress σ_t as the ordinate and extension ratio $\lambda = L/L_0$ as the abscissa. From Eqn. 6, the engineering stress σ_e corresponding to any

³Here percent strain was used for ϵ_t ; this produces the same value for n but a different A than if full rather than percentage values were used.

value of true stress σ_t is slope of a secant line drawn from origin ($\lambda = 0$, not $\lambda = 1$) to intersect the $\sigma_t - \lambda$ curve at σ_t .

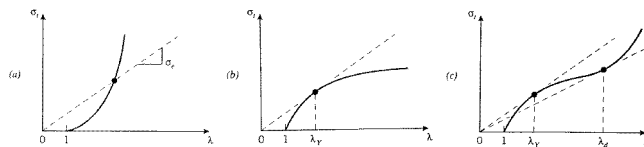


Figure 10: Considère construction. (a) True stress-strain curve with no tangents - no necking or drawing. (b) One tangent - necking but not drawing. (c) Two tangents - necking and drawing.

Among the many possible shapes the true stress-strain curves could assume, let us consider the concave up, concave down, and sigmoidal shapes shown in Fig. 10. These differ in the number of tangent points that can be found for the secant line, and produce the following yield characteristics:

- (a) *No tangents:* Here the curve is always concave upward as in part (a) of Fig. 10, so the slope of the secant line rises continuously. Therefore the engineering stress rises as well, without showing a yield drop. Eventually fracture intercedes, so a true stress-strain curve of this shape identifies a material that fractures before it yields.
- (b) *One tangent:* The curve is concave downward as in part (b) of Fig. 10, so a secant line reaches a tangent point at $\lambda = \lambda_Y$. The slope of the secant line, and therefore the engineering stress as well, begins to fall at this point. This is then the yield stress σ_Y seen as a maximum in stress on a conventional stress-strain curve, and λ_Y is the extension ratio at yield. The yielding process begins at some adventitious location in the gage length of the specimen, and continues at that location rather than being initiated elsewhere because the secant modulus has been reduced at the first location. The specimen is now flowing at a single location with decreasing resistance, leading eventually to failure. Ductile metals such as aluminum fail in this way, showing a marked reduction in cross sectional area at the position of yield and eventual fracture.
- (c) *Two tangents:* For sigmoidal stress-strain curves as in part (c) of Fig. 10, the engineering stress begins to fall at an extension ration λ_Y , but then rises again at λ_d . As in the previous one-tangent case, material begins to yield at a single position when $\lambda = \lambda_Y$, producing a neck that in turn implies a nonuniform distribution of strain along the gage length. Material at the neck location then stretches to λ_d , after which the engineering stress there would have to rise to stretch it further. But this stress is greater than that needed to stretch material at the edge of the neck from λ_Y to λ_d , so material already in the neck stops stretching and the neck propagates outward from the initial yield location. Only material within the neck shoulders is being stretched during propagation, with material inside the necked-down region holding constant at λ_d , the material’s “natural draw ratio,” and material outside holding at λ_Y . When all the material has been drawn into the necked region, the stress begins to rise uniformly in the specimen until eventually fracture occurs.

The increase in strain hardening rate needed to sustain the drawing process in semicrystalline polymers arises from a dramatic transformation in the material’s microstructure. These materials are initially “spherulitic,” containing flat lamellar crystalline plates, perhaps 10 nm

thick, arranged radially outward in a spherical domain. As the induced strain increases, these spherulites are first deformed in the straining direction. As the strain increases further, the spherulites are broken apart and the lamellar fragments rearranged with a dominantly axial molecular orientation to become what is known as the fibrillar microstructure. With the strong covalent bonds now dominantly lined up in the load-bearing direction, the material exhibits markedly greater strengths and stiffnesses — by perhaps an order of magnitude — than in the original material. This structure requires a much higher strain hardening rate for increased strain, causing the upturn and second tangent in the true stress-strain curve.

Strain energy

The area under the $\sigma_e - \epsilon_e$ curve up to a given value of strain is the total mechanical energy per unit volume consumed by the material in straining it to that value. This is easily shown as follows:

$$U^* = \frac{1}{V} \int P dL = \int_0^L \frac{P}{A_0} \frac{dL}{L_0} = \int_0^\epsilon \sigma d\epsilon \quad (9)$$

In the absence of molecular slip and other mechanisms for energy dissipation, this mechanical energy is stored reversibly within the material as strain energy. When the stresses are low enough that the material remains in the elastic range, the strain energy is just the triangular area in Fig. 11:

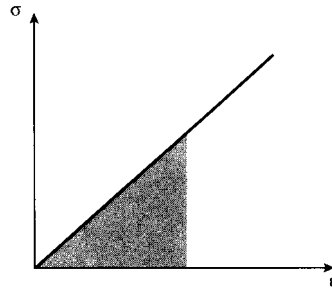


Figure 11: Strain energy = area under stress-strain curve.

Note that the strain energy increases quadratically with the stress or strain; i.e. that as the strain increases the energy stored by a given increment of additional strain grows as the square of the strain. This has important consequences, one example being that an archery bow cannot be simply a curved piece of wood to work well. A real bow is initially straight, then bent when it is strung; this stores substantial strain energy in it. When it is bent further on drawing the arrow back, the energy available to throw the arrow is very much greater than if the bow were simply carved in a curved shape without actually bending it.

Figure 12 shows schematically the amount of strain energy available for two equal increments of strain $\Delta\epsilon$, applied at different levels of existing strain.

The area up to the yield point is termed the *modulus of resilience*, and the total area up to fracture is termed the *modulus of toughness*; these are shown in Fig. 13. The term “modulus” is used because the units of strain energy per unit volume are $\text{N}\cdot\text{m}/\text{m}^3$ or N/m^2 , which are the same as stress or modulus of elasticity. The term “resilience” alludes to the concept that up to the point of yielding, the material is unaffected by the applied stress and upon unloading

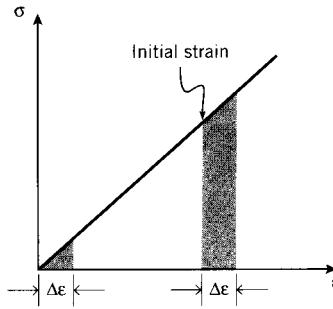


Figure 12: Energy associated with increments of strain

Table 1: Energy absorption of various materials.

Material	Maximum Strain, %	Maximum Stress, MPa	Modulus of Toughness, MJ/m ³	Density kg/m ³	Max. Energy J/kg
Ancient Iron	0.03	70	0.01	7,800	1.3
Modern spring steel	0.3	700	1.0	7,800	130
Yew wood	0.3	120	0.5	600	900
Tendon	8.0	70	2.8	1,100	2,500
Rubber	300	7	10.0	1,200	8,000

will return to its original shape. But when the strain exceeds the yield point, the material is deformed irreversibly, so that some residual strain will persist even after unloading. The modulus of resilience is then the quantity of energy the material can absorb without suffering damage. Similarly, the modulus of toughness is the energy needed to completely fracture the material. Materials showing good impact resistance are generally those with high moduli of toughness.

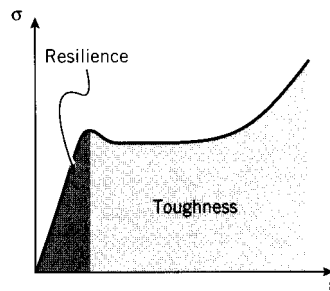


Figure 13: Moduli of resilience and toughness.

Table 1⁴ lists energy absorption values for a number of common materials. Note that natural and polymeric materials can provide extremely high energy absorption per unit weight.

During loading, the area under the stress-strain curve is the strain energy per unit volume absorbed by the material. Conversely, the area under the unloading curve is the energy released by the material. In the elastic range, these areas are equal and no net energy is absorbed. But

⁴J.E. Gordon, *Structures, or Why Things Don't Fall Down*, Plenum Press, New York, 1978.

if the material is loaded into the plastic range as shown in Fig. 14, the energy absorbed exceeds the energy released and the difference is dissipated as heat.

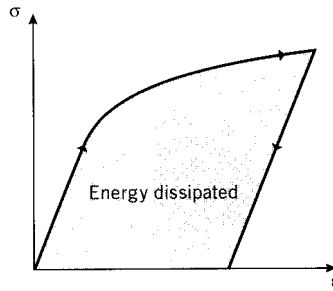


Figure 14: Energy loss = area under stress-strain loop.

Compression

The above discussion is concerned primarily with simple tension, i.e. uniaxial loading that increases the interatomic spacing. However, as long as the loads are sufficiently small (stresses less than the proportional limit), in many materials the relations outlined above apply equally well if loads are placed so as to put the specimen in compression rather than tension. The expression for deformation and a given load $\delta = PL/AE$ applies just as in tension, with negative values for δ and P indicating compression. Further, the modulus E is the same in tension and compression to a good approximation, and the stress-strain curve simply extends as a straight line into the third quadrant as shown in Fig. 15.

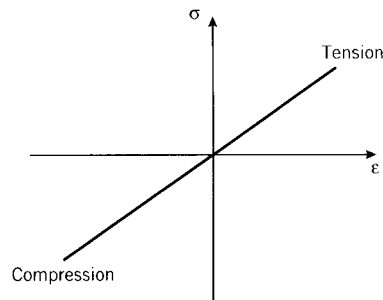


Figure 15: Stress-strain curve in tension and compression.

There are some practical difficulties in performing stress-strain tests in compression. If excessively large loads are mistakenly applied in a tensile test, perhaps by wrong settings on the testing machine, the specimen simply breaks and the test must be repeated with a new specimen. But in compression, a mistake can easily damage the load cell or other sensitive components, since even after specimen failure the loads are not necessarily relieved.

Specimens loaded cyclically so as to alternate between tension and compression can exhibit hysteresis loops if the loads are high enough to induce plastic flow (stresses above the yield stress). The enclosed area in the loop seen in Fig. 16 is the strain energy per unit volume released as heat in each loading cycle. This is the well-known tendency of a wire that is being

bent back and forth to become quite hot at the region of plastic bending. The temperature of the specimen will rise according to the magnitude of this internal heat generation and the rate at which the heat can be removed by conduction within the material and convection from the specimen surface.

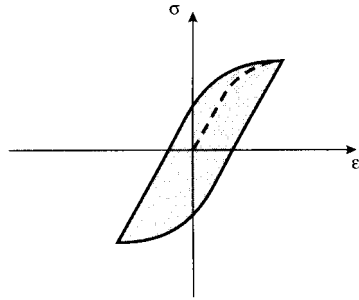


Figure 16: Hysteresis loop.

Specimen failure by cracking is inhibited in compression, since cracks will be closed up rather than opened by the stress state. A number of important materials are much stronger in compression than in tension for this reason. Concrete, for example, has good compressive strength and so finds extensive use in construction in which the dominant stresses are compressive. But it has essentially no strength in tension, as cracks in sidewalks and building foundations attest: tensile stresses appear as these structures settle, and cracks begin at very low tensile strain in unreinforced concrete.

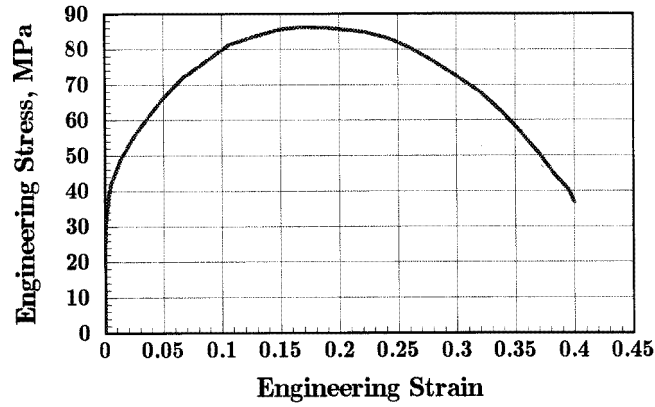
References

1. Boyer, H.F., *Atlas of Stress-Strain Curves*, ASM International, Metals Park, Ohio, 1987.
2. Courtney, T.H., *Mechanical Behavior of Materials*, McGraw-Hill, New York, 1990.
3. Hayden, H.W., W.G. Moffatt and J. Wulff, *The Structure and Properties of Materials: Vol. III Mechanical Behavior*, Wiley, New York, 1965.

Problems

1. The figure below shows the engineering stress-strain curve for pure polycrystalline aluminum; the numerical data for this figure are in the file `aluminum.txt`, which can be imported into a spreadsheet or other analysis software. For this material, determine (a) Young's modulus, (b) the 0.2% offset yield strength, (c) the Ultimate Tensile Strength (UTS), (d) the modulus of resilience, and (e) the modulus of toughness.
2. Develop the relations given in Eqn. 6:

$$\sigma_t = \sigma_e (1 + \epsilon_e) = \sigma_e \lambda, \quad \epsilon_t = \ln(1 + \epsilon_e) = \ln \lambda$$



Prob. 1

3. Using the relations of Eqn. 6, plot the true stress-strain curve for aluminum (using data from Prob.1) up to the strain of neck formation.
4. Replot the the results of the previous problem using log-log axes as in Fig. 9 to determine the parameters A and n in Eqn. 8 for aluminum.
5. Using Eqn. 8 with parameters $A = 800$ MPa, $n = 0.2$, plot the engineering stress-strain curve up to a strain of $\epsilon_e = 0.4$. Does the material neck? Explain why the curve is or is not valid at strains beyond necking.
6. Using the parameters of the previous problem, use the condition $(d\sigma_e/d\epsilon_e)_{\text{neck}} = 0$ to show that the engineering strain at necking is $\epsilon_{e,\text{neck}} = 0.221$.
7. Use a Considère construction (plot σ_t vs. λ , as in Fig. 10) to verify the result of the previous problem.
8. Elastomers (rubber) have stress-strain relations of the form

$$\sigma_e = \frac{E}{3} \left(\lambda - \frac{1}{\lambda^2} \right),$$

where E is the initial modulus. Use the Considère construction to show whether this material will neck, or draw.

9. Show that a power-law material (one obeying Eqn. 8) necks when the true strain ϵ_t becomes equal to the strain-hardening exponent n .
10. Show that the UTS (engineering stress at incipient necking) for a power-law material (Eqn. 8) is

$$\sigma_f = \frac{An^n}{e^n}$$

11. Show that the strain energy $U = \int \sigma d\epsilon$ can be computed using either engineering or true values of stress and strain, with equal result.

12. Show that the strain energy needed to neck a power-law material (Eqn.8) is

$$U = \frac{An^{n+1}}{n+1}$$

TRUSSES

David Roylance
Department of Materials Science and Engineering
Massachusetts Institute of Technology
Cambridge, MA 02139

June 8, 2000

Introduction

A truss is an assemblage of long, slender structural elements that are connected at their ends. Trusses find substantial use in modern construction, for instance as towers (see Fig. 1), bridges, scaffolding, etc. In addition to their practical importance as useful structures, truss elements have a dimensional simplicity that will help us extend further the concepts of mechanics introduced in the modules dealing with uniaxial response. This module will also use trusses to introduce important concepts in statics and numerical analysis that will be extended in later modules to more general problems.



Figure 1: Truss tower supporting the NASA wind turbine generator at Oahu, Hawaii.

Example 1

Trusses are often used to stiffen structures, and most people are familiar with the often very elaborate systems of cross-bracing used in bridges. The truss bracing used to stiffen the towers of suspension bridges against buckling are hard to miss, but not everyone notices the vertical truss panels on most such bridges that serve to stiffen the deck against flexural and torsional deformation.

Many readers will have seen the very famous movie, taken on November 7, 1940, by Barney Elliott of The Camera Shop in Tacoma, Washington. The wind was gusting up to 42 mph that day, and induced a

sequence of spectacular undulations and eventual collapse of the Tacoma Narrows bridge¹. This bridge was built using relatively short I-beams for deck stiffening rather than truss panels, reportedly for aesthetic reasons; bridge designs of the period favored increasingly slender and graceful-appearing structures. Even during construction, the bridge became well known for its alarming tendency to sway in the wind, earning it the local nickname “Galloping Gertie.”

Truss stiffeners were used when the bridge was rebuilt in 1950, and the new bridge was free of the oscillations that led to the collapse of its predecessor. This is a good example of one important use of trusses, but it is probably an even better example of the value of caution and humility in engineering. The glib answers often given for the original collapse — resonant wind gusts, von Karman vortices, etc. — are not really satisfactory beyond the obvious statement that the deck was not stiff enough. Even today, knowledgeable engineers argue about the very complicated structural dynamics involved. Ultimately, many uncertainties exist even in designs completed using very modern and elaborate techniques. A wise designer will never fully trust a theoretical result, computer-generated or not, and will take as much advantage of experience and intuition as possible.

Statics analysis of forces

Newton observed that a mass accelerates according to the vector sum of forces applied to it: $\sum \mathbf{F} = m\mathbf{a}$. (Vector quantities indicated by boldface type.) In structures that are anchored so as to prevent motion, there is obviously no acceleration and the forces must sum to zero. This vector equation has as many scalar components as the dimensionality of the problem; for two-dimensional cases we have:

$$\sum F_x = 0 \tag{1}$$

$$\sum F_y = 0 \tag{2}$$

where F_x and F_y are the components of \mathbf{F} in the x and y cartesian coordinate directions. These two equations, which we can interpret as constraining the structure against translational motion in the x and y directions, allow us to solve for at most two unknown forces in structural problems. If the structure is constrained against rotation as well as translation, we can add a *moment equation* that states that the sum of moments or torques in the x - y plane must also add to zero:

$$\sum M_{xy} = 0 \tag{3}$$

In two dimensions, then, we have three equations of static equilibrium that can be used to solve for unknown forces. In three dimensions, a third force equation and two more moment equations are added, for a total of six:

$\sum F_x = 0$	$\sum M_{xy} = 0$	(4)
$\sum F_y = 0$	$\sum M_{xz} = 0$	
$\sum F_z = 0$	$\sum M_{yz} = 0$	

These equations can be applied to the structure as a whole, or we can (conceptually) remove a piece of the structure and consider the forces acting on the removed piece. A sketch of the

¹An interactive instructional videodisk of the Tacoma Narrows Bridge collapse is available from Wiley Educational Software (ISBN 0-471-87320-9).

piece, showing all forces acting on it, is called a *free body diagram*. If the number of unknown forces in the diagram is equal to or less than the number of available static equilibrium equations, the unknowns can be solved in a straightforward manner; such problems are termed *statically determinate*. Note that these equilibrium equations do not assume anything about the material from which the structure is made, so the resulting forces are also independent of the material.

In the analyses to be considered here, the truss elements are assumed to be joined together by pins or other such connections that allow free rotation around the joint. As seen in the free-body diagram of Fig. 2, this inability to resist rotation implies that the force acting on a truss element's pin joint must be in the element's axial direction: any transverse component would tend to cause rotation, and if the element is to be in static equilibrium the moment equation forces the transverse component to vanish. If the element ends were to be welded or bolted rather than simply pinned, the end connection could transmit transverse forces and bending moments into the element. Such a structure would then be called a *frame* rather than a truss, and its analysis would have to include bending effects. Such structures will be treated in the Module on Bending.

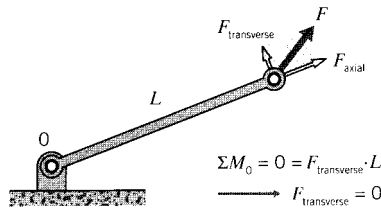


Figure 2: Pinned elements cannot support transverse loads.

Knowing that the force in each truss element must be in the element's axial direction is the key to solving for the element forces in trusses that contain many elements. Each element meeting at a pin joint will pull or push on the pin depending on whether the element is in tension or compression, and since the pin must be in static equilibrium the sum of all element forces acting on the pin must equal the force that is externally applied to the pin:

$$\sum_e \mathbf{F}_i^e = \mathbf{F}_i$$

Here the e superscript indicates the vector force supplied by the element on the i^{th} pin in the truss and \mathbf{F}_i is the force externally applied to that pin. The summation is over all the elements connected to the pin.

Example 2

The very simple two-element truss often found in high school physics books and shown in Fig. 3 can be analyzed this way. Intuition tells us that the upper element, connecting joints A and B , is in tension while element BC is in compression. In more complicated problems it is not always possible to determine the sign of the element force by inspection, but it doesn't matter. In sketching the free body diagrams for the pins, the load can be drawn in either direction; if the guess turns out to be wrong, the solution will give a negative value for the force magnitude.

The unknown forces on the connecting pin B are in the direction of the elements attached to it, and since there are only two such forces they may be determined from the two static equilibrium force equations:

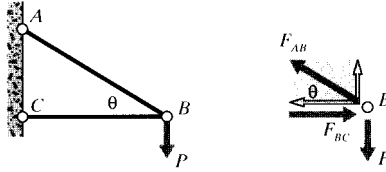


Figure 3: A two-element truss.

$$\sum F_y = 0 = +F_{AB} \sin \theta - P \Rightarrow F_{AB} = \frac{P}{\sin \theta}$$

$$\sum F_x = 0 = -F_{AB} \cos \theta + F_{BC} \Rightarrow F_{BC} = F_{AB} \cos \theta = \frac{P}{\tan \theta}$$

In more complicated trusses, the general approach is to start at a pin joint containing no more than two elements having unknown forces, and then work from joint to joint using the element forces from the previous step to reduce the number of unknowns. Consider the 6-element truss shown in Fig. 4, in which the joints and elements are numbered as indicated, with the element numbers appearing in circles. Joint 3 is a natural starting point, since only forces F_2 and F_5 appear as unknowns. Once F_5 is found, an analysis of joint 5 has only forces F_4 and F_6 as unknowns. Finally, the free-body diagram of node 2 can be completed, since only F_1 and F_3 are now unknown. The force analysis is then complete.

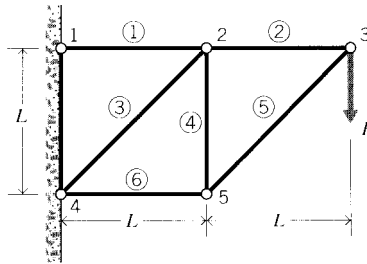


Figure 4: A six-element truss.

There are often many ways to complete problems such as this, perhaps with some being easier than others. Another approach might be to start at one of the joints at the wall; i.e. joint 1 or joint 4. The problem as originally stated gives these joints as having fixed displacements rather than specified forces. This is an example of a *mixed boundary value problem*, with some parts of the boundary having specified forces and the remaining parts having specified displacements. Such problems are generally more difficult, and require more mathematical information for their solution than problems having only one or the other type of boundary condition. However, in the *statically determinate* problems, the structure can be converted to a load-only type by invoking static equilibrium on the structure as a whole. The fixed-displacement boundary conditions are then replaced by *reaction forces* that are set up at the points of constraint.

Moment equilibrium equations were not useful in the joint-by-joint analysis described earlier, since individual elements cannot support moments. But as seen in Fig. 5, we can consider the

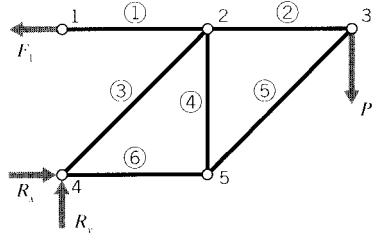


Figure 5: Free-body diagram of six-element truss

6-element truss as a whole and take moments around joint 4. With counterclockwise-tending moments being positive, this gives

$$\sum M_4 = 0 = F_1 \times L - P \times 2L \Rightarrow F_1 = 2P$$

The force F_1 is the force applied by the wall to joint 1, and this is obviously equal to the tensile force in element 1. There can be no vertical component of this reaction force, since the element forces must be axial and only element 1 is connected to joint 1. At joint 4, reaction forces R_x and R_y can act in both the x and y directions since element 3 is not perpendicular to the wall. These reaction forces can be found by invoking horizontal and vertical equilibrium:

$$\sum F_x = 0 = -F_1 + R_x \Rightarrow R_x = F_1 = 2P$$

$$\sum F_y = 0 = +R_y - P \Rightarrow R_y = P$$

A joint-by-joint analysis can now be started from joint 4, since only two unknown forces act there (see Fig. 6). For vertical equilibrium, $F_3 \cos 45 = P$, so $F_3 = \sqrt{2}P$. Then for horizontal equilibrium $F_6 + F_3 \cos 45 = 2P$, so $F_6 = P$. Now moving to joint 5, horizontal equilibrium gives $F_5 \cos 45 = P$ so $F_5 = F_3 = \sqrt{2}P$, and vertical equilibrium gives $F_4 = F_5 \cos 45$ so $F_4 = P$. Finally, at joint 3 horizontal equilibrium gives $F_2 = F_5 \cos 45$ so $F_2 = P$.

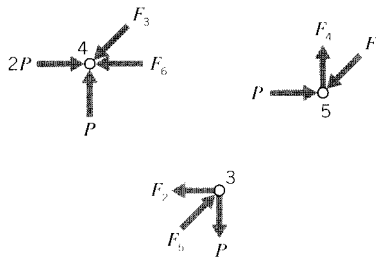


Figure 6: Individual joint diagrams.

In actual truss design, once each element's force is known its cross-sectional area can then be calculated so as to keep the element stress according to $\sigma = P/A$ safely less than the material's yield point. Elements in compression, however, must be analyzed for buckling as well, since their ratios of EI to L^2 are generally low. The buckling load can be increased substantially by bracing the element against sideward deflection, and this bracing is evident in most bridges

and cranes. Also, the truss elements are usually held together by welded or bolted joints rather than pins. These joints can carry some bending moments, which helps stiffen the truss against buckling.

Deflections

It may be important in some applications that the truss be stiff enough to keep the deformations inside specified limits. Astronomical telescopes are an example, since deflection of the structure supporting the optical assemblies can degrade the focusing ability of the instrument. A typical derrick or bridge, however, is probably more likely to be strength rather than stiffness-critical, so it might appear deflections would be relatively unimportant. However, it will be seen that consideration of deflections is necessary to solve the great number of structures that are *not* statically determinate. The following sections treat truss deflections for both these reasons.

Geometrical approach

Once the axial force in each truss element is known, the individual element deformations follow directly using $\delta = PL/AE$. The deflection of any point in the truss can then be determined geometrically, invoking the requirement that the elements remain pinned together at their attachment points. In the symmetric two-element truss shown in Fig. 7, joint B will obviously deflect downward vertically. The relation between the the axial deformation δ of the elements and the vertical deflection of the joint δ_v is then seen to be

$$\delta_v = \frac{\delta}{\cos \theta}$$

It is assumed here that the deformation is small enough that the gross aspects of the geometry are essentially unchanged; in this case, that the angle θ is the same before and after the load is applied.

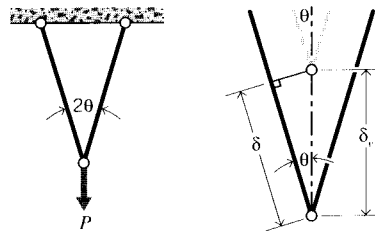


Figure 7: Two-element truss.

In geometrical analyses of more complicated trusses, it is sometimes convenient to visualize unpinning the elements at a selected joint, letting the elements elongate or shrink according to the axial force they are transmitting, and then swinging them around the still-pinned joint until the pin locations match up again. The motion of the unpinned ends would trace out circular paths, but if the deflections are small the path can be approximated as a straight line perpendicular to the element axis. The joint position can then be computed from Pythagorean relationships.

In the earlier two-element truss shown in Fig. 3, we had $P_{AB} = P/\sin \theta$ and $P_{BC} = P/\tan \theta$. If the pin at joint B were removed, the element deflections would be

$$\delta_{AB} = \frac{P}{\sin \theta} \left(\frac{L}{AE} \right)_{AB} \quad (\text{tension})$$

$$\delta_{BC} = \frac{P}{\tan \theta} \left(\frac{L}{AE} \right)_{BC} \quad (\text{compression})$$

The total downward deflection of joint B is then

$$\begin{aligned} \delta_v &= \delta_1 + \delta_2 = \frac{\delta_{AB}}{\sin \theta} + \frac{\delta_{BC}}{\tan \theta} \\ &= \frac{P}{\sin^2 \theta} \left(\frac{L}{AE} \right)_{AB} + \frac{P}{\tan^2 \theta} \left(\frac{L}{AE} \right)_{BC} \end{aligned}$$

These deflections are shown in Fig. 8.

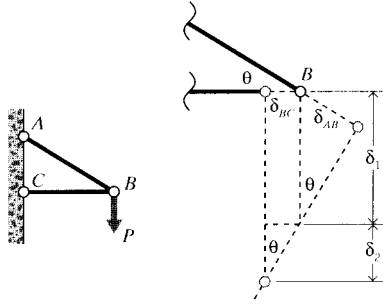


Figure 8: Displacements in the two-element truss.

The horizontal deflection δ_h of the pin is easier to compute, since it is just the contraction of element BC :

$$\delta_h = \delta_{BC} = \frac{P}{\tan \theta} \left(\frac{L}{AE} \right)_{BC}$$

Energy approach

The geometrical approach to truss deformation analysis can be rather tedious, especially as problems become larger. Many problems can be solved more easily using a strain energy rather than force-at-a-point approach. The total strain energy U in a single elastically loaded truss element is

$$U = \int P d\delta$$

The increment of deformation $d\delta$ is related to a corresponding increment of load dP by

$$\delta = \frac{PL}{AE} \Rightarrow d\delta = \frac{L}{AE} dP$$

The strain energy is then

$$U = \int P \frac{L}{AE} dP = \frac{P^2 L}{2AE}$$

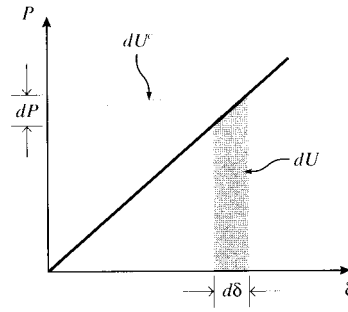


Figure 9: Increments of strain and complimentary strain energy.

The *incremental* increase in strain energy corresponding to an increase in deformation $d\delta$ is just $dU = P d\delta$. If the force-elongation curve is linear, this is identical to the increase in the quantity called the *complimentary* strain energy: $dU^c = \delta dP$. These quantities are depicted in Fig. 9. Now consider a system with many joints, subjected to a number of loads acting at different joints. If we were to increase the i^{th} load slightly while holding all the other loads constant, the increase in the total complimentary energy of the system would be

$$dU^c = \delta_i dP_i$$

where δ_i is the displacement that would occur at the location of P_i , moving in the same direction as the force vector for P_i . Rearranging,

$$\delta_i = \frac{\partial U^c}{\partial P_i}$$

and since $U^c = U$:

$$\boxed{\delta_i = \frac{\partial U}{\partial P_i}} \quad (5)$$

Hence the displacement at a given point is the derivative of the total strain energy with respect to the load acting at that point. This provides the basis of an extremely useful method of displacement analysis known as *Castigliano's Theorem*², which can be stated for truss problems as the following recipe:

1. Let the load applied at the joint whose deformation is sought, in the direction of the desired deformation, be written as an algebraic variable, say Q . If the load is known numerically, replace the number with a letter. If there is no load at the desired location and direction, put an imaginary one there that will be set to zero at the end of the problem.
2. Solve for the forces $F_i(Q)$ in each truss element, each of which may be dependent on the load Q assigned in the previous step.
3. Use these forces to compute the strain energy for each element, and sum the energies in each element to obtain the total strain energy for the truss:

²From the 1873 thesis of the Italian engineer Alberto Castigliano (1847–1884), at the Turin Polytechnical Institute.

$$U_{tot} = \sum_i U_i = \sum_i \frac{F_i^2 L_i}{2A_i E_i} \quad (6)$$

Each term in this summation may contain the variable Q .

4. The deformation *congruent* to Q , i.e. the deformation at the point where Q is applied and in the same direction as Q , is then

$$\delta_Q = \frac{\partial U_{tot}}{\partial Q} = \sum_i \frac{F_i L_i}{A_i E_i} \frac{\partial F_i(Q)}{\partial Q} \quad (7)$$

5. The load Q is replaced by its numerical value, if known. Or by zero, if it was an imaginary load in the first place.

Applying this method to the vertical deflection of the two-element truss of Fig. 3, the problem already has a force in the required direction, the applied downward load P . The forces have already been shown to be $P_{AB} = P/\sin\theta$ and $P_{BC} = P/\tan\theta$, so the vertical deflection can be written immediately as

$$\begin{aligned} \delta_v &= P_{AB} \left(\frac{L}{AE} \right)_{AB} \frac{\partial P_{AB}}{\partial P} + P_{BC} \left(\frac{L}{AE} \right)_{BC} \frac{\partial P_{BC}}{\partial P} \\ &= \frac{P}{\sin\theta} \left(\frac{L}{AE} \right)_{AB} \frac{1}{\sin\theta} + \frac{P}{\tan\theta} \left(\frac{L}{AE} \right)_{AB} \frac{1}{\sin\theta} + \frac{P}{\tan\theta} \left(\frac{AE}{L} \right)_{BC} \frac{1}{\tan\theta} \end{aligned}$$

This is identical to the expression obtained from geometric considerations. The energy method didn't save too many algebraic steps in this case, but it avoided having to visualize and idealize the displacements geometrically.

If the horizontal displacement at joint B is desired, the method requires that a horizontal force exist at that point. One isn't given, so we place an imaginary one there, say Q . The truss is then reanalyzed statically to find how the element forces are influenced by this new force Q . The upper element force is $P_{AB} = P/\sin\theta$ as before, and the lower element force becomes $P_{BC} = P/\tan\theta - Q$. Repeating the Castigliano process, but now differentiating with respect to Q :

$$\begin{aligned} \delta_h &= P_{AB} \left(\frac{L}{AE} \right)_{AB} \frac{\partial P_{AB}}{\partial Q} + P_{BC} \left(\frac{L}{AE} \right)_{BC} \frac{\partial P_{BC}}{\partial Q} \\ &= \frac{P}{\sin\theta} \left(\frac{L}{AE} \right)_{AB} \cdot 0 + \left(\frac{P}{\tan\theta} - Q \right) \left(\frac{L}{AE} \right)_{BC} (-1) \end{aligned}$$

The first term vanishes upon differentiation since Q did not appear in the expression for P_{AB} . This is the method's way of noticing that the horizontal deflection is determined completely by the contraction of element BC . Upon setting $Q = 0$, the final result is

$$\delta_h = -\frac{P}{\tan\theta} \left(\frac{AE}{L} \right)_{BC}$$

as before.

Example 3

Consider the 6-element truss of Fig. 4 whose individual element forces were found earlier by free body diagrams. We are seeking the vertical deflection of node 3, which is congruent to the force P . Using Castigliano's method, this deflection is the derivative of the total strain energy with respect to P . Equivalently, we can differentiate the strain energy of each element with respect to P individually, and then add the contributions of each element to obtain the final result:

$$\delta_P = \frac{\partial}{\partial P} \sum_i \frac{F_i^2 L_i}{2A_i E_i} = \sum_i \left(\frac{F_i L_i}{A_i E_i} \frac{\partial F_i}{\partial P} \right)$$

To systemize this approach, we can form a table of needed parameters as follows:

i	F_i	$\frac{L_i}{A_i E_i}$	$\frac{\partial F_i}{\partial P}$	$\frac{F_i L_i}{A_i E_i} \frac{\partial F_i}{\partial P}$
1	$2P$	L/AE	2	$4PL/AE$
2	P	L/AE	1	PL/AE
3	$\sqrt{2}P$	$\sqrt{2}L/AE$	$\sqrt{2}$	$2.83PL/AE$
4	P	L/AE	1	PL/AE
5	$\sqrt{2}P$	$\sqrt{2}L/AE$	$\sqrt{2}$	$2.83PL/AE$
6	P	L/AE	1	PL/AE
$\delta_P = \sum =$				$12.7PL/AE$

If for instance we have as numerical parameters $P = 1000$ lbs, $L = 100$ in, $E = 30$ Mpsi and $A = 0.5$ in², then $\delta_P = 0.0844$ in.

Statically indeterminate trusses

It has already been noted that that the element forces in the truss problems treated up to now do not depend on the properties of the materials used in their construction, just as the stress in a simple tension test is independent of the material. This result, which certainly makes the problem easier to solve, is a consequence of the earlier problems being statically determinate; i.e. able to be solved using only the equations of static equilibrium. Statical determinacy, then, is an important aspect of the difficulty we can expect in solving the problem. Not all problems are statically determinate, and one consequence of this indeterminacy is that the forces in the structure *may* depend on the material properties.

After performing a static analysis of the truss as a whole to find reaction forces at the supports, we typically try to find the element forces using the joint-at-a-time method described above. However, there can be at most two unknown forces at a pin joint in a two-dimensional truss problem if the joint is to be solved using statics alone, since the moment equation does not provide usable information in this case. If more unknowns are present no matter in which order the truss joints are analyzed, then a number of additional equations equal to the remaining unknowns must be found. These extra equations are those enforcing compatibility of the various joint displacements, each of which must be such as to keep the truss joints pinned together.

Example 4

A simple example, just two truss elements acting in parallel as shown in Fig. 10, will show the approach needed. Here the compatibility condition is just

$$\delta_A = \delta_B$$

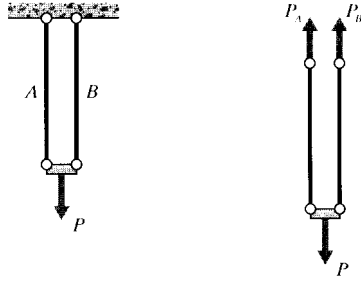


Figure 10: Two truss elements in parallel.

The individual element displacements are related to the element forces by $\delta = PL/AE$, which is material-dependent and can be termed a *constitutive* equation because it reflects the material's mechanical constitution. Combining this with the compatibility condition gives

$$\frac{P_A L}{A_A E_A} = \frac{P_B L}{A_B E_B} \Rightarrow P_B = P_A \frac{A_B E_B}{A_A E_A}$$

Finally, the individual element forces must add up to the total applied load P in order to satisfy equilibrium:

$$P = P_A + P_B = P_A + P_A \frac{A_B E_B}{A_A E_A} \Rightarrow P_A = P \left(\frac{1}{1 + \left(\frac{A_B E_B}{A_A E_A} \right)} \right)$$

Note that the final answer in the above example depends on the element dimensions and material stiffnesses, as promised. Here the geometrical compatibility condition was very simple and obvious, namely that the displacements of the two element end joints were identical. In more complex trusses these relations can be subtle, but tend to become more evident with practice.

Three different types of relations were used in the above problem: a *compatibility* equation, stating how the structure must deform kinematically in order to remain connected; a *constitutive* equation, embodying the stress-strain response of the material; and an *equilibrium* equation, stating that the forces must sum to zero if acceleration is to be avoided. These three concepts, made somewhat more general mathematically to handle geometrically more elaborate problems, underlie all of solid mechanics.

In the Module on Elastic Response, we noted that the stress in a tensile specimen is determined only by considerations of static equilibrium, being given by $\sigma = P/A$ independent of the material properties. We see now that the statical determinacy depends, among other things, on the material being *homogeneous*, i.e. identical throughout. If the tensile specimen is composed of two subunits each having different properties, the stresses will be allocated differently among the two units, and the stresses will not be uniform. Whenever a stress or deformation formula is copied out of a handbook, the user must be careful to note the limitations of the underlying theory. The handbook formulae are usually applicable only to homogeneous materials in their linear elastic range, and higher-order theories must be used when these conditions are not met.

Example 5

Figure 11(a) shows another statically indeterminate truss, with three elements having the same area and

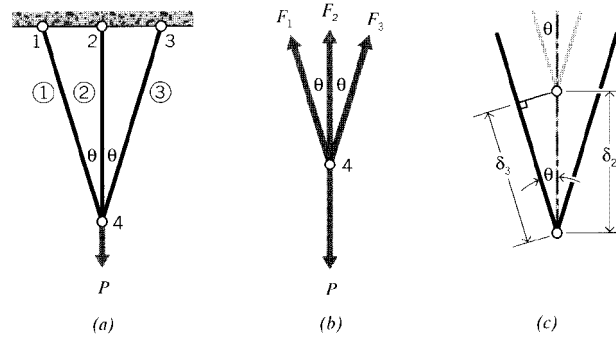


Figure 11: (a) Three-element statically indeterminate truss. (b) Free-body diagram of node 4. (c) Deflections at node 4.

modulus, but different lengths, meeting at a common node. At a glance, we can see node 4 has three elements meeting there whose forces are unknown, and this is one more than the useful equations of static equilibrium will be able to handle. This is also evident in the free-body diagram of Fig. 11(b): horizontal and vertical equilibrium gives

$$\sum F_x = 0 = -F_1 + F_2 \rightarrow F_1 = F_2$$

$$\sum F_y = 0 = -P + F_2 + F_1 \cos \theta + F_3 \cos \theta \rightarrow F_2 + 2F_3 \cos \theta = P \quad (8)$$

These two equations are clearly not sufficient to determine the unknowns F_1, F_2, F_3 . We need another equation, and it's provided by requiring the deformation be such as to keep the truss pinned together at node 4. Since the symmetry of the problems tells us that the deflection there is straight downward, the diagram in Fig. 11(c) can be used. And since the deflection is small relative to the lengths of the elements, the angle of element 3 remains essentially unchanged after deformation. This lets us write

$$\delta_3 = \delta_2 \cos \theta$$

or

$$\frac{F_3 L_3}{A_3 E_3} = \frac{F_2 L_2}{A_2 E_2} \cos \theta$$

Using $A_2 = A_3$, $E_2 = E_3$, $L_3 = L$, and $L_2 = L \cos \theta$, this becomes

$$F_3 = F_2 \cos^2 \theta$$

Solving this simultaneously with Eqn. 8, we obtain

$$F_2 = \frac{P}{1 + 2 \cos^3 \theta}, \quad F_3 = \frac{P \cos^2 \theta}{1 + 2 \cos^3 \theta}$$

Note that the modulus E does not appear in this result, even though the problem is statically indeterminate. If the elements had different stiffnesses, however, the cancellation of E would not have occurred.

Matrix analysis of trusses

The joint-by-joint free-body analysis of trusses is tedious for large and complicated structures, especially if static indeterminacy requires that displacement compatibility be considered along with static equilibrium. However, even statically indeterminate trusses can be solved quickly and reliably for both forces and displacements by a straightforward numerical procedure known as *matrix structural analysis*. This method is a forerunner of the more general computer method named *finite element analysis* (FEA), which has come to dominate much of engineering analysis in the past two decades. The foundations of matrix analysis will be outlined here, primarily as an introduction to the more general use of FEA in stress analysis.

Matrix analysis of trusses operates by considering the stiffness of each truss element one at a time, and then using these stiffnesses to determine the forces that are set up in the truss elements by the displacements of the joints, usually called “nodes” in finite element analysis. Then noting that the sum of the forces contributed by each element to a node must equal the force that is externally applied to that node, we can assemble a sequence of linear algebraic equations in which the nodal displacements are the unknowns and the applied nodal forces are known quantities. These equations are conveniently written in matrix form, which gives the method its name:

$$\begin{bmatrix} K_{11} & K_{12} & \cdots & K_{1n} \\ K_{21} & K_{22} & \cdots & K_{2n} \\ \vdots & \vdots & \ddots & \vdots \\ K_{n1} & K_{n2} & \cdots & K_{nn} \end{bmatrix} \begin{Bmatrix} u_1 \\ u_2 \\ \vdots \\ u_n \end{Bmatrix} = \begin{Bmatrix} f_1 \\ f_2 \\ \vdots \\ f_n \end{Bmatrix}$$

Here u_i and f_j indicate the deflection at the i^{th} node and the force at the j^{th} node (these would actually be vector quantities, with subcomponents along each coordinate axis). The K_{ij} coefficient array is called the *global stiffness matrix*, with the ij component being physically the influence of the j^{th} displacement on the i^{th} force. The matrix equations can be abbreviated as

$$K_{ij}u_j = f_i \quad \text{or} \quad \mathbf{Ku} = \mathbf{f} \quad (9)$$

using either subscripts or boldface to indicate vector and matrix quantities.

Either the force externally applied or the displacement is known at the outset for each node, and it is impossible to specify simultaneously both an arbitrary displacement *and* a force on a given node. These prescribed nodal forces and displacements are the boundary conditions of the problem. It is the task of analysis to determine the forces that accompany the imposed displacements, and the displacements at the nodes where known external forces are applied.

Stiffness matrix for a single truss element

As a first step in developing a set of matrix equations that describe truss systems, we need a relationship between the forces and displacements at each end of a single truss element. Consider such an element in the $x - y$ plane as shown in Fig. 12, attached to nodes numbered i and j and inclined at an angle θ from the horizontal.

Considering the elongation vector δ to be resolved in directions along and transverse to the element, the elongation in the truss element can be written in terms of the differences in the displacements of its end points:

$$\delta = (u_j \cos \theta + v_j \sin \theta) - (u_i \cos \theta + v_i \sin \theta)$$

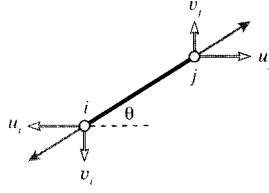


Figure 12: Individual truss element.

where u and v are the horizontal and vertical components of the deflections, respectively. (The displacements at node i drawn in Fig. 12 are negative.) This relation can be written in matrix form as:

$$\delta = \begin{bmatrix} -c & -s & c & s \end{bmatrix} \begin{Bmatrix} u_i \\ v_i \\ u_j \\ v_j \end{Bmatrix}$$

Here $c = \cos \theta$ and $s = \sin \theta$.

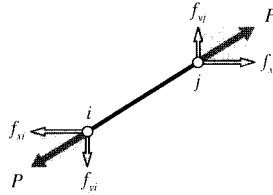


Figure 13: Components of nodal force.

The axial force P that accompanies the elongation δ is given by Hooke's law for linear elastic bodies as $P = (AE/L)\delta$. The horizontal and vertical nodal forces are shown in Fig. 13; these can be written in terms of the total axial force as:

$$\begin{aligned} \begin{Bmatrix} f_{xi} \\ f_{yi} \\ f_{xj} \\ f_{yj} \end{Bmatrix} &= \begin{Bmatrix} -c \\ -s \\ c \\ s \end{Bmatrix} P = \begin{Bmatrix} -c \\ -s \\ c \\ s \end{Bmatrix} \frac{AE}{L} \delta \\ &= \begin{Bmatrix} -c \\ -s \\ c \\ s \end{Bmatrix} \frac{AE}{L} \begin{bmatrix} -c & -s & c & s \end{bmatrix} \begin{Bmatrix} u_i \\ v_i \\ u_j \\ v_j \end{Bmatrix} \end{aligned}$$

Carrying out the matrix multiplication:

$$\boxed{\begin{Bmatrix} f_{xi} \\ f_{yi} \\ f_{xj} \\ f_{yj} \end{Bmatrix} = \frac{AE}{L} \begin{bmatrix} c^2 & cs & -c^2 & -cs \\ cs & s^2 & -cs & -s^2 \\ -c^2 & -cs & c^2 & cs \\ -cs & -s^2 & cs & s^2 \end{bmatrix} \begin{Bmatrix} u_i \\ v_i \\ u_j \\ v_j \end{Bmatrix}} \quad (10)$$

The quantity in brackets, multiplied by AE/L , is known as the “element stiffness matrix” k_{ij} . Each of its terms has a physical significance, representing the contribution of one of the displacements to one of the forces. The global system of equations is formed by combining the element stiffness matrices from each truss element in turn, so their computation is central to the method of matrix structural analysis. The principal difference between the matrix truss method and the general finite element method is in how the element stiffness matrices are formed; most of the other computer operations are the same.

Assembly of multiple element contributions

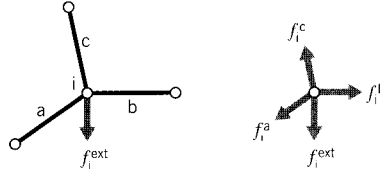


Figure 14: Element contributions to total nodal force.

The next step is to consider an assemblage of many truss elements connected by pin joints. Each element meeting at a joint, or node, will contribute a force there as dictated by the displacements of both that element’s nodes (see Fig. 14). To maintain static equilibrium, all element force contributions f_i^{elem} at a given node must sum to the force f_i^{ext} that is externally applied at that node:

$$f_i^{ext} = \sum_{elem} f_i^{elem} = \left(\sum_{elem} k_{ij}^{elem} u_j \right) = \left(\sum_{elem} k_{ij}^{elem} \right) u_j = K_{ij} u_j$$

Each element stiffness matrix k_{ij}^{elem} is added to the appropriate location of the overall, or “global” stiffness matrix K_{ij} that relates all of the truss displacements and forces. This process is called “assembly.” The index numbers in the above relation must be the “global” numbers assigned to the truss structure as a whole. However, it is generally convenient to compute the individual element stiffness matrices using a local scheme, and then to have the computer convert to global numbers when assembling the individual matrices.

Example 6

The assembly process is at the heart of the finite element method, and it is worthwhile to do a simple case by hand to see how it really works. Consider the two-element truss problem of Fig. 7, with the nodes being assigned arbitrary “global” numbers from 1 to 3. Since each node can in general move in two directions, there are $3 \times 2 = 6$ total degrees of freedom in the problem. The global stiffness matrix will then be a 6×6 array relating the six displacements to the six externally applied forces. Only one of the displacements is unknown in this case, since all but the vertical displacement of node 2 (degree of freedom number 4) is constrained to be zero. Figure 15 shows a workable listing of the global numbers, and also “local” numbers for each individual element.

Using the local numbers, the 4×4 element stiffness matrix of each of the two elements can be evaluated according to Eqn. 10. The inclination angle is calculated from the nodal coordinates as

$$\theta = \tan^{-1} \frac{y_2 - y_1}{x_2 - x_1}$$

The resulting matrix for element 1 is:

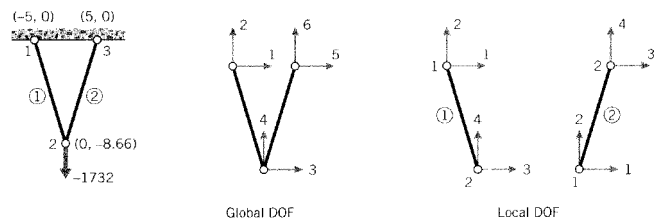


Figure 15: Global and local numbering for the two-element truss.

$$k^{(1)} = \begin{bmatrix} 25.00 & -43.30 & -25.00 & 43.30 \\ -43.30 & 75.00 & 43.30 & -75.00 \\ -25.00 & 43.30 & 25.00 & -43.30 \\ 43.30 & -75.00 & -43.30 & 75.00 \end{bmatrix} \times 10^3$$

and for element 2:

$$k^{(2)} = \begin{bmatrix} 25.00 & 43.30 & -25.00 & -43.30 \\ 43.30 & 75.00 & -43.30 & -75.00 \\ -25.00 & -43.30 & 25.00 & 43.30 \\ -43.30 & -75.00 & 43.30 & 75.00 \end{bmatrix} \times 10^3$$

(It is important the units be consistent; here lengths are in inches, forces in pounds, and moduli in psi. The modulus of both elements is $E = 10$ Mpsi and both have area $A = 0.1 \text{ in}^2$.) These matrices have rows and columns numbered from 1 to 4, corresponding to the local degrees of freedom of the element. However, each of the local degrees of freedom can be matched to one of the global degrees of the overall problem. By inspection of Fig. 15, we can form the following table that maps local to global numbers:

local	global, element 1	global, element 2
1	1	3
2	2	4
3	3	5
4	4	6

Using this table, we see for instance that the second degree of freedom for element 2 is the fourth degree of freedom in the global numbering system, and the third local degree of freedom corresponds to the fifth global degree of freedom. Hence the value in the second row and third column of the element stiffness matrix of element 2, denoted $k_{23}^{(2)}$, should be added into the position in the fourth row and fifth column of the 6×6 global stiffness matrix. We write this as

$$k_{23}^{(2)} \longrightarrow K_{4,5}$$

Each of the sixteen positions in the stiffness matrix of each of the two elements must be added into the global matrix according to the mapping given by the table. This gives the result

$$K = \begin{bmatrix} k_{11}^{(1)} & k_{12}^{(1)} & k_{13}^{(1)} & k_{14}^{(1)} & 0 & 0 \\ k_{21}^{(1)} & k_{22}^{(1)} & k_{23}^{(1)} & k_{24}^{(1)} & 0 & 0 \\ k_{31}^{(1)} & k_{32}^{(1)} & k_{33}^{(1)} + k_{11}^{(2)} & k_{34}^{(1)} + k_{12}^{(2)} & k_{13}^{(2)} & k_{14}^{(2)} \\ k_{41}^{(1)} & k_{42}^{(1)} & k_{43}^{(1)} + k_{21}^{(2)} & k_{44}^{(1)} + k_{22}^{(2)} & k_{23}^{(2)} & k_{24}^{(2)} \\ 0 & 0 & k_{31}^{(2)} & k_{32}^{(2)} & k_{33}^{(2)} & k_{34}^{(2)} \\ 0 & 0 & k_{41}^{(2)} & k_{42}^{(2)} & k_{43}^{(2)} & k_{44}^{(2)} \end{bmatrix}$$

This matrix premultiplies the vector of nodal displacements according to Eqn. 9 to yield the vector of externally applied nodal forces. The full system equations, taking into account the known forces and displacements, are then

$$10^3 \begin{bmatrix} 25.0 & -43.3 & -25.0 & 43.3 & 0.0 & 0.00 \\ -43.3 & 75.0 & 43.3 & -75.0 & 0.0 & 0.00 \\ -25.0 & 43.3 & 50.0 & 0.0 & -25.0 & -43.30 \\ 43.3 & -75.0 & 0.0 & 150.0 & -43.3 & -75.00 \\ 0.0 & 0.0 & -25.0 & -43.3 & 25.0 & 43.30 \\ 0.0 & 0.0 & -43.3 & -75.0 & 43.3 & 75.00 \end{bmatrix} \begin{bmatrix} 0 \\ 0 \\ 0 \\ u_4 \\ 0 \\ 0 \end{bmatrix} = \begin{bmatrix} f_1 \\ f_2 \\ f_3 \\ -1732 \\ f_5 \\ f_5 \end{bmatrix}$$

Note that either the force or the displacement for each degree of freedom is known, with the accompanying displacement or force being unknown. Here only one of the displacements (u_4) is unknown, but in most problems the unknown displacements far outnumber the unknown forces. Note also that only those elements that are physically connected to a given node can contribute a force to that node. In most cases, this results in the global stiffness matrix containing many zeroes corresponding to nodal pairs that are not spanned by an element. Effective computer implementations will take advantage of the matrix sparseness to conserve memory and reduce execution time.

In larger problems the matrix equations are solved for the unknown displacements and forces by Gaussian reduction or other techniques. In this two-element problem, the solution for the single unknown displacement can be written down almost from inspection. Multiplying out the fourth row of the system, we have

$$0 + 0 + 0 + 150 \times 10^3 u_4 + 0 + 0 = -1732$$

$$u_4 = -1732/150 \times 10^3 = -0.01155 \text{ in}$$

Now any of the unknown forces can be obtained directly. Multiplying out the first row for instance gives

$$0 + 0 + 0 + (43.4)(-0.0115) \times 10^3 + 0 + 0 = f_1$$

$$f_1 = -500 \text{ lb}$$

The negative sign here indicates the horizontal force on global node #1 is to the left, opposite the direction assumed in Fig. 15.

The process of cycling through each element to form the element stiffness matrix, assembling the element matrix into the correct positions in the global matrix, solving the equations for displacements and then back-multiplying to compute the forces, and printing the results can be automated to make a very versatile computer code.

Larger-scale truss (and other) finite element analysis are best done with a dedicated computer code, and an excellent one for learning the method is available from the web at www-cse.ucsd.edu/users/atkinson/felt/. This code, named **felt**, was authored by Jason Gobat and Darren Atkinson for educational use, and incorporates a number of novel features to promote user-friendliness. Complete information describing this code, as well as the C-language source and a number of trial runs and auxiliary code modules is available via their web pages. If you have access to X-window workstations, a graphical shell named **velvet** is available as well.

Example 7

To illustrate how this code operates for a somewhat larger problem, consider the six-element truss of Fig. 4, analyzed earlier both by the joint-at-a-time free body analysis approach and by Castigliano's method. The truss is redrawn in Fig. 16 by the **velvet** graphical interface.

The input dataset, which can be written manually or developed graphically in **velvet**, employs parsing techniques to simplify what can be a very tedious and error-prone step in finite element analysis. The dataset for this 6-element truss is:

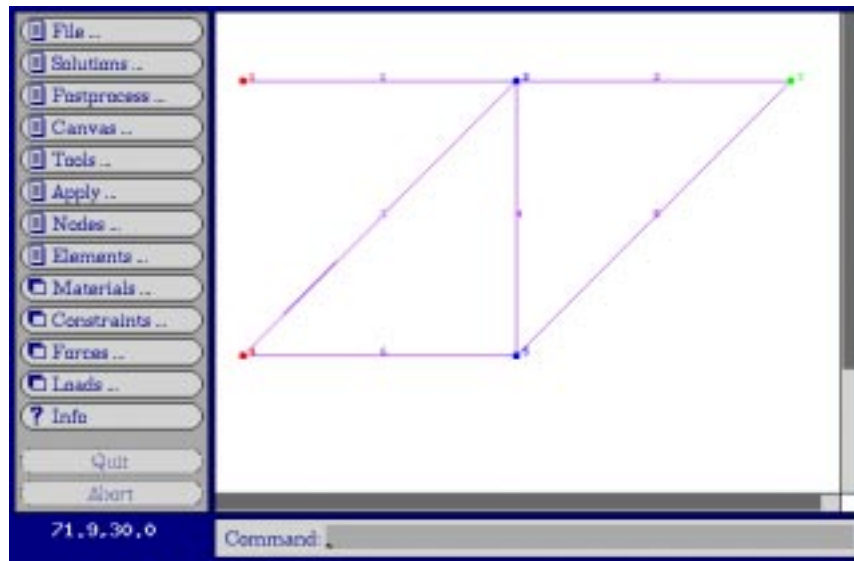


Figure 16: The six-element truss.

problem description

nodes=5 elements=6

nodes

1 x=0 y=100 z=0 constraint=pin
 2 x=100 y=100 z=0 constraint=planar
 3 x=200 y=100 z=0 force=P
 4 x=0 y=0 z=0 constraint=pin
 5 x=100 y=0 z=0 constraint=planar

truss elements

1 nodes=[1,2] material=steel
 2 nodes=[2,3]
 3 nodes=[4,2]
 4 nodes=[2,5]
 5 nodes=[5,3]
 6 nodes=[4,5]

material properties

steel E=3e+07 A=0.5

distributed loads

constraints

free Tx=u Ty=u Tz=u Rx=u Ry=u Rz=u
 pin Tx=c Ty=c Tz=c Rx=u Ry=u Rz=u
 planar Tx=u Ty=u Tz=c Rx=u Ry=u Rz=u

forces

P Fy=-1000

end

The meaning of these lines should be fairly evident on inspection, although the `felt` documentation should be consulted for more detail. The output produced by `felt` for these data is:

** **

Nodal Displacements

Node #	DOF 1	DOF 2	DOF 3	DOF 4	DOF 5	DOF 6
1	0	0	0	0	0	0
2	0.013333	-0.03219	0	0	0	0
3	0.02	-0.084379	0	0	0	0
4	0	0	0	0	0	0
5	-0.0066667	-0.038856	0	0	0	0

Element Stresses

1:	4000
2:	2000
3:	-2828.4
4:	2000
5:	-2828.4
6:	-2000

Reaction Forces

Node #	DOF	Reaction Force
1	Tx	-2000
1	Ty	0
1	Tz	0
2	Tz	0
3	Tz	0
4	Tx	2000
4	Ty	1000
4	Tz	0
5	Tz	0

Material Usage Summary

Material: steel
 Number: 6
 Length: 682.8427
 Mass: 0.0000

Total mass: 0.0000

Note that the vertical displacement of node 3 (the DOF 2 value) is -0.0844, the same value obtained earlier in Example 3. Figure 17 shows the `velvet` graphical output for the truss deflections (greatly magnified).

Problems

1. A rigid beam of length L rests on two supports that resist vertical motion, and is loaded by a vertical force F a distance a from the left support. Draw a free body diagram for

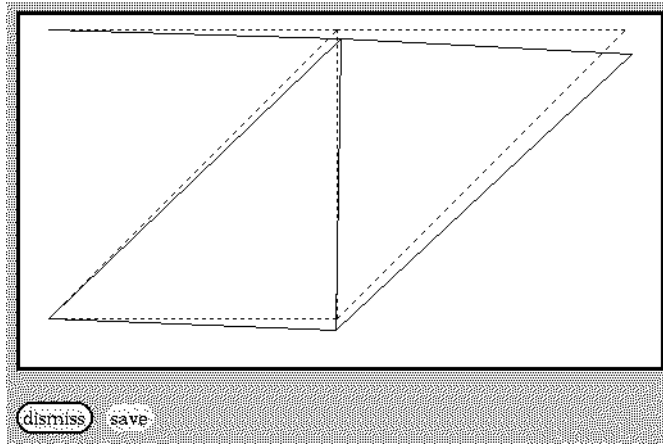
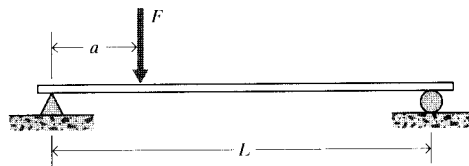


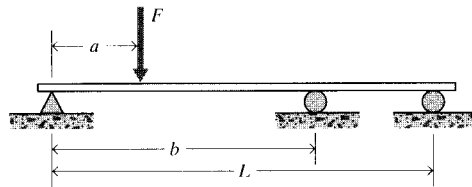
Figure 17: The 6-element truss in its original and deformed shape.

the beam, replacing the supports by the reaction forces R_1 and R_2 that they exert on the beam. Solve for the reaction forces in terms of F , a , and L .



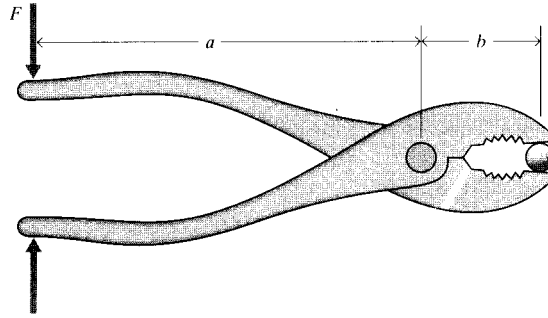
Prob. 1

2. A third support is added to the beam of the previous problem. Draw the free-body diagram for this case, and write the equilibrium equations available to solve for the reaction forces at each support. Is it possible to solve for all the reaction forces?



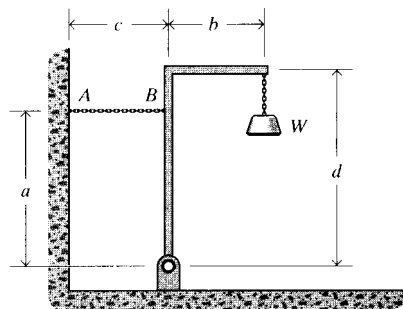
Prob. 2

3. The handles of a pair of pliers are squeezed with a force F . Draw a free-body diagram for one of the pliers' arms. What is the force exerted on an object gripped between the pliers' faces?
4. An object of weight W is suspended from a frame as shown. What is the tension in the



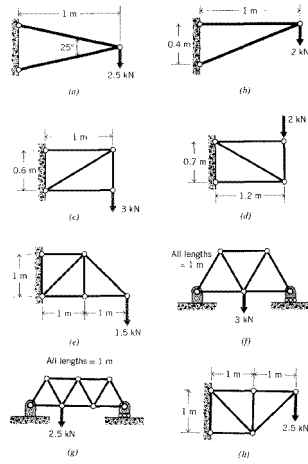
Prob. 3

restraining cable AB ?

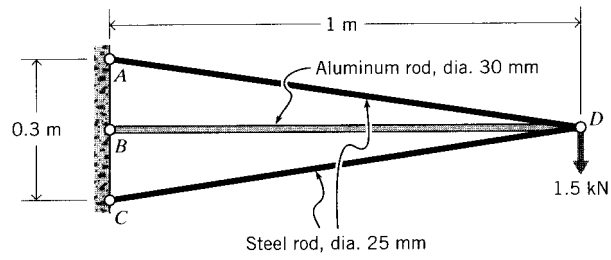


Prob. 4

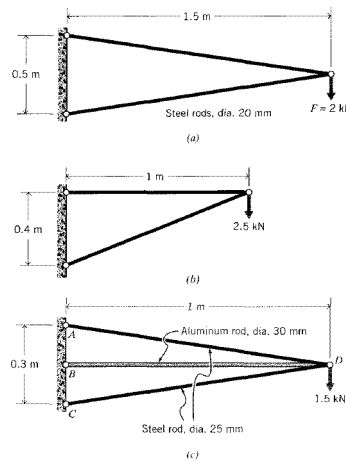
5. (a) – (h) Determine the force in each element of the trusses drawn below.
6. (a) – (h) Using geometrical considerations, determine the deflection of the loading point (the point at which the load is applied, in the direction of the load) for the trusses in Prob. 5. All elements are constructed of 20 mm diameter round carbon steel rods.
7. (a) – (h) Same as Prob. 6, but using Castigliano's theorem.
8. (a) – (h) Same as Prob. 6, but using finite element analysis.
9. Find the element forces and deflection at the loading point for the truss shown, using the method of your own choice.
10. (a) – (c) Write out the global stiffness matrices for the trusses listed below, and solve for the unknown forces and displacements.
11. Two truss elements of equal initial length L_0 are connected horizontally. Assuming the elements remain linearly elastic at all strains, determine the downward deflection y as a function of a load F applied transversely to the joint.



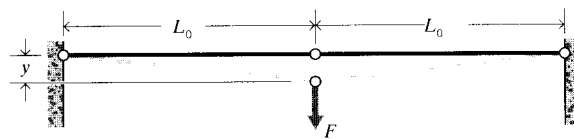
Prob. 5



Prob. 9



Prob. 10



Prob. 11

PRESSURE VESSELS

David Roylance
Department of Materials Science and Engineering
Massachusetts Institute of Technology
Cambridge, MA 02139

August 23, 2001

Introduction

A good deal of the Mechanics of Materials can be introduced entirely within the confines of uniaxially stressed structural elements, and this was the goal of the previous modules. But of course the real world is three-dimensional, and we need to extend these concepts accordingly. We now take the next step, and consider those structures in which the loading is still simple, but where the stresses and strains now require a second dimension for their description. Both for their value in demonstrating two-dimensional effects and also for their practical use in mechanical design, we turn to a slightly more complicated structural type: the thin-walled pressure vessel.

Structures such as pipes or bottles capable of holding internal pressure have been very important in the history of science and technology. Although the ancient Romans had developed municipal engineering to a high order in many ways, the very need for their impressive system of large aqueducts for carrying water was due to their not yet having pipes that could maintain internal pressure. Water *can* flow uphill when driven by the hydraulic pressure of the reservoir at a higher elevation, but without a pressure-containing pipe an aqueduct must be constructed so the water can run downhill all the way from the reservoir to the destination.

Airplane cabins are another familiar example of pressure-containing structures. They illustrate very dramatically the importance of proper design, since the atmosphere in the cabin has enough energy associated with its relative pressurization compared to the thin air outside that catastrophic crack growth is a real possibility. A number of fatal commercial tragedies have resulted from this, particularly famous ones being the Comet aircraft that disintegrated in flight in the 1950's¹ and the loss of a 5-meter section of the roof in the first-class section of an Aloha Airlines B737 in April 1988²

In the sections to follow, we will outline the means of determining stresses and deformations in structures such as these, since this is a vital first step in designing against failure.

Stresses

In two dimensions, the state of stress at a point is conveniently illustrated by drawing four perpendicular lines that we can view as representing four adjacent planes of atoms taken from an arbitrary position within the material. The planes on this “stress square” shown in Fig. 1 can be identified by the orientations of their normals; the upper horizontal plane is a $+y$ plane, since

¹T. Bishop, “Fatigue and the Comet Disasters,” *Metal Progress*, Vol. 67, pp. 79–85, May 1955.

²E.E. Murphy, “Aging Aircraft: Too Old to Fly?” *IEEE Spectrum*, pp. 28–31, June 1989.

its normal points in the $+y$ direction. The vertical plane on the right is a $+x$ plane. Similarly, the left vertical and lower horizontal planes are $-y$ and $-x$, respectively.

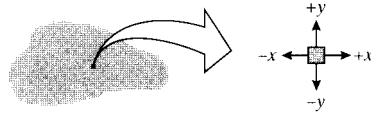


Figure 1: State of stress in two dimensions: the stress square.

The sign convention in common use regards tensile stresses as positive and compressive stresses as negative. A positive tensile stress acting in the x direction is drawn on the $+x$ face as an arrow pointed in the $+x$ direction. But for the stress square to be in equilibrium, this arrow must be balanced by another acting on the $-x$ face and pointed in the $-x$ direction. Of course, these are not two separate stresses, but simply indicate the stress state is one of uniaxial tension. A positive stress is therefore indicated by a $+$ arrow on a $+$ face, or a $-$ arrow on a $-$ face. Compressive stresses are the reverse: a $-$ arrow on a $+$ face or a $+$ arrow on a $-$ face. A stress state with both positive and negative components is shown in Fig. 2.

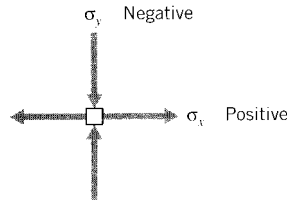


Figure 2: The sign convention for normal stresses.

Consider now a simple spherical vessel of radius r and wall thickness b , such as a round balloon. An internal pressure p induces equal biaxial tangential tensile stresses in the walls, which can be denoted using spherical $r\theta\phi$ coordinates as σ_θ and σ_ϕ .

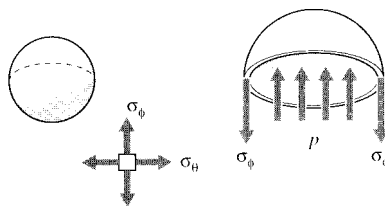


Figure 3: Wall stresses in a spherical pressure vessel.

The magnitude of these stresses can be determined by considering a free body diagram of half the pressure vessel, including its pressurized internal fluid (see Fig. 3). The fluid itself is assumed to have negligible weight. The internal pressure generates a force of $pA = p(\pi r^2)$ acting on the fluid, which is balanced by the force obtained by multiplying the wall stress times its area, $\sigma_\phi(2\pi r b)$. Equating these:

$$p(\pi r^2) = \sigma_\phi(2\pi r b)$$

$$\boxed{\sigma_\phi = \frac{pr}{2b}} \quad (1)$$

Note that this is a statically determined result, with no dependence on the material properties. Further, note that the stresses in any two orthogonal circumferential directions are the same; i.e. $\sigma_\phi = \sigma_\theta$.

The accuracy of this result depends on the vessel being “thin-walled,” i.e. $r \gg b$. At the surfaces of the vessel wall, a radial stress σ_r must be present to balance the pressure there. But the inner-surface radial stress is equal to p , while the circumferential stresses are p times the ratio $(r/2b)$. When this ratio is large, the radial stresses can be neglected in comparison with the circumferential stresses.

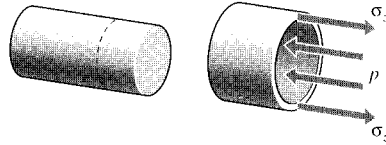


Figure 4: Free-body diagram for axial stress in a closed-end vessel.

The stresses σ_z in the axial direction of a cylindrical pressure vessel with closed ends are found using this same approach as seen in Fig. 4, and yielding the same answer:

$$p(\pi r^2) = \sigma_z(2\pi r)b$$

$$\boxed{\sigma_z = \frac{pr}{2b}} \quad (2)$$

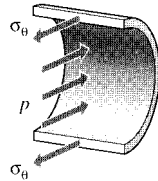


Figure 5: Hoop stresses in a cylindrical pressure vessel.

However, a different view is needed to obtain the circumferential or “hoop” stresses σ_θ . Considering an axial section of unit length, the force balance for Fig. 5 gives

$$2\sigma_\theta(b \cdot 1) = p(2r \cdot 1)$$

$$\boxed{\sigma_\theta = \frac{pr}{b}} \quad (3)$$

Note the hoop stresses are twice the axial stresses. This result — different stresses in different directions — occurs more often than not in engineering structures, and shows one of the

compelling advantages for engineered materials that can be made stronger in one direction than another (the property of *anisotropy*). If a pressure vessel constructed of conventional isotropic material is made thick enough to keep the hoop stresses below yield, it will be twice as strong as it needs to be in the axial direction. In applications placing a premium on weight this may well be something to avoid.

Example 1

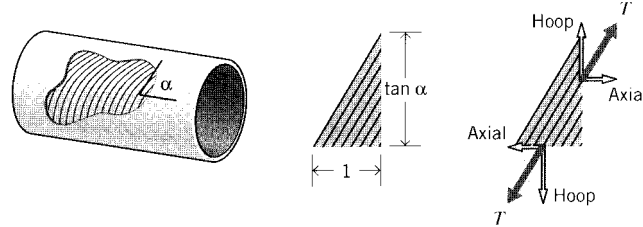


Figure 6: Filament-wound cylindrical pressure vessel.

Consider a cylindrical pressure vessel to be constructed by *filament winding*, in which fibers are laid down at a prescribed helical angle α (see Fig. 6). Taking a free body of unit axial dimension along which n fibers transmitting tension T are present, the circumferential distance cut by these same n fibers is then $\tan \alpha$. To balance the hoop and axial stresses, the fiber tensions must satisfy the relations

$$\text{hoop : } nT \sin \alpha = \frac{pr}{b}(1)(b)$$

$$\text{axial : } nT \cos \alpha = \frac{pr}{2b}(\tan \alpha)(b)$$

Dividing the first of these expressions by the second and rearranging, we have

$$\tan^2 \alpha = 2, \quad \alpha = 54.7^\circ$$

This is the “magic angle” for filament wound vessels, at which the fibers are inclined just enough toward the circumferential direction to make the vessel twice as strong circumferentially as it is axially. Firefighting hoses are also braided at this same angle, since otherwise the nozzle would jump forward or backward when the valve is opened and the fibers try to align themselves along the correct direction.

Deformation: the Poisson effect

When a pressure vessel has open ends, such as with a pipe connecting one chamber with another, there will be no axial stress since there are no end caps for the fluid to push against. Then only the hoop stress $\sigma_\theta = pr/b$ exists, and the corresponding hoop strain is given by Hooke’s Law as:

$$\epsilon_\theta = \frac{\sigma_\theta}{E} = \frac{pr}{bE}$$

Since this strain is the change in circumference δ_C divided by the original circumference $C = 2\pi r$ we can write:

$$\delta_C = C\epsilon_\theta = 2\pi r \frac{pr}{bE}$$

The change in circumference and the corresponding change in radius δ_r are related by $\delta_r = \delta_C/2\pi$, so the radial expansion is:

$$\delta_r = \frac{pr^2}{bE} \quad (4)$$

This is analogous to the expression $\delta = PL/AE$ for the elongation of a uniaxial tensile specimen.

Example 2

Consider a *compound cylinder*, one having a cylinder of brass fitted snugly inside another of steel as shown in Fig. 7 and subjected to an internal pressure of $p = 2$ MPa.

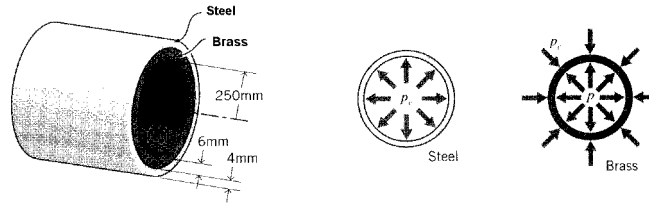


Figure 7: A compound pressure vessel.

When the pressure is put inside the inner cylinder, it will naturally try to expand. But the outer cylinder pushes back so as to limit this expansion, and a “contact pressure” p_c develops at the interface between the two cylinders. The inner cylinder now expands according to the difference $p - p_c$, while the outer cylinder expands as demanded by p_c alone. But since the two cylinders are obviously going to remain in contact, it should be clear that the radial expansions of the inner and outer cylinders must be the same, and we can write

$$\delta_b = \delta_s \rightarrow \frac{(p - p_c)r_b^2}{E_b b_b} = \frac{p_c r_s^2}{E_s b_s}$$

where the a and s subscripts refer to the brass and steel cylinders respectively.

Substituting numerical values and solving for the unknown contact pressure p_c :

$$p_c = 976 \text{ KPa}$$

Now knowing p_c , we can calculate the radial expansions and the stresses if desired. For instance, the hoop stress in the inner brass cylinder is

$$\sigma_{\theta,b} = \frac{(p - p_c)r_b}{b_b} = 62.5 \text{ MPa} \quad (= 906 \text{ psi})$$

Note that the stress is no longer independent of the material properties (E_b and E_s), depending as it does on the contact pressure p_c which in turn depends on the material stiffnesses. This loss of statical determinacy occurs here because the problem has a mixture of some load boundary values (the internal pressure) and some displacement boundary values (the constraint that both cylinders have the same radial displacement.)

If a cylindrical vessel has closed ends, both axial and hoop stresses appear together, as given by Eqns. 2 and 3. Now the deformations are somewhat subtle, since a positive (tensile) strain in one direction will also contribute a negative (compressive) strain in the other direction, just as stretching a rubber band to make it longer in one direction makes it thinner in the other

directions (see Fig. 8). This lateral contraction accompanying a longitudinal extension is called the *Poisson effect*,³ and the *Poisson's ratio* is a material property defined as

$$\nu = \frac{-\epsilon_{\text{lateral}}}{\epsilon_{\text{longitudinal}}} \quad (5)$$

where the minus sign accounts for the sign change between the lateral and longitudinal strains. The stress-strain, or “constitutive,” law of the material must be extended to include these effects, since the strain in any given direction is influenced by not only the stress in that direction, but also by the Poisson strains contributed by the stresses in the other two directions.

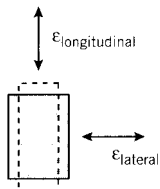


Figure 8: The Poisson effect.

A material subjected only to a stress σ_x in the x direction will experience a strain in that direction given by $\epsilon_x = \sigma_x/E$. A stress σ_y acting alone in the y direction will induce an x -direction strain given from the definition of Poisson's ratio of $\epsilon_x = -\nu\epsilon_y = -\nu(\sigma_y/E)$. If the material is subjected to both stresses σ_x and σ_y at once, the effects can be superimposed (since the governing equations are *linear*) to give:

$$\epsilon_x = \frac{\sigma_x}{E} - \frac{\nu\sigma_y}{E} = \frac{1}{E}(\sigma_x - \nu\sigma_y) \quad (6)$$

Similarly for a strain in the y direction:

$$\epsilon_y = \frac{\sigma_y}{E} - \frac{\nu\sigma_x}{E} = \frac{1}{E}(\sigma_y - \nu\sigma_x) \quad (7)$$

The material is in a state of *plane stress* if no stress components act in the third dimension (the z direction, here). This occurs commonly in thin sheets loaded in their plane. The z components of stress vanish at the surfaces because there are no forces acting externally in that direction to balance them, and these components do not have sufficient specimen distance in the thin through-thickness dimension to build up to appreciable levels. However, a state of plane stress is *not* a state of plane strain. The sheet will experience a strain in the z direction equal to the Poisson strain contributed by the x and y stresses:

$$\epsilon_z = -\frac{\nu}{E}(\sigma_x + \sigma_y) \quad (8)$$

In the case of a closed-end cylindrical pressure vessels, Eqn. 6 or 7 can be used directly to give the hoop strain as

$$\epsilon_\theta = \frac{1}{E}(\sigma_\theta - \nu\sigma_z) = \frac{1}{E}\left(\frac{pr}{b} - \nu\frac{pr}{2b}\right)$$

³After the French mathematician Simeon Denis Poisson, (1781–1840).

$$= \frac{pr}{bE} \left(1 - \frac{\nu}{2}\right)$$

The radial expansion is then

$$\delta_r = r\epsilon_\theta = \frac{pr^2}{bE} \left(1 - \frac{\nu}{2}\right) \quad (9)$$

Note that the radial expansion is reduced by the Poisson term; the axial deformation contributes a shortening in the radial direction.

Example 3

It is common to build pressure vessels by using bolts to hold end plates on an open-ended cylinder, as shown in Fig. 9. Here let's say for example the cylinder is made of copper alloy, with radius $R = 5''$, length $L = 10''$ and wall thickness $b_c = 0.1''$. Rigid plates are clamped to the ends by nuts threaded on four $3/8''$ diameter steel bolts, each having 15 threads per inch. Each of the nuts is given an additional $1/2$ turn beyond the just-snug point, and we wish to estimate the internal pressure that will just cause incipient leakage from the vessel.

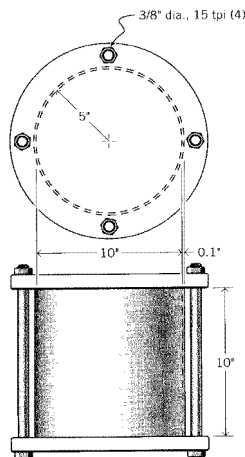


Figure 9: A bolt-clamped pressure vessel.

As pressure p inside the cylinder increases, a force $F = p(\pi R^2)$ is exerted on the end plates, and this is reacted equally by the four restraining bolts; each thus feels a force F_b given by

$$F_b = \frac{p(\pi R^2)}{4}$$

The bolts then stretch by an amount δ_b given by:

$$\delta_b = \frac{F_b L}{A_b E_b}$$

It's tempting to say that the vessel will start to leak when the bolts have stretched by an amount equal to the original tightening; i.e. $1/2$ turn/15 turns per inch. But as p increases, the cylinder itself is deforming as well; it experiences a radial expansion according to Eqn. 4. The radial expansion by itself doesn't cause leakage, but it is accompanied by a Poisson contraction δ_c in the axial direction. This means the bolts don't have to stretch as far before the restraining plates are lifted clear. (Just as leakage begins, the plates are no longer pushing on the cylinder, so the axial loading of the plates on the cylinder becomes zero and is not needed in the analysis.)

The relations governing leakage, in addition to the above expressions for δ_b and F_b are therefore:

$$\delta_b + \delta_c = \frac{1}{2} \times \frac{1}{15}$$

where here the subscripts b and c refer to the bolts and the cylinder respectively. The axial deformation δ_c of the cylinder is just L times the axial strain ϵ_z , which in turn is given by an expression analogous to Eqn. 7:

$$\delta_c = \epsilon_z L = \frac{L}{E_c} [\sigma_z - \nu \sigma_\theta]$$

Since σ_z becomes zero just as the plate lifts off and $\sigma_\theta = pR/b_c$, this becomes

$$\delta_c = \frac{L}{E_c} \frac{\nu p R}{b_c}$$

Combining the above relations and solving for p , we have

$$p = \frac{2 A_b E_b E_c b_c}{15 R L (\pi R E_c b_c + 4 \nu A_b E_b)}$$

On substituting the geometrical and materials numerical values, this gives

$$p = 496 \text{ psi}$$

The Poisson's ratio is a dimensionless parameter that provides a good deal of insight into the nature of the material. The major classes of engineered structural materials fall neatly into order when ranked by Poisson's ratio:

Material Class	Poisson's Ratio ν
Ceramics	0.2
Metals	0.3
Plastics	0.4
Rubber	0.5

(The values here are approximate.) It will be noted that the most brittle materials have the lowest Poisson's ratio, and that the materials appear to become generally more flexible as the Poisson's ratio increases. The ability of a material to contract laterally as it is extended longitudinally is related directly to its molecular mobility, with rubber being liquid-like and ceramics being very tightly bonded.

The Poisson's ratio is also related to the compressibility of the material. The *bulk modulus* K , also called the modulus of compressibility, is the ratio of the hydrostatic pressure p needed for a unit relative decrease in volume $\Delta V/V$:

$$K = \frac{-p}{\Delta V/V} \tag{10}$$

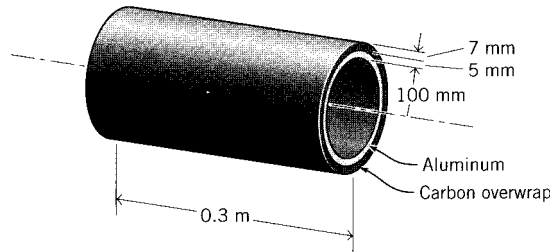
where the minus sign indicates that a compressive pressure (traditionally considered positive) produces a negative volume change. It can be shown that for isotropic materials the bulk modulus is related to the elastic modulus and the Poisson's ratio as

$$K = \frac{E}{3(1 - 2\nu)} \tag{11}$$

This expression becomes unbounded as ν approaches 0.5, so that rubber is essentially incompressible. Further, ν cannot be larger than 0.5, since that would mean volume would *increase* on the application of positive pressure. A ceramic at the lower end of Poisson's ratios, by contrast, is so tightly bonded that it is unable to rearrange itself to "fill the holes" that are created when a specimen is pulled in tension; it has no choice but to suffer a volume increase. Paradoxically, the tightly bonded ceramics have lower bulk moduli than the very mobile elastomers.

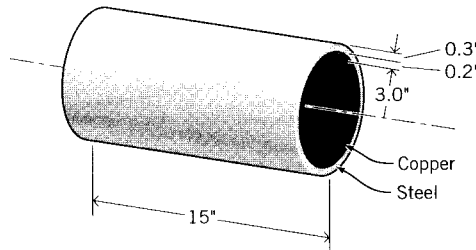
Problems

1. A closed-end cylindrical pressure vessel constructed of carbon steel has a wall thickness of 0.075", a diameter of 6", and a length of 30". What are the hoop and axial stresses σ_θ, σ_z when the cylinder carries an internal pressure of 1500 psi? What is the radial displacement δ_r ?
2. What will be the safe pressure of the cylinder in the previous problem, using a factor of safety of two?
3. A compound pressure vessel with dimensions as shown is constructed of an aluminum inner layer and a carbon-overwrapped outer layer. Determine the circumferential stresses (σ_θ) in the two layers when the internal pressure is 15 MPa. The modulus of the graphite layer in the circumferential direction is 15.5 GPa.



Prob. 3

4. A copper cylinder is fitted snugly inside a steel one as shown. What is the contact pressure generated between the two cylinders if the temperature is increased by 10°C? What if the copper cylinder is on the outside?



Prob. 4

5. Three cylinders are fitted together to make a compound pressure vessel. The inner cylinder is of carbon steel with a thickness of 2 mm, the central cylinder is of copper alloy with

a thickness of 4 mm, and the outer cylinder is of aluminum with a thickness of 2 mm. The inside radius of the inner cylinder is 300 mm, and the internal pressure is 1.4 MPa. Determine the radial displacement and circumferential stress in the inner cylinder.

6. A pressure vessel is constructed with an open-ended steel cylinder of diameter 6", length 8", and wall thickness 0.375". The ends are sealed with rigid end plates held by four 1/4" diameter bolts. The bolts have 18 threads per inch, and the retaining nuts have been tightened 1/4 turn beyond their just-snug point before pressure is applied. Find the internal pressure that will just cause incipient leakage from the vessel.
7. An aluminum cylinder, with 1.5" inside radius and thickness 0.1", is to be fitted inside a steel cylinder of thickness 0.25". The inner radius of the steel cylinder is 0.005" smaller than the outer radius of the aluminum cylinder; this is called an *interference fit*. In order to fit the two cylinders together initially, the inner cylinder is shrunk by cooling. By how much should the temperature of the aluminum cylinder be lowered in order to fit it inside the steel cylinder? Once the assembled compound cylinder has warmed to room temperature, how much contact pressure is developed between the aluminum and the steel?
8. Assuming the material in a spherical rubber balloon can be modeled as linearly elastic with modulus E and Poisson's ratio $\nu = 0.5$, show that the internal pressure p needed to expand the balloon varies with the radial expansion ratio $\lambda_r = r/r_0$ as

$$\frac{pr_0}{4Eb_0} = \frac{1}{\lambda_r^2} - \frac{1}{\lambda_r^3}$$

where b_0 is the initial wall thickness. Plot this function and determine its critical values.

9. Repeat the previous problem, but using the constitutive relation for rubber:

$${}^t\sigma_x = \frac{E}{3} \left(\lambda_x^2 - \frac{1}{\lambda_x^2 \lambda_y^2} \right)$$

10. What pressure is needed to expand a balloon, initially 3" in diameter and with a wall thickness of 0.1", to a diameter of 30"? The balloon is constructed of a rubber with a specific gravity of 0.9 and a molecular weight between crosslinks of 3000 g/mol. The temperature is 20°.
11. After the balloon of the previous problem has been inflated, the temperature is increased by 25C. How do the pressure and radius change?

SHEAR AND TORSION

David Roylance
Department of Materials Science and Engineering
Massachusetts Institute of Technology
Cambridge, MA 02139

June 23, 2000

Introduction

Torsionally loaded shafts are among the most commonly used structures in engineering. For instance, the drive shaft of a standard rear-wheel drive automobile, depicted in Fig. 1, serves primarily to transmit torsion. These shafts are almost always hollow and circular in cross section, transmitting power from the transmission to the differential joint at which the rotation is diverted to the drive wheels. As in the case of pressure vessels, it is important to be aware of design methods for such structures purely for their inherent usefulness. However, we study them here also because they illustrate the role of shearing stresses and strains.

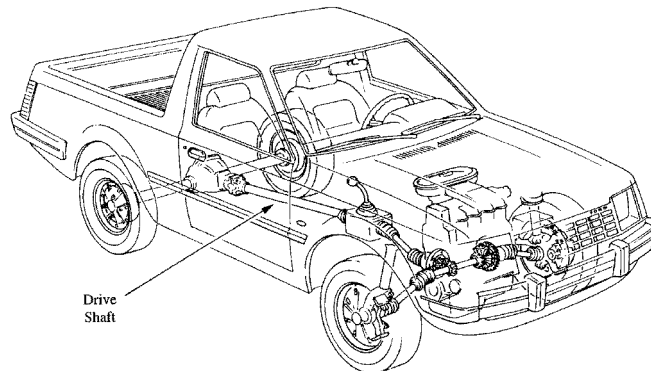


Figure 1: A drive shaft.

Shearing stresses and strains

Not all deformation is elongational or compressive, and we need to extend our concept of strain to include “shearing,” or “distortional,” effects. To illustrate the nature of shearing distortions, first consider a square grid inscribed on a tensile specimen as depicted in Fig. 2(a). Upon uniaxial loading, the grid would be deformed so as to increase the length of the lines in the tensile loading direction and contract the lines perpendicular to the loading direction. However, the lines remain perpendicular to one another. These are termed *normal* strains, since planes normal to the loading direction are moving apart.

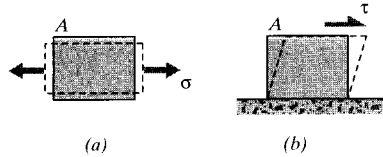


Figure 2: (a) Normal and (b) shearing deformations.

Now consider the case illustrated in Fig. 2(b), in which the load P is applied *transversely* to the specimen. Here the horizontal lines tend to *slide* relative to one another, with line lengths of the originally square grid remaining unchanged. The vertical lines tilt to accommodate this motion, so the originally right angles between the lines are distorted. Such a loading is termed *direct shear*. Analogously to our definition of normal stress as force per unit area¹, or $\sigma = P/A$, we write the *shear stress* τ as

$$\tau = \frac{P}{A}$$

This expression is identical to the expression for normal stress, but the different symbol τ reminds us that the loading is transverse rather than extensional.

Example 1

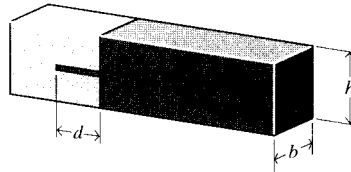


Figure 3: Tongue-and-groove adhesive joint.

Two timbers, of cross-sectional dimension $b \times h$, are to be glued together using a tongue-and-groove joint as shown in Fig. 3, and we wish to estimate the depth d of the glue joint so as to make the joint approximately as strong as the timber itself.

The axial load P on the timber acts to shear the glue joint, and the shear stress in the joint is just the load divided by the total glue area:

$$\tau = \frac{P}{2bd}$$

If the bond fails when τ reaches a maximum value τ_f , the load at failure will be $P_f = (2bd)\tau_f$. The load needed to fracture the timber in tension is $P_f = bh\sigma_f$, where σ_f is the ultimate tensile strength of the timber. Hence if the glue joint and the timber are to be equally strong we have

$$(2bd)\tau_f = bh\sigma_f \rightarrow d = \frac{h\sigma_f}{2\tau_f}$$

¹See Module 1, Introduction to Elastic Response

Normal stresses act to pull parallel planes within the material apart or push them closer together, while shear stresses act to slide planes along one another. Normal stresses promote crack formation and growth, while shear stresses underlie yield and plastic slip. The shear stress can be depicted on the stress square as shown in Fig. 4(a); it is traditional to use a half-arrowhead to distinguish shear stress from normal stress. The yx subscript indicates the stress is on the y plane in the x direction.

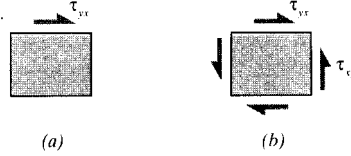


Figure 4: Shear stress.

The τ_{yx} arrow on the $+y$ plane must be accompanied by one in the opposite direction on the $-y$ plane, in order to maintain horizontal equilibrium. But these two arrows by themselves would tend to cause a clockwise rotation, and to maintain moment equilibrium we must also add two vertical arrows as shown in Fig. 4(b); these are labeled τ_{xy} , since they are on x planes in the y direction. For rotational equilibrium, the magnitudes of the horizontal and vertical stresses must be equal:

$$\tau_{yx} = \tau_{xy} \quad (1)$$

Hence any shearing that tends to cause tangential sliding of horizontal planes is accompanied by an equal tendency to slide vertical planes as well. Note that all of these are positive by our earlier convention of $+$ arrows on $+$ faces being positive. A positive state of shear stress, then, has arrows meeting at the upper right and lower left of the stress square. Conversely, arrows in a negative state of shear meet at the lower right and upper left.

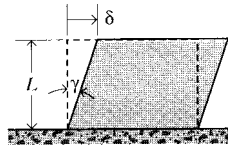


Figure 5: Shear strain.

The strain accompanying the shear stress τ_{xy} is a *shear strain* denoted γ_{xy} . This quantity is a deformation per unit length just as was the normal strain ϵ , but now the displacement is transverse to the length over which it is distributed (see Fig. 5). This is also the distortion or change in the right angle:

$$\frac{\delta}{L} = \tan \gamma \approx \gamma \quad (2)$$

This angular distortion is found experimentally to be linearly proportional to the shear stress at sufficiently small loads, and the shearing counterpart of Hooke's Law can be written as

$$\tau_{xy} = G\gamma_{xy} \quad (3)$$

where G is a material property called the *shear modulus*. for *isotropic* materials (properties same in all directions), there is no Poisson-type effect to consider in shear, so that the shear strain is not influenced by the presence of normal stresses. Similarly, application of a shearing stress has no influence on the normal strains. For plane stress situations (no normal or shearing stress components in the z direction), the constitutive equations as developed so far can be written:

$$\boxed{\begin{aligned}\epsilon_x &= \frac{1}{E} (\sigma_x - \nu\sigma_y) \\ \epsilon_y &= \frac{1}{E} (\sigma_y - \nu\sigma_x) \\ \gamma_{xy} &= \frac{1}{G} \tau_{xy}\end{aligned}} \quad (4)$$

It will be shown later that for isotropic materials, only two of the material constants here are independent, and that

$$\boxed{G = \frac{E}{2(1 + \nu)}} \quad (5)$$

Hence if any two of the three properties E , G , or ν , are known, the other is determined.

Statics - Twisting Moments

Twisting moments, or torques, are forces acting through distances (“lever arms”) so as to promote rotation. The simple example is that of using a wrench to tighten a nut on a bolt as shown in Fig. 6: if the bolt, wrench, and force are all perpendicular to one another, the moment is just the force F times the length l of the wrench: $T = F \cdot l$. This relation will suffice when the geometry of torsional loading is simple as in this case, when the torque is applied “straight”.

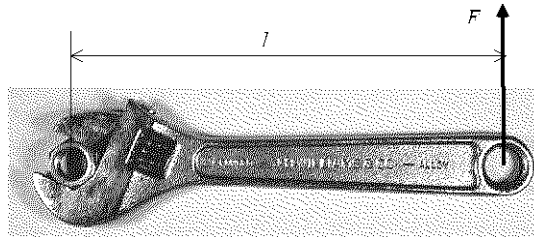


Figure 6: Simple torque: $T = F \times l$.

Often, however, the geometry of the applied moment is a bit more complicated. Consider a not-uncommon case where for instance a spark plug must be loosened and there just isn't room to put a wrench on it properly. Here a swiveled socket wrench might be needed, which can result in the lever arm not being perpendicular to the spark plug axis, and the applied force (from your hand) not being perpendicular to the lever arm. Vector algebra can make the geometrical calculations easier in such cases. Here the *moment vector* around a point O is obtained by crossing the vector representation of the lever arm \mathbf{r} from O with the force vector \mathbf{F} :

$$\mathbf{T} = \mathbf{r} \times \mathbf{F} \quad (6)$$

This vector is in a direction given by the right hand rule, and is normal to the plane containing the point O and the force vector. The torque tending to loosen the spark plug is then the component of this moment vector along the plug axis:

$$T = \mathbf{i} \cdot (\mathbf{r} \times \mathbf{F}) \quad (7)$$

where \mathbf{i} is a unit vector along the axis. The result, a torque or twisting moment *around an axis*, is a *scalar* quantity.

Example 2

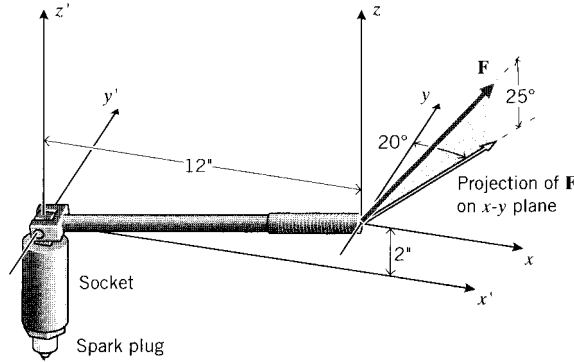


Figure 7: Working on your good old car - trying to get the spark plug out.

We wish to find the effective twisting moment on a spark plug, where the force applied to a swivel wrench that is skewed away from the plug axis as shown in Fig. 7. An $x'y'z'$ Cartesian coordinate system is established with z' being the spark plug axis; the free end of the wrench is $2''$ above the $x'y'$ plane perpendicular to the plug axis, and $12''$ away from the plug along the x' axis. A 15 lb force is applied to the free end at a skewed angle of 25° vertical and 20° horizontal.

The force vector applied to the free end of the wrench is

$$\mathbf{F} = 15(\cos 25 \sin 20 \mathbf{i} + \cos 25 \cos 20 \mathbf{j} + \sin 25 \mathbf{k})$$

The vector from the axis of rotation to the applied force is

$$\mathbf{r} = 12\mathbf{i} + 0\mathbf{j} + 2\mathbf{k}$$

where $\mathbf{i}, \mathbf{j}, \mathbf{k}$, are the unit vectors along the x, y, z axes. The moment vector around the point O is then

$$\mathbf{T}_O = \mathbf{r} \times \mathbf{F} = (-25.55\mathbf{i} - 66.77\mathbf{j} + 153.3\mathbf{k})$$

and the scalar moment along the axis z' is

$$T_{z'} = \mathbf{k} \cdot (\mathbf{r} \times \mathbf{F}) = 153.3 \text{ in} - \text{lb}$$

This is the torque that will loosen the spark plug, if you're luckier than I am with cars.

Shafts in torsion are used in almost all rotating machinery, as in our earlier example of a drive shaft transmitting the torque of an automobile engine to the wheels. When the car is operating at constant speed (not accelerating), the torque on a shaft is related to its rotational speed ω and the power W being transmitted:

$$W = T\omega \quad (8)$$

Geared transmissions are usually necessary to keep the engine speed in reasonable bounds as the car speeds up, and the gearing must be considered in determining the torques applied to the shafts.

Example 3

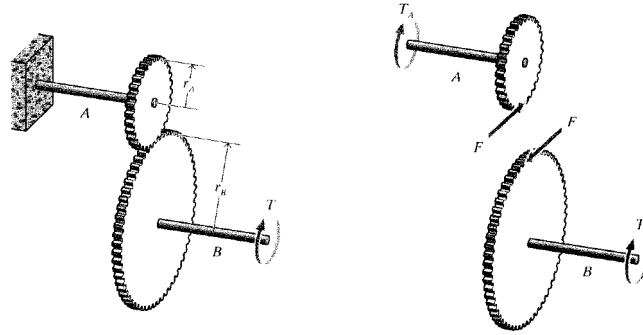


Figure 8: Two-gear assembly.

Consider a simple two-shaft gearing as shown in Fig. 8, with one end of shaft A clamped and the free end of shaft B loaded with a moment T . Drawing free-body diagrams for the two shafts separately, we see the force F transmitted at the gear periphery is just that which keeps shaft B in rotational equilibrium:

$$F \cdot r_B = T$$

This same force acts on the periphery of gear A , so the torque T_A experienced by shaft A is

$$T_A = F \cdot r_A = T \cdot \frac{r_A}{r_B}$$

Torsional Stresses and Displacements

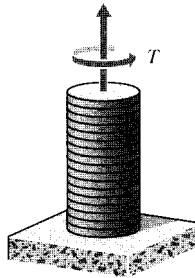


Figure 9: Poker-chip visualization of torsional deformation.

The stresses and deformations induced in a circular shaft by a twisting moment can be found by what is sometimes called the *direct method* of stress analysis. Here an expression of

the geometrical form of displacement in the structure is proposed, after which the kinematic, constitutive, and equilibrium equations are applied sequentially to develop expressions for the strains and stresses. In the case of simple twisting of a circular shaft, the geometric statement is simply that the circular symmetry of the shaft is maintained, which implies in turn that plane cross sections remain plane, without warping. As depicted in Fig. 9, the deformation is like a stack of poker chips that rotate relative to one another while remaining flat. The sequence of direct analysis then takes the following form:

1. *Geometrical statement:* To quantify the geometry of deformation, consider an increment of length dz from the shaft as seen in Fig. 10, in which the top rotates relative to the bottom by an increment of angle $d\theta$. The relative tangential displacement of the top of a vertical line drawn at a distance r from the center is then:

$$\delta = r d\theta \quad (9)$$

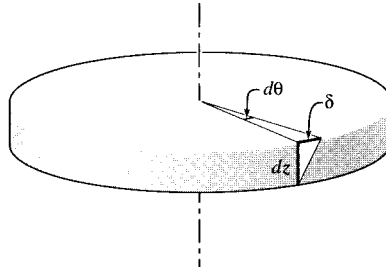


Figure 10: Incremental deformation in torsion.

2. *Kinematic or strain-displacement equation:* The geometry of deformation fits exactly our earlier description of shear strain, so we can write:

$$\gamma_{z\theta} = \frac{\delta}{dz} = r \frac{d\theta}{dz} \quad (10)$$

The subscript indicates a shearing of the z plane (the plane normal to the z axis) in the θ direction. As with the shear stresses, $\gamma_{z\theta} = \gamma_{\theta z}$, so the order of subscripts is arbitrary.

3. *Constitutive equation:* If the material is in its linear elastic regime, the shear stress is given directly from Hooke's Law as:

$$\tau_{\theta z} = G\gamma_{\theta z} = Gr \frac{d\theta}{dz} \quad (11)$$

The sign convention here is that positive twisting moments (moment vector along the $+z$ axis) produce positive shear stresses and strains. However, it is probably easier simply to intuit in which direction the applied moment will tend to slip adjacent horizontal planes. Here the upper ($+z$) plane is clearly being twisted to the right relative to the lower ($-z$) plane, so the upper arrow points to the right. The other three arrows are then determined as well.

4. *Equilibrium equation:* In order to maintain rotational equilibrium, the sum of the moments contributed by the shear stress acting on each differential area dA on the cross section must balance the applied moment T as shown in Fig. 11:

$$T = \int_A \tau_{\theta z} r dA = \int_A Gr \frac{d\theta}{dz} r dA = G \frac{d\theta}{dz} \int_A r^2 dA$$

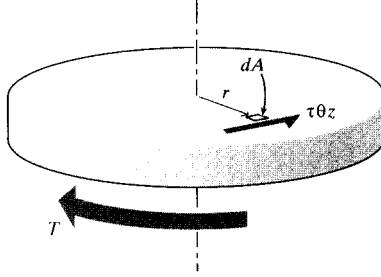


Figure 11: Torque balance.

The quantity $\int r^2 dA$ is the polar moment of inertia J , which for a hollow circular cross section is calculated as

$$J = \int_{R_i}^{R_o} r^2 2\pi r dr = \frac{\pi(R_o^4 - R_i^4)}{2} \quad (12)$$

where R_i and R_o are the inside and outside radii. For solid shafts, $R_i = 0$. The quantity $d\theta/dz$ can now be found as

$$\frac{d\theta}{dz} = \frac{T}{GJ} \rightarrow \theta = \int_z \frac{T}{JG} dz$$

Since in the simple twisting case under consideration the quantities T, J, G are constant along z , the angle of twist can be written as

$$\frac{d\theta}{dz} = \text{constant} = \frac{\theta}{L}$$

$$\boxed{\theta = \frac{TL}{GJ}} \quad (13)$$

This is analogous to the expression $\delta = PL/AE$ for the elongation of a uniaxial tensile specimen.

5. An explicit formula for the stress can be obtained by using this in Eqn. 11:

$$\tau_{\theta z} = Gr \frac{d\theta}{dz} = Gr \frac{\theta}{L} = \frac{Gr TL}{L GJ}$$

$$\boxed{\tau_{\theta z} = \frac{Tr}{J}} \quad (14)$$

Note that the material property G has canceled from this final expression for stress, so that the stresses are independent of the choice of material. Earlier, we have noted that stresses are independent of materials properties in certain pressure vessels and truss elements, and this was due to those structures being statically determinate. The shaft in torsion is not statically indeterminate, however; we had to use geometrical considerations and a statement of material linear elastic response as well as static equilibrium in obtaining the result. Since the material properties do not appear in the resulting equation for stress, it is easy to forget that the derivation depended on geometrical and material linearity. It is always important to keep in mind the assumptions used in derivations such as this, and be on guard against using the result in instances for which the assumptions are not justified.

For instance, we might twist a shaft until it breaks at a final torque of $T = T_f$, and then use Eqn. 14 to compute an apparent ultimate shear strength: $\tau_f = T_f r / J$. However, the material may very well have been stressed beyond its elastic limit in this test, and the assumption of material linearity may not have been valid at failure. The resulting value of τ_f obtained from the elastic analysis is therefore fictitious unless proven otherwise, and could be substantially different than the actual stress. The fictitious value might be used, however, to estimate failure torques in shafts of the same material but of different sizes, since the actual failure stress would scale with the fictitious stress in that case. The fictitious failure stress calculated using the elastic analysis is often called the *modulus of rupture in torsion*.

Eqn. 14 shows one reason why most drive shafts are hollow, since there isn't much point in using material at the center where the stresses are zero. Also, for a given quantity of material the designer will want to maximize the moment of inertia by placing the material as far from the center as possible. This is a powerful tool, since J varies as the fourth power of the radius.

Example 4

An automobile engine is delivering 100 hp (horsepower) at 1800 rpm (revolutions per minute) to the drive shaft, and we wish to compute the shearing stress. From Eqn. 8, the torque on the shaft is

$$T = \frac{W}{\omega} = \frac{100 \text{ hp} \left(\frac{1}{1.341 \times 10^{-3}} \right) \frac{\text{N}\cdot\text{m}}{\text{s}\cdot\text{hp}}}{1800 \frac{\text{rev}}{\text{min}} 2\pi \frac{\text{rad}}{\text{rev}} \left(\frac{1}{60} \right) \frac{\text{min}}{\text{s}}} = 396 \text{ N}\cdot\text{m}$$

The present drive shaft is a solid rod with a circular cross section and a diameter of $d = 10$ mm. Using Eqn. 14, the maximum stress occurs at the outer surface of the rod as is

$$\tau_{\theta z} = \frac{Tr}{J}, \quad r = d/2, \quad J = \pi(d/2)^4/2$$

$$\tau_{\theta z} = 252 \text{ MPa}$$

Now consider what the shear stress would be if the shaft were made annular rather than solid, keeping the amount of material the same. The outer-surface shear stress for an annular shaft with outer radius r_o and inner radius r_i is

$$\tau_{\theta z} = \frac{Tr_o}{J}, \quad J = \frac{\pi}{2} (r_o^4 - r_i^4)$$

To keep the amount of material in the annular shaft the same as in the solid one, the cross-sectional areas must be the same. Since the cross-sectional area of the solid shaft is $A_0 = \pi r^2$, the inner radius r_i of an annular shaft with outer radius r_o and area A_0 is found as

$$A_0 = \pi (r_o^2 - r_i^2) \rightarrow r_i = \sqrt{r_o^2 - (A_0/\pi)}$$

Evaluating these equations using the same torque and with $r_o = 30$ mm, we find $r_i = 28.2$ mm (a 1.8 mm wall thickness) and a stress of $\tau_{\theta z} = 44.5$ MPa. This is an 82% reduction in stress. The value of r in the elastic shear stress formula went up when we went to the annular rather than solid shaft, but this was more than offset by the increase in moment of inertia J , which varies as r^4 .

Example 5

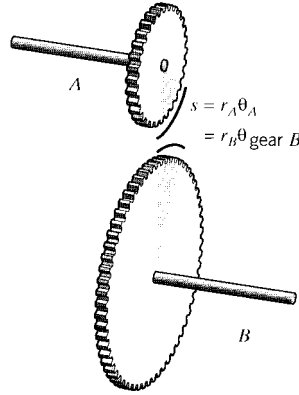


Figure 12: Rotations in the two-gear assembly.

Just as with trusses, the angular displacements in systems of torsion rods may be found from direct geometrical considerations. In the case of the two-rod geared system described earlier, the angle of twist of rod A is

$$\theta_A = \left(\frac{L}{GJ} \right)_A T_A = \left(\frac{L}{GJ} \right)_A T \cdot \frac{r_A}{r_B}$$

This rotation will be experienced by gear A as well, so a point on its periphery will sweep through an arc S of

$$S = \theta_A r_A = \left(\frac{L}{GJ} \right)_A T \cdot \frac{r_A}{r_B} \cdot r_A$$

Since gears A and B are connected at their peripheries, gear B will rotate through an angle of

$$\theta_{gear B} = \frac{S}{r_B} = \left(\frac{L}{GJ} \right)_A T \cdot \frac{r_A}{r_B} \cdot \frac{r_A}{r_B}$$

(See Fig. 11). Finally, the total angular displacement at the end of rod B is the rotation of gear B plus the twist of rod B itself:

$$\theta = \theta_{gear B} + \theta_{rod B} = \left(\frac{L}{GJ} \right)_A T \left(\frac{r_A}{r_B} \right)^2 + \left(\frac{L}{GJ} \right)_B T$$

Energy method for rotational displacement

The angular deformation may also be found using Castigliano's Theorem², and in some problems this approach may be easier. The strain energy per unit volume in a material subjected to elastic shearing stresses τ and strains γ arising from simple torsion is:

$$U^* = \int \tau d\gamma = \frac{1}{2}\tau\gamma = \frac{\tau^2}{2G} = \frac{1}{2G} \left(\frac{Tr}{J}\right)^2$$

This is then integrated over the specimen volume to obtain the total energy:

$$U = \int_V U^* dV = \int_L \int_A \frac{1}{2G} \left(\frac{Tr}{J}\right)^2 dA dz = \int_L \frac{T^2}{2GJ^2} \int_A r^2 dA dz$$

$$U = \int_L \frac{T^2}{2GJ} dz$$

(15)

If T , G , and J are constant along the length z , this becomes simply

$$U = \frac{T^2 L}{2GJ}$$
(16)

which is analogous to the expression $U = P^2 L / 2AE$ for tensile specimens.

In torsion, the angle θ is the generalized displacement congruent to the applied moment T , so Castigliano's theorem is applied for a single torsion rod as

$$\theta = \frac{\partial U}{\partial T} = \frac{TL}{GJ}$$

as before.

Example 6

Consider the two shafts geared together discussed earlier (Fig. 11). The energy method requires no geometrical reasoning, and follows immediately once the torques transmitted by the two shafts is known. Since the torques are constant along the lengths, we can write

$$U = \sum_i \left(\frac{T^2 L}{2GJ}\right)_i = \left(\frac{L}{2GJ}\right)_A \left(T \frac{r_A}{r_B}\right)^2 + \left(\frac{L}{2GJ}\right)_B T^2$$
$$\theta = \frac{\partial U}{\partial T} = \left(\frac{L}{GJ}\right)_A \left(T \cdot \frac{r_A}{r_B}\right) \left(\frac{r_A}{r_B}\right) + \left(\frac{L}{GJ}\right)_B T$$

Noncircular sections: the Prandtl membrane analogy

Shafts with noncircular sections are not uncommon. Although a circular shape is optimal from a stress analysis view, square or prismatic shafts may be easier to produce. Also, round shafts often have keyways or other geometrical features needed in order to join them to gears. All of this makes it necessary to be able to cope with noncircular sections. We will outline one means of doing this here, partly for its inherent usefulness and partly to introduce a type of

²Castigliano's Theorem is introduced in the Module 5, Trusses.

experimental stress analysis. Later modules will expand on these methods, and will present a more complete treatment of the underlying mathematical theory.

The lack of axial symmetry in noncircular sections renders the direct approach that led to Eqn. 14 invalid, and a thorough treatment must attack the differential governing equations of the problem mathematically. These equations will be discussed in later modules, but suffice it to say that they can be difficult to solve in closed form for arbitrarily shaped cross sections. The advent of finite element and other computer methods to solve these equations numerically has removed this difficulty to some degree, but one important limitation of numerical solutions is that they usually fail to provide intuitive insight as to why the stress distributions are the way they are: they fail to provide hints as to how the stresses might be modified favorably by design changes, and this intuition is one of the designer’s most important tools.

In an elegant insight, Prandtl³ pointed out that the stress distribution in torsion can be described by a “Poisson” differential equation, identical in form to that describing the deflection of a flexible membrane supported and pressurized from below⁴. This provides the basis of the *Prandtl membrane analogy*, which was used for many years to provide a form of experimental stress analysis for noncircular shafts in torsion. Although this experimental use has been supplanted by the more convenient computer methods, the analogy provides a visualization of torsionally induced stresses that can provide the sort of design insight we seek.

The analogy works such that the shear stresses in a torsionally loaded shaft of arbitrary cross section are proportional to the *slope* of a suitably inflated flexible membrane. The membrane is clamped so that its edges follow a shape similar to that of the noncircular section, and then displaced by air pressure. Visualize a horizontal sheet of metal with a circular hole in it, a sheet of rubber placed below the hole, and the rubber now made to bulge upward by pressure acting from beneath the plate (see Fig. 13). The bulge will be steepest at the edges and horizontal at its center; i.e. its slope will be zero at the center and largest at the edges, just as the stresses in a twisted circular shaft.

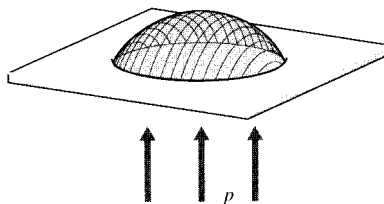


Figure 13: Membrane inflated through a circular hole.

It is not difficult to visualize that if the hole were square as in Fig. 14 rather than round, the membrane would be forced to lie flat (have zero slope) in the corners, and would have the steepest slopes at the midpoints of the outside edges. This is just what the stresses do. One good reason for not using square sections for torsion rods, then, is that the corners carry no stress and are therefore wasted material. The designer could remove them without consequence, the decision just being whether the cost of making circular rather than square shafts is more or less than the cost of the wasted material. To generalize the lesson in stress analysis, a *protruding* angle is not dangerous in terms of stress, only wasteful of material.

But conversely, an *entrant* angle can be extremely dangerous. A sharp notch cut into the

³Ludwig Prandtl (1875–1953) is best known for his pioneering work in aerodynamics.

⁴J.P. Den Hartog, *Advanced Strength of Materials*, McGraw-Hill, New York, 1952

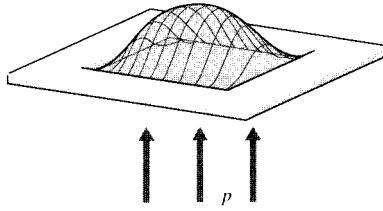
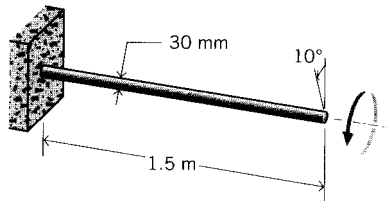


Figure 14: Membrane inflated through a square hole.

shaft is like a knife edge cutting into the rubber membrane, causing the rubber to be almost vertical. Such notches or keyways are notorious stress risers, very often acting as the origination sites for fatigue cracks. They may be necessary in some cases, but the designer must be painfully aware of their consequences.

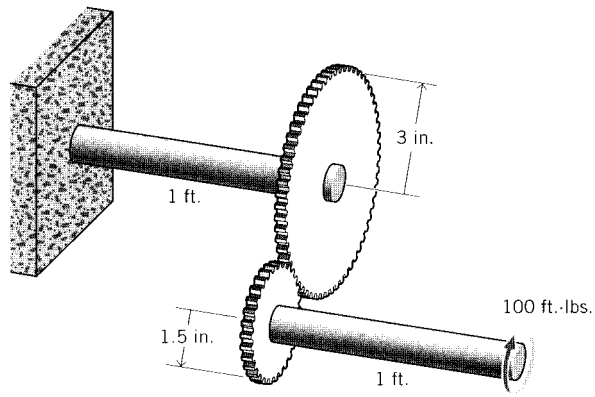
Problems

1. A torsion bar 1.5 m in length and 30 mm in diameter is clamped at one end, and the free end is twisted through an angle of 10° . Find the maximum torsional shear stress induced in the bar.

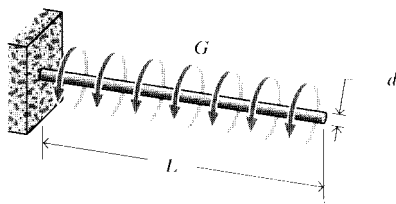


Prob. 1

2. The torsion bar of Prob. 1 fails when the applied torque is 1500 N-m. What is the modulus of rupture in torsion? Is this the same as the material's maximum shear stress?
3. A solid steel drive shaft is to be capable of transmitting 50 hp at 500 rpm. What should its diameter be if the maximum torsional shear stress is to be kept less than half the tensile yield strength?
4. How much power could the shaft of Prob. 3 transmit (at the same maximum torsional shear stress) if the same quantity of material were used in an annular rather than a solid shaft? Take the inside diameter to be half the outside diameter.
5. Two shafts, each 1 ft long and 1 in diameter, are connected by a 2:1 gearing, and the free end is loaded with a 100 ft-lb torque. Find the angle of twist at the loaded end.
6. A shaft of length L , diameter d , and shear modulus G is loaded with a uniformly distributed twisting moment of T_0 (N-m/m). (The twisting moment $T(x)$ at a distance x from the free end is therefore T_0x .) Find the angle of twist at the free end.
7. A composite shaft 3 ft in length is constructed by assembling an aluminum rod, 2 in diameter, over which is bonded an annular steel cylinder of 0.5 in wall thickness. Determine



Prob. 5



Prob. 6

the maximum torsional shear stress when the composite cylinder is subjected to a torque of 10,000 in-lb.

8. Sketch the shape of a membrane inflated through a round section containing an entrant keyway shape.

The Kinematic Equations

David Roylance
Department of Materials Science and Engineering
Massachusetts Institute of Technology
Cambridge, MA 02139

September 19, 2000

Introduction

The *kinematic* or *strain-displacement* equations describe how the strains – the stretching and distortion – within a loaded body relate to the body’s displacements. The displacement components in the x , y , and z directions are denoted by the vector $\mathbf{u} \equiv u_i \equiv (u, v, w)$, and are functions of position within the body: $\mathbf{u} = \mathbf{u}(x, y, z)$. If all points within the material experience the same displacement ($\mathbf{u} = \text{constant}$), the structure moves as a rigid body, but does not stretch or deform internally. For stretching to occur, points within the body must experience *different* displacements.

Infinitesimal strain

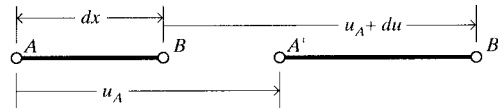


Figure 1: Incremental deformation.

Consider two points A and B separated initially by a small distance dx as shown in Fig. 1, and experiencing motion in the x direction. If the displacement at point A is u_A , the displacement at B can be expressed by a Taylor’s series expansion of $u(x)$ around the point $x = A$:

$$u_B = u_A + du = u_A + \frac{\partial u}{\partial x} dx$$

where here the expansion has been truncated after the second term. The *differential* motion δ between the two points is then

$$\delta = u_B - u_A = \left(u_A + \frac{\partial u}{\partial x} dx \right) - u_A = \frac{\partial u}{\partial x} dx$$

In our concept of stretching as being the differential displacement per unit length, the x component of strain is then

$$\boxed{\epsilon_x = \frac{\delta}{dx} = \frac{\partial u}{\partial x}} \quad (1)$$

Hence the strain is a *displacement gradient*. Applying similar reasoning to differential motion in the y direction, the y -component of strain is the gradient of the vertical displacement v with respect to y :

$$\boxed{\epsilon_y = \frac{\partial v}{\partial y}} \quad (2)$$

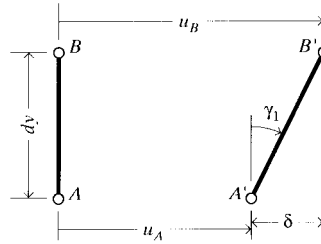


Figure 2: Shearing distortion.

The distortion of the material, which can be described as the change in originally right angles, is the sum of the tilts imparted to vertical and horizontal lines. As shown in Fig. 2, the tilt of an originally vertical line is the relative horizontal displacement of two nearby points along the line:

$$\delta = u_B - u_A = \left(u_A + \frac{\partial u}{\partial y} dy \right) - u_A = \frac{\partial u}{\partial y} dy$$

The change in angle is then

$$\gamma_1 \approx \tan \gamma_1 = \frac{\delta}{dy} = \frac{\partial u}{\partial y}$$

Similarly (see Fig. 3), the tilt γ_2 of an originally horizontal line is the gradient of v with respect to x . The shear strain in the xy plane is then

$$\boxed{\gamma_{xy} = \gamma_1 + \gamma_2 = \frac{\partial v}{\partial x} + \frac{\partial u}{\partial y}} \quad (3)$$

This notation, using ϵ for normal strain and γ for shearing strain, is sometimes known as the “classical” description of strain.

Matrix Formulation

The “indicial notation” described in the Module on Matrix and Index Notation provides a concise method of writing out all the components of three-dimensional states of strain:

$$\boxed{\epsilon_{ij} = \frac{1}{2} \left(\frac{\partial u_i}{\partial x_j} + \frac{\partial u_j}{\partial x_i} \right) \equiv \frac{1}{2} (u_{i,j} + u_{j,i})} \quad (4)$$

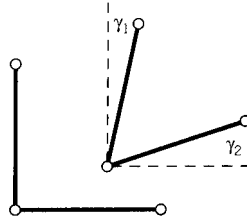


Figure 3: Shearing strain.

where the comma denotes differentiation with respect to the following spatial variable. This double-subscript index notation leads naturally to a matrix arrangement of the strain components, in which the i - j component of the strain becomes the matrix element in the i^{th} row and the j^{th} column:

$$\epsilon_{ij} = \begin{bmatrix} \frac{\partial u}{\partial x} & \frac{1}{2} \left(\frac{\partial u}{\partial y} + \frac{\partial v}{\partial x} \right) & \frac{1}{2} \left(\frac{\partial u}{\partial z} + \frac{\partial w}{\partial x} \right) \\ \frac{1}{2} \left(\frac{\partial u}{\partial y} + \frac{\partial v}{\partial x} \right) & \frac{\partial v}{\partial y} & \frac{1}{2} \left(\frac{\partial v}{\partial z} + \frac{\partial w}{\partial y} \right) \\ \frac{1}{2} \left(\frac{\partial u}{\partial z} + \frac{\partial w}{\partial x} \right) & \frac{1}{2} \left(\frac{\partial v}{\partial z} + \frac{\partial w}{\partial y} \right) & \frac{\partial w}{\partial z} \end{bmatrix} \quad (5)$$

Note that the strain matrix is symmetric, i.e. $\epsilon_{ij} = \epsilon_{ji}$. This symmetry means that there are six rather than nine independent strains, as might be expected in a 3×3 matrix. Also note that the indicial description of strain yields the same result for the normal components as in the classical description: $\epsilon_{11} = \epsilon_x$. However, the indicial components of shear strain are half their classical counterparts: $\epsilon_{12} = \gamma_{xy}/2$.

In still another useful notational scheme, the classical strain-displacement equations can be written out in a vertical list, similar to a vector:

$$\begin{Bmatrix} \epsilon_x \\ \epsilon_y \\ \epsilon_z \\ \gamma_{yz} \\ \gamma_{xz} \\ \gamma_{xy} \end{Bmatrix} = \begin{Bmatrix} \partial u / \partial x \\ \partial v / \partial y \\ \partial w / \partial z \\ \partial v / \partial z + \partial w / \partial y \\ \partial u / \partial z + \partial w / \partial x \\ \partial u / \partial y + \partial v / \partial x \end{Bmatrix}$$

This vector-like arrangement of the strain components is for convenience only, and is sometimes called a *pseudovector*. Strain is actually a *second-rank tensor*, like stress or moment of inertia, and has mathematical properties very different than those of vectors. The ordering of the elements in the pseudovector form is arbitrary, but it is conventional to list them as we have here by moving down the diagonal of the strain matrix of Eqn. 5 from upper left to lower right, then move up the third column, and finally move one column to the left on the first row; this gives the ordering 1,1; 2,2; 3,3; 2,3; 1,3; 1,2.

Following the rules of matrix multiplication, the strain pseudovector can also be written in

terms of the displacement vector as

$$\begin{pmatrix} \epsilon_x \\ \epsilon_y \\ \epsilon_z \\ \gamma_{yz} \\ \gamma_{xz} \\ \gamma_{xy} \end{pmatrix} = \begin{bmatrix} \partial/\partial x & 0 & 0 \\ 0 & \partial/\partial y & 0 \\ 0 & 0 & \partial/\partial z \\ 0 & \partial/\partial z & \partial/\partial y \\ \partial/\partial z & 0 & \partial/\partial x \\ \partial/\partial y & \partial/\partial x & 0 \end{bmatrix} \begin{pmatrix} u \\ v \\ w \end{pmatrix} \quad (6)$$

The matrix in brackets above, whose elements are differential operators, can be abbreviated as **L**:

$$\mathbf{L} = \begin{bmatrix} \partial/\partial x & 0 & 0 \\ 0 & \partial/\partial y & 0 \\ 0 & 0 & \partial/\partial z \\ 0 & \partial/\partial z & \partial/\partial y \\ \partial/\partial z & 0 & \partial/\partial x \\ \partial/\partial y & \partial/\partial x & 0 \end{bmatrix} \quad (7)$$

The strain-displacement equations can then be written in the concise ‘‘pseudovector-matrix’’ form:

$$\boxed{\boldsymbol{\epsilon} = \mathbf{L}\mathbf{u}} \quad (8)$$

Equations such as this must be used in a well-defined context, as they apply only when the somewhat arbitrary pseudovector listing of the strain components is used.

Volumetric strain

Since the normal strain is just the change in length per unit of original length, the new length L' after straining is found as

$$\epsilon = \frac{L' - L_0}{L_0} \Rightarrow L' = (1 + \epsilon)L_0 \quad (9)$$

If a cubical volume element, originally of dimension abc , is subjected to normal strains in all three directions, the change in the element’s volume is

$$\begin{aligned} \frac{\Delta V}{V} &= \frac{a'b'c' - abc}{abc} = \frac{a(1 + \epsilon_x)b(1 + \epsilon_y)c(1 + \epsilon_z) - abc}{abc} \\ &= (1 + \epsilon_x)(1 + \epsilon_y)(1 + \epsilon_z) - 1 \approx \epsilon_x + \epsilon_y + \epsilon_z \end{aligned} \quad (10)$$

where products of strains are neglected in comparison with individual values. The volumetric strain is therefore the sum of the normal strains, i.e. the sum of the diagonal elements in the strain matrix (this is also called the *trace* of the matrix, or $\text{Tr}[\boldsymbol{\epsilon}]$). In index notation, this can be written simply

$$\frac{\Delta V}{V} = \epsilon_{kk}$$

This is known as the volumetric, or ‘‘dilatational’’ component of the strain.

Example 1

To illustrate how volumetric strain is calculated, consider a thin sheet of steel subjected to strains in its plane given by $\epsilon_x = 3$, $\epsilon_y = -4$, and $\gamma_{xy} = 6$ (all in $\mu\text{in}/\text{in}$). The sheet is not in plane strain, since it can undergo a Poisson strain in the z direction given by $\epsilon_z = -\nu(\epsilon_x + \epsilon_y) = -0.3(3 - 4) = 0.3$. The total state of strain can therefore be written as the matrix

$$[\epsilon] = \begin{bmatrix} 3 & 6 & 0 \\ 6 & -4 & 0 \\ 0 & 0 & 0.3 \end{bmatrix} \times 10^{-6}$$

where the brackets on the $[\epsilon]$ symbol emphasize that the matrix rather than pseudovector form of the strain is being used. The volumetric strain is:

$$\frac{\Delta V}{V} = (3 - 4 + 0.3) \times 10^{-6} = -0.7 \times 10^{-6}$$

Engineers often refer to “microinches” of strain; they really mean microinches per inch. In the case of volumetric strain, the corresponding (but awkward) unit would be micro-cubic-inches per cubic inch.

Finite strain

The infinitesimal strain-displacement relations given by Eqns. 3.1–3.3 are used in the vast majority of mechanical analyses, but they do not describe stretching accurately when the displacement gradients become large. This often occurs when polymers (especially elastomers) are being considered. Large strains also occur during deformation processing operations, such as stamping of steel automotive body panels. The kinematics of large displacement or strain can be complicated and subtle, but the following section will outline a simple description of *Lagrangian* finite strain to illustrate some of the concepts involved.

Consider two orthogonal lines OB and OA as shown in Fig. 4, originally of length dx and dy , along the x - y axes, where for convenience we set $dx = dy = 1$. After strain, the endpoints of these lines move to new positions $A_1O_1B_1$ as shown. We will describe these new positions using the coordinate scheme of the original x - y axes, although we could also allow the new positions to define a new set of axes. In following the motion of the lines with respect to the original positions, we are using the so-called *Lagrangian* viewpoint. We could alternately have used the final positions as our reference; this is the *Eulerian* view often used in fluid mechanics.

After straining, the distance dx becomes

$$(dx)' = \left(1 + \frac{\partial u}{\partial x}\right) dx$$

Using our earlier “small” thinking, the x -direction strain would be just $\partial u/\partial x$. But when the strains become larger, we must also consider that the upward motion of point B_1 relative to O_1 , that is $\partial v/\partial x$, also helps stretch the line OB . Considering both these effects, the Pythagorean theorem gives the new length O_1B_1 as

$$O_1B_1 = \sqrt{\left(1 + \frac{\partial u}{\partial x}\right)^2 + \left(\frac{\partial v}{\partial x}\right)^2}$$

We now define our Lagrangian strain as

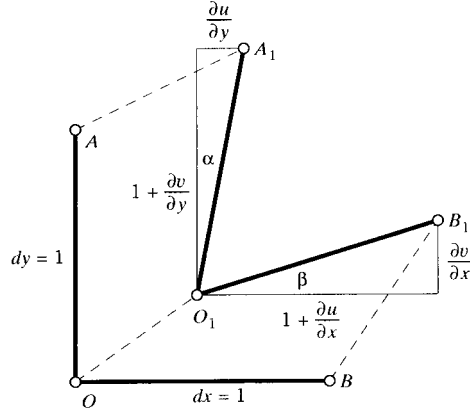


Figure 4: Finite displacements.

$$\begin{aligned}\epsilon_x &= \frac{O_1B_1 - OB}{OB} = O_1B_1 - 1 \\ &= \sqrt{1 + 2\frac{\partial u}{\partial x} + \left(\frac{\partial u}{\partial x}\right)^2 + \left(\frac{\partial v}{\partial x}\right)^2} - 1\end{aligned}$$

Using the series expansion $\sqrt{1+x} = 1 + x/2 + x^2/8 + \dots$ and neglecting terms beyond first order, this becomes

$$\begin{aligned}\epsilon_x &\approx \left\{ 1 + \frac{1}{2} \left[2\frac{\partial u}{\partial x} + \left(\frac{\partial u}{\partial x}\right)^2 + \left(\frac{\partial v}{\partial x}\right)^2 \right] \right\} - 1 \\ &= \frac{\partial u}{\partial x} + \frac{1}{2} \left[\left(\frac{\partial u}{\partial x}\right)^2 + \left(\frac{\partial v}{\partial x}\right)^2 \right]\end{aligned}\quad (11)$$

Similarly, we can show

$$\epsilon_y = \frac{\partial v}{\partial y} + \frac{1}{2} \left[\left(\frac{\partial v}{\partial y}\right)^2 + \left(\frac{\partial u}{\partial y}\right)^2 \right]\quad (12)$$

$$\gamma_{xy} = \frac{\partial u}{\partial y} + \frac{\partial v}{\partial x} + \frac{\partial u}{\partial y} \frac{\partial u}{\partial x} + \frac{\partial v}{\partial y} \frac{\partial v}{\partial x}\quad (13)$$

When the strains are sufficiently small that the quadratic terms are negligible compared with the linear ones, these reduce to the infinitesimal-strain expressions shown earlier.

Example 2

The displacement function $u(x)$ for a tensile specimen of uniform cross section and length L , fixed at one end and subjected to a displacement δ at the other, is just the linear relation

$$u(x) = \left(\frac{x}{L}\right) \delta$$

The Lagrangian strain is then given by Eqn. 11 as

$$\epsilon_x = \frac{\delta}{L} + \frac{1}{2} \left(\frac{\delta}{L} \right)^2$$

The first term is the familiar small-strain expression, with the second nonlinear term becoming more important as δ becomes larger. When $\delta = L$, i.e. the conventional strain is 100%, there is a 50% difference between the conventional and Lagrangian strain measures.

The Lagrangian strain components can be generalized using index notation as

$$\epsilon_{ij} = \frac{1}{2}(u_{i,j} + u_{j,i} + u_{r,i} u_{r,j}).$$

A pseudovector form is also convenient occasionally:

$$\begin{aligned} \begin{Bmatrix} \epsilon_x \\ \epsilon_y \\ \gamma_{xy} \end{Bmatrix} &= \begin{Bmatrix} u_{,x} \\ v_{,y} \\ u_{,y} + v_{,x} \end{Bmatrix} + \frac{1}{2} \begin{bmatrix} u_{,x} & v_{,x} & 0 & 0 \\ 0 & 0 & u_{,y} & v_{,y} \\ u_{,y} & v_{,y} & u_{,x} & v_{,x} \end{bmatrix} \begin{Bmatrix} u_{,x} \\ v_{,x} \\ u_{,y} \\ v_{,y} \end{Bmatrix} \\ &= \left(\begin{bmatrix} \partial/\partial x & 0 \\ 0 & \partial/\partial y \\ \partial/\partial y & \partial/\partial x \end{bmatrix} + \frac{1}{2} \begin{bmatrix} u_{,x} & v_{,x} & 0 & 0 \\ 0 & 0 & u_{,y} & v_{,y} \\ u_{,y} & v_{,y} & u_{,x} & v_{,x} \end{bmatrix} \begin{bmatrix} \partial/\partial x & 0 \\ 0 & \partial/\partial x \\ \partial/\partial y & 0 \\ 0 & \partial/\partial y \end{bmatrix} \right) \begin{Bmatrix} u \\ v \end{Bmatrix} \end{aligned}$$

which can be abbreviated

$$\boldsymbol{\epsilon} = [\mathbf{L} + \mathbf{A}(\mathbf{u})] \mathbf{u} \quad (14)$$

The matrix $\mathbf{A}(\mathbf{u})$ contains the nonlinear effect of large strain, and becomes negligible when strains are small.

Problems

1. Write out the abbreviated strain-displacement equation $\boldsymbol{\epsilon} = \mathbf{L}\mathbf{u}$ (Eqn. 8) for two dimensions.
2. Write out the components of the Lagrangian strain tensor in three dimensions:

$$\epsilon_{ij} = \frac{1}{2}(u_{i,j} + u_{j,i} + u_{r,i} u_{r,j})$$

3. Show that for small strains the fractional volume change is the trace of the infinitesimal strain tensor:

$$\frac{\Delta V}{V} \equiv \epsilon_{kk} = \epsilon_x + \epsilon_y + \epsilon_z$$

4. When the material is incompressible, show the extension ratios are related by

$$\lambda_x \lambda_y \lambda_z = 1$$

5. Show that the kinematic (strain-displacement) relations in for polar coordinates can be written

$$\epsilon_r = \frac{\partial u_r}{\partial r}$$

$$\epsilon_\theta = \frac{1}{r} \frac{\partial u_\theta}{\partial \theta} + \frac{u_r}{r}$$

$$\gamma_{r\theta} = \frac{1}{r} \frac{\partial u_r}{\partial \theta} + \frac{\partial u_\theta}{\partial r} - \frac{u_\theta}{r}$$

The Equilibrium Equations

David Roylance
Department of Materials Science and Engineering
Massachusetts Institute of Technology
Cambridge, MA 02139

September 26, 2000

Introduction

The kinematic relations described in Module 8 are purely geometric, and do not involve considerations of material behavior. The equilibrium relations to be discussed in this module have this same independence from the material. They are simply Newton's law of motion, stating that in the absence of acceleration all of the forces acting on a body (or a piece of it) must balance. This allows us to state how the stress within a body, but evaluated just below the surface, is related to the external force applied to the surface. It also governs how the stress varies from position to position within the body.

Cauchy stress

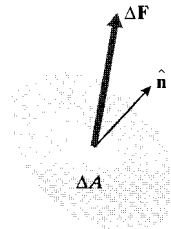


Figure 1: Traction vector.

In earlier modules, we expressed the normal stress as force per unit area acting perpendicularly to a selected area, and a shear stress was a force per unit area acting transversely to the area. To generalize this concept, consider the situation depicted in Fig. 1, in which a *traction vector* \mathbf{T} acts on an arbitrary plane within or on the external boundary of the body, and at an arbitrary direction with respect to the orientation of the plane. The traction is a simple force vector having magnitude and direction, but its magnitude is expressed in terms of force per unit of area:

$$\mathbf{T} = \lim_{\Delta A \rightarrow 0} \left(\frac{\Delta \mathbf{F}}{\Delta A} \right) \quad (1)$$

where ΔA is the magnitude of the area on which $\Delta \mathbf{F}$ acts. The *Cauchy*¹ stresses, which are a generalization of our earlier definitions of stress, are the forces per unit area acting on the Cartesian x , y , and z planes to balance the traction. In two dimensions this balance can be written by drawing a simple free body diagram with the traction vector acting on an area of arbitrary size A (Fig. 2), remembering to obtain the forces by multiplying by the appropriate area.

$$\sigma_x(A \cos \theta) + \tau_{xy}(A \sin \theta) = T_x A$$

$$\tau_{xy}(A \cos \theta) + \sigma_y(A \sin \theta) = T_y A$$

Canceling the factor A , this can be written in matrix form as

$$\begin{bmatrix} \sigma_x & \tau_{xy} \\ \tau_{xy} & \sigma_y \end{bmatrix} \begin{Bmatrix} \cos \theta \\ \sin \theta \end{Bmatrix} = \begin{Bmatrix} T_x \\ T_y \end{Bmatrix} \quad (2)$$

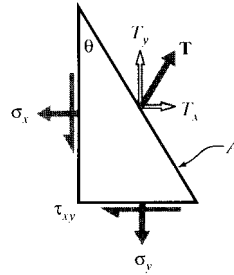


Figure 2: Cauchy stress.

Example 1

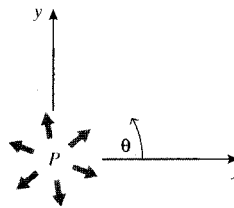


Figure 3: Constant pressure on internal circular boundary.

Consider a circular cavity containing an internal pressure p . The components of the traction vector are then $T_x = -p \cos \theta$, $T_y = -p \sin \theta$. The Cartesian Cauchy stresses in the material at the boundary must then satisfy the relations

$$\sigma_x \cos \theta + \tau_{xy} \sin \theta = -p \cos \theta$$

¹Baron Augustin-Louis Cauchy (1789–1857) was a prolific French engineer and mathematician.

$$\tau_{xy} \cos \theta + \sigma_y \sin \theta = -p \sin \theta$$

At $\theta = 0$, $\sigma_x = -p, \sigma_y = \tau_{xy} = 0$; at $\theta = \pi/2$, $\sigma_y = -p, \sigma_x = \tau_{xy} = 0$. The shear stress τ_{xy} vanishes for $\theta = 0$ or $\pi/2$; in Module 10 it will be seen that the normal stresses σ_x and σ_y are therefore *principal* stresses at those points.

The vector $(\cos \theta, \sin \theta)$ on the left hand side of Eqn. 2 is also the vector $\hat{\mathbf{n}}$ of direction cosines of the normal to the plane on which the traction acts, and serves to define the orientation of this plane. This matrix equation, which is sometimes called *Cauchy's relation*, can be abbreviated as

$$\boxed{[\boldsymbol{\sigma}] \hat{\mathbf{n}} = \mathbf{T}} \quad (3)$$

The brackets here serve as a reminder that the stress is being written as the square matrix of Eqn. 2 rather than in pseudovector form. This relation serves to define the stress concept as an entity that relates the traction (a vector) acting on an arbitrary surface to the orientation of the surface (another vector). The stress is therefore of a higher degree of abstraction than a vector, and is technically a *second-rank tensor*. The difference between vectors (first-rank tensors) and second-rank tensors shows up in how they *transform* with respect to coordinate rotations, which is treated in Module 10. As illustrated by the previous example, Cauchy's relation serves both to define the stress and to compute its magnitude at boundaries where the tractions are known.

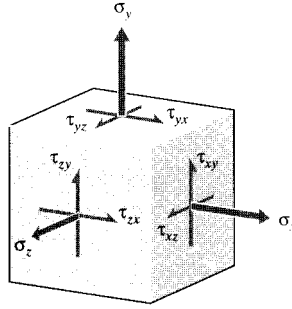


Figure 4: Cartesian Cauchy stress components in three dimensions.

In three dimensions, the matrix form of the stress state shown in Fig. 4 is the symmetric 3×3 array obtained by an obvious extension of the one in Eqn. 2:

$$\boxed{[\boldsymbol{\sigma}] = \sigma_{ij} = \begin{bmatrix} \sigma_x & \tau_{xy} & \tau_{xz} \\ \tau_{xy} & \sigma_y & \tau_{yz} \\ \tau_{xz} & \tau_{yz} & \sigma_z \end{bmatrix}} \quad (4)$$

The element in the i^{th} row and the j^{th} column of this matrix is the stress on the i^{th} face in the j^{th} direction. Moment equilibrium requires that the stress matrix be symmetric, so the order of subscripts of the off-diagonal shearing stresses is immaterial.

Differential governing equations

Determining the variation of the stress components as functions of position within the interior of a body is obviously a principal goal in stress analysis. This is a type of *boundary value problem* often encountered in the theory of differential equations, in which the *gradients* of the variables, rather than the explicit variables themselves, are specified. In the case of stress, the gradients are governed by conditions of static equilibrium: the stresses cannot change arbitrarily between two points A and B , or the material between those two points may not be in equilibrium.

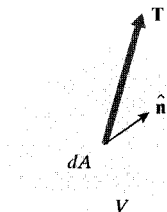


Figure 5: Traction vector \mathbf{T} acting on differential area dA with direction cosines $\hat{\mathbf{n}}$.

To develop this idea formally, we require that the integrated value of the surface traction \mathbf{T} over the surface A of an arbitrary volume element dV within the material (see Fig. 5) must sum to zero in order to maintain static equilibrium :

$$0 = \int_A \mathbf{T} dA = \int_A [\boldsymbol{\sigma}] \hat{\mathbf{n}} dA$$

Here we assume the lack of gravitational, centripetal, or other “body” forces acting on material within the volume. The surface integral in this relation can be converted to a volume integral by Gauss’ divergence theorem²:

$$\int_V \nabla [\boldsymbol{\sigma}] dV = 0$$

Since the volume V is arbitrary, this requires that the integrand be zero:

$$\nabla [\boldsymbol{\sigma}] = 0 \tag{5}$$

For Cartesian problems in three dimensions, this expands to:

$$\boxed{\begin{aligned} \frac{\partial \sigma_x}{\partial x} + \frac{\partial \tau_{xy}}{\partial y} + \frac{\partial \tau_{xz}}{\partial z} &= 0 \\ \frac{\partial \tau_{xy}}{\partial x} + \frac{\partial \sigma_y}{\partial y} + \frac{\partial \tau_{yz}}{\partial z} &= 0 \\ \frac{\partial \tau_{xz}}{\partial x} + \frac{\partial \tau_{yz}}{\partial y} + \frac{\partial \sigma_z}{\partial z} &= 0 \end{aligned}} \tag{6}$$

Using index notation, these can be written:

$$\sigma_{ij,j} = 0 \tag{7}$$

²Gauss’ Theorem states that $\int_A X \hat{\mathbf{n}} dA = \int_V \nabla X dV$ where X is a scalar, vector, or tensor quantity.

Or in pseudovector-matrix form, we can write

$$\begin{bmatrix} \frac{\partial}{\partial x} & 0 & 0 & 0 & \frac{\partial}{\partial z} & \frac{\partial}{\partial y} \\ 0 & \frac{\partial}{\partial y} & 0 & \frac{\partial}{\partial z} & 0 & \frac{\partial}{\partial x} \\ 0 & 0 & \frac{\partial}{\partial z} & \frac{\partial}{\partial y} & \frac{\partial}{\partial x} & 0 \end{bmatrix} \begin{Bmatrix} \sigma_x \\ \sigma_y \\ \sigma_z \\ \tau_{yz} \\ \tau_{xz} \\ \tau_{xy} \end{Bmatrix} = \begin{Bmatrix} 0 \\ 0 \\ 0 \end{Bmatrix} \quad (8)$$

Noting that the differential operator matrix in the brackets is just the transform of the one that appeared in Eqn. 7 of Module 8, we can write this as:

$$\mathbf{L}^T \boldsymbol{\sigma} = \mathbf{0} \quad (9)$$

Example 2

It isn't hard to come up with functions of stress that satisfy the equilibrium equations; any constant will do, since the stress gradients will then be identically zero. The catch is that they must satisfy the boundary conditions as well, and this complicates things considerably. Later modules will outline several approaches to solving the equations directly, but in some simple cases a solution can be seen by inspection.

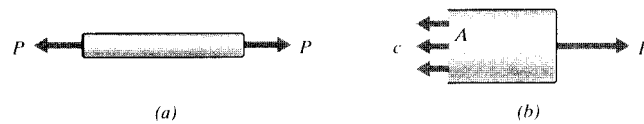


Figure 6: A tensile specimen.

Consider a tensile specimen subjected to a load P as shown in Fig. 6. A trial solution that certainly satisfies the equilibrium equations is

$$[\boldsymbol{\sigma}] = \begin{bmatrix} c & 0 & 0 \\ 0 & 0 & 0 \\ 0 & 0 & 0 \end{bmatrix}$$

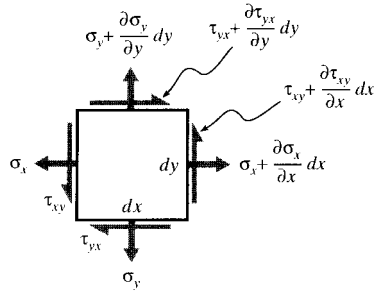
where c is a constant we must choose so as to satisfy the boundary conditions. To maintain horizontal equilibrium in the free-body diagram of Fig. 6(b), it is immediately obvious that $cA = P$, or $\sigma_x = c = P/A$. This familiar relation was used in Module 1 to define the stress, but we see here that it can be viewed as a consequence of equilibrium considerations rather than a basic definition.

Problems

1. Determine whether the following stress state satisfies equilibrium:

$$[\boldsymbol{\sigma}] = \begin{bmatrix} 2x^3y^2 & -2x^2y^3 \\ -2x^2y^3 & xy^4 \end{bmatrix}$$

2. Develop the two-dimensional form of the Cartesian equilibrium equations by drawing a free-body diagram of an infinitesimal section:



Prob. 2

3. Use the free body diagram of the previous problem to show that $\tau_{xy} = \tau_{yx}$.
4. Use a free-body diagram approach to show that in polar coordinates the equilibrium equations are

$$\frac{\partial \sigma_r}{\partial r} + \frac{1}{r} \frac{\partial \tau_{r\theta}}{\partial \theta} + \frac{\sigma_r - \sigma_\theta}{r} = 0$$

$$\frac{\partial \tau_{r\theta}}{\partial r} + \frac{1}{r} \frac{\partial \sigma_\theta}{\partial \theta} + 2 \frac{\tau_{r\theta}}{r} = 0$$

5. Develop the above equations for equilibrium in polar coordinates by transforming the Cartesian equations using

$$x = r \cos \theta$$

$$y = r \sin \theta$$

6. The *Airy stress function* $\phi(x, y)$ is defined such that the Cartesian Cauchy stresses are

$$\sigma_x = \frac{\partial^2 \phi}{\partial y^2}, \quad \sigma_y = \frac{\partial^2 \phi}{\partial x^2}, \quad \tau_{xy} = -\frac{\partial^2 \phi}{\partial x \partial y}$$

Show that the stresses obtained from this procedure satisfy the equilibrium equations.

Transformation of Stresses and Strains

David Roylance
Department of Materials Science and Engineering
Massachusetts Institute of Technology
Cambridge, MA 02139

May 14, 2001

Introduction

One of the most common problems in mechanics of materials involves *transformation of axes*. For instance, we may know the stresses acting on xy planes, but are really more interested in the stresses acting on planes oriented at, say, 30° to the x axis as seen in Fig. 1, perhaps because these are close-packed atomic planes on which sliding is prone to occur, or is the angle at which two pieces of lumber are glued together in a “scarf” joint. We seek a means to transform the stresses to these new $x'y'$ planes.

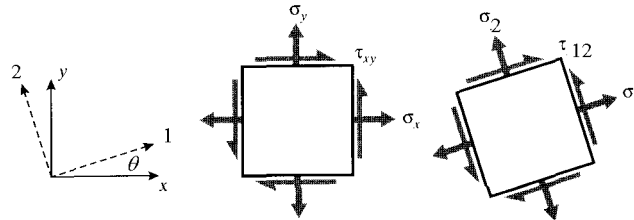


Figure 1: Rotation of axes in two dimensions.

These transformations are vital in analyses of stress and strain, both because they are needed to compute critical values of these entities and also because the tensorial nature of stress and strain is most clearly seen in their transformation properties. Other entities, such as moment of inertia and curvature, also transform in a manner similar to stress and strain. All of these are *second-rank tensors*, an important concept that will be outlined later in this module.

Direct approach

The rules for stress transformations can be developed directly from considerations of static equilibrium. For illustration, consider the case of uniaxial tension shown in Fig. 2 in which all stresses other than σ_y are zero. A free body diagram is then constructed in which the specimen is “cut” along the inclined plane on which the stresses, labeled $\sigma_{y'}$ and $\tau_{x'y'}$, are desired. The key here is to note that the area on which these transformed stresses act is different than the area normal to the y axis, so that both the areas and the forces acting on them need to be “transformed.” Balancing forces in the y' direction (the direction normal to the inclined plane):

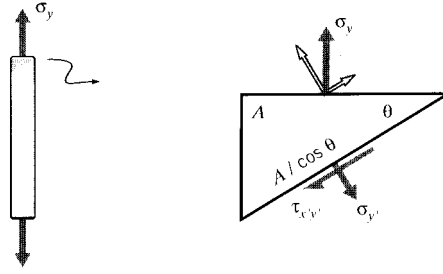


Figure 2: An inclined plane in a tensile specimen.

$$(\sigma_y A) \cos \theta = \sigma_{y'} \left(\frac{A}{\cos \theta} \right)$$

$$\sigma_{y'} = \sigma_y \cos^2 \theta \quad (1)$$

Similarly, a force balance in the tangential direction gives

$$\tau_{x'y'} = \sigma_y \sin \theta \cos \theta \quad (2)$$

Example 1

Consider a unidirectionally reinforced composite ply with strengths $\hat{\sigma}_1$ in the fiber direction, $\hat{\sigma}_2$ in the transverse direction, and $\hat{\tau}_{12}$ in shear. As the angle θ between the fiber direction and an applied tensile stress σ_y is increased, the stress in the fiber direction will decrease according to Eqn. 1. If the ply were to fail by fiber fracture alone, the stress $\sigma_{y,b}$ needed to cause failure would *increase* with misalignment according to $\sigma_{y,b} = \hat{\sigma}_1 / \cos^2 \theta$.

However, the shear stresses as given by Eqn. 2 *increase* with θ , so the σ_y stress needed for shear failure drops. The strength $\sigma_{y,b}$ is the smaller of the stresses needed to cause fiber-direction or shear failure, so the strength becomes limited by shear after only a few degrees of misalignment. In fact, a 15° off-axis tensile specimen has been proposed as a means of measuring intralaminar shear strength. When the orientation angle approaches 90°, failure is dominated by the transverse strength. The experimental data shown in Fig. 3 are for glass-epoxy composites¹, which show good but not exact agreement with these simple expressions.

A similar approach, but generalized to include stresses σ_x and τ_{xy} on the original xy planes as shown in Fig. 4 (see Prob. 2) gives:

$$\begin{cases} \sigma_{x'} &= \sigma_x \cos^2 \theta + \sigma_y \sin^2 \theta + 2\tau_{xy} \sin \theta \cos \theta \\ \sigma_{y'} &= \sigma_x \sin^2 \theta + \sigma_y \cos^2 \theta - 2\tau_{xy} \sin \theta \cos \theta \\ \tau_{x'y'} &= (\sigma_y - \sigma_x) \sin \theta \cos \theta + \tau_{xy}(\cos^2 \theta - \sin^2 \theta) \end{cases} \quad (3)$$

These relations can be written in pseudovector-matrix form as

$$\begin{Bmatrix} \sigma_{x'} \\ \sigma_{y'} \\ \tau_{x'y'} \end{Bmatrix} = \begin{bmatrix} c^2 & s^2 & 2sc \\ s^2 & c^2 & -2sc \\ -sc & sc & c^2 - s^2 \end{bmatrix} \begin{Bmatrix} \sigma_x \\ \sigma_y \\ \tau_{xy} \end{Bmatrix} \quad (4)$$

¹R.M. Jones, *Mechanics of Composite Materials*, McGraw-Hill, 1975.

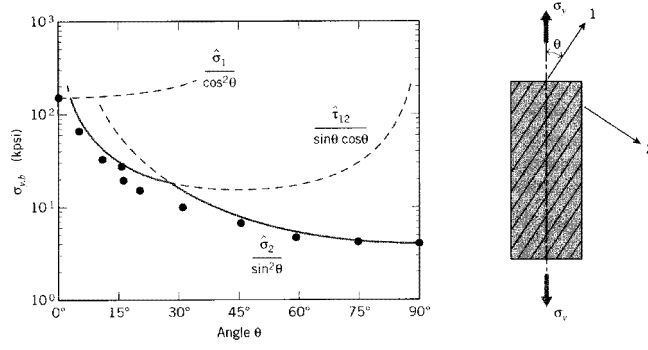


Figure 3: Stress applied at an angle to the fibers in a one-dimensional ply.

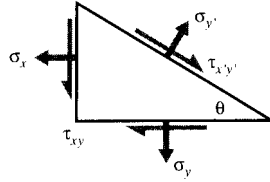


Figure 4: Stresses on inclined plane.

where $c = \cos \theta$ and $s = \sin \theta$. This can be abbreviated as

$$\boldsymbol{\sigma}' = \mathbf{A}\boldsymbol{\sigma} \quad (5)$$

where \mathbf{A} is the transformation matrix in brackets above. This expression would be valid for three dimensional as well as two dimensional stress states, although the particular form of \mathbf{A} given in Eqn. 4 is valid in two dimensions only (plane stress), and for Cartesian coordinates.

Using either mathematical or geometric arguments (see Probs. 3 and 4), it can be shown that the components of infinitesimal strain transform by *almost* the same relations:

$$\begin{Bmatrix} \epsilon_{x'} \\ \epsilon_{y'} \\ \frac{1}{2}\gamma_{x'y'} \end{Bmatrix} = \mathbf{A} \begin{Bmatrix} \epsilon_x \\ \epsilon_y \\ \frac{1}{2}\gamma_{xy} \end{Bmatrix} \quad (6)$$

The factor of 1/2 on the shear components arises from the classical definition of shear strain, which is twice the tensorial shear strain. This introduces some awkwardness into the transformation relations, some of which can be reduced by defining the *Reuter's matrix* as

$$[\mathbf{R}] = \begin{bmatrix} 1 & 0 & 0 \\ 0 & 1 & 0 \\ 0 & 0 & 2 \end{bmatrix} \quad \text{or} \quad [\mathbf{R}]^{-1} = \begin{bmatrix} 1 & 0 & 0 \\ 0 & 1 & 0 \\ 0 & 0 & \frac{1}{2} \end{bmatrix} \quad (7)$$

We can now write:

$$\begin{Bmatrix} \epsilon_{x'} \\ \epsilon_{y'} \\ \gamma_{x'y'} \end{Bmatrix} = \mathbf{R} \begin{Bmatrix} \epsilon_{x'} \\ \epsilon_{y'} \\ \frac{1}{2}\gamma_{x'y'} \end{Bmatrix} = \mathbf{R}\mathbf{A} \begin{Bmatrix} \epsilon_x \\ \epsilon_y \\ \frac{1}{2}\gamma_{xy} \end{Bmatrix} = \mathbf{R}\mathbf{A}\mathbf{R}^{-1} \begin{Bmatrix} \epsilon_x \\ \epsilon_y \\ \gamma_{xy} \end{Bmatrix}$$

Or

$$\boldsymbol{\epsilon}' = \mathbf{R}\mathbf{A}\mathbf{R}^{-1}\boldsymbol{\epsilon} \quad (8)$$

As can be verified by expanding this relation, the transformation equations for strain can also be obtained from the stress transformation equations (e.g. Eqn. 3) by replacing σ with ϵ and τ with $\gamma/2$:

$$\begin{array}{l} \epsilon_{x'} = \epsilon_x \cos^2 \theta + \epsilon_y \sin^2 \theta + \gamma_{xy} \sin \theta \cos \theta \\ \epsilon_{y'} = \epsilon_x \sin^2 \theta + \epsilon_y \cos^2 \theta - \gamma_{xy} \sin \theta \cos \theta \\ \gamma_{x'y'} = 2(\epsilon_y - \epsilon_x) \sin \theta \cos \theta + \gamma_{xy}(\cos^2 \theta - \sin^2 \theta) \end{array} \quad (9)$$

Example 2

Consider the biaxial strain state

$$\boldsymbol{\epsilon} = \begin{Bmatrix} \epsilon_{x'} \\ \epsilon_{y'} \\ \gamma_{x'y'} \end{Bmatrix} = \begin{Bmatrix} 0.01 \\ -0.01 \\ 0 \end{Bmatrix}$$

The state of strain $\boldsymbol{\epsilon}'$ referred to axes rotated by $\theta = 45^\circ$ from the x - y axes can be computed by matrix multiplication as:

$$\mathbf{A} = \begin{bmatrix} c^2 & s^2 & 2sc \\ s^2 & c^2 & -2sc \\ -sc & sc & c^2 - s^2 \end{bmatrix} = \begin{bmatrix} 0.5 & 0.5 & 1.0 \\ 0.5 & 0.5 & -1.0 \\ -0.5 & 0.5 & 0.0 \end{bmatrix}$$

Then

$$\begin{aligned} \boldsymbol{\epsilon}' &= \mathbf{R}\mathbf{A}\mathbf{R}^{-1}\boldsymbol{\epsilon} \\ &= \begin{bmatrix} 1.0 & 0.0 & 0.0 \\ 0.0 & 1.0 & 0.0 \\ 0.0 & 0.0 & 2.0 \end{bmatrix} \begin{bmatrix} 0.5 & 0.5 & 1.0 \\ 0.5 & 0.5 & -1.0 \\ -0.5 & 0.5 & 0.0 \end{bmatrix} \begin{bmatrix} 1.0 & 0.0 & 0.0 \\ 0.0 & 1.0 & 0.0 \\ 0.0 & 0.0 & 0.5 \end{bmatrix} = \begin{Bmatrix} 0.00 \\ 0.00 \\ -0.02 \end{Bmatrix} \end{aligned}$$

Obviously, the matrix multiplication method is tedious unless matrix-handling software is available, in which case it becomes very convenient.

Mohr's circle

Everyday experience with such commonplace occurrences as pushing objects at an angle gives us all a certain intuitive sense of how vector transformations work. Second-rank tensor transformations seem more abstract at first, and a device to help visualize them is of great value. As it happens, the transformation equations have a famous (among engineers) graphical interpretation known as *Mohr's circle*². The Mohr procedure is justified mathematically by using the trigonometric double-angle relations to show that Eqns. 3 have a circular representation (see Prob. 5), but it can probably best be learned simply by memorizing the following recipe³:

²Presented in 1900 by the German engineer Otto Mohr (1835–1918).

³An interactive web demonstration of Mohr's circle construction is available at <http://web.mit.edu/course/3/3.11/www/java/mohr.html>.

1. Draw the stress square, noting the values on the x and y faces; Fig. 5(a) shows a hypothetical case for illustration. *For the purpose of Mohr's circle only*, regard a shear stress acting in a clockwise-rotation sense as being positive, and counter-clockwise as negative. The shear stresses on the x and y faces must then have opposite signs. The normal stresses are positive in tension and negative in compression, as usual.

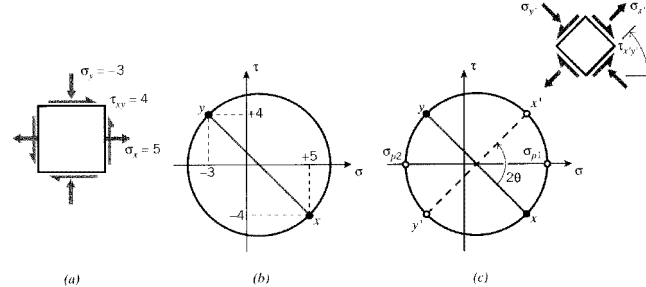


Figure 5: Stress square (a) and Mohr's circle (b) for $\sigma_x = +5$, $\sigma_y = -3$, $\tau_{xy} = +4$. (c) Stress state on inclined plane.

2. Construct a graph with τ as the ordinate (y axis) and σ as abscissa, and plot the stresses on the x and y faces of the stress square as two points on this graph. Since the shear stresses on these two faces are the negative of one another, one of these points will be above the σ -axis exactly as far as the other is below. It is helpful to label the two points as x and y .
3. Connect these two points with a straight line. It will cross the σ axis at the line's midpoint. This point will be at $(\sigma_x + \sigma_y)/2$, which in our illustration is $[5 + (-3)]/2 = 1$.
4. Place the point of a compass at the line's midpoint, and set the pencil at the end of the line. Draw a circle with the line as a diameter. The completed circle for our illustrative stress state is shown in Fig. 5(b).
5. To determine the stresses on a stress square that has been rotated through an angle θ with respect to the original square, rotate the diametral line *in the same direction* through *twice* this angle; i.e. 2θ . The new end points of the line can now be labeled x' and y' , and their σ - τ values are the stresses on the rotated x' - y' axes as shown in Fig. 5(c).

There is nothing mysterious or magical about the Mohr's circle; it is simply a device to help visualize how stresses and other second-rank tensors change when the axes are rotated.

It is clear in looking at the Mohr's circle in Fig. 5(c) that there is something special about axis rotations that cause the diametral line to become either horizontal or vertical. In the first case, the normal stresses assume maximal values and the shear stresses are zero. These normal stresses are known as the *principal* stresses, σ_{p1} and σ_{p2} , and the planes on which they act are the *principal* planes. If the material is prone to fail by tensile cracking, it will do so by cracking along the principal planes when the value of σ_{p1} exceeds the tensile strength.

Example 3

It is instructive to use a Mohr's circle construction to predict how a piece of blackboard chalk will break in torsion, and then verify it in practice. The torsion produces a state of pure shear as shown in Fig. 6,

which causes the principal planes to appear at $\pm 45^\circ$ to the chalk's long axis. The crack will appear transverse to the principal tensile stress, producing a spiral-like failure surface. (As the crack progresses into the chalk, the state of pure shear is replaced by a more complicated stress distribution, so the last part of the failure surface deviates from this ideal path to one running along the axial direction.) This is the same type of fracture that occurred all too often in skiers' femurs, before the advent of modern safety bindings.

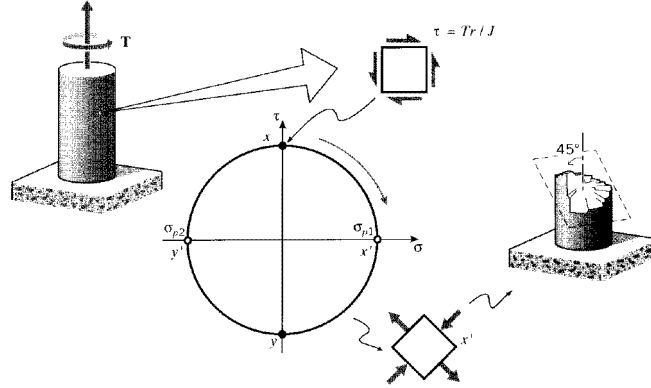


Figure 6: Mohr's circle for simple torsion.

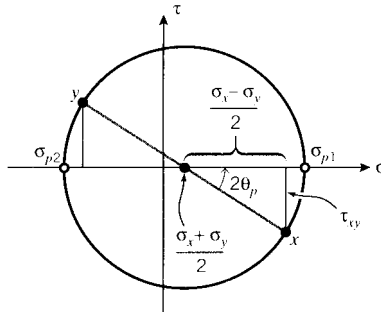


Figure 7: Principal stresses on Mohr's circle.

By direct Pythagorean construction as shown in Fig. 7, the Mohr's circle shows that the angle from the x - y axes to the principal planes is

$$\tan 2\theta_p = \frac{\tau_{xy}}{(\sigma_x - \sigma_y)/2} \quad (10)$$

and the values of the principal stresses are

$$\sigma_{p1,p1} = \frac{\sigma_x + \sigma_y}{2} \pm \sqrt{\left(\frac{\sigma_x - \sigma_y}{2}\right)^2 + \tau_{xy}^2} \quad (11)$$

where the first term above is the σ -coordinate of the circle's center, and the second is its radius.

When the Mohr's circle diametral line is vertical, the shear stresses become maximum, equal in magnitude to the radius of the circle:

$$\tau_{\max} = \sqrt{\left(\frac{\sigma_x - \sigma_y}{2}\right)^2 + \tau_{xy}^2} = \frac{\sigma_{p1} - \sigma_{p2}}{2} \quad (12)$$

The points of maximum shear are 90° away from the principal stress points on the Mohr's circle, so on the actual specimen the planes of maximum shear are 45° from the principal planes. The molecular sliding associated with yield is driven by shear, and usually takes place on the planes of maximum shear. A tensile specimen has principal planes along and transverse to its loading direction, so shear slippage will occur on planes $\pm 45^\circ$ from the loading direction. These slip planes can often be observed as "shear bands" on the specimen.

Note that normal stresses may appear on the planes of maximum shear, so the situation is not quite the converse of the principal planes, on which the shear stresses vanish while the normal stresses are maximum. If the normal stresses happen to vanish on the planes of maximum shear, the stress state is said to be one of "pure shear," such as is induced by simple torsion. A state of pure shear is therefore one for which a rotation of axes exists such that the normal stresses vanish, which is possible only if the center of the Mohr's circle is at the origin, i.e. $(\sigma_x + \sigma_y)/2 = 0$. More generally, a state of pure shear is one in which the trace of the stress (and strain) matrix vanishes.

Example 4

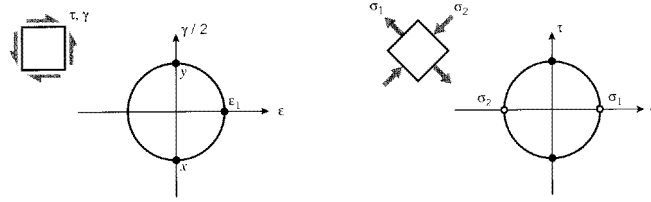


Figure 8: Strain and stress Mohr's circles for simple shear.

Mohr's circles can be drawn for strains as well as stresses, with shear strain plotted on the ordinate and normal strain on the abscissa. However, the ordinate must be $\gamma/2$ rather than just γ , due to the way classical infinitesimal strains are defined. Consider a state of pure shear with strain γ and stress τ as shown in Fig. 8, such as might be produced by placing a circular shaft in torsion. A Mohr's circle for strain quickly shows the principal strain, on a plane 45° away, is given by $\epsilon_1 = \gamma/2$. Hooke's law for shear gives $\tau = G\gamma$, so $\epsilon_1 = \tau/2G$. The principal strain is also related to the principal stresses by

$$\epsilon_1 = \frac{1}{E}(\sigma_1 - \nu\sigma_2)$$

The Mohr's circle for stress gives $\sigma_1 = -\sigma_2 = \tau$, so this can be written

$$\frac{\tau}{2G} = \frac{1}{E}[\tau - \nu(-\tau)]$$

Canceling τ and rearranging, we have the relation among elastic constants stated earlier without proof:

$$G = \frac{E}{2(1 + \nu)}$$

General approach

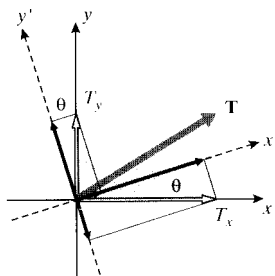


Figure 9: Transformation of vectors.

Another approach to the stress transformation equations, capable of easy extension to three dimensions, starts with the familiar relations by which *vectors* are transformed in two dimensions (see Fig. 9):

$$T_{x'} = T_x \cos \theta + T_y \sin \theta$$

$$T_{y'} = -T_x \sin \theta + T_y \cos \theta$$

In matrix form, this is

$$\begin{Bmatrix} T_{x'} \\ T_{y'} \end{Bmatrix} = \begin{bmatrix} \cos \theta & \sin \theta \\ -\sin \theta & \cos \theta \end{bmatrix} \begin{Bmatrix} T_x \\ T_y \end{Bmatrix}$$

or

$$\mathbf{T}' = \mathbf{a}\mathbf{T} \tag{13}$$

where \mathbf{a} is another transformation matrix that serves to transform the vector components in the original coordinate system to those in the primed system. In index-notation terms, this could also be denoted a_{ij} , so that

$$T'_i = a_{ij}T_j$$

The individual elements of a_{ij} are the cosines of the angles between the i^{th} primed axis and the j^{th} unprimed axis.

It can be shown by direct examination that the \mathbf{a} matrix has the useful property that its inverse equals its transpose; i.e., $\mathbf{a}^{-1} = \mathbf{a}^T$. We can multiply Eqn. 13 by \mathbf{a}^T to give

$$\mathbf{a}^T\mathbf{T}' = (\mathbf{a}^T\mathbf{a})\mathbf{T} = \mathbf{T} \tag{14}$$

so the transformation can go from primed to unprimed, or the reverse.

These relations can be extended to yield an expression for transformation of stresses (or strains, or moments of inertia, or other similar quantities). Recall Cauchy's relation in matrix form:

$$[\boldsymbol{\sigma}]\hat{\mathbf{n}} = \mathbf{T}$$

Using Eqn. 14 to transform the $\hat{\mathbf{n}}$ and \mathbf{T} vectors into their primed counterparts, we have

$$[\boldsymbol{\sigma}]\mathbf{a}^T\hat{\mathbf{n}}' = \mathbf{a}^T\mathbf{T}'$$

Multiplying through by \mathbf{a} :

$$(\mathbf{a}[\boldsymbol{\sigma}]\mathbf{a}^T)\hat{\mathbf{n}}' = (\mathbf{a}\mathbf{a}^T)\mathbf{T}' = \mathbf{T}'$$

This is just Cauchy's relation again, but in the primed coordinate frame. The quantity in parentheses must therefore be $[\boldsymbol{\sigma}']$:

$$[\boldsymbol{\sigma}'] = \mathbf{a}[\boldsymbol{\sigma}]\mathbf{a}^T \quad (15)$$

Therefore, transformation of stresses and can be done by pre- and postmultiplying by the same transformation matrix applicable to vector transformation. This can also be written out using index notation, which provides another illustration of the transformation differences between scalars (zero-rank tensors), vectors (first-rank tensors), and second-rank tensors:

$$\begin{aligned} \text{rank 0:} & \quad b' = b \\ \text{rank 1:} & \quad T'_i = a_{ij}T_j \\ \text{rank 2:} & \quad \sigma'_{ij} = a_{ij}a_{kl}\sigma_{kl} \end{aligned} \quad (16)$$

In practical work, it is not always a simple matter to write down the nine elements of the \mathbf{a} matrix needed in Eqn. 15. The squares of the components of $\hat{\mathbf{n}}$ for any given plane must sum to unity, and in order for the three planes of the transformed stress cube to be mutually perpendicular the dot product between any two plane normals must vanish. So not just any nine numbers will make sense. Obtaining \mathbf{a} is made much easier by using "Euler angles" to describe axis transformations in three dimensions.

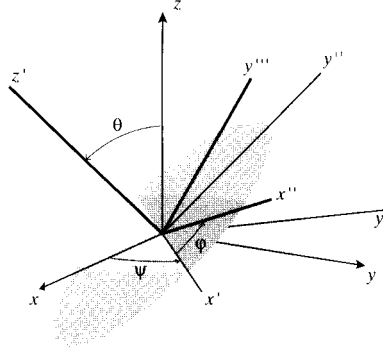


Figure 10: Transformation in terms of Euler angles.

As shown in Fig. 10, the final transformed axes are visualized as being achieved in three steps: first, rotate the original x - y - z axes by an angle ψ (psi) around the z -axis to obtain a new frame we may call x' - y' - z . Next, rotate this new frame by an angle θ about the x' axis to obtain another frame we can call x' - y'' - z' . Finally, rotate this frame by an angle ϕ (phi) around the z' axis to obtain the final frame x'' - y''' - z' . These three transformations correspond to the transformation matrix

$$\mathbf{a} = \begin{bmatrix} \cos \psi & \sin \psi & 0 \\ -\sin \psi & \cos \psi & 0 \\ 0 & 0 & 1 \end{bmatrix} \begin{bmatrix} 1 & 0 & 0 \\ 0 & \cos \theta & \sin \theta \\ 0 & -\sin \theta & \cos \theta \end{bmatrix} \begin{bmatrix} \cos \phi & \sin \phi & 0 \\ -\sin \phi & \cos \phi & 0 \\ 0 & 0 & 1 \end{bmatrix}$$

This multiplication would certainly be a pain if done manually, but is a natural for a computational approach.

Example 5

The output below shows a computer evaluation of a three-dimensional stress transformation, in this case using MapleTM symbolic mathematics software.

```
# read linear algebra library
> with(linalg):
# Define Euler-angle transformation matrices:
> a1:=array(1..3,1..3,[[cos(psi),sin(psi),0],[-sin(psi),cos(psi),0],[0,0
> ,1]]);
           [cos(psi)   sin(psi)   0]
      a1 := [-sin(psi)  cos(psi)   0]
           [ 0         0         1]
> a2:=array(1..3,1..3,[[1,0,0],[0,cos(theta),sin(theta)],[0,-sin(theta),
> cos(theta)]]);
           [1         0         0   ]
      a2 := [0   cos(theta)  sin(theta)]
           [0  -sin(theta)  cos(theta)]
> a3:=array(1..3,1..3,[[cos(phi),sin(phi),0],[-sin(phi),cos(phi),0],[0,0
> ,1]]);
           [cos(phi)   sin(phi)   0]
      a3 := [-sin(phi)  cos(phi)   0]
           [ 0         0         1]
# Overall transformation matrix (multiply individual Euler matrices):
> a:=a1&*a2&*a3;
           a := (a1 &* a2) &* a3
# Set precision and read in Euler angles (converted to radians); here
# we are rotating 30 degrees around the z axis only.
> Digits:=4;psi:=0;theta:=30*(Pi/180);phi:=0;
           Digits := 4
           psi := 0
           theta := 1/6 Pi
           phi := 0
# Display transformation matrix for these angles: "evalf" evaluates the
# matrix element, and "map" applies the evaluation to each element of
# the matrix.
> aa:=map(evalf,evalm(a));
           [1.    0.    0. ]
      aa := [0.   .8660  .5000]
           [0.   -.5000  .8660]
# Define the stress matrix in the unprimed frame:
> sigma:=array(1..3,1..3,[[1,2,3],[2,4,5],[3,5,6]]);
           [1  2  3]
      sigma := [2  4  5]
           [3  5  6]
# The stress matrix in the primed frame is then given by Eqn. 15:
> 'sigma_prime'=map(evalf,evalm(aa&*sigma&*transpose(aa)));
           [ 1.    3.232  1.598]
sigma_prime = [3.232  8.830  3.366]
           [1.598  3.366  1.170]
```

Principal stresses and planes in three dimensions

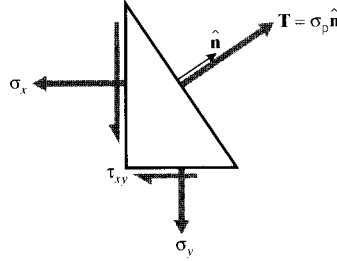


Figure 11: Traction vector normal to principal plane.

The Mohr's circle procedure is not capable of finding principal stresses for three-dimensional stress states, and a more general method is needed. In three dimensions, we seek orientations of axes such that no shear stresses appear, leaving only normal stresses in three orthogonal directions. The vanishing of shear stresses on a plane means that the stress vector \mathbf{T} is normal to the plane, illustrated in two dimensions in Fig. 11. The traction vector can therefore be written as

$$\mathbf{T} = \sigma_p \hat{\mathbf{n}}$$

where σ_p is a simple scalar quantity, the *magnitude* of the stress vector. Using this in Cauchy's relation:

$$\boldsymbol{\sigma} \hat{\mathbf{n}} = \mathbf{T} = \sigma_p \hat{\mathbf{n}}$$

$$(\boldsymbol{\sigma} - \sigma_p \mathbf{I}) \hat{\mathbf{n}} = \mathbf{0} \quad (17)$$

Here \mathbf{I} is the unit matrix. This system will have a nontrivial solution ($\hat{\mathbf{n}} \neq \mathbf{0}$) only if its determinant is zero:

$$|\boldsymbol{\sigma} - \sigma_p \mathbf{I}| = \begin{vmatrix} \sigma_x - \sigma_p & \tau_{xy} & \tau_{xz} \\ \tau_{xy} & \sigma_y - \sigma_p & \tau_{yz} \\ \tau_{xz} & \tau_{yz} & \sigma_z - \sigma_p \end{vmatrix} = 0$$

Expanding the determinant yields a cubic polynomial equation in σ_p :

$$f(\sigma_p) = \sigma_p^3 - I_1 \sigma_p^2 + I_2 \sigma_p - I_3 = 0 \quad (18)$$

This is the *characteristic equation* for stress, where the coefficients are

$$I_1 = \sigma_x + \sigma_y + \sigma_z = \sigma_{kk} \quad (19)$$

$$I_2 = \sigma_x \sigma_y + \sigma_x \sigma_z + \sigma_y \sigma_z - \tau_{xy}^2 - \tau_{yz}^2 - \tau_{xz}^2 = \frac{1}{2} (\sigma_{ii} \sigma_{jj} - \sigma_{ij} \sigma_{ij}) \quad (20)$$

$$I_3 = \det |\sigma| = \frac{1}{3}\sigma_{ij}\sigma_{jk}\sigma_{ki} \quad (21)$$

These I parameters are known as the *invariants* of the stress state; they do not change with transformation of the coordinates and can be used to characterize the overall nature of the stress. For instance I_1 , which has been identified earlier as the trace of the stress matrix, will be seen in a later section to be a measure of the tendency of the stress state to induce hydrostatic dilation or compression. We have already noted that the stress state is one of pure shear if its trace vanishes.

Since the characteristic equation is cubic in σ_p , it will have three roots, and it can be shown that all three roots must be real. These roots are just the principal stresses σ_{p1} , σ_{p2} , and σ_{p3} .

Example 6

Consider a state of simple shear with $\tau_{xy} = 1$ and all other stresses zero:

$$[\sigma] = \begin{bmatrix} 0 & 1 & 0 \\ 1 & 0 & 0 \\ 0 & 0 & 0 \end{bmatrix}$$

The invariants are

$$I_1 = 0, \quad I_2 = -1, \quad I_3 = 0$$

and the characteristic equation is

$$\sigma_p^3 - \sigma_p = 0$$

This equation has roots of (-1,0,1) corresponding to principal stresses $\sigma_{p1} = 1$, $\sigma_{p2} = 0$, $\sigma_{p3} = -1$, and is plotted in Fig. 12. This is the same stress state considered in Example 4, and the roots of the characteristic equation agree with the principal values shown by the Mohr's circle.

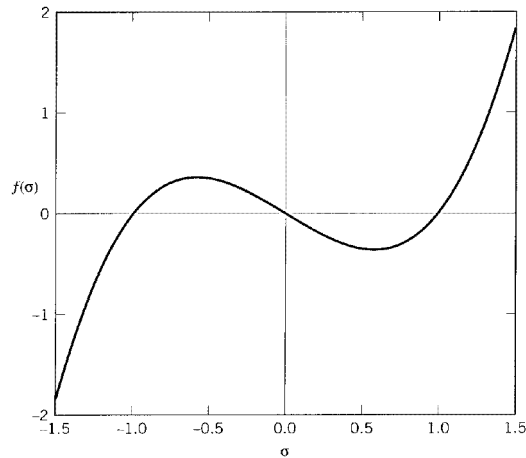


Figure 12: The characteristic equation for $\tau_{xy} = 1$, all other stresses zero.

Problems

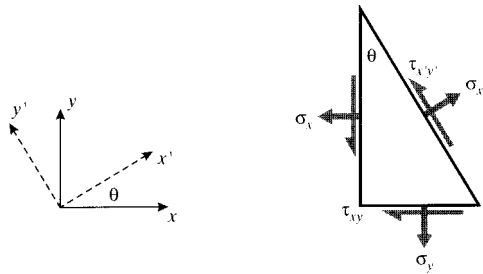
1. Develop an expression for the stress needed to cause transverse failure in a unidirectionally oriented composite as a function of the angle between the load direction and the fiber direction, and show this function in a plot of strength versus θ .
2. Use a free-body force balance to derive the two-dimensional Cartesian stress transformation equations as

$$\begin{aligned}\sigma_{x'} &= \sigma_x \cos^2 \theta + \sigma_y \sin^2 \theta + 2\tau_{xy} \sin \theta \cos \theta \\ \sigma_{y'} &= \sigma_x \sin^2 \theta + \sigma_y \cos^2 \theta - 2\tau_{xy} \sin \theta \cos \theta \\ \tau_{x'y'} &= (\sigma_y - \sigma_x) \sin \theta \cos \theta + \tau_{xy}(\cos^2 \theta - \sin^2 \theta)\end{aligned}$$

Or

$$\begin{Bmatrix} \sigma_{x'} \\ \sigma_{y'} \\ \tau_{x'y'} \end{Bmatrix} = \begin{bmatrix} c^2 & s^2 & 2sc \\ s^2 & c^2 & -2sc \\ -sc & sc & c^2 - s^2 \end{bmatrix} \begin{Bmatrix} \sigma_x \\ \sigma_y \\ \tau_{xy} \end{Bmatrix}$$

where $c = \cos \theta$ and $s = \sin \theta$.



Prob. 2

3. Develop mathematical relations for displacements and gradients along transformed axes of the form

$$u' = u \cos \theta + v \sin \theta$$

$$\frac{\partial}{\partial x'} = \frac{\partial}{\partial x} \cdot \frac{\partial x}{\partial x'} + \frac{\partial}{\partial y} \cdot \frac{\partial y}{\partial x'} = \frac{\partial}{\partial x} \cdot \cos \theta + \frac{\partial}{\partial y} \cdot \sin \theta$$

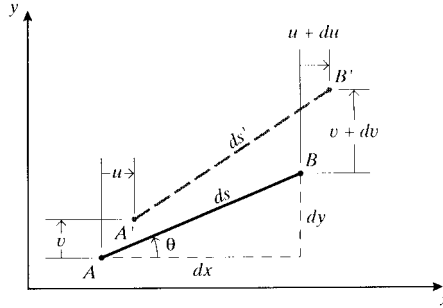
with analogous expressions for v' and $\partial/\partial y'$. Use these to obtain the strain transformation equations (Eqn. 6).

4. Consider a line segment AB of length $ds^2 = dx^2 + dy^2$, oriented at an angle θ from the Cartesian $x - y$ axes as shown. Let the differential displacement of end B relative to end A be

$$du = \frac{\partial u}{\partial x} dx + \frac{\partial u}{\partial y} dy$$

$$dv = \frac{\partial v}{\partial x} dx + \frac{\partial v}{\partial y} dy$$

Use this geometry to derive the strain transformation equations (Eqn. 6), where the x' axis is along line AB .



Prob. 4

5. Employ double-angle trigonometric relations to show that the two-dimensional Cartesian stress transformation equations can be written in the form

$$\begin{aligned}\sigma_{x'} &= \frac{\sigma_x + \sigma_y}{2} + \frac{\sigma_x - \sigma_y}{2} \cos 2\theta + \tau_{xy} \sin 2\theta \\ \tau_{x'y'} &= -\frac{\sigma_x - \sigma_y}{2} \sin 2\theta + \tau_{xy} \cos 2\theta \\ \sigma_{y'} &= \frac{\sigma_x + \sigma_y}{2} + \frac{\sigma_x - \sigma_y}{2} \cos 2\theta - \tau_{xy} \sin 2\theta\end{aligned}$$

Use these relations to justify the Mohr's circle construction.

6. Use matrix multiplication (Eqns. 5 or 8) to transform the following stress and strain states to axes rotated by $\theta = 30^\circ$ from the original x - y axes.

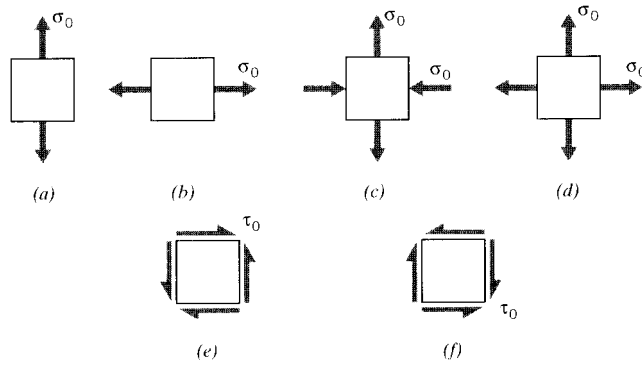
(a)

$$\boldsymbol{\sigma} = \begin{Bmatrix} 1.0 \\ -2.0 \\ 3.0 \end{Bmatrix}$$

(b)

$$\boldsymbol{\epsilon} = \begin{Bmatrix} 0.01 \\ -0.02 \\ 0.03 \end{Bmatrix}$$

7. Sketch the Mohr's circles for each of the stress states shown in the figure below.
8. Construct Mohr's circle solutions for the transformations of Prob. 6.
9. Draw the Mohr's circles and determine the magnitudes of the principal stresses for the following stress states. Denote the principal stress state on a suitably rotated stress square.
- (a) $\sigma_x = 30$ MPa, $\sigma_y = -10$ MPa, $\tau_{xy} = 25$ MPa.
- (b) $\sigma_x = -30$ MPa, $\sigma_y = -90$ MPa, $\tau_{xy} = -40$ MPa.
- (c) $\sigma_x = -10$ MPa, $\sigma_y = 20$ MPa, $\tau_{xy} = -15$ MPa.



Prob. 7

10. Show that the values of principal stresses given by Mohr's circle agree with those obtained mathematically by setting to zero the derivatives of the stress with respect to the transformation angle.
11. For the 3-dimensional stress state $\sigma_x = 25$, $\sigma_y = -15$, $\sigma_z = -30$, $\tau_{yz} = 20$, $\tau_{xz} = 10$, $\tau_{xy} = 30$ (all in MPa):
 - (a) Determine the stress state for Euler angles $\psi = 20^\circ$, $\theta = 30^\circ$, $\phi = 25^\circ$.
 - (b) Plot the characteristic equation.
 - (c) Determine the principal stresses.

Constitutive Equations

David Roylance
Department of Materials Science and Engineering
Massachusetts Institute of Technology
Cambridge, MA 02139

October 4, 2000

Introduction

The modules on kinematics (Module 8), equilibrium (Module 9), and tensor transformations (Module 10) contain concepts vital to Mechanics of Materials, but they do not provide insight on the role of the material itself. The kinematic equations relate strains to displacement gradients, and the equilibrium equations relate stress to the applied tractions on loaded boundaries and also govern the relations among stress gradients within the material. In three dimensions there are six kinematic equations and three equilibrium equations, for a total of nine. However, there are fifteen variables: three displacements, six strains, and six stresses. We need six more equations, and these are provided by the material's *constitutive* relations: six expressions relating the stresses to the strains. These are a sort of mechanical equation of state, and describe how the material is *constituted mechanically*.

With these constitutive relations, the vital role of the material is reasserted: The elastic constants that appear in this module are material properties, subject to control by processing and microstructural modification as outlined in Module 2. This is an important tool for the engineer, and points up the necessity of considering design *of* the material as well as *with* the material.

Isotropic elastic materials

In the general case of a linear relation between components of the strain and stress tensors, we might propose a statement of the form

$$\epsilon_{ij} = S_{ijkl} \sigma_{kl}$$

where the S_{ijkl} is a *fourth-rank* tensor. This constitutes a sequence of nine equations, since each component of ϵ_{ij} is a linear combination of all the components of σ_{ij} . For instance:

$$\epsilon_{23} = S_{2311} \sigma_{11} + S_{2312} \sigma_{12} + \cdots + S_{2333} \sigma_{33}$$

Based on each of the indices of S_{ijkl} taking on values from 1 to 3, we might expect a total of 81 independent components in S . However, both ϵ_{ij} and σ_{ij} are symmetric, with six rather than nine independent components each. This reduces the number of S components to 36, as can be seen from a linear relation between the pseudovector forms of the strain and stress:

$$\begin{pmatrix} \epsilon_x \\ \epsilon_y \\ \epsilon_z \\ \gamma_{yz} \\ \gamma_{xz} \\ \gamma_{xy} \end{pmatrix} = \begin{bmatrix} S_{11} & S_{12} & \cdots & S_{16} \\ S_{21} & S_{22} & \cdots & S_{26} \\ \vdots & \vdots & \ddots & \vdots \\ S_{61} & S_{26} & \cdots & S_{66} \end{bmatrix} \begin{pmatrix} \sigma_x \\ \sigma_y \\ \sigma_z \\ \tau_{yz} \\ \tau_{xz} \\ \tau_{xy} \end{pmatrix} \quad (1)$$

It can be shown¹ that the \mathbf{S} matrix in this form is also symmetric. It therefore it contains only 21 independent elements, as can be seen by counting the elements in the upper right triangle of the matrix, including the diagonal elements ($1 + 2 + 3 + 4 + 5 + 6 = 21$).

If the material exhibits symmetry in its elastic response, the number of independent elements in the \mathbf{S} matrix can be reduced still further. In the simplest case of an *isotropic* material, whose stiffnesses are the same in all directions, only *two* elements are independent. We have earlier shown that in two dimensions the relations between strains and stresses in isotropic materials can be written as

$$\begin{aligned} \epsilon_x &= \frac{1}{E} (\sigma_x - \nu \sigma_y) \\ \epsilon_y &= \frac{1}{E} (\sigma_y - \nu \sigma_x) \\ \gamma_{xy} &= \frac{1}{G} \tau_{xy} \end{aligned} \quad (2)$$

along with the relation

$$G = \frac{E}{2(1 + \nu)}$$

Extending this to three dimensions, the pseudovector-matrix form of Eqn. 1 for isotropic materials is

$$\begin{pmatrix} \epsilon_x \\ \epsilon_y \\ \epsilon_z \\ \gamma_{yz} \\ \gamma_{xz} \\ \gamma_{xy} \end{pmatrix} = \begin{bmatrix} \frac{1}{E} & \frac{-\nu}{E} & \frac{-\nu}{E} & 0 & 0 & 0 \\ \frac{-\nu}{E} & \frac{1}{E} & \frac{-\nu}{E} & 0 & 0 & 0 \\ \frac{-\nu}{E} & \frac{-\nu}{E} & \frac{1}{E} & 0 & 0 & 0 \\ 0 & 0 & 0 & \frac{1}{G} & 0 & 0 \\ 0 & 0 & 0 & 0 & \frac{1}{G} & 0 \\ 0 & 0 & 0 & 0 & 0 & \frac{1}{G} \end{bmatrix} \begin{pmatrix} \sigma_x \\ \sigma_y \\ \sigma_z \\ \tau_{yz} \\ \tau_{xz} \\ \tau_{xy} \end{pmatrix} \quad (3)$$

The quantity in brackets is called the *compliance matrix* of the material, denoted \mathbf{S} or S_{ij} . It is important to grasp the physical significance of its various terms. Directly from the rules of matrix multiplication, the element in the i^{th} row and j^{th} column of S_{ij} is the contribution of the j^{th} stress to the i^{th} strain. For instance the component in the 1,2 position is the contribution of the y -direction stress to the x -direction strain: multiplying σ_y by $1/E$ gives the y -direction strain generated by σ_y , and then multiplying this by $-\nu$ gives the Poisson strain induced in the x direction. The zero elements show the lack of coupling between the normal and shearing components.

The isotropic constitutive law can also be written using index notation as (see Prob. 1)

$$\epsilon_{ij} = \frac{1 + \nu}{E} \sigma_{ij} - \frac{\nu}{E} \delta_{ij} \sigma_{kk} \quad (4)$$

where here the indicial form of strain is used and G has been eliminated using $G = E/2(1 + \nu)$. The symbol δ_{ij} is the *Kronecker delta*, described in the Module on Matrix and Index Notation.

¹G.M. Mase, *Schaum's Outline of Theory and Problems of Continuum Mechanics*, McGraw-Hill, 1970.

If we wish to write the stresses in terms of the strains, Eqns. 3 can be inverted. In cases of plane stress ($\sigma_z = \tau_{xz} = \tau_{yz} = 0$), this yields

$$\begin{Bmatrix} \sigma_x \\ \sigma_y \\ \tau_{xy} \end{Bmatrix} = \frac{E}{1-\nu^2} \begin{bmatrix} 1 & \nu & 0 \\ \nu & 1 & 0 \\ 0 & 0 & (1-\nu)/2 \end{bmatrix} \begin{Bmatrix} \epsilon_x \\ \epsilon_y \\ \gamma_{xy} \end{Bmatrix} \quad (5)$$

where again G has been replaced by $E/2(1+\nu)$. Or, in abbreviated notation:

$$\boldsymbol{\sigma} = \mathbf{D}\boldsymbol{\epsilon} \quad (6)$$

where $\mathbf{D} = \mathbf{S}^{-1}$ is the *stiffness matrix*.

Hydrostatic and distortional components

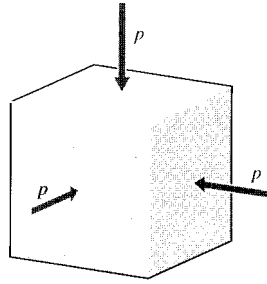


Figure 1: Hydrostatic compression.

A state of hydrostatic compression, depicted in Fig. 1, is one in which no shear stresses exist and where all the normal stresses are equal to the hydrostatic pressure:

$$\sigma_x = \sigma_y = \sigma_z = -p$$

where the minus sign indicates that compression is conventionally positive for pressure but negative for stress. For this stress state it is obviously true that

$$\frac{1}{3}(\sigma_x + \sigma_y + \sigma_z) = \frac{1}{3}\sigma_{kk} = -p$$

so that the hydrostatic pressure is the negative *mean normal stress*. This quantity is just one third of the stress invariant I_1 , which is a reflection of hydrostatic pressure being the same in all directions, not varying with axis rotations.

In many cases other than direct hydrostatic compression, it is still convenient to “dissociate” the hydrostatic (or “dilatational”) component from the stress tensor:

$$\sigma_{ij} = \frac{1}{3}\sigma_{kk}\delta_{ij} + \Sigma_{ij} \quad (7)$$

Here Σ_{ij} is what is left over from σ_{ij} after the hydrostatic component is subtracted. The Σ_{ij} tensor can be shown to represent a state of pure shear, i.e. there exists an axis transformation such that all normal stresses vanish (see Prob. 5). The Σ_{ij} is called the distortional, or deviatoric,

component of the stress. Hence all stress states can be thought of as having two components as shown in Fig. 2, one purely extensional and one purely distortional. This concept is convenient because the material response to these stress components is very different ways. For instance, plastic and viscous flow is driven dominantly by distortional components, with the hydrostatic component causing only elastic deformation.

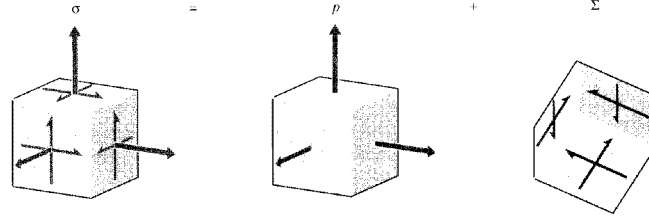


Figure 2: Dilatational and deviatoric components of the stress tensor.

Example 1

Consider the stress state

$$\sigma = \begin{bmatrix} 5 & 6 & 7 \\ 6 & 8 & 9 \\ 7 & 9 & 2 \end{bmatrix}, \text{ GPa}$$

The mean normal stress is $\sigma_{kk}/3 = (5 + 8 + 2)/3 = 5$, so the stress decomposition is

$$\sigma = \frac{1}{3} \sigma_{kk} \delta_{ij} + \Sigma_{ij} = \begin{bmatrix} 5 & 0 & 0 \\ 0 & 5 & 0 \\ 0 & 0 & 5 \end{bmatrix} + \begin{bmatrix} 0 & 6 & 7 \\ 6 & 3 & 9 \\ 7 & 9 & -3 \end{bmatrix}$$

It is not obvious that the deviatoric component given in the second matrix represents pure shear, since there are nonzero components on its diagonal. However, a stress transformation using Euler angles $\psi = \phi = 0, \theta = -9.22^\circ$ gives the stress state

$$\Sigma' = \begin{bmatrix} 0.00 & 4.80 & 7.87 \\ 4.80 & 0.00 & 9.49 \\ 7.87 & 9.49 & 0.00 \end{bmatrix}$$

The hydrostatic component of stress is related to the volumetric strain through the modulus of compressibility ($-p = K \Delta V/V$), so

$$\frac{1}{3} \sigma_{kk} = K \epsilon_{kk} \quad (8)$$

Similarly to the stress, the strain can also be dissociated as

$$\epsilon_{ij} = \frac{1}{3} \epsilon_{kk} \delta_{ij} + e_{ij}$$

where e_{ij} is the deviatoric component of strain. The deviatoric components of stress and strain are related by the material's shear modulus:

$$\Sigma_{ij} = 2G e_{ij} \quad (9)$$

where the factor 2 is needed because tensor descriptions of strain are half the classical strains for which values of G have been tabulated. Writing the constitutive equations in the form of Eqns. 8 and 9 produces a simple form without the coupling terms in the conventional E - ν form.

Example 2

Using the stress state of the previous example along with the elastic constants for steel ($E = 207$ GPa, $\nu = 0.3$, $K = E/3(1 - 2\nu) = 173$ GPa, $G = E/2(1 + \nu) = 79.6$ GPa), the dilatational and distortional components of strain are

$$\delta_{ij}\epsilon_{kk} = \frac{\delta_{ij}\sigma_{kk}}{3K} = \begin{bmatrix} 0.0289 & 0 & 0 \\ 0 & 0.0289 & 0 \\ 0 & 0 & 0.0289 \end{bmatrix}$$

$$e_{ij} = \frac{\Sigma_{ij}}{2G} = \begin{bmatrix} 0 & 0.0378 & 0.0441 \\ 0.0378 & 0.0189 & 0.0567 \\ 0.0441 & 0.0567 & -0.0189 \end{bmatrix}$$

The total strain is then

$$\epsilon_{ij} = \frac{1}{3}\epsilon_{kk}\delta_{ij} + e_{ij} = \begin{bmatrix} 0.00960 & 0.0378 & 0.0441 \\ 0.0378 & 0.0285 & 0.0567 \\ 0.0441 & 0.0567 & -0.00930 \end{bmatrix}$$

If we evaluate the total strain using Eqn. 4, we have

$$\epsilon_{ij} = \frac{1+\nu}{E}\sigma_{ij} - \frac{\nu}{E}\delta_{ij}\sigma_{kk} = \begin{bmatrix} 0.00965 & 0.0377 & 0.0440 \\ 0.0377 & 0.0285 & 0.0565 \\ 0.0440 & 0.0565 & -0.00915 \end{bmatrix}$$

These results are the same, differing only by roundoff error.

Finite strain model

When deformations become large, geometrical as well as material nonlinearities can arise that are important in many practical problems. In these cases the analyst must employ not only a different strain measure, such as the Lagrangian strain described in Module 8, but also different stress measures (the “Second Piola-Kirchoff stress” replaces the Cauchy stress when Lagrangian strain is used) and different stress-strain constitutive laws as well. A treatment of these formulations is beyond the scope of these modules, but a simple nonlinear stress-strain model for rubbery materials will be outlined here to illustrate some aspects of finite strain analysis. The text by Bathe² provides a more extensive discussion of this area, including finite element implementations.

In the case of small displacements, the strain ϵ_x is given by the expression:

$$\epsilon_x = \frac{1}{E} [\sigma_x - \nu(\sigma_y + \sigma_z)]$$

For the case of elastomers with $\nu = 0.5$, this can be rewritten in terms of the mean stress $\sigma_m = (\sigma_x + \sigma_y + \sigma_z)/3$ as:

$$2\epsilon_x = \frac{3}{E}(\sigma_x - \sigma_m)$$

²K.-J. Bathe, *Finite Element Procedures in Engineering Analysis*, Prentice-Hall, 1982.

For the large-strain case, the following analogous stress-strain relation has been proposed:

$$\lambda_x^2 = 1 + 2\epsilon_x = \frac{3}{E}(\sigma_x - \sigma_m^*) \quad (10)$$

where here ϵ_x is the Lagrangian strain and σ_m^* is a parameter not necessarily equal to σ_m . The σ_m^* parameter can be found for the case of uniaxial tension by considering the transverse contractions $\lambda_y = \lambda_z$:

$$\lambda_y^2 = \frac{3}{E}(\sigma_y - \sigma_m^*)$$

Since for rubber $\lambda_x\lambda_y\lambda_z = 1$, $\lambda_y^2 = 1/\lambda_x$. Making this substitution and solving for σ_m^* :

$$\sigma_m^* = \frac{-E\lambda_y^2}{3} = \frac{-E}{3\lambda_x}$$

Substituting this back into Eqn. 10,

$$\lambda_x^2 = \frac{3}{E} \left[\sigma_x - \frac{E}{3\lambda_x} \right]$$

Solving for σ_x ,

$$\sigma_x = \frac{E}{3} \left(\lambda_x^2 - \frac{1}{\lambda_x} \right)$$

Here the stress $\sigma_x = F/A$ is the “true” stress based on the actual (contracted) cross-sectional area. The “engineering” stress $\sigma_e = F/A_0$ based on the original area $A_0 = A\lambda_x$ is:

$$\sigma_e = \frac{\sigma_x}{\lambda_x} = G \left(\lambda_x - \frac{1}{\lambda_x^2} \right)$$

where $G = E/2(1 + \nu) = E/3$ for $\nu = 1/2$. This result is the same as that obtained in Module 2 by considering the force arising from the reduced entropy as molecular segments spanning crosslink sites are extended. It appears here from a simple hypothesis of stress-strain response, using a suitable measure of finite strain.

Anisotropic materials

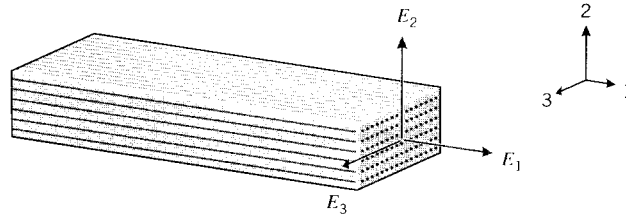


Figure 3: An orthotropic material.

If the material has a texture like wood or unidirectionally-reinforced fiber composites as shown in Fig. 3, the modulus E_1 in the fiber direction will typically be larger than those in the transverse directions (E_2 and E_3). When $E_1 \neq E_2 \neq E_3$, the material is said to be *orthotropic*.

It is common, however, for the properties in the plane transverse to the fiber direction to be isotropic to a good approximation ($E_2 = E_3$); such a material is called *transversely isotropic*. The elastic constitutive laws must be modified to account for this anisotropy, and the following form is an extension of Eqn. 3 for transversely isotropic materials:

$$\begin{Bmatrix} \epsilon_1 \\ \epsilon_2 \\ \gamma_{12} \end{Bmatrix} = \begin{bmatrix} 1/E_1 & -\nu_{21}/E_2 & 0 \\ -\nu_{12}/E_1 & 1/E_2 & 0 \\ 0 & 0 & 1/G_{12} \end{bmatrix} \begin{Bmatrix} \sigma_1 \\ \sigma_2 \\ \tau_{12} \end{Bmatrix} \quad (11)$$

The parameter ν_{12} is the *principal Poisson's ratio*; it is the ratio of the strain induced in the 2-direction by a strain applied in the 1-direction. This parameter is not limited to values less than 0.5 as in isotropic materials. Conversely, ν_{21} gives the strain induced in the 1-direction by a strain applied in the 2-direction. Since the 2-direction (transverse to the fibers) usually has much less stiffness than the 1-direction, it should be clear that a given strain in the 1-direction will usually develop a much larger strain in the 2-direction than will the same strain in the 2-direction induce a strain in the 1-direction. Hence we will usually have $\nu_{12} > \nu_{21}$. There are five constants in the above equation (E_1 , E_2 , ν_{12} , ν_{21} and G_{12}). However, only four of them are independent; since the S matrix is symmetric, $\nu_{21}/E_2 = \nu_{12}/E_1$.

A table of elastic constants and other properties for widely used anisotropic materials can be found in the Module on Composite Ply Properties.

The simple form of Eqn. 11, with zeroes in the terms representing coupling between normal and shearing components, is obtained only when the axes are aligned along the *principal material directions*; i.e. along and transverse to the fiber axes. If the axes are oriented along some other direction, all terms of the compliance matrix will be populated, and the symmetry of the material will not be evident. If for instance the fiber direction is off-axis from the loading direction, the material will develop shear strain as the fibers try to orient along the loading direction as shown in Fig. 4. There will therefore be a coupling between a normal stress and a shearing strain, which never occurs in an isotropic material.

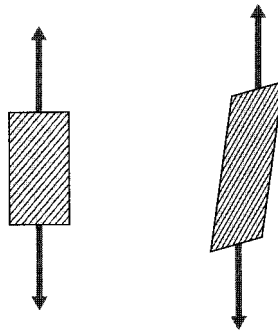


Figure 4: Shear-normal coupling.

The transformation law for compliance can be developed from the transformation laws for strains and stresses, using the procedures described in Module 10 (Transformations). By successive transformations, the pseudovector form for strain in an arbitrary x - y direction shown in Fig. 5 is related to strain in the 1-2 (principal material) directions, then to the stresses in the 1-2 directions, and finally to the stresses in the x - y directions. The final grouping of transformation matrices relating the x - y strains to the x - y stresses is then the transformed compliance matrix

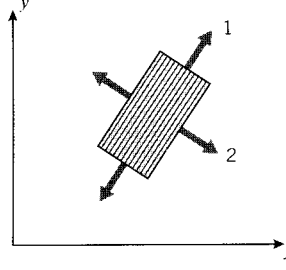


Figure 5: Axis transformation for constitutive equations.

in the x - y direction:

$$\begin{aligned} \begin{Bmatrix} \epsilon_x \\ \epsilon_y \\ \gamma_{xy} \end{Bmatrix} &= \mathbf{R} \begin{Bmatrix} \epsilon_x \\ \epsilon_y \\ \frac{1}{2}\gamma_{xy} \end{Bmatrix} = \mathbf{R}\mathbf{A}^{-1} \begin{Bmatrix} \epsilon_1 \\ \epsilon_2 \\ \frac{1}{2}\gamma_{12} \end{Bmatrix} = \mathbf{R}\mathbf{A}^{-1}\mathbf{R}^{-1} \begin{Bmatrix} \epsilon_1 \\ \epsilon_2 \\ \gamma_{12} \end{Bmatrix} \\ &= \mathbf{R}\mathbf{A}^{-1}\mathbf{R}^{-1}\mathbf{S} \begin{Bmatrix} \sigma_1 \\ \sigma_2 \\ \tau_{12} \end{Bmatrix} = \mathbf{R}\mathbf{A}^{-1}\mathbf{R}^{-1}\mathbf{S}\mathbf{A} \begin{Bmatrix} \sigma_x \\ \sigma_y \\ \tau_{xy} \end{Bmatrix} \equiv \bar{\mathbf{S}} \begin{Bmatrix} \sigma_x \\ \sigma_y \\ \tau_{xy} \end{Bmatrix} \end{aligned}$$

where $\bar{\mathbf{S}}$ is the *transformed compliance matrix* relative to x - y axes. Here \mathbf{A} is the transformation matrix, and \mathbf{R} is the Reuter's matrix defined in the Module on Tensor Transformations. The inverse of $\bar{\mathbf{S}}$ is $\bar{\mathbf{D}}$, the stiffness matrix relative to x - y axes:

$$\boxed{\bar{\mathbf{S}} = \mathbf{R}\mathbf{A}^{-1}\mathbf{R}^{-1}\mathbf{S}\mathbf{A}, \quad \bar{\mathbf{D}} = \bar{\mathbf{S}}^{-1}} \quad (12)$$

Example 3

Consider a ply of Kevlar-epoxy composite with a stiffnesses $E_1 = 82$, $E_2 = 4$, $G_{12} = 2.8$ (all GPa) and $\nu_{12} = 0.25$. The compliance matrix \mathbf{S} in the 1-2 (material) direction is:

$$\mathbf{S} = \begin{bmatrix} 1/E_1 & -\nu_{21}/E_2 & 0 \\ -\nu_{12}/E_1 & 1/E_2 & 0 \\ 0 & 0 & 1/G_{12} \end{bmatrix} = \begin{bmatrix} .1220 \times 10^{-10} & -.3050 \times 10^{-11} & 0 \\ -.3050 \times 10^{-11} & .2500 \times 10^{-9} & 0 \\ 0 & 0 & .3571 \times 10^{-9} \end{bmatrix}$$

If the ply is oriented with the fiber direction (the “1” direction) at $\theta = 30^\circ$ from the x - y axes, the appropriate transformation matrix is

$$\mathbf{A} = \begin{bmatrix} c^2 & s^2 & 2sc \\ s^2 & c^2 & -2sc \\ -sc & sc & c^2 - s^2 \end{bmatrix} = \begin{bmatrix} .7500 & .2500 & .8660 \\ .2500 & .7500 & -.8660 \\ -.4330 & .4330 & .5000 \end{bmatrix}$$

The compliance matrix relative to the x - y axes is then

$$\bar{\mathbf{S}} = \mathbf{R}\mathbf{A}^{-1}\mathbf{R}^{-1}\mathbf{S}\mathbf{A} = \begin{bmatrix} .8830 \times 10^{-10} & -.1970 \times 10^{-10} & -.1222 \times 10^{-9} \\ -.1971 \times 10^{-10} & .2072 \times 10^{-9} & -.8371 \times 10^{-10} \\ -.1222 \times 10^{-9} & -.8369 \times 10^{-10} & -.2905 \times 10^{-9} \end{bmatrix}$$

Note that this matrix is symmetric (to within numerical roundoff error), but that nonzero coupling values exist. A user not aware of the internal composition of the material would consider it completely anisotropic.

The apparent engineering constants that would be observed if the ply were tested in the x - y rather than 1-2 directions can be found directly from the transformed $\bar{\mathbf{S}}$ matrix. For instance, the apparent elastic modulus in the x direction is $E_x = 1/\bar{\mathbf{S}}_{1,1} = 1/(.8830 \times 10^{-10}) = 11.33$ GPa.

Problems

- Expand the indicial forms of the governing equations for solid elasticity in three dimensions:

$$\text{equilibrium : } \sigma_{ij,j} = 0$$

$$\text{kinematic : } \epsilon_{ij} = (u_{i,j} + u_{j,i})/2$$

$$\text{constitutive : } \epsilon_{ij} = \frac{1+\nu}{E}\sigma_{ij} - \frac{\nu}{E}\delta_{ij}\sigma_{kk} + \alpha\delta_{ij}\Delta T$$

where α is the coefficient of linear thermal expansion and ΔT is a temperature change.

- Write out the compliance matrix \mathbf{S} of Eqn. 3 for polycarbonate using data in the Module on Material Properties.
 - Use matrix inversion to obtain the stiffness matrix \mathbf{D} .
 - Use matrix multiplication to obtain the stresses needed to induce the strains

$$\boldsymbol{\epsilon} = \begin{Bmatrix} \epsilon_x \\ \epsilon_y \\ \epsilon_z \\ \gamma_{yz} \\ \gamma_{xz} \\ \gamma_{xy} \end{Bmatrix} = \begin{Bmatrix} 0.02 \\ 0.0 \\ 0.03 \\ 0.01 \\ 0.025 \\ 0.0 \end{Bmatrix}$$

- Write out the compliance matrix \mathbf{S} of Eqn.3 for an aluminum alloy using data in the Module on Material Properties.
 - Use matrix inversion to obtain the stiffness matrix \mathbf{D} .
 - Use matrix multiplication to obtain the stresses needed to induce the strains

$$\boldsymbol{\epsilon} = \begin{Bmatrix} \epsilon_x \\ \epsilon_y \\ \epsilon_z \\ \gamma_{yz} \\ \gamma_{xz} \\ \gamma_{xy} \end{Bmatrix} = \begin{Bmatrix} 0.01 \\ 0.02 \\ 0.0 \\ 0.0 \\ 0.15 \\ 0.0 \end{Bmatrix}$$

- Given the stress tensor

$$\sigma_{ij} = \begin{bmatrix} 1 & 2 & 3 \\ 2 & 4 & 5 \\ 3 & 5 & 7 \end{bmatrix} \quad (\text{MPa})$$

- Dissociate σ_{ij} into deviatoric and dilatational parts Σ_{ij} and $(1/3)\sigma_{kk}\delta_{ij}$.

(b) Given $G = 357$ MPa and $K = 1.67$ GPa, obtain the deviatoric and dilatational strain tensors e_{ij} and $(1/3)\epsilon_{kk}\delta_{ij}$.

(c) Add the deviatoric and dilatational strain components obtained above to obtain the total strain tensor ϵ_{ij} .

(d) Compute the strain tensor ϵ_{ij} using the alternate form of the elastic constitutive law for isotropic elastic solids:

$$\epsilon_{ij} = \frac{1 + \nu}{E}\sigma_{ij} - \frac{\nu}{E}\delta_{ij}\sigma_{kk}$$

Compare the result with that obtained in (c).

5. Provide an argument that any stress matrix having a zero trace can be transformed to one having only zeroes on its diagonal; i.e. the deviatoric stress tensor Σ_{ij} represents a state of pure shear.
6. Write out the x - y two-dimensional compliance matrix $\bar{\mathbf{S}}$ and stiffness matrix $\bar{\mathbf{D}}$ (Eqn. 12) for a single ply of graphite/epoxy composite with its fibers aligned along the x axes.
7. Write out the x - y two-dimensional compliance matrix $\bar{\mathbf{S}}$ and stiffness matrix $\bar{\mathbf{D}}$ (Eqn. 12) for a single ply of graphite/epoxy composite with its fibers aligned 30° from the x axis.

Statics of Bending: Shear and Bending Moment Diagrams

David Roylance
Department of Materials Science and Engineering
Massachusetts Institute of Technology
Cambridge, MA 02139

November 15, 2000

Introduction

Beams are long and slender structural elements, differing from truss elements in that they are called on to support transverse as well as axial loads. Their attachment points can also be more complicated than those of truss elements: they may be bolted or welded together, so the attachments can transmit bending moments or transverse forces into the beam. Beams are among the most common of all structural elements, being the supporting frames of airplanes, buildings, cars, people, and much else.

The nomenclature of beams is rather standard: as shown in Fig. 1, L is the length, or span; b is the width, and h is the height (also called the *depth*). The cross-sectional shape need not be rectangular, and often consists of a vertical *web* separating horizontal *flanges* at the top and bottom of the beam¹.

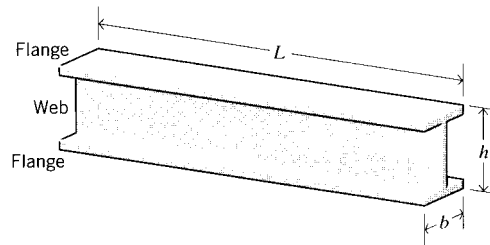


Figure 1: Beam nomenclature.

As will be seen in Modules 13 and 14, the stresses and deflections induced in a beam under bending loads vary along the beam's length and height. The first step in calculating these quantities and their spatial variation consists of constructing *shear* and *bending moment* diagrams, $V(x)$ and $M(x)$, which are the internal shearing forces and bending moments induced in the beam, plotted along the beam's length. The following sections will describe how these diagrams are made.

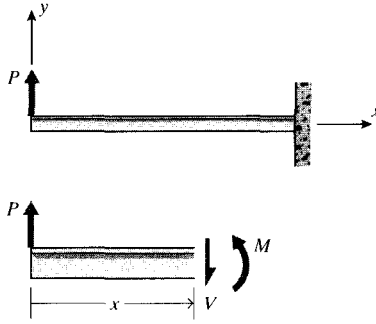


Figure 2: A cantilevered beam.

Free-body diagrams

As a simple starting example, consider a beam clamped (“cantilevered”) at one end and subjected to a load P at the free end as shown in Fig. 2. A free body diagram of a section cut transversely at position x shows that a shear force V and a moment M must exist on the cut section to maintain equilibrium. We will show in Module 13 that these are the resultants of shear and normal stresses that are set up on internal planes by the bending loads. As usual, we will consider section areas whose normals point in the $+x$ direction to be positive; then shear forces pointing in the $+y$ direction on $+x$ faces will be considered positive. Moments whose vector direction as given by the right-hand rule are in the $+z$ direction (vector out of the plane of the paper, or tending to cause counterclockwise rotation in the plane of the paper) will be positive when acting on $+x$ faces. Another way to recognize positive bending moments is that they cause the bending shape to be concave upward. For this example beam, the statics equations give:

$$\sum F_y = 0 = V + P \Rightarrow V = \text{constant} = -P \quad (1)$$

$$\sum M_0 = 0 = -M + Px \Rightarrow M = M(x) = Px \quad (2)$$

Note that the moment increases with distance from the loaded end, so the magnitude of the maximum value of M compared with V increases as the beam becomes longer. This is true of most beams, so shear effects are usually more important in beams with small length-to-height ratios.

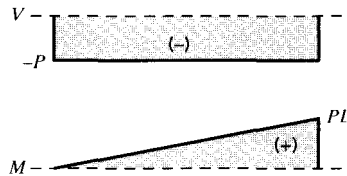


Figure 3: Shear and bending moment diagrams.

¹There is a standardized protocol for denoting structural steel beams; for instance W 8 × 40 indicates a wide-flange beam with a nominal depth of 8” and weighing 40 lb/ft of length

As stated earlier, the stresses and deflections will be shown to be functions of V and M , so it is important to be able to compute how these quantities vary along the beam's length. Plots of $V(x)$ and $M(x)$ are known as *shear* and *bending moment diagrams*, and it is necessary to obtain them before the stresses can be determined. For the end-loaded cantilever, the diagrams shown in Fig. 3 are obvious from Eqns. 1 and 2.

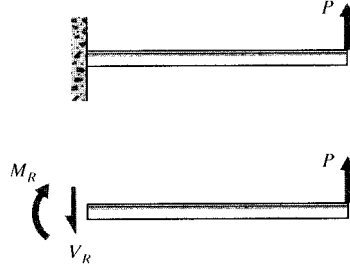


Figure 4: Wall reactions for the cantilevered beam.

It was easiest to analyze the cantilevered beam by beginning at the free end, but the choice of origin is arbitrary. It is not always possible to guess the easiest way to proceed, so consider what would have happened if the origin were placed at the wall as in Fig. 4. Now when a free body diagram is constructed, forces must be placed at the origin to replace the reactions that were imposed by the wall to keep the beam in equilibrium with the applied load. These reactions can be determined from free-body diagrams of the beam as a whole (if the beam is statically determinate), and must be found before the problem can proceed. For the beam of Fig. 4:

$$\sum F_y = 0 = -V_R + P \Rightarrow V_R = P$$

$$\sum M_o = 0 = M_R - PL \Rightarrow M_R = PL$$

The shear and bending moment at x are then

$$V(x) = V_R = P = \text{constant}$$

$$M(x) = M_R - V_R x = PL - Px$$

This choice of origin produces some extra algebra, but the $V(x)$ and $M(x)$ diagrams shown in Fig. 5 are the same as before (except for changes of sign): V is constant and equal to P , and M varies linearly from zero at the free end to PL at the wall.

Distributed loads

Transverse loads may be applied to beams in a distributed rather than at-a-point manner as depicted in Fig. 6, which might be visualized as sand piled on the beam. It is convenient to describe these distributed loads in terms of *force per unit length*, so that $q(x) dx$ would be the load applied to a small section of length dx by a distributed load $q(x)$. The shear force $V(x)$ set up in reaction to such a load is

$$V(x) = - \int_{x_0}^x q(\xi) d\xi \tag{3}$$

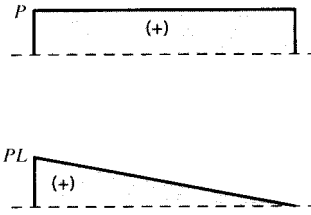


Figure 5: Alternative shear and bending moment diagrams for the cantilevered beam.

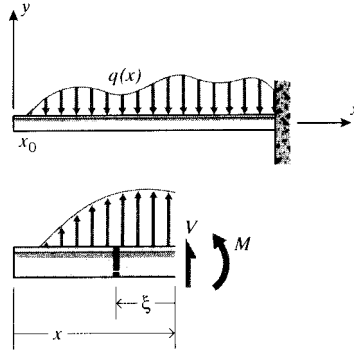


Figure 6: A distributed load and a free-body section.

where x_0 is the value of x at which $q(x)$ begins, and ξ is a dummy length variable that looks backward from x . Hence $V(x)$ is the area under the $q(x)$ diagram up to position x . The moment balance is obtained considering the increment of load $q(\xi) d\xi$ applied to a small width $d\xi$ of beam, a distance ξ from point x . The incremental moment of this load around point x is $q(\xi) \xi d\xi$, so the moment $M(x)$ is

$$M = \int_{x_0}^x q(\xi) \xi d\xi \quad (4)$$

This can be related to the centroid of the area under the $q(x)$ curve up to x , whose distance from x is

$$\bar{\xi} = \frac{\int q(\xi) \xi d\xi}{\int q(\xi) d\xi}$$

Hence Eqn. 4 can be written

$$M = Q\bar{\xi} \quad (5)$$

where $Q = \int q(\xi) d\xi$ is the area. Therefore, the distributed load $q(x)$ is statically equivalent to a concentrated load of magnitude Q placed at the centroid of the area under the $q(x)$ diagram.

Example 1

Consider a simply-supported beam carrying a triangular and a concentrated load as shown in Fig. 7. For

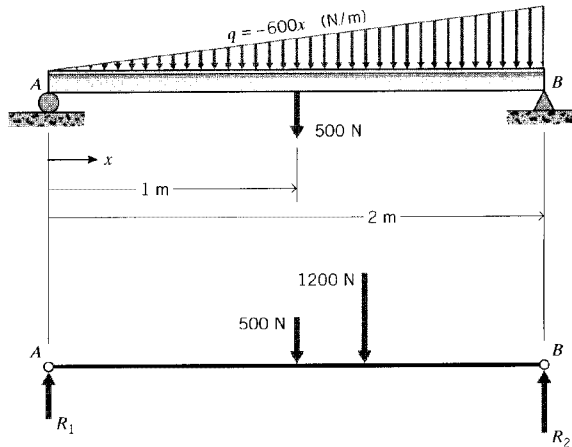


Figure 7: Distributed and concentrated loads.

the purpose of determining the support reaction forces R_1 and R_2 , the distributed triangular load can be replaced by its static equivalent. The magnitude of this equivalent force is

$$Q = \int_0^2 (-600x) dx = -1200$$

The equivalent force acts through the centroid of the triangular area, which is $2/3$ of the distance from its narrow end (see Prob. 1). The reaction R_2 can now be found by taking moments around the left end:

$$\sum M_A = 0 = -500(1) - (1200)(2/3) + R_2(2) \rightarrow R_2 = 650$$

The other reaction can then be found from vertical equilibrium:

$$\sum F_y = 0 = R_1 - 500 - 1200 + 650 = 1050$$

Successive integration method

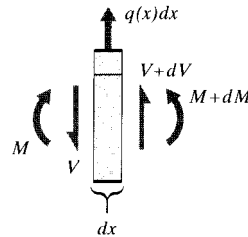


Figure 8: Relations between distributed loads and internal shear forces and bending moments.

We have already noted in Eqn. 3 that the shear curve is the negative integral of the loading curve. Another way of developing this is to consider a free body balance on a small increment

of length dx over which the shear and moment changes from V and M to $V + dV$ and $M + dM$ (see Fig. 8). The distributed load $q(x)$ can be taken as constant over the small interval, so the force balance is:

$$\sum F_y = 0 = V + dV + q dx - V = 0$$

$$\boxed{\frac{dV}{dx} = -q} \quad (6)$$

or

$$\boxed{V(x) = - \int q(x) dx} \quad (7)$$

which is equivalent to Eqn. 3. A moment balance around the center of the increment gives

$$\sum M_o = (M + dM) + (V + dV) \frac{dx}{2} + V \frac{dx}{2} - M$$

As the increment dx is reduced to the limit, the term containing the higher-order differential $dV dx$ vanishes in comparison with the others, leaving

$$\boxed{\frac{dM}{dx} = -V} \quad (8)$$

or

$$\boxed{M(x) = - \int V(x) dx} \quad (9)$$

Hence the value of the shear curve at any axial location along the beam is equal to the negative of the slope of the moment curve at that point, and the value of the moment curve at any point is equal to the negative of the area under the shear curve up to that point.

The shear and moment curves can be obtained by successive integration of the $q(x)$ distribution, as illustrated in the following example.

Example 2

Consider a cantilevered beam subjected to a negative distributed load $q(x) = -q_0 = \text{constant}$ as shown in Fig. 9; then

$$V(x) = - \int q(x) dx = q_0 x + c_1$$

where c_1 is a constant of integration. A free body diagram of a small sliver of length near $x = 0$ shows that $V(0) = 0$, so the c_1 must be zero as well. The moment function is obtained by integrating again:

$$M(x) = - \int V(x) dx = -\frac{1}{2} q_0 x^2 + c_2$$

where c_2 is another constant of integration that is also zero, since $M(0) = 0$.

Admittedly, this problem was easy because we picked one with null boundary conditions, and with only one loading segment. When concentrated or distributed loads are found at different

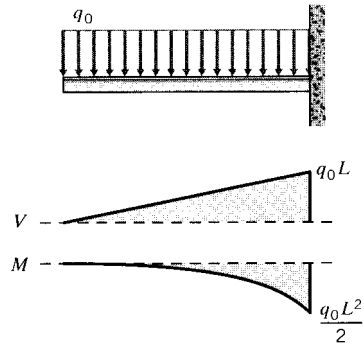


Figure 9: Shear and moment distributions in a cantilevered beam.

positions along the beam, it is necessary to integrate over each section between loads separately. Each integration will produce an unknown constant, and these must be determined by invoking the continuity of slopes and deflections from section to section. This is a laborious process, but one that can be made much easier using *singularity functions* that will be introduced shortly.

It is often possible to sketch V and M diagrams without actually drawing free body diagrams or writing equilibrium equations. This is made easier because the curves are integrals or derivatives of one another, so graphical sketching can take advantage of relations among slopes and areas.

These rules can be used to work gradually from the $q(x)$ curve to $V(x)$ and then to $M(x)$. Wherever a concentrated load appears on the beam, the $V(x)$ curve must jump by that value, but in the opposite direction; similarly, the $M(x)$ curve must jump discontinuously wherever a couple is applied to the beam.

Example 3

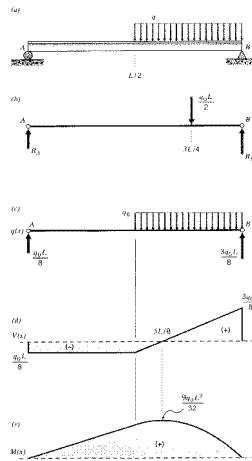


Figure 10: A simply supported beam.

To illustrate this process, consider a simply-supported beam of length L as shown in Fig. 10, loaded

over half its length by a negative distributed load $q = -q_0$. The solution for $V(x)$ and $M(x)$ takes the following steps:

1. The reactions at the supports are found from static equilibrium. Replacing the distributed load by a concentrated load $Q = -q_0(L/2)$ at the midpoint of the q distribution (Fig. 10(b)) and taking moments around A :

$$R_B L = \left(\frac{q_0 L}{2}\right) \left(\frac{3L}{4}\right) \Rightarrow R_B = \frac{3q_0 L}{8}$$

The reaction at the right end is then found from a vertical force balance:

$$R_A = \frac{q_0 L}{2} - R_B = \frac{q_0 L}{8}$$

Note that only two equilibrium equations were available, since a horizontal force balance would provide no relevant information. Hence the beam will be statically indeterminate if more than two supports are present.

The $q(x)$ diagram is then just the beam with the end reactions shown in Fig. 10(c).

2. Beginning the shear diagram at the left, V immediately jumps down to a value of $-q_0 L/8$ in opposition to the discontinuously applied reaction force at A ; it remains at this value until $x = L/2$ as shown in Fig. 10(d).
3. At $x = L/2$, the $V(x)$ curve starts to rise with a constant slope of $+q_0$ as the area under the $q(x)$ distribution begins to accumulate. When $x = L$, the shear curve will have risen by an amount $q_0 L/2$, the total area under the $q(x)$ curve; its value is then $(-q_0 L/8) + (q_0 L/2) = (3q_0 L/8)$. The shear curve then drops to zero in opposition to the reaction force $R_B = (3q_0 L/8)$. (The V and M diagrams should always close, and this provides a check on the work.)
4. The moment diagram starts from zero as shown in Fig. 10(e), since there is no discontinuously applied moment at the left end. It moves upward at a constant slope of $+q_0 L/8$, the value of the shear diagram in the first half of the beam. When $x = L/2$, it will have risen to a value of $q_0 L^2/16$.
5. After $x = L/2$, the slope of the moment diagram starts to fall as the value of the shear diagram rises. The moment diagram is now parabolic, always being one order higher than the shear diagram. The shear diagram crosses the $V = 0$ axis at $x = 5L/8$, and at this point the slope of the moment diagram will have dropped to zero. The maximum value of M is $9q_0 L^2/32$, the total area under the V curve up to this point.
6. After $x = 5L/8$, the moment diagram falls parabolically, reaching zero at $x = L$.

Singularity functions

This special family of functions provides an automatic way of handling the irregularities of loading that usually occur in beam problems. They are much like conventional polynomial factors, but with the property of being zero until “activated” at desired points along the beam. The formal definition is

$$f_n(x) = \langle x - a \rangle^n = \begin{cases} 0, & x < a \\ (x - a)^n, & x > a \end{cases} \quad (10)$$

where $n = -2, -1, 0, 1, 2, \dots$. The function $\langle x - a \rangle^0$ is a unit step function, $\langle x - a \rangle_{-1}$ is a concentrated load, and $\langle x - a \rangle_{-2}$ is a concentrated couple. The first five of these functions are sketched in Fig. 11.

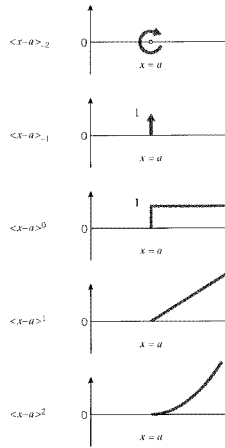


Figure 11: Singularity functions.

The singularity functions are integrated much like conventional polynomials:

$$\int_{-\infty}^x \langle x - a \rangle^n dx = \frac{\langle x - a \rangle^{n+1}}{n + 1} \quad n \geq 0 \quad (11)$$

However, there are special integration rules for the $n = -1$ and $n = -2$ members, and this special handling is emphasized by using subscripts for the n index:

$$\int_{-\infty}^x \langle x - a \rangle_{-2} dx = \langle x - a \rangle_{-1} \quad (12)$$

$$\int_{-\infty}^x \langle x - a \rangle_{-1} dx = \langle x - a \rangle^0 \quad (13)$$

Example 4

Applying singularity functions to the beam of Example 4.3, the loading function would be written

$$q(x) = +\frac{q_0 L}{8} \langle x - 0 \rangle_{-1} - q_0 \langle x - \frac{L}{2} \rangle^0$$

The reaction force at the right end could also be included, but it becomes activated only as the problem is over. Integrating once:

$$V(x) = - \int q(x) dx = -\frac{q_0 L}{8} \langle x \rangle^0 + q_0 \langle x - \frac{L}{2} \rangle^1$$

The constant of integration is included automatically here, since the influence of the reaction at A has been included explicitly. Integrating again:

$$M(x) = - \int V(x) dx = \frac{q_0 L}{8} \langle x \rangle^1 - \frac{q_0}{2} \langle x - \frac{L}{2} \rangle^2$$

Examination of this result will show that it is the same as that developed previously.

Maple™ symbolic manipulation software provides an efficient means of plotting these functions. The following shows how the moment equation of this example might be plotted, using the Heaviside function to provide the singularity.


```

# Define function sfn in terms of a and n
>sfn:=proc(a,n) (x-a)^n*Heaviside(x-a) end;

      sfn := proc(a, n) (x - a)^n*Heaviside(x - a) end proc

# Input moment equation using singularity functions
>M(x):=(q*L/8)*sfn(0,1)-(q/2)*sfn(L/2,2);

      M(x) := 1/8 q L x Heaviside(x)
              2
              - 1/2 q (x - 1/2 L) Heaviside(x - 1/2 L)

# Provide numerical values for q and L:
>q:=1: L:=10:

# Plot function
>plot(M(x),x=0..10);

```

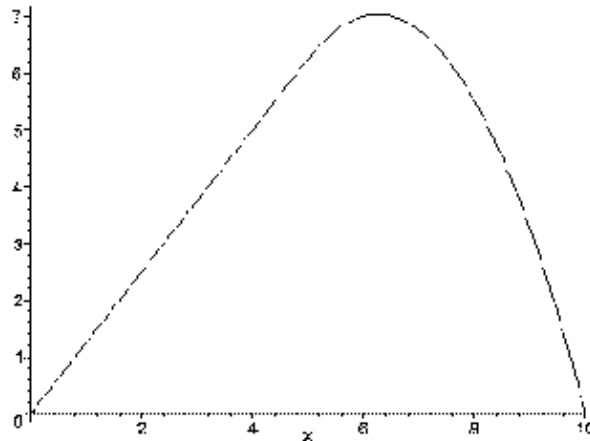
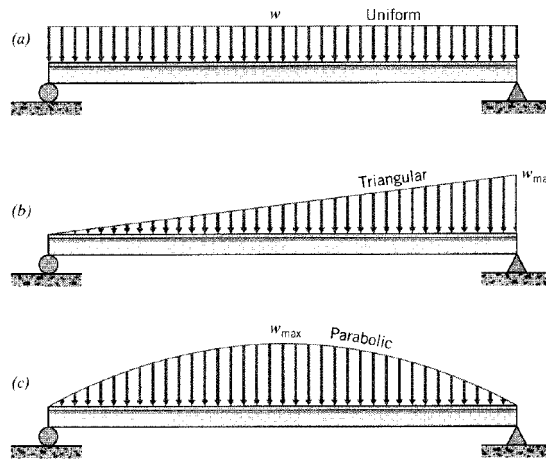


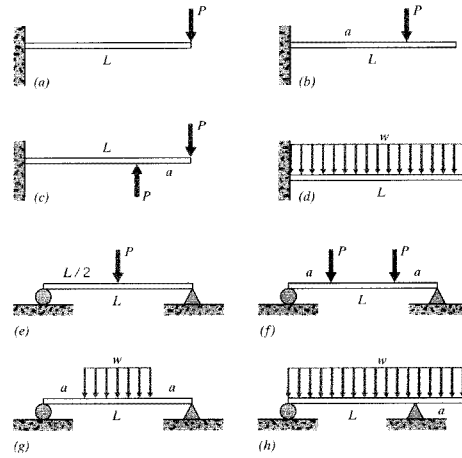
Figure 12: Maple singularity plot

Problems

- (a)–(c) Locate the magnitude and position of the force equivalent to the loading distributions shown here.
- (a)–(c) Determine the reaction forces at the supports of the cases in Prob. 1.
- (a)–(h) Sketch the shear and bending moment diagrams for the load cases shown here.
- (a)–(h) Write singularity-function expressions for the shear and bending moment distributions for the cases in Prob. 3.
- (a)–(h) Use Maple (or other) software to plot the shear and bending moment distributions for the cases in Prob. 3, using the values (as needed) $L = 25$ in, $a = 5$ in, $w = 10$ lb/in, $P = 150$ lb.

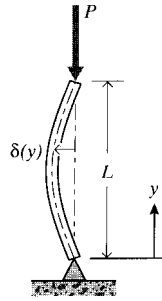


Prob. 1

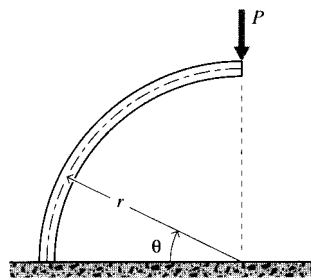


Prob. 3

6. The transverse deflection of a beam under an axial load P is taken to be $\delta(y) = \delta_0 \sin(y\pi/L)$, as shown here. Determine the bending moment $M(y)$ along the beam.
7. Determine the bending moment $M(\theta)$ along the circular curved beam shown.



Prob. 6



Prob. 7

STRESSES IN BEAMS

David Roylance
Department of Materials Science and Engineering
Massachusetts Institute of Technology
Cambridge, MA 02139

November 21, 2000

Introduction

Understanding of the stresses induced in beams by bending loads took many years to develop. Galileo worked on this problem, but the theory as we use it today is usually credited principally to the great mathematician Leonard Euler (1707–1783). As will be developed below, beams develop normal stresses in the lengthwise direction that vary from a maximum in tension at one surface, to zero at the beam's midplane, to a maximum in compression at the opposite surface. Shear stresses are also induced, although these are often negligible in comparison with the normal stresses when the length-to-height ratio of the beam is large. The procedures for calculating these stresses for various loading conditions and beam cross-section shapes are perhaps the most important methods to be found in introductory Mechanics of Materials, and will be developed in the sections to follow. This theory requires that the user be able to construct shear and bending moment diagrams for the beam, as developed for instance in Module 12.

Normal Stresses

A beam subjected to a positive bending moment will tend to develop a concave-upward curvature. Intuitively, this means the material near the top of the beam is placed in compression along the x direction, with the lower region in tension. At the transition between the compressive and tensile regions, the stress becomes zero; this is the *neutral axis* of the beam. If the material tends to fail in tension, like chalk or glass, it will do so by crack initiation and growth from the lower tensile surface. If the material is strong in tension but weak in compression, it will fail at the top compressive surface; this might be observed in a piece of wood by a compressive buckling of the outer fibers.

We seek an expression relating the magnitudes of these axial normal stresses to the shear and bending moment within the beam, analogously to the shear stresses induced in a circular shaft by torsion. In fact, the development of the needed relations follows exactly the same direct approach as that used for torsion:

1. *Geometrical statement:* We begin by stating that originally transverse planes within the beam remain planar under bending, but rotate through an angle θ about points on the neutral axis as shown in Fig. 1. For small rotations, this angle is given approximately by

the x -derivative of the beam's vertical deflection function $v(x)$ ¹:

$$u = -yv_{,x} \quad (1)$$

where the comma indicates differentiation with respect to the indicated variable ($v_{,x} \equiv dv/dx$). Here y is measured positive upward from the neutral axis, whose location within the beam has not yet been determined.

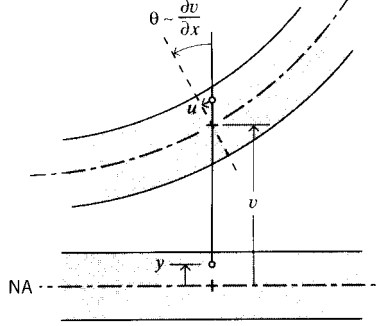


Figure 1: Geometry of beam bending.

2. *Kinematic equation:* The x -direction normal strain ϵ_x is then the gradient of the displacement:

$$\epsilon_x = \frac{du}{dx} = -yv_{,xx} \quad (2)$$

Note that the strains are zero at the neutral axis where $y = 0$, negative (compressive) above the axis, and positive (tensile) below. They increase in magnitude linearly with y , much as the shear strains increased linearly with r in a torsionally loaded circular shaft. The quantity $v_{,xx} \equiv d^2v/dx^2$ is the spatial rate of change of the slope of the beam deflection curve, the “slope of the slope.” This is called the *curvature* of the beam.

3. *Constitutive equation:* The stresses are obtained directly from Hooke’s law as

$$\sigma_x = E\epsilon_x = -yEv_{,xx} \quad (3)$$

This restricts the applicability of this derivation to linear elastic materials. Hence the axial normal stress, like the strain, increases linearly from zero at the neutral axis to a maximum at the outer surfaces of the beam.

4. *Equilibrium relations:* Since there are no axial (x -direction) loads applied externally to the beam, the total axial force generated by the normal σ_x stresses (shown in Fig. 2) must be zero. This can be expressed as

¹The exact expression for curvature is

$$\frac{d\theta}{ds} = \frac{d^2v/dx^2}{[1 + (dv/dx)^2]^{3/2}}$$

This gives $\theta \approx dv/dx$ when the squared derivative in the denominator is small compared to 1.

$$\sum F_x = 0 = \int_A \sigma_x dA = \int_A -yEv_{,xx} dA$$

which requires that

$$\int_A y dA = 0$$

The distance \bar{y} from the neutral axis to the centroid of the cross-sectional area is

$$\bar{y} = \frac{\int_A y dA}{\int_A dA}$$

Hence $\bar{y} = 0$, i.e. the neutral axis is coincident with the centroid of the beam cross-sectional area. This result is obvious on reflection, since the stresses increase at the same linear rate, above the axis in compression and below the axis in tension. Only if the axis is exactly at the centroidal position will these stresses balance to give zero net horizontal force and keep the beam in horizontal equilibrium.

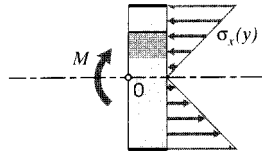


Figure 2: Moment and force equilibrium in the beam.

The normal stresses in compression and tension are balanced to give a zero net horizontal force, but they also produce a net clockwise moment. This moment must equal the value of $M(x)$ at that value of x , as seen by taking a moment balance around point O :

$$\sum M_O = 0 = M + \int_A \sigma_x \cdot y dA$$

$$M = \int_A (yEv_{,xx}) \cdot y dA = Ev_{,xx} \int_A y^2 dA \quad (4)$$

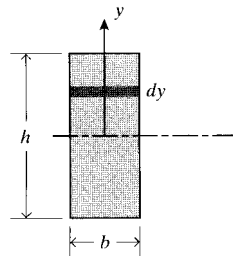


Figure 3: Moment of inertia for a rectangular section.

The quantity $\int y^2 dA$ is the rectangular moment of inertia with respect to the centroidal axis, denoted I . For a rectangular cross section of height h and width b as shown in Fig. 3 this is:

$$I = \int_{-h/2}^{h/2} y^2 b dy = \frac{bh^3}{12} \quad (5)$$

Solving Eqn. 4 for $v_{,xx}$, the beam curvature is

$$\boxed{v_{,xx} = \frac{M}{EI}} \quad (6)$$

5. An explicit formula for the stress can be obtained by using this in Eqn. 3:

$$\boxed{\sigma_x = -yE \frac{M}{EI} = \frac{-My}{I}} \quad (7)$$

The final expression for stress, Eqn. 7, is similar to $\tau_{\theta z} = Tr/J$ for twisted circular shafts: the stress varies linearly from zero at the neutral axis to a maximum at the outer surface, it varies inversely with the moment of inertia of the cross section, and it is independent of the material's properties. Just as a designer will favor annular drive shafts to maximize the polar moment of inertia J , beams are often made with wide flanges at the upper and lower surfaces to increase I .

Example 1

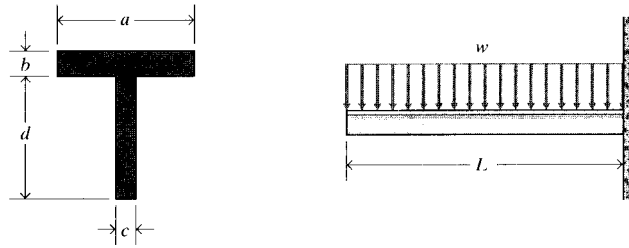


Figure 4: A cantilevered T-beam.

Consider a cantilevered T-beam with dimensions as shown in Fig. 4, carrying a uniform loading of w N/m. The maximum bending moment occurs at the wall, and is easily found to be $M_{max} = (wL)(L/2)$. The stress is then given by Eqn. 7, which requires that we know the location of the neutral axis (since y and I are measured from there).

The distance \bar{y} from the bottom of the beam to the centroidal neutral axis can be found using the “composite area theorem” (see Prob. 1). This theorem states that the distance from an arbitrary axis to the centroid of an area made up of several subareas is the sum of the subareas times the distance to their individual centroids, divided by the sum of the subareas (i.e. the total area):

$$\bar{y} = \frac{\sum_i A_i \bar{y}_i}{\sum_i A_i}$$

For our example, this is

$$\bar{y} = \frac{(d/2)(cd) + (d + b/2)(ab)}{cd + ab}$$

The moments of inertia of the individual parts of the compound area with respect to their own centroids are just $ab^3/12$ and $cd^3/12$. These moments can be referenced to the horizontal axis through the centroid of the compound area using the “parallel axis theorem” (see Prob. 3). This theorem states that the moment of inertia $I_{z'}$ of an area A , relative to any arbitrary axis z' parallel to an axis through the centroid but a distance d from it, is the moment of inertia relative to the centroidal axis I_z plus the product of the area A and the square of the distance d :

$$I_{z'} = I_z + Ad^2$$

For our example, this is

$$I^{(1)} = \frac{ab^3}{12} + (ab) \left(d + \frac{b}{2} - \bar{y} \right)^2$$

$$I^{(2)} = \frac{cd^3}{12} + (cd) \left(\frac{d}{2} - \bar{y} \right)^2$$

The moment of inertia of the entire compound area, relative to its centroid, is then the sum of these two contributions:

$$I = I^{(1)} + I^{(2)}$$

The maximum stress is then given by Eqn. 7 using this value of I and $y = \bar{y}/2$ (the distance from the neutral axis to the outer fibers), along with the maximum bending moment M_{max} . The result of these substitutions is

$$\sigma_x = \frac{(3d^2c + 6abd + 3ab^2)wL^2}{2c^2d^4 + 8abcd^3 + 12ab^2cd^2 + 8ab^3cd + 2a^2b^4}$$

In practice, each step would likely be reduced to a numerical value rather than working toward an algebraic solution.

In pure bending (only bending moments applied, no transverse or longitudinal forces), the only stress is σ_x as given by Eqn. 7. All other stresses are zero ($\sigma_y = \sigma_z = \tau_{xy} = \tau_{xz} = \tau_{yz} = 0$). However, strains other than ϵ_x are present, due to the Poisson effect. This does not generate shear strain ($\gamma_{xy} = \gamma_{xz} = \gamma_{yz} = 0$), but the normal strains are

$$\epsilon_x = \frac{1}{E}[\sigma_x - \nu(\sigma_y + \sigma_z)] = \frac{\sigma_x}{E}$$

$$\epsilon_y = \frac{1}{E}[\sigma_y - \nu(\sigma_x + \sigma_z)] = -\nu \frac{\sigma_x}{E}$$

$$\epsilon_z = \frac{1}{E}[\sigma_z - \nu(\sigma_x + \sigma_y)] = -\nu \frac{\sigma_x}{E}$$

The strains can also be written in terms of curvatures. From Eqn. 2, the curvature along the beam is

$$v_{,xx} = -\frac{\epsilon_x}{y}$$

This is accompanied by a curvature transverse to the beam axis given by

$$v_{,zz} = -\frac{\epsilon_z}{y} = \frac{\nu\epsilon_x}{y} = -\nu v_{,xx}$$

This transverse curvature, shown in Fig. 5, is known as *anticlastic curvature*; it can be seen by bending a “Pink Pearl” type eraser in the fingers.

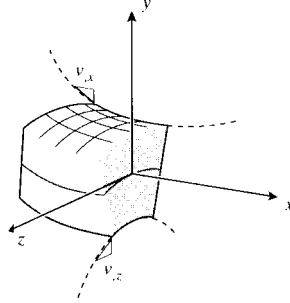


Figure 5: Anticlastic curvature.

As with tension and torsion structures, bending problems can often be done more easily with energy methods. Knowing the stress from Eqn. 7, the strain energy due to bending stress U_b can be found by integrating the strain energy per unit volume $U^* = \sigma^2/2E$ over the specimen volume:

$$\begin{aligned} U_b &= \int_V U^* dV = \int_L \int_A \frac{\sigma_x^2}{2E} dA dL \\ &= \int_L \int_A \frac{1}{2E} \left(\frac{-My}{I} \right)^2 dA dL = \int_L \frac{M^2}{2EI^2} \int_A y^2 dA dL \end{aligned}$$

Since $\int_A y^2 dA = I$, this becomes

$$\boxed{U_b = \int_L \frac{M^2 dL}{2EI}} \quad (8)$$

If the bending moment is constant along the beam (definitely *not* the usual case), this becomes

$$U = \frac{M^2 L}{2EI}$$

This is another analog to the expression for uniaxial tension, $U = P^2 L/2AE$.

Buckling

Long slender columns placed in compression are prone to fail by buckling, in which the column develops a kink somewhere along its length and quickly collapses unless the load is relaxed. This is actually a bending phenomenon, driven by the bending moment that develops if and when the beam undergoes a transverse deflection. Consider a beam loaded in axial compression and pinned at both ends as shown in Fig. 6. Now let the beam be made to deflect transversely by an amount v , perhaps by an adventitious sideward load or even an irregularity in the beam’s cross section. Positions along the beam will experience a moment given by

$$M(x) = Pv(x) \quad (9)$$

The beam's own stiffness will act to restore the deflection and recover a straight shape, but the effect of the bending moment is to deflect the beam *more*. It's a battle over which influence wins out. If the tendency of the bending moment to increase the deflection dominates over the ability of the beam's elastic stiffness to resist bending, the beam will become unstable, continuing to bend at an accelerating rate until it fails.

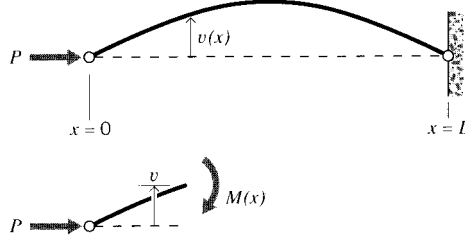


Figure 6: Imminent buckling in a beam.

The bending moment is related to the beam curvature by Eqn. 6, so combining this with Eqn. 9 gives

$$v_{,xx} = \frac{P}{EI} v \quad (10)$$

Of course, this governing equation is satisfied identically if $v = 0$, i.e. the beam is straight. We wish to look beyond this trivial solution, and ask if the beam could adopt a *bent* shape that would also satisfy the governing equation; this would imply that the stiffness is insufficient to restore the unbent shape, so that the beam is beginning to buckle. Equation 10 will be satisfied by functions that are proportional to their own second derivatives. Trigonometric functions have this property, so candidate solutions will be of the form

$$v = c_1 \sin \sqrt{\frac{P}{EI}} x + c_2 \cos \sqrt{\frac{P}{EI}} x$$

It is obvious that c_2 must be zero, since the deflection must go to zero at $x = 0$ and L . Further, the sine term must go to zero at these two positions as well, which requires that the length L be exactly equal to a multiple of the half wavelength of the sine function:

$$\sqrt{\frac{P}{EI}} L = n\pi, \quad n = 1, 2, 3, \dots$$

The lowest value of P leading to the deformed shape corresponds to $n = 1$; the critical buckling load P_{cr} is then:

$$\boxed{P_{cr} = \frac{\pi^2 EI}{L^2}} \quad (11)$$

Note the dependency on L^2 , so the buckling load drops with the square of the length.

This strong dependency on length shows why crossbracing is so important in preventing buckling. If a brace is added at the beam's midpoint as shown in Fig. 7 to eliminate deflection

there, the buckling shape is forced to adopt a wavelength of L rather than $2L$. This is equivalent to making the beam half as long, which increases the critical buckling load by a factor of four.

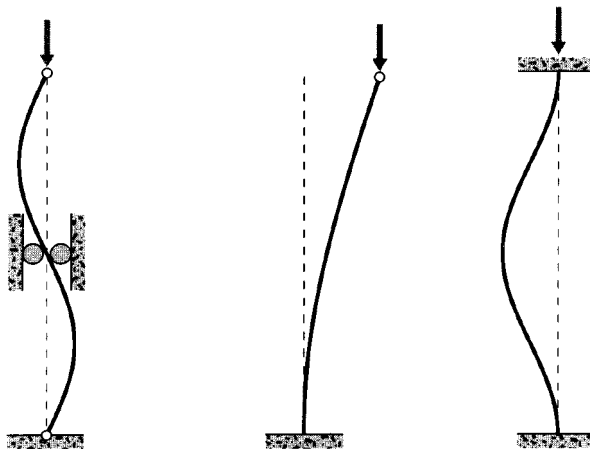


Figure 7: Effect of lateral support and end conditions on beam buckling.

Similar reasoning can be used to assess the result of having different support conditions. If for instance the beam is cantilevered at one end but unsupported at the other, its buckling shape will be a quarter sine wave. This is equivalent to making the beam twice as long as the case with both ends pinned, so the buckling load will go *down* by a factor of four. Cantilevering *both* ends forces a full-wave shape, with the same buckling load as the pinned beam with a midpoint support.

Shear stresses

Transverse loads bend beams by inducing axial tensile and compressive normal strains in the beam's x -direction, as discussed above. In addition, they cause shear effects that tend to slide vertical planes tangentially to one another as depicted in Fig. 8, much like sliding playing cards past one another. The stresses τ_{xy} associated with this shearing effect add up to the vertical shear force we have been calling V , and we now seek to understand how these stresses are distributed over the beam's cross section. The shear stress on vertical planes must be accompanied by an equal stress on horizontal planes since $\tau_{xy} = \tau_{yx}$, and these horizontal shearing stresses must become zero at the upper and lower surfaces of the beam unless a traction is applied there to balance them. Hence they must reach a maximum somewhere within the beam.

The variation of this horizontal shear stress with vertical position y can be determined by examining a free body of width dx cut from the beam a distance y above neutral axis as shown in Fig. 9. The moment on the left vertical face is $M(x)$, and on the right face it has increased to $M + dM$. Since the horizontal normal stresses are directly proportional to the moment ($\sigma_x = My/I$), any increment in moment dM over the distance dx produces an imbalance in the horizontal force arising from the normal stresses. This imbalance must be compensated by a shear stress τ_{xy} on the horizontal plane at y . The horizontal force balance is written as

$$\tau_{xy} b dx = \int_{A'} \frac{dM \xi}{I} dA'$$

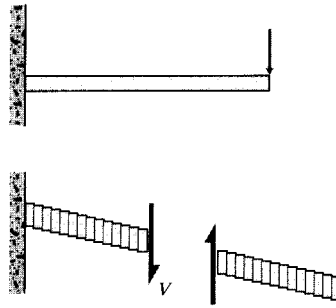


Figure 8: Shearing displacements in beam bending.

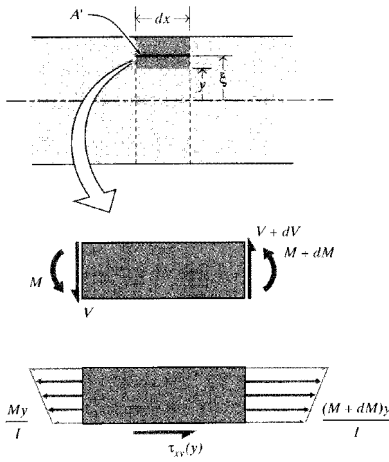


Figure 9: Shear and bending moment in a differential length of beam.

where b is the width of the beam at y , ξ is a dummy height variable ranging from y to the outer surface of the beam, and A' is the cross-sectional area between the plane at y and the outer surface. Using $dM = V dx$ from Eqn. 8 of Module 12, this becomes

$$\tau_{xy} = \frac{V}{Ib} \int_{A'} \xi dA' = \frac{VQ}{Ib} \quad (12)$$

where here $Q(y) = \int_{A'} \xi dA' = \bar{\xi}A'$ is the first moment of the area above y about the neutral axis.

The parameter $Q(y)$ is notorious for confusing persons new to beam theory. To determine it for a given height y relative to the neutral axis, begin by sketching the beam cross section, and draw a horizontal line at the position y at which Q is sought (Fig. 10 shows a rectangular beam of constant width b and height h for illustration). Note the area A' between this line and the outer surface (indicated by cross-hatching in Fig. 10). Now compute the distance $\bar{\xi}$ from the neutral axis to the centroid of A' . The parameter $Q(y)$ is the product of A' and $\bar{\xi}$; this is the first moment of the area A' with respect to the centroidal axis. For the rectangular beam, it is

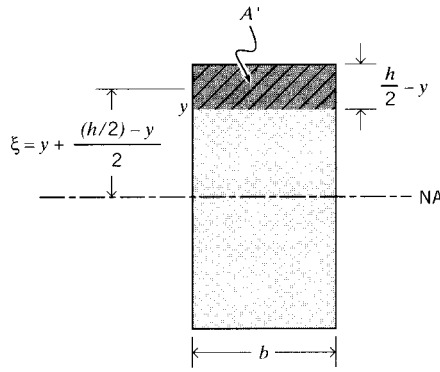


Figure 10: Section of a rectangular beam.

$$Q = A' \bar{\xi} = \left[b \left(\frac{h}{2} - y \right) \right] \left[y + \frac{1}{2} \left(\frac{h}{2} - y \right) \right] = \frac{b}{2} \left(\frac{h^2}{4} - y^2 \right)$$

Note that $Q(y)$, and therefore $\tau_{xy}(y)$ as well, is parabolic, being maximum at the neutral axis ($y = 0$) and zero at the outer surface ($y = h/2$). Using $I = bh^3/12$ for the rectangular beam, the maximum shear stress as given by Eqn. 12 is

$$\tau_{xy,max} = \tau_{xy}|_{y=0} = \frac{3V}{2bh}$$

(Keep in mind that the above two expressions for Q and $\tau_{xy,max}$ are for rectangular cross section only; sections of other shapes will have different results.) These shear stresses are most important in beams that are short relative to their height, since the bending moment usually increases with length and the shear force does not (see Prob. 11). One standard test for interlaminar shear strength² is to place a short beam in bending and observe the load at which cracks develop along the midplane.

Example 2

Since the normal stress is maximum where the horizontal shear stress is zero (at the outer fibers), and the shear stress is maximum where the normal stress is zero (at the neutral axis), it is often possible to consider them one at a time. However, the juncture of the web and the flange in I and T beams is often a location of special interest, since here both stresses can take on substantial values.

Consider the T beam seen previously in Example 1, and examine the location at point A shown in Fig. 11, in the web immediately below the flange. Here the width b in Eqn. 12 is the dimension labeled c ; since the beam is thin here the shear stress τ_{xy} will tend to be large, but it will drop dramatically in the flange as the width jumps to the larger value a . The normal stress at point A is computed from $\sigma_x = My/I$, using $y = d - \bar{y}$. This value will be almost as large as the outer-fiber stress if the flange thickness b is small compared with the web height d . The Mohr's circle for the stress state at point A would then have appreciable contributions from both σ_x and τ_{xy} , and can result in a principal stress larger than at either the outer fibers or the neutral axis.

This problem provides a good review of the governing relations for normal and shear stresses in beams, and is also a natural application for symbolic-manipulation computer methods. Using Maple software, we might begin by computing the location of the centroidal axis:

²“Apparent Horizontal Shear Strength of Reinforced Plastics by Short Beam Method,” ASTM D2344, American Society for Testing and Materials.

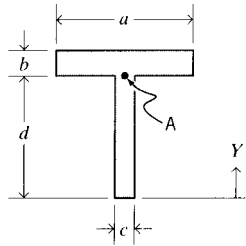


Figure 11: Section of T beam.

```
> ybar := ((d/2)*c*d) + ( (d+(b/2) )*a*b )/( c*d + a*b );
```

Here the “>” symbol is the Maple prompt, and the “;” is needed by Maple to end the command. The maximum shear force and bending moment (present at the wall) are defined in terms of the distributed load and the beam length as

```
> V := w*L;
> M := -(w*L)*(L/2);
```

For plotting purposes, it will be convenient to have a height variable Y measured from the bottom of the section. The relations for normal stress, shear stress, and the first principal stress are functions of Y ; these are defined using the Maple “procedure” command:

```
> sigx := proc (Y) -M*(Y-ybar)/Iz end;
> tauxy := proc (Y) V*Q(Y)/(Iz*B(Y) ) end;
> sigp1 := proc (Y) (sigx(Y)/2) + sqrt( (sigx(Y)/2)^2 + (tauxy(Y))^2 ) end;
```

The moment of inertia I_z is computed as

```
> I1 := (a*b^3)/12 + a*b* (d+(b/2)-ybar)^2;
> I2 := (c*d^3)/12 + c*d* ((d/2)-ybar)^2;
> Iz := I1+I2;
```

The beam width B is defined to take the appropriate value depending on whether the variable Y is in the web or the flange:

```
> B:= proc (Y) if Y<d then B:=c else B:=a fi end;
```

The command “fi” (“if” spelled backwards) is used to end an if-then loop. The function $Q(Y)$ is defined for the web and the flange separately:

```
> Q:= proc (Y) if Y<d then
>   int( (yy-ybar)*c,yy=Y..d) + int( (yy-ybar)*a,yy=d..(d+b) )
> else
>   int( (yy-ybar)*a,yy=Y.. (d+b) )
> fi end;
```

Here “int” is the Maple command for integration, and yy is used as the dummy height variable. The numerical values of the various parameters are defined as

```
> a:=3: b:=1/4: c:=1/4: d:=3-b: L:=8: w:=100:
```

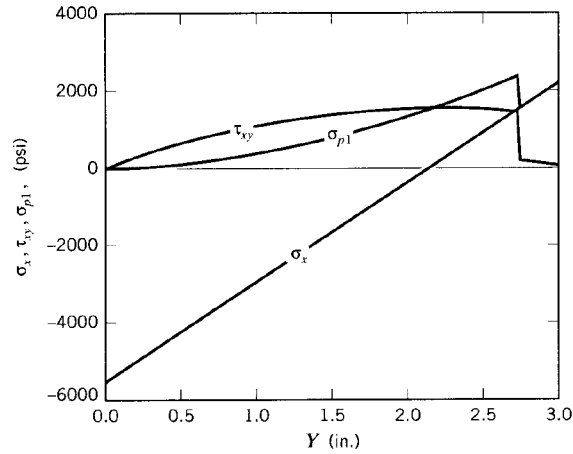


Figure 12: Stresses at the web-flange junction in a short cantilevered T beam subjected to uniform loading.

Finally, the stresses can be graphed using the Maple plot command

```
> plot({sigx,tauxy,sigp1},Y=0..3,sigx=-500..2500);
```

The resulting plot is shown in Fig. 12.

Example 3

In the previous example, we were interested in the variation of stress as a function of height in a beam of irregular cross section. Another common design or analysis problem is that of the variation of stress not only as a function of height but also of distance along the span dimension of the beam. The shear and bending moments $V(x)$ and $M(x)$ vary along this dimension, and so naturally do the stresses $\sigma_x(x, y)$ and $\tau_{xy}(x, y)$ that depend on them according to Eqns. 7 and 12.

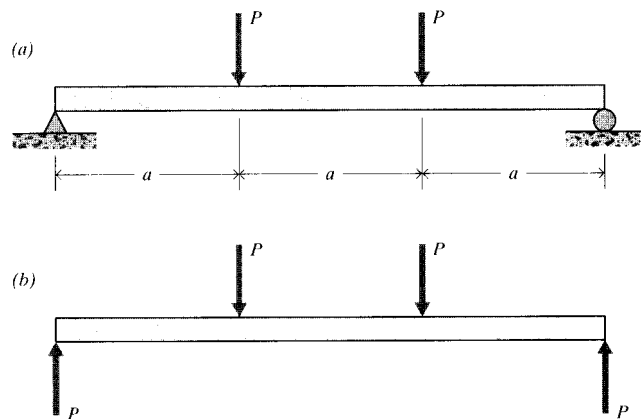


Figure 13: (a) Beam in four-point bending. (b) Free-body diagram.

Consider a short beam of rectangular cross section subjected to four-point loading as seen in Fig. 13. The loading, shear, and bending moment functions are:

$$q(x) = P\langle x \rangle_{-1} - P\langle x - a \rangle_{-1} - P\langle x - 2a \rangle_{-1} + P\langle x - 3a \rangle_{-1}$$

$$V(x) = - \int q(x) dx = -P\langle x \rangle^0 + P\langle x - a \rangle^0 + P\langle x - 2a \rangle^0 - P\langle x - 3a \rangle^0$$

$$M(x) = - \int V(x) dx = P\langle x \rangle^1 - P\langle x - a \rangle^1 - P\langle x - 2a \rangle^1 + P\langle x - 3a \rangle^1$$

The shear and normal stresses can be determined as functions of x and y directly from these functions, as well as such parameters as the principal stress. Since σ_y is zero everywhere, the principal stress is

$$\sigma_{p1} = \frac{\sigma_x}{2} + \sqrt{\left(\frac{\sigma_x}{2}\right)^2 + \tau_{xy}^2}$$

One way to visualize the x - y variation of σ_{p1} is by means of a 3D surface plot, which can be prepared easily by Maple. For the numerical values $P = 100, a = h = 10, b = 3$, we could use the expressions (Maple responses removed for brevity):

```
> # use Heaviside for singularity functions
> readlib(Heaviside);
> sfm := proc(x,a,n) (x-a)^n * Heaviside(x-a) end;
> # define shear and bending moment functions
> V:=(x)-> -P*sfn(x,0,0)+P*sfn(x,a,0)+P*sfn(x,2*a,0)-P*sfn(x,3*a,0);
> M:=(x)-> P*sfn(x,0,1)-P*sfn(x,a,1)-P*sfn(x,2*a,1)+P*sfn(x,3*a,1);
> # define shear stress function
> tau:=V(x)*Q/(Iz*b);
> Q:=(b/2)*( h^2/4 -y^2);
> Iz:=b*h^3/12;
> # define normal stress function
> sig:=M(x)*y/Iz;
> # define principal stress
> sigp:=(sig/2) + sqrt( (sig/2)^2 + tau^2 );
> # define numerical parameters
> P:=100;a:=10;h:=10;b:=3;
> # make plot
> plot3d(sigp,x=0..3*a,y=-h/2 .. h/2);
```

The resulting plot is shown in Fig. 14. The dominance of the parabolic shear stress is evident near the beam ends, since here the shear force is at its maximum value but the bending moment is small (plot the shear and bending moment diagrams to confirm this). In the central part of the beam, where $a < x < 2a$, the shear force vanishes and the principal stress is governed only by the normal stress σ_x , which varies linearly from the beam's neutral axis. The first principal stress is zero in the compressive lower part of this section, since here the normal stress σ_x is negative and the right edge of the Mohr's circle must pass through the zero value of the other normal stress σ_y . Working through the plot of Fig. 14 is a good review of the beam stress formulas.

Problems

1. Derive the composite area theorem for determining the centroid of a compound area.

$$\bar{y} = \frac{\sum_i A_i \bar{y}_i}{\sum_i A_i}$$

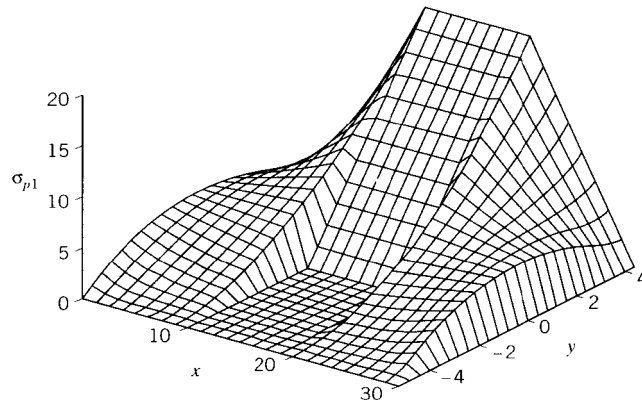
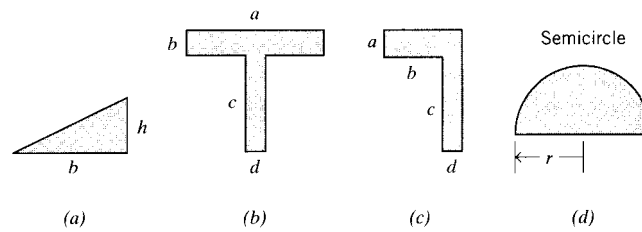


Figure 14: Variation of principal stress σ_{p1} in four-point bending.

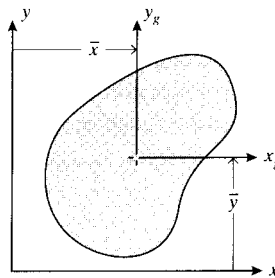


Prob. 2

2. (a)–(d) Locate the centroids of the areas shown.
3. Derive the “parallel-axis theorem” for moments of inertia of a plane area:

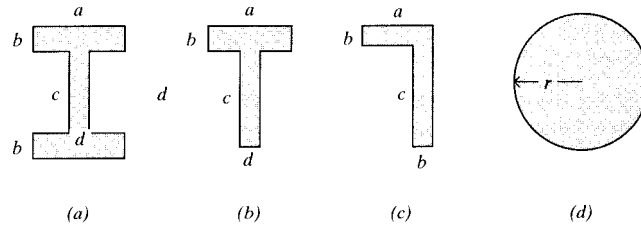
$$I_x = I_{xg} + A\bar{y}^2$$

$$I_y = I_{yg} + A\bar{x}^2$$



Prob. 3

4. (a)–(d) Determine the moment of inertia relative to the horizontal centroidal axis of the areas shown.



Prob. 4

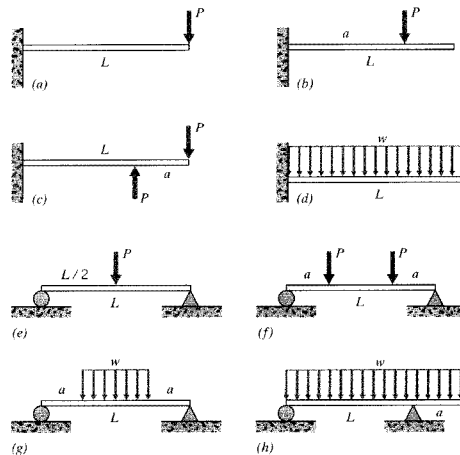
5. Show that the moment of inertia transforms with respect to axis rotations exactly as does the stress:

$$I_{x'} = I_x \cos^2 \theta + I_y \sin^2 \theta - 2I_{xy} \sin \theta \cos \theta$$

where I_x and I_y are the moments of inertia relative to the x and y axes respectively and I_{xy} is the *product of inertia* defined as

$$I_{xy} = \int_A xy \, dA$$

6. (a)–(h) Determine the maximum normal stress σ_x in the beams shown here, using the values (as needed) $L = 25$ in, $a = 5$ in, $w = 10$ lb/in, $P = 150$ lb. Assume a rectangular cross-section of width $b = 1$ in and height $h = 2$ in.



Prob. 6

7. Justify the statement in ASTM test D790, “Standard Test Methods for Flexural Properties of Unreinforced and Reinforced Plastics and Electrical Insulating Materials,” which reads:

When a beam of homogeneous, elastic material is tested in flexure as a simple beam supported at two points and loaded at the midpoint, the maximum stress in the outer fibers occurs at midspan. This stress may be calculated for any point on the load-deflection curve by the following equation:

$$S = 3PL/2bd^2$$

where S = stress in the outer fibers at midspan, MPa; P = load at a given point on the load-deflection curve; L = support span, mm; b = width of beam tested, mm; and d = depth of beam tested, mm.

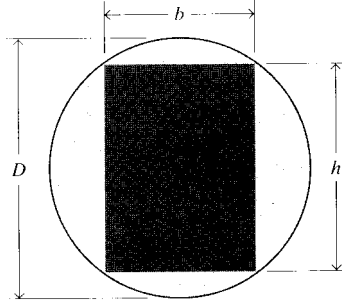
8. Justify the statement in ASTM test D790, "Standard Test Methods for Flexural Properties of Unreinforced and Reinforced Plastics and Electrical Insulating Materials," which reads:

The tangent modulus of elasticity, often called the "modulus of elasticity," is the ratio, within the elastic limit of stress to corresponding strain and shall be expressed in megapascals. It is calculated by drawing a tangent to the steepest initial straight-line portion of the load-deflection curve and using [the expression:]

$$E_b = L^3 m / 4bd^3$$

where E_b = modulus of elasticity in bending, MPa; L = support span, mm; d = depth of beam tested, mm; and m = slope of the tangent to the initial straight-line portion of the load-deflection curve, N/mm of deflection.

9. A rectangular beam is to be milled from circular stock as shown. What should be the ratio of height to width (b/h) to as to minimize the stresses when the beam is put into bending?

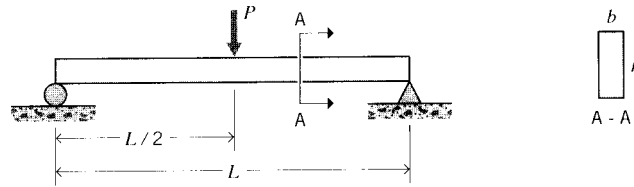


Prob. 9

10. (a)–(h) Determine the maximum shear τ_{xy} in the beams of Prob. 6, , using the values (as needed) $L = 25$ in, $a = 5$ in, $w = 10$ lb/in, $P = 150$ lb. Assume a rectangular cross-section of width $b = 1$ in and height $h = 2$ in.
11. Show that the ratio of maximum shearing stress to maximum normal stress in a beam subjected to 3-point bending is

$$\frac{\tau}{\sigma} = \frac{h}{2L}$$

Hence the importance of shear stress increases as the beam becomes shorter in comparison with its height.



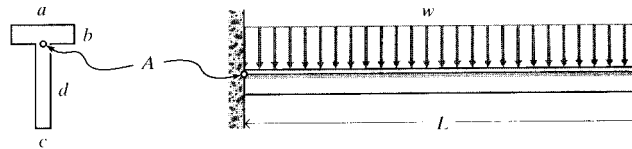
Prob. 11

12. Read the ASTM test D4475, “Standard Test Method for Apparent Horizontal Shear Strength of Pultruded Reinforced Plastic Rods By The Short-Beam Method,” and justify the expression given there for the apparent shear strength:

$$S = 0.849P/d^2$$

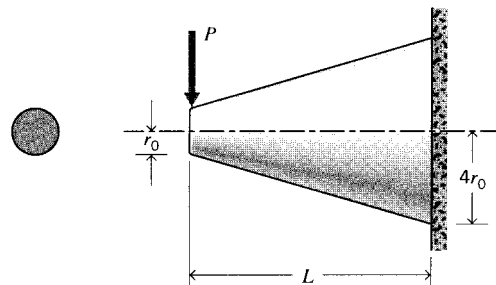
where S = apparent shear strength, N/m², (or psi); P = breaking load, N, (or lbf); and d = diameter of specimen, m (or in.).

13. For the T beam shown here, with dimensions $L = 3$, $a = 0.05$, $b = 0.005$, $c = 0.005$, $d = 0.7$ (all in m) and a loading distribution of $w = 5000$ N/m, determine the principal and maximum shearing stress at point A.



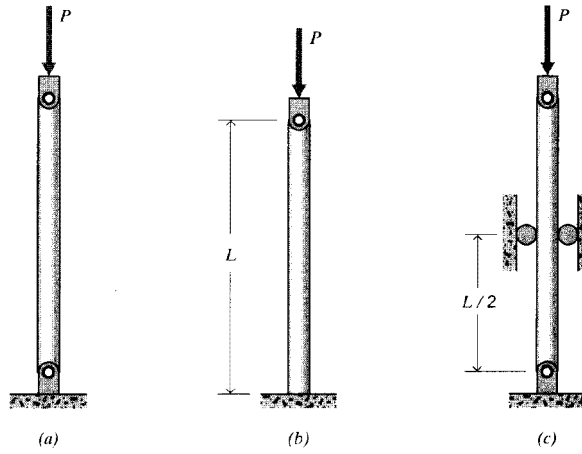
Prob. 13

14. Determine the maximum normal stress in a cantilevered beam of circular cross section whose radius varies linearly from $4r_0$ to r_0 in a distance L , loaded with a force P at the free end.



Prob. 14

15. A carbon steel column has a length $L = 1$ m and a circular cross section of diameter $d = 20$ mm. Determine the critical buckling load P_c for the case of (a) both ends pinned, (b) one end cantilevered, (c) both ends pinned but supported laterally at the midpoint.



Prob. 15

16. A carbon steel column has a length $L = 1$ m and a circular cross section. Determine the diameter d at which the column has an equal probability of buckling or yielding in compression.

Beam Displacements

David Roylance
Department of Materials Science and Engineering
Massachusetts Institute of Technology
Cambridge, MA 02139

November 30, 2000

Introduction

We want to be able to predict the deflection of beams in bending, because many applications have limitations on the amount of deflection that can be tolerated. Another common need for deflection analysis arises from materials testing, in which the transverse deflection induced by a bending load is measured. If we know the relation expected between the load and the deflection, we can “back out” the material properties (specifically the modulus) from the measurement. We will show, for instance, that the deflection at the midpoint of a beam subjected to “three-point bending” (beam loaded at its center and simply supported at its edges) is

$$\delta_P = \frac{PL^3}{48EI}$$

where the length L and the moment of inertia I are geometrical parameters. If the ratio of δ_P to P is measured experimentally, the modulus E can be determined. A stiffness measured this way is called the *flexural modulus*.

There are a number of approaches to the beam deflection problem, and many texts spend a good deal of print on this subject. The following treatment outlines only a few of the more straightforward methods, more with a goal of understanding the general concepts than with developing a lot of facility for doing them manually. In practice, design engineers will usually consult handbook tabulations of deflection formulas as needed, so even before the computer age many of these methods were a bit academic.

Multiple integration

In Module 12, we saw how two integrations of the loading function $q(x)$ produces first the shear function $V(x)$ and then the moment function $M(x)$:

$$V = - \int q(x) dx + c_1 \tag{1}$$

$$M = - \int V(x) dx + c_2 \tag{2}$$

where the constants of integration c_1 and c_2 are evaluated from suitable boundary conditions on V and M . (If singularity functions are used, the boundary conditions are included explicitly and the integration constants c_1 and c_2 are identically zero.) From Eqn. 6 in Module 13, the curvature

$v_{,xx}(x)$ is just the moment divided by the section modulus EI . Another two integrations then give

$$v_{,x}(x) = \frac{1}{EI} \int M(x) dx + c_3 \quad (3)$$

$$v(x) = \int v_{,x}(x) dx + c_4 \quad (4)$$

where c_3 and c_4 are determined from boundary conditions on slope or deflection.

Example 1

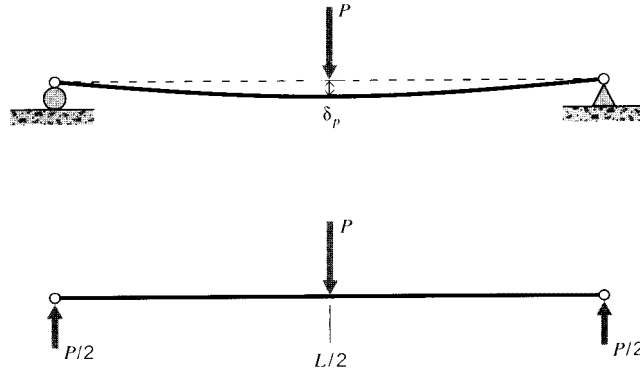


Figure 1: Three-point bending.

As an illustration of this process, consider the case of “three-point bending” shown in Fig. 1. This geometry is often used in materials testing, as it avoids the need to clamp the specimen to the testing apparatus. If the load P is applied at the midpoint, the reaction forces at A and B are equal to half the applied load. The loading function is then

$$q(x) = \frac{P}{2} \langle x \rangle_{-1} - P \langle x - \frac{L}{2} \rangle_{-1}$$

Integrating according to the above scheme:

$$V(x) = -\frac{P}{2} \langle x \rangle^0 + P \langle x - \frac{L}{2} \rangle^0$$

$$M(x) = \frac{P}{2} \langle x \rangle^1 - P \langle x - \frac{L}{2} \rangle^1 \quad (5)$$

$$EIv_{,x}(x) = \frac{P}{4} \langle x \rangle^2 - \frac{P}{2} \langle x - \frac{L}{2} \rangle^2 + c_3$$

From symmetry, the beam has zero slope at the midpoint. Hence $v_{,x} = 0$ @ $x = L/2$, so c_3 can be found to be $-PL^2/16$. Integrating again:

$$EIv(x) = \frac{P}{12} \langle x \rangle^3 - \frac{P}{6} \langle x - \frac{L}{2} \rangle^3 - \frac{PL^2x}{16} + c_4$$

The deflection is zero at the left end, so $c_4 = 0$. Rearranging, the beam deflection is given by

$$v = \frac{P}{48EI} \left[4x^3 - 3L^2x - 8\left(x - \frac{L}{2}\right)^3 \right] \quad (6)$$

The maximum deflection occurs at $x = L/2$, which we can evaluate just before the singularity term activates. Then

$$\boxed{\delta_{\max} = \frac{PL^3}{48EI}} \quad (7)$$

This expression is much used in flexural testing, and is the example used to begin this module.

Before the loading function $q(x)$ can be written, the reaction forces at the beam supports must be determined. If the beam is statically determinate, as in the above example, this can be done by invoking the equations of static equilibrium. Static determinacy means only two reaction forces or moments can be present, since we have only a force balance in the direction transverse to the beam axis and one moment equation available. A simply supported beam (one resting on only two supports) or a simply cantilevered beam are examples of such determinate beams; in the former case there is one reaction force at each support, and in the latter case there is one transverse force and one moment at the clamped end.

Of course, there is no stringent engineering reason to limit the number of beam supports to those sufficient for static equilibrium. Adding “extra” supports will limit deformations and stresses, and this will often be worthwhile in spite of the extra construction expense. But the analysis is now a bit more complicated, since not all of the unknown reactions can be found from the equations of static equilibrium. In these statically indeterminate cases it will be necessary to invoke geometrical constraints to develop enough equations to solve the problem.

This is done by writing the slope and deflection equations, carrying the unknown reaction forces and moments as undetermined parameters. The slopes and deflections are then set to their known values at the supports, and the resulting equations solved for the unknowns. If for instance a beam is resting on three supports, there will be three unknown reaction forces, and we will need a total of five equations: three for the unknown forces and two more for the constants of integration that arise when the slope and deflection equations are written. Two of these equations are given by static equilibrium, and three more are obtained by setting the deflections at the supports to zero. The following example illustrates the procedure, which is straightforward although tedious if done manually.

Example 2

Consider a triply-supported beam of length $L = 15$ as shown in Fig. 2, carrying a constant uniform load of $w = -10$. There are not sufficient equilibrium equations to determine the reaction forces R_a , R_b , and R_c , so these are left as unknowns while multiple integration is used to develop a deflection equation:

$$\begin{aligned} q(x) &= R_a \langle x \rangle_{-1} + R_b \langle x - 7.5 \rangle_{-1} + R_c \langle x - 15 \rangle_{-1} - 10 \langle x \rangle^0 \\ V(x) &= - \int q(x) dx = -R_a \langle x \rangle^0 - R_b \langle x - 7.5 \rangle^0 - R_c \langle x - 15 \rangle^0 + 10 \langle x \rangle^1 \\ M(x) &= - \int V(x) dx = R_a \langle x \rangle^1 + R_b \langle x - 7.5 \rangle^1 + R_c \langle x - 15 \rangle^1 - \frac{10}{2} \langle x \rangle^2 \\ EIy'(x) &= \int M(x) dx = \frac{R_a}{2} \langle x \rangle^2 + \frac{R_b}{2} \langle x - 7.5 \rangle^2 + \frac{R_c}{2} \langle x - 15 \rangle^2 - \frac{10}{6} \langle x \rangle^3 + c_1 \end{aligned}$$

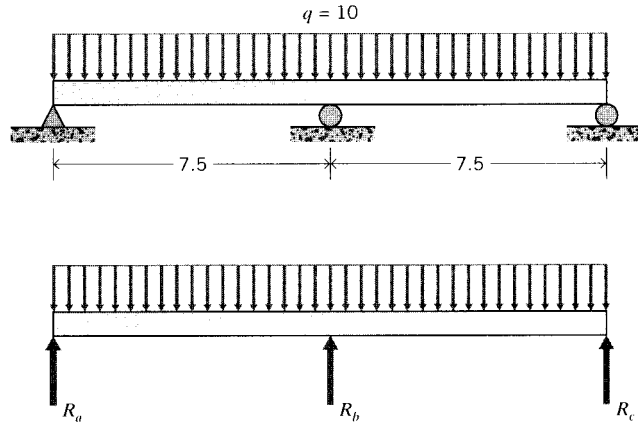


Figure 2: Uniformly loaded beam resting on three supports.

$$EIy(x) = \int EIy'(x) dx = \frac{R_a}{6}\langle x \rangle^3 + \frac{R_b}{6}\langle x - 7.5 \rangle^3 + \frac{R_c}{6}\langle x - 15 \rangle^3 - \frac{10}{24}\langle x \rangle^4 + c_1x + c_2$$

These equations have 5 unknowns: R_a , R_b , R_c , c_1 , and c_2 . These must be obtained from the two equilibrium equations

$$\begin{aligned} \sum F_y = 0 &= R_a + R_b + R_c - qL \\ \sum M_a = 0 &= qL\frac{L}{2} - R_b\frac{L}{2} - R_cL \end{aligned}$$

and the three known zero displacements at the supports

$$y(0) = y(L/2) = y(L) = 0$$

Although the process is straightforward, there is a lot of algebra to wade through. Statically indeterminate beams tend to generate tedious mathematics, but fortunately this can be reduced greatly by modern software. Follow how easily this example is handled by the Maple V package (some of the Maple responses removed for brevity):

```
> # read the library containing the Heaviside function
> readlib(Heaviside);
> # use the Heaviside function to define singularity functions;
> #   sfm(x,a,n) is same as <x-a>^n
> sfm := proc(x,a,n) (x-a)^n * Heaviside(x-a) end;
> # define the deflection function:
> y := (x)-> (Ra/6)*sfm(x,0,3)+(Rb/6)*sfm(x,7.5,3)+(Rc/6)*sfm(x,15,3)
>   -(10/24)*sfm(x,0,4)+c1*x+c2;
> # Now define the five constraint equations; first vertical equilibrium:
> eq1 := 0=Ra+Rb+Rc-(10*15);
> # rotational equilibrium:
> eq2 := 0=(10*15*7.5)-Rb*7.5-Rc*15;
> # Now the three zero displacements at the supports:
> eq3 := y(0)=0;
> eq4 := y(7.5)=0;
> eq5 := y(15)=0;
> # set precision; 4 digits is enough:
```

```

> Digits:=4;
> # solve the 5 equations for the 5 unknowns:
> solve({eq1,eq2,eq3,eq4,eq5},{Ra,Rb,Rc,c1,c2});
      {c2 = 0, c1 = -87.82, Rb = 93.78, Ra = 28.11, Rc = 28.11}
> # assign the known values for plotting purposes:
> c1:=-87.82;c2:=0;Ra:=28.11;Rb:=93.78;Rc:=28.11;
> # the equation of the deflection curve is:
> y(x);
      3              3
      4.686 x Heaviside(x) + 15.63 (x - 7.5) Heaviside(x - 7.5)
      3              4
      + 4.686 (x - 15) Heaviside(x - 15) - 5/12 x Heaviside(x) - 87.82 x
> # plot the deflection curve:
> plot(y(x),x=0..15);
> # The maximum deflection occurs at the quarter points:
> y(15/4);
      -164.7

```

The plot of the deflection curve is shown in Fig. 3.

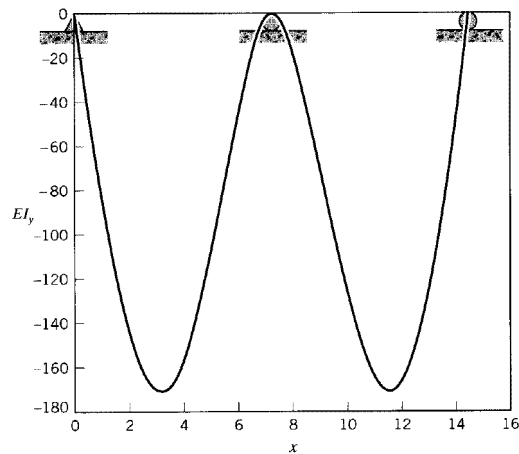


Figure 3: Deflection curve $EIy(x)$ for uniformly loaded triply-supported beam (Note difference in horizontal and vertical scales).

Energy method

The strain energy in bending as given by Eqn. 8 of Module 13 can be used to find deflections, and this may be more convenient than successive integration if the deflection at only a single point is desired. Castigliano's Theorem gives the deflection congruent to a load P as

$$\delta_P = \frac{\partial U}{\partial P} = \frac{\partial}{\partial P} \int_L \frac{M^2 dx}{2EI}$$

It is usually more convenient to do the differentiation before the integration, since this lowers the order of the expression in the integrand:

$$\delta_P = \int_L \frac{M}{EI} \frac{\partial M}{\partial P} dx$$

where here E and I are assumed not to vary with x .

The shear contribution to bending can be obtained similarly. Knowing the shear stress $\tau = VQ/Ib$ (omitting the xy subscript on τ for now), the strain energy due to shear U_s can be written

$$U_s = \int_V \frac{\tau^2}{2G} dV = \int_L \frac{V^2}{2GI} \left[\int_A \frac{Q^2}{E^2} dA \right] dx$$

The integral over the cross-sectional area A is a purely geometrical factor, and we can write

$$U_s = \int_L \frac{V^2 f_s}{2GA} dA \quad (8)$$

where the f_s is a dimensionless *form factor for shear* defined as

$$f_s = \frac{A}{I^2} \int_A \frac{Q^2}{b^2} dA \quad (9)$$

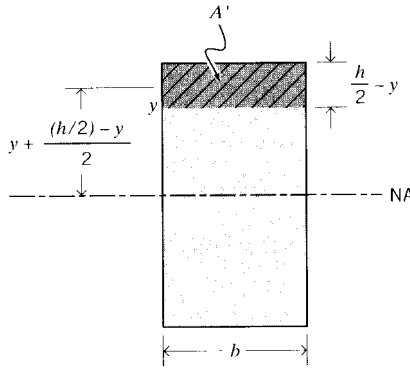


Figure 4: Rectangular beam section.

Evaluating f_s for rectangular sections for illustration (see Fig. 4), we have in that case

$$\begin{aligned} A &= bh, & I &= \frac{bh^3}{12} \\ Q &= \left[y + \frac{(h/2) - y}{2} \right] \left[b \left(\frac{h}{2} - y \right) \right] \\ f_s &= \frac{(bh)}{(bh^3/12)^2} \int_{-h/2}^{h/2} \frac{1}{b^2} Q dy = \frac{6}{5} \end{aligned}$$

Hence f_s is the same for all rectangular sections, regardless of their particular dimensions. Similarly, it can be shown (see Prob. 3) that for solid circular sections $f_s = 10/9$ and for hollow circular sections $f_s = 2$.

Example 3

If for instance we are seeking the deflection under the load P in the three-point bending example done earlier, we can differentiate the moment given in Eqn. 5 to obtain

$$\frac{\partial M}{\partial P} = \frac{1}{2}\langle x \rangle^1 - \langle x - \frac{L}{2} \rangle^1$$

Then

$$\delta_P = \frac{1}{EI} \int_L \left(\frac{P}{2}\langle x \rangle^1 - P\langle x - \frac{L}{2} \rangle^1 \right) \left(\frac{1}{2}\langle x \rangle^1 - \langle x - \frac{L}{2} \rangle^1 \right) dx$$

Expanding this and adjusting the limits of integration to account for singularity functions that have not been activated:

$$\begin{aligned} \delta_P &= \frac{P}{EI} \left\{ \int_0^L \frac{x^2}{4} dx + \int_{L/2}^L \left[-x \left(x - \frac{L}{2} \right) + \left(x - \frac{L}{2} \right)^2 \right] dx \right\} \\ &= -\frac{PL^3}{48EI} \end{aligned}$$

as before.

The contribution of shear to the deflection can be found by using $V = P/2$ in the equation for strain energy. For the case of a rectangular beam with $f_s = 6/5$ we have:

$$\begin{aligned} U_s &= \frac{(P/2)^2(6/5)}{2GA} L \\ \delta_{P,s} &= \frac{\partial U_s}{\partial P} = \frac{6PL}{20GA} \end{aligned}$$

The shear contribution can be compared with the bending contribution by replacing A with $12I/h^2$ (since $A = bh$ and $I = bh^3/12$). Then the ratio of the shear to bending contributions is

$$\frac{PLh^2/40GI}{PL^3/24EI} = \frac{3h^2E}{5L^2G}$$

Hence the importance of the shear term scales as $(h/L)^2$, i.e. quadratically as the span-to-depth ratio.

The energy method is often convenient for systems having complicated geometries and combined loading. For slender shafts transmitting axial, torsional, bending and shearing loads the strain energy is

$$\boxed{U = \int_L \left(\frac{P^2}{2EA} + \frac{T^2}{2GJ} + \frac{M^2}{2EI} + \frac{V^2 f_s}{2GA} \right) dx} \quad (10)$$

Example 4

Consider a cantilevered circular beam as shown in Fig. 5 that tapers from radius r_1 to r_2 over the length L . We wish to determine the deflection caused by a force F applied to the free end of the beam, at an angle θ from the horizontal. Turning to Maple to avoid the algebraic tedium, the dimensional parameters needed in Eqn. 10 are defined as:

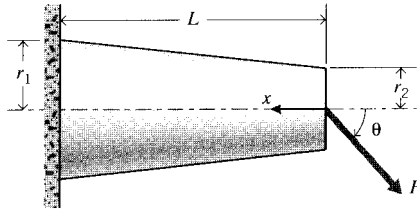


Figure 5: Tapered circular beam.

```

> r := proc (x) r1 + (r2-r1)*(x/L) end;
> A := proc (r) Pi*(r(x))^2 end;
> Iz := proc (r) Pi*(r(x))^4 /4 end;
> Jp := proc (r) Pi*(r(x))^4 /2 end;

```

where $r(x)$ is the radius, $A(r)$ is the section area, I_z is the rectangular moment of inertia, and J_p is the polar moment of inertia. The axial, bending, and shear loads are given in terms of F as

```

> P := F* cos(theta);
> V := F* sin(theta);
> M := proc (x) -F* sin(theta) * x end;

```

The strain energies corresponding to tension, bending and shear are

```

> U1 := P^2/(2*E*A(r));
> U2 := (M(x))^2/(2*E*Iz(r));
> U3 := V^2*(10/9)/(2*G*A(r));
> U := int( U1+U2+U3, x=0..L);

```

Finally, the deflection congruent to the load F is obtained by differentiating the total strain energy:

```

> dF := diff(U,F);

```

The result of these manipulations yields

$$\delta_F = \frac{LF [12 L^2 G - 12 GL^2 \cos^2 \theta + 9 Gr_2^2 \cos^2 \theta + 10 r_2^2 E - 10 r_2^2 E \cos^2 \theta]}{9 r_1 r_2^3 E \pi G}$$

This displacement is in the direction of the applied force F ; the horizontal and vertical deflections of the end of the beam are then

$$\begin{aligned} \delta_x &= \delta_F \cos \theta \\ \delta_y &= \delta_F \sin \theta \end{aligned}$$

Superposition

In practice, many beams will be loaded in a complicated manner consisting of several concentrated or distributed loads acting at various locations along the beam. Although these multiple-load cases can be solved from scratch using the methods described above, it is often easier to solve the problem by superposing solutions of simpler problems whose solutions are tabulated. Fig. 6 gives an abbreviated collection of deflection formulas¹ that will suffice for many problems. The superposition approach is valid since the governing equations are linear; hence the response to a combination of loads is the sum of the responses that would be generated by each separate load acting alone.

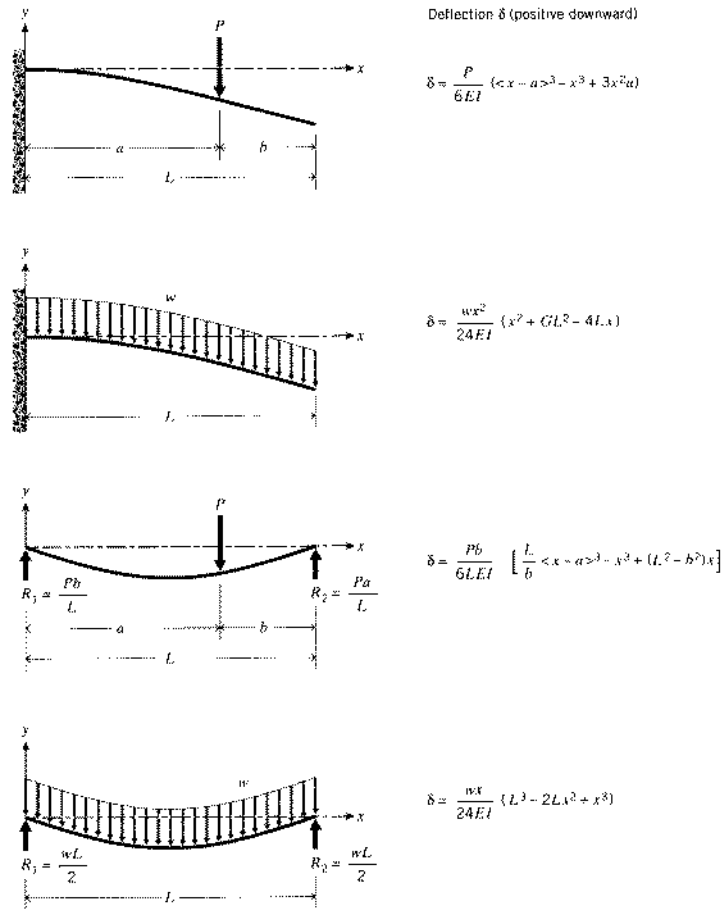


Figure 6: Deflections for cantilevered and simply-supported beams, under concentrated and distributed loading.

Example 5

We wish to find the equation of the deflection curve for a simply-supported beam loaded in symmetric four-point bending as shown in Fig. 7. From Fig. 6, the deflection of a beam with a single load at a

¹A more exhaustive listing is available in W.C. Young, *Roark's Formulas for Stress and Strain*, McGraw-Hill, New York, 1989.

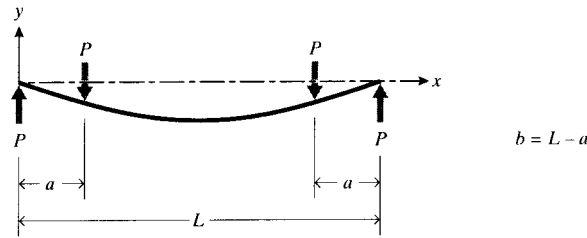


Figure 7: Four-point bending.

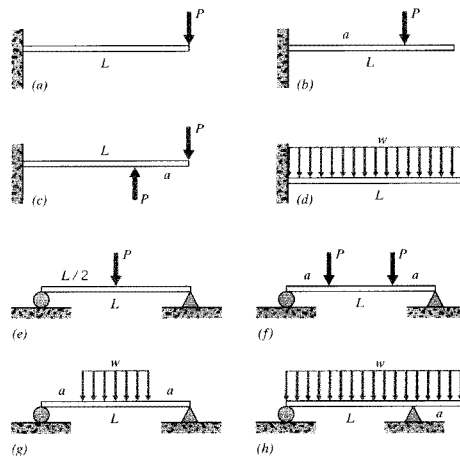
distance a from the left end is $\delta(x) = \frac{Pb}{6LEI} \left[\frac{L}{b} \langle x - a \rangle^3 - x^3 + (L^2 - b^2) x \right]$. Our present problem is just two such loads acting simultaneously, so we have

$$\delta(x) = \frac{P(L-a)}{6LEI} \left[\frac{L}{L-a} \langle x - a \rangle^3 - x^3 + (L^2 - (L-a)^2) x \right] + \frac{Pa}{6LEI} \left[\frac{L}{a} \langle x - (L-a) \rangle^3 - x^3 + (L^2 - a^2) x \right]$$

In some cases the designer may not need the entire deflection curve, and superposition of tabulated results for maximum deflection and slope is equally valid.

Problems

- (a)–(h) Write expressions for the slope and deflection curves of the beams shown here.

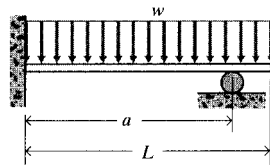


Prob. 1

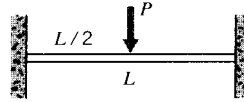
- (a)–(h) Use MapleV (or other) software to plot the slope and deflection curves for the beams in Prob. 1, using the values (as needed) $L = 25$ in, $a = 15$ in, $w = 10$ lb/in, $P = 150$ lb.
- Show that the shape factor for shear for a circular cross section is

$$f_s = \frac{A}{I^2} \int_A \frac{Q}{b^2} dA = \frac{10}{9}$$

4. (a)–(b) Determine the deflection curves for the beams shown here. Plot these curves for the values (as needed) $L = 25$ in, $a = 5$ in, $w = 10$ lb/in, $P = 150$ lb.



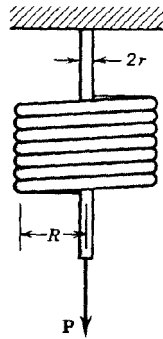
(a)



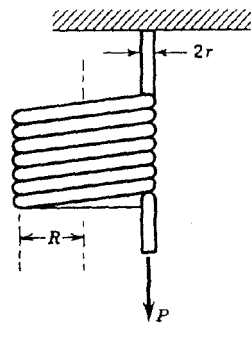
(b)

Prob. 4

5. (a) Determine the deflection of a coil spring under the influence of an axial force F , including the contribution of bending, direct shear, and torsional shear effects. Using $r = 1$ mm and $R = 10$ mm, compute the relative magnitudes of the three contributions.
 (b) Repeat the solution in (a), but take the axial load to be placed at the outer radius of the coil.



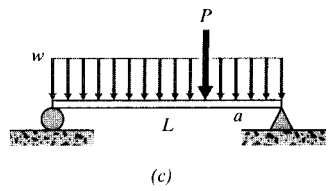
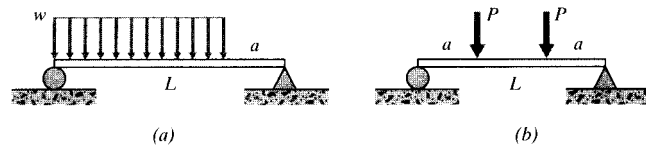
(a)



(b)

Prob. 5

6. (a)–(c) Use the method of superposition to write expressions for the deflection curve $\delta(x)$ for the cases shown here.



Prob. 6

LAMINATED COMPOSITE PLATES

David Roylance
Department of Materials Science and Engineering
Massachusetts Institute of Technology
Cambridge, MA 02139

February 10, 2000

Introduction

This document is intended to outline the mechanics of fiber-reinforced laminated plates, leading to a computational scheme that relates the in-plane strain and curvature of a laminate to the tractions and bending moments imposed on it. Although this is a small part of the overall field of fiber-reinforced composites, or even of laminate theory, it is an important technique that should be understood by all composites engineers.

In the sections to follow, we will review the constitutive relations for isotropic materials in matrix form, then show that the extension to transversely isotropic composite laminae is very straightforward. Since each ply in a laminate may be oriented arbitrarily, we will then show how the elastic properties of the individual laminae can be transformed to a common direction. Finally, we will balance the individual ply stresses against the applied tractions and moments to develop matrix governing relations for the laminate as a whole.

The calculations for laminate mechanics are best done by computer, and algorithms are outlined for elastic laminates, laminates exhibiting thermal expansion effects, and laminates exhibiting viscoelastic response.

Isotropic linear elastic materials

As shown in elementary texts on Mechanics of Materials (*cf.* Roylance 1996¹), the Cartesian strains resulting from a state of plane stress ($\sigma_z = \tau_{xz} = \tau_{yz} = 0$) are

$$\epsilon_x = \frac{1}{E} (\sigma_x - \nu\sigma_y)$$

$$\epsilon_y = \frac{1}{E} (\sigma_y - \nu\sigma_x)$$

$$\gamma_{xy} = \frac{1}{G} \tau_{xy}$$

In plane stress there is also a strain in the z direction due to the Poisson effect: $\epsilon_z = -\nu(\sigma_x + \sigma_y)$; this strain component will be ignored in the sections to follow. In the above relations there are three elastic constants: the Young's modulus E , Poisson's ratio ν , and the shear modulus

¹See References listed at the end of this document.

G . However, for isotropic materials there are only two independent elastic constants, and for instance G can be obtained from E and ν as

$$G = \frac{E}{2(1 + \nu)}$$

Using matrix notation, these relations can be written as

$$\begin{Bmatrix} \epsilon_x \\ \epsilon_y \\ \gamma_{xy} \end{Bmatrix} = \begin{bmatrix} 1/E & -\nu/E & 0 \\ -\nu/E & 1/E & 0 \\ 0 & 0 & 1/G \end{bmatrix} \begin{Bmatrix} \sigma_x \\ \sigma_y \\ \tau_{xy} \end{Bmatrix} \quad (1)$$

The quantity in brackets is called the *compliance matrix* of the material, denoted \mathbf{S} or S_{ij} . It is important to grasp the physical significance of its various terms. Directly from the rules of matrix multiplication, the element in the i^{th} row and j^{th} column of S_{ij} is the contribution of the j^{th} stress to the i^{th} strain. For instance the component in the 1,2 position is the contribution of the y -direction stress to the x -direction strain: multiplying σ_y by $1/E$ gives the y -direction strain generated by σ_y , and then multiplying this by $-\nu$ gives the Poisson strain induced in the x direction. The zero elements show the lack of coupling between the normal and shearing components.

If we wish to write the stresses in terms of the strains, Eqn. 1 can be inverted to give:

$$\begin{Bmatrix} \sigma_x \\ \sigma_y \\ \tau_{xy} \end{Bmatrix} = \frac{E}{1 - \nu^2} \begin{bmatrix} 1 & \nu & 0 \\ \nu & 1 & 0 \\ 0 & 0 & (1 - \nu)/2 \end{bmatrix} \begin{Bmatrix} \epsilon_x \\ \epsilon_y \\ \gamma_{xy} \end{Bmatrix} \quad (2)$$

where here G has been replaced by $E/2(1 + \nu)$. This relation can be abbreviated further as:

$$\boldsymbol{\sigma} = \mathbf{D}\boldsymbol{\epsilon} \quad (3)$$

where $\mathbf{D} = \mathbf{S}^{-1}$ is the *stiffness matrix*. Note that the Young's modulus can be recovered by taking the reciprocal of the 1,1 element of the compliance matrix \mathbf{S} , but that the 1,1 position of the stiffness matrix \mathbf{D} contains Poisson effects and is not equal to E .

Anisotropic Materials

If the material has a texture like wood or unidirectionally-reinforced fiber composites as shown in Fig. 1, the modulus E_1 in the fiber direction will typically be larger than those in the transverse directions (E_2 and E_3). When $E_1 \neq E_2 \neq E_3$, the material is said to be *orthotropic*. It is common, however, for the properties in the plane transverse to the fiber direction to be isotropic to a good approximation ($E_2 = E_3$); such a material is called *transversely isotropic*. The elastic constitutive laws must be modified to account for this anisotropy, and the following form is an extension of the usual equations of isotropic elasticity to transversely isotropic materials:

$$\begin{Bmatrix} \epsilon_1 \\ \epsilon_2 \\ \gamma_{12} \end{Bmatrix} = \begin{bmatrix} 1/E_1 & -\nu_{21}/E_2 & 0 \\ -\nu_{12}/E_1 & 1/E_2 & 0 \\ 0 & 0 & 1/G_{12} \end{bmatrix} \begin{Bmatrix} \sigma_1 \\ \sigma_2 \\ \tau_{12} \end{Bmatrix} \quad (4)$$

The parameter ν_{12} is the *principal Poisson's ratio*; it is the ratio of the strain induced in the 2-direction by a strain applied in the 1-direction. This parameter is not limited to values less than 0.5 as in isotropic materials. Conversely, ν_{21} gives the strain induced in the 1-direction by

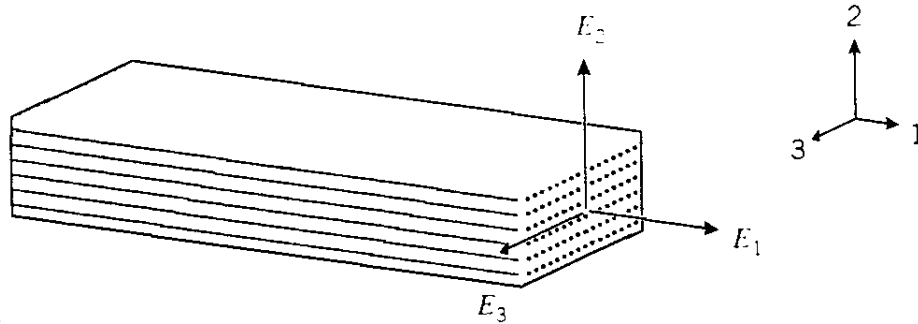


Figure 1: An orthotropic material.

a strain applied in the 2-direction. Since the 2-direction (transverse to the fibers) usually has much less stiffness than the 1-direction, a given strain in the 1-direction will usually develop a much larger strain in the 2-direction than will the same strain in the 2-direction induce a strain in the 1-direction. Hence we will usually have $\nu_{12} > \nu_{21}$. There are five constants in the above equation (E_1 , E_2 , ν_{12} , ν_{21} and G_{12}). However, only four of them are independent; since the S matrix is symmetric, we have $\nu_{21}/E_2 = \nu_{12}/E_1$.

The simple form of Eqn. 4, with zeroes in the terms representing coupling between normal and shearing components, is obtained only when the axes are aligned along the *principal material directions*; i.e. along and transverse to the fiber axes. If the axes are oriented along some other direction, all terms of the compliance matrix will be populated, and the symmetry of the material will not be evident. If for instance the fiber direction is off-axis from the loading direction, the material will develop shear strain as the fibers try to orient along the loading direction. There will therefore be a coupling between a normal stress and a shearing strain, which does not occur in an isotropic material.

Transformation of Axes

It is important to be able to transform the axes to and from the “laboratory” $x - y$ frame to a natural material frame in which the axes might be labeled 1 – 2 corresponding to the fiber and transverse directions as shown in Fig. 2.

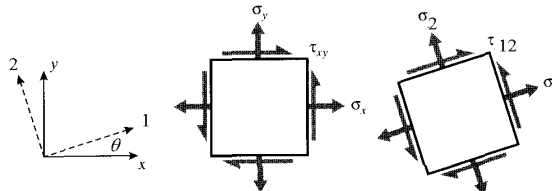


Figure 2: Rotation of axes.

As shown in elementary textbooks, the transformation law for Cartesian Cauchy stress can

be written:

$$\begin{aligned}\sigma_1 &= \sigma_x \cos^2 \theta + \sigma_y \sin^2 \theta + 2\tau_{xy} \sin \theta \cos \theta \\ \sigma_2 &= \sigma_x \sin^2 \theta + \sigma_y \cos^2 \theta - 2\tau_{xy} \sin \theta \cos \theta \\ \tau_{12} &= (\sigma_y - \sigma_x) \sin \theta \cos \theta + \tau_{xy}(\cos^2 \theta - \sin^2 \theta)\end{aligned}\quad (5)$$

Where θ is the angle from the x axis to the 1 (fiber) axis. These relations can be written in matrix form as

$$\begin{Bmatrix} \sigma_1 \\ \sigma_2 \\ \tau_{12} \end{Bmatrix} = \begin{bmatrix} c^2 & s^2 & 2sc \\ s^2 & c^2 & -2sc \\ -sc & sc & c^2 - s^2 \end{bmatrix} \begin{Bmatrix} \sigma_x \\ \sigma_y \\ \tau_{xy} \end{Bmatrix}\quad (6)$$

where $c = \cos \theta$ and $s = \sin \theta$. This can be abbreviated as

$$\boldsymbol{\sigma}' = \mathbf{A}\boldsymbol{\sigma}\quad (7)$$

where \mathbf{A} is the transformation matrix in brackets above. This expression could be applied to three-dimensional as well as two-dimensional stress states, although the particular form of \mathbf{A} given in Eqn. 6 is valid in two dimensions only (plane stress), and for Cartesian coordinates.

Using either mathematical or geometric arguments, it can be shown that the components of infinitesimal strain transform by *almost* the same relations:

$$\begin{Bmatrix} \epsilon_1 \\ \epsilon_2 \\ \frac{1}{2}\gamma_{12} \end{Bmatrix} = \mathbf{A} \begin{Bmatrix} \epsilon_x \\ \epsilon_y \\ \frac{1}{2}\gamma_{xy} \end{Bmatrix}\quad (8)$$

The factor of 1/2 on the shear components arises from the classical definition of shear strain, which is twice the tensorial shear strain. This introduces some awkwardness into the transformation relations, which can be reduced by introducing the *Reuter's matrix*, defined as

$$[\mathbf{R}] = \begin{bmatrix} 1 & 0 & 0 \\ 0 & 1 & 0 \\ 0 & 0 & 2 \end{bmatrix} \quad \text{or} \quad [\mathbf{R}]^{-1} = \begin{bmatrix} 1 & 0 & 0 \\ 0 & 1 & 0 \\ 0 & 0 & \frac{1}{2} \end{bmatrix}\quad (9)$$

We can now write:

$$\begin{Bmatrix} \epsilon_1 \\ \epsilon_2 \\ \gamma_{12} \end{Bmatrix} = \mathbf{R} \begin{Bmatrix} \epsilon_1 \\ \epsilon_2 \\ \frac{1}{2}\gamma_{12} \end{Bmatrix} = \mathbf{R}\mathbf{A} \begin{Bmatrix} \epsilon_x \\ \epsilon_y \\ \frac{1}{2}\gamma_{xy} \end{Bmatrix} = \mathbf{R}\mathbf{A}\mathbf{R}^{-1} \begin{Bmatrix} \epsilon_x \\ \epsilon_y \\ \gamma_{xy} \end{Bmatrix}$$

Or

$$\boldsymbol{\epsilon}' = \mathbf{R}\mathbf{A}\mathbf{R}^{-1}\boldsymbol{\epsilon}\quad (10)$$

The transformation law for compliance can now be developed from the transformation laws for strains and stresses. By successive transformations, the strain in an arbitrary x - y direction is related to strain in the 1-2 (principal material) directions, then to the stresses in the 1-2 directions, and finally to the stresses in the x - y directions. The final grouping of transformation matrices relating the x - y strains to the x - y stresses is then the transformed compliance matrix in the x - y direction:

$$\begin{aligned} \begin{Bmatrix} \epsilon_x \\ \epsilon_y \\ \gamma_{xy} \end{Bmatrix} &= \mathbf{R} \begin{Bmatrix} \epsilon_x \\ \epsilon_y \\ \frac{1}{2}\gamma_{xy} \end{Bmatrix} = \mathbf{R}\mathbf{A}^{-1} \begin{Bmatrix} \epsilon_1 \\ \epsilon_2 \\ \frac{1}{2}\gamma_{12} \end{Bmatrix} = \mathbf{R}\mathbf{A}^{-1}\mathbf{R}^{-1} \begin{Bmatrix} \epsilon_1 \\ \epsilon_2 \\ \gamma_{12} \end{Bmatrix} \\ &= \mathbf{R}\mathbf{A}^{-1}\mathbf{R}^{-1}\mathbf{S} \begin{Bmatrix} \sigma_1 \\ \sigma_2 \\ \tau_{12} \end{Bmatrix} = \mathbf{R}\mathbf{A}^{-1}\mathbf{R}^{-1}\mathbf{S}\mathbf{A} \begin{Bmatrix} \sigma_x \\ \sigma_y \\ \tau_{xy} \end{Bmatrix} \equiv \overline{\mathbf{S}} \begin{Bmatrix} \sigma_x \\ \sigma_y \\ \tau_{xy} \end{Bmatrix} \end{aligned}$$

where $\overline{\mathbf{S}}$ is the *transformed compliance matrix* relative to x - y axes. The inverse of $\overline{\mathbf{S}}$ is $\overline{\mathbf{D}}$, the stiffness matrix relative to x - y axes:

$$\boxed{\overline{\mathbf{S}} = \mathbf{R}\mathbf{A}^{-1}\mathbf{R}^{-1}\mathbf{S}\mathbf{A}, \quad \overline{\mathbf{D}} = \overline{\mathbf{S}}^{-1}} \quad (11)$$

Example 1

Consider a ply of Kevlar-epoxy composite with a stiffnesses $E_1 = 82$, $E_2 = 4$, $G_{12} = 2.8$ (all GPa) and $\nu_{12} = 0.25$. oriented at 30° from the x axis. The stiffness in the x direction can be found as the reciprocal of the 1,1 element of the transformed compliance matrix $\overline{\mathbf{S}}$, as given by Eqn. 11. The following shows how this can be done with Maple symbolic mathematics software (edited for brevity):

```
Read linear algebra package
> with(linalg):
Define compliance matrix
> S:=matrix(3,3,[ [1/E[1], -nu[21]/E[2], 0], [-nu[12]/E[1], 1/E[2], 0], [0,0,1/G[12]]]);
Numerical parameters for Kevlar-epoxy
> Digits:=4;unprotect(E);E[1]:=82e9;E[2]:=4e9;G[12]:=2.8e9;nu[12]:= .25;
nu[21]:=nu[12]*E[2]/E[1];
Compliance matrix evaluated
> S2:=map(eval,S);
```

$$S2 := \begin{bmatrix} .1220 \cdot 10^{-10} & -.3050 \cdot 10^{-11} & 0 \\ -.3049 \cdot 10^{-11} & .2500 \cdot 10^{-9} & 0 \\ 0 & 0 & .3571 \cdot 10^{-9} \end{bmatrix}$$

```
Transformation matrix
> A:=matrix(3,3,[ [c^2,s^2,2*s*c], [s^2,c^2,-2*s*c], [-s*c,s*c,c^2-s^2]]);
Trigonometric relations and angle
> s:=sin(theta);c:=cos(theta);theta:=30*Pi/180;
Transformation matrix evaluated
> A2:=evalf(map(eval,A));
```

$$A2 := \begin{bmatrix} .7500 & .2500 & .8660 \\ .2500 & .7500 & -.8660 \\ -.4330 & .4330 & .5000 \end{bmatrix}$$

```
Reuter's matrix
> R:=matrix(3,3,[ [1,0,0], [0,1,0], [0,0,2]]);
Transformed compliance matrix
> Sbar:=evalf(evalm( R &* inverse(A2) &* inverse(R) &* S2 &* A2 ));
```

$$S_{bar} := \begin{bmatrix} .8828 \cdot 10^{-10} & -.1968 \cdot 10^{-10} & -.1222 \cdot 10^{-9} \\ -.1969 \cdot 10^{-10} & .2071 \cdot 10^{-9} & -.8370 \cdot 10^{-10} \\ -.1222 \cdot 10^{-9} & -.8377 \cdot 10^{-10} & .2905 \cdot 10^{-9} \end{bmatrix}$$

Stiffness in x-direction
 > 'E[x]'=1/Sbar[1,1];

$$E_x = .1133 \cdot 10^{11}$$

Note that the transformed compliance matrix is symmetric (to within numerical roundoff error), but that nonzero coupling values exist. A user not aware of the internal composition of the material would consider it completely anisotropic.

Laminated composite plates

One of the most common forms of fiber-reinforced composite materials is the crossplied laminate, in which the fabricator “lays up” a sequence of unidirectionally reinforced “plies” as indicated in Fig. 3. Each ply is typically a thin (approximately 0.2 mm) sheet of collimated fibers impregnated with an uncured epoxy or other thermosetting polymer matrix material. The orientation of each ply is arbitrary, and the layup sequence is tailored to achieve the properties desired of the laminate. In this section we outline how such laminates are designed and analyzed.

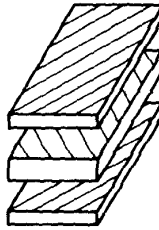


Figure 3: A 3-ply symmetric laminate.

“Classical Laminate Theory” is an extension of the theory for bending of homogeneous plates, but with an allowance for in-plane tractions in addition to bending moments, and for the varying stiffness of each ply in the analysis. In general cases, the determination of the tractions and moments at a given location will require a solution of the general equations for equilibrium and displacement compatibility of plates. This theory is treated in a number of standard texts², and will not be discussed here.

We begin by assuming a knowledge of the tractions \mathbf{N} and moments \mathbf{M} applied to a plate at a position x, y , as shown in Fig. 4:

$$\mathbf{N} = \begin{Bmatrix} N_x \\ N_y \\ N_{xy} \end{Bmatrix} \quad \mathbf{M} = \begin{Bmatrix} M_x \\ M_y \\ M_{xy} \end{Bmatrix} \quad (12)$$

²cf. S. Timoshenko and S. Woinowsky-Krieger, *Theory of Plates and Shells*, McGraw-Hill, New York, 1959.

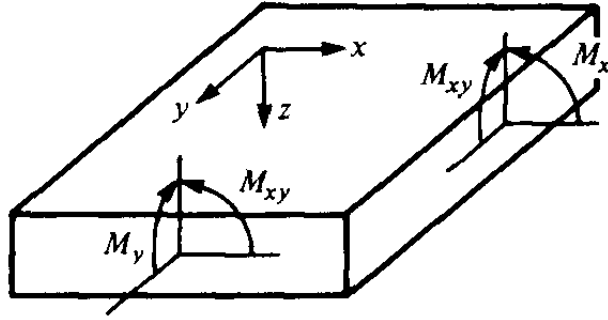


Figure 4: Applied moments in plate bending.

It will be convenient to normalize these tractions and moments by the width of the plate, so they have units of N/m and N-m/m, or simply N, respectively. Coordinates x and y are the directions in the plane of the plate, and z is customarily taken as positive downward. The deflection in the z direction is termed w , also taken as positive downward.

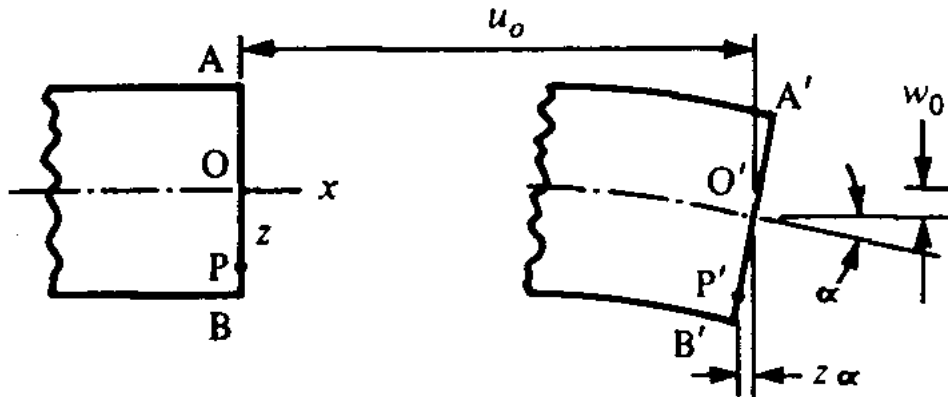


Figure 5: Displacement of a point in a plate (from Powell, 1983).

Analogously with the Euler assumption for beams, the *Kirshchoff assumption* for plate bending takes initially straight vertical lines to remain straight but rotate around the midplane ($z = 0$). As shown in Fig. 5, the horizontal displacements u and v in the x and y directions due to rotation can be taken to a reasonable approximation from the rotation angle and distance from midplane, and this rotational displacement is added to the midplane displacement (u_0, v_0):

$$u = u_0 - z w_{0,x} \quad (13)$$

$$v = v_0 - z w_{0,y} \quad (14)$$

The strains are just the gradients of the displacements; using matrix notation these can be written

$$\boldsymbol{\epsilon} = \begin{Bmatrix} \epsilon_x \\ \epsilon_y \\ \gamma_{xy} \end{Bmatrix} = \begin{Bmatrix} u_{,x} \\ v_{,y} \\ u_{,y} + v_{,x} \end{Bmatrix} = \begin{Bmatrix} u_{0,x} - z w_{0,xx} \\ v_{0,y} - z w_{0,yy} \\ (u_{0,y} + v_{0,x}) - 2z w_{0,xy} \end{Bmatrix} = \boldsymbol{\epsilon}^0 + z \boldsymbol{\kappa} \quad (15)$$

where $\boldsymbol{\epsilon}^0$ is the midplane strain and $\boldsymbol{\kappa}$ is the vector of second derivatives of the displacement, called the *curvature*:

$$\boldsymbol{\kappa} = \begin{Bmatrix} \kappa_x \\ \kappa_y \\ \kappa_{xy} \end{Bmatrix} = \begin{Bmatrix} -w_{0,xx} \\ -w_{0,yy} \\ -2w_{0,xy} \end{Bmatrix}$$

The component κ_{xy} is a *twisting* curvature, stating how the x -direction midplane slope changes with y (or equivalently how the y -direction slope changes with x).

The stresses relative to the x - y axes are now determined from the strains, and this must take consideration that each ply will in general have a different stiffness, depending on its own properties and also its orientation with respect to the x - y axes. This is accounted for by computing the transformed stiffness matrix $\bar{\mathbf{D}}$ as described in the previous section (Eqn. 11). Recall that the ply stiffnesses as given by Eqn. 4 are those along the fiber and transverse directions of that particular ply. The properties of each ply must be transformed to a common x - y axes, chosen arbitrarily for the entire laminate. The stresses at any vertical position are then:

$$\boldsymbol{\sigma} = \bar{\mathbf{D}}\boldsymbol{\epsilon} = \bar{\mathbf{D}}\boldsymbol{\epsilon}^0 + z\bar{\mathbf{D}}\boldsymbol{\kappa} \quad (16)$$

where here $\bar{\mathbf{D}}$ is the transformed stiffness of the ply at the position at which the stresses are being computed.

Each of these ply stresses must add to balance the traction per unit width \mathbf{N} :

$$\mathbf{N} = \int_{-h/2}^{+h/2} \boldsymbol{\sigma} dz = \sum_{k=1}^N \int_{z_k}^{z_{k+1}} \boldsymbol{\sigma}_k dz \quad (17)$$

where $\boldsymbol{\sigma}_k$ is the stress in the k th ply and z_k is the distance from the laminate midplane to the bottom of the k th ply. Using Eqn. 16 to write the stresses in terms of the mid-plane strains and curvatures:

$$\mathbf{N} = \sum_{k=1}^N \left(\int_{z_k}^{z_{k+1}} \bar{\mathbf{D}}\boldsymbol{\epsilon}^0 dz + \int_{z_k}^{z_{k+1}} \bar{\mathbf{D}}\boldsymbol{\kappa} z dz \right) \quad (18)$$

The curvature $\boldsymbol{\kappa}$ and midplane strain $\boldsymbol{\epsilon}^0$ are constant throughout z , and the transformed stiffness $\bar{\mathbf{D}}$ does not change within a given ply. Removing these quantities from within the integrals:

$$\mathbf{N} = \sum_{k=1}^N \left(\bar{\mathbf{D}}\boldsymbol{\epsilon}^0 \int_{z_k}^{z_{k+1}} dz + \bar{\mathbf{D}}\boldsymbol{\kappa} \int_{z_k}^{z_{k+1}} z dz \right) \quad (19)$$

After evaluating the integrals, this expression can be written in the compact form:

$$\mathbf{N} = \mathcal{A}\boldsymbol{\epsilon}^0 + \mathcal{B}\boldsymbol{\kappa} \quad (20)$$

where \mathcal{A} is an ‘‘extensional stiffness matrix’’ defined as:

$$\mathcal{A} = \sum_{k=1}^N \overline{\mathcal{D}}(z_{k+1} - z_k) \quad (21)$$

and \mathcal{B} is a “coupling stiffness matrix” defined as:

$$\mathcal{B} = \frac{1}{2} \sum_{k=1}^N \overline{\mathcal{D}}(z_{k+1}^2 - z_k^2) \quad (22)$$

The rationale for the names “extensional” and “coupling” is suggested by Eqn. 20. The \mathcal{A} matrix gives the influence of an extensional mid-plane strain ϵ^0 on the inplane traction \mathbf{N} , and the \mathcal{B} matrix gives the contribution of a curvature $\boldsymbol{\kappa}$ to the traction. It may not be obvious why bending the plate will require an in-plane traction, or conversely why pulling the plate in its plane will cause it to bend. But visualize the plate containing plies all of the same stiffness, except for some very low-modulus plies somewhere above its midplane. When the plate is pulled, the more compliant plies above the midplane will tend to stretch more than the stiffer plies below the midplane. The top half of the laminate stretches more than the bottom half, so it takes on a concave-downward curvature.

Similarly, the moment resultants per unit width must be balanced by the moments contributed by the internal stresses:

$$\mathbf{M} = \int_{-h/2}^{+h/2} \boldsymbol{\sigma} z \, dz = \mathcal{B}\epsilon^0 + \mathcal{D}\boldsymbol{\kappa} \quad (23)$$

where \mathcal{D} is a “bending stiffness matrix” defined as:

$$\mathcal{D} = \frac{1}{3} \sum_{k=1}^N \overline{\mathcal{D}}(z_{k+1}^3 - z_k^3) \quad (24)$$

The complete set of relations between applied forces and moments, and the resulting mid-plane strains and curvatures, can be summarized as a single matrix equation:

$$\begin{Bmatrix} \mathbf{N} \\ \mathbf{M} \end{Bmatrix} = \begin{bmatrix} \mathcal{A} & \mathcal{B} \\ \mathcal{B} & \mathcal{D} \end{bmatrix} \begin{Bmatrix} \epsilon^0 \\ \boldsymbol{\kappa} \end{Bmatrix} \quad (25)$$

The $\mathcal{A}/\mathcal{B}/\mathcal{B}/\mathcal{D}$ matrix in brackets is the *laminate stiffness matrix*, and its inverse will be the *laminate compliance matrix*.

The presence of nonzero elements in the coupling matrix \mathcal{B} indicates that the application of an in-plane traction will lead to a curvature or warping of the plate, or that an applied bending moment will also generate an extensional strain. These effects are usually undesirable. However, they can be avoided by making the laminate *symmetric* about the midplane, as examination of Eqn. 22 can reveal. (In some cases, this extension-curvature coupling can be used as an interesting design feature. For instance, it is possible to design a composite propeller blade whose angle of attack changes automatically with its rotational speed: increased speed increases the in-plane centripetal loading, which induces a twist into the blade.)

The above relations provide a straightforward (although tedious, unless a computer is used) means of determining stresses and displacements in laminated composites subjected to in-plane traction or bending loads:

1. For each material type in the stacking sequence, obtain by measurement or micromechanical estimation the four independent anisotropic parameters appearing in Eqn. 4: (E_1 , E_2 , ν_{12} , and G_{12}).
2. Using Eqn. 11, transform the compliance matrix for each ply from the ply's principal material directions to some convenient reference axes that will be used for the laminate as a whole.
3. Invert the transformed compliance matrix to obtain the transformed (relative to x - y axes) stiffness matrix $\bar{\mathbf{D}}$.
4. Add each ply's contribution to the \mathcal{A} , \mathcal{B} and \mathcal{D} matrices as prescribed by Eqns. 21, 22 and 24.
5. Input the prescribed tractions \mathbf{N} and bending moments \mathbf{M} , and form the system equations given by Eqn. 25.
6. Solve the resulting system for the unknown values of in-plane strain $\boldsymbol{\epsilon}^0$ and curvature $\boldsymbol{\kappa}$.
7. Use Eqn. 16 to determine the ply stresses for each ply in the laminate in terms of $\boldsymbol{\epsilon}^0$, $\boldsymbol{\kappa}$ and z . These will be the stresses relative to the x - y axes.
8. Use Eqn. 6 to transform the x - y stresses back to the principal material axes (parallel and transverse to the fibers).
9. If desired, the individual ply stresses can be used in a suitable failure criterion to assess the likelihood of that ply failing. The *Tsai-Hill* criterion is popularly used for this purpose:

$$\left(\frac{\sigma_1}{\hat{\sigma}_1}\right)^2 - \frac{\sigma_1\sigma_2}{\hat{\sigma}_1^2} + \left(\frac{\sigma_2}{\hat{\sigma}_2}\right)^2 + \left(\frac{\tau_{12}}{\hat{\tau}_{12}}\right)^2 = 1 \quad (26)$$

Here $\hat{\sigma}_1$ and $\hat{\sigma}_2$ are the ply tensile strengths parallel to and along the fiber direction, and $\hat{\tau}_{12}$ is the intralaminar ply strength. This criterion predicts failure whenever the left-hand-side of the above equation equals or exceeds unity.

Example 2

The laminate analysis outlined above has been implemented in a code named `plate`, and this example demonstrates the use of this code in determining the stiffness of a two-ply 0/90 layup of graphite/epoxy composite. Here each of the two plies is given a thickness of 0.5, so the total laminate height will be unity. The laminate theory assumes a unit width, so the overall stiffness and compliance matrices will be based on a unit cross section.

```
> plate
assign properties for lamina type 1...

enter modulus in fiber direction...
  (enter -1 to stop): 230e9
enter modulus in transverse direction: 6.6e9
enter principal Poisson ratio: .25
enter shear modulus: 4.8e9
enter ply thickness: .5
assign properties for lamina type 2...
```

```

enter modulus in fiber direction...
  (enter -1 to stop): -1
define layup sequence, starting at bottom...
  (use negative material set number to stop)

enter material set number for ply number  1: 1
enter ply angle: 0

enter material set number for ply number  2: 1
enter ply angle: 90

enter material set number for ply number  3: -1

laminate stiffness matrix:

    0.1185E+12  0.1653E+10  0.2942E+04  -0.2798D+11  0.0000D+00  0.7354D+03
    0.1653E+10  0.1185E+12  0.1389E+06  0.0000D+00  0.2798D+11  0.3473D+05
    0.2942E+04  0.1389E+06  0.4800E+10  0.7354D+03  0.3473D+05  0.0000D+00

   -0.2798E+11  0.0000E+00  0.7354E+03  0.9876D+10  0.1377D+09  0.2451D+03
    0.0000E+00  0.2798E+11  0.3473E+05  0.1377D+09  0.9876D+10  0.1158D+05
    0.7354E+03  0.3473E+05  0.0000E+00  0.2451D+03  0.1158D+05  0.4000D+09

laminate compliance matrix:

    0.2548E-10 -0.3554E-12 -0.1639E-16  0.7218D-10  0.7125D-19 -0.6022D-16
   -0.3554E-12  0.2548E-10 -0.2150E-15  0.3253D-18 -0.7218D-10 -0.1228D-15
   -0.1639E-16 -0.2150E-15  0.2083E-09  -0.6022D-16 -0.1228D-15  0.2228D-19

    0.7218E-10  0.1084E-18 -0.6022E-16  0.3058D-09 -0.4265D-11 -0.1967D-15
    0.6214E-22 -0.7218E-10 -0.1228E-15  -0.4265D-11  0.3058D-09 -0.2580D-14
   -0.6022E-16 -0.1228E-15  0.2228E-19  -0.1967D-15 -0.2580D-14  0.2500D-08

```

Note that this unsymmetric laminate generates nonzero values in the coupling matrix \mathcal{B} , as expected. The stiffness is equal in the x and y directions, as can be seen by examining the 1,1 and 2,2 elements of the laminate compliance matrix. The effective modulus is $E_x = E_y = 1/0.2548 \times 10^{-10} = 39.2$ GPa. However, the laminate is not isotropic, as can be found by rerunning `plate` with the 0/90 layup oriented at a different angle from the $x - y$ axes.

Temperature Effects

There are a number of improvements one might consider for the plate code described above: it could be extended to include interlaminar shear stresses between plies, it could incorporate a database of commercially available prepreg and core materials, or the user interface could be made “friendlier” and graphically-oriented. Many such features are available in commercial codes, or could be added by the user, and will not be discussed further here. However, thermal expansion effects are so important in application that a laminate code almost *must* have this feature to be usable, and the general approach will be outlined here.

In general, an increase in temperature ΔT causes a thermal expansion given by the well-known relation $\epsilon_T = \alpha \Delta T$, where ϵ_T is the thermally-induced strain and α is the coefficient of

linear thermal expansion. This thermal strain is obtained without needing to apply stress, so that when Hooke's law is used to compute the stress from the strain the thermal component is subtracted first: $\sigma = E(\epsilon - \alpha\Delta T)$. The thermal expansion causes normal strain only, so shearing components of strain are unaffected. Equation 3 can thus be extended as

$$\boldsymbol{\sigma} = \mathbf{D}(\boldsymbol{\epsilon} - \boldsymbol{\epsilon}_T)$$

where the thermal strain vector in the 1 – 2 coordinate frame is

$$\boldsymbol{\epsilon}_T = \begin{Bmatrix} \alpha_1 \\ \alpha_2 \\ 0 \end{Bmatrix} \Delta T$$

Here α_1 and α_2 are the anisotropic thermal expansion coefficients in the fiber and transverse directions. Transforming to common $x - y$ axes, this relation becomes:

$$\begin{Bmatrix} \sigma_x \\ \sigma_y \\ \tau_{xy} \end{Bmatrix} = \begin{bmatrix} \bar{D}_{11} & \bar{D}_{12} & \bar{D}_{13} \\ \bar{D}_{12} & \bar{D}_{22} & \bar{D}_{23} \\ \bar{D}_{13} & \bar{D}_{23} & \bar{D}_{33} \end{bmatrix} \left\{ \begin{bmatrix} \epsilon_x \\ \epsilon_y \\ \gamma_{xy} \end{bmatrix} - \begin{bmatrix} \alpha_x \\ \alpha_y \\ \alpha_{xy} \end{bmatrix} \Delta T \right\} \quad (27)$$

The subscripts on the \bar{D} elements refer to row and column positions within the stiffness matrix rather than coordinate directions; the over-bar serves as a reminder that these elements refer to $x-y$ axes. The thermal expansion vector on the right-hand side ($\boldsymbol{\alpha} = \alpha_x, \alpha_y, \alpha_{xy}$) is essentially a strain vector, and so can be obtained from $(\alpha_1, \alpha_2, 0)$ as in Eqn. 10:

$$\boldsymbol{\alpha} = \begin{Bmatrix} \alpha_x \\ \alpha_y \\ \alpha_{xy} \end{Bmatrix} = \mathbf{R}\mathbf{A}^{-1}\mathbf{R}^{-1} \begin{Bmatrix} \alpha_1 \\ \alpha_2 \\ 0 \end{Bmatrix}$$

Note that in the common $x-y$ direction, thermal expansion induces both normal and shearing strains.

The previous temperature-independent development can now be repeated, modified only by carrying along the thermal expansion terms. As before, the strain vector for any position z from the midplane is given in terms of the midplane strain $\boldsymbol{\epsilon}^0$ and curvature $\boldsymbol{\kappa}$ by

$$\boldsymbol{\epsilon} = \boldsymbol{\epsilon}^0 + z\boldsymbol{\kappa}$$

The corresponding stress is then

$$\boldsymbol{\sigma} = \bar{\mathbf{D}}(\boldsymbol{\epsilon}^0 + z\boldsymbol{\kappa} - \boldsymbol{\alpha}\Delta T)$$

Balancing the stresses against the applied tractions and moments as before:

$$\mathbf{N} = \int \boldsymbol{\sigma} dz = \mathcal{A}\boldsymbol{\epsilon}^0 + \mathcal{B}\boldsymbol{\kappa} - \int \bar{\mathbf{D}}\boldsymbol{\alpha}\Delta T dz$$

$$\mathbf{M} = \int \boldsymbol{\sigma} z dz = \mathcal{B}\boldsymbol{\epsilon}^0 + \mathcal{D}\boldsymbol{\kappa} - \int \bar{\mathbf{D}}\boldsymbol{\alpha}\Delta T z dz$$

This result is identical to that of Eqns. 20 and 23, other than the addition of the integrals representing the “thermal loads.” This permits temperature-dependent problems to be handled by an “equivalent mechanical formulation;” the overall governing equations can be written as

$$\begin{Bmatrix} \bar{\mathbf{N}} \\ \bar{\mathbf{M}} \end{Bmatrix} = \begin{bmatrix} \mathbf{A} & \mathbf{B} \\ \mathbf{B} & \mathbf{D} \end{bmatrix} \begin{Bmatrix} \boldsymbol{\epsilon}^0 \\ \boldsymbol{\kappa} \end{Bmatrix}, \quad \text{or} \quad \begin{Bmatrix} \boldsymbol{\epsilon}^0 \\ \boldsymbol{\kappa} \end{Bmatrix} = \begin{bmatrix} \mathbf{A} & \mathbf{B} \\ \mathbf{B} & \mathbf{D} \end{bmatrix}^{-1} \begin{Bmatrix} \bar{\mathbf{N}} \\ \bar{\mathbf{M}} \end{Bmatrix} \quad (28)$$

where the “equivalent thermal loads” are given as

$$\begin{aligned} \bar{\mathbf{N}} &= \mathbf{N} + \int \bar{\mathbf{D}}\boldsymbol{\alpha}\Delta T dz \\ \bar{\mathbf{M}} &= \mathbf{M} + \int \bar{\mathbf{D}}\boldsymbol{\alpha}\Delta T z dz \end{aligned}$$

The extension of the `plate` code to accommodate thermal effects thus consists of modifying the 6×1 loading vector by adding the two 3×1 vector integrals in the above expression.

Viscoelastic Effects

Since the matrix of many composite laminates is polymeric, the designer may need to consider the possibility of viscoelastic stress relaxation or creep during loading. Any such effect will probably not be large, since the fibers that bear most of the load are not usually viscoelastic. Further, the matrix material is usually used well below its glass transition temperature, and will act in a glassy elastic mode.

Some applications may not be so simple, however. If the laminate is used at elevated temperature, and if stresses act in directions not supported by the reinforcing fibers, relaxation effects may be observed. Figure 6 shows creep measured in a T300/5208 unidirectional graphite-epoxy laminate³, loaded transversely to the fibers at 149°C. Even in this almost-worst case scenario, the creep strains are relatively small (less than 10% of the elastic strain), but Fig. 6 does show that relaxation effects may be important in some situations.

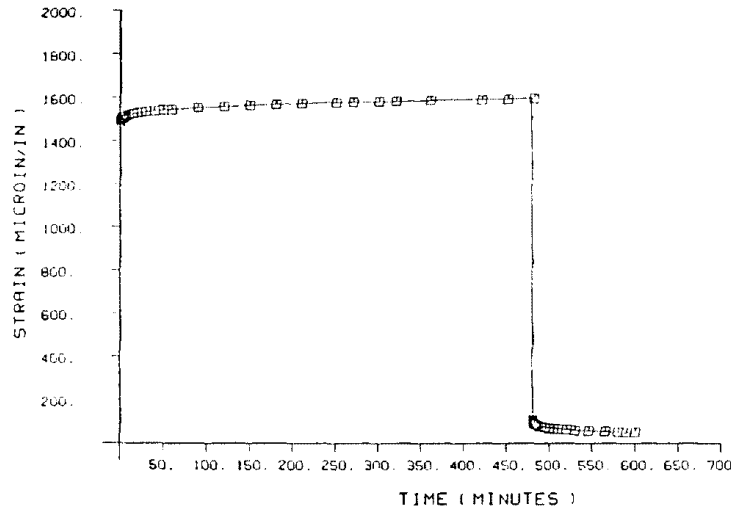


Figure 6: Creep/creep-recovery response of graphite-epoxy laminate.

³M.E. Tuttle and H.F. Brinson, “Prediction of Long-Term Creep Compliance of General Composite Laminates,” *Experimental Mechanics*, p. 89, March 1986.

The Tuttle-Brinson paper cited above describes a time-stepping computational scheme that can be used to model these viscoelastic laminate effects, and a simplified form of their method will be outlined here. The viscoelastic creep strain occurring in a given ply during a time increment dt can be calculated from the stress in the ply at that time, assuming the ply to be free of adjoining plies; this gives an *independent-ply creep strain*. This strain will act to relax the ply stress.

Of course, the plies are not free to strain arbitrarily, and the proper strain compatibility can be reestablished by calculating the external loads that would produce elastic strains equal to the independent-ply creep strains. These loads are summed over all plies in the laminate to give an *equivalent laminate creep load*. This load is applied to the laminate to compute a set of compatible strains and curvatures, termed the *equivalent-laminate creep strain*. This strain is added to the initial elastic strain in computing the stress on a given ply, while the independent-ply creep strain is subtracted.

The following list develops these steps in more detail:

1. The elastic mid-plane strains and curvatures are solved for the specified bending moments and tractions, using the glassy moduli of the various plies. From Eqn. 25:

$$\begin{Bmatrix} \epsilon^0 \\ \kappa \end{Bmatrix} = \begin{bmatrix} \mathbf{A} & \mathbf{B} \\ \mathbf{B} & \mathbf{D} \end{bmatrix}^{-1} \begin{Bmatrix} \mathbf{N} \\ \mathbf{M} \end{Bmatrix}$$

2. The elastic strain in each ply is then obtained from Eqn. 15. For the k^{th} ply, with center at coordinate z , this is:

$$\epsilon_{p-e-xy} = \epsilon^0 + z\kappa$$

where the $p-e-xy$ subscript indicates *ply, elastic*, strain in the $x-y$ direction. The elastic ply strains relative to the 1-2 (fiber-transverse) directions are given by the transformation of Eqn. 10:

$$\epsilon_{p-e-12} = \mathbf{R}\mathbf{A}\mathbf{R}^{-1}\epsilon_{p-e-xy}$$

These first two steps are performed by the elastic `plate` code, and the adaptation to viscoelastic response consists of adding the following steps.

3. The current ply stress σ_{k-12} in the 1-2 directions is:

$$\sigma_{k-12} = \mathbf{D}[\epsilon_{p-e-12} + (\epsilon_{p-lc-12} - \epsilon_{p-c-12})]$$

The quantity $\epsilon_{p-lc-12} - \epsilon_{p-c-12}$ is the difference between the *equivalent laminate creep strain* and the *independent-ply creep strain*. The quantities $\epsilon_{p-lc-12}$ and ϵ_{p-c-12} are set to zero initially, but are updated in steps 4 and 8 below to account for viscoelastic relaxation.

4. The current ply stress is then used in an appropriate viscoelastic model to compute the creep that would occur if the ply were free to strain independently of the adjoining plies; this is termed the *independent ply creep strain*. For a simple Voigt model, the current value of creep strain can be updated from its value in the previous time step as:

$$\epsilon_{p-c-12}^t = \sigma_{k-12} C_v (1 - e^{-dt/\tau}) + \epsilon_{p-c-12}^{t-1} e^{-dt/\tau}$$

where the superscripts on strain indicate values at the current and previous time steps. Here C_v is the viscoelastic creep compliance and τ is a relaxation time. A creep strain

equal to C_v will develop in addition to the initial elastic strain in the laminate, and a fraction $2/e$ of this creep strain will develop in a time τ . Different values of C_v will be used for the fiber, transverse, and shear strain components due to the anisotropy of the ply.

5. The stresses in the 1-2 and x - y directions that would be needed to develop the independent-ply creep strains *if the ply were elastic* are

$$\boldsymbol{\sigma}_{k\text{-}12} = \mathbf{D}\boldsymbol{\epsilon}_{p\text{-}c\text{-}12}$$

$$\boldsymbol{\sigma}_{k\text{-}xy} = \mathbf{A}^{-1}\boldsymbol{\sigma}_{k\text{-}12}$$

6. These equivalent elastic ply stresses are summed over all plies in the laminate to build up an *equivalent laminate creep load*. The contribution of the k^{th} ply is:

$$\mathbf{N}_c = \mathbf{N}_c + t_k\boldsymbol{\sigma}_{k\text{-}xy}$$

$$\mathbf{M}_c = \mathbf{M}_c + t_k z \boldsymbol{\sigma}_{k\text{-}xy},$$

where t_k is the thickness of the k^{th} ply and z is its centerline coordinate.

7. An *equivalent laminate creep strain* is then computed from the elastic compliance matrix and the equivalent laminate creep loads as

$$\begin{Bmatrix} \boldsymbol{\epsilon}_{lc}^0 \\ \boldsymbol{\kappa}_{lc} \end{Bmatrix} = \begin{bmatrix} \mathcal{A} & \mathcal{B} \\ \mathcal{B} & \mathcal{D} \end{bmatrix}^{-1} \begin{Bmatrix} \mathbf{N}_c \\ \mathbf{M}_c \end{Bmatrix}$$

8. The *ply laminate creep strain* in the x - y and 1-2 directions are

$$\boldsymbol{\epsilon}_{p\text{-}lc\text{-}xy} = \boldsymbol{\epsilon}_{lc}^0 + z\boldsymbol{\kappa}_{lc}$$

$$\boldsymbol{\epsilon}_{p\text{-}lc\text{-}12} = \mathbf{R}\mathbf{A}\mathbf{R}^{-1}\boldsymbol{\epsilon}_{p\text{-}lc\text{-}xy}$$

9. Finally, the time is incremented ($t \leftarrow t + dt$) and another time cycle is computed starting at step 3.

Example 3

As an illustration of the above algorithm, consider a simple model laminate with one isotropic ply. The elastic constants are $E = 100$ (arbitrary units) and $\nu = 0.25$, and a unit stress is applied in the x -direction. The initial x -direction strain is therefore $\epsilon_{x,0} = \sigma_x/E = 0.01$. In this isotropic test case, the code calculates the shear modulus as $G = E/2(1 + \nu)$. The creep strain is governed by a parameter v_{frac} , which sets the Voigt creep compliance C_v to v_{frac}/E_2 in the transverse direction, v_{frac}/G_{12} for shear components, and zero in the fiber direction (assuming only elastic response along the fibers.)

Figure 7 shows the creep strain history of this laminate for a relaxation time of $\tau = 1000$ s. The code steps linearly in log time, in this case with four time steps per decade. The creep strain is the strain over and beyond the initial elastic strain, which transitions from zero to $C_v\epsilon_{x,0} = 5 \times 10^{-4}$ as time progresses through the relaxation time.

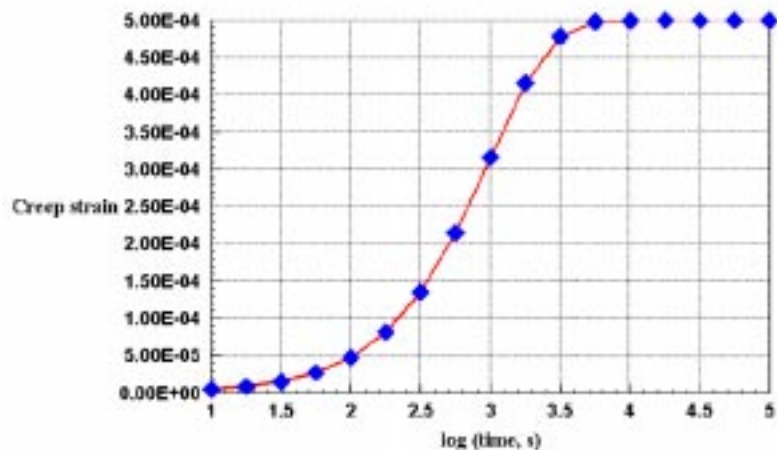


Figure 7: Creep strain history in model laminate.

References

1. Ashton, J.E., J.C. Halpin and P.H. Petit, *Primer on Composite Materials: Analysis*, Technomic Press, Westport, CT, 1969.
2. Jones, R.M., *Mechanics of Composite Materials*, McGraw-Hill, New York, 1975.
3. Powell, P.C, *Engineering with Polymers*, Chapman and Hall, London, 1983.
4. Roylance, D., *Mechanics of Materials*, Wiley & Sons, New York, 1996.

Problems

1. Write out the x - y two-dimensional compliance matrix $\bar{\mathbf{S}}$ and stiffness matrix $\bar{\mathbf{D}}$ (Eqn. 11) for a single ply of graphite/epoxy composite with its fibers aligned along the x - y axes.
2. Write out the x - y two-dimensional compliance matrix $\bar{\mathbf{S}}$ and stiffness matrix $\bar{\mathbf{D}}$ (Eqn. 11) for a single ply of graphite/epoxy composite with its fibers aligned 30° from the x axis.
3. Plot the effective Young's modulus, measured along the x - axis, of a single unidirectional ply of graphite-epoxy composite as a function of the angle between the ply fiber direction and the x -axis.
4. Using a programming language of your choice, write a laminate code similar to the `plate` code mentioned in the text, and verify it by computing the laminate stiffness and compliance matrices given in Ex. 2.
5. A $(60^\circ/0^\circ/-60^\circ)^S$ layup (the S superscript indicates the plies are repeated to give a symmetric laminate) is an example of what are called "quasi-isotropic" laminates, having equal stiffnesses in the x and y directions, regardless of the laminate orientation. Verify that this is so for two laminate orientations, one having the 0° plies oriented along the x axis and the other with the 0° plies oriented at 30° from the x axis.

Mechanical Properties of Composite Materials

The following table lists physical and mechanical property values for representative ply and core materials widely used in fiber-reinforced composite laminates. Ply properties are taken from F.P.Gerstle, "Composites," *Encyclopedia of Polymer Science and Engineering*, Wiley, New York, 1991, which should be consulted for data from a wider range of materials. See also G. Lubin, *Handbook of Composites*, Van Nostrand, New York, 1982.

	S-glass/ epoxy	Kevlar/ epoxy	HM Graphite/ epoxy	Pine	Rohacell 51 rigid foam
Elastic Properties:					
E_1 , GPa	55	80	230	13.4	0.07
E_2 , GPa	16	5.5	6.6	0.55	0.07
G_{12} , GPa	7.6	2.1	4.8	0.83	0.021
ν_{12}	0.26	0.31	0.25	0.30	
Tensile Strengths:					
σ_1 , MPa	1800	2000	1100	78	1.9
σ_2 , Mpa	40	20	21	2.1	1.9
σ_{12} , MPa	80	40	65	6.2	0.8
Compressive Strengths:					
σ_1 , MPa	690	280	620	33	0.9
σ_2 , MPa	140	140	170	3.0	0.9
Physical Properties:					
α_1 , $10^{-6}/^{\circ}\text{C}$	2.1	-4.0	-0.7		33
α_2 , $10^{-6}/^{\circ}\text{C}$	6.3	60	28		33
Volume fraction	0.7	0.54	0.7		
Thickness, mm	0.15	0.13	0.13		
Density, Mg/m^3	2.0	1.38	1.63	0.55	0.05

Closed-Form Solutions

David Roylance
Department of Materials Science and Engineering
Massachusetts Institute of Technology
Cambridge, MA 02139

February 21, 2001

Introduction

During most of its historical development, the science of Mechanics of Materials relied principally on closed-form (not computational) mathematical theorists. Much of their work represents mathematical intuition and skill of a very high order, challenging even for advanced researchers of today. This theory is taught primarily in graduate subjects, but is outlined here both to provide some background that will be useful in the Module on Fracture and as a preliminary introduction to these more advanced subjects.

Governing equations

We have earlier shown (see Module 9) how the spatial gradients of the six Cauchy stresses are related by three *equilibrium* equations that can be written in pseudovector form as

$$\mathbf{L}^T \boldsymbol{\sigma} = \mathbf{0} \quad (1)$$

These are augmented by six *constitutive* equations which can be written for linear elastic materials as (see Module 11)

$$\boldsymbol{\sigma} = \mathbf{D}\boldsymbol{\epsilon} \quad (2)$$

and six *kinematic* or strain-displacement equations (Module 8)

$$\boldsymbol{\epsilon} = \mathbf{L}\mathbf{u} \quad (3)$$

These fifteen equations must be satisfied by the fifteen independent functions (three displacements \mathbf{u} , six strains $\boldsymbol{\epsilon}$, and six stresses $\boldsymbol{\sigma}$). These functions must also satisfy boundary conditions on displacement

$$\mathbf{u} = \hat{\mathbf{u}} \quad \text{on} \quad \Gamma_u \quad (4)$$

where Γ_u is the portion of the boundary on which the displacements $\mathbf{u} = \hat{\mathbf{u}}$ are prescribed. The remainder of the boundary must then have prescribed tractions $\mathbf{T} = \hat{\mathbf{T}}$, on which the stresses must satisfy Cauchy's relation:

$$\boldsymbol{\sigma}\hat{\mathbf{n}} = \hat{\mathbf{T}} \quad \text{on} \quad \Gamma_T \quad (5)$$

In the familiar cantilevered beam shown in Fig. 1, the region of the beam at the wall constitutes Γ_u , having specified (zero) displacement and slope. All other points on the beam boundary make up Γ_T , with a load of P at the loading point A and a specified load of zero elsewhere.

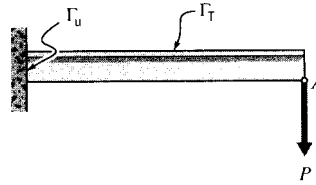


Figure 1: Cantilevered beam.

With structures such as the beam that have simple geometries, solutions can be obtained by the direct method we have used in earlier modules: an expression for the displacements is written, from which the strains and stresses can be obtained, and the stresses then balanced against the externally applied loads. (Problem 2 provides another example of this process.) In situations not having this geometrical simplicity, the analyst must carry out a mathematical solution, seeking functions of stress, strain and displacement that satisfy both the governing equations and the boundary conditions.

Currently, practical problems are likely to be solved by computational approximation, but it is almost always preferable to obtain a closed-form solution if at all possible. The mathematical result will show the functional importance of the various parameters, such as loading conditions or material properties, in a way a numerical solution cannot, and is therefore more useful in guiding design decisions. For this reason, the designer should always begin an analysis of load-bearing structures by searching for closed-form solutions of the given, or similar, problem. Several compendia of such solutions are available, the book by Roark¹ being a useful example.

However, there is always a danger in performing this sort of “handbook engineering” blindly, and this section is intended partly to illustrate the mathematical concepts that underlie many of these published solutions. It is probably true that most of the problems that can be solved mathematically have already been completed; these are the classical problems of applied mechanics, and they often require a rather high level of mathematical sophistication. The classic text by Timoshenko and Goodier² is an excellent source for further reading in this area.

The Airy stress function

Expanding the kinematic or strain-displacement equations (Eqn. 3) in two dimensions gives the familiar forms:

$$\begin{aligned}\epsilon_x &= \frac{\partial u}{\partial x} \\ \epsilon_y &= \frac{\partial v}{\partial y} \\ \gamma_{xy} &= \frac{\partial v}{\partial x} + \frac{\partial u}{\partial y}\end{aligned}\tag{6}$$

¹W.C. Young, *Roark’s Formulas for Stress and Strain*, McGraw-Hill, New York, 1989.

²S. Timoshenko and J.N. Goodier, *Theory of Elasticity*, McGraw-Hill, New York, 1951.

Since three strains (ϵ_x , ϵ_y , γ_{xy}) are written in terms of only two displacements (u , v), they cannot be specified arbitrarily; a relation must exist between the three strains. If ϵ_x is differentiated twice by dx , ϵ_y twice by dy , and γ_{xy} by dx and then dy we have directly

$$\frac{\partial^2 \epsilon_x}{\partial y^2} + \frac{\partial^2 \epsilon_y}{\partial x^2} = \frac{\partial^2 \gamma_{xy}}{\partial x \partial y} \quad (7)$$

In order for the displacements to be so differentiable, they must be continuous functions, which means physically that the body must deform in a *compatible* manner, i.e. without developing cracks or overlaps. For this reason Eqn. 7 is called the *compatibility* equation for strains, since the continuity of the body is guaranteed if the strains satisfy it.

The compatibility equation can be written in terms of the stresses rather than the strains by recalling the constitutive equations for elastic plane stress:

$$\begin{aligned} \epsilon_x &= \frac{1}{E}(\sigma_x - \nu\sigma_y) \\ \epsilon_y &= \frac{1}{E}(\sigma_y - \nu\sigma_x) \\ \gamma_{xy} &= \frac{1}{G}\tau_{xy} = \frac{2(1+\nu)}{E}\tau_{xy} \end{aligned} \quad (8)$$

Substituting these in Eqn. 7 gives

$$\frac{\partial^2}{\partial y^2}(\sigma_x - \nu\sigma_y) + \frac{\partial^2}{\partial x^2}(\sigma_y - \nu\sigma_x) = 2(1+\nu)\frac{\partial^2 \tau_{xy}}{\partial x \partial y} \quad (9)$$

Stresses satisfying this relation guarantee compatibility of strain.

The stresses must also satisfy the equilibrium equations, which in two dimensions can be written

$$\begin{aligned} \frac{\partial \sigma_x}{\partial x} + \frac{\partial \tau_{xy}}{\partial y} &= 0 \\ \frac{\partial \tau_{xy}}{\partial x} + \frac{\partial \sigma_y}{\partial y} &= 0 \end{aligned} \quad (10)$$

As a means of simplifying the search for functions whose derivatives obey these rules, G.B. Airy (1801–1892) defined a *stress function* ϕ from which the stresses could be obtained by differentiation:

$$\begin{aligned} \sigma_x &= \frac{\partial^2 \phi}{\partial y^2} \\ \sigma_y &= \frac{\partial^2 \phi}{\partial x^2} \\ \tau_{xy} &= -\frac{\partial^2 \phi}{\partial x \partial y} \end{aligned} \quad (11)$$

Direct substitution will show that stresses obtained from this procedure will automatically satisfy the equilibrium equations. This maneuver is essentially limited to two-dimensional problems, but with that proviso it provides a great simplification in searching for valid functions for the stresses.

Now substituting these into Eqn. 9, we have

$$\frac{\partial^4 \phi}{\partial x^4} + 2 \frac{\partial^4 \phi}{\partial x^2 \partial y^2} + \frac{\partial^4 \phi}{\partial y^4} \equiv \nabla^2(\nabla^2 \phi) \equiv \nabla^4 \phi = 0 \quad (12)$$

Any function $\phi(x, y)$ that satisfies this relation will satisfy the governing relations for equilibrium, geometric compatibility, and linear elasticity. Of course, many functions could be written that satisfy the compatibility equation; for instance setting $\phi = 0$ would always work. But to make the solution correct for a particular stress analysis, the boundary conditions on stress and displacement must be satisfied as well. This is usually a much more difficult undertaking, and no general solution that works for all cases exists. It can be shown, however, that a solution satisfying both the compatibility equation and the boundary conditions is unique; i.e. that it is the *only* correct solution.

Stresses around a circular hole

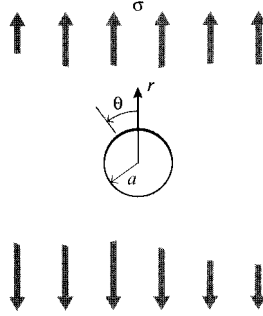


Figure 2: Circular hole in a uniaxially stressed plate

To illustrate the use of the Airy function approach, we will outline the important work of Kirsch³, who obtained a solution for the influence on the stresses of a hole placed in the material. This is vitally important in analyzing such problems as rivet holes used in joining, and the effect of a manufacturing void in initiating failure. Consider a thin sheet as illustrated in Fig. 2, infinite in lateral dimensions but containing a circular hole of radius a , and subjected to a uniaxial stress σ . Using circular r, θ coordinates centered on the hole, the compatibility equation for ϕ is

$$\nabla^4 \phi = \left(\frac{\partial^2}{\partial r^2} + \frac{1}{r} \frac{\partial}{\partial r} + \frac{1}{r^2} \frac{\partial^2}{\partial \theta^2} \right) \left(\frac{\partial^2 \phi}{\partial r^2} + \frac{1}{r} \frac{\partial \phi}{\partial r} + \frac{1}{r^2} \frac{\partial^2 \phi}{\partial \theta^2} \right) = 0 \quad (13)$$

In these circular coordinates, the stresses are obtained from ϕ as

$$\begin{aligned} \sigma_r &= \frac{1}{r} \frac{\partial \phi}{\partial r} + \frac{1}{r^2} \frac{\partial^2 \phi}{\partial \theta^2} \\ \sigma_\theta &= \frac{\partial^2 \phi}{\partial r^2} \\ \tau_{r\theta} &= -\frac{\partial}{\partial r} \left(\frac{1}{r} \frac{\partial \phi}{\partial \theta} \right) \end{aligned} \quad (14)$$

³G. Kirsch, *VDI*, vol. 42, 1898; described in Timoshenko & Goodier, *op. cit.*.

We now seek a function $\phi(r, \theta)$ that satisfies Eqn. 13 and also the boundary conditions of the problem. On the periphery of the hole the radial and shearing stresses must vanish, since no external tractions exist there:

$$\sigma_r = \tau_{r\theta} = 0, \quad r = a \quad (15)$$

Far from the hole, the stresses must become the far-field value σ ; the Mohr procedure gives the radial and tangential stress components in circular coordinates as

$$\left. \begin{aligned} \sigma_r &= \frac{\sigma}{2}(1 + \cos 2\theta) \\ \sigma_\theta &= \frac{\sigma}{2}(1 - \cos 2\theta) \\ \tau_{r\theta} &= \frac{\sigma}{2} \sin 2\theta \end{aligned} \right\} r \rightarrow \infty \quad (16)$$

Since the normal stresses vary circumferentially as $\cos 2\theta$ (removing temporarily the $\sigma/2$ factor) and the shear stresses vary as $\sin 2\theta$, an acceptable stress function could be of the form

$$\phi = f(r) \cos 2\theta \quad (17)$$

When this is substituted into Eqn. 13, an ordinary differential equation in $f(r)$ is obtained:

$$\left(\frac{d^2}{dr^2} + \frac{1}{r} \frac{d}{dr} - \frac{4}{r^2} \right) \left(\frac{d^2 f}{dr^2} + \frac{1}{r} \frac{df}{dr} - \frac{4f}{r^2} \right) = 0$$

This has the general solution

$$f(r) = Ar^2 + Br^4 + C \frac{1}{r^2} + D \quad (18)$$

The stress function obtained from Eqns. 17 and 18 is now used to write expressions for the stresses according to Eqn. 14, and the constants determined using the boundary conditions in Eqns. 15 and 16; this gives

$$A = -\frac{\sigma}{4}, \quad B = 0, \quad C = -\frac{a^4 \sigma}{4}, \quad D = \frac{a^2 \sigma}{2}$$

Substituting these values into the expressions for stress and replacing the $\sigma/2$ that was temporarily removed, the final expressions for the stresses are

$$\begin{aligned} \sigma_r &= \frac{\sigma}{2} \left(1 - \frac{a^2}{r^2} \right) + \frac{\sigma}{2} \left(1 + \frac{3a^4}{r^4} - \frac{4a^2}{r^2} \right) \cos 2\theta \\ \sigma_\theta &= \frac{\sigma}{2} \left(1 + \frac{a^2}{r^2} \right) - \frac{\sigma}{2} \left(1 + \frac{3a^4}{r^4} \right) \cos 2\theta \\ \tau_{r\theta} &= -\frac{\sigma}{2} \left(1 - \frac{3a^4}{r^4} + \frac{2a^2}{r^2} \right) \sin 2\theta \end{aligned} \quad (19)$$

As seen in the plot of Fig. 3, the stress reaches a maximum value of $(\sigma_\theta)_{\max} = 3\sigma$ at the periphery of the hole ($r = a$), at a diametral position transverse to the loading direction ($\theta = \pi/2$). The *stress concentration factor*, or SCF, for this problem is therefore 3. The x -direction stress falls to zero at the position $\theta = \pi/2$, $r = a$, as it must to satisfy the stress-free boundary condition at the periphery of the hole.

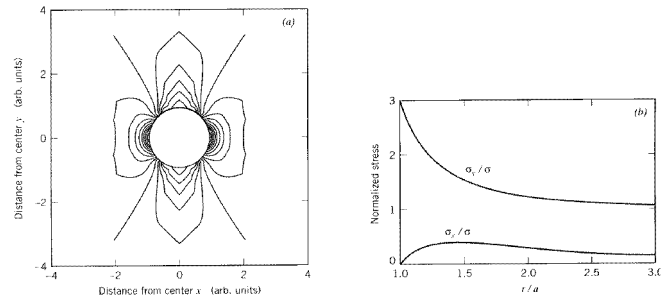


Figure 3: Stresses near circular hole. (a) Contours of σ_y (far-field stress applied in y -direction). (b) Variation of σ_y and σ_x along $\theta = \pi/2$ line.

Note that in the case of a circular hole the SCF does not depend on the size of the hole: any hole, no matter how small, increases the local stresses near the hole by a factor of three. This is a very serious consideration in the design of structures that must be drilled and riveted in assembly. This is the case in construction of most jetliner fuselages, the skin of which must withstand substantial stresses as the differential cabin pressure is cycled by approximately 10 psig during each flight. The high-stress region near the rivet holes has a dangerous propensity to incubate fatigue cracks, and several catastrophic aircraft failures have been traced to exactly this cause.

Note also that the stress concentration effect is confined to the region quite close to the hole, with the stresses falling to their far-field values within three or so hole diameters. This is a manifestation of *St. Venant's principle*⁴, which is a common-sense statement that the influence of a perturbation in the stress field is largely confined to the region of the disturbance. This principle is extremely useful in engineering approximations, but of course the stress concentration near the disturbance itself must be kept in mind.

When at the beginning of this section we took the size of the plate to be “infinite in lateral extent,” we really meant that the stress conditions at the plate edges were far enough away from the hole that they did not influence the stress state near the hole. With the Kirsch solution now in hand, we can be more realistic about this: the plate must be three or so times larger than the hole, or the Kirsch solution will be unreliable.

Complex functions

In many problems of practical interest, it is convenient to use stress functions as complex functions of two variables. We will see that these have the ability to satisfy the governing equations automatically, leaving only adjustments needed to match the boundary conditions. For this reason, complex-variable methods play an important role in theoretical stress analysis, and even in this introductory treatment we wish to illustrate the power of the method. To outline a few necessary relations, consider z to be a complex number in Cartesian coordinates x and y or polar coordinates r and θ as

$$z = x + iy = re^{i\theta} \quad (20)$$

⁴The French scientist Barré de Saint-Venant (1797–1886) is one of the great pioneers in mechanics of materials.

where $i = \sqrt{-1}$. An *analytic function* $f(z)$ is one whose derivatives depend on z only, and takes the form

$$f(z) = \alpha + i\beta \quad (21)$$

where α and β are real functions of x and y . It is easily shown that α and β satisfy the *Cauchy-Riemann* equations:

$$\frac{\partial\alpha}{\partial x} = \frac{\partial\beta}{\partial y} \quad \frac{\partial\alpha}{\partial y} = -\frac{\partial\beta}{\partial x} \quad (22)$$

If the first of these is differentiated with respect to x and the second with respect to y , and the results added, we obtain

$$\frac{\partial^2\alpha}{\partial x^2} + \frac{\partial^2\alpha}{\partial y^2} \equiv \nabla^2\alpha = 0 \quad (23)$$

This is *Laplace's equation*, and any function that satisfies this equation is termed a *harmonic* function. Equivalently, α could have been eliminated in favor of β to give $\nabla^2\beta = 0$, so both the real and imaginary parts of any complex function provide solutions to Laplace's equation. Now consider a function of the form $x\psi$, where ψ is harmonic; it can be shown by direct differentiation that

$$\nabla^4(x\psi) = 0 \quad (24)$$

i.e. any function of the form $x\psi$, where ψ is harmonic, satisfies Eqn. 12, and many thus be used as a stress function. Similarly, it can be shown that $y\psi$ and $(x^2+y^2)\psi = r^2\psi$ are also suitable, as is ψ itself. In general, a suitable stress function can be obtained from any two analytic functions ψ and χ according to

$$\phi = \text{Re} [(x - iy)\psi(z) + \chi(z)] \quad (25)$$

where "Re" indicates the real part of the complex expression. The stresses corresponding to this function ϕ are obtained as

$$\begin{aligned} \sigma_x + \sigma_y &= 4 \text{Re } \psi'(z) \\ \sigma_y - \sigma_x + 2i\tau_{xy} &= 2[\bar{z}\psi''(z) + \chi''(z)] \end{aligned} \quad (26)$$

where the primes indicate differentiation with respect to z and the overbar indicates the *conjugate function* obtained by replacing i with $-i$; hence $\bar{z} = x - iy$.

Stresses around an elliptical hole

In a development very important to the theory of fracture, Inglis⁵ used complex potential functions to extend Kirsch's work to treat the stress field around a plate containing an elliptical rather than circular hole. This permits crack-like geometries to be treated by making the minor axis of the ellipse small. It is convenient to work in elliptical α, β coordinates, as shown in Fig. 4, defined as

$$x = c \cosh \alpha \cos \beta, \quad y = c \sinh \alpha \sin \beta \quad (27)$$

⁵C.E. Inglis, "Stresses in a Plate Due to the Presence of Cracks and Sharp Corners," *Transactions of the Institution of Naval Architects*, Vol. 55, London, 1913, pp. 219-230.

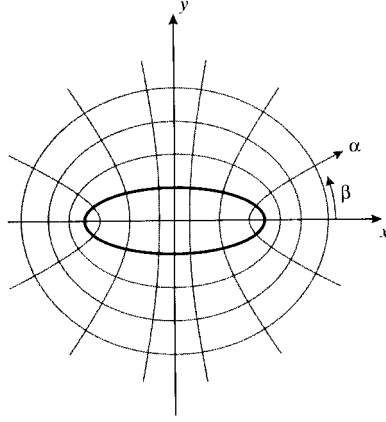


Figure 4: Elliptical coordinates.

where c is a constant. If β is eliminated this is seen in turn to be equivalent to

$$\frac{x^2}{\cosh^2 \alpha} + \frac{y^2}{\sinh^2 \alpha} = c^2 \quad (28)$$

On the boundary of the ellipse $\alpha = \alpha_0$, so we can write

$$c \cosh \alpha_0 = a, \quad c \sinh \alpha_0 = b \quad (29)$$

where a and b are constants. On the boundary, then

$$\frac{x^2}{a^2} + \frac{y^2}{b^2} = 1 \quad (30)$$

which is recognized as the Cartesian equation of an ellipse, with a and b being the major and minor radii. The elliptical coordinates can be written in terms of complex variables as

$$z = c \cosh \zeta, \quad \zeta = \alpha + i\beta \quad (31)$$

As the boundary of the ellipse is traversed, α remains constant at α_0 while β varies from 0 to 2π . Hence the stresses must be periodic in β with period 2π , while becoming equal to the far-field uniaxial stress $\sigma_y = \sigma, \sigma_x = \tau_{xy} = 0$ far from the ellipse; Eqn. 26 then gives

$$\left. \begin{aligned} 4 \operatorname{Re} \psi'(z) &= \sigma \\ 2[\bar{z}\psi''(z) + \chi''(z)] &= \sigma \end{aligned} \right\} \zeta \rightarrow \infty \quad (32)$$

These boundary conditions can be satisfied by potential functions in the forms

$$\begin{aligned} 4\psi(z) &= Ac \cosh \zeta + Bc \sinh \zeta \\ 4\chi(z) &= Cc^2\zeta + Dc^2 \cosh 2\zeta + Ec^2 \sinh 2\zeta \end{aligned}$$

where A, B, C, D, E are constants to be determined from the boundary conditions. When this is done the complex potentials are given as

$$4\psi(z) = \sigma c[(1 + e^{2\alpha_0}) \sinh \zeta - e^{2\alpha_0} \cosh \zeta]$$

$$4\chi(z) = -\sigma c^2 \left[(\cosh 2\alpha_0 - \cosh \pi)\zeta + \frac{1}{2}e^{2\alpha_0} - \cosh 2 \left(\zeta - \alpha_0 - i\frac{\pi}{2} \right) \right]$$

The stresses σ_x , σ_y , and τ_{xy} can be obtained by using these in Eqns. 26. However, the amount of labor in carrying out these substitutions isn't to be sneezed at, and before computers were generally available the Inglis solution was of somewhat limited use in probing the nature of the stress field near crack tips.

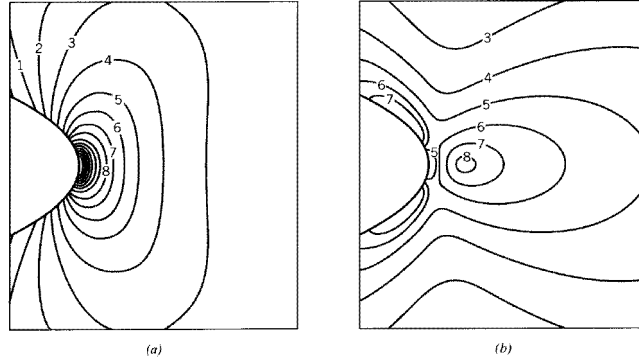


Figure 5: Stress field in the vicinity of an elliptical hole, with uniaxial stress applied in y -direction. (a) Contours of σ_y , (b) Contours of σ_x .

Figure 5 shows stress contours computed by Cook and Gordon⁶ from the Inglis equations. A strong stress concentration of the stress σ_y is noted at the periphery of the hole, as would be expected. The horizontal stress σ_x goes to zero at this same position, as it must to satisfy the boundary conditions there. Note however that σ_x exhibits a mild stress concentration (one fifth of that for σ_y , it turns out) a little distance away from the hole. If the material has planes of weakness along the y direction, for instance as between the fibrils in wood or many other biological structures, the stress σ_x could cause a split to open up in the y direction just ahead of the main crack. This would act to blunt and arrest the crack, and thus impart a measure of toughness to the material. This effect is sometimes called the *Cook-Gordon toughening mechanism*.

The mathematics of the Inglis solution are simpler at the surface of the elliptical hole, since here the normal component σ_α must vanish. The tangential stress component can then be computed directly:

$$(\sigma_\beta)_{\alpha=\alpha_0} = \sigma e^{2\alpha_0} \left[\frac{\sinh 2\alpha_0(1 + e^{-2\alpha_0})}{\cosh 2\alpha_0 - \cos 2\beta} - 1 \right]$$

The greatest stress occurs at the end of the major axis ($\cos 2\beta = 1$):

$$(\sigma_\beta)_{\beta=0,\pi} = \sigma_y = \sigma \left(1 + 2\frac{a}{b} \right) \quad (33)$$

This can also be written in terms of the radius of curvature ρ at the tip of the major axis as

$$\sigma_y = \sigma \left(1 + 2\sqrt{\frac{a}{\rho}} \right) \quad (34)$$

⁶J.E. Gordon, *The Science of Structures and Materials*, Scientific American Library, New York, 1988.

This result is immediately useful: it is clear that large cracks are worse than small ones (the local stress increases with crack size a), and it is also obvious that sharp voids (decreasing ρ) are worse than rounded ones. Note also that the stress σ_y increases without limit as the crack becomes sharper ($\rho \rightarrow 0$), so the concept of a stress concentration factor becomes difficult to use for very sharp cracks. When the major and minor axes of the ellipse are the same ($b = a$), the result becomes identical to that of the circular hole outlined earlier.

Stresses near a sharp crack

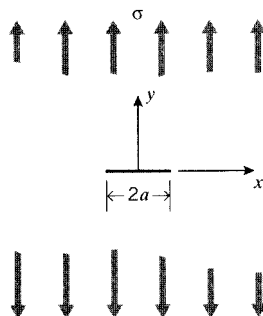


Figure 6: Sharp crack in an infinite sheet.

The Inglis solution is difficult to apply, especially as the crack becomes sharp. A more tractable and now more widely used approach was developed by Westergaard⁷, which treats a sharp crack of length $2a$ in a thin but infinitely wide sheet (see Fig. 6). The stresses that act perpendicularly to the crack free surfaces (the crack “flanks”) must be zero, while at distances far from the crack they must approach the far-field imposed stresses. Consider a harmonic function $\phi(z)$, with first and second derivatives $\phi'(z)$ and $\phi''(z)$, and first and second integrals $\bar{\phi}(z)$ and $\bar{\bar{\phi}}(z)$. Westergaard constructed a stress function as

$$\Phi = \operatorname{Re} \bar{\bar{\phi}}(z) + y \operatorname{Im} \bar{\phi}(z) \quad (35)$$

It can be shown directly that the stresses derived from this function satisfy the equilibrium, compatibility, and constitutive relations. The function $\phi(z)$ needed here is a harmonic function such that the stresses approach the far-field value of σ at infinity, but are zero at the crack flanks except at the crack tip where the stress becomes unbounded:

$$\sigma_y = \begin{cases} \sigma, & x \rightarrow \pm\infty, \quad -a < x < +a, y = 0 \\ \infty, & x = \pm a \end{cases}$$

These conditions are satisfied by complex functions of the form

$$\phi(z) = \frac{\sigma}{\sqrt{1 - a^2/z^2}} \quad (36)$$

⁷Westergaard, H.M., “Bearing Pressures and Cracks,” *Transactions, Am. Soc. Mech. Engrs., Journal of Applied Mechanics*, Vol. 5, p. 49, 1939.

This gives the needed singularity for $z = \pm a$, and the other boundary conditions can be verified directly as well. The stresses are now found by suitable differentiations of the stress function; for instance

$$\sigma_y = \frac{\partial^2 \Phi}{\partial x^2} = \operatorname{Re} \phi(z) + y \operatorname{Im} \phi'(z)$$

In terms of the distance r from the crack tip, this becomes

$$\sigma_y = \sigma \sqrt{\frac{a}{2r}} \cdot \cos \frac{\theta}{2} \left(1 + \sin \frac{\theta}{2} \sin \frac{3\theta}{2} \right) + \dots \quad (37)$$

where these are the initial terms of a series approximation. Near the crack tip, when $r \ll a$, we can write

$$(\sigma_y)_{y=0} = \sigma \sqrt{\frac{a}{2r}} \equiv \frac{K}{\sqrt{2\pi r}} \quad (38)$$

where $K = \sigma \sqrt{\pi a}$ is the *stress intensity factor*, with units of $\text{Nm}^{-3/2}$ or $\text{psi}\sqrt{\text{in}}$. (The factor π seems redundant here since it appears to the same power in both the numerator and denominator, but it is usually included as written here for agreement with the older literature.) We will see in the Module on Fracture that the stress intensity factor is a commonly used measure of the driving force for crack propagation, and thus underlies much of modern fracture mechanics. The dependency of the stress on distance from the crack is singular, with a $1/\sqrt{r}$ dependency. The K factor scales the intensity of the overall stress distribution, with the stress always becoming unbounded as the crack tip is approached.

Problems

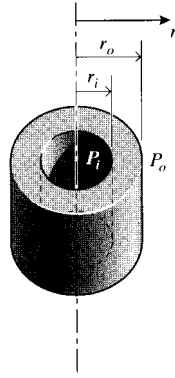
1. Expand the governing equations (Eqns. 1—3) in two Cartesian dimensions. Identify the unknown functions. How many equations and unknowns are there?
2. Consider a thick-walled pressure vessel of inner radius r_i and outer radius r_o , subjected to an internal pressure p_i and an external pressure p_o . Assume a trial solution for the radial displacement of the form $u(r) = Ar + B/r$; this relation can be shown to satisfy the governing equations for equilibrium, strain-displacement, and stress-strain governing equations.
 - (a) Evaluate the constants A and B using the boundary conditions

$$\sigma_r = -p_i \text{ @ } r = r_i, \quad \sigma_r = -p_o \text{ @ } r = r_o$$

- (b) Then show that

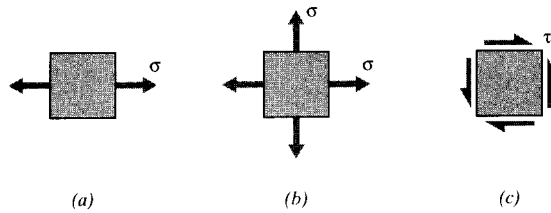
$$\sigma_r(r) = -\frac{p_i [(r_o/r)^2 - 1] + p_o [(r_o/r_i)^2 - (r_o/r)^2]}{(r_o/r_i)^2 - 1}$$

3. Justify the boundary conditions given in Eqns. 14 for stress in circular coordinates ($\sigma_r, \sigma_\theta, \tau_{xy}$) appropriate to a uniaxially loaded plate containing a circular hole.
4. Show that the Airy function $\phi(x, y)$ defined by Eqns. 11 satisfies the equilibrium equations.



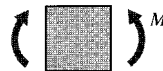
Prob. 2

5. Show that stress functions in the form of quadratic or cubic polynomials ($\phi = a_2x^2 + b_2xy + c_2y^2$ and $\phi = a_3x^3 + b_3x^2y + c_3xy^2 + d_3y^3$) automatically satisfy the governing relation $\nabla^4\phi = 0$.
6. Write the stresses $\sigma_x, \sigma_y, \tau_{xy}$ corresponding to the quadratic and cubic stress functions of the previous problem.
7. Choose the constants in the quadratic stress function of the previous two problems so as to represent (a) simple tension, (b) biaxial tension, and (c) pure shear of a rectangular plate.



Prob. 7

8. Choose the constants in the cubic stress function of the previous problems so as to represent pure bending induced by couples applied to vertical sides of a rectangular plate.



Prob. 8

9. Consider a cantilevered beam of rectangular cross section and width $b = 1$, loaded at the free end ($x = 0$) with a force P . At the free end, the boundary conditions on stress can be written $\sigma_x = \sigma_y = 0$, and

$$\int_{-h/2}^{h/2} \tau_{xy} dy = P$$

The horizontal edges are not loaded, so we also have that $\tau_{xy} = 0$ at $y = \pm h/2$.

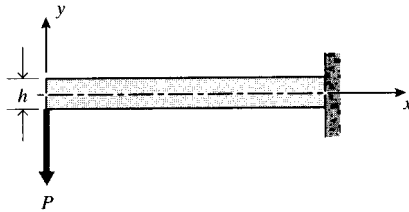
(a) Show that these conditions are satisfied by a stress function of the form

$$\phi = b_2xy + d_4xy^3$$

(b) Evaluate the constants to show that the stresses can be written

$$\sigma_x = \frac{Pxy}{I}, \quad \sigma_y = 0, \quad \tau_{xy} = \frac{P}{2I} \left[\left(\frac{h}{2} \right)^2 - y^2 \right]$$

in agreement with the elementary theory of beam bending (Module 13).



Prob. 9

Experimental Strain Analysis

David Roylance
Department of Materials Science and Engineering
Massachusetts Institute of Technology
Cambridge, MA 02139

February 23, 2001

Introduction

As was seen in previous modules, stress analysis even of simple-appearing geometries can lead to complicated mathematical maneuvering. Actual articles — engine crankshafts, medical prostheses, tennis rackets, etc. — have boundary shapes that cannot easily be described mathematically, and even if they were it would be extremely difficult to fit solutions of the governing equations to them. One approach to this impasse is the experimental one, in which we seek to construct a physical laboratory model that somehow reveals the stresses in a measurable way.

It is the nature of forces and stresses that they cannot be measured directly. It is the *effect* of a force that is measurable: when we weigh an object on a spring scale, we are actually measuring the stretching of the spring, and then calculating the force from Hooke's law. Experimental *stress* analysis, then, is actually experimental *strain* analysis. The difficulty is that strains in the linear elastic regime are almost always small, on the order of 1% or less, and the art in this field is that of detecting and interpreting small displacements. We look for phenomena that exhibit large and measurable changes due to small and difficult-to-measure displacements. There a number of such techniques, and three of these will be outlined briefly in the sections to follow. A good deal of methodology has been developed around these and other experimental methods, and both further reading¹ and laboratory practice would be required to put become competent in this area.

Strain gages

The term “strain gage” usually refers to a thin wire or foil, folded back and forth on itself and bonded to the specimen surface as seen in Fig. 1, that is able to generate an electrical measure of strain in the specimen. As the wire is stretched along with the specimen, the wire's electrical resistance R changes both because its length L is increased and its cross-sectional area A is reduced. For many resistors, these variables are related by the simple expression discovered in 1856 by Lord Kelvin:

$$R = \frac{\rho L}{A}$$

¹*Manual on Experimental Stress Analysis*, Third Edition, Society of Experimental Stress Analysis (now Society of Experimental Mechanics), 1978.

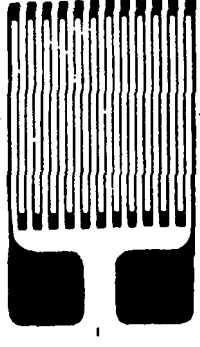


Figure 1: Wire resistance strain gage.

where here ρ is the material's *resistivity*. To express the effect of a strain $\epsilon = dL/L$ in the wire's long direction on the electrical resistance, assume a circular wire with $A = \pi r^2$ and take logarithms:

$$\ln R = \ln \rho + \ln L - (\ln \pi + 2 \ln r)$$

The total differential of this expression gives

$$\frac{dR}{R} = \frac{d\rho}{\rho} + \frac{dL}{L} - 2\frac{dr}{r}$$

Since

$$\epsilon_r = \frac{dr}{r} = -\nu \frac{dL}{L}$$

then

$$\frac{dR}{R} = \frac{d\rho}{\rho} + (1 + 2\nu) \frac{dL}{L}$$

P.W. Bridgeman (1882–1961) in 1929 studied the effect of volume change on electrical resistance and found these to vary proportionally:

$$\frac{d\rho}{\rho} = \alpha_R \frac{dV}{V}$$

where α_R is the constant of proportionality between resistance change and volume change. Writing the volume change in terms of changes in length and area, this becomes

$$\frac{d\rho}{\rho} = \alpha_R \left(\frac{dL}{L} + \frac{dA}{A} \right) = \alpha_R (1 - 2\nu) \frac{dL}{L}$$

Hence

$$\frac{dR/R}{\epsilon} = (1 + 2\nu) + \alpha_R (1 - 2\nu) \tag{1}$$

This quantity is called the *gage factor*, GF. Constantan, a 45/55 nickel/copper alloy, has $\alpha_R = 1.13$ and $\nu = 0.3$, giving $GF \approx 2.0$. This material also has a low temperature coefficient of resistivity, which reduces the temperature sensitivity of the strain gage.

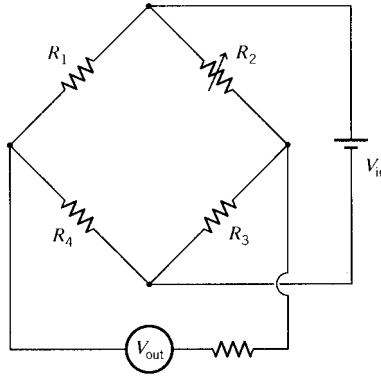


Figure 2: Wheatstone bridge circuit for strain gages.

A change in resistance of only 2%, which would be generated by a gage with $GF = 2$ at 1% strain, would not be noticeable on a simple ohmmeter. For this reason strain gages are almost always connected to a Wheatstone-bridge circuit as seen in Fig. 2. The circuit can be adjusted by means of the variable resistance R_2 to produce a zero output voltage V_{out} before strain is applied to the gage. Typically the gage resistance is approximately 350Ω and the excitation voltage is near 10V. When the gage resistance is changed by strain, the bridge is unbalanced and a voltage appears on the output according to the relation

$$\frac{V_{out}}{V_{in}} = \frac{\Delta R}{2R_0}$$

where R_0 is the nominal resistance of the four bridge elements. The output voltage is easily measured because it is a deviation from zero rather than being a relatively small change superimposed on a much larger quantity; it can thus be amplified to suit the needs of the data acquisition system.

Temperature compensation can be achieved by making a bridge element on the opposite side of the bridge from the active gage, say R_3 , an inactive gage that is placed near the active gage but not bonded to the specimen. Resistance changes in the active gage due to temperature will then be offset by an equal resistance change in the other arm of the bridge.

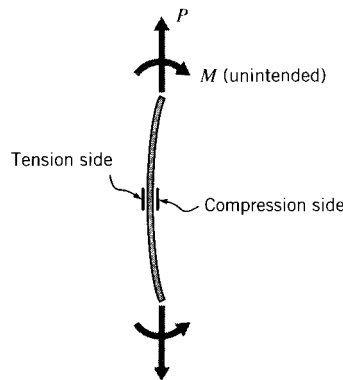


Figure 3: Cancellation of bending effects.

It is often difficult to mount a tensile specimen in the testing machine without inadvertently applying bending in addition to tensile loads. If a single gage were applied to the convex-outward side of the specimen, its reading would be erroneously high. Similarly, a gage placed on the concave-inward or compressive-tending side would read low. These bending errors can be eliminated by using an active gage on each side of the specimen as shown in Fig. 3 and wiring them on the same side of the Wheatstone bridge, e.g. R_1 and R_4 . The tensile component of bending on one side of the specimen is accompanied by an equal but compressive component on the other side, and these will generate equal but opposite resistance changes in R_1 and R_4 . The effect of bending will therefore cancel, and the gage combination will measure only the tensile strain (with doubled sensitivity, since both R_1 and R_4 are active).

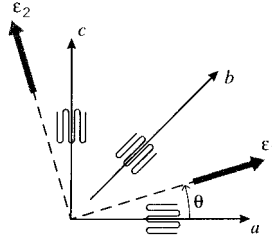


Figure 4: Strain rosette.

The strain in the gage direction can be found directly from the gage factor (Eqn. 1). When the direction of principal stress is unknown, strain gage *rosettes* are useful; these employ multiple gages on the same film backing, oriented in different directions. The rectangular three-gage rosette shown in Fig. 4 uses two gages oriented perpendicularly, and a third gage oriented at 45° to the first two.

Example 1

A three-gage rosette gives readings $\epsilon_0 = 150\mu$, $\epsilon_{45} = 200\mu$, and $\epsilon_{90} = -100\mu$ (here the μ symbol indicates micrometers per meter). If we align the x and y axis along the 0° and 90° gage directions, then ϵ_x and ϵ_y are measured directly, since these are ϵ_0 and ϵ_{90} respectively. To determine the shear strain γ_{xy} , we use the rule for strain transformation to write the normal strain at 45° :

$$\epsilon_{45} = 200\mu = \epsilon_x \cos^2 45 + \epsilon_y \sin^2 45 + \gamma_{xy} \sin 45 \cos 45$$

Substituting the known values for ϵ_x and ϵ_y , and solving,

$$\gamma_{xy} = 350\mu$$

The principal strains can now be found as

$$\epsilon_{1,2} = \frac{\epsilon_x + \epsilon_y}{2} \pm \sqrt{\left(\frac{\epsilon_x - \epsilon_y}{2}\right)^2 + \left(\frac{\gamma_{xy}}{2}\right)^2} = 240\mu, -190\mu$$

The angle from the x -axis to the principal plane is

$$\tan 2\theta_p = \frac{\gamma_{xy}/2}{(\epsilon_x - \epsilon_y)/2} \rightarrow \theta_p = 27.2^\circ$$

The stresses can be found from the strains from the material constitutive relations; for instance for steel with $E = 205$ GPa and $\nu = .3$ the principal stress is

$$\sigma_1 = \frac{E}{1 - \nu^2}(\epsilon_1 + \nu\epsilon_2) = 41.2 \text{ MPa}$$

For the specific case of a 0-45-90 rosette, the orientation of the principal strain axis can be given directly by²

$$\tan 2\theta = \frac{2\epsilon_b - \epsilon_a - \epsilon_c}{\epsilon_a - \epsilon_c} \quad (2)$$

and the principal strains are

$$\epsilon_{1,2} = \frac{\epsilon_a + \epsilon_c}{2} \pm \sqrt{\frac{(\epsilon_a - \epsilon_b)^2 + (\epsilon_b - \epsilon_c)^2}{2}} \quad (3)$$

Graphical solutions based on Mohr's circles are also useful for reducing gage output data.

Strain gages are used very extensively, and critical structures such as aircraft may be instrumented with hundreds of gages during testing. Each gage must be bonded carefully to the structure, and connected by its two leads to the signal conditioning unit that includes the excitation voltage source and the Wheatstone bridge. This can obviously be a major instrumentation chore, with computer-aided data acquisition and reduction a practical necessity.

Photoelasticity

Wire-resistance strain gages are probably the principal device used in experimental stress analysis today, but they have the disadvantage of monitoring strain only at a single location. Photoelasticity and moire methods, to be outlined in the following sections, are more complicated in concept and application but have the ability to provide *full-field* displays of the strain distribution. The intuitive insight from these displays can be so valuable that it may be unnecessary to convert them to numerical values, although the conversion can be done if desired.

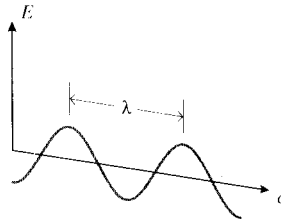


Figure 5: Light propagation.

Photoelasticity employs a property of many transparent polymers and inorganic glasses called *birefringence*. To explain this phenomenon, recall the definition of *refractive index*, n , which is the ratio of the speed of light v in the medium to that in vacuum c :

$$n = \frac{v}{c} \quad (4)$$

²M. Hetenyi, ed., *Handbook of Experimental Stress Analysis*, Wiley, New York, 1950.

As the light beam travels in space (see Fig. 5), its electric field vector E oscillates up and down at an angular frequency ω in a fixed plane, termed the *plane of polarization* of the beam. (The wavelength of the light is $\lambda = 2\pi c/\omega$.) A birefringent material is one in which the refractive index depends on the orientation of plane of polarization, and magnitude of the birefringence is the difference in indices:

$$\Delta n = n_{\perp} - n_{\parallel}$$

where n_{\perp} and n_{\parallel} are the refractive indices on the two planes. Those two planes that produce the maximum Δn are the *principal optical planes*. As shown in Fig. 6, a birefringent material can be viewed simplistically as a Venetian blind that resolves an arbitrarily oriented electric field vector into two components, one on each of the two principal optical planes, after which each component will transit the material at a different speed according to Eqn. 4. The two components will eventually exit the material, again traveling at the same speed but having been shifted in phase from one another by an amount related to the difference in transit times.

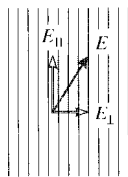


Figure 6: Venetian-blind model of birefringence.

A *photoelastic* material is one in which the birefringence depends on the applied stress, and many such materials can be described to a good approximation by the *stress-optical law*

$$\Delta n = C(\lambda)(\sigma_1 - \sigma_2) \quad (5)$$

where C is the *stress-optical coefficient*, and the quantity in the second parentheses is the difference between the two principal stresses in the plane normal to the light propagation direction; this is just twice the maximum shear stress in that plane. The stress-optical coefficient is generally a function of the wavelength λ .

The stress distribution in an irregularly shaped body can be viewed by replicating the actual structure (probably scaled up or down in size for convenience) in a birefringent material such as epoxy. If the structure is statically determinate, the stresses in the model will be the same as that in the actual structure, in spite of the differences in modulus. To make the birefringence effect visible, the model is placed between crossed polarizers in an apparatus known as a *polariscope*. (Polarizers such as Polaroid, a polymer sheet containing oriented iodide crystals, are essentially just birefringent materials that pass only light polarized in the polarizer's principal optical plane.)

The radiation source can produce either conventional white (polychromatic) or filtered (monochromatic) light. The electric field vector of light striking the first polarizer with an arbitrary orientation can be resolved into two components as shown in Fig. 7, one in the polarization direction and the other perpendicular to it. The polarizer will block the transverse component, allowing the parallel component to pass through to the specimen. This polarized component can be written

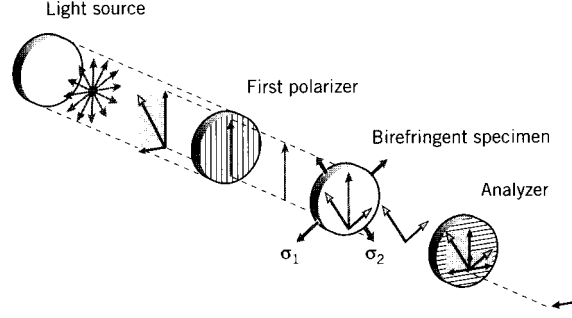


Figure 7: The circular polariscope.

$$u_P = A \cos \omega t$$

where u_P is the field intensity at time t . The birefringent specimen will resolve this component into two further components, along each of the principal stress directions; these can be written as

$$u_1 = A \cos \alpha \cos \omega t$$

$$u_2 = A \sin \alpha \cos \omega t$$

where α is the (unknown) angle the principal stress planes makes with the polarization direction. Both of these new components pass through the specimen, but at different speeds as given by Eqn. 5. After traveling through the specimen a distance h with velocities v_1 and v_2 , they emerge as

$$u'_1 = A \cos \alpha \cos \omega [t - (h/v_1)]$$

$$u'_2 = A \sin \alpha \cos \omega [t - (h/v_2)]$$

These two components then fall on the second polarizer, oriented at 90° to the first and known as the *analyzer*. Each is again resolved into further components parallel and perpendicular to the analyzer axis, and the perpendicular components blocked while the parallel components passed through. The transmitted component can be written as

$$\begin{aligned} u_A &= -u'_1 \sin \alpha + u'_2 \cos \alpha \\ &= -A \sin \alpha \cos \alpha \left[\cos \omega \left(t - \frac{h}{v_1} \right) - \cos \omega \left(t - \frac{h}{v_2} \right) \right] \\ &= A \sin 2\alpha \sin \omega \left(\frac{h}{2v_1} - \frac{h}{2v_2} \right) \sin \omega \left(t - \frac{h}{2v_1} - \frac{h}{2v_2} \right) \end{aligned}$$

This is of the form $u_A = A' \sin(\omega t - \delta)$, where A' is an amplitude and δ is a phase angle. Note that the amplitude is zero, so that no light will be transmitted, if either $\alpha = 0$ or if

$$\frac{2\pi c}{\lambda} \left(\frac{h}{2v_1} - \frac{h}{2v_2} \right) = 0, \pi, 2\pi, \dots \quad (6)$$

The case for which $\alpha = 0$ occurs when the principal stress planes are aligned with the polarizer-analyzer axes. All positions on the model at which this is true thus produce an extinction of the transmitted light. These are seen as dark bands called *isoclinics*, since they map out lines of constant inclination of the principal stress axes. These contours can be photographed at a sequence of polarization orientations, if desired, to give an even more complete picture of stress directions.

Positions of zero stress produce extinction as well, since then the retardation is zero and the two light components exiting the analyzer cancel one another. The neutral axis of a beam in bending, for instance, shows as a black line in the observed field. As the stress at a given location is increased from zero, the increasing phase shift between the two components causes the cancellation to be incomplete, and light is observed. Eventually, as the stress is increased still further, the retardation will reach $\delta = \pi$, and extinction occurs again. This produces another dark fringe in the observed field. In general, alternating light areas and dark fringes are seen, corresponding to increasing orders of extinction.

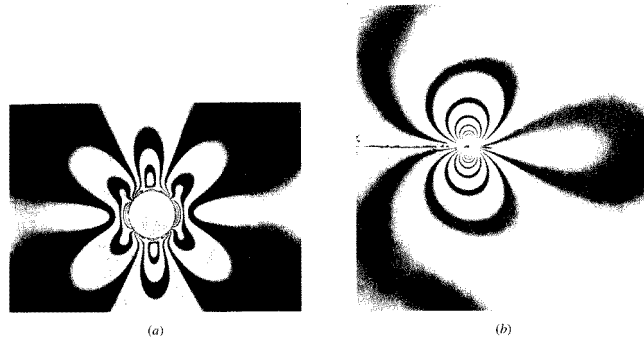


Figure 8: Photoelastic patterns for stress around (a) a circular hole and (b) a sharp crack.

Close fringe spacing indicates a steep stress gradient, similar to elevation lines on a geographical contour map; Fig. 8 shows the patterns around circular and a sharp-crack stress risers. It may suffice simply to observe the locations of high fringe density to note the presence of stress concentrations, which could then be eliminated by suitable design modifications (such as rounding corners or relocating abrupt geometrical discontinuities from high-stress regions). If white rather than monochromatic light is used, brightly colored lines rather than dark fringes are observed, with each color being the complement of that color that has been brought into extinction according to Eqn. 4. These bands of constant color are termed *isochromatics*.

Converting the fringe patterns to numerical stress values is usually straightforward but tedious, since the fringes are related to the stress difference $\sigma_1 - \sigma_2$ rather than a single stress. At a free boundary, however, the stress components normal to the boundary must be zero, which means that the stress tangential to the boundary is a principal stress and is therefore given directly by the fringe order there. The reduction of photoelastic patterns to numerical values usually involves beginning at these free surfaces, and then working gradually into the interior of the body using a graphical procedure.

Moire

The term “moire” is spelled with a small “m” and derives not from someone’s name but from the name of a silk fabric that shows patterns of light and dark bands. Bands of this sort are also developed by the superposition of two almost-identical gratings, such as might be seen when looking through two window screens slightly rotated from one another. Figure 9 demonstrates that fringes are developed if the two grids have different spacing as well as different orientations. The fringes change dramatically for even small motions or strains in the gratings, and this visual amplification of motion can be used in detecting and quantifying strain in the specimen.

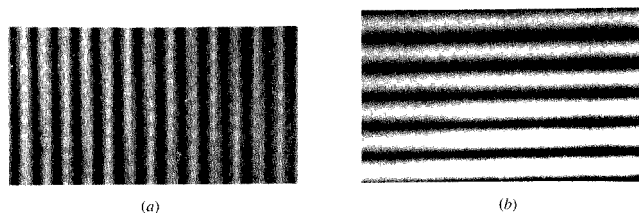


Figure 9: Moire fringes developed by difference in line pitch (a) and line orientation (b). (Prof. Fu-Pen Chiang, SUNY-Stony Brook.)

As a simple illustration of moire strain analysis, assume a grating of vertical lines of spacing p (the “specimen” grating) is bonded to the specimen and that this is observed by looking through another “reference” grating of the same period but not bonded to the specimen. Now let the specimen undergo a strain, so that the specimen grating is stretched to a period of p' . A dark fringe will appear when the lines from the two gratings superimpose, and this will occur when $N(p' - p) = p$, since after N lines on the specimen grid the incremental gap $(p' - p)$ will have accumulated to one reference pitch distance p . The distance S between the fringes is then

$$S = Np' = \frac{pp'}{p' - p} \quad (7)$$

The normal strain ϵ_x in the horizontal direction is now given directly from the fringe spacing as

$$\epsilon_x = \frac{p' - p}{p} = \frac{p}{S} \quad (8)$$

Fringes will also develop if the specimen grid undergoes a rotation relative to the reference grid: if the rotation is small, then

$$\frac{p}{S} = \tan \theta \approx \theta$$

$$S = \frac{p}{\theta}$$

This angle is also the shear strain γ_{xy} , so

$$\gamma_{xy} = \theta = \frac{p}{S} \quad (9)$$

More generally, consider the interference fringes that develop between a vertical reference grid and an arbitrarily displaced specimen grid (originally vertical). The zeroth-order ($N = 0$) fringe is that corresponding to positions having zero horizontal displacement, the first-order ($N = 1$)

fringe corresponds to horizontal motions of exactly one pitch distance, etc. The horizontal displacement is given directly by the fringe order as $u = Np$, from which the strain is given by

$$\epsilon_x = \frac{\partial u}{\partial x} = p \frac{\partial N}{\partial x} \quad (10)$$

so the strain is given as the slope of the fringe.

Similarly, a moire pattern developed between two originally horizontal grids, characterized by fringes $N' = 0, 1, 2, \dots$ gives the vertical strains:

$$\epsilon_y = \frac{\partial v}{\partial y} = \frac{\partial(N'p)}{\partial y} = p \frac{\partial N'}{\partial y} \quad (11)$$

The shearing strains are found from the slopes of both the u -field and v -field fringes:

$$\gamma_{xy} = p \left(\frac{\partial N}{\partial y} + \frac{\partial N'}{\partial x} \right) \quad (12)$$

Figure 10 shows the fringes corresponding to vertical displacements around a circular hole in a plate subjected to loading in the y -direction. The vertical strain ϵ_y is proportional to the y -distance between these fringes, each of which is a contour of constant vertical displacement. This strain is largest along the x -axis at the periphery of the hole, and smallest along the y -axis at the periphery of the hole.

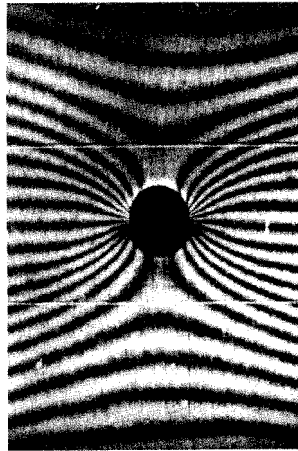


Figure 10: Moire patterns of the vertical displacements of a bar with a hole under pure tension. (Prof. Fu-Pen Chiang, SUNY-Stony Brook.)

Problems

1. A $0^\circ/45^\circ/90^\circ$ three-arm strain gage rosette bonded to a steel specimen gives readings $\epsilon_0 = 175\mu$, $\epsilon_{45} = 150\mu$, and $\epsilon_{90} = -120\mu$. Determine the principal stresses and the orientation of the principal planes at the gage location.
2. Repeat the previous problem, but with gage readings $\epsilon_0 = 150\mu$, $\epsilon_{45} = 200\mu$, and $\epsilon_{90} = 125\mu$.

Finite Element Analysis

David Roylance
Department of Materials Science and Engineering
Massachusetts Institute of Technology
Cambridge, MA 02139

February 28, 2001

Introduction

Finite element analysis (FEA) has become commonplace in recent years, and is now the basis of a multibillion dollar per year industry. Numerical solutions to even very complicated stress problems can now be obtained routinely using FEA, and the method is so important that even introductory treatments of Mechanics of Materials – such as these modules – should outline its principal features.

In spite of the great power of FEA, the disadvantages of computer solutions must be kept in mind when using this and similar methods: they do not necessarily reveal how the stresses are influenced by important problem variables such as materials properties and geometrical features, and errors in input data can produce wildly incorrect results that may be overlooked by the analyst. Perhaps the most important function of theoretical modeling is that of sharpening the designer’s intuition; users of finite element codes should plan their strategy toward this end, supplementing the computer simulation with as much closed-form and experimental analysis as possible.

Finite element codes are less complicated than many of the word processing and spreadsheet packages found on modern microcomputers. Nevertheless, they are complex enough that most users do not find it effective to program their own code. A number of prewritten commercial codes are available, representing a broad price range and compatible with machines from microcomputers to supercomputers¹. However, users with specialized needs should not necessarily shy away from code development, and may find the code sources available in such texts as that by Zienkiewicz² to be a useful starting point. Most finite element software is written in Fortran, but some newer codes such as `felt` are in C or other more modern programming languages.

In practice, a finite element analysis usually consists of three principal steps:

1. *Preprocessing*: The user constructs a *model* of the part to be analyzed in which the geometry is divided into a number of discrete subregions, or “elements,” connected at discrete points called “nodes.” Certain of these nodes will have fixed displacements, and others will have prescribed loads. These models can be extremely time consuming to prepare, and commercial codes vie with one another to have the most user-friendly graphical “pre-processor” to assist in this rather tedious chore. Some of these preprocessors can overlay a mesh on a preexisting CAD file, so that finite element analysis can be done conveniently as part of the computerized drafting-and-design process.

¹C.A. Brebbia, ed., *Finite Element Systems, A Handbook*, Springer-Verlag, Berlin, 1982.

²O.C. Zienkiewicz and R.L. Taylor, *The Finite Element Method*, McGraw-Hill Co., London, 1989.

2. *Analysis*: The dataset prepared by the preprocessor is used as input to the finite element code itself, which constructs and solves a system of linear or nonlinear algebraic equations

$$\mathbf{K}_{ij}\mathbf{u}_j = \mathbf{f}_i$$

where \mathbf{u} and \mathbf{f} are the displacements and externally applied forces at the nodal points. The formation of the \mathbf{K} matrix is dependent on the type of problem being attacked, and this module will outline the approach for truss and linear elastic stress analyses. Commercial codes may have very large element libraries, with elements appropriate to a wide range of problem types. One of FEA's principal advantages is that many problem types can be addressed with the same code, merely by specifying the appropriate element types from the library.

3. *Postprocessing*: In the earlier days of finite element analysis, the user would pore through reams of numbers generated by the code, listing displacements and stresses at discrete positions within the model. It is easy to miss important trends and hot spots this way, and modern codes use graphical displays to assist in visualizing the results. A typical postprocessor display overlays colored contours representing stress levels on the model, showing a full-field picture similar to that of photoelastic or moire experimental results.

The operation of a specific code is usually detailed in the documentation accompanying the software, and vendors of the more expensive codes will often offer workshops or training sessions as well to help users learn the intricacies of code operation. One problem users may have even after this training is that the code tends to be a "black box" whose inner workings are not understood. In this module we will outline the principles underlying most current finite element stress analysis codes, limiting the discussion to linear elastic analysis for now. Understanding this theory helps dissipate the black-box syndrome, and also serves to summarize the analytical foundations of solid mechanics.

Matrix analysis of trusses

Pin-jointed trusses, discussed more fully in Module 5, provide a good way to introduce FEA concepts. The static analysis of trusses can be carried out exactly, and the equations of even complicated trusses can be assembled in a matrix form amenable to numerical solution. This approach, sometimes called "matrix analysis," provided the foundation of early FEA development.

Matrix analysis of trusses operates by considering the stiffness of each truss element one at a time, and then using these stiffnesses to determine the forces that are set up in the truss elements by the displacements of the joints, usually called "nodes" in finite element analysis. Then noting that the sum of the forces contributed by each element to a node must equal the force that is externally applied to that node, we can assemble a sequence of linear algebraic equations in which the nodal displacements are the unknowns and the applied nodal forces are known quantities. These equations are conveniently written in matrix form, which gives the method its name:

$$\begin{bmatrix} K_{11} & K_{12} & \cdots & K_{1n} \\ K_{21} & K_{22} & \cdots & K_{2n} \\ \vdots & \vdots & \ddots & \vdots \\ K_{n1} & K_{n2} & \cdots & K_{nn} \end{bmatrix} \begin{Bmatrix} u_1 \\ u_2 \\ \vdots \\ u_n \end{Bmatrix} = \begin{Bmatrix} f_1 \\ f_2 \\ \vdots \\ f_n \end{Bmatrix}$$

Here u_i and f_j indicate the deflection at the i^{th} node and the force at the j^{th} node (these would actually be vector quantities, with subcomponents along each coordinate axis). The K_{ij} coefficient array is called the *global stiffness matrix*, with the ij component being physically the influence of the j^{th} displacement on the i^{th} force. The matrix equations can be abbreviated as

$$K_{ij}u_j = f_i \quad \text{or} \quad \mathbf{K}\mathbf{u} = \mathbf{f} \quad (1)$$

using either subscripts or boldface to indicate vector and matrix quantities.

Either the force externally applied or the displacement is known at the outset for each node, and it is impossible to specify simultaneously both an arbitrary displacement *and* a force on a given node. These prescribed nodal forces and displacements are the boundary conditions of the problem. It is the task of analysis to determine the forces that accompany the imposed displacements, and the displacements at the nodes where known external forces are applied.

Stiffness matrix for a single truss element

As a first step in developing a set of matrix equations that describe truss systems, we need a relationship between the forces and displacements at each end of a single truss element. Consider such an element in the $x - y$ plane as shown in Fig. 1, attached to nodes numbered i and j and inclined at an angle θ from the horizontal.

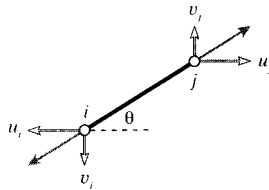


Figure 1: Individual truss element.

Considering the elongation vector δ to be resolved in directions along and transverse to the element, the elongation in the truss element can be written in terms of the differences in the displacements of its end points:

$$\delta = (u_j \cos \theta + v_j \sin \theta) - (u_i \cos \theta + v_i \sin \theta)$$

where u and v are the horizontal and vertical components of the deflections, respectively. (The displacements at node i drawn in Fig. 1 are negative.) This relation can be written in matrix form as:

$$\delta = \begin{bmatrix} -c & -s & c & s \end{bmatrix} \begin{Bmatrix} u_i \\ v_i \\ u_j \\ v_j \end{Bmatrix}$$

Here $c = \cos \theta$ and $s = \sin \theta$.

The axial force P that accompanies the elongation δ is given by Hooke's law for linear elastic bodies as $P = (AE/L)\delta$. The horizontal and vertical nodal forces are shown in Fig. 2; these can be written in terms of the total axial force as:

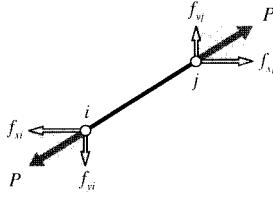


Figure 2: Components of nodal force.

$$\begin{aligned} \begin{Bmatrix} f_{xi} \\ f_{yi} \\ f_{xj} \\ f_{yj} \end{Bmatrix} &= \begin{Bmatrix} -c \\ -s \\ c \\ s \end{Bmatrix} P = \begin{Bmatrix} -c \\ -s \\ c \\ s \end{Bmatrix} \frac{AE}{L} \delta \\ &= \begin{Bmatrix} -c \\ -s \\ c \\ s \end{Bmatrix} \frac{AE}{L} \begin{bmatrix} -c & -s & c & s \end{bmatrix} \begin{Bmatrix} u_i \\ v_i \\ u_j \\ v_j \end{Bmatrix} \end{aligned}$$

Carrying out the matrix multiplication:

$$\begin{Bmatrix} f_{xi} \\ f_{yi} \\ f_{xj} \\ f_{yj} \end{Bmatrix} = \frac{AE}{L} \begin{bmatrix} c^2 & cs & -c^2 & -cs \\ cs & s^2 & -cs & -s^2 \\ -c^2 & -cs & c^2 & cs \\ -cs & -s^2 & cs & s^2 \end{bmatrix} \begin{Bmatrix} u_i \\ v_i \\ u_j \\ v_j \end{Bmatrix} \quad (2)$$

The quantity in brackets, multiplied by AE/L , is known as the “element stiffness matrix” k_{ij} . Each of its terms has a physical significance, representing the contribution of one of the displacements to one of the forces. The global system of equations is formed by combining the element stiffness matrices from each truss element in turn, so their computation is central to the method of matrix structural analysis. The principal difference between the matrix truss method and the general finite element method is in how the element stiffness matrices are formed; most of the other computer operations are the same.

Assembly of multiple element contributions

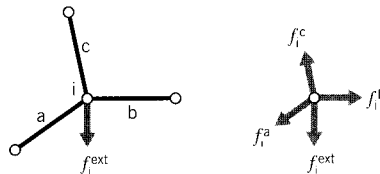


Figure 3: Element contributions to total nodal force.

The next step is to consider an assemblage of many truss elements connected by pin joints. Each element meeting at a joint, or node, will contribute a force there as dictated by the displacements of both that element’s nodes (see Fig. 3). To maintain static equilibrium, all

element force contributions f_i^{elem} at a given node must sum to the force f_i^{ext} that is externally applied at that node:

$$f_i^{ext} = \sum_{elem} f_i^{elem} = \left(\sum_{elem} k_{ij}^{elem} u_j \right) = \left(\sum_{elem} k_{ij}^{elem} \right) u_j = K_{ij} u_j$$

Each element stiffness matrix k_{ij}^{elem} is added to the appropriate location of the overall, or “global” stiffness matrix K_{ij} that relates all of the truss displacements and forces. This process is called “assembly.” The index numbers in the above relation must be the “global” numbers assigned to the truss structure as a whole. However, it is generally convenient to compute the individual element stiffness matrices using a local scheme, and then to have the computer convert to global numbers when assembling the individual matrices.

Example 1

The assembly process is at the heart of the finite element method, and it is worthwhile to do a simple case by hand to see how it really works. Consider the two-element truss problem of Fig. 4, with the nodes being assigned arbitrary “global” numbers from 1 to 3. Since each node can in general move in two directions, there are $3 \times 2 = 6$ total degrees of freedom in the problem. The global stiffness matrix will then be a 6×6 array relating the six displacements to the six externally applied forces. Only one of the displacements is unknown in this case, since all but the vertical displacement of node 2 (degree of freedom number 4) is constrained to be zero. Figure 4 shows a workable listing of the global numbers, and also “local” numbers for each individual element.

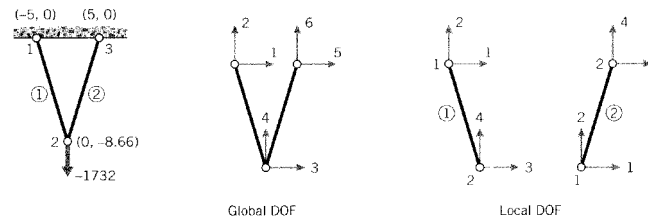


Figure 4: Global and local numbering for the two-element truss.

Using the local numbers, the 4×4 element stiffness matrix of each of the two elements can be evaluated according to Eqn. 2. The inclination angle is calculated from the nodal coordinates as

$$\theta = \tan^{-1} \frac{y_2 - y_1}{x_2 - x_1}$$

The resulting matrix for element 1 is:

$$k^{(1)} = \begin{bmatrix} 25.00 & -43.30 & -25.00 & 43.30 \\ -43.30 & 75.00 & 43.30 & -75.00 \\ -25.00 & 43.30 & 25.00 & -43.30 \\ 43.30 & -75.00 & -43.30 & 75.00 \end{bmatrix} \times 10^3$$

and for element 2:

$$k^{(2)} = \begin{bmatrix} 25.00 & 43.30 & -25.00 & -43.30 \\ 43.30 & 75.00 & -43.30 & -75.00 \\ -25.00 & -43.30 & 25.00 & 43.30 \\ -43.30 & -75.00 & 43.30 & 75.00 \end{bmatrix} \times 10^3$$

(It is important the units be consistent; here lengths are in inches, forces in pounds, and moduli in psi. The modulus of both elements is $E = 10$ Mpsi and both have area $A = 0.1$ in².) These matrices have rows and columns numbered from 1 to 4, corresponding to the local degrees of freedom of the element.

However, each of the local degrees of freedom can be matched to one of the global degrees of the overall problem. By inspection of Fig. 4, we can form the following table that maps local to global numbers:

local	global, element 1	global, element 2
1	1	3
2	2	4
3	3	5
4	4	6

Using this table, we see for instance that the second degree of freedom for element 2 is the fourth degree of freedom in the global numbering system, and the third local degree of freedom corresponds to the fifth global degree of freedom. Hence the value in the second row and third column of the element stiffness matrix of element 2, denoted $k_{23}^{(2)}$, should be added into the position in the fourth row and fifth column of the 6×6 global stiffness matrix. We write this as

$$k_{23}^{(2)} \longrightarrow K_{4,5}$$

Each of the sixteen positions in the stiffness matrix of each of the two elements must be added into the global matrix according to the mapping given by the table. This gives the result

$$K = \begin{bmatrix} k_{11}^{(1)} & k_{12}^{(1)} & k_{13}^{(1)} & k_{14}^{(1)} & 0 & 0 \\ k_{21}^{(1)} & k_{22}^{(1)} & k_{23}^{(1)} & k_{24}^{(1)} & 0 & 0 \\ k_{31}^{(1)} & k_{32}^{(1)} & k_{33}^{(1)} + k_{11}^{(2)} & k_{34}^{(1)} + k_{12}^{(2)} & k_{13}^{(2)} & k_{14}^{(2)} \\ k_{41}^{(1)} & k_{42}^{(1)} & k_{43}^{(1)} + k_{21}^{(2)} & k_{44}^{(1)} + k_{22}^{(2)} & k_{23}^{(2)} & k_{24}^{(2)} \\ 0 & 0 & k_{31}^{(2)} & k_{32}^{(2)} & k_{33}^{(2)} & k_{34}^{(2)} \\ 0 & 0 & k_{41}^{(2)} & k_{42}^{(2)} & k_{43}^{(2)} & k_{44}^{(2)} \end{bmatrix}$$

This matrix premultiplies the vector of nodal displacements according to Eqn. 1 to yield the vector of externally applied nodal forces. The full system equations, taking into account the known forces and displacements, are then

$$10^3 \begin{bmatrix} 25.0 & -43.3 & -25.0 & 43.3 & 0.0 & 0.00 \\ -43.3 & 75.0 & 43.3 & -75.0 & 0.0 & 0.00 \\ -25.0 & 43.3 & 50.0 & 0.0 & -25.0 & -43.30 \\ 43.3 & -75.0 & 0.0 & 150.0 & -43.3 & -75.00 \\ 0.0 & 0.0 & -25.0 & -43.3 & 25.0 & 43.30 \\ 0.0 & 0.0 & -43.3 & -75.0 & 43.3 & 75.00 \end{bmatrix} \begin{Bmatrix} 0 \\ 0 \\ 0 \\ u_4 \\ 0 \\ 0 \end{Bmatrix} = \begin{Bmatrix} f_1 \\ f_2 \\ f_3 \\ -1732 \\ f_5 \\ f_5 \end{Bmatrix}$$

Note that either the force or the displacement for each degree of freedom is known, with the accompanying displacement or force being unknown. Here only one of the displacements (u_4) is unknown, but in most problems the unknown displacements far outnumber the unknown forces. Note also that only those elements that are physically connected to a given node can contribute a force to that node. In most cases, this results in the global stiffness matrix containing many zeroes corresponding to nodal pairs that are not spanned by an element. Effective computer implementations will take advantage of the matrix sparseness to conserve memory and reduce execution time.

In larger problems the matrix equations are solved for the unknown displacements and forces by Gaussian reduction or other techniques. In this two-element problem, the solution for the single unknown displacement can be written down almost from inspection. Multiplying out the fourth row of the system, we have

$$0 + 0 + 0 + 150 \times 10^3 u_4 + 0 + 0 = -1732$$

$$u_4 = -1732/150 \times 10^3 = -0.01155 \text{ in}$$

Now any of the unknown forces can be obtained directly. Multiplying out the first row for instance gives

$$0 + 0 + 0 + (43.4)(-0.0115) \times 10^3 + 0 + 0 = f_1$$

$$f_1 = -500 \text{ lb}$$

The negative sign here indicates the horizontal force on global node #1 is to the left, opposite the direction assumed in Fig. 4.

The process of cycling through each element to form the element stiffness matrix, assembling the element matrix into the correct positions in the global matrix, solving the equations for displacements and then back-multiplying to compute the forces, and printing the results can be automated to make a very versatile computer code.

Larger-scale truss (and other) finite element analysis are best done with a dedicated computer code, and an excellent one for learning the method is available from the web at <http://felt.sourceforge.net/>. This code, named **felt**, was authored by Jason Gobat and Darren Atkinson for educational use, and incorporates a number of novel features to promote user-friendliness. Complete information describing this code, as well as the C-language source and a number of trial runs and auxiliary code modules is available via their web pages. If you have access to X-window workstations, a graphical shell named **velvet** is available as well.

Example 2

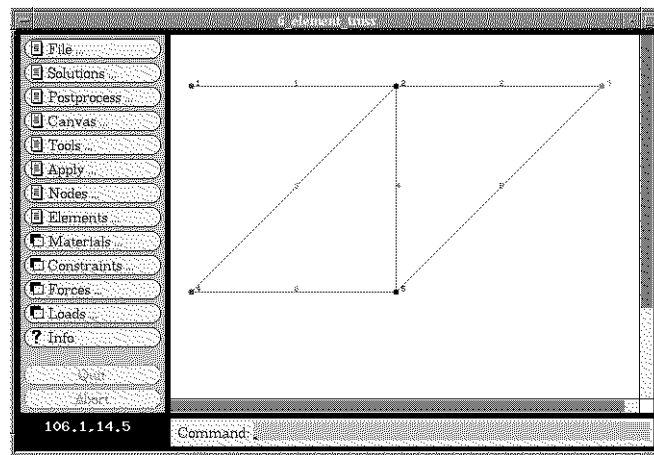


Figure 5: The six-element truss, as developed in the **velvet/felt** FEA graphical interface.

To illustrate how this code operates for a somewhat larger problem, consider the six-element truss of Fig. 5, which was analyzed in Module 5 both by the joint-at-a-time free body analysis approach and by Castigliano's method.

The input dataset, which can be written manually or developed graphically in **velvet**, employs parsing techniques to simplify what can be a very tedious and error-prone step in finite element analysis. The dataset for this 6-element truss is:

```
problem description
nodes=5 elements=6

nodes
1 x=0 y=100 z=0 constraint=pin
```



```

2 x=100 y=100 z=0 constraint=planar
3 x=200 y=100 z=0 force=P
4 x=0 y=0 z=0 constraint=pin
5 x=100 y=0 z=0 constraint=planar

```

truss elements

```

1 nodes=[1,2] material=steel
2 nodes=[2,3]
3 nodes=[4,2]
4 nodes=[2,5]
5 nodes=[5,3]
6 nodes=[4,5]

```

material properties

```
steel E=3e+07 A=0.5
```

distributed loads

constraints

```

free Tx=u Ty=u Tz=u Rx=u Ry=u Rz=u
pin Tx=c Ty=c Tz=c Rx=u Ry=u Rz=u
planar Tx=u Ty=u Tz=c Rx=u Ry=u Rz=u

```

forces

```
P Fy=-1000
```

end

The meaning of these lines should be fairly evident on inspection, although the `felt` documentation should be consulted for more detail. The output produced by `felt` for these data is:

** **

Nodal Displacements

Node #	DOF 1	DOF 2	DOF 3	DOF 4	DOF 5	DOF 6
1	0	0	0	0	0	0
2	0.013333	-0.03219	0	0	0	0
3	0.02	-0.084379	0	0	0	0
4	0	0	0	0	0	0
5	-0.0066667	-0.038856	0	0	0	0

Element Stresses

```

1:      4000
2:      2000
3:     -2828.4
4:      2000
5:     -2828.4
6:     -2000

```

Reaction Forces

Node #	DOF	Reaction Force
--------	-----	----------------

1	Tx	-2000
1	Ty	0
1	Tz	0
2	Tz	0
3	Tz	0
4	Tx	2000
4	Ty	1000
4	Tz	0
5	Tz	0

Material Usage Summary

Material: steel
Number: 6
Length: 682.8427
Mass: 0.0000

Total mass: 0.0000

The vertical displacement of node 3 (the DOF 2 value) is -0.0844, the same value obtained by the closed-form methods of Module 5. Figure 6 shows the *velvet* graphical output for the truss deflections (greatly magnified).

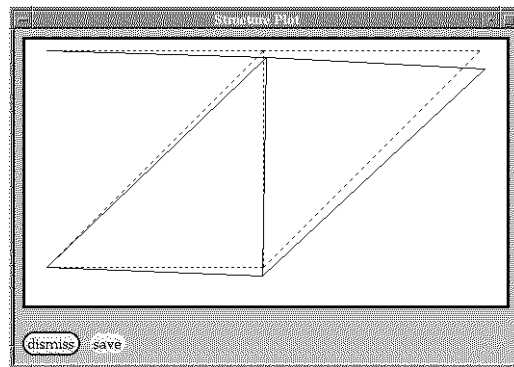


Figure 6: The 6-element truss in its original and deformed shape.

General Stress Analysis

The element stiffness matrix could be formed exactly for truss elements, but this is not the case for general stress analysis situations. The relation between nodal forces and displacements are not known in advance for general two- or three-dimensional stress analysis problems, and an approximate relation must be used in order to write out an element stiffness matrix.

In the usual “displacement formulation” of the finite element method, the governing equations are combined so as to have only displacements appearing as unknowns; this can be done by using the Hookean constitutive equations to replace the stresses in the equilibrium equations by the strains, and then using the kinematic equations to replace the strains by the displacements. This gives

$$\mathbf{L}^T \boldsymbol{\sigma} = \mathbf{L}^T \mathbf{D} \boldsymbol{\epsilon} = \mathbf{L}^T \mathbf{D} \mathbf{L} \mathbf{u} = \mathbf{0} \tag{3}$$

Of course, it is often impossible to solve these equations in closed form for the irregular boundary conditions encountered in practical problems. However, the equations are amenable to discretization and solution by numerical techniques such as finite differences or finite elements.

Finite element methods are one of several approximate numerical techniques available for the solution of engineering boundary value problems. Problems in the mechanics of materials often lead to equations of this type, and finite element methods have a number of advantages in handling them. The method is particularly well suited to problems with irregular geometries and boundary conditions, and it can be implemented in general computer codes that can be used for many different problems.

To obtain a numerical solution for the stress analysis problem, let us postulate a function $\tilde{\mathbf{u}}(x, y)$ as an approximation to \mathbf{u} :

$$\tilde{\mathbf{u}}(x, y) \approx \mathbf{u}(x, y) \quad (4)$$

Many different forms might be adopted for the approximation $\tilde{\mathbf{u}}$. The finite element method discretizes the solution domain into an assemblage of subregions, or “elements,” each of which has its own approximating functions. Specifically, the approximation for the displacement $\tilde{\mathbf{u}}(x, y)$ within an element is written as a combination of the (as yet unknown) displacements at the nodes belonging to that element:

$$\tilde{\mathbf{u}}(x, y) = N_j(x, y)\mathbf{u}_j \quad (5)$$

Here the index j ranges over the element’s nodes, \mathbf{u}_j are the nodal displacements, and the N_j are “interpolation functions.” These interpolation functions are usually simple polynomials (generally linear, quadratic, or occasionally cubic polynomials) that are chosen to become unity at node j and zero at the other element nodes. The interpolation functions can be evaluated at any position within the element by means of standard subroutines, so the approximate displacement at any position within the element can be obtained in terms of the nodal displacements directly from Eqn. 5.

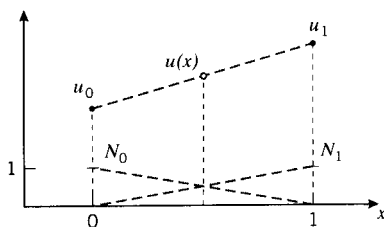


Figure 7: Interpolation in one dimension.

The interpolation concept can be illustrated by asking how we might guess the value of a function $u(x)$ at an arbitrary point x located between two nodes at $x = 0$ and $x = 1$, assuming we know somehow the nodal values $u(0)$ and $u(1)$. We might assume that as a reasonable approximation $u(x)$ simply varies linearly between these two values as shown in Fig. 7, and write

$$u(x) \approx \tilde{u}(x) = u_0(1 - x) + u_1(x)$$

or

$$\tilde{u}(x) = u_0 N_0(x) + u_1 N_1(x), \quad \begin{cases} N_0(x) = (1 - x) \\ N_1(x) = x \end{cases}$$

Here the N_0 and N_1 are the linear interpolation functions for this one-dimensional approximation. Finite element codes have subroutines that extend this interpolation concept to two and three dimensions.

Approximations for the strain and stress follow directly from the displacements:

$$\tilde{\boldsymbol{\epsilon}} = \mathbf{L}\tilde{\mathbf{u}} = \mathbf{L}N_j\mathbf{u}_j \equiv \mathbf{B}_j\mathbf{u}_j \quad (6)$$

$$\tilde{\boldsymbol{\sigma}} = \mathbf{D}\tilde{\boldsymbol{\epsilon}} = \mathbf{D}\mathbf{B}_j\mathbf{u}_j \quad (7)$$

where $\mathbf{B}_j(x, y) = \mathbf{L}N_j(x, y)$ is an array of derivatives of the interpolation functions:

$$\mathbf{B}_j = \begin{bmatrix} N_{j,x} & 0 \\ 0 & N_{j,y} \\ N_{j,y} & N_{j,x} \end{bmatrix} \quad (8)$$

A “virtual work” argument can now be invoked to relate the nodal displacement \mathbf{u}_j appearing at node j to the forces applied externally at node i : if a small, or “virtual,” displacement $\delta\mathbf{u}_i$ is superimposed on node i , the increase in strain energy δU within an element connected to that node is given by:

$$\delta U = \int_V \delta\boldsymbol{\epsilon}^T \boldsymbol{\sigma} dV \quad (9)$$

where V is the volume of the element. Using the approximate strain obtained from the interpolated displacements, $\delta\tilde{\boldsymbol{\epsilon}} = \mathbf{B}_i\delta\mathbf{u}_i$ is the approximate virtual increase in strain induced by the virtual nodal displacement. Using Eqn. 7 and the matrix identity $(\mathbf{A}\mathbf{B})^T = \mathbf{B}^T\mathbf{A}^T$, we have:

$$\delta U = \delta\mathbf{u}_i^T \int_V \mathbf{B}_i^T \mathbf{D}\mathbf{B}_j dV \mathbf{u}_j \quad (10)$$

(The nodal displacements $\delta\mathbf{u}_i^T$ and \mathbf{u}_j are not functions of x and y , and so can be brought from inside the integral.) The increase in strain energy δU must equal the work done by the nodal forces; this is:

$$\delta W = \delta\mathbf{u}_i^T \mathbf{f}_i \quad (11)$$

Equating Eqns. 10 and 11 and canceling the common factor $\delta\mathbf{u}_i^T$, we have:

$$\boxed{\left[\int_V \mathbf{B}_i^T \mathbf{D}\mathbf{B}_j dV \right] \mathbf{u}_j = \mathbf{f}_i} \quad (12)$$

This is of the desired form $\mathbf{k}_{ij}\mathbf{u}_j = \mathbf{f}_i$, where $\mathbf{k}_{ij} = \int_V \mathbf{B}_i^T \mathbf{D}\mathbf{B}_j dV$ is the element stiffness.

Finally, the integral in Eqn. 12 must be replaced by a numerical equivalent acceptable to the computer. Gauss-Legendre numerical integration is commonly used in finite element codes for this purpose, since that technique provides a high ratio of accuracy to computing effort. Stated briefly, the integration consists of evaluating the integrand at optimally selected integration points within the element, and forming a weighted summation of the integrand values at these points. In the case of integration over two-dimensional element areas, this can be written:

$$\int_A f(x, y) dA \approx \sum_l f(x_l, y_l) w_l \quad (13)$$

The location of the sampling points x_l, y_l and the associated weights w_l are provided by standard subroutines. In most modern codes, these routines map the element into a convenient shape, determine the integration points and weights in the transformed coordinate frame, and then map the results back to the original frame. The functions N_j used earlier for interpolation can be used for the mapping as well, achieving a significant economy in coding. This yields what are known as “numerically integrated isoparametric elements,” and these are a mainstay of the finite element industry.

Equation 12, with the integral replaced by numerical integrations of the form in Eqn. 13, is the finite element counterpart of Eqn. 3, the differential governing equation. The computer will carry out the analysis by looping over each element, and within each element looping over the individual integration points. At each integration point the components of the element stiffness matrix \mathbf{k}_{ij} are computed according to Eqn. 12, and added into the appropriate positions of the \mathbf{K}_{ij} global stiffness matrix as was done in the assembly step of matrix truss method described in the previous section. It can be appreciated that a good deal of computation is involved just in forming the terms of the stiffness matrix, and that the finite element method could never have been developed without convenient and inexpensive access to a computer.

Stresses around a circular hole

We have considered the problem of a uniaxially loaded plate containing a circular hole in previous modules, including the theoretical Kirsch solution (Module 16) and experimental determinations using both photoelastic and moire methods (Module 17). This problem is of practical importance — for instance, we have noted the dangerous stress concentration that appears near rivet holes — and it is also quite demanding in both theoretical and numerical analyses. Since the stresses rise sharply near the hole, a finite element grid must be refined there in order to produce acceptable results.

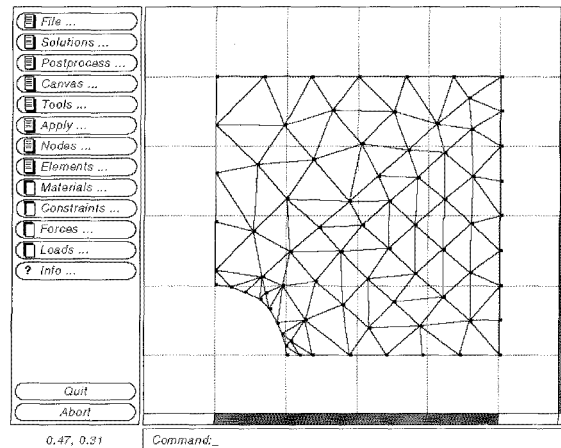


Figure 8: Mesh for circular-hole problem.

Figure 8 shows a mesh of three-noded triangular elements developed by the `felt-velvet`

graphical FEA package that can be used to approximate the displacements and stresses around a uniaxially loaded plate containing a circular hole. Since both theoretical and experimental results for this stress field are available as mentioned above, the circular-hole problem is a good one for becoming familiar with code operation.

The user should take advantage of symmetry to reduce problem size whenever possible, and in this case only one quadrant of the problem need be meshed. The center of the hole is kept fixed, so the symmetry requires that nodes along the left edge be allowed to move vertically but not horizontally. Similarly, nodes along the lower edge are constrained vertically but left free to move horizontally. Loads are applied to the nodes along the upper edge, with each load being the resultant of the far-field stress acting along half of the element boundaries between the given node and its neighbors. (The far-field stress is taken as unity.) Portions of the `felt` input dataset for this problem are:

```

problem description
nodes=76 elements=116

nodes
1  x=1 y=-0 z=0 constraint=slide_x
2  x=1.19644 y=-0 z=0
3  x=0.984562 y=0.167939 z=0 constraint=free
4  x=0.940634 y=0.335841 z=0
5  x=1.07888 y=0.235833 z=0
.
.
.
72 x=3.99602 y=3.01892 z=0
73 x=3.99602 y=3.51942 z=0
74 x=3.33267 y=4 z=0
75 x=3.57706 y=3.65664 z=0
76 x=4 y=4 z=0

CSTPlaneStress elements
1  nodes=[13,12,23] material=steel
2  nodes=[67,58,55]
6  nodes=[50,41,40]
.
.
.
7  nodes=[68,67,69] load=load_case_1
8  nodes=[68,58,67]
9  nodes=[57,58,68] load=load_case_1
10 nodes=[57,51,58]
11 nodes=[52,51,57] load=load_case_1
12 nodes=[37,39,52] load=load_case_1
13 nodes=[39,51,52]
.
.
.
116 nodes=[2,3,1]

material properties
steel E=2.05e+11 nu=0.33 t=1

distributed loads
load_case_1 color=red direction=GlobalY values=(1,1) (3,1)

```

```

constraints
free Tx=u Ty=u Tz=u Rx=u Ry=u Rz=u
slide_x color=red Tx=u Ty=c Tz=c Rx=u Ry=u Rz=u
slide_y color=red Tx=c Ty=u Tz=c Rx=u Ry=u Rz=u

end

```

The y -displacements and vertical stresses σ_y are contoured in Fig. 9(a) and (b) respectively; these should be compared with the photoelastic and moire analyses given in Module 17, Figs. 8 and 10(a). The stress at the integration point closest to the x -axis at the hole is computed to be $\sigma_{y,max} = 3.26$, 9% larger than the theoretical value of 3.00. In drawing the contours of Fig. 9b, the postprocessor extrapolated the stresses to the nodes by fitting a least-squares plane through the stresses at all four integration points within the element. This produces an even higher value for the stress concentration factor, 3.593. The user must be aware that graphical postprocessors smooth results that are themselves only approximations, so numerical inaccuracy is a real possibility. Refining the mesh, especially near the region of highest stress gradient at the hole meridian, would reduce this error.

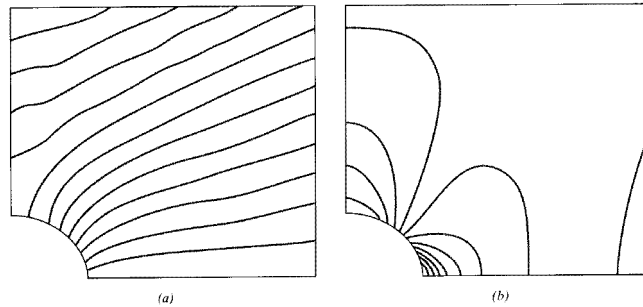
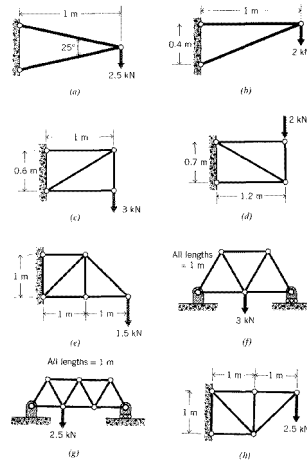


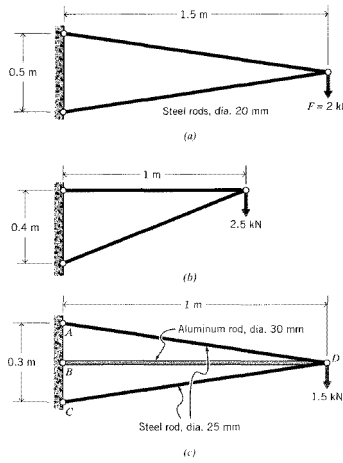
Figure 9: Vertical displacements (a) and stresses (b) as computed for the mesh of Fig. 8.

Problems

1. (a) – (h) Use FEA to determine the force in each element of the trusses drawn below.
2. (a) – (c) Write out the global stiffness matrices for the trusses listed below, and solve for the unknown forces and displacements. For each element assume $E = 30$ Mpsi and $A = 0.1$ in².
3. Obtain a plane-stress finite element solution for a cantilevered beam with a single load at the free end. Use arbitrarily chosen (but reasonable) dimensions and material properties. Plot the stresses σ_x and τ_{xy} as functions of y at an arbitrary station along the span; also plot the stresses given by the elementary theory of beam bending (c.f. Module 13) and assess the magnitude of the numerical error.
4. Repeat the previous problem, but with a symmetrically-loaded beam in three-point bending.

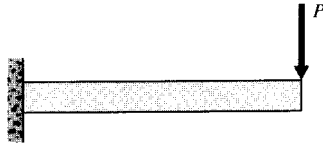


Prob. 1

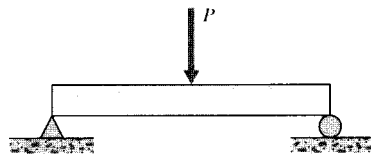


Prob. 2

- Use axisymmetric elements to obtain a finite element solution for the radial stress in a thick-walled pressure vessel (using arbitrary geometry and material parameters). Compare the results with the theoretical solution (c.f. Prob. 2 in Module 16).



Prob. 3



Prob. 4

ENGINEERING VISCOELASTICITY

David Roylance
Department of Materials Science and Engineering
Massachusetts Institute of Technology
Cambridge, MA 02139

October 24, 2001

1 Introduction

This document is intended to outline an important aspect of the mechanical response of polymers and polymer-matrix composites: the field of *linear viscoelasticity*. The topics included here are aimed at providing an instructional introduction to this large and elegant subject, and should not be taken as a thorough or comprehensive treatment. The references appearing either as footnotes to the text or listed separately at the end of the notes should be consulted for more thorough coverage.

Viscoelastic response is often used as a probe in polymer science, since it is sensitive to the material's chemistry and microstructure. The concepts and techniques presented here are important for this purpose, but the principal objective of this document is to demonstrate how linear viscoelasticity can be incorporated into the general theory of mechanics of materials, so that structures containing viscoelastic components can be designed and analyzed.

While not all polymers are viscoelastic to any important practical extent, and even fewer are *linearly* viscoelastic¹, this theory provides a usable engineering approximation for many applications in polymer and composites engineering. Even in instances requiring more elaborate treatments, the linear viscoelastic theory is a useful starting point.

2 Molecular Mechanisms

When subjected to an applied stress, polymers may deform by either or both of two fundamentally different atomistic mechanisms. The lengths and angles of the chemical bonds connecting the atoms may distort, moving the atoms to new positions of greater internal energy. This is a small motion and occurs very quickly, requiring only $\approx 10^{-12}$ seconds.

If the polymer has sufficient molecular mobility, larger-scale rearrangements of the atoms may also be possible. For instance, the relatively facile rotation around backbone carbon-carbon single bonds can produce large changes in the conformation of the molecule. Depending on the mobility, a polymer molecule can extend itself in the direction of the applied stress, which decreases its conformational entropy (the molecule is less “disordered”). Elastomers — rubber — respond almost wholly by this entropic mechanism, with little distortion of their covalent bonds or change in their internal energy.

¹For an overview of *nonlinear* viscoelastic theory, see for instance W.N. Findley et al., *Creep and Relaxation of Nonlinear Viscoelastic Materials*, Dover Publications, New York, 1989.

The combined first and second laws of thermodynamics state how an increment of mechanical work $f dx$ done on the system can produce an increase in the internal energy dU or a decrease in the entropy dS :

$$f dx = dU - T dS \quad (1)$$

Clearly, the relative importance of the entropic contribution increases with temperature T , and this provides a convenient means of determining experimentally whether the material's stiffness is energetic or entropic in origin. The retractive force needed to hold a rubber band at fixed elongation will increase with increasing temperature, as the increased thermal agitation will make the internal structure more vigorous in its natural attempts to restore randomness. But the retractive force in a stretched steel specimen — which shows little entropic elasticity — will decrease with temperature, as thermal expansion will act to relieve the internal stress.

In contrast to the instantaneous nature of the energetically controlled elasticity, the conformational or entropic changes are processes whose rates are sensitive to the local molecular mobility. This mobility is influenced by a variety of physical and chemical factors, such as molecular architecture, temperature, or the presence of absorbed fluids which may swell the polymer. Often, a simple mental picture of “free volume” — roughly, the space available for molecular segments to act cooperatively so as to carry out the motion or reaction in question — is useful in intuiting these rates.

These rates of conformational change can often be described with reasonable accuracy by Arrhenius-type expressions of the form

$$\text{rate} \propto \exp \frac{-E^\ddagger}{RT} \quad (2)$$

where E^\ddagger is an apparent activation energy of the process and $R = 8.314\text{J/mol} - ^\circ\text{K}$ is the Gas Constant. At temperatures much above the “*glass transition temperature*,” labeled T_g in Fig. 1, the rates are so fast as to be essentially instantaneous, and the polymer acts in a rubbery manner in which it exhibits large, instantaneous, and fully reversible strains in response to an applied stress.

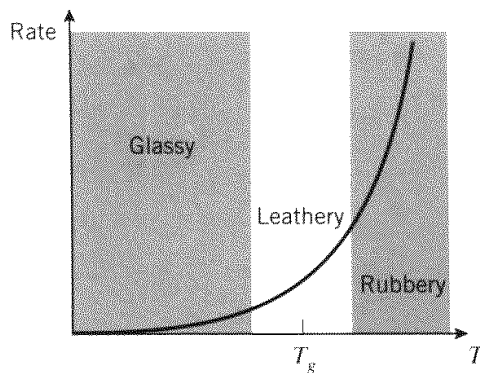


Figure 1: Temperature dependence of rate.

Conversely, at temperatures much less than T_g , the rates are so slow as to be negligible. Here the chain uncoiling process is essentially “frozen out,” so the polymer is able to respond only by bond stretching. It now responds in a “glassy” manner, responding instantaneously

and reversibly but being incapable of being strained beyond a few percent before fracturing in a brittle manner.

In the range near T_g , the material is midway between the glassy and rubbery regimes. Its response is a combination of viscous fluidity and elastic solidity, and this region is termed “leathery,” or, more technically, “viscoelastic”. The value of T_g is an important descriptor of polymer thermomechanical response, and is a fundamental measure of the material’s propensity for mobility. Factors that enhance mobility, such as absorbed diluents, expansive stress states, and lack of bulky molecular groups, all tend to produce lower values of T_g . The transparent polyvinyl butyral film used in automobile windshield laminates is an example of a material that is used in the viscoelastic regime, as viscoelastic response can be a source of substantial energy dissipation during impact.

At temperatures well below T_g , when entropic motions are frozen and only elastic bond deformations are possible, polymers exhibit a relatively high modulus, called the “glassy modulus” E_g , which is on the order of 3 GPa (400 kpsi). As the temperature is increased through T_g , the stiffness drops dramatically, by perhaps two orders of magnitude, to a value called the “rubbery modulus” E_r . In elastomers that have been permanently crosslinked by sulphur vulcanization or other means, the value of E_r is determined primarily by the crosslink density; the kinetic theory of rubber elasticity gives the relation as

$$\sigma = NRT \left(\lambda - \frac{1}{\lambda^2} \right) \quad (3)$$

where σ is the stress, N is the crosslink density (mol/m³), and $\lambda = L/L_0$ is the extension ratio. Differentiation of this expression gives the slope of the stress-strain curve at the origin as $E_r = 3NRT$.

If the material is not crosslinked, the stiffness exhibits a short plateau due to the ability of molecular entanglements to act as network junctions; at still higher temperatures the entanglements slip and the material becomes a viscous liquid. Neither the glassy nor the rubbery modulus depends strongly on time, but in the vicinity of the transition near T_g time effects can be very important. Clearly, a plot of modulus versus temperature, such as is shown in Fig. 2, is a vital tool in polymer materials science and engineering. It provides a map of a vital engineering property, and is also a fingerprint of the molecular motions available to the material.

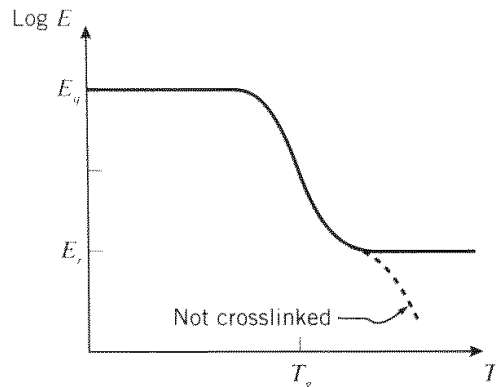


Figure 2: A generic modulus-temperature map for polymers.

3 Phenomenological Aspects

Experimentally, one seeks to characterize materials by performing simple laboratory tests from which information relevant to actual in-use conditions may be obtained. In the case of viscoelastic materials, mechanical characterization often consists of performing uniaxial tensile tests similar to those used for elastic solids, but modified so as to enable observation of the time dependency of the material response. Although many such “viscoelastic tensile tests” have been used, one most commonly encounters only three: creep, stress relaxation, and dynamic (sinusoidal) loading.

Creep

The creep test consists of measuring the time dependent strain $\epsilon(t) = \delta(t)/L_0$ resulting from the application of a steady uniaxial stress σ_0 as illustrated in Fig. 3. These three curves are the strains measured at three different stress levels, each one twice the magnitude of the previous one.

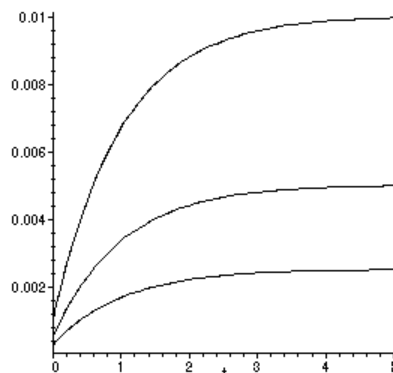


Figure 3: Creep strain at various constant stresses.

Note in Fig. 3 that when the stress is doubled, the resulting strain is doubled over its full range of time. This occurs if the material is *linear* in its response. If the strain-stress relation is linear, the strain resulting from a stress $a\sigma$, where a is a constant, is just the constant a times the strain resulting from σ alone. Mathematically,

$$\epsilon(a\sigma) = a\epsilon(\sigma)$$

This is just a case of “double the stress, double the strain.”

If the creep strains produced at a given time are plotted as the abscissa against the applied stress as the ordinate, an “isochronous” stress-strain curve would be produced. If the material is linear, this “curve” will be a straight line, with a slope that increases as the chosen time is decreased.

For linear materials, the family of strain histories $\epsilon(t)$ obtained at various constant stresses may be superimposed by normalizing them based on the applied stress. The ratio of strain to stress is called the “compliance” C , and in the case of time-varying strain arising from a constant stress the ratio is the “creep compliance”:

$$C_{crp}(t) = \frac{\epsilon(t)}{\sigma_0}$$

A typical form of this function is shown in Fig. 4, plotted against the logarithm of time. Note that the logarithmic form of the plot changes the shape of the curve drastically, stretching out the short-time portion of the response and compressing the long-time region. Upon loading, the material strains initially to the “glassy” compliance C_g ; this is the elastic deformation corresponding to bond distortion. In time, the compliance rises to an equilibrium or “rubbery” value C_r , corresponding to the rubbery extension of the material. The value along the abscissa labeled “ $\log \tau$ ” marks the inflection from rising to falling slope, and τ is called the “relaxation time” of the creep process.

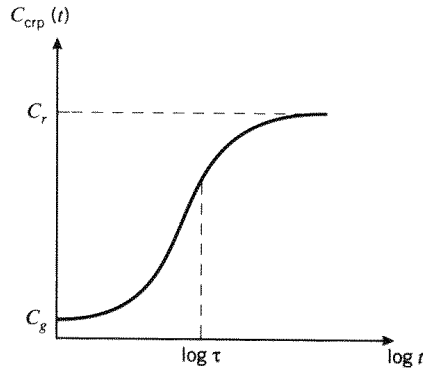


Figure 4: The creep compliance function $C_{crp}(t)$.

Stress relaxation

Another common test, easily conducted on Instron or other displacement-controlled machines, consists of monitoring the time-dependent stress resulting from a steady strain as seen in Fig. 5. This is the converse of Fig. 3; here the stress curves correspond to three different levels of constant strain, each one twice the magnitude of the previous one.

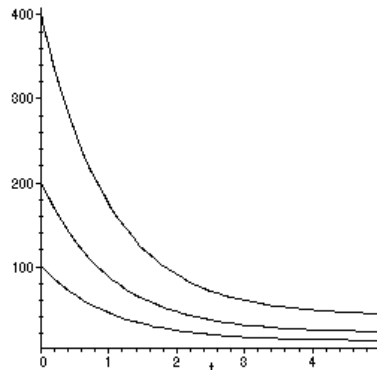


Figure 5: Measurement of relaxation response.

Analogously with creep compliance, one may superimpose the relaxation curves by means of the “relaxation modulus,” defined as $E_{rel}(t) = \sigma(t)/\epsilon_0$, plotted against $\log t$ in Fig. 6. At short times, the stress is at a high plateau corresponding to a “glassy” modulus E_g , and

then falls exponentially to a lower equilibrium “rubbery” modulus E_r as the polymer molecules gradually accommodate the strain by conformational extension rather than bond distortion.

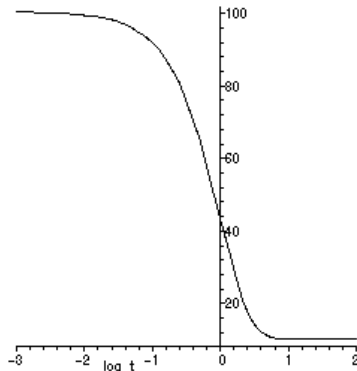


Figure 6: The stress relaxation modulus $E_{rel}(t)$. Here $E_g = 100$, $E_r = 10$, and $\tau = 1$.

Creep and relaxation are both manifestations of the same molecular mechanisms, and one should expect that E_{rel} and C_{crp} are related. However even though $E_g = 1/C_g$ and $E_r = 1/C_r$, in general $E_{rel}(t) \neq 1/C_{crp}(t)$. In particular, the relaxation response moves toward its equilibrium value more quickly than does the creep response.

Dynamic loading

Creep and stress relaxation tests are convenient for studying material response at long times (minutes to days), but less accurate at shorter times (seconds and less). Dynamic tests, in which the stress (or strain) resulting from a sinusoidal strain (or stress) is measured, are often well-suited for filling out the “short-time” range of polymer response. When a viscoelastic material is subjected to a sinusoidally varying stress, a steady state will eventually be reached² in which the resulting strain is also sinusoidal, having the same angular frequency but retarded in phase by an angle δ ; this is analogous to the delayed strain observed in creep experiments. The strain lags the stress by the phase angle δ , and this is true even if the strain rather than the stress is the controlled variable.

If the origin along the time axis is selected to coincide with a time at which the strain passes through its maximum, the strain and stress functions can be written as:

$$\epsilon = \epsilon_0 \cos \omega t \quad (4)$$

$$\sigma = \sigma_0 \cos(\omega t + \delta) \quad (5)$$

Using an algebraic maneuver common in the analysis of reactive electrical circuits and other harmonic systems, it is convenient to write the stress function as a complex quantity σ^* whose real part is in phase with the strain and whose imaginary part is 90° out of phase with it:

$$\sigma^* = \sigma'_0 \cos \omega t + i \sigma''_0 \sin \omega t \quad (6)$$

Here $i = \sqrt{-1}$ and the asterisk denotes a complex quantity as usual.

²The time needed for the initial transient effect to die out will itself be dependent on the material’s viscoelastic response time, and in some situations this can lead to experimental errors. Problem 5 develops the full form of the dynamic response, including the initial transient term.

It can be useful to visualize the observable stress and strain as the projection on the real axis of vectors rotating in the complex plane at a frequency ω . If we capture their positions just as the strain vector passes the real axis, the stress vector will be ahead of it by the phase angle δ as seen in Fig. 7.

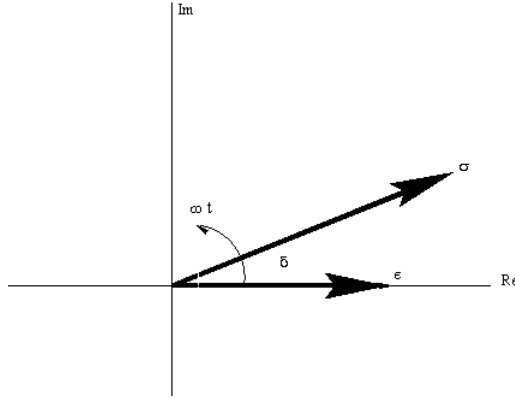


Figure 7: The “rotating-vector” representation of harmonic stress and strain.

Figure 7 makes it easy to develop the relations between the various parameters in harmonic relations:

$$\tan \delta = \sigma_0'' / \sigma_0' \quad (7)$$

$$|\sigma^*| = \sigma_0 = \sqrt{(\sigma_0')^2 + (\sigma_0'')^2} \quad (8)$$

$$\sigma_0' = \sigma_0 \cos \delta \quad (9)$$

$$\sigma_0'' = \sigma_0 \sin \delta \quad (10)$$

We can use this complex form of the stress function to define two different dynamic moduli, both being ratios of stress to strain as usual but having very different molecular interpretations and macroscopic consequences. The first of these is the “real,” or “storage,” modulus, defined as the ratio of the in-phase stress to the strain:

$$E' = \sigma_0' / \epsilon_0 \quad (11)$$

The other is the “imaginary,” or “loss,” modulus, defined as the ratio of the out-of-phase stress to the strain:

$$E'' = \sigma_0'' / \epsilon_0 \quad (12)$$

Example 1

The terms “storage” and “loss” can be understood more readily by considering the mechanical work done per loading cycle. The quantity $\int \sigma d\epsilon$ is the strain energy per unit volume (since $\sigma = \text{force/area}$ and $\epsilon = \text{distance/length}$). Integrating the in-phase and out-of-phase components separately:

$$W = \oint \sigma d\epsilon = \oint \sigma \frac{d\epsilon}{dt} dt \quad (13)$$

$$= \int_0^{2\pi/\omega} (\sigma_0' \cos \omega t)(-\epsilon_0 \omega \sin \omega t) dt + \int_0^{2\pi/\omega} (\sigma_0'' \sin \omega t)(-\epsilon_0 \omega \sin \omega t) dt \quad (14)$$

$$= 0 - \pi \sigma_0'' \epsilon_0 \quad (15)$$

Note that the in-phase components produce no net work when integrated over a cycle, while the out-of-phase components result in a net dissipation per cycle equal to:

$$W_{dis} = \pi \sigma_0'' \epsilon_0 = \pi \sigma_0 \epsilon_0 \sin \delta \quad (16)$$

This should be interpreted to illustrate that the strain energy associated with the in-phase stress and strain is reversible; i.e. that energy which is stored in the material during a loading cycle can be recovered without loss during unloading. Conversely, energy supplied to the material by the out-of-phase components is converted irreversibly to heat.

The maximum energy stored by the in-phase components occurs at the quarter-cycle point, and this maximum stored energy is:

$$\begin{aligned} W_{st} &= \int_0^{\pi/2\omega} (\sigma_0' \cos \omega t)(-\epsilon_0 \omega \sin \omega t) dt \\ &= -\frac{1}{2} \sigma_0' \epsilon_0 = -\frac{1}{2} \sigma_0 \epsilon_0 \cos \delta \end{aligned} \quad (17)$$

The relative dissipation – the ratio of W_{dis}/W_{st} – is then related to the phase angle by:

$$\frac{W_{dis}}{W_{st}} = 2\pi \tan \delta \quad (18)$$

We will also find it convenient to express the harmonic stress and strain functions as exponentials:

$$\sigma = \sigma_0^* e^{i\omega t} \quad (19)$$

$$\epsilon = \epsilon_0^* e^{i\omega t} \quad (20)$$

The $e^{i\omega t}$ factor follows from the Euler relation $e^{i\theta} = \cos \theta + i \sin \theta$, and writing both the stress and the strain as complex numbers removes the restriction of placing the origin at a time of maximum strain as was done above. The complex modulus can now be written simply as:

$$E^* = \sigma_0^*/\epsilon_0^* \quad (21)$$

4 Mathematical Models for Linear Viscoelastic Response

4.1 The Maxwell Spring-Dashpot Model

The time dependence of viscoelastic response is analogous to the time dependence of reactive electrical circuits, and both can be described by identical ordinary differential equations in time. A convenient way of developing these relations while also helping visualize molecular motions employs “spring-dashpot” models. These mechanical analogs use “Hookean” springs, depicted in Fig. 8 and described by

$$\sigma = k\epsilon$$

where σ and ϵ are analogous to the spring force and displacement, and the spring constant k is analogous to the Young’s modulus E ; k therefore has units of N/m². The spring models the instantaneous bond deformation of the material, and its magnitude will be related to the fraction of mechanical energy stored reversibly as strain energy.



Figure 8: Hookean spring (left) and Newtonian dashpot (right).

The entropic uncoiling process is fluidlike in nature, and can be modeled by a “Newtonian dashpot” also shown in Fig. 8, in which the stress produces not a strain but a strain *rate*:

$$\sigma = \eta \dot{\epsilon}$$

Here the overdot denotes time differentiation and η is a viscosity with units of N-s/m². In many of the relations to follow, it will be convenient to employ the ratio of viscosity to stiffness:

$$\tau = \frac{\eta}{k}$$

The unit of τ is time, and it will be seen that this ratio is a useful measure of the response time of the material’s viscoelastic response.



Figure 9: The Maxwell model.

The “Maxwell” solid shown in Fig. 9 is a mechanical model in which a Hookean spring and a Newtonian dashpot are connected in series. The spring should be visualized as representing the elastic or energetic component of the response, while the dashpot represents the conformational or entropic component. In a series connection such as the Maxwell model, the stress on each element is the same and equal to the imposed stress, while the total strain is the sum of the strain in each element:

$$\sigma = \sigma_s = \sigma_d$$

$$\epsilon = \epsilon_s + \epsilon_d$$

Here the subscripts s and d represent the spring and dashpot, respectively. In seeking a single equation relating the stress to the strain, it is convenient to differentiate the strain equation and then write the spring and dashpot strain rates in terms of the stress:

$$\dot{\epsilon} = \dot{\epsilon}_s + \dot{\epsilon}_d = \frac{\dot{\sigma}}{k} + \frac{\sigma}{\eta}$$

Multiplying by k and using $\tau = \eta/k$:

$$\boxed{k\dot{\epsilon} = \dot{\sigma} + \frac{1}{\tau}\sigma} \quad (22)$$

This expression is a “constitutive” equation for our fictitious Maxwell material, an equation that relates the stress to the strain. Note that it contains time derivatives, so that simple constant of

proportionality between stress and strain does not exist. The concept of “modulus” – the ratio of stress to strain – must be broadened to account for this more complicated behavior.

Eqn. 22 can be solved for the stress $\sigma(t)$ once the strain $\epsilon(t)$ is specified, or for the strain if the stress is specified. Two examples will illustrate this process:

Example 2

In a stress relaxation test, a constant strain ϵ_0 acts as the “input” to the material, and we seek an expression for the resulting time-dependent stress; this is depicted in Fig. 10.

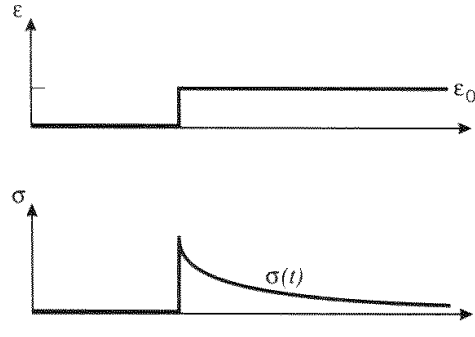


Figure 10: Strain and stress histories in the stress relaxation test.

Since in stress relaxation $\dot{\epsilon} = 0$, Eqn. 22 becomes

$$\frac{d\sigma}{dt} = -\frac{1}{\tau}\sigma$$

Separating variables and integrating:

$$\int_{\sigma_0}^{\sigma} \frac{d\sigma}{\sigma} = -\frac{1}{\tau} \int_0^t dt$$

$$\ln \sigma - \ln \sigma_0 = -\frac{t}{\tau}$$

$$\sigma(t) = \sigma_0 \exp(-t/\tau)$$

Here the significance of $\tau \equiv \eta/k$ as a characteristic “relaxation time” is evident; it is physically the time needed for the stress to fall to $1/e$ of its initial value. It is also the time at which the stress function passes through an inflection when plotted against log time.

The relaxation modulus E_{rel} may be obtained from this relation directly, noting that initially only the spring will deform and the initial stress and strain are related by $\sigma_0 = k\epsilon_0$. So

$$E_{rel}(t) = \frac{\sigma(t)}{\epsilon_0} = \frac{\sigma_0}{\epsilon_0} \exp(-t/\tau)$$

$$\boxed{E_{rel}(t) = k \exp(-t/\tau)} \quad (23)$$

This important function is plotted schematically in Fig. 11. The two adjustable parameters in the model, k and τ , can be used to force the model to match an experimental plot of the relaxation modulus at two points. The spring stiffness k would be set to the initial or glass modulus E_g , and τ would be chosen to force the value k/e to match the experimental data at $t = \tau$.

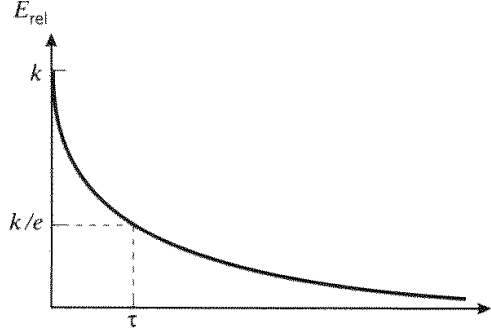


Figure 11: Relaxation modulus for the Maxwell model.

The relaxation time τ is strongly dependent on temperature and other factors that effect the mobility of the material, and is roughly inverse to the rate of molecular motion. Above T_g , τ is very short; below T_g , it is very long. More detailed consideration of the temperature dependence will be given in a later section, in the context of “thermorheologically simple” materials.

Example 3

In the case of the dynamic response, the time dependency of both the stress and the strain are of the form $\exp(i\omega t)$. All time derivatives will therefore contain the expression $(i\omega) \exp(i\omega t)$, so Eqn. 22 gives:

$$k(i\omega) \epsilon_0^* \exp(i\omega t) = \left(i\omega + \frac{1}{\tau_j} \right) \sigma_0^* \exp(i\omega t)$$

The complex modulus E^* is then

$$E^* = \frac{\sigma_0^*}{\epsilon_0^*} = \frac{k(i\omega)}{i\omega + \frac{1}{\tau_j}} = \frac{k(i\omega\tau)}{1 + i\omega\tau} \quad (24)$$

This equation can be manipulated algebraically (multiply and divide by the complex conjugate of the denominator) to yield:

$$E^* = \frac{k\omega^2\tau^2}{1 + \omega^2\tau^2} + i \frac{k\omega\tau}{1 + \omega^2\tau^2} \quad (25)$$

In Eq. 25, the real and imaginary components of the complex modulus are given explicitly; these are the “Debye” relations also important in circuit theory.

4.2 The Standard Linear Solid (Maxwell Form)

Most polymers do not exhibit the unrestricted flow permitted by the Maxwell model, although it might be a reasonable model for Silly Putty or warm tar. Therefore Eqn. 23 is valid only for a very limited set of materials. For more typical polymers whose conformational change is eventually limited by the network of entanglements or other types of junction points, more elaborate spring-dashpot models can be used effectively.

Placing a spring in parallel with the Maxwell unit gives a very useful model known as the “Standard Linear Solid” (S.L.S.) shown in Fig. 12. This spring has stiffness k_e , so named because

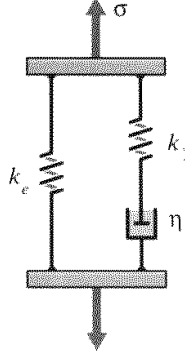


Figure 12: The Maxwell form of the Standard Linear Solid.

it provides an “equilibrium” or rubbery stiffness that remains after the stresses in the Maxwell arm have relaxed away as the dashpot extends.

In this arrangement, the Maxwell arm and the parallel spring k_e experience the same strain, and the total stress σ is the sum of the stress in each arm: $\sigma = \sigma_e + \sigma_m$. It is awkward to solve for the stress σ_m in the Maxwell arm using Eqn. 22, since that contains both the stress and its time derivative. The Laplace transformation is very convenient in this and other viscoelasticity problems, because it reduces differential equations to algebraic ones. Appendixes A lists some transform pairs encountered often in these problems.

Since the stress and strain are zero as the origin is approached from the left, the transforms of the time derivatives are just the Laplace variable s times the transforms of the functions; denoting the transformed functions with an overline, we have $\mathcal{L}(\dot{\epsilon}) = s\bar{\epsilon}$ and $\mathcal{L}(\dot{\sigma}) = s\bar{\sigma}$. Then writing the transform of an expression such as Eqn. 22 is done simply by placing a line over the time-dependent functions, and replacing the time-derivative overdot by an s coefficient:

$$k\dot{\epsilon} = \dot{\sigma}_m + \frac{1}{\tau}\sigma_m \longrightarrow k_1 s\bar{\epsilon} = s\bar{\sigma}_m + \frac{1}{\tau}\bar{\sigma}_m$$

Solving for $\bar{\sigma}_m$:

$$\bar{\sigma}_m = \frac{k_1 s}{s + \frac{1}{\tau}} \bar{\epsilon} \quad (26)$$

Adding the stress $\bar{\sigma}_e = k_e \bar{\epsilon}$ in the equilibrium spring, the total stress is:

$$\bar{\sigma} = k_e \bar{\epsilon} + \frac{k_1 s}{s + \frac{1}{\tau}} \bar{\epsilon} = \left\{ k_e + \frac{k_1 s}{s + \frac{1}{\tau}} \right\} \bar{\epsilon}$$

This result can be written

$$\boxed{\bar{\sigma} = \mathcal{E} \bar{\epsilon}} \quad (27)$$

where for this model the parameter \mathcal{E} is

$$\mathcal{E} = k_e + \frac{k_1 s}{s + \frac{1}{\tau}} \quad (28)$$

Eqn. 27, which is clearly reminiscent of Hooke's Law $\sigma = E\epsilon$ but in the Laplace plane, is called the *associated viscoelastic constitutive equation*. Here the specific expression for \mathcal{E} is that of the Standard Linear Solid model, but other models could have been used as well.

For a given strain input function $\epsilon(t)$, we obtain the resulting stress function in three steps:

1. Obtain an expression for the transform of the strain function, $\bar{\epsilon}(s)$.
2. Form the algebraic product $\bar{\sigma}(s) = \mathcal{E}\bar{\epsilon}(s)$.
3. Obtain the inverse transform of the result to yield the stress function in the time plane.

Example 4

In the case of stress relaxation, the strain function $\epsilon(t)$ is treated as a constant ϵ_0 times the ‘‘Heaviside’’ or ‘‘unit step’’ function $u(t)$:

$$\epsilon(t) = \epsilon_0 u(t), \quad u(t) = \begin{cases} 0, & t < 0 \\ 1, & t \geq 0 \end{cases}$$

This has the Laplace transform

$$\bar{\epsilon} = \frac{\epsilon_0}{s}$$

Using this in Eqn. 27 and dividing through by ϵ_0 , we have

$$\frac{\bar{\sigma}}{\epsilon_0} = \frac{k_e}{s} + \frac{k_1}{s + \frac{1}{\tau}}$$

Since $\mathcal{L}^{-1} 1/(s + a) = e^{-at}$, this can be inverted directly to give

$$\boxed{\frac{\sigma(t)}{\epsilon_0} \equiv E_{rel}(t) = k_e + k_1 \exp(-t/\tau)} \quad (29)$$

This function, which is just that of the Maxwell model shifted upward by an amount k_e , was used to generate the curve shown in Fig. 6.

Example 5

The form of Eqn. 27 is convenient when the stress needed to generate a given strain is desired. It is somewhat awkward when the strain generated by a given stress is desired, since then the parameter \mathcal{E} appears in the denominator:

$$\bar{\epsilon} = \frac{\bar{\sigma}}{\mathcal{E}} = \frac{\bar{\sigma}}{k_e + \frac{k_1 s}{s + \frac{1}{\tau}}}$$

This is more difficult to invert, and in such cases symbolic manipulation software such as MapleTM can be helpful. For instance, if we want to compute the creep compliance of the Maxwell Standard Linear Solid, we could write:

```
read transformation library
> with(inttrans):
define governing equation
> eq1:=sigbar=EE*epsbar;
Constant stress sig0:
> sigbar:=laplace(sig0,t,s);
```

```

EE viscoelastic operator - Maxwell S.L.S. model
> EE:= k[e]+k[1]*s/(s+1/tau);
Solve governing equation for epsbar and invert:
> C[crp](t):=simplify((invlaplace(solve(eq1,epsbar),s,t))/sig0);

```

$$C[crp](t) := - \frac{-k[e] - k[1] + k[1] \exp\left(-\frac{k[e] t}{\tau (k[e] + k[1])}\right)}{k[e] (k[e] + k[1])}$$

This result can be written as

$$\boxed{C_{crp}(t) = C_g + (C_r - C_g) \left(1 - e^{-t/\tau_c}\right)} \quad (30)$$

where

$$C_g = \frac{1}{k_e + k_1}, \quad C_r = \frac{1}{k_e}, \quad \tau_c = \tau \left(\frac{k_e + k_1}{k_e}\right)$$

The glassy compliance C_g is the compliance of the two springs k_e and k_1 acting in parallel, and the rubbery compliance C_r is that of spring k_e alone, as expected. Less obvious is that the characteristic time for creep τ_c (sometimes called the “retardation” time) is longer than the characteristic time for relaxation τ , by a factor equal to the ratio of the glassy to the rubbery modulus. This is a general result, not restricted to the particular model used.

A less awkward form for compliance problems is produced when “Voigt-type” rather than Maxwell-type models are used; see problems 7 and 8.

The Standard Linear Solid is a three-parameter model capable of describing the general features of viscoelastic relaxation: k_e and k_1 are chosen to fit the glassy and rubbery moduli, and τ is chosen to place the relaxation in the correct time interval:

$$k_e = E_r \quad (31)$$

$$k_1 = E_g - E_r \quad (32)$$

$$\tau = t @ E_{rel} = \left(E_r + \frac{1}{e}(E_g - E_r)\right) \quad (33)$$

This forces the S.L.S. prediction to match the experimental data at three points, but the ability of the model to fit the experimental data over the full range of the relaxation is usually poor. The relaxation modulus predicted by the S.L.S. drops from E_g to E_r in approximately two decades³ of time, which is generally too abrupt a transition.

4.3 The Wiechert Model

A real polymer does not relax with a single relaxation time as predicted by the previous models. Molecular segments of varying length contribute to the relaxation, with the simpler and shorter segments relaxing much more quickly than the long ones. This leads to a distribution of relaxation times, which in turn produces a relaxation spread over a much longer time than

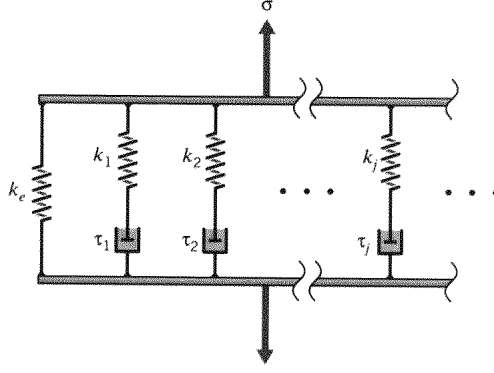


Figure 13: The Wiechert model.

can be modeled accurately with a single relaxation time. When the engineer considers it necessary to incorporate this effect, the Wiechert model illustrated in Fig. 13 can have as many spring-dashpot Maxwell elements as are needed to approximate the distribution satisfactorily.

The total stress σ transmitted by the model is the stress in the isolated spring (of stiffness k_e) plus that in each of the Maxwell spring-dashpot arms:

$$\sigma = \sigma_e + \sum_j \sigma_j$$

From Eqn. 26, the stress in the Maxwell arm is

$$\bar{\sigma}_j = \frac{k_j s \bar{\epsilon}}{\left(s + \frac{1}{\tau_j}\right)}$$

Then

$$\boxed{\bar{\sigma} = \bar{\sigma}_e + \sum_j \bar{\sigma}_j = \left\{ k_e + \sum_j \frac{k_j s}{\left(s + \frac{1}{\tau_j}\right)} \right\} \bar{\epsilon}} \quad (34)$$

The quantity in braces is the viscoelastic modulus operator \mathcal{E} defined in Eqn. 27 for the Wiechert model.

Example 6

In stress relaxation tests, we have

$$\epsilon(t) = \epsilon_0 \Rightarrow \bar{\epsilon}(s) = \epsilon_0/s$$

$$\bar{\sigma}(s) = \mathcal{E}(s)\bar{\epsilon}(s) = \left\{ k_e + \sum_j \frac{k_j s}{s + \frac{1}{\tau_j}} \right\} \frac{\epsilon_0}{s} = \left\{ \frac{k_e}{s} + \sum_j \frac{k_j}{s + \frac{1}{\tau_j}} \right\} \epsilon_0$$

³A “decade” of time in our context is a multiple of ten, say from 10^3 to 10^4 seconds, rather than a span of ten years.

$$\sigma(t) = \mathcal{L}^{-1}[\bar{\sigma}(s)] = \left\{ k_e + \sum_j k_j \exp\left(\frac{-t}{\tau_j}\right) \right\} \epsilon_0 \quad (35)$$

Dividing by ϵ_0 , the relaxation modulus is

$$E_{rel}(t) = k_e + \sum_j k_j \exp\left(\frac{-t}{\tau_j}\right) \quad (36)$$

The material constants in this expression (k_e and the various k_j and τ_j) can be selected by forcing the predicted values of $E_{rel}(t)$ as given by Eqn. 36 to match those determined experimentally. Prob. 19 provides an example of such a procedure.

Example 7

Consider the stress function resulting from a constant-strain-rate test:

$$\epsilon = R_\epsilon t \longrightarrow \bar{\epsilon}(s) = R_\epsilon / s^2$$

where R_ϵ is the strain rate. Then

$$\begin{aligned} \bar{\sigma}(s) = \mathcal{E}(s)\bar{\epsilon}(s) &= \left[k_e + \sum_j \frac{k_j s}{s + \frac{1}{\tau_j}} \right] \frac{R_\epsilon}{s^2} = \frac{k_e R_\epsilon}{s^2} + \sum_j \frac{k_j R_\epsilon}{s \left(s + \frac{1}{\tau_j} \right)} \\ \sigma(t) &= k_e R_\epsilon t + \sum_j k_j R_\epsilon \tau_j [1 - \exp(-t/\tau_j)] \end{aligned} \quad (37)$$

Note that the stress-time function, and hence the stress-strain curve, is not linear. It is not true, therefore, that a curved stress-strain diagram implies that the material response is nonlinear. It is also interesting to note that the slope of the constant-strain-rate stress-strain curve is related to the value of the relaxation modulus evaluated at the same time:

$$\begin{aligned} \frac{d\sigma}{d\epsilon} &= \frac{d\sigma}{dt} \cdot \frac{dt}{d\epsilon} = \frac{d\sigma}{dt} \cdot \frac{1}{R_\epsilon} = \left[k_e R_\epsilon + \sum_j k_j R_\epsilon \exp(-t/\tau_j) \right] \frac{1}{R_\epsilon} \\ &= \left[k_e + \sum_j k_j \exp(-t/\tau_j) \right] \equiv E_{rel}(t) |_{t=\epsilon/R_\epsilon} \end{aligned} \quad (38)$$

Example 8

It may be that the input strain function is not known as a mathematical expression, or its mathematical expression may be so complicated as to make the transform process intractable. In those cases, one may return to the differential constitutive equation and recast it in finite-difference form so as to obtain a numerical solution. Recall that the stress in the j th arm of the Wiechert model is given by

$$\frac{d\sigma_j}{dt} + \frac{1}{\tau_j} \sigma_j = k_j \frac{d\epsilon}{dt} \quad (39)$$

This can be written in finite difference form as

$$\frac{\sigma_j^t - \sigma_j^{t-1}}{\Delta t} + \frac{1}{\tau_j} \sigma_j^t = k_j \frac{\epsilon^t - \epsilon^{t-1}}{\Delta t} \quad (40)$$

where the superscripts t and $t-1$ indicate values before and after the passage of a small time increment Δt . Solving for σ_j^t :

$$\sigma_j^t = \frac{1}{1 + (\Delta t/\tau_j)} [k_j(\epsilon^t - \epsilon^{t-1}) + \sigma_j^{t-1}] \quad (41)$$

Now summing over all arms of the model and adding the stress in the equilibrium spring:

$$\sigma^t = k_e \epsilon^t + \sum_j \frac{k_j(\epsilon^t - \epsilon^{t-1}) + \sigma_j^{t-1}}{1 + (\Delta t/\tau_j)} \quad (42)$$

This constitutes a recursive algorithm which the computer can use to calculate successive values of σ^t beginning at $t = 0$. In addition to storing the various k_j and τ_j which constitute the material description, the computer must also keep the previous values of each arm stress (the σ_j^{t-1}) in storage.

4.4 The Boltzman Superposition Integral

As seen in the previous sections, linear viscoelasticity can be stated in terms of mechanical models constructed from linear springs and dashpots. These models generate constitutive relations that are ordinary differential equations; see Probs. 13 and 14 as examples of this. However, integral equations could be used as well, and this integral approach is also used as a starting point for viscoelastic theory.

Integrals are summing operations, and this view of viscoelasticity takes the response of the material at time t to be the sum of the responses to excitations imposed at all previous times. The ability to sum these individual responses requires the material to obey a more general statement of linearity than we have invoked previously, specifically that the response to a number of individual excitations be the sum of the responses that would have been generated by each excitation acting alone. Mathematically, if the stress due to a strain $\epsilon_1(t)$ is $\sigma(\epsilon_1)$ and that due to a different strain $\epsilon_2(t)$ is $\sigma(\epsilon_2)$, then the stress due to both strains is $\sigma(\epsilon_1 + \epsilon_2) = \sigma(\epsilon_1) + \sigma(\epsilon_2)$. Combining this with the condition for multiplicative scaling used earlier, we have as a general statement of linear viscoelasticity:

$$\sigma(a\epsilon_1 + b\epsilon_2) = a\sigma(\epsilon_1) + b\sigma(\epsilon_2) \quad (43)$$

The ‘‘Boltzman Superposition Integral’’ statement of linear viscoelastic response follows from this definition. Consider the stress $\sigma_1(t)$ at time t due to the application of a small strain $\Delta\epsilon_1$ applied at a time ξ_1 previous to t ; this is given directly from the definition of the relaxation modulus as

$$\sigma_1(t) = E_{rel}(t - \xi_1)\Delta\epsilon_1$$

Similarly, the stress $\sigma_2(t)$ due to a strain increment $\Delta\epsilon_2$ applied at a different time ξ_2 is

$$\sigma_2(t) = E_{rel}(t - \xi_2)\Delta\epsilon_2$$

If the material is linear, the total stress at time t due to both strain increments together can be obtained by superposition of these two individual effects:

$$\sigma(t) = \sigma_1(t) + \sigma_2(t) = E_{rel}(t - \xi_1)\Delta\epsilon_1 + E_{rel}(t - \xi_2)\Delta\epsilon_2$$

As the number of applied strain increments increases so as to approach a continuous distribution, this becomes:

$$\begin{aligned}\sigma(t) &= \sum_j \sigma_j(t) = \sum_j E_{rel}(t - \xi_j)\Delta\epsilon_j \\ \longrightarrow \sigma(t) &= \int_{-\infty}^t E_{rel}(t - \xi) d\epsilon = \int_{-\infty}^t E_{rel}(t - \xi) \frac{d\epsilon(\xi)}{d\xi} d\xi\end{aligned}\quad (44)$$

Example 9

In the case of constant strain rate ($\epsilon(t) = R_\epsilon t$) we have

$$\frac{d\epsilon(\xi)}{d\xi} = \frac{d(R_\epsilon \xi)}{d\xi} = R_\epsilon$$

For S.L.S. materials response ($E_{rel}(t) = k_e + k_1 \exp[-t/\tau]$),

$$E_{rel}(t - \xi) = k_e + k_1 e^{-\frac{(t-\xi)}{\tau}}$$

Eqn. 44 gives the stress as

$$\sigma(t) = \int_0^t \left(k_e + k_1 e^{-\frac{(t-\xi)}{\tau}} \right) R_\epsilon d\xi$$

Maple statements for carrying out these operations might be:

```
define relaxation modulus for S.L.S.
>Erel:=k[e]+k[1]*exp(-t/tau);
define strain rate
>eps:=R*t;
integrand for Boltzman integral
>integrand:=subs(t=t-xi,Erel)*diff(subs(t=xi,eps),xi);
carry out integration
>'sigma(t) '=int(integrand,xi=0..t);
```

which gives the result:

$$\sigma(t) = k_e R_\epsilon t + k_1 R_\epsilon \tau [1 - \exp(-t/\tau)]$$

This is identical to Eqn. 37, with one arm in the model.

The Boltzman integral relation can be obtained formally by recalling that the transformed relaxation modulus is related simply to the associated viscoelastic modulus in the Laplace plane as

$$\text{stress relaxation : } \epsilon(t) = \epsilon_0 u(t) \rightarrow \bar{\epsilon} = \frac{\epsilon_0}{s}$$

$$\bar{\sigma} = \mathcal{E} \bar{\epsilon} = \mathcal{E} \frac{\epsilon_0}{s}$$

$$\frac{\bar{\sigma}}{\epsilon_0} = \bar{E}_{rel}(s) = \frac{1}{s} \mathcal{E}(s)$$

Since $s\bar{f} = \bar{\dot{f}}$, the following relations hold:

$$\bar{\sigma} = \mathcal{E}\bar{\epsilon} = s\bar{E}_{rel}\bar{\epsilon} = \bar{\dot{E}}_{rel}\bar{\epsilon} = \bar{E}_{rel}\bar{\dot{\epsilon}}$$

The last two of the above are of the form for which the convolution integral transform applies (see Appendix A), so the following four equivalent relations are obtained immediately:

$$\begin{aligned}\sigma(t) &= \int_0^t E_{rel}(t-\xi)\dot{\epsilon}(\xi) d\xi \\ &= \int_0^t E_{rel}(\xi)\dot{\epsilon}(t-\xi) d\xi \\ &= \int_0^t \dot{E}_{rel}(t-\xi)\epsilon(\xi) d\xi \\ &= \int_0^t \dot{E}_{rel}(\xi)\epsilon(t-\xi) d\xi\end{aligned}\tag{45}$$

These relations are forms of Duhamel's formula, where $E_{rel}(t)$ can be interpreted as the stress $\sigma(t)$ resulting from a unit input of strain. If stress rather than strain is the input quantity, then an analogous development leads to

$$\epsilon(t) = \int_0^t C_{crp}(t-\xi)\dot{\sigma}(\xi) d\xi\tag{46}$$

where $C_{crp}(t)$, the strain response to a unit stress input, is the quantity defined earlier as the creep compliance. The relation between the creep compliance and the relaxation modulus can now be developed as:

$$\begin{aligned}\bar{\sigma} &= s\bar{E}_{rel}\bar{\epsilon} \\ \bar{\epsilon} &= s\bar{C}_{crp}\bar{\sigma} \\ \bar{\sigma}\bar{\epsilon} &= s^2\bar{E}_{rel}\bar{C}_{crp}\bar{\epsilon}\bar{\sigma} \longrightarrow \bar{E}_{rel}\bar{C}_{crp} = \frac{1}{s^2} \\ \int_0^t E_{rel}(t-\xi)C_{crp}(\xi) d\xi &= \int_0^t E_{rel}(\xi)C_{crp}(t-\xi) d\xi = t\end{aligned}$$

It is seen that one must solve an integral equation to obtain a creep function from a relaxation function, or vice versa. This deconvolution process may sometimes be performed analytically (probably using Laplace transforms), and in intractable cases some use has been made of numerical approaches.

4.5 Effect of Temperature

As mentioned at the outset (*cf.* Eqn. 2), temperature has a dramatic influence on rates of viscoelastic response, and in practical work it is often necessary to adjust a viscoelastic analysis for varying temperature. This strong dependence of temperature can also be useful in experimental characterization: if for instance a viscoelastic transition occurs too quickly at room temperature for easy measurement, the experimenter can lower the temperature to slow things down.

In some polymers, especially "simple" materials such as polyisobutylene and other amorphous thermoplastics that have few complicating features in their microstructure, the relation

between time and temperature can be described by correspondingly simple models. Such materials are termed “thermorheologically simple”.

For such simple materials, the effect of lowering the temperature is simply to shift the viscoelastic response (plotted against log time) to the right without change in shape. This is equivalent to increasing the relaxation time τ , for instance in Eqns. 29 or 30, without changing the glassy or rubbery moduli or compliances. A “time-temperature shift factor” $a_T(T)$ can be defined as the horizontal shift that must be applied to a response curve, say $C_{crp}(t)$, measured at an arbitrary temperature T in order to move it to the curve measured at some reference temperature T_{ref} .

$$\log(a_T) = \log \tau(T) - \log \tau(T_{ref}) \quad (47)$$

This shifting is shown schematically in Fig. 14.

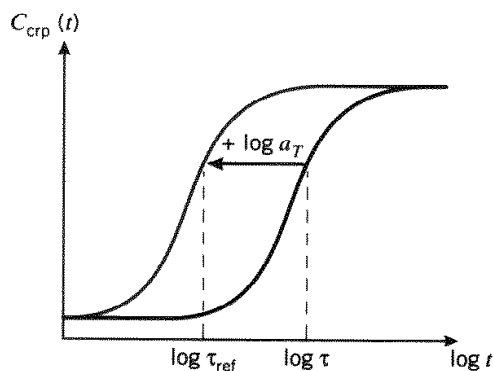


Figure 14: The time-temperature shifting factor.

In the above we assume a single relaxation time. If the model contains multiple relaxation times, thermorheological simplicity demands that all have the same shift factor, since otherwise the response curve would change shape as well as position as the temperature is varied.

If the relaxation time obeys an Arrhenius relation of the form $\tau(T) = \tau_0 \exp(E^\dagger/RT)$, the shift factor is easily shown to be (see Prob. 17)

$$\log a_T = \frac{E^\dagger}{2.303R} \left(\frac{1}{T} - \frac{1}{T_{ref}} \right) \quad (48)$$

Here the factor $2.303 = \ln 10$ is the conversion between natural and base 10 logarithms, which are commonly used to facilitate graphical plotting using log paper.

While the Arrhenius kinetic treatment is usually applicable to secondary polymer transitions, many workers feel the glass-rubber primary transition appears governed by other principles. A popular alternative is to use the “W.L.F.” equation at temperatures near or above the glass temperature:

$$\log a_T = \frac{-C_1(T - T_{ref})}{C_2 + (T - T_{ref})} \quad (49)$$

Here C_1 and C_2 are arbitrary material constants whose values depend on the material and choice of reference temperature T_{ref} . It has been found that if T_{ref} is chosen to be T_g , then C_1 and C_2 often assume “universal” values applicable to a wide range of polymers:

$$\log a_T = \frac{-17.4(T - T_g)}{51.6 + (T - T_g)} \quad (50)$$

where T is in Celsius. The original W.L.F. paper⁴ developed this relation empirically, but rationalized it in terms of free-volume concepts.

A series of creep or relaxation data taken over a range of temperatures can be converted to a single “master curve” via this horizontal shifting. A particular curve is chosen as reference, then the other curves shifted horizontally to obtain a single curve spanning a wide range of log time as shown in Fig. 15. Curves representing data obtained at temperatures lower than the reference temperature appear at longer times, to the right of the reference curve, so will have to shift left; this is a *positive* shift as we have defined the shift factor in Eqn. 47. Each curve produces its own value of a_T , so that a_T becomes a tabulated function of temperature. The master curve is valid only at the reference temperature, but it can be used at other temperatures by shifting it by the appropriate value of $\log a_T$.

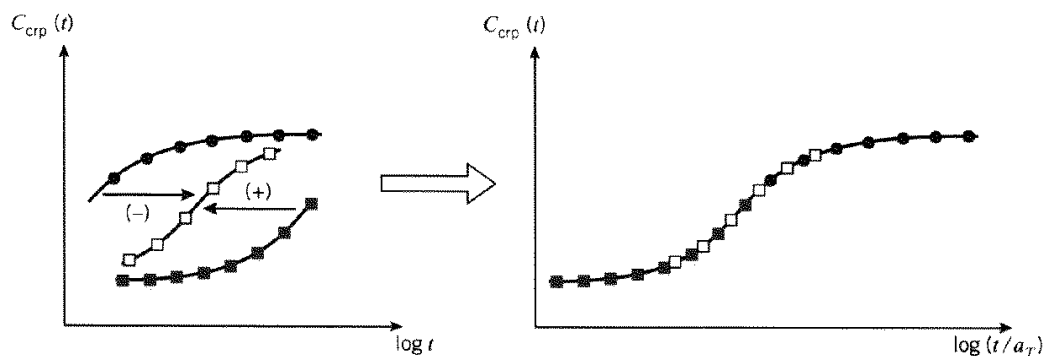


Figure 15: Time-temperature superposition.

The labeling of the abscissa as $\log(t/a_T) = \log t - \log a_t$ in Fig. 15 merits some discussion. Rather than shifting the master curve to the right for temperatures less than the reference temperature, or to the left for higher temperatures, it is easier simply to renumber the axis, increasing the numbers for low temperatures and decreasing them for high. The label therefore indicates that the numerical values on the horizontal axis have been adjusted for temperature by subtracting the log of the shift factor. Since lower temperatures have positive shift factors, the numbers are smaller than they need to be and have to be *increased* by the appropriate shift factor. Labeling axes this way is admittedly ambiguous and tends to be confusing, but the correct adjustment is easily made by remembering that lower temperatures slow the creep rate, so times (t) to be made longer by increasing the numbers on the axis. Conversely for higher temperatures, the numbers must be made smaller.

Example 10

We wish to find the extent of creep in a two-temperature cycle that consists of $t_1 = 10$ hours at 20°C followed by $t_2 = 5$ minutes at 50°C . The log shift factor for 50°C , relative to a reference temperature of 20°C , is known to be -2.2 .

⁴M.L. Williams, R.F. Landel, and J.D. Ferry, *J. Am. Chem. Soc.*, Vol. 77, No. 14, pp. 3701–3707, 1955.

Using the given shift factor, we can adjust the time of the second temperature at 50°C to an equivalent time t'_2 at 20°C as follows:

$$t'_2 = \frac{t_2}{a_T} = \frac{5 \text{ min}}{10^{-2.2}} = 792 \text{ min} = 13.2 \text{ h}$$

Hence 5 minutes at 50°C is equivalent to over 13 h at 20°C. The total effective time is then the sum of the two temperature steps:

$$t' = t_1 + t'_2 = 10 + 13.2 = 23.2 \text{ h}$$

The total creep can now be evaluated by using this effective time in a suitable relation for creep, for instance Eqn. 30.

The effective-time approach to response at varying temperatures can be extended to an arbitrary number of temperature steps:

$$t' = \sum_j t'_j = \sum_j \left(\frac{t_j}{a_T(T_j)} \right)$$

For time-dependent temperatures in general, we have $T = T(t)$, so a_T becomes an implicit function of time. The effective time can be written for continuous functions as

$$t' = \int_0^t \frac{d\xi}{a_T(\xi)} \quad (51)$$

where ξ is a dummy time variable. This approach, while perhaps seeming a bit abstract, is of considerable use in modeling time-dependent materials response. Factors such as damage due to applied stress or environmental exposure can accelerate or retard the rate of a given response, and this change in rate can be described by a time-expansion factor similar to a_T but dependent on other factors in addition to temperature.

Example 11

Consider a hypothetical polymer with a relaxation time measured at 20°C of $\tau = 10$ days, and with glassy and rubbery moduli $E_g = 100$, $E_r = 10$. The polymer can be taken to obey the W.L.F. equation to a reasonable accuracy, with $T_g = 0^\circ\text{C}$. We wish to compute the relaxation modulus in the case of a temperature that varies sinusoidally $\pm 5^\circ$ around 20°C over the course of a day. This can be accomplished by using the effective time as computed from Eqn. 51 in Eqn. 29, as shown in the following Maple commands:

```
define WLF form of log shift factor
>log_aT:=-17.4*(T-Tg)/(51.6+(T-Tg));
find offset; want shift at 20C to be zero
>Digits:=4;Tg:=0;offset:=evalf(subs(T=20,log_aT));
add offset to WLF
>log_aT:=log_aT-offset;
define temperature function
>T:=20+5*cos(2*Pi*t);
get shift factor; take antilog
>aT:=10^log_aT;
replace time with dummy time variable xi
>aT:=subs(t=xi,aT);
get effective time t'
>t_prime:=int(1/aT,xi=0..t);
```

```

define relaxation modulus
>Erel:=ke+k1*exp(-t_prime/tau);
define numerical parameters
>ke:=10;k1:=90;tau:=10;
plot result
>plot(Erel,t=0..10);

```

The resulting plot is shown in Fig. 16.

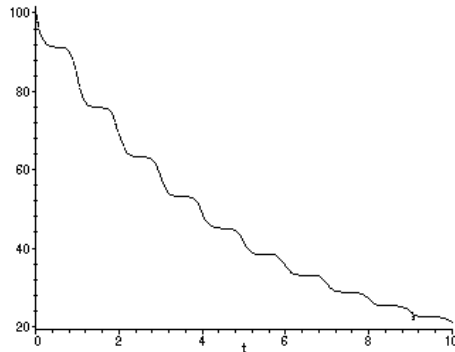


Figure 16: Relaxation modulus with time-varying temperature.

5 Viscoelastic Stress Analysis

5.1 Multiaxial Stress States

The viscoelastic expressions above have been referenced to a simple stress state in which a specimen is subjected to uniaxial tension. This loading is germane to laboratory characterization tests, but the information obtained from these tests must be cast in a form that allows application to the multiaxial stress states that are encountered in actual design.

Many formulae for stress and displacement in structural mechanics problems are cast in forms containing the Young's modulus E and the Poisson's ratio ν . To adapt these relations for viscoelastic response, one might observe both longitudinal and transverse response in a tensile test, so that both $E(t)$ and $\nu(t)$ could be determined. Models could then be fit to both deformation modes to find the corresponding viscoelastic operators \mathcal{E} and \mathcal{N} . However, it is often more convenient to use the shear modulus G and the bulk modulus K rather than E and ν , which can be done using the relations valid for isotropic linear elastic materials:

$$E = \frac{9GK}{3K + G} \quad (52)$$

$$\nu = \frac{3K - 2G}{6K + 2G} \quad (53)$$

These important relations follow from geometrical or equilibrium arguments, and do not involve considerations of time-dependent response. Since the Laplace transformation affects time and not spatial parameters, the corresponding viscoelastic operators obey analogous relations in the Laplace plane:

$$\mathcal{E}(s) = \frac{9\mathcal{G}(s)\mathcal{K}(s)}{3\mathcal{K}(s) + \mathcal{G}(s)}$$

$$\mathcal{N}(s) = \frac{3\mathcal{K}(s) - 2\mathcal{G}(s)}{6\mathcal{K}(s) + 2\mathcal{G}(s)}$$

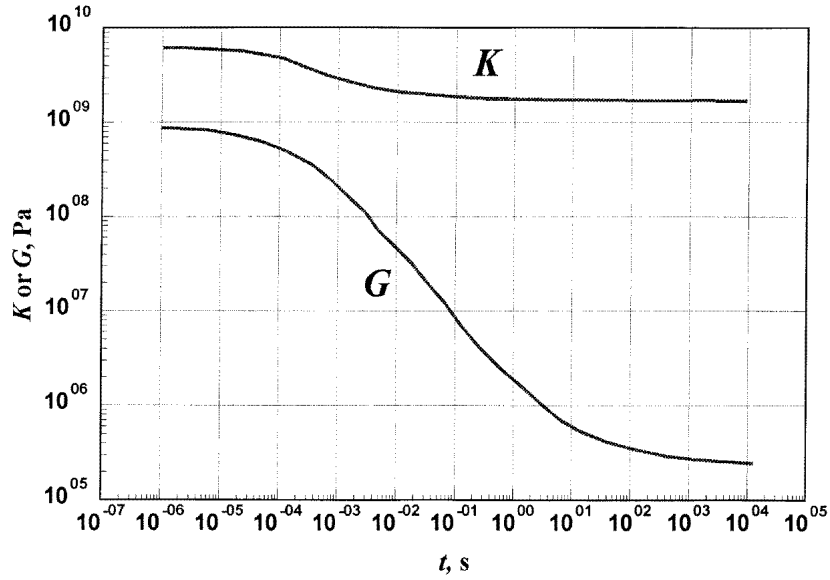


Figure 17: Relaxation moduli of polyisobutylene in dilation (K) and shear (G). From Huang, M.G., Lee, E.H., and Rogers, T.G., “On the Influence of Viscoelastic Compressibility in Stress Analysis,” *Stanford University Technical Report No. 140* (1963).

These substitutions are useful because $K(t)$ is usually much larger than $G(t)$, and $K(t)$ usually experiences much smaller relaxations than $G(t)$ (see Fig. 17). These observations lead to idealizations of compressibility that greatly simplify analysis. First, if one takes $K_{rel} = K_e$ to be finite but constant (only shear response viscoelastic), then

$$\mathcal{K} = s\overline{K}_{rel} = s\frac{K_e}{s} = K_e$$

$$\mathcal{G} = \frac{3K_e\mathcal{E}}{9K_e - \mathcal{E}}$$

Secondly, if K is assumed not only constant but infinite (material incompressible, no hydrostatic deformation), then

$$\mathcal{G} = \frac{\mathcal{E}}{3}$$

$$\mathcal{N} = \nu = \frac{1}{2}$$

Example 12

The shear modulus of polyvinyl chloride (PVC) is observed to relax from a glassy value of $G_g = 800$ MPa to a rubbery value of $G_r = 1.67$ MPa. The relaxation time at 75°C is approximately $\tau = 100$ s, although the transition is much broader than would be predicted by a single relaxation time model. But assuming a standard linear solid model as an approximation, the shear operator is

$$\mathcal{G} = G_r + \frac{(G_g - G_r)s}{s + \frac{1}{\tau}}$$

The bulk modulus is constant to a good approximation at $K_e = 1.33$ GPa. These data can be used to predict the time dependence of the Poisson's ratio, using the expression

$$\mathcal{N} = \frac{3K_e - 2\mathcal{G}}{6K_e + 2\mathcal{G}}$$

On substituting the numerical values and simplifying, this becomes

$$\mathcal{N} = 0.25 + \frac{9.97 \times 10^8}{4.79 \times 10^{11}s + 3.99 \times 10^9}$$

The “relaxation” Poisson's ratio — the time-dependent strain in one direction induced by a constant strain in a transverse direction — is then

$$\bar{\nu}_{rel} = \frac{\mathcal{N}}{s} = \frac{0.25}{s} + \frac{1}{s} \left(\frac{9.97 \times 10^8}{4.79 \times 10^{11}s + 3.99 \times 10^9} \right)$$

Inverting, this gives

$$\nu_{rel} = 0.5 - 0.25e^{-t/120}$$

This function is plotted in Fig. 18. The Poisson's ratio is seen to *rise* from a glassy value of 0.25 to a rubbery value of 0.5 as the material moves from the glassy to the rubbery regime over time. Note that the time constant of 120 s in the above expression is not the same as the relaxation time τ for the pure shear response.

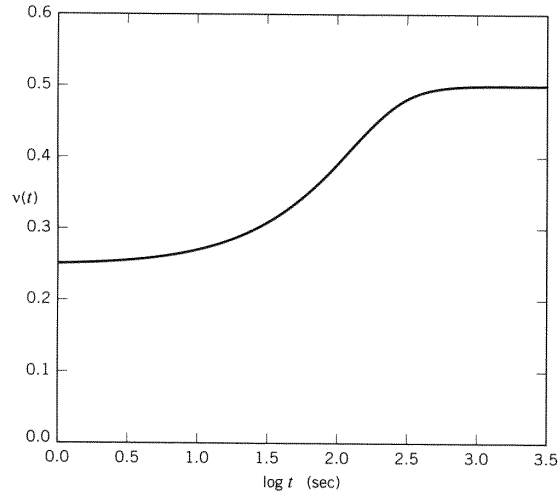


Figure 18: Time dependence of Poisson's ratio for PVC at 75°C , assuming viscoelastic shear response and elastic hydrostatic response.

In the case of material isotropy (properties not dependent on direction of measurement), at most two viscoelastic operators — say \mathcal{G} and \mathcal{K} — will be necessary for a full characterization of the material. For materials exhibiting lower orders of symmetry more descriptors will be necessary: a transversely isotropic material requires four constitutive descriptors, an orthotropic material requires nine, and a triclinic material twenty-one. If the material is both viscoelastic and anisotropic, these are the number of viscoelastic operators that will be required. Clearly, the analyst must be discerning in finding the proper balance between realism and practicality in choosing models.

5.2 Superposition

Fortunately, it is often unnecessary to start from scratch in solving structural mechanics problems that involve viscoelastic materials. We will outline two convenient methods for adapting standard solutions for linear elastic materials to the viscoelastic case, and the first of these is based on the Boltzman superposition principle. We will illustrate this with a specific example, that of the thin-walled pressure vessel.

Polymers such as polybutylene and polyvinyl chloride are finding increasing use in plumbing and other liquid delivery systems, and these materials exhibit measurable viscoelastic time dependency in their mechanical response. It is common to ignore these rate effects in design of simple systems by using generous safety factors. However, in more critical situations the designer may wish extend the elastic theory outlined in standard texts to include material viscoelasticity.

One important point to stress at the outset is that in many cases, the stress distribution does not depend on the material properties and consequently is not influenced by viscoelasticity. For instance, the “hoop” stress σ_θ in an open-ended cylindrical pressure vessel is

$$\sigma_\theta = \frac{pr}{b}$$

where p is the internal pressure, r is the vessel radius, and b is the wall thickness. If the material happens to be viscoelastic, this relation — which contains no material constants — applies without change.

However, the displacements — for instance the increase in radius δ_r — are affected, increasing with time as the strain in the material increases via molecular conformational change. For an open-ended cylindrical vessel with linear elastic material, the radial expansion is

$$\delta_r = \frac{pr^2}{bE}$$

The elastic modulus in the denominator indicates that the radial expansion will increase as material loses stiffness through viscoelastic response. In quantifying this behavior, it is convenient to replace the modulus E by the compliance $C = 1/E$. The expression for radial expansion now has the material constant in the numerator:

$$\delta_r = \frac{pr^2}{b} C \tag{54}$$

If the pressure p is constant, viscoelasticity enters the problem only through the material compliance C , which must be made a suitable time-dependent function. (Here we assume that values of r and b can be treated as constant, which will be usually be valid to a good approximation.) The value of δ_r at time t is then simply the factor (pr^2/b) times the value of $C(t)$ at that time.

The function $C(t)$ needed here is the material's *creep compliance*, the time-dependent strain exhibited by the material in response to an imposed unit tensile stress: $C_{crp} = \epsilon(t)/\sigma_0$. The standard linear solid, as given by Eqn. 30, gives the compliance as

$$C_{crp}(t) = C_g + (C_r - C_g) (1 - e^{-t/\tau}) \quad (55)$$

where here it is assumed that the stress is applied at time $t = 0$. The radial expansion of a pressure vessel, subjected to a constant internal pressure p_0 and constructed of a material for which the S.L.S. is a reasonable model, is then

$$\delta_r(t) = \frac{p_0 r^2}{b} \left[C_g + (C_r - C_g) (1 - e^{-t/\tau}) \right] \quad (56)$$

This function is shown schematically in Fig. 19.

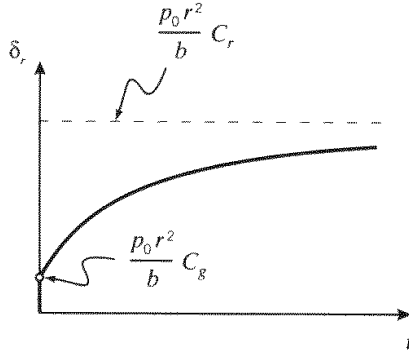


Figure 19: Creep of open-ended pressure vessel subjected to constant internal pressure.

The situation is a bit more complicated if both the internal pressure and the material compliance are time-dependent. It is incorrect simply to use the above equation with the value of p_0 replaced by the value of $p(t)$ at an arbitrary time, because the radial expansion at time t is influenced by the pressure at previous times as well as the pressure at the current time.

The correct procedure is to “fold” the pressure and compliance functions together in a convolution integral as was done in developing the Boltzman Superposition Principle. This gives:

$$\delta_r(t) = \frac{r^2}{b} \int_{-\infty}^t C_{crp}(t - \xi) \dot{p}(\xi) d\xi \quad (57)$$

Example 13

Let the internal pressure be a constantly increasing “ramp” function, so that $p = R_p t$, with R_p being the rate of increase; then we have $\dot{p}(\xi) = R_p$. Using the standard linear solid of Eqn. 55 for the creep compliance, the stress is calculated from the convolution integral as

$$\begin{aligned} \delta_r(t) &= \frac{r^2}{b} \int_0^t \left[C_g + (C_r - C_g) (1 - e^{-(t-\xi)/\tau}) \right] R_p d\xi \\ &= \frac{r^2}{b} \left[R_p t C_r - R_p \tau (C_r - C_g) (1 - e^{-t/\tau}) \right] \end{aligned}$$

This function is plotted in Fig. 20, for a hypothetical material with parameters $C_g = 1/3 \times 10^5 \text{ psi}^{-1}$, $C_r = 1/3 \times 10^4 \text{ psi}^{-1}$, $b = 0.2 \text{ in}$, $r = 2 \text{ in}$, $\tau = 1 \text{ month}$, and $R_p = 100 \text{ psi/month}$. Note that the creep rate increases from an initial value $(r^2/b)R_pC_g$ to a final value $(r^2/b)R_pC_r$ as the glassy elastic components relax away.

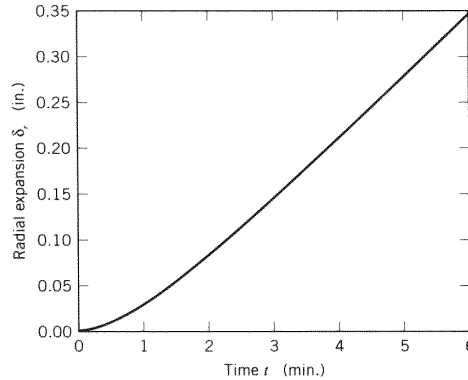


Figure 20: Creep $\delta_r(t)$ of hypothetical pressure vessel for constantly increasing internal pressure.

When the pressure vessel has closed ends and must therefore resist axial as well as hoop stresses, the radial expansion is $\delta_r = (pr^2/bE)[1 - (\nu/2)]$. The extension of this relation to viscoelastic material response *and* a time-dependent pressure is another step up in complexity. Now *two* material descriptors, E and ν , must be modeled by suitable time-dependent functions, and then folded into the pressure function. The superposition approach described above could be used here as well, but with more algebraic complexity. The “viscoelastic correspondence principle” to be presented in below is often more straightforward, but the superposition concept is very important in understanding time-dependent materials response.

5.3 The viscoelastic correspondence principle

In elastic materials, the boundary tractions and displacements may depend on time as well as position without affecting the solution: time is carried only as a parameter, since no time derivatives appear in the governing equations. With viscoelastic materials, the constitutive or stress-strain equation is replaced by a time-differential equation, which complicates the subsequent solution. In many cases, however, the field equations possess certain mathematical properties that permit a solution to be obtained relatively easily⁵. The “viscoelastic correspondence principle” to be outlined here works by adapting a previously available elastic solution to make it applicable to viscoelastic materials as well, so that a new solution from scratch is unnecessary.

If a mechanics problem — the structure, its materials, and its boundary conditions of traction and displacement — is subjected to the Laplace transformation, it will often be the case that none of the spatial aspects of its description will be altered: the problem will appear the same, at least spatially. Only the time-dependent aspects, namely the material properties, will be altered. The Laplace-plane version of problem can then be interpreted as representing a stress analysis

⁵E.H. Lee, “Viscoelasticity,” *Handbook of Engineering Mechanics*, W. Flugge, ed., McGraw-Hill, New York, 1962, Chap. 53.

problem for an elastic body of the same shape as the viscoelastic body, so that a solution for an elastic body will apply to a corresponding viscoelastic body as well, but in the Laplace plane.

There is an exception to this correspondence, however: although the physical shape of the body is unchanged upon passing to the Laplace plane, the boundary conditions for traction or displacement may be altered spatially on transformation. For instance, if the imposed traction is $\hat{T} = \cos(xt)$, then $\bar{T} = s/(s^2 + x^2)$; this is obviously of a different spatial form than the original untransformed function. However, functions that can be written as separable space and time factors will not change spatially on transformation:

$$\hat{T}(x, t) = f(x)g(t) \Rightarrow \bar{T} = f(x)\bar{g}(s)$$

This means that the stress analysis problems whose boundary constraints are independent of time or at worst are separable functions of space and time will *look* the same in both the actual and Laplace planes. In the Laplace plane, the problem is then geometrically identical with an “associated” elastic problem.

Having reduced the viscoelastic problem to an associated elastic one by taking transforms, the vast library of elastic solutions may be used: one looks up the solution to the associated elastic problem, and then performs a Laplace inversion to return to the time plane. The process of viscoelastic stress analysis employing transform methods is usually called the “correspondence principle”, which can be stated as the following recipe:

1. Determine the nature of the associated elastic problem. If the spatial distribution of the boundary and body-force conditions is unchanged on transformation - a common occurrence - then the associated elastic problem appears exactly like the original viscoelastic one.
2. Determine the solution to this associated elastic problem. This can often be done by reference to standard handbooks⁶ or texts on the theory of elasticity⁷.
3. Recast the elastic constants appearing in the elastic solution in terms of suitable viscoelastic operators. As discussed in Section 5.1, it is often convenient to replace E and ν with G and K , and then replace the G and K by their viscoelastic analogs:

$$\left. \begin{array}{l} E \\ \nu \end{array} \right\} \longrightarrow \left\{ \begin{array}{l} G \longrightarrow \mathcal{G} \\ K \longrightarrow \mathcal{K} \end{array} \right.$$

4. Replace the applied boundary and body force constraints by their transformed counterparts:

$$\begin{aligned} \hat{\mathbf{T}} &\Rightarrow \bar{\mathbf{T}} \\ \hat{\mathbf{u}} &\Rightarrow \bar{\mathbf{u}} \end{aligned}$$

where $\hat{\mathbf{T}}$ and $\hat{\mathbf{u}}$ are imposed tractions and displacements, respectively.

5. Invert the expression so obtained to obtain the solution to the viscoelastic problem in the time plane.

⁶For instance, W.C. Young, *Roark's Formulas for Stress and Strain*, McGraw-Hill, Inc., New York, 1989.

⁷For instance, S. Timoshenko and J.N. Goodier, *Theory of Elasticity*, McGraw-Hill, Inc., New York, 1951.

If the elastic solution contains just two time-dependent quantities in the numerator, such as in Eqn. 54, the correspondence principle is equivalent to the superposition method of the previous section. Using the pressure-vessel example, the correspondence method gives

$$\delta_r = \frac{pr^2C}{b} \rightarrow \bar{\delta}_r(s) = \frac{r^2}{b}\bar{p}C$$

Since $C = s\bar{C}_{crp}$, the transform relation for convolution integrals gives

$$\delta_r(t) = \mathcal{L}^{-1}\left(\frac{r^2}{b}s\bar{C}_{crp}\cdot\bar{p}\right) = \mathcal{L}^{-1}\left(\frac{r^2}{b}\bar{C}_{crp}\cdot\bar{p}\right) = \frac{r^2}{b}\int_{-\infty}^t C_{crp}(t-\xi)\dot{p}(\xi)d\xi$$

as before. However, the correspondence principle is more straightforward in problems having a complicated mix of time-dependent functions, as demonstrated in the following example.

Example 14

The elastic solution for the radial expansion of a closed-end cylindrical pressure vessel of radius r and thickness b is

$$\delta_r = \frac{pr^2}{bE}\left(1 - \frac{\nu}{2}\right)$$

Following the correspondence-principle recipe, the associated solution in the Laplace plane is

$$\bar{\delta}_r = \frac{\bar{p}r^2}{b\mathcal{E}}\left(1 - \frac{\mathcal{N}}{2}\right)$$

In terms of hydrostatic and shear response functions, the viscoelastic operators are:

$$\mathcal{E}(s) = \frac{9\mathcal{G}(s)\mathcal{K}(s)}{3\mathcal{K}(s) + \mathcal{G}(s)}$$

$$\mathcal{N}(s) = \frac{3\mathcal{K}(s) - 2\mathcal{G}(s)}{6\mathcal{K}(s) + 2\mathcal{G}(s)}$$

In Example 12, we considered a PVC material at 75°C that to a good approximation was elastic in hydrostatic response and viscoelastic in shear. Using the standard linear solid model, we had

$$\mathcal{K} = K_e, \quad \mathcal{G} = G_r + \frac{(G_g - G_r)s}{s + \frac{1}{\tau}}$$

where $K_e = 1.33$ GPa, $G_g = 800$ MPa, $G_r = 1.67$ MPa, and $\tau = 100$ s.

For constant internal pressure $p(t) = p_0$, $\bar{p} = p_0/s$. All these expressions must be combined, and the result inverted. Maple commands for this problem might be:

```
define shear operator
> G:=Gr+((Gg-Gr)*s)/(s+(1/tau));
define Poisson operator
> N:=(3*K-2*G)/(6*K+2*G);
define modulus operator
> Eop:=(9*G*K)/(3*K+G);
define pressure operator
> pbar:=p0/s;
get d1, radial displacement (in Laplace plane)
> d1:=(pbar*r^2)*(1-(N/2))/(b*Eop);
read Maple library for Laplace transforms
> readlib(inttrans);
invert transform to get d2, radial displacement in real plane
> d2:=invlaplace(d1,s,t);
```

After some manual rearrangement, the radial displacement $\delta_r(t)$ can be written in the form

$$\delta_r(t) = \frac{r^2 p_0}{b} \left[\left(\frac{1}{4G_r} + \frac{1}{6K} \right) - \left(\frac{1}{4G_r} - \frac{1}{4G_g} \right) e^{-t/\tau_c} \right]$$

where the creep retardation time is $\tau_c = \tau(G_g/G_r)$. Continuing the Maple session:

```
define numerical parameters
> Gg:=800*10^6; Gr:=1.67*10^6; tau:=100; K:=1.33*10^9;
> r:=.05; b:=.005; p0:=2*10^5;
resulting expression for radial displacement
> d2;
      - .01494 exp( - .00002088 t) + .01498
```

A log-log plot of this function is shown in Fig. 21. Note that for this problem the effect of the small change in Poisson's ratio ν during the transition is negligible in comparison with the very large change in the modulus E , so that a nearly identical result would have been obtained simply by letting $\nu = \text{constant} = 0.5$. On the other hand, it isn't appreciably more difficult to include the time dependence of ν if symbolic manipulation software is available.

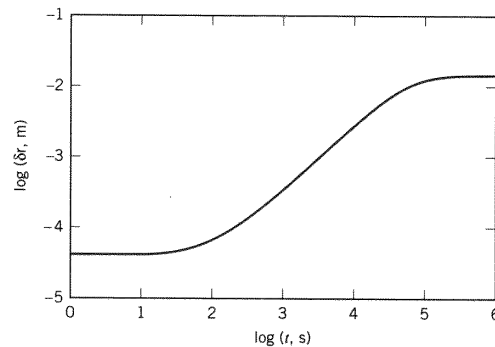


Figure 21: Creep response of PVC pressure vessel.

6 Additional References

1. Aklonis, J.J., MacKnight, W.J., and Shen, M., *Introduction to Polymer Viscoelasticity*, Wiley-Interscience, New York, 1972.
2. Christensen, R.M., *Theory of Viscoelasticity*, 2nd ed., Academic Press, New York, 1982.
3. Ferry, J.D., *Viscoelastic Properties of Polymers*, 3rd ed., Wiley & Sons, New York, 1980.
4. Flugge, W., *Viscoelasticity*, Springer-Verlag, New York, 1975.
5. McCrum, N.G, Read, B.E., and Williams, G., *Anelastic and Dielectric in Polymeric Solids*, Wiley & Sons, London, 1967. Available from Dover Publications, New York.
6. Tschoegl, N.W., *The Phenomenological Theory of Linear Viscoelastic Behavior*, Springer-Verlag, Heidelberg, 1989.

7. Tschoegl, N.W., "Time Dependence in Materials Properties: An Overview," *Mechanics of Time-Dependent Materials*, Vol. 1, pp. 3–31, 1997.
8. Williams, M.L., "Structural Analysis of Viscoelastic Materials," *AIAA Journal*, p. 785, May 1964.

7 Problems

1. Plot the functions $e^{-t/\tau}$ and $1 - e^{-t/\tau}$ versus $\log_{10} t$ from $t = 10^{-2}$ to $t = 10^2$. Have two curves on the plot for each function, one for $\tau = 1$ and one for $\tau = 10$.
2. Determine the apparent activation energy in (E^\dagger in Eqn. 2) for a viscoelastic relaxation in which the initial rate is observed to double when the temperature is increased from 20°C to 30°C. (Answer: $E^\dagger = 51$ kJ/mol.)
3. Determine the crosslink density N and segment molecular weight M_c between crosslinks for a rubber with an initial modulus $E = 1000$ psi at 20°C and density 1.1 g/cm³. (Answer: $N = 944$ mol/m³, $M_c = 1165$ g/mol.)
4. Expand the exponential forms for the dynamic stress and strain ($\sigma(t) = \sigma_0^* e^{i\omega t}$, $\epsilon(t) = \epsilon_0^* e^{i\omega t}$) and show that

$$E^* = \frac{\sigma(t)}{\epsilon(t)} = \frac{\sigma_0 \cos \delta}{\epsilon_0} + i \frac{\sigma_0 \sin \delta}{\epsilon_0},$$

where δ is the phase angle between the stress and strain.

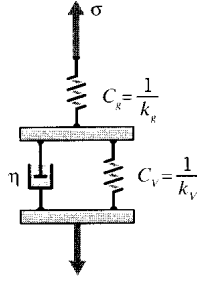
5. Using the relation $\bar{\sigma} = \mathcal{E}\bar{\epsilon}$ for the case of dynamic loading ($\epsilon(t) = \epsilon_0 \cos \omega t$) and S.L.S. material response ($\mathcal{E} = k_e + k_1 s / (s + \frac{1}{\tau})$), solve for the time-dependent stress $\sigma(t)$. Use this solution to identify the steady-state components of the complex modulus $E^* = E' + iE''$, and the transient component as well. Answer:

$$E^* = \frac{k_1}{1 + \omega^2 \tau^2} e^{-t/\tau} + \left(k_e + \frac{k_1 \omega^2 \tau^2}{1 + \omega^2 \tau^2} \right) \cos \omega t - \left(\frac{k_1 \omega \tau}{1 + \omega^2 \tau^2} \right) \sin \omega t$$

6. For the Standard Linear Solid with parameters $k_e = 25$, $k_1 = 50$, and $\tau_1 = 1$, plot E' and E'' versus $\log \omega$ in the range $10^{-2} < \omega \tau_1 < 10^2$. Also plot E'' versus E' in this same range, using ordinary rather than logarithmic axes and the same scale for both axes (Argand diagram).
7. Show that the viscoelastic law for the "Voigt" form of the Standard Linear Solid (a spring of stiffness $k_v = 1/C_v$ in parallel with a dashpot of viscosity η , and this combination in series with another spring of stiffness $k_g = 1/C_g$) can be written

$$\bar{\epsilon} = \mathcal{C}\bar{\sigma}, \quad \text{with} \quad \mathcal{C} = \left[C_g + \frac{C_v}{\tau \left(s + \frac{1}{\tau} \right)} \right]$$

where $\tau = \eta/k_v$.

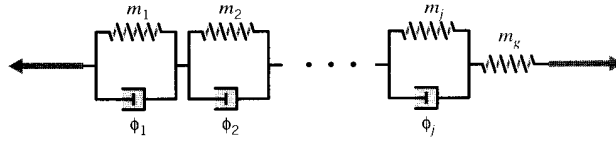


Prob. 7

8. Show that the creep compliance of the Voigt SLS model of Prob. 7 is

$$C_{crp} = C_g + C_v (1 - e^{-t/\tau})$$

9. In cases where the stress rather than the strain is prescribed, the Kelvin model - a series arrangement of Voigt elements - is preferable to the Wiechert model:



Prob. 9

where $\phi_j = 1/\eta_j = \dot{\epsilon}_j/\sigma_{dj}$ and $m_j = 1/k_j = \epsilon_j/\sigma_{sj}$. Using the relations $\epsilon = \epsilon_g + \sum_j \epsilon_j$, $\sigma = \sigma_{sj} + \sigma_{dj}$, $\tau_j = m_j/\phi_j$, show the associated viscoelastic constitutive equation to be:

$$\bar{\epsilon} = \left[m_g + \sum_j \frac{m_j}{\tau_j \left(s + \frac{1}{\tau_j} \right)} \right] \bar{\sigma}$$

and for this model show the creep compliance to be:

$$C_{crp}(t) = \frac{\epsilon(t)}{\sigma_0} = m_g + \sum_j m_j (1 - e^{-t/\tau_j})$$

10. For a simple Voigt model ($C_g=0$ in Prob. 7), show that the strain $\epsilon^{t+\Delta t}$ at time $t + \Delta t$ can be written in terms of the strain ϵ^t at time t and the stress σ^t acting during the time increment Δt as

$$\epsilon^{t+\Delta t} = C_v \sigma^t (1 - e^{-\Delta t/\tau}) + \epsilon^t e^{-\Delta t/\tau}$$

Use this algorithm to plot the creep strain arising from a constant stress $\sigma = 100$ versus $\log t = (1, 5)$ for $C_v = 0.05$ and $\tau = 1000$.

11. Plot the strain response $\epsilon(t)$ to a load-unload stress input defined as

$$\sigma(t) = \begin{cases} 0, & t < 1 \\ 1, & 1 < t < 4.5 \\ -1, & 4.5 < t < 5 \\ 0, & t > 5 \end{cases}$$

The material obeys the SLS compliance law (Eqn. 30) with $C_g = 5$, $C_r = 10$, and $\tau = 2$.

12. Using the Maxwell form of the standard linear solid with $k_e = 10$, $k_1 = 100$ and $\eta = 1000$:
 - a) Plot $E_{rel}(t)$ and $E_{crp}(t) = 1/C_{crp}(t)$ versus log time. b) Plot $[E_{crp}(t) - E_{rel}(t)]$ versus log time. c) Compare the relaxation time with the retardation time (the time when the argument of the exponential becomes -1 , for relaxation and creep respectively). Speculate on why one is shorter than the other.
13. Show that a Wiechert model with two Maxwell arms (Eqn. 34) is equivalent to the second-order ordinary differential equation

$$a_2\ddot{\sigma} + a_1\dot{\sigma} + a_0\sigma = b_2\ddot{\epsilon} + b_1\dot{\epsilon} + b_0\epsilon$$

where

$$\begin{aligned} a_2 &= \tau_1\tau_2, & a_1 &= \tau_1 + \tau_2, & a_0 &= 1 \\ b_2 &= \tau_1\tau_2(k_e + k_1 + k_2), & b_1 &= k_e(\tau_1 + \tau_2) + k_1\tau_1 + k_2\tau_2, & b_0 &= k_e \end{aligned}$$

14. For a viscoelastic material defined by the differential constitutive equation:

$$15\ddot{\sigma} + 8\dot{\sigma} + \sigma = 105\ddot{\epsilon} + 34\dot{\epsilon} + \epsilon,$$

write an expression for the relaxation modulus in the Prony-series form (Eqn. 36). (Answer: $E_{rel} = 1 + 2e^{-t/3} + 4e^{-t/5}$)

15. For the simple Maxwell element, verify that

$$\int_0^t E_{rel}(\xi) D_{crp}(t - \xi) d\xi = t$$

16. Evaluate the Boltzman integral

$$\sigma(t) = \int_0^t E_{rel}(t - \xi)\dot{\epsilon}(\xi) d\xi$$

to determine the response of the Standard Linear Solid to sinusoidal straining ($\epsilon(t) = \cos(\omega t)$)

17. Derive Eqn. 48 by using the Arrhenius expression for relaxation time to subtract the log relaxation time at an arbitrary temperature T from that at a reference temperature T_{ref} .
18. Using isothermal stress relaxation data at various temperatures, shift factors have been measured for a polyurethane material as shown in the table below:

$T, ^\circ C$	$\log_{10} a_T$
+5	-0.6
0	0
-5	0.8
-10	1.45
-15	2.30
-20	3.50
-25	4.45
-30	5.20

- (a) Plot $\log a_T$ vs. $1/T(^{\circ}K)$; compute an average activation energy using Eqn 48. (Answer: $E^\ddagger = 222$ kJ/mol.)
- (b) Plot $\log a_T$ vs. $T(^{\circ}C)$ and compare with WLF equation (Eqn. 50), with $T_g = -35^{\circ}C$. (Note that $T_{ref} = 0 \neq T_g$.)
19. After time-temperature shifting, a master relaxation curve at $0^{\circ}C$ for the polyurethane of Prob. 18 gives the following values of $E_{rel}(t)$ at various times:

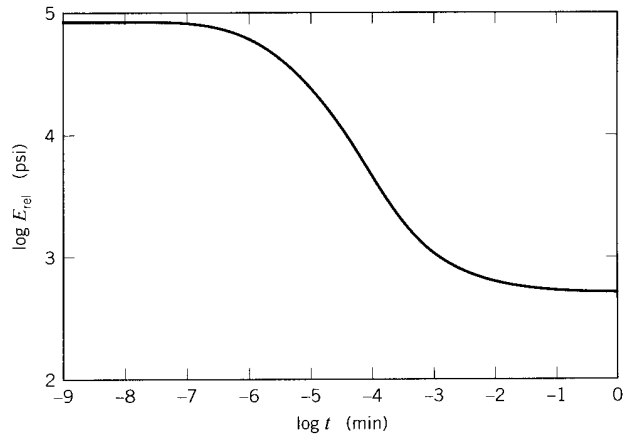
$\log(t, \text{min})$	$E_{rel}(t), \text{psi}$
-6	56,280
-5	22,880
-4	4,450
-3	957
-2	578
-1	481
0	480

- (a) In Eqn. 36, choose $k_e = E_{rel}(t = 0) = 480$.
- (b) Choose values of τ_j to match the times given in the above table from 10^{-6} to 10^{-1} (a process called “collocation”).
- (c) Determine appropriate values for the spring stiffnesses k_j corresponding to each τ_j so as to make Eqn. 36 match the experimental values of $E_{rel}(t)$. This can be done by setting up and solving a sequence of linear algebraic equations with the k_j as unknowns:

$$\sum_{j=1}^6 k_j e^{-t_i/\tau_j} = E_{rel}(t_i) - k_e, \quad i = 1, 6$$

Note that the coefficient matrix is essentially triangular, which facilitates manual solution in the event a computer is not available.

- (d) Adjust the value of k_1 so that the sum of all the spring stiffnesses equals the glassy modulus $E_g = 91,100$ psi.
- (e) Plot the relaxation modulus predicted by the model from $\log t = -8$ to 0.
20. Plot the relaxation (constant strain) values of modulus E and Poisson’s ratio ν for the polyisobutylene whose dilatational and shear response is shown in Fig. 17. Assume S.L.S. models for both dilatation and shear.

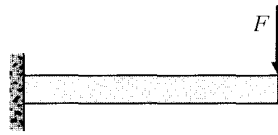


Prob. 19

21. The elastic solution for the stress $\sigma_x(x, y)$ and vertical deflection $v(x, y)$ in a cantilevered beam of length L and moment of inertia I , loaded at the free end with a force F , is

$$\sigma_x(x, y) = \frac{F(L-x)y}{I}, \quad v(x, y) = \frac{Fx^2}{6EI}(3L-x)$$

Determine the viscoelastic counterparts of these relations using both the superposition and correspondence methods, assuming S.L.S. behavior for the material compliance (Eqn. 30).



Prob. 21

22. A polymer with viscoelastic properties as given in Fig. 17 is placed in a rigid circular die and loaded with a pressure $\sigma_y = 1$ MPa. Plot the transverse stress $\sigma_x(t)$ and the axial strain $\epsilon_y(t)$ over $\log t = -5$ to 1. The elastic solution is

$$\sigma_x = \frac{\nu\sigma_y}{1-\nu}, \quad \epsilon_y = \frac{(1+\nu)(1-2\nu)}{E(1-\nu)}\sigma_y$$

A Laplace Transformations

Basic definition:

$$\mathcal{L}f(t) = \bar{f}(s) = \int_0^{\infty} f(t) e^{-st} dt$$

Fundamental properties:

$$\mathcal{L}[c_1 f_1(t) + c_2 f_2(t)] = c_2 \bar{f}_1(s) + c_1 \bar{f}_2(s)$$

$$\mathcal{L} \left[\frac{\partial f}{\partial t} \right] = s \bar{f}(s) - f(0^-)$$

Some useful transform pairs:

$f(t)$	$\bar{f}(s)$
$u(t)$	$1/s$
t^n	$n!/s^{n+1}$
e^{-at}	$1/(s+a)$
$\frac{1}{a}(1 - e^{-at})$	$1/s(s+a)$
$\frac{t}{a} - \frac{1}{a^2}(1 - e^{-at})$	$1/s^2(s+a)$

Here $u(t)$ is the Heaviside or unit step function, defined as

$$u(t) = \begin{cases} 0, & t < 0 \\ 1, & t \geq 0 \end{cases}$$

The convolution integral:

$$\mathcal{L}f \cdot \mathcal{L}g = \bar{f} \cdot \bar{g} = \mathcal{L} \left[\int_0^t f(t-\xi) g(\xi) d\xi \right] = \mathcal{L} \left[\int_0^t f(\xi) g(t-\xi) d\xi \right]$$

Yield and Plastic Flow

David Roylance
Department of Materials Science and Engineering
Massachusetts Institute of Technology
Cambridge, MA 02139

October 15, 2001

Introduction

In our overview of the tensile stress-strain curve in Module 4, we described yield as a permanent molecular rearrangement that begins at a sufficiently high stress, denoted σ_Y in Fig. 1. The yielding process is very material-dependent, being related directly to molecular mobility. It is often possible to control the yielding process by optimizing the materials processing in a way that influences mobility. General purpose polystyrene, for instance, is a weak and brittle plastic often credited with giving plastics a reputation for shoddiness that plagued the industry for years. This occurs because polystyrene at room temperature has so little molecular mobility that it experiences brittle fracture at stresses less than those needed to induce yield with its associated ductile flow. But when that same material is blended with rubber particles of suitable size and composition, it becomes so tough that it is used for batting helmets and ultra-durable children's toys. This magic is done by control of the yielding process. Yield control to balance strength against toughness is one of the most important aspects of materials engineering for structural applications, and all engineers should be aware of the possibilities.

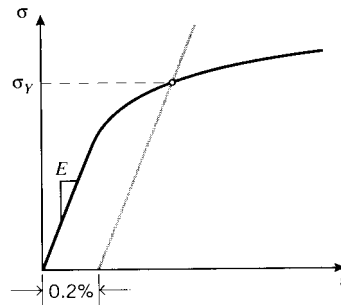


Figure 1: Yield stress σ_Y as determined by the 0.2% offset method.

Another important reason for understanding yield is more prosaic: if the material is not allowed to yield, it is not likely to fail. This is not true of brittle materials such as ceramics that fracture before they yield, but in most of the tougher structural materials no damage occurs before yield. It is common design practice to size the structure so as to keep the stresses in the elastic range, short of yield by a suitable safety factor. We therefore need to be able to predict

when yielding will occur in general multidimensional stress states, given an experimental value of σ_Y .

Fracture is driven by *normal* stresses, acting to separate one atomic plane from another. Yield, conversely, is driven by *shearing* stresses, sliding one plane along another. These two distinct mechanisms are illustrated in Fig. 2. Of course, bonds must be broken during the sliding associated with yield, but unlike in fracture are allowed to reform in new positions. This process can generate substantial change in the material, even leading eventually to fracture (as in bending a metal rod back and forth repeatedly to break it). The “plastic” deformation that underlies yielding is essentially a viscous flow process, and follows kinetic laws quite similar to liquids. Like flow in liquids, plastic flow usually takes place without change in volume, corresponding to Poisson’s ratio $\nu = 1/2$.

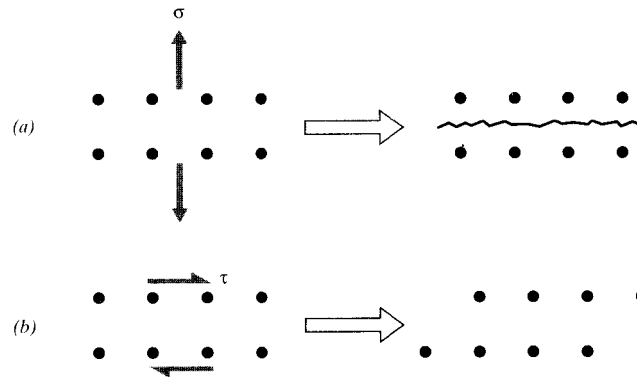


Figure 2: Cracking is caused by normal stresses (a), sliding is caused by shear stresses (b).

Multiaxial stress states

The yield stress σ_Y is usually determined in a tensile test, where a single uniaxial stress acts. However, the engineer must be able to predict when yield will occur in more complicated real-life situations involving multiaxial stresses. This is done by use of a *yield criterion*, an observation derived from experimental evidence as to just what it is about the stress state that causes yield. One of the simplest of these criteria, known as the maximum shear stress or *Tresca* criterion, states that yield occurs when the maximum shear stress reaches a critical value $\tau_{max} = k$. The numerical value of k for a given material could be determined directly in a pure-shear test, such as torsion of a circular shaft, but it can also be found indirectly from the tension test as well. As shown in Fig. 3, Mohr’s circle shows that the maximum shear stress acts on a plane 45° away from the tensile axis, and is half the tensile stress in magnitude; then $k = \sigma_Y/2$.

In cases of plane stress, Mohr’s circle gives the maximum shear stress *in that plane* as half the difference of the principal stresses:

$$\tau_{max} = \frac{\sigma_{p1} - \sigma_{p2}}{2} \quad (1)$$

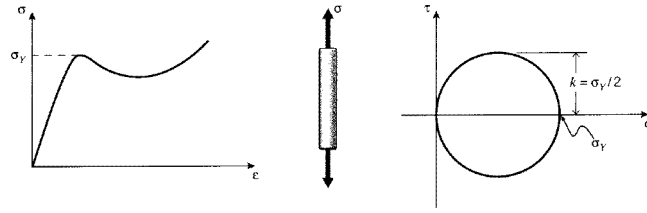


Figure 3: Mohr's circle construction for yield in uniaxial tension.

Example 1

Using $\sigma_{p1} = \sigma_\theta = pr/b$ and $\sigma_{p2} = \sigma_z = pr/2b$ in Eqn. 1, the shear stress in a cylindrical pressure vessel with closed ends is¹

$$\tau_{max,\theta z} = \frac{1}{2} \left(\frac{pr}{b} - \frac{pr}{2b} \right) = \frac{pr}{4b}$$

where the θz subscript indicates a shear stress in a plane tangential to the vessel wall. Based on this, we might expect the pressure vessel to yield when

$$\tau_{max,\theta z} = k = \frac{\sigma_Y}{2}$$

which would occur at a pressure of

$$p_Y = \frac{4b\tau_{max,\theta z}}{r} \stackrel{?}{=} \frac{2b\sigma_Y}{r}$$

However, this analysis is in error, as can be seen by drawing Mohr's circles not only for the θz plane but for the θr and rz planes as well as shown in Fig. 4.

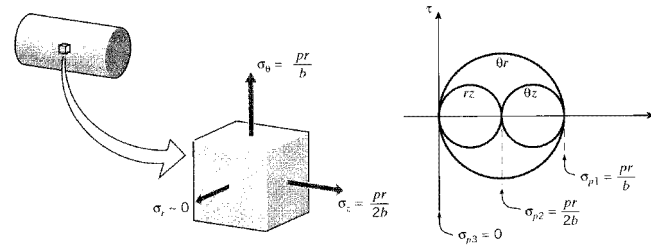


Figure 4: Principal stresses and Mohr's circle for closed-end pressure vessel

The shear stresses in the θr plane are seen to be twice those in the θz plane, since in the θr plane the second principal stress is zero:

$$\tau_{max,\theta r} = \frac{1}{2} \left(\frac{pr}{b} - 0 \right) = \frac{pr}{2b}$$

Yield will therefore occur in the θr plane at a pressure of $b\sigma_Y/r$, half the value needed to cause yield in the θz plane. Failing to consider the shear stresses acting in this third direction would lead to a seriously underdesigned vessel.

Situations similar to this example occur in plane stress whenever the principal stresses in the xy plane are of the same sign (both tensile or both compressive). The maximum shear stress,

¹See Module 6.

which controls yield, is half the *difference* between the principal stresses; if they are both of the same sign, an even larger shear stress will occur on the perpendicular plane containing the larger of the principal stresses in the xy plane.

This concept can be used to draw a “yield locus” as shown in Fig. 5, an envelope in σ_1 - σ_2 coordinates outside of which yield is predicted. This locus obviously crosses the coordinate axes at values corresponding to the tensile yield stress σ_Y . In the I and III quadrants the principal stresses are of the same sign, so according to the maximum shear stress criterion yield is determined by the difference between the larger principal stress and zero. In the II and IV quadrants the locus is given by $\tau_{max} = |\sigma_1 - \sigma_2|/2 = \sigma_Y/2$, so $\sigma_1 - \sigma_2 = \text{const}$; this gives straight diagonal lines running from σ_Y on one axis to σ_Y on the other.

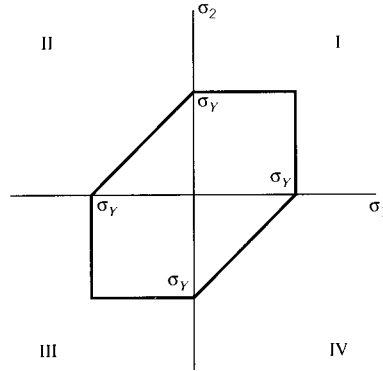


Figure 5: Yield locus for the maximum-shear stress criterion.

Example 2

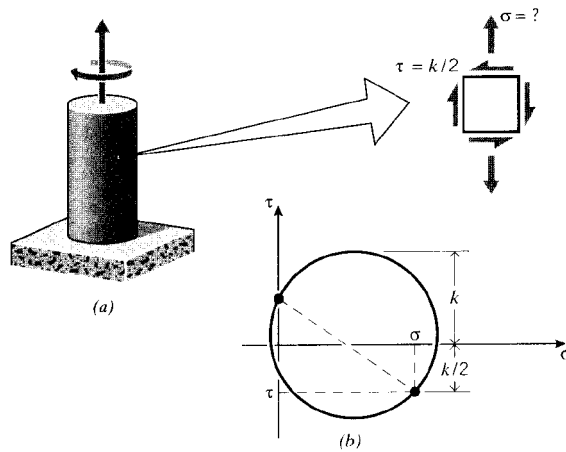


Figure 6: (a) Circular shaft subjected to simultaneous twisting and tension. (b) Mohr's circle construction.

A circular shaft is subjected to a torque of half that needed to cause yielding as shown in Fig. 6; we now ask what tensile stress could be applied simultaneously without causing yield.

A Mohr's circle is drawn with shear stress $\tau = k/2$ and unknown tensile stress σ . Using the Tresca maximum-shear yield criterion, yield will occur when σ is such that

$$\begin{aligned}\tau_{max} = k &= \sqrt{\left(\frac{\sigma}{2}\right)^2 + \left(\frac{k}{2}\right)^2} \\ \sigma &= \sqrt{3}k\end{aligned}$$

The Tresca criterion is convenient to use in practice, but a somewhat better fit to experimental data can often be obtained from the “von Mises” criterion, in which the driving force for yield is the strain energy associated with the deviatoric components of stress. The *von Mises stress* (also called the *equivalent* or *effective* stress) is defined as

$$\sigma_M = \sqrt{\frac{1}{2} [(\sigma_x - \sigma_y)^2 + (\sigma_x - \sigma_z)^2 + (\sigma_y - \sigma_z)^2 + 6(\tau_{xy} + \tau_{yz} + \tau_{xz})]}$$

In terms of the principal stresses this is

$$\sigma_M = \sqrt{\frac{1}{2} [(\sigma_1 - \sigma_2)^2 + (\sigma_1 - \sigma_3)^2 + (\sigma_2 - \sigma_3)^2]}$$

where the stress differences in parentheses are proportional to the maximum shear stresses on the three principal planes². (Since the quantities are squared, the order of stresses inside the parentheses is unimportant.) The Mises stress can also be written in compact form in terms of the second invariant of the deviatoric stress tensor Σ_{ij} :

$$\sigma_M = \sqrt{3\Sigma_{ij}\Sigma_{ij}/2} \tag{2}$$

It can be shown that this is proportional to the total distortional strain energy in the material, and also to the shear stress τ_{oct} on the “octahedral” plane oriented equally to the 1-2-3 axes. The von Mises stress is the driving force for damage in many ductile engineering materials, and is routinely computed by most commercial finite element stress analysis codes.

The value of von Mises stress $\sigma_{M,Y}$ needed to cause yield can be determined from the tensile yield stress σ_Y , since in tension at the yield point we have $\sigma_1 = \sigma_Y$, $\sigma_2 = \sigma_3 = 0$. Then

$$\sigma_{M,Y} = \sqrt{\frac{1}{2} [(\sigma_Y - 0)^2 + (\sigma_Y - 0)^2 + (0 - 0)^2]} = \sigma_Y$$

Hence the value of von Mises stress needed to cause yield is the same as the simple tensile yield stress.

The shear yield stress k can similarly be found by inserting the principal stresses corresponding to a state of pure shear in the Mises equation. Using $k = \sigma_1 = -\sigma_3$ and $\sigma_2 = 0$, we have

$$\begin{aligned}\sqrt{\frac{1}{2} [(k - 0)^2 + (k + k)^2 + (0 - k)^2]} &= \sqrt{\frac{6k^2}{2}} = \sigma_Y \\ k &= \frac{\sigma_Y}{\sqrt{3}}\end{aligned}$$

²Some authors use a factor other than 1/2 within the radical. This is immaterial, since it will be absorbed by the calculation of the critical value of σ_M .

Note that this result is different than the Tresca case, in which we had $k = \sigma_Y/2$.

The von Mises criterion can be plotted as a yield locus as well. Just as the Tresca criterion, it must pass through σ_Y on each axis. However, it plots as an ellipse rather than the prismatic shape of the Tresca criterion (see Fig. 7).

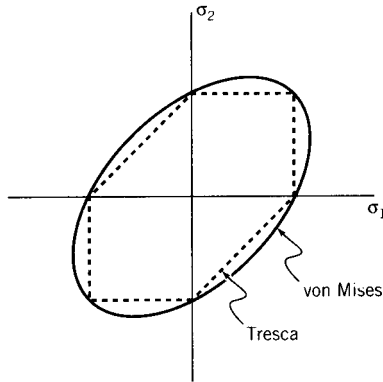


Figure 7: Yield locus for the von Mises criterion.

Effect of hydrostatic pressure

Since in the discussion up to now yield has been governed only by shear stress, it has not mattered whether a uniaxial stress is compressive or tensile; yield occurs when $\sigma = \pm\sigma_Y$. This corresponds to the hydrostatic component of the stress $-p = (\sigma_x + \sigma_y + \sigma_z)/3$ having no influence on yield, which is observed experimentally to be valid for slip in metallic systems. Polymers, however, are much more resistant to yielding in compressive stress states than in tension. The atomistic motions underlying slip in polymers can be viewed as requiring “free volume” as the molecular segments move, and this free volume is diminished by compressive stresses. It is thus difficult to form solid polymers by deformation processing such as stamping and forging in the same way steel can be shaped; this is one reason the vast majority of automobile body panels continue to be made of steel rather than plastic.

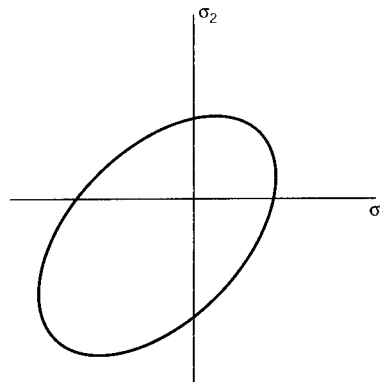


Figure 8: Effect of pressure on the von Mises yield envelope.

This dependency on hydrostatic stress can be modeled by modifying the yield criterion to state that yield occurs when

$$\tau_{max} \text{ or } \sigma_M \geq \tau_0 + Ap \quad (3)$$

where τ_0 and A are constants. As p increases (the hydrostatic component of stress becomes more positive) the shear stress needed for yield becomes greater as well, since there is less free volume and more hindrance to molecular motion. The effect of this modification is to slide the von Mises ellipse to extend less into the I quadrant and more into the III quadrant as shown in Fig. 8. This shows graphically that greater stresses are needed for yield in compression, and lesser stresses in tension.

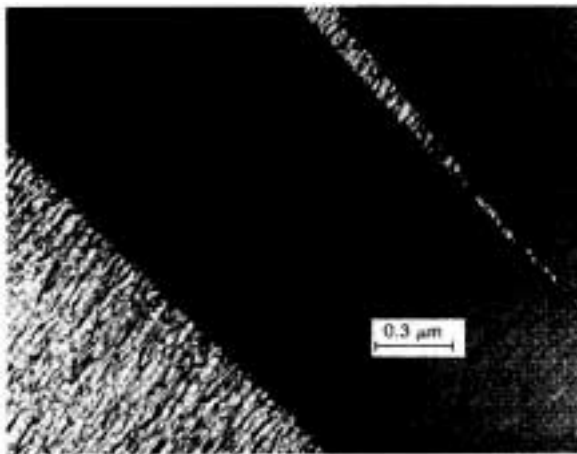


Figure 9: A craze in polystyrene (from R. Kambour, “Crazing,” *Encyclopedia of Polymer Science and Engineering*, Wiley-Interscience, 1991).

Several amorphous glassy polymers — notably polystyrene, polymethylmethacrylate, and polycarbonate — are subject to a yield mechanism termed “crazing” in which long elongated voids are created within the material by a tensile cavitation process. Figure 9 shows a craze in polystyrene, grown in plasticizing fluid near T_g . The voids, or crazes, are approximately 1000Å thick and microns or more in length, and appear visually to be much like conventional cracks. They differ from cracks, however, in that the broad faces of the crazes are spanned by a great many elongated fibrils that have been drawn from the polymer as the craze opens. The fibril formation requires shear flow, but the process is also very dependent on free volume. A successful multiaxial stress criterion for crazing that incorporates both these features has been proposed³ of the form

$$\sigma_1 - \sigma_2 = A(T) + \frac{B(T)}{\sigma_1 + \sigma_2}$$

The left hand side of this relation is proportional to the shear stress, and the denominator in the second term on the right hand side is related to the hydrostatic component of the stress. As the hydrostatic tension increases, the shear needed to cause crazing decreases. The parameters A and B are adjustable, and both depend on temperature. This relation plots as a batwing on the yield locus diagram as seen in Fig. 10, approaching a 45° diagonal drawn through the II

³S. Sternstein and L. Ongchin, *Polymer Preprints*, **10**, 1117, 1969.

and IV quadrants. Crazing occurs to the right of the curve; note that crazing never occurs in compressive stress fields.

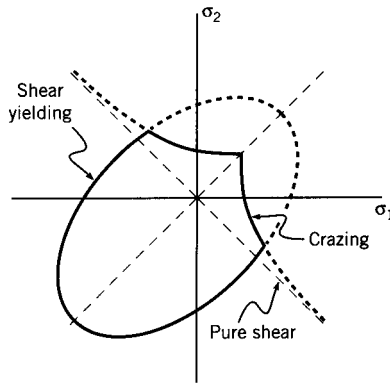


Figure 10: The Sternstein envelopes for crazing and pressure-inhibited shear yielding.

Crazing is a yield mechanism, but it also precipitates brittle fracture as the craze height increases and the fibrils are brought to rupture. The point where the craze locus crosses the shear yielding locus is therefore a type of mechanically induced ductile-brittle transition, as the failure mode switches from shear yielding to craze embrittlement. Environmental agents such as acetone that expand the free volume in these polymers greatly exacerbate the tendency for craze brittleness. Conversely, modifications such as rubber particle inclusions that stabilize the crazes and prevent them from becoming true cracks can provide remarkable toughness. Rubber particles not only stabilize crazes, they also cause a great increase in the number of crazes, so the energy absorption of craze formation can add to the toughness as well. This is the basis of the “high impact polystyrene,” or HIPS, mentioned at the outset of this chapter.

Effect of rate and temperature

The yield process can be viewed as competing with fracture, and whichever process has the lowest stress requirements will dominate. As the material is made less and less mobile, for instance by lowering the temperature or increasing the number and tightness of chemical bonds, yielding becomes more and more difficult. The fracture process is usually much less dependent on mobility. Both yield and fracture stresses usually increase with decreasing temperature, but yield is more temperature-dependent (see Fig. 11). This implies that below a critical temperature (called the ductile-brittle transition temperature T_{DB}) the material will fracture before it yields. Several notable failures in ships and pipelines have occurred during winter temperatures when the steels used in their manufacture were stressed below their T_{DB} and were thus unable to resist catastrophic crack growth. In polymers, the ductile-brittle transition temperature is often coincident with the glass transition temperature. Clearly, we need an engineering model capable of showing how yield depends on temperature, and one popular approach is outlined below.

Yield processes are thermally activated, stress driven motions, much like the flow of viscous liquids. Even without going into much detail as to the specifics of the motions, it is possible to write down quite effective expressions for the dependency of these motions on strain rate and temperature. In the Eyring view of thermally activated processes, an energy barrier E_Y^* must be overcome for the motion to proceed. (We shall use the asterisk superscript to indicate activation

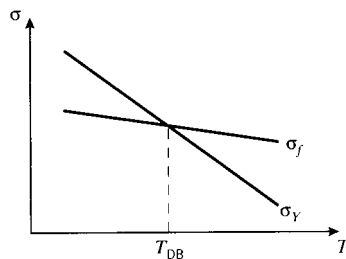


Figure 11: Schematic illustration of the temperature dependence of yield and fracture stress.

parameters, and the Y subscript here indicates the yield process.) A stress acts to lower the barrier when it acts in the direction of flow, and to raise it when it opposes the flow.

Consider now a constant strain rate test ($\dot{\epsilon} = \text{const}$), in which the stress rises until yield occurs at $\sigma = \sigma_Y$. At the yield point we have $d\sigma/d\epsilon = 0$, so a fluidlike state is achieved in which an increment of strain can occur without a corresponding incremental increase in stress. Analogously with rate theories for viscous flow, an Eyring rate equation can be written for the yielding process as

$$\dot{\epsilon} = \dot{\epsilon}_0 \exp \frac{-(E_Y^* - \sigma_Y V^*)}{kT} \quad (4)$$

Here k is Boltzman's constant and V^* is a factor governing the effectiveness of the stress in reducing the activation barrier. It must have units of volume for the product $\sigma_Y V^*$ to have units of energy, and is called the "activation volume" of the process. Taking logs and rearranging,

$$\frac{\sigma_Y}{T} = \frac{E_Y^*}{V^* T} + \left(\frac{k}{V^*} \right) \ln \left(\frac{\dot{\epsilon}}{\dot{\epsilon}_0} \right)$$

Hence plots of σ_Y/T versus $\ln \dot{\epsilon}$ should be linear with a slope k/V^* as seen in Fig. 12, from which the activation volume may be computed. The horizontal spacing between two lines at differing temperatures T_1 and T_2 gives the activation energy:

$$E_Y^* = \frac{k (\ln \dot{\epsilon}^{T_2} - \ln \dot{\epsilon}^{T_1})}{\left(\frac{1}{T_1} - \frac{1}{T_2} \right)}$$

Apparent activation volumes in polymers are on the order of 5000\AA^3 , much larger than a single repeat unit. This is taken to indicate that yield in polymers involves the cooperative motion of several hundred repeat units.

Example 3

The yield stress for polycarbonate is reported at 60 MPa at room-temperature ($23^\circ\text{C} = 296^\circ\text{K}$), and we wish to know its value at 0°C (273°K), keeping the strain rate the same.

This can be accomplished by writing Eqn. 4 out twice, once for each temperature, and then dividing one by the other. The parameters $\dot{\epsilon}$ and $\dot{\epsilon}_0$ cancel, leaving

$$1 = \exp \left(\frac{E_Y^* - \sigma_Y^{273} V^*}{R(273)} - \frac{E_Y^* - \sigma_Y^{296} V^*}{R(296)} \right)$$

From the data in Fig. 12, the yield activation parameters are $E_Y^* = 309 \text{ kJ/mol}$, $V^* = 3.9 \times 10^{-3} \text{ m}^3/\text{mol}$. Using these along with $R = 8.314 \text{ J/mol}$ and $\sigma_Y^{296} = 60 \times 10^6 \text{ N/m}^2$, we have

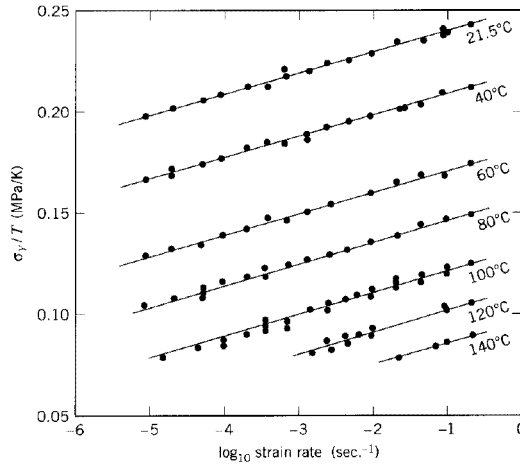


Figure 12: Eyring plot showing dependence of yield strength on temperature and strain rate in polycarbonate (from N.G. McCrum, C.P. Buckley and C.B. Bucknall, *Principles of Polymer Engineering*, Oxford University Press, 1988).

$$\sigma_Y^{273} = 61.5 \text{ MPa}$$

Continuum plasticity

Plasticity theory, which seeks to determine stresses and displacements in structures all or part of which have been stressed beyond the yield point, is an important aspect of solid mechanics. The situation is both materially and geometrically nonlinear, so it is not a trivial undertaking. However, in such areas as metal forming, plasticity theory has provided valuable insight. We will outline only a few aspects of this field in the following paragraphs, to introduce some of the fundamental concepts that the reader can extend in future study.

Plastic deformation

A useful idealization in modeling plastic behavior takes the material to be linearly elastic up to the yield point as shown in Fig. 13, and then “perfectly plastic” at strains beyond yield. Strains up to yield (the line between points *a* and *b*) are recoverable, and the material unloads along the same elastic line it followed during loading; this is conventional elastic response. But if the material is strained beyond yield (point *b*), the “plastic” straining beyond *b* takes place at constant stress and is unrecoverable. If the material is strained to point *c* and then unloaded, it follows the path *cd* (a line parallel to the original elastic line *ab*) rather than returning along *cba*. When the stress has been brought to zero (point *d*), the plastic strain *ad* remains as a *residual* strain.

Plastic deformation can generate “residual” stresses in structures, internal stresses that remain even after the external loads are removed. To illustrate this, consider two rods having different stress-strain curves, connected in parallel (so their strains are always equal) as shown in Fig. 14. When the rods are strained up to the yield point of rod *B* (point *a* on the strain

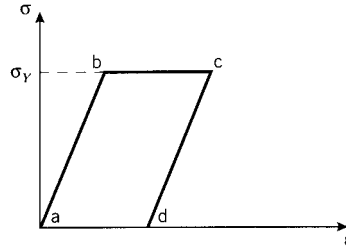


Figure 13: The elastic-perfectly plastic idealization of plastic deformation.

axis), rod A will have experienced an amount of permanent plastic deformation ϵ^p . When the applied load is removed, rod B unloads along its original stress-strain curve, but rod A follows a path parallel to its original elastic line. When rod A reaches zero stress (point b), rod B will still be in tension (point c). In order for the load transmitted by the rods together to come to zero, rod B will pull rod A into compression until $-\sigma_B = \sigma_A$ as indicated by points d and e . Residual stresses are left in the rods, and the assembly as a whole is left with a residual tensile strain.

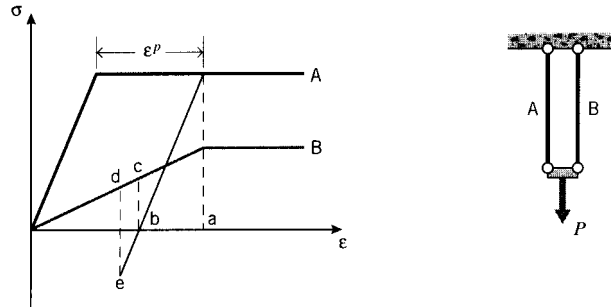


Figure 14: Plastic deformation of two-bar assembly.

Compressive residual stress can be valuable if the structure must bear tensile loads. Similarly to how rapid quenching can be used to make safety glass by putting the surfaces in compression, plastic deformation can be used to create favorable compressive stresses. One famous such technique is called “autofrettage;” this is a method used to strengthen cannon barrels against bursting by pressurizing them from the inside so as to bring the inner portion of the barrel into the plastic range. When the pressure is removed, the inner portions are left with a compressive residual stress just as with bar A in the above example.

Wire drawing

To quantify the plastic flow process in more detail, consider next the “drawing” of wire⁴, in which wire is pulled through a reducing die so as to reduce its cross-sectional area from A_0 to A as shown in Fig. 15. Since volume is conserved during plastic deformation, this corresponds to an axial elongation of $L/L_0 = A_0/A$. Considering the stress state to be simple uniaxial tension, we have

⁴G.W. Rowe, *Elements of Metalworking Theory*, Edward Arnold, London, 1979.

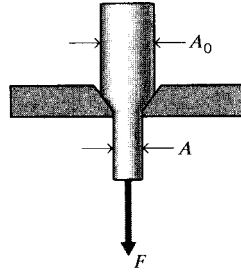


Figure 15: Wire drawing.

$$\sigma_1 = \sigma_Y, \quad \sigma_2 = \sigma_3 = 0$$

where 1 denotes the direction along the wire and 2 and 3 are the transverse directions. The work done in stretching the wire by an increment of length dL , per unit volume of material, is

$$dU = \frac{dW}{AL} = \frac{\sigma_Y A dL}{AL}$$

Integrating this from L_0 to L to obtain the total work:

$$U = \int_{L_0}^L dU = \frac{F dL}{AL} = \sigma_Y \ln \frac{L}{L_0}$$

The quantity $\ln(L/L_0)$ is the *logarithmic strain* ϵ_T introduced in Module 4 (Stress-Strain Curves).

Example 4

The logarithmic strain can be written in terms of either length increase or area reduction, due to the constancy of volume during plastic deformation: $\epsilon_T = \ln(L/L_0) = \ln(A_0/A)$. In terms of diameter reduction, the relation $A = \pi d^2/4$ leads to

$$\epsilon_T = \ln \left(\frac{\pi d_0^2/4}{\pi d^2/4} \right) = 2 \ln \left(\frac{d_0}{d} \right)$$

Taking the pearlite cell size to shrink commensurately with the diameter, we expect the wire strength σ_f to vary according to the Hall-Petch relation with $1/\sqrt{d}$. The relation between wire strength and logarithmic drawing strain is then

$$\sigma_f \propto \frac{\exp(\epsilon_T/4)}{\sqrt{d_0}}$$

The work done by the constant pulling force F in drawing an initial length L_0 of wire to a new length L is $W = FL$. This must equal the work per unit volume done in the die, multiplied by the total volume of wire:

$$FL = (AL) \sigma_Y \ln \frac{L}{L_0}$$

Written in terms of area reduction, this is

$$F = A \sigma_Y \ln \frac{A_0}{A}$$

This simple result is useful in estimating the requirements of wire drawing, even though it neglects the actual complicated flow field within the die and the influence of friction at the die walls. Both friction at the surface and constraints to flow within the field raise the force needed in drawing, but the present analysis serves to establish a lower-limit approximation. It is often written in terms of the drawing stress $\sigma_1 = F/A$ and the area reduction ratio $r = (A_0 - A)/A_0 = 1 - (A/A_0)$:

$$\sigma_1 = \sigma_Y \ln \frac{1}{1-r}$$

Note that the draw stress for a small area reduction is less than the tensile yield stress. In fact, the maximum area reduction that can be achieved in a single pass can be estimated by solving for the value of r which brings the draw stress up to the value of the yield stress, which it obviously cannot exceed. This calculation gives

$$\ln \frac{1}{1-r_{max}} = 1 \Rightarrow r_{max} = 1 - \frac{1}{e} = 0.63$$

Hence the maximum area reduction is approximately 63%, assuming perfect lubrication at the die. This lower-bound treatment gives an optimistic result, but is not far from the approximately 50% reduction often used as a practical limit. If the material hardens during drawing, the maximum reduction can be slightly greater.

Slip-line fields

In cases of plane strain, there is a graphical technique called *slip-line theory*⁵ which permits a more detailed examination of plastic flow fields and the loads needed to create them. Friction and internal flow constraints can be included, so upper-bound approximations are obtained that provide more conservative estimates of the forces needed in deformation. Considerable experience is needed to become proficient in this method, but the following will outline some of the basic ideas.

Consider plane strain in the 1-3 plane, with no strain in the 2-direction. There is a Poisson stress in the 2-direction, given by

$$\epsilon_2 = 0 = \frac{1}{E}[\sigma_2 - \nu(\sigma_1 + \sigma_3)]$$

Since $\nu = 1/2$ in plastic flow,

$$\sigma_2 = \frac{1}{2}(\sigma_1 + \sigma_3)$$

The hydrostatic component of stress is then

$$p = \frac{1}{3}(\sigma_1 + \sigma_2 + \sigma_3) = \frac{1}{2}(\sigma_1 + \sigma_3) = \sigma_2$$

Hence the Poisson stress σ_2 in the zero-strain direction is the average of the other two stresses σ_1 and σ_3 , and also equal to the hydrostatic component of stress. The stress state can be specified in terms of the maximum shear stress, which is just k during plastic flow, and the superimposed hydrostatic pressure p :

$$\sigma_1 = -p + k, \quad \sigma_2 = -p \quad \sigma_3 = -p - k$$

⁵W. Johnson and P.B. Mellor, *Plasticity for Mechanical Engineers*, Van Nostrand Co., New York, 1962.

Since the shear stress is equal to k everywhere, the problem is one of determining the directions of k (the direction of maximum shear, along which slip occurs), and the magnitude of p .

The graphical technique involves sketching lines that lie along the directions of k . Since maximum shear stresses act on two orthogonal planes, there will be two sets of these lines, always perpendicular to one another and referred to as α -lines and β -lines. The direction of these lines is specified by an inclination angle ϕ . Any convenient inclination can be used for the $\phi = 0$ datum, and the identification of α - vs. β -lines is such as to make the shear stress positive according to the usual convention. As the pressure p varies from point to point, there is a corresponding variation of the angle ϕ , given by the *Hencky equations* as

$$p + 2k\phi = C_1 = \text{constant, along an } \alpha\text{-line}$$

$$p - 2k\phi = C_2 = \text{constant, along a } \beta\text{-line}$$

Hence the pressure can be determined from the curvature of the sliplines, once the constant is known.

The slip-line field must obey certain constraints at boundaries:

1. *Free surfaces*: Since there can be no stress normal to a free surface, we can put $\sigma_3 = 0$ there and then

$$p = k, \quad \sigma_1 = -p - k = -2k$$

Hence the pressure is known to be just the shear yield strength at a free surface. Furthermore, since the directions normal and tangential to the surface are principal directions, the directions of maximum shear must be inclined at 45° to the surface.

2. *Frictionless surface*: The shear stress must be zero tangential to a frictionless surface, which again means that the tangential and normal directions must be principal directions. Hence the slip lines must meet the surface at 45° . However, there will in general be a stress acting normal to the surface, so $\sigma_3 \neq 0$ and thus p will not be equal to k .
3. *Perfectly rough surface*: If the friction is so high as to prevent any tangential motion at the surface, the shearing must be maximum in a direction that is also tangential to the surface. One set of slip lines must then be tangential to the surface, and the other set normal to it.

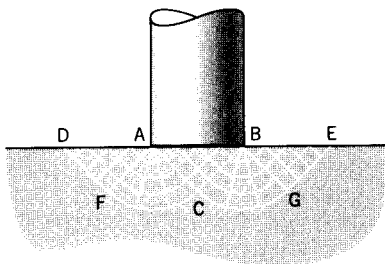


Figure 16: Slip-line construction for a flat indentation.

Consider a flat indenter of width b being pressed into a semi-infinite block, with negligible friction (see Fig. 16). Since the sliplines must meet the indenter surface at 45° , we can draw a

triangular flow field ABC . Since all lines in this region are straight, there can be no variation in the pressure p , and the field is one of “constant state.” This cannot be the full extent of the field, however, since it would be constrained both vertically and laterally by rigid metal. The field must extend to the free surfaces adjacent to the punch, so that downward motion under the punch can be compensated by upward flow adjacent to it. Two more triangular regions ADF and BEG are added that satisfy the boundary conditions at free surfaces, and these are connected to the central triangular regions by “fans” AFC and BCG . Fans are very useful in slip-line constructions; they are typically centered on singularities such as points A and B where there is no defined normal to the surface.

The pressure on the punch needed to establish this field can be determined from the sliplines, and this is one of their principal uses. Since BE is a free surface, $\sigma_3 = 0$ there and $p = k$. The pressure remains constant along line EG since ϕ is unchanging, but as ϕ decreases along the curve GC (the line curves clockwise), the pressure must increase according to the Hencky equation. At point C it has rotated through $-\pi/2$ so the pressure there is

$$p_C + 2k\phi = p_C + 2k\left(-\frac{\pi}{2}\right) = \text{constant} = p_G = k$$

$$p_C = k(1 + \pi)$$

The pressure remains unchanged along lines CA and CB , so the pressure along the punch face is also $k(1 + \pi)$. The total stress acting upward on the punch face is therefore

$$\sigma_1 = p + k = 2k\left(1 + \frac{\pi}{2}\right)$$

The ratio of punch pressure to the tensile yield strength $2k$ is

$$\frac{\sigma_1}{2k} = 1 + \frac{\pi}{2} = 2.571$$

The factor 2.571 represents the increase over the tensile yield strength caused by the geometrical constraints on the flow field under the punch.

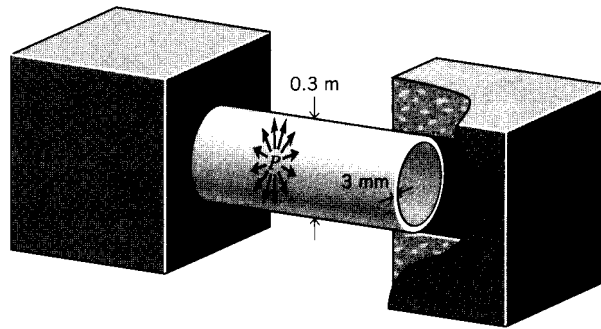
The *Brinell Hardness Test* is similar to the punch yielding scenario above, but uses a hard steel sphere instead of a flat indenter. The Brinell hardness H is calculated as the load applied to the punch divided by the projected area of the indentation. Analysis of the Brinell test differs somewhat in geometry, but produces a result not much different than that of the flat punch:

$$\frac{H}{\sigma_Y} \approx 2.8 - 2.9$$

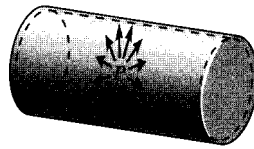
This relation is very useful in estimating the yield strength of metals by simple nondestructive indentation hardness tests.

Problems

1. An open-ended pressure vessel is constructed of aluminum, with diameter 0.3 m and wall thickness 3 mm. (Open-ended in this context means that both ends of the vessel are connected to other structural parts able to sustain pressure, as in a hose connected between two reservoirs.) Determine the internal pressure at which the vessel will yield according to the (a) Tresca and (b) von Mises criteria.

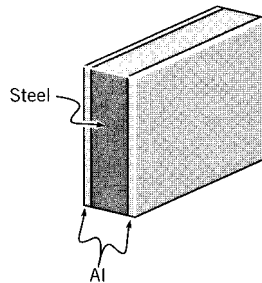


Prob. 1



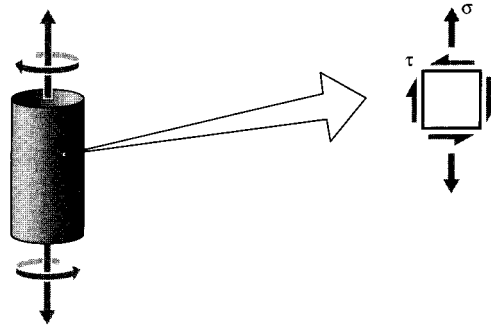
Prob. 2

2. Repeat the previous problem, but with the pressure vessel now being closed-ended.
3. A steel plate is clad with a thin layer of aluminum on both sides at room temperature, and the temperature then raised. At what temperature increase ΔT will the aluminum yield?



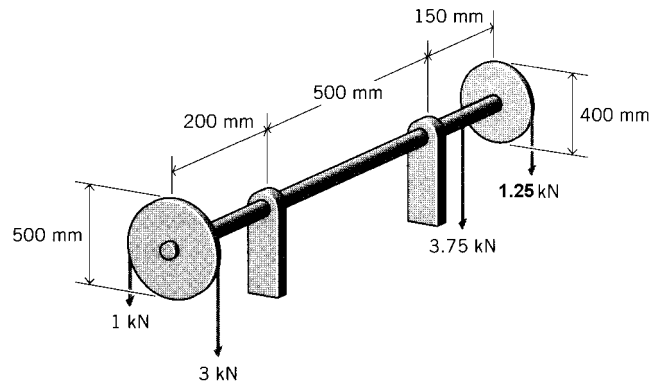
Prob. 3

4. If the temperature in the previous problem is raised 40°C beyond the value at which yielding occurs, and is thereafter lowered back to room temperature, what is the residual stress left in the aluminum?
5. Copper alloy is subjected to the stress state $\sigma_x = 100, \sigma_y = -200, \tau_{xy} = 100$ (all in MPa). Determine whether yield will occur according to the (a) Tresca and (b) von Mises criterion.
6. Repeat the previous problem, but with the stress state $\sigma_x = 190, \sigma_y = 90, \tau_{xy} = 120$ (all in MPa)
7. A thin-walled tube is placed in simultaneous tension and torsion, causing a stress state as shown here. Construct a plot of τ/σ_Y vs. σ/σ_Y at which yield will occur according to the (a) Tresca and (b) von Mises criterion. (σ_Y is the tensile yield stress.)



Prob. 7

8. A solid circular steel shaft is loaded by belt pulleys at both ends as shown. Determine the diameter of the shaft required to avoid yield according to the von Mises criterion, with a factor of safety of 2.



Prob. 8

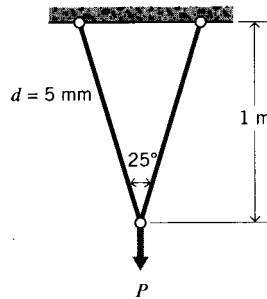
9. For polycarbonate, the kinetic parameters in Eqn. 4 are found to be $\dot{\epsilon}_0 = 448 \text{ s}^{-1}$, $E_Y^* = 309 \text{ kJ/mol}$, and $V^* = 3.9 \times 10^{-3} \text{ m}^3/\text{mol}$. Find the yield stress σ_Y at a strain rate of $\dot{\epsilon} = 10^2 \text{ s}^{-1}$ and temperature 40°C .
10. Yield stresses (in MPa) have been measured at various strain rates and temperatures as follows:

	$\dot{\epsilon} = 10^{-3} \text{ s}^{-1}$	$\dot{\epsilon} = 10^{-1} \text{ s}^{-1}$
$T = 0^\circ\text{C}$	54.1	62.7
$T = 40^\circ\text{C}$	42.3	52.1

Determine the activation volume for the yield process. What physical significance might this parameter have?

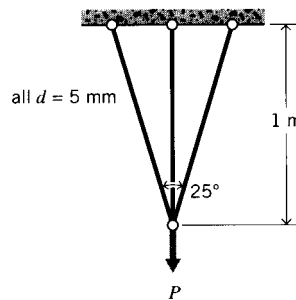
11. The yield stress of a polymer is measured to be 20 MPa at a temperature of 300K and a strain rate of 10^{-3} s^{-1} . When the strain rate is doubled from this value, the yield stress is observed to increase by 10%. What is the apparent activation volume for yield in this case?

12. Show the von Mises stress can be written in index notation as $\sigma_M = \sqrt{3\Sigma_{ij}\Sigma_{ij}/2}$
13. A sample of linear polyethylene was tested in uniaxial loading at $T = 23^\circ \text{ C}$ and $\dot{\epsilon} = 10^{-3} \text{ s}^{-1}$. The yield stress σ_Y was found to be 30.0 MPa in tension and 31.5 MPa in compression. Determine the pressure-dependency constant A in Eqn. 3.
14. A circular shaft of radius R is subjected to a torque T .
- What value of T will be just large enough to induce yielding at the outer surface?
 - As the value of T is increased beyond the level found in (a), determine the radius r_e within which the material is still in the elastic range.
 - What value of T will make the shaft fully plastic; i.e. $r_e = 0$?
15. A two-element truss frame is constructed of steel with the geometry shown. What load P can the frame support without yielding in either element?



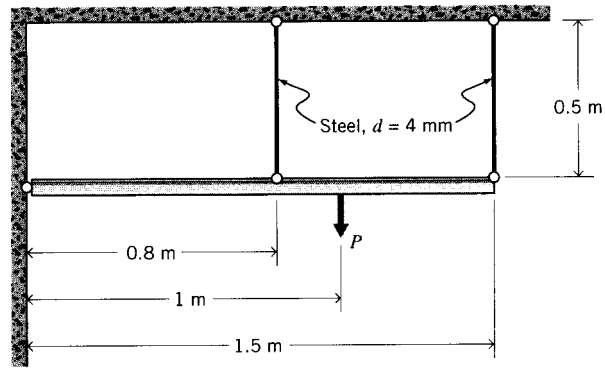
Prob. 15

16. A three-element truss frame is constructed of steel with the geometry shown. What load P can the frame support before all three elements have yielded?



Prob. 16

17. If the frame of the previous problem is loaded until all three members have yielded and the load then reduced to zero, find the residual stress in the central element.
18. A rigid beam is hinged at one end as shown and supported by two vertical rods as shown.
- What load P can the structure support before both vertical rods have yielded?
 - What is the residual stress in the vertical rods after the load has been reduced to zero?



Prob. 18

19. Estimate the drawing force required to reduce the diameter of a 0.125" aluminum rod by 50% in a wire-drawing operation.

The Dislocation Basis of Yield and Creep

David Roylance
Department of Materials Science and Engineering
Massachusetts Institute of Technology
Cambridge, MA 02139

March 22, 2001

Introduction

Phenomenological treatments such those outlined in the Module on Yield and Plastic Flow (Module 20) are very useful for engineering predictions, but they provide only limited insight to the molecular mechanisms underlying yield. Molecular understanding is a higher level of insight, and also guides processing adjustments that can optimize the material. As discussed in the Module on Atomistics of Elasticity (Module 2), the high level of order present in crystalline materials lead to good atomistic models for the stiffness. Early workers naturally sought an atomistic treatment of the yield process as well. This turned out to be a much more subtle problem than might have been anticipated, and required hypothesizing a type of crystalline defect — the “dislocation” — to explain the experimentally observed results. Dislocation theory permits a valuable intuitive understanding of yielding in crystalline materials, and explains how yielding can be controlled by alloying and heat treatment. It is one of the principal triumphs of the last century of materials science.

Theoretical yield strength

In yield, atoms slide tangentially from one equilibrium position to another. The forces required to bring this about are given by the bond energy function, which is the anharmonic curve resulting from the balance of attractive and repulsive atomic forces described in Module 2. The force needed to displace the atom from equilibrium is the derivative of the energy function, being zero at the equilibrium position (see Fig. 1). As a simplifying assumption, let us approximate the force function with a harmonic expression, and write

$$\tau = \tau_{max} \sin \left(2\pi \frac{x}{a} \right)$$

where a is the interatomic spacing. The stress reaches a maximum a quarter of the distance between the two positions, dropping to zero at the metastable position midway between them. After that, the stress changes sign, meaning that force is required to hold the atom back as it tries to fall toward the new equilibrium position. Using $\gamma = x/a$ as the shear strain, the maximum shear stress τ_{max} can be related to the shear modulus G as

$$\frac{d\tau}{d\gamma} = \frac{d\tau}{dx} \frac{dx}{d\gamma} = a \frac{d\tau}{dx} = a \tau_{max} \frac{2\pi}{a} \cos \frac{2\pi x}{a}$$

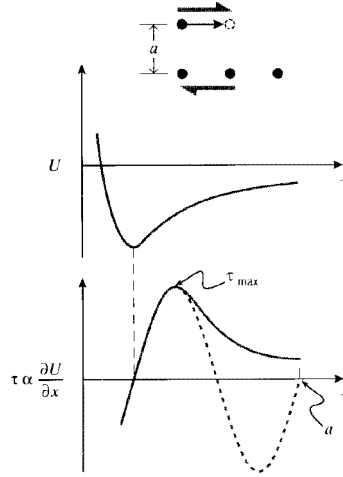


Figure 1: Atomistic energy and stress functions.

$$G = \left. \frac{d\tau}{d\gamma} \right|_{\gamma \rightarrow 0} = \tau_{max} \cdot 2\pi$$

This implies a shear stress at yield of $\tau_{max} = G/2\pi \approx G/10$, which would be on the order of 10 GPa. Measured values are 10–100 MPa, so the theoretical value is 2 to 3 orders of magnitude too large. More elaborate derivations give a somewhat smaller value for the theoretical yield stress, but still much larger than what is observed experimentally.

Edge, screw, and mixed dislocations

A rationale for the apparently low experimental values for the yield strengths of crystalline materials was proposed independently by Taylor, Polanyi and Orowan in 1934. These workers realized that it was not necessary to slip entire planes of atoms past one another to deform the material plastically, a process that would require breaking all the bonds connecting the planes simultaneously. The stress needed to do this would be very high, on the order of $G/10$ as described above. But it isn't necessary to move all the atoms at once; only a few at a time need to move, requiring a much smaller stress. Analogously to the way an inchworm moves, only those atoms lying in a plane above a single line might be displaced one atomic spacing. This would force the plane of atoms previously there into a midway position as shown in Fig. 2, creating an “extra” plane of atoms halfway between the normal equilibrium positions. The termination of this plane then constitutes a line defect in the crystal known as a *dislocation*¹.

Viewed end-on as seen in Fig. 3, it can be appreciated that the extra plane of atoms creates a region of compression near the plane but above the dislocation line, and a tensile region below it. In a “soft” crystal whose interatomic bonds are relatively compliant, the distortion extends an appreciable distance from the dislocation. Conversely, in “hard” crystals with stiffer bonds the distortion is confined to a smaller region near the dislocation. The face-centered cubic (fcc) metals such as copper and gold have close-packed planes (those with (111) Miller indices), which

¹For an extended discussion of the geometrical aspects of crystal dislocations, see S.M. Allen and E.L. Thomas, *The Structure of Materials*, John Wiley & Sons, New York, 1999.

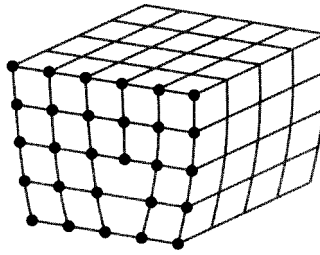


Figure 2: The edge dislocation.

corresponds to large distances between those planes. This gives rise to relatively soft interplanar bonds, so that the dislocation width is large. The dislocation width is substantially smaller in the body centered cubic (bcc) metals such as iron and steel, smaller still in ionically bonded ceramics, and even smaller in covalently bonded ceramics.

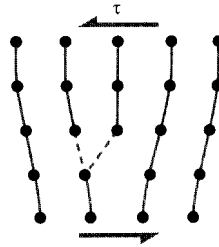


Figure 3: Dislocation motion.

The dislocation associated with this extra plane of atoms can be moved easily, since only a small adjustment in position is required to break the bonds on the next plane over and allow them to form on the originally “extra” plane. Now the third plane is the extra one, and the dislocation will have moved by one atomic position. Slip is obviously made much easier if dislocation motion is available to the material. In fact, it first appears the dislocation concept does *too* good a job in explaining crystal plasticity, since the dislocation is in a balanced metastable position and should be capable of being moved either left or right with a vanishingly small force. If this were true, the crystal would have essentially *no* shear strength.

However, as the dislocation moves it drags with it the regions of compressive and tensile distortion in the lattice around it. This is accompanied by a sort of frictional drag, giving rise to a resistance to dislocation motion known as the *Peierls* force. This force is dependent on such factors as the crystal type and the temperature, and this plays an important role in determining the material’s yield stress. As seen in Table 1, materials with wide dislocations have low Peierls forces, since the distortion is spread out over a large volume and is much less intense at its core.

Table 1 also indicates that the effect of temperature on the Peierls force is low for fcc materials having wide dislocations, and this results in a small temperature dependency of the yield stress. Conversely, materials with narrow and intense dislocation fields have high Peierls forces with a large temperature sensitivity of the yield stress, with higher temperatures facilitating dislocation mobility and thus reducing the yield strength. Among the important consequences of these factors is the dangerous tendency of steel to become brittle at low temperatures; as the temperature is lowered, the yield stress can rise to such high levels that brittle fracture

Table 1: Relationship between dislocation width and yield strength temperature sensitivity (from R.W. Hertzberg, *Deformation and Fracture Mechanics of Engineering Materials*, John Wiley & Sons, 1976).

Material	Crystal Type	Dislocation Width	Peierls Stress	Yield Strength Temperature Sensitivity
Metal	fcc	wide	very small	negligible
Metal	bcc	narrow	moderate	strong
Ceramic	ionic	narrow	large	strong
Ceramic	covalent	very narrow	very large	strong

intervenes.

Dislocations can have geometries other than the simple edge dislocation shown in Fig. 3. A more general view is provided by considering displacing a portion of the atoms in a “slip plane” $acfg$ a distance \bar{b} , as shown in Fig. 4. The vector \bar{b} is also a measure of the magnitude and direction of the crystal dislocation, and is known as the *Burgers’ vector*. The boundary between slipped and unslipped atoms on the slip plane is the dislocation line, shown as a dotted line. At position e , the dislocation line is perpendicular to the Burgers’ vector, so these two quantities lie in the slip plane. A dislocation so situated is called an *edge* dislocation, and is constrained to move only in the slip plane defined by the dislocation line and the Burgers’ vector.

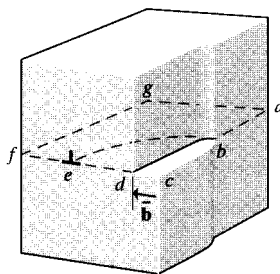


Figure 4: The mixed dislocation.

At position b , a spiral-like defect is formed such that a circular transit around the dislocation line ends on a plane a distance \bar{b} from the starting point. Now the defect is known as a *screw* dislocation. The dislocation line is now parallel to the Burgers’ vector, so these two quantities do not define a unique slip plane the way an edge dislocation does. A screw dislocation can therefore *cross-slip* to another easy-glide plane passing through the dislocation line, and this mechanism enables screw dislocations to maneuver around obstacles that might otherwise impede their motion. Edge dislocations are more easily pinned, since they must “climb” by diffusion of vacancies to surmount obstacles as illustrated in Fig. 5.

As the curved dislocation line is traversed from point b to point e , the dislocation changes gradually from screw to edge character. At intermediate points the dislocation has both edge and screw character, and is known as a *mixed* dislocation.

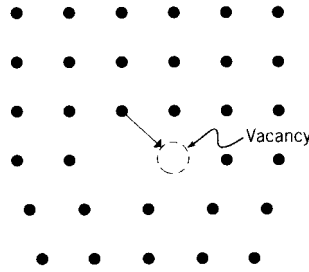


Figure 5: Dislocation climb by vacancy diffusion.

Dislocation-controlled yield

Single crystals tend to slip on their most closely packed planes, and in directions of minimum atomic separation distance. The distances between planes is maximum for the close-packed planes, so these are the most loosely bonded. Slip in close-packed directions minimizes the distance the stresses need to displace the slipping atoms. Both of these act to minimize the energy needed for slip. There are 12 such slip systems in the face-centered cubic (fcc) systems; using Miller indices, these are the $\{111\}$ planes and the $\langle 110 \rangle$ directions. There are 4 independent nonparallel (111) planes, and 3 independent $[110]$ directions in each plane.

Table 2: Critical Resolved shear stress for single crystals of various materials.

Material	crystal type	slip system	τ_{crss} , MPa
Nickel	fcc	$\{111\} \langle 110 \rangle$	5.7
Copper	fcc	$\{111\} \langle 110 \rangle$	0.98
Gold	fcc	$\{111\} \langle 110 \rangle$	0.90
Silver	fcc	$\{111\} \langle 110 \rangle$	0.60
Magnesium	hcp	$\{1101\} \langle 001 \rangle$	0.81
NaCl	cubic	$\{110\} \langle 110 \rangle$	0.75

Slip occurs when the shear stress on the slip plane, and in the slip direction, reaches a value τ_{crss} , the *critical resolved shear stress*; experimental values for τ_{crss} are listed in Table 2 for a number of single crystal materials. The resolved shear stress corresponding to an arbitrary stress state can be computed using the transformation relations of Module 10. In a simple tension test it can be written by inspection of Fig. 6 as

$$\tau_{rss} = \frac{P \cos \theta}{A_s} = \frac{P \cos \theta}{A_0 / \cos \phi} = \sigma (\cos \theta \cos \phi) \equiv \frac{\sigma}{m}$$

where m is a structure factor dependent on the orientation of the slip system relative to the applied tensile stress. For single crystals of arbitrary alignment, the yield stress will then be of the form

$$\sigma_Y = \tau_{crss} \cdot m \tag{1}$$

This is known as “Schmid’s Law,” and m is the “Schmid factor.”

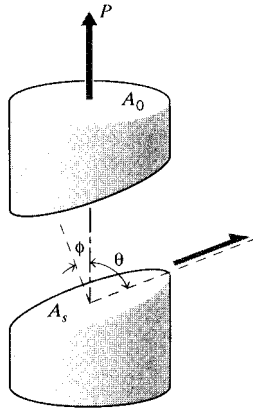


Figure 6: Critical resolved shear stress.

The yield stress will generally be higher in polycrystalline materials, since many of the grains will be oriented unfavorably (have high Schmid factors). Equation 1 can be modified for polycrystalline systems as

$$\sigma_Y = \tau_{crss} \cdot \bar{m}$$

where \bar{m} is an equivalent Schmid factor that is generally somewhat higher than a simple average over all the individual grains; for fcc and bcc systems $\bar{m} \approx 3$.

Strain energy in dislocations

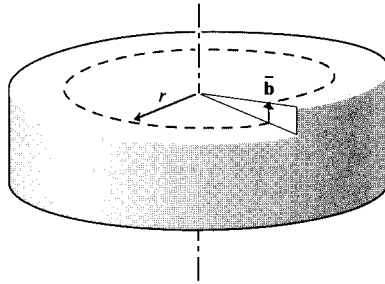


Figure 7: Shear strain associated with a screw dislocation.

Many calculations in dislocation mechanics are done more easily with energy concepts than with Newtonian force-displacement approaches. As seen in Fig. 7, the shear strain associated with a screw dislocation is the deflection \bar{b} divided by the circumference of a circular path around the dislocation core:

$$\gamma = \frac{\bar{b}}{2\pi r} \quad (2)$$

where r is the distance from the dislocation core. Assuming Hookean elasticity, the corresponding strain energy per unit volume is

$$U = \int \tau d\gamma = \frac{1}{2}\tau\gamma = \frac{G\gamma^2}{2} = \frac{G\bar{b}^2}{8\pi^2r^2}$$

The total strain energy associated with the screw dislocation is now obtained by integrating this over the volume around the dislocation:

$$U_{screw} = \int U dV = l \cdot \int_{r_0}^r \frac{G\bar{b}^2}{8\pi^2r^2} 2\pi r dr$$

where here l is the length of the dislocation line and r_0 is the radius of the dislocation “core” inside which the energy is neglected. (Mathematically, the energy density increases without bound inside the core; however its volume becomes very small.) Taking $l = 1$ to obtain energy per unit length and carrying out the integration,

$$\boxed{U_{screw} = \frac{G\bar{b}^2}{4\pi} \ln \frac{r}{r_0} \approx G\bar{b}^2} \quad (3)$$

This last approximation should be read “scales as,” since it is arbitrary to select the limiting value r so that $\ln \frac{r}{r_0} \approx 4\pi$. The important conclusion is that the dislocation energy increases linearly with the shear modulus G and quadratically with the Burgers’ vector \bar{b} . A similar expression can be obtained for the strain energy per unit length of edge dislocation; it can be shown that

$$\boxed{U_{edge} = \frac{G\bar{b}^2}{1-\nu}} \quad (4)$$

where ν is the Poisson’s ratio.

The dislocation energy represents an increase in the total energy of the system, which the material will try to eliminate if possible. For instance, two dislocations of opposite sign will be attracted to one another, since their strain fields will tend to cancel and lower the energy. Conversely, two dislocations of same sign will repel one another. The force of this attraction or repulsion will scale as

$$F dr = dU \Rightarrow F_{screw} \approx \frac{G\bar{b}^2}{r}$$

where here r is the distance between dislocations.

Dislocation motion and hardening

The ductility of crystalline materials is determined by dislocation mobility, and factors that impede dislocation motion can produce dramatic increases in the material’s yield strength. This increased resistance to plastic flow also raises the indentation hardness of the material, so strengthening of this sort is known as *hardening*. Alloying elements, grain boundaries, and even dislocations themselves can provide this impediment, and these provide the means by which the materials technologist controls yield. A thorough treatment of these important concepts must be left to subjects in physical metallurgy, but the following paragraphs will provide a brief introduction to some of them.

When one dislocation, moving on its slip plane under the influence of a driving shear stress, passes through another a “jog” will be created in the second dislocation as shown in Fig. 8.

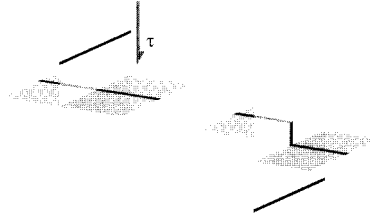


Figure 8: A dislocation jog.

The portion of the dislocation line in the jog is now no longer on its original glide plane, and is “pinned” in position. If the dislocation concentration is large, these jogs become a powerful impediment to plastic flow by dislocation motion. Paradoxically, the very dislocations that permit plastic flow in the first place can impede it if they become too numerous.

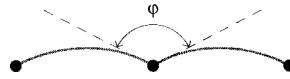


Figure 9: Dislocation bowing.

When a moving dislocation becomes pinned by jogs or other impediments, the shear stress τ that had been driving the dislocation now causes the line segment between the obstacles to bow forward as shown in Fig. 9, with an angle ϕ between adjacent segments. The extra length of the bowed line represents an increase in the strain energy of the dislocation, and if the shear stress were not present the line would straighten out to reduce this energy. The line acts similarly to an elastic band, with a “line tension” T that acts to return the line to a straight shortest-distance path between pinning points. The units of dislocation energy per unit length (N-m/m) are the same as simple tension, and we can write

$$T = \frac{\partial E}{\partial l} \approx Gb^2$$

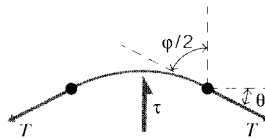


Figure 10: Force balance on dislocation segment.

As shown in Fig. 10, a free-body diagram of the line segment between two pinning points gives a force balance of the form

$$2T \sin \frac{d\theta}{2} = \tau \bar{b} \cdot r d\theta$$

where here r is the radius of curvature of the line (not the distance from the dislocation, as in Eqn. 2). Rearranging and canceling the $d\theta$ factor,

$$\tau = \frac{G\bar{b}}{r} \quad (5)$$

This relation gives the curvature of the dislocation in terms of the shear stress acting on it. The maximum shear stress is that needed to bend the dislocation into a semicircle (smallest r), after which the dislocation expands spontaneously. When the loops meet, annihilation occurs at that point, spawning a new dislocation line embedded in a circular loop. The process can be repeated with the new dislocation as well, and by this mechanism a large number of dislocations can be spawned as shown in Fig. 11. This is the “Frank-Read” source, and is an important means by which dislocations can multiply during plastic deformation. The increasing number of dislocations leads to more and more entanglements, with jogs acting as pinning points.

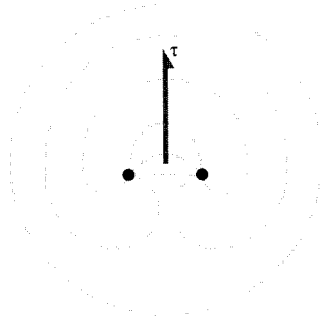


Figure 11: The Frank-Read dislocation source.

Equation 5 also provides an estimate of the influence of dislocation density on yield strength. If the obstacles pinning dislocation motion are “soft” the dislocation will be able to overcome them at relatively low driving stress, corresponding to a low critical angle ϕ_c . But as the obstacle becomes “harder,” i.e. provides more resistance to dislocation motion, the angle approaches zero and the radius of curvature becomes on the order of the obstacle spacing L . The shear stress needed to overcome such obstacles is then

$$\tau \approx \frac{G\bar{b}}{L}$$

When the hard obstacles arise from jogs created by intersections with other dislocations, the obstacle spacing L can be written in terms of the dislocation density. If the number of dislocations passing through a unit area is ρ , the number of dislocations encountered in moving along a straight line will be proportional to $\sqrt{\rho}$. The spacing between them is proportional to the reciprocal of this, so $\tau \propto G\bar{b}\sqrt{\rho}$. The yield stress is then the stress τ_0 needed to move dislocations in the absence of interfering dislocations, plus that needed to break through the obstacles; this can be written as

$$\boxed{\tau_Y = \tau_0 + AG\bar{b}\sqrt{\rho}} \quad (6)$$

where A is a constant that has been found to vary between 0.3 and 0.6 for a number of fcc, bcc and polycrystalline metals as well as some ionic crystals. Experimental corroboration of this relation is provided in Fig. 12.

The action of plastic flow therefore creates new dislocations by Frank-Read and other sources, which makes the material harder and harder, i.e. increasingly resistant to further plastic flow.

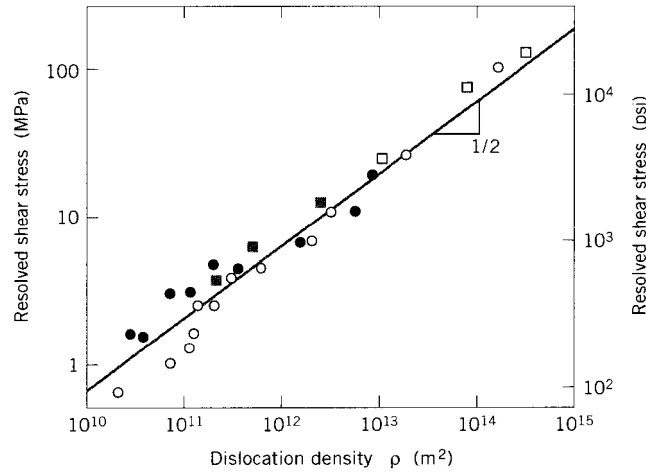


Figure 12: Effect of dislocation density ρ on critical resolved shear stress (for copper single and polycrystals, from T.H. Courtney, *Mechanical Behavior of Materials*, McGraw-Hill, 1990).

Eventually the yield stress for continued deformation becomes larger than the fracture stress, and the material will now break before it deforms further. If continued working of the material is desired, the number of dislocations must be reduced, for instance by thermal annealing. Annealing can produce *recovery* (dislocation climb around obstacles by vacancy diffusion) or recrystallization of new dislocation-free grains.

Grain boundaries act to impede dislocation motion, since the slip systems in adjoining grains will usually not line up; increases in yield strength arising from this mechanism are called *boundary strengthening*. Fine-grained metals have increased grain boundary area and thus have higher yield strengths than coarse-grained ones. The influence of grain size can often be described by the *Hall-Petch* formula

$$\sigma_Y = \sigma_0 + k_Y d^{-1/2} \quad (7)$$

where σ_0 is the lattice friction stress needed to move dislocations and K is a constant. This relation is essentially empirical, but it can be rationalized by viewing the second term as being related to the stress needed to activate a new mobile dislocation in the unfavorably oriented grain.

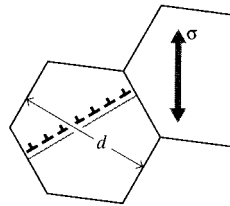


Figure 13: Dislocation pileup at a grain boundary.

As dislocations pile up against the boundary in the originally deforming grain, they act much like a crack whose length scales with the grain size d as shown in Fig. 13: the larger

the grain, the more dislocations in the pileup, the larger the virtual crack. Since the stress in front of a sharp crack of length a scales² as \sqrt{a} , the stress in front of the crack containing the dislocation pileup is increased by a factor that scales with \sqrt{d} . When this stress exceeds that needed to generate a new dislocation the unfavorably oriented grain begins to deform by dislocation motion. This stress diminishes according to $d^{-1/2}$ as the size of the original grain is scaled down, thus strengthening the metal according to the Hall-Petch relationship. Grain size is determined by the balance between nucleation and growth rates as the metal is solidified, and these are in turn controllable by the cooling rates imposed. This is an important example of processing-structure-property control available to the materials technologist.

A related phenomenon accounts for the very high strengths (≈ 4 GPa, or 600 kpsi) of piano wire, a eutectoid steel that has been drawn through a sequence of reducing dies to obtain a small final diameter. The “pearlitic” structure obtained on cooling this steel through the eutectoid temperature is a two-phase mixture of Fe_3C (“cementite”) in bcc iron (“ferrite”). As the diameter is reduced during drawing, the ferrite cells are reduced as well, forming a structure analogous to a fine-grained metal. The cell boundaries restrict dislocation motion, leading to the very high yield strengths.

Impurity atoms in solid solution can also serve to harden a crystalline material by impeding dislocation motion; this is called *solution strengthening*. An impurity atom smaller than the atoms of the host lattice will create an approximately spherical tensile field around itself which will attract the compressive regions around mobile dislocations, and a larger impurity atom will tend to trap the tensile region of nearby dislocations. On average, the population of dislocations will maneuver so as to lower their strain energies by associating with the nonuniform strain fields around impurities. This association impedes dislocation motion, which inhibits plastic flow and increases the yield stress.

Solution hardening is not usually an especially effective strengthening mechanism in commercial materials, largely because the solubility of impurity atoms is not sufficient to generate an appreciable number of obstacles. One important exception to this is the iron-carbon, or steel, system. If steel at approximately the eutectoid carbon composition (0.8% C) is cooled rapidly from above the eutectoid temperature of 723°C , the carbon atoms can become trapped in the iron lattice at much higher concentrations than bcc iron’s equilibrium carbon solubility would normally allow. (This tendency for trapping can be enhanced by alloying elements such as chromium and molybdenum, which have an affinity for carbon and thus reduce its ability to diffuse away.) To accommodate these metastable impurity atoms, the iron lattice transforms to a body-centered tetragonal form named *martensite* (see Fig. 14), with a strong nonspherical strain field around the carbon atoms. These tetragonal distortions are very effective impediments to dislocation motion, making martensite an extremely hard phase. The periodic water quenches a blacksmith uses during metalworking is done (perhaps without the smith knowing why it works) to tailor the material’s hardness by developing martensitic inclusions in the steel.

Martensite is so hard and brittle that the rapidly quenched steel must usually be *tempered* by heating it to approximately 400°C for an hour or so. This allows diffusion of carbon to take place, creating a dispersion of cementite inclusions; it also permits recovery of the dislocations present in the martensite. The resulting material is much tougher than the as-formed martensitic steel, but still retains a high strength level due to the strengthening effect of the carbide inclusions.

²See Module 16.

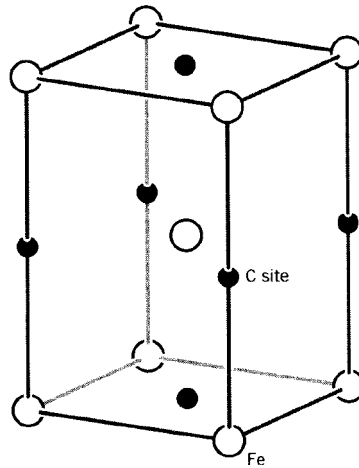


Figure 14: The body-centered tetragonal structure of martensite.

Kinetics of creep in crystalline materials

“Creep” is the term used to describe the tendency of many materials to exhibit continuing deformation even though the stress is held constant. Viscoelastic polymers exhibit creep, as was discussed in Module 19. However, creep also occurs in polycrystalline metallic and ceramic systems, most importantly when the the temperature is higher than approximately half their absolute melting temperature. This high-temperature creep can occur at stresses less than the yield stress, but is related to this module’s discussion of dislocation-controlled yield since dislocation motion often underlies the creep process as well.

High-temperature creep is of concern in such applications as jet engines or nuclear reactors. This form of creep often consists of three distinct regimes as seen in Fig. 15: *primary* creep, in which the material appears to harden so the creep rate diminishes with time; *secondary* or steady state creep, in which hardening and softening mechanisms appear to balance to produce a constant creep rate $\dot{\epsilon}_{II}$; and *tertiary* creep in which the material softens until creep rupture occurs. The entire creep curve reflects a competition between hardening mechanisms such as dislocation pileup, and mechanisms such as dislocation climb and cross-slip which are termed *recovery* and which augment dislocation mobility.

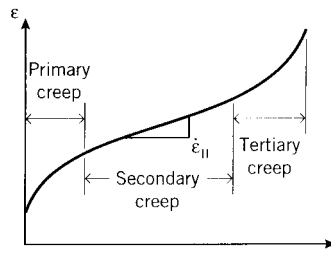


Figure 15: The three stages of creep.

In most applications the secondary regime consumes most of the time to failure, so much of

the modeling effort has been directed to this stage. The secondary creep rate $\dot{\epsilon}_{II}$ can often be described by a general nonlinear expression of the form

$$\dot{\epsilon}_{II} = A\sigma^m \exp \frac{-E_c^*}{RT} \quad (8)$$

where A and m are adjustable constants, E_c^* is an apparent activation energy for creep, σ is the stress, R is the Gas Constant (to be replaced by Boltzman's constant if a molar basis is not used) and T is the absolute temperature. This is known as the *Weertman-Dorn equation*.

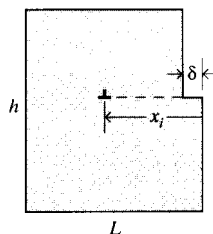


Figure 16: Dislocation motion and creep rate.

The plastic flow rate is related directly to dislocation velocity, which can be visualized by considering a section of material of height h and width L as shown in Fig. 16. A single dislocation, having traveled in the width direction for the full distance L will produce a transverse deformation of $\delta_i = \bar{b}$. If the dislocation has propagated through the crystal only a fraction x_i/L of the width, the deformation can be reduced by this same fraction: $\delta_i = \bar{b}(x_i/L)$. The total deformation in the crystal is then the sum of the deformations contributed by each dislocation:

$$\delta = \sum_i \delta_i = \sum_i \bar{b}(x_i/L)$$

The shear strain is the ratio of the transverse deformation to the height over which it is distributed:

$$\gamma = \frac{\delta}{h} = \frac{\bar{b}}{Lh} \sum_i x_i$$

The value $\sum_i x_i$ can be replaced by the quantity $N\bar{x}$, where N is the number of dislocations in the crystal segment and \bar{x} is the average propagation distance. We can then write

$$\gamma = \rho \bar{b} \bar{x}$$

where $\rho = N/Lh$ is the dislocation density in the crystal. The shear strain *rate* $\dot{\gamma}$ is then obtained by differentiation:

$$\dot{\gamma} = \rho \bar{b} v \quad (9)$$

where $v = \dot{\bar{x}}$ is the average dislocation velocity. Hence the creep rate scales directly with the dislocation velocity.

To investigate the temperature and stress dependence of this velocity, we consider rate at which dislocations can overcome obstacles to be yet another example of a thermally activated, stress aided rate process and write an Eyring equation for the creep rate:

$$\dot{\epsilon} \propto v \propto \exp \frac{-(E_d^* - \sigma V^*)}{kT} - \exp \frac{-(E_d^* + \sigma V^*)}{kT}$$

where V^* is an apparent activation volume. The second term here indicates that the activation barrier for motion in the direction of stress is augmented by the stress, and diminished for motions in the opposite direction. When we discussed yielding the stress was sufficiently high that motion in the direction opposing flow could be neglected. Here we are interested in creep taking place at relatively low stresses and at high temperature, so that reverse flow can be appreciable. Factoring,

$$\dot{\epsilon} \propto \exp \frac{-E_d^*}{RT} \left(\exp \frac{+\sigma V^*}{RT} - \exp \frac{-\sigma V^*}{RT} \right)$$

Since $\sigma V^* \ll RT$, we can neglect quadratic and higher order terms in the series expansion $e^x = 1 + x + (x^2/2!) + (x^3/3!) + \dots$ to give

$$\dot{\epsilon} = A \left(\frac{\sigma V^*}{RT} \right) \exp \frac{-(E_d^*)}{RT}$$

If now we neglect the temperature dependence in the preexponential factor in comparison with the much stronger temperature dependence of the exponential itself, this model predicts a creep rate in agreement with the Weertman-Dorn equation with $m = 1$.

Creep by dislocation glide occurs over the full range of temperatures from absolute zero to the melting temperature, although the specific equation developed above contains approximations valid only at higher temperature. The stresses needed to drive dislocation glide are on the order of a tenth the theoretical shear strength of $G/10$. At lower stresses the creep rate is lower, and becomes limited by the rate at which dislocations can climb over obstacles by vacancy diffusion. This is hinted at in the similarity of the activation energies for creep and self diffusion as shown in Fig. 17. (Note that these values also correlate with the tightness of the bond energy functions, as discussed in Module 1; diffusion is impeded in more tightly-bonded lattices.) Vacancy diffusion is another stress-aided thermally activated rate process, again leading to models in agreement with the Weertman-Dorn equation.

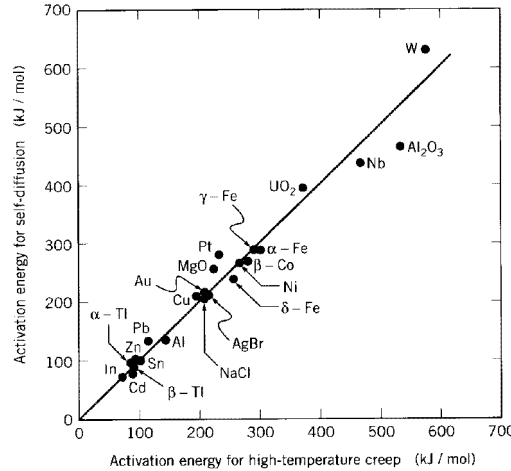


Figure 17: Correlation of activation energies for diffusion and creep.

Problems

1. The yield stresses σ_Y have been measured using steel and aluminum specimens of various grain sizes, as follows:

Material	d, μ	σ_Y , MPa
steel	60.5	160
	136	130
aluminum	11.1	235
	100	225

- (a) Determine the coefficients σ_0 and k_Y in the Hall-Petch relation (Eqn. 7) for these two materials.
- (b) Determine the yield stress in each material for a grain size of $d = 30\mu$.

Statistics of Fracture

David Roylance
Department of Materials Science and Engineering
Massachusetts Institute of Technology
Cambridge, MA 02139

March 30, 2001

Introduction

One particularly troublesome aspect of fracture, especially in high-strength and brittle materials, is its *variability*. The designer must be able to cope with this, and limit stresses to those which reduce the *probability* of failure to an acceptably low level. Selection of an acceptable level of risk is a difficult design decision itself, obviously being as close to zero as possible in cases where human safety is involved but higher in doorknobs and other inexpensive items where failure is not too much more than a nuisance. The following sections will not replace a thorough study of statistics, but will introduce at least some of the basic aspects of statistical theory needed in design against fracture. The text by Collins¹ includes an extended treatment of statistical analysis of fracture and fatigue data, and is recommended for further reading.

Basic statistical measures

The value of tensile strength σ_f cited in materials property handbooks is usually the *arithmetic mean*, simply the sum of a number of individual strength measurements divided by the number of specimens tested:

$$\overline{\sigma_f} = \frac{1}{N} \sum_{i=1}^N \sigma_{f,i} \quad (1)$$

where the overline denotes the mean and $\sigma_{f,i}$ is the measured strength of the i^{th} (out of N) individual specimen. Of course, not all specimens have strengths exactly equal to the mean; some are weaker, some are stronger. There are several measures of how widely scattered is the distribution of strengths, one important one being the sample *standard deviation*, a sort of root mean square average of the individual deviations from the mean:

$$s = \sqrt{\frac{1}{N-1} \sum_{i=1}^N (\overline{\sigma_f} - \sigma_{x,i})^2} \quad (2)$$

The significance of s to the designer is usually in relation to how large it is compared to the mean, so the *coefficient of variation*, or C.V., is commonly used:

¹Collins, J.A., *Failure of Materials in Mechanical Design*, Wiley, 1993.

$$\text{C.V.} = \frac{s}{\bar{\sigma}_f}$$

This is often expressed as a percentage. Coefficients of variation for tensile strength are commonly in the range of 1–10%, with values much over that indicating substantial inconsistency in the specimen preparation or experimental error.

Example 1

In order to illustrate the statistical methods to be outlined in this Module, we will use a sequence of thirty measurements of the room-temperature tensile strength of a graphite/epoxy composite². These data (in kpsi) are: 72.5, 73.8, 68.1, 77.9, 65.5, 73.23, 71.17, 79.92, 65.67, 74.28, 67.95, 82.84, 79.83, 80.52, 70.65, 72.85, 77.81, 72.29, 75.78, 67.03, 72.85, 77.81, 75.33, 71.75, 72.28, 79.08, 71.04, 67.84, 69.2, 71.53. Another thirty measurements from the same source, but taken at 93°C and -59°C, are given in Probs. 2 and 3, and can be subjected to the same treatments as homework.

There are several computer packages available for doing statistical calculations, and most of the procedures to be outlined here can be done with spreadsheets. The Microsoft Excel functions for mean and standard deviation are `average()` and `stdev()`, where the arguments are the range of cells containing the data. These give for the above data

$$\bar{\sigma}_f = 73.28, \quad s = 4.63 \text{ (kpsi)}$$

The coefficient of variation is $\text{C.V.} = (4.63/73.28) \times 100\% = 6.32\%$.

The normal distribution

A more complete picture of strength variability is obtained if the number of individual specimen strengths falling in a discrete strength interval $\Delta\sigma_f$ is plotted versus σ_f in a *histogram* as shown in Fig. 1; the maximum in the histogram will be near the mean strength and its width will be related to the standard deviation.

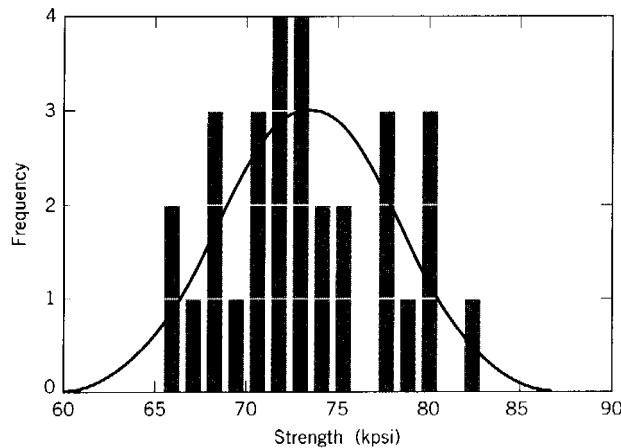


Figure 1: Histogram and normal distribution function for the strength data of Example 1.

²P. Shyprykevich, *ASTM STP 1003*, pp. 111–135, 1989.

As the number of specimens increases, the histogram can be drawn with increasingly finer $\Delta\sigma_f$ increments, eventually forming a smooth *probability distribution function*, or “pdf”. The mathematical form of this function is up to the material (and also the test method in some cases) to decide, but many phenomena in nature can be described satisfactorily by the *normal*, or *Gaussian*, function:

$$f(X) = \frac{1}{\sqrt{2\pi}} \exp \frac{-X^2}{2}, \quad X = \frac{\sigma_f - \bar{\sigma}_f}{s} \quad (3)$$

Here X is the *standard normal variable*, and is simply how many standard deviations an individual specimen strength is away from the mean. The factor $1/\sqrt{2\pi}$ normalizes the function so that its integral is unity, which is necessary if the specimen is to have a 100% chance of failing at *some* stress. In this expression we have assumed that the measure of standard deviation determined from Eqn. 2 based on a discrete number of specimens is acceptably close to the “true” value that would be obtained if every piece of material in the universe could somehow be tested.

The normal distribution function $f(X)$ plots as the “bell curve” familiar to all grade-conscious students. Its integral, known as the *cumulative distribution function* or $P_f(X)$, is also used commonly; its ordinate is the probability of fracture, also the fraction of specimens having a strength lower than the associated abscissal value. Since the normal pdf has been normalized, the cumulative function rises with an S-shaped or sigmoidal shape to approach unity at large values of X . The two functions $f(X)$ and $F(X)$ are plotted in Fig. 2, and tabulated in Tables 1 and 2 of the Appendix attached to this module. (Often the probability of survival $P_s = 1 - P_f$ is used as well; this curve begins at near unity and falls in a sigmoidal shape toward zero as the applied stress increases.)

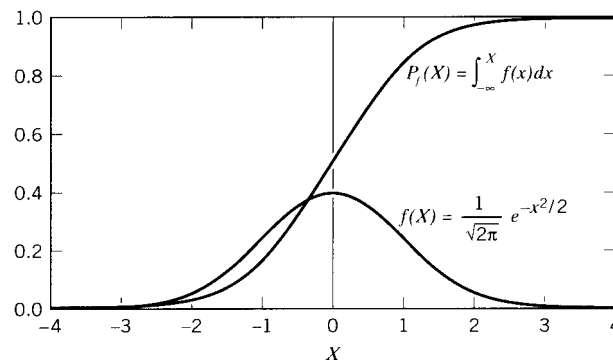


Figure 2: Differential $f(X)$ and cumulative $P_f(X)$ normal probability functions.

One convenient means of determining whether or not a particular set of measurements is normally distributed involves using special graph paper (a copy is included in the Appendix) whose ordinate has been distorted to make the sigmoidal cumulative distribution P_f plot as a straight line. (Sometimes it is easier to work with straight lines on curvy paper than curvy lines on straight paper.) Experimental data are ranked from lowest to highest, and each assigned a rank based on the fraction of strengths having higher values. If the ranks are assigned as $i/(N + 1)$, where i is the position of a datum in the ordered list and N is the number of specimens, the ranks are always greater than zero and less than one; this facilitates plotting.

The degree to which these rank-strength data plot as straight lines on normal probability paper is then a visual measure of how well the data are described by a normal distribution. The

best-fit straight line through the points passes the 50% cumulative fraction line at the sample mean, and its slope gives the standard distribution. Plotting several of these lines, for instance for different processing conditions of a given material, is a convenient way to characterize the strength differences arising from the two conditions (See Prob. 2).

Example 2

For our thirty-specimen test population, the ordered and ranked data are:

i	$\sigma_{f,i}$	$P_f = \frac{i}{N+1}$
1	65.50	0.0323
2	65.67	0.0645
3	67.03	0.0968
4	67.84	0.1290
5	67.95	0.1613
6	68.10	0.1935
7	69.20	0.2258
8	70.65	0.2581
9	71.04	0.2903
10	71.17	0.3226
11	71.53	0.3548
12	71.75	0.3871
13	72.28	0.4194
14	72.29	0.4516
15	72.5	0.4839
16	72.85	0.5161
17	72.85	0.5484
18	73.23	0.5806
19	73.80	0.6129
20	74.28	0.6452
21	75.33	0.6774
22	75.78	0.7097
23	77.81	0.7419
24	77.81	0.7742
25	77.90	0.8065
26	79.08	0.8387
27	79.83	0.8710
28	79.92	0.9032
29	80.52	0.9355
30	82.84	0.9677

When these are plotted using probability scaling on the ordinate, the graph in Fig. 3 is obtained.

The normal distribution function has been characterized thoroughly, and it is possible to infer a great deal of information from it for strength distributions that are close to normal. For instance, the cumulative normal distribution function (cdf) tabulated in Table 2 of the Appendix shows that that 68.3% of all members of a normal distribution lie within $\pm 1s$ of the mean, 95% lie within $\pm 1.96s$, and 99.865% lie within $\pm 3s$. It is common practice in much aircraft design to take $\bar{\sigma}_f - 3s$ as the safe fracture strength; then almost 99.9% of all specimens will have a strength at least this high. This doesn't really mean one out of every thousand airplane wings are unsafe; within the accuracy of the theory, 0.1% is a negligible number, and the $3s$

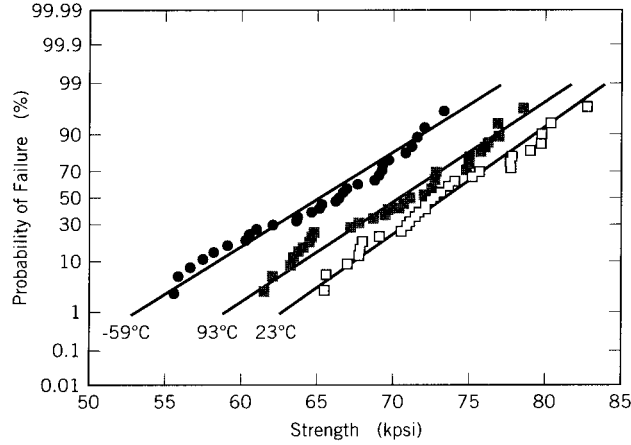


Figure 3: Probability plot of cumulative probability of failure for the strength data of Example 1. Also shown are test data taken at higher and lower temperature.

tolerance includes essentially the entire population³. Having to reduce the average strength by $3s$ in design can be a real penalty for advanced materials such as composites that have high strengths but also high variability due to their processing methods being relatively undeveloped. This is a major factor limiting the market share of these advanced materials.

Beyond the visual check of the linearity of the probability plot, several “goodness-of-fit” tests are available to assess the degree to which the population can reasonably be defined by the normal (or some other) distribution function. The “Chi-square” test is often used for this purpose. Here a test statistic measuring how far the observed data deviate from those expected from a normal distribution, or any other proposed distribution, is

$$\begin{aligned}\chi^2 &= \sum \frac{(\text{observed} - \text{expected})^2}{\text{expected}} \\ &= \sum_{i=1}^N \frac{(n_i - Np_i)^2}{Np_i}\end{aligned}$$

where n_i is the number of specimens actually failing in a strength increment $\Delta\sigma_{f,i}$, N is the total number of specimens, and p_i is the probability expected from the assumed distribution of a specimen having having a strength in that increment.

Example 3

To apply the Chi-square test to our 30-test population, we begin by counting the number of strengths falling in selected strength increments, much as if we were constructing a histogram. We choose five increments to obtain reasonable counts in each increment. The number *expected* to fall in each increment is determined from the normal pdf table, and the square of the difference calculated.

³“Six-sigma” has become a popular goal in manufacturing, which means that only one part out of approximately a billion will fail to meet specification.

Lower Limit	Upper Limit	Observed Frequency	Expected Frequency	Chisquare
0	69.33	7	5.9	0.198
69.33	72.00	5	5.8	0.116
72.00	74.67	8	6.8	0.214
74.67	77.33	2	5.7	2.441
77.33	∞	8	5.7	0.909

$\chi^2 = 3.878$

The number of degrees of freedom for this Chi-square test is 4; this is the number of increments less one, since we have the constraint that $n_1 + n_2 + n_3 + n_5 = 30$.

Interpolating in the Chi-Square Distribution Table (Table 3 in the Appendix), we find that a fraction 0.44 of normally distributed populations can be expected to have χ^2 statistics of up to 3.88. Hence, it seems reasonable that our population can be viewed as normally distributed.

Usually, we ask the question the other way around: is the computed χ^2 so large that only a small fraction — say 5% — of normally distributed populations would have χ^2 values that high or larger? If so, we would reject the hypothesis that our population is normally distributed.

From the χ^2 Table, we read that $\alpha = 0.05$ for $\chi^2 = 9.488$, where α is the fraction of the χ^2 population with values of χ^2 greater than 9.488. Equivalently, values of χ^2 above 9.488 would imply that there is less than a 5% chance that a population described by a normal distribution would have the computed χ^2 value. Our value of 3.878 is substantially less than this, and we are justified in claiming our data to be normally distributed.

Several governmental and voluntary standards-making organizations have worked to develop standardized procedures for generating statistically allowable property values for design of critical structures⁴. One such procedure defines the “B-allowable” strength as that level for which we have 95% confidence that 90% of all specimens will have at least that strength. (The use of *two* percentages here may be confusing. We mean that if we were to measure the strengths of 100 groups each containing 10 specimens, at least 95 of these groups would have at least 9 specimens whose strengths exceed the B-allowable.) In the event the normal distribution function is found to provide a suitable description of the population, the B-basis value can be computed from the mean and standard deviation using the formula

$$B = \bar{\sigma}_f - k_B s$$

where k_b is $n^{-1/2}$ times the 95th quantile of the “noncentral t-distribution;” this factor is tabulated, but can be approximated by the formula

$$k_b = 1.282 + \exp(0.958 - 0.520 \ln N + 3.19/N)$$

Example 4

In the case of the previous 30-test example, k_B is computed to be 1.78, so this is less conservative than the $3s$ guide. The B-basis value is then

$$B = 73.28 - (1.78)(4.632) = 65.05$$

Having a distribution function available lets us say something about the confidence we can have in how reliably we have measured the mean strength, based on a necessarily limited number

⁴*Military Handbook 17B*, Army Materials Technology Laboratory, Part I, Vol. 1, 1987.

of individual strength tests. A famous and extremely useful result in mathematical statistics states that, if the mean of a distribution is measured N times, the *distribution of the means* will have its own standard deviation s_m that is related to the mean of the underlying distribution s and *the number of determinations*, N as

$$s_m = \frac{s}{\sqrt{N}} \quad (4)$$

This result can be used to establish *confidence limits*. Since 95% of all measurements of a normally distributed population lie within 1.96 standard deviations from the mean, the ratio $\pm 1.96s/\sqrt{N}$ is the range over which we can expect 95 out of 100 measurements of the mean to fall. So even in the presence of substantial variability we can obtain measures of mean strength to any desired level of confidence; we simply make more measurements to increase the value of N in the above relation. The “error bars” often seen in graphs of experimental data are not always labeled, and the reader must be somewhat cautious: they are *usually* standard deviations, but they may indicate maximum and minimum values, and occasionally they are 95% confidence limits. The significance of these three is obviously quite different.

Example 5

Equation 4 tells us that were we to repeat the 30-test sequence of the previous example over and over (obviously with new specimens each time), 95% of the measured sample means would lie within the interval

$$73.278 - \frac{(1.96)(4.632)}{\sqrt{30}}, \quad 73.278 + \frac{(1.96)(4.632)}{\sqrt{30}} = 71.62, 74.94$$

The t distribution

The “ t ” distribution, tabulated in Table 4 of the Appendix, is similar to the normal distribution, plotting as a bell-shaped curve centered on the mean. It has several useful applications to strength data. When there are few specimens in the sample, the t -distribution should be used in preference to the normal distribution in computing confidence limits. As seen in the table, the t -value for the 95th percentile and the 29 degrees of freedom of our 30-test sample in Example 3 is 2.045. (The number of degrees of freedom is one less than the total specimen count, since the sum of the number of specimens having each recorded strength is constrained to be the total number of specimens.) The 2.045 factor replaces 1.96 in this example, without much change in the computed confidence limits. As the number of specimens increases, the t -value approaches 1.96. For fewer specimens the factor deviates substantially from 1.96; it is 2.571 for $n = 5$ and 3.182 for $n = 3$.

The t distribution is also useful in deciding whether two test samplings indicate significant differences in the populations they are drawn from, or whether any difference in, say, the means of the two samplings can be ascribed to expected statistical variation in what are two essentially identical populations. For instance, Fig. 3 shows the cumulative failure probability for graphite-epoxy specimens tested at three different temperatures, and it appears that the mean strength is reduced somewhat by high temperatures and even more by low temperatures. But are these differences real, or merely statistical scatter?

This question can be answered by computing a value for t using the means and standard deviations of any two of the samples, according to the formula

$$t = \frac{|\bar{\sigma}_{f1} - \bar{\sigma}_{f2}|}{\sqrt{\frac{s_1^2}{n_1-1} + \frac{s_2^2}{n_2-1}}} \quad (5)$$

This statistic is known to have a t distribution if the deviations s_1 and s_2 are not too different. The mean and standard deviation of the -59°C data shown in Fig. 3 are 65.03 and 5.24 respectively. Using Eqn. 5 to compare the room-temperature (23°C) and -59°C data, the t -statistic is

$$t = \frac{(73.28 - 65.03)}{\sqrt{\frac{(4.63)^2}{29} + \frac{(5.24)^2}{29}}} = 6.354$$

From Table 4 in the Appendix, we now look up the value of t for 29 degrees of freedom corresponding to 95% (or some other value, as desired) of the population. We do this by scanning the column for $F(t) = 0.975$ rather than 0.95, since the t distribution is symmetric and another 0.025 fraction of the population lies beyond $t = -0.975$. The t value for 95% ($F(t) = 0.975$) and 29 degrees of freedom is 2.045.

This result means that were we to select repeatedly any two arbitrary 30-specimen samples from a single population, 95% of these selections would have t -statistics as computed with Eqn. 5 less than 2.045; only 5% would produce larger values of t . Since the 6.354 t -statistic for the -59°C and 23°C samplings is much greater than 2.045, we can conclude that it is very unlikely that the two sets of data are from the same population. Conversely, we conclude that the two datasets are in fact statistically independent, and that temperature has a statistically significant effect on the strength.

The Weibull distribution

Large specimens tend to have lower average strengths than small ones, simply because large ones are more likely to contain a flaw large enough to induce fracture at a given applied stress. This effect can be measured directly, for instance by plotting the strengths of fibers versus the fiber circumference as in Fig. 4. For similar reasons, brittle materials tend to have higher strengths when tested in flexure than in tension, since in flexure the stresses are concentrated in a smaller region near the outer surfaces.

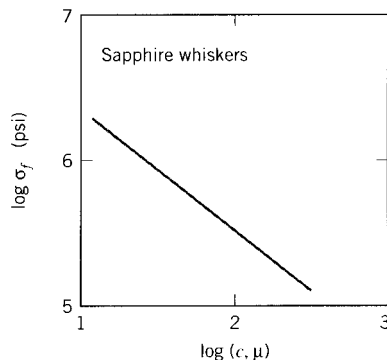


Figure 4: Effect of circumference c on fracture strength σ_f for sapphire whiskers. From L.J. Broutman and R.H. Krock, *Modern Composite Materials*, Addison-Wesley, 1967.

The hypothesis of the size effect led to substantial development effort in the statistical analysis community of the 1930's and 40's, with perhaps the most noted contribution being that of W. Weibull⁵ in 1939. Weibull postulated that the probability of survival at a stress σ , i.e. the probability that the specimen volume does not contain a flaw large enough to fail under the stress σ , could be written in the form

$$P_s(\sigma) = \exp \left[- \left(\frac{\sigma}{\sigma_0} \right)^m \right] \quad (6)$$

Weibull selected the form of this expression for its mathematical convenience rather than some fundamental understanding, but it has been found over many trials to describe fracture statistics well. The parameters σ_0 and m are adjustable constants; Fig. 5 shows the form of the Weibull function for two values of the parameter m . Materials with greater variability have smaller values of m ; steels have $m \approx 100$, while ceramics have $m \approx 10$. This parameter can be related to the coefficient of variation; to a reasonable approximation, $m \approx 1.2/\text{C.V.}$

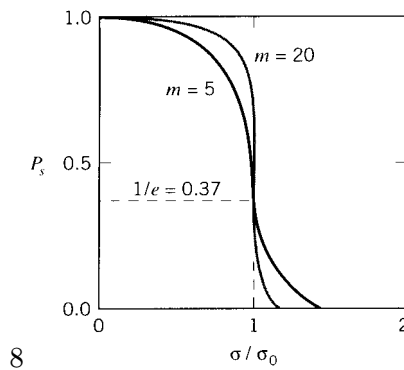


Figure 5: The Weibull function.

A variation on the normal probability paper graphical method outlined earlier can be developed by taking logarithms of Eqn. 6:

$$\ln P_s = - \left(\frac{\sigma}{\sigma_0} \right)^m$$

$$\ln(\ln P_s) = -m \ln \left(\frac{\sigma}{\sigma_0} \right)$$

Hence the double logarithm of the probability of exceeding a particular strength σ versus the logarithm of the strength should plot as a straight line with slope m .

Example 6

Again using the 30-test sample of the previous examples, an estimate of the σ_0 parameter can be obtained by plotting the survival probability (1 minus the rank) and noting the value of σ_f at which P_s drops to $1/e = 0.37$; this gives $\sigma_0 \approx 74$. (A more accurate regression method gives 75.46.) A tabulation of the double logarithm of P_s against the logarithm of σ_f/σ_0 is then

⁵See B. Epstein, *J. Appl. Phys.*, Vol. 19, p. 140, 1948 for a useful review of the statistical treatment of the size effect in fracture, and for a summary of extreme-value statistics as applied to fracture problems.

i	$\sigma_{f,i}$	$\ln \ln(1/P_s)$	$\ln(\sigma_{f,i}/\sigma_0)$
1	65.50	-3.4176	-0.1416
2	65.67	-2.7077	-0.1390
3	67.03	-2.2849	-0.1185
4	67.84	-1.9794	-0.1065
5	67.95	-1.7379	-0.1048
6	68.10	-1.5366	-0.1026
7	69.20	-1.3628	-0.0866
8	70.65	-1.2090	-0.0659
9	71.04	-1.0702	-0.0604
10	71.17	-0.9430	-0.0585
11	71.53	-0.8250	-0.0535
12	71.75	-0.7143	-0.0504
13	72.28	-0.6095	-0.0431
14	72.29	-0.5095	-0.0429
15	72.50	-0.4134	-0.0400
16	72.85	-0.3203	-0.0352
17	72.85	-0.2295	-0.0352
18	73.23	-0.1404	-0.0300
19	73.80	-0.0523	-0.0222
20	74.28	0.0355	-0.0158
21	75.33	0.1235	-0.0017
22	75.78	0.2125	0.0042
23	77.81	0.3035	0.0307
24	77.81	0.3975	0.0307
25	77.90	0.4961	0.0318
26	79.08	0.6013	0.0469
27	79.83	0.7167	0.0563
28	79.92	0.8482	0.0574
29	80.52	1.0083	0.0649
30	82.84	1.2337	0.0933

The Weibull plot of these data is shown in Fig. 6; the regression slope is 17.4.

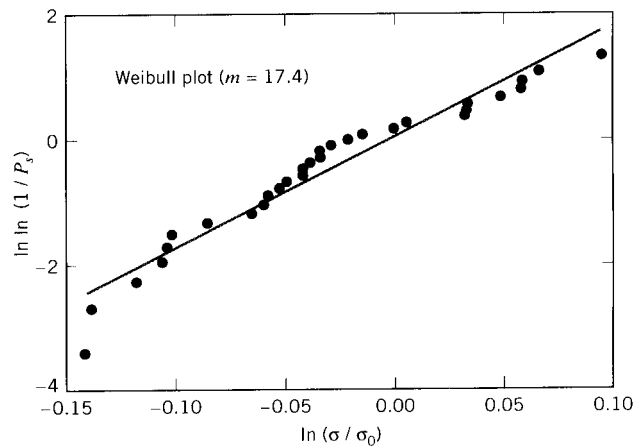


Figure 6: Weibull plot.

Similarly to the B-basis design allowable for the normal distribution, the B-allowable can also be computed from the Weibull parameters m and σ_0 . The procedure is⁶:

$$B = Q \exp \left[\frac{-V}{m\sqrt{N}} \right]$$

where Q and V are

$$Q = \sigma_0 (0.10536)^{1/m}$$

$$V = 3.803 + \exp \left[1.79 - 0.516 \ln(N) + \frac{5.1}{N} \right]$$

Example 7

The B-allowable is computed for the 30-test population as

$$Q = 75.46 (0.10536)^{1/17.4m} = 66.30$$

$$V = 3.803 + \exp \left[1.79 - 0.516 \ln(30) + \frac{5.1}{30} \right] = 5.03$$

$$B = 66.30 \exp \left[\frac{-5.03}{17.4\sqrt{30}} \right] = 62.89$$

This value is somewhat lower than the 65.05 obtained as the normal-distribution B-allowable, so in this case the Weibull method is a bit more lenient.

The Weibull equation can be used to predict the magnitude of the size effect. If for instance we take a reference volume V_0 and express the volume of an arbitrary specimen as $V = nV_0$, then the probability of failure at volume V is found by multiplying $P_s(V)$ by itself n times:

$$P_s(V) = [P_s(V_0)]^n = [P_s(V_0)]^{V/V_0}$$

$$\boxed{P_s(V) = \exp -\frac{V}{V_0} \left(\frac{\sigma}{\sigma_0} \right)^m} \quad (7)$$

Hence the probability of failure increases exponentially with the specimen volume. This is another danger in simple scaling, beyond the area vs. volume argument we outlined in Module 1.

Example 8

Solving Eqn. 7, the stress for a given probability of survival is

$$\sigma = \left[\frac{-\ln(P_s)}{(V/V_0)} \right]^{\frac{1}{n}} \sigma_0$$

Using $\sigma_0 = 75.46$ and $n = 17.4$ for the 30-specimen population, the stress for $P_s = .5$ and $V/V_0 = 1$ is $\sigma = 73.9$ kpsi. If now the specimen size is doubled, so that $V/V_0 = 2$, the probability of survival at this stress as given by Eqn. 7 drops to $P_s = 0.25$. If on the other hand the specimen size is halved ($V/V_0 = 0.5$), the probability of survival rises to $P_s = 0.71$.

⁶S.W. Rust, et al., *ASTM STP 1003*, p. 136, 1989. (Also Military Handbook 17.)

A final note of caution, a bit along the lines of the famous Mark Twain aphorism about there being “lies, damned lies, and statistics:” it is often true that populations of simple tensile or other laboratory specimens can be well described by classical statistical distributions. This should not be taken to imply that more complicated structures such as bridges and airplanes can be so neatly described. For instance, one aircraft study cited by Gordon⁷ found failures to occur randomly and uniformly over a wide range extending both above and below the statistically-based design safe load. Any real design, especially for structures that put human life at risk, must be checked in every reasonable way the engineer can imagine. This will include proof testing to failure, consideration of the worst possible environmental factors, consideration of construction errors resulting from difficult-to-manufacture designs, and so on almost without limit. Experience, caution and common sense will usually be at least as important as elaborate numerical calculations.

Problems

1. Ten strength measurements have produced a mean tensile strength of $\bar{\sigma}_f = 100$ MPa, with 95% confidence limits of ± 8 MPa. How many additional measurements would be necessary to reduce the confidence limits by half, assuming the mean and standard deviation of the measurements remains unchanged?
2. The thirty measurements of the tensile strength of graphite/epoxy composite listed in Example 1 were made at room temperature. Thirty additional tests conducted at 93°C gave the values (in kpsi): 63.40, 69.70, 72.80, 63.60, 71.20, 72.07, 76.97, 70.94, 76.22, 64.65, 62.08, 61.53, 70.53, 72.88, 74.90, 78.61, 68.72, 72.87, 64.49, 75.12, 67.80, 72.68, 75.09, 67.23, 64.80, 75.84, 63.87, 72.46, 69.54, 76.97. For these data:
 - (a) Determine the arithmetic mean, standard deviation, and coefficient of variation.
 - (b) Determine the 95% confidence limits on the mean strength.
 - (c) Determine whether the average strengths at 23°C and 93°C are statistically different.
 - (d) Determine the normal and Weibull B-allowable strengths.
 - (e) Plot the cumulative probability of failure P_f vs. the failure stress on normal probability paper.
 - (f) Do the data appear to be distributed normally, based on the χ^2 test?
 - (g) Plot the cumulative probability of survival P_s vs. the failure stress on Weibull probability paper.
 - (h) Determine the Weibull parameters σ_0 and m .
 - (i) Estimate how the mean strength would change if the specimens were made ten times smaller, or ten times larger.
3. Repeat the previous problem, but using data for -59°C: 55.62, 55.91, 56.73, 57.54, 58.28, 59.23, 60.39, 60.62, 61.1, 62.1, 63.69, 63.8, 64.7, 65.2, 65.33, 66.39, 66.43, 66.72, 67.05, 67.76, 68.84, 69.15, 69.3, 69.37, 69.82, 70.94, 71.39, 71.74, 72.2, 73.46.

⁷J.E. Gordon, *Structures*, Plenum Press, 1978.

Appendix - Statistical Tables and Paper

Following are several standard tables and graph papers that can be used in performing statistical calculations, in the event suitable software is not available.

1. Normal Distribution Table
2. Cumulative Normal Distribution Table
3. Chi-Square Table
4. t -Distribution
5. Normal Probability Paper
6. Weibull Paper

Maximum C^2 values for $\alpha =$

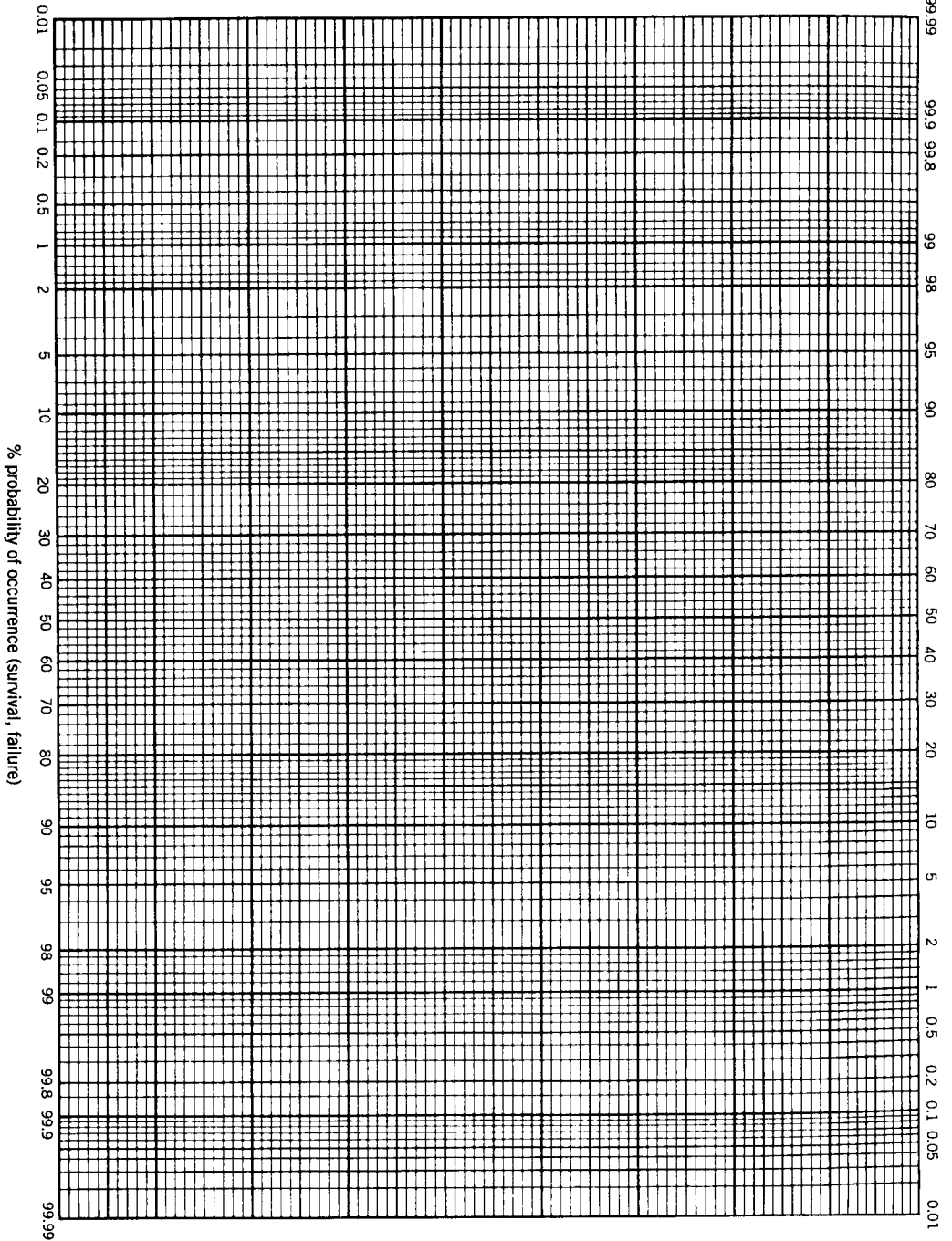
Degrees of Freedom	0.995	0.990	0.975	0.950	0.900	0.750	0.500	0.250	0.100	0.050	0.025	0.010	0.005
1	0.0000393	0.000157	0.000982	0.00393	0.0158	0.102	0.455	1.32	2.71	3.84	5.02	6.63	7.88
2	0.0100	0.0201	0.0506	0.103	0.211	0.575	1.390	2.77	4.61	5.99	7.38	9.21	10.6
3	0.0717	0.115	0.216	0.352	0.584	1.21	2.37	4.11	6.25	7.81	9.35	11.3	12.8
4	0.207	0.297	0.484	0.711	1.06	1.92	3.36	5.39	7.78	9.49	11.1	13.3	14.9
5	0.412	0.554	0.831	1.15	1.61	2.67	4.35	6.63	9.24	11.1	12.8	15.1	16.7
6	0.676	0.872	1.24	1.64	2.20	3.45	5.35	7.84	10.6	12.6	14.4	16.8	18.5
7	0.989	1.24	1.69	2.17	2.83	4.25	6.35	9.04	12.0	14.1	16.0	18.5	20.3
8	1.34	1.65	2.18	2.73	3.49	5.07	7.34	10.2	13.4	15.5	17.5	20.1	22.0
9	1.73	2.09	2.70	3.33	4.17	5.90	8.34	11.4	14.7	16.9	19.0	21.7	23.6
10	2.16	2.56	3.25	3.94	4.87	6.74	9.34	12.5	16.0	18.3	20.5	23.2	25.2
11	2.60	3.05	3.82	4.57	5.58	7.58	10.3	13.7	17.3	19.7	21.9	24.7	26.8
12	3.07	3.57	4.40	5.23	6.30	8.44	11.3	14.8	18.5	21.0	23.3	26.2	28.3
13	3.57	4.11	5.01	5.89	7.04	9.30	12.3	16.0	19.8	22.4	24.7	27.7	29.8
14	4.07	4.66	5.63	6.57	7.79	10.2	13.3	17.1	21.1	23.7	26.1	29.1	31.3
15	4.60	5.23	6.26	7.26	8.55	11.0	14.3	18.2	22.3	25.0	27.5	30.6	32.8
16	5.14	5.81	6.91	7.96	9.31	11.9	15.3	19.4	23.5	26.3	28.8	32.0	34.3
17	5.70	6.41	7.56	8.67	10.1	12.8	16.3	20.5	24.8	27.6	30.2	33.4	35.7
18	6.26	7.01	8.23	9.39	10.9	13.7	17.3	21.6	26.0	28.9	31.5	34.8	37.2
19	6.84	7.63	8.91	10.1	11.7	14.6	18.3	22.7	27.2	30.1	32.9	36.2	38.6
20	7.43	8.26	9.59	10.9	12.4	15.5	19.3	23.8	28.4	31.4	34.2	37.6	40.0
21	8.03	8.90	10.3	11.6	13.2	16.3	20.3	24.9	29.6	32.7	35.5	38.9	41.4
22	8.64	9.54	11.0	12.3	14.0	17.2	21.3	26.0	30.8	33.9	36.8	40.3	42.8
23	9.26	10.20	11.7	13.1	14.8	18.1	22.3	27.1	32.0	35.2	38.1	41.6	44.2
24	9.89	10.90	12.4	13.8	15.7	19.0	23.3	28.2	33.2	36.4	39.4	43.0	45.6
25	10.50	11.50	13.1	14.6	16.5	19.9	24.3	29.3	34.4	37.7	40.6	44.3	46.9
26	11.20	12.20	13.8	15.4	17.3	20.8	25.3	30.4	35.6	38.9	41.9	45.6	48.3
27	11.80	12.90	14.6	16.2	18.1	21.7	26.3	31.5	36.7	40.1	43.2	47.0	49.6
28	12.50	13.60	15.3	16.9	18.9	22.7	27.3	32.6	37.9	41.3	44.5	48.3	51.0
29	13.10	14.30	16.0	17.7	19.8	23.6	28.3	33.7	39.1	42.6	45.7	49.6	52.3
30	13.80	15.00	16.8	18.5	20.6	24.5	29.3	34.8	40.3	43.8	47.0	50.9	53.7

t-Distribution**Percentile**

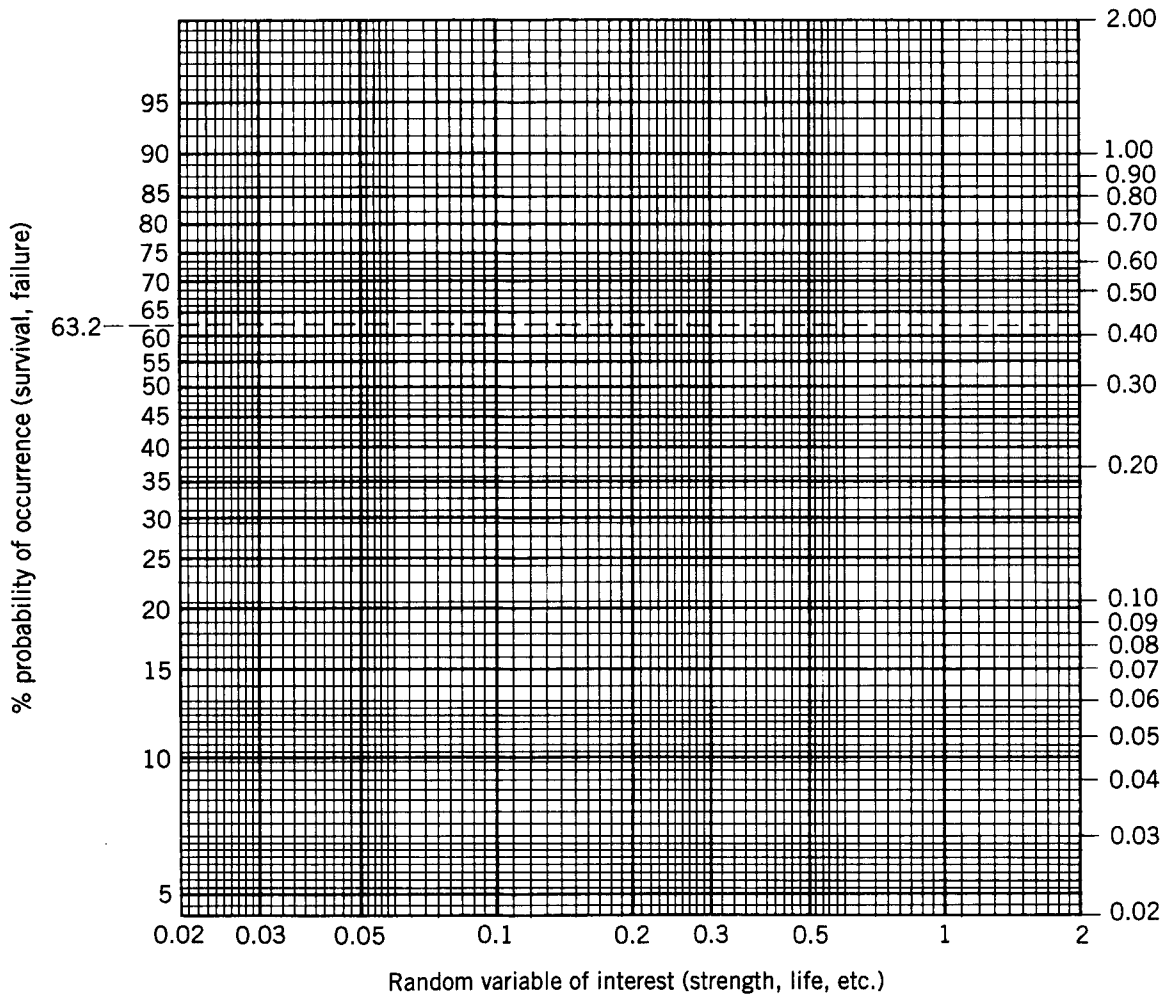
Degrees of Freedom	50	80	90	95	98	99	99.90
1	1.000	3.078	6.314	12.706	31.821	63.657	636.610
2	0.816	1.886	2.920	4.303	6.965	9.925	31.598
3	0.765	1.638	2.353	3.182	4.541	5.841	12.941
4	0.741	1.533	2.132	2.776	3.747	4.604	8.610
5	0.727	1.476	2.015	2.571	3.365	4.032	6.859
6	0.718	1.440	1.943	2.447	3.143	3.707	5.959
7	0.711	1.415	1.895	2.365	2.998	3.499	5.405
8	0.706	1.397	1.860	2.306	2.896	3.355	5.041
9	0.703	1.383	1.833	2.262	2.821	3.250	4.781
10	0.700	1.372	1.812	2.228	2.764	3.169	4.587
11	0.697	1.363	1.796	2.201	2.718	3.106	4.437
12	0.695	1.356	1.782	2.179	2.681	3.055	4.318
13	0.694	1.350	1.771	2.160	2.650	3.012	4.221
14	0.692	1.345	1.761	2.145	2.624	2.977	4.140
15	0.691	1.341	1.753	2.131	2.602	2.947	4.073
16	0.690	1.337	1.746	2.120	2.583	2.921	4.015
17	0.689	1.333	1.740	2.110	2.567	2.898	3.965
18	0.688	1.330	1.734	2.101	2.552	2.878	3.922
19	0.688	1.328	1.729	2.093	2.539	2.861	3.883
20	0.687	1.325	1.725	2.086	2.528	2.845	3.850
21	0.686	1.323	1.721	2.080	2.518	2.831	3.819
22	0.686	1.321	1.717	2.074	2.508	2.819	3.792
23	0.685	1.319	1.714	2.069	2.500	2.807	3.767
24	0.685	1.318	1.711	2.064	2.492	2.797	3.745
25	0.684	1.316	1.708	2.060	2.485	2.787	3.725
26	0.684	1.315	1.706	2.056	2.479	2.779	3.707
27	0.684	1.314	1.703	2.052	2.473	2.771	3.690
28	0.683	1.313	1.701	2.048	2.467	2.763	3.674
29	0.683	1.311	1.699	2.045	2.462	2.756	3.659
30	0.683	1.310	1.697	2.042	2.457	2.750	3.646
40	0.681	1.303	1.684	2.021	2.423	2.704	3.551
60	0.679	1.296	1.671	2.000	2.390	2.660	3.460
120	0.677	1.289	1.658	1.980	2.358	2.617	3.373
infinity	0.674	1.282	1.645	1.960	2.326	2.576	3.291

5. Normal Probability Paper

Random variable of interest (strength, life, etc.)



6. Weibull Paper



Introduction to Fracture Mechanics

David Roylance
Department of Materials Science and Engineering
Massachusetts Institute of Technology
Cambridge, MA 02139

June 14, 2001

Introduction

In 1983, the National Bureau of Standards (now the National Institute for Science and Technology) and Battelle Memorial Institute¹ estimated the costs for failure due to fracture to be \$119 billion per year in 1982 dollars. The dollars are important, but the cost of many failures in human life and injury is infinitely more so.

Failures have occurred for many reasons, including uncertainties in the loading or environment, defects in the materials, inadequacies in design, and deficiencies in construction or maintenance. Design against fracture has a technology of its own, and this is a very active area of current research. This module will provide an introduction to an important aspect of this field, since without an understanding of fracture the methods in stress analysis discussed previously would be of little use. We will focus on fractures due to simple tensile overstress, but the designer is cautioned again about the need to consider absolutely as many factors as possible that might lead to failure, especially when life is at risk.

The Module on the Dislocation Basis of Yield (Module 21) shows how the strength of structural metals – particularly steel – can be increased to very high levels by manipulating the microstructure so as to inhibit dislocation motion. Unfortunately, this renders the material increasingly brittle, so that cracks can form and propagate catastrophically with very little warning. An unfortunate number of engineering disasters are related directly to this phenomenon, and engineers involved in structural design must be aware of the procedures now available to safeguard against brittle fracture.

The central difficulty in designing against fracture in high-strength materials is that the presence of cracks can modify the local stresses to such an extent that the elastic stress analyses done so carefully by the designers are insufficient. When a crack reaches a certain critical length, it can propagate catastrophically through the structure, *even though the gross stress is much less than would normally cause yield or failure in a tensile specimen*. The term “fracture mechanics” refers to a vital specialization within solid mechanics in which the presence of a crack is assumed, and we wish to find quantitative relations between the crack length, the material’s inherent resistance to crack growth, and the stress at which the crack propagates at high speed to cause structural failure.

¹R.P. Reed et al., NBS Special Publication 647-1, Washington, 1983.

The energy-balance approach

When A.A. Griffith (1893–1963) began his pioneering studies of fracture in glass in the years just prior to 1920, he was aware of Inglis' work in calculating the stress concentrations around elliptical holes², and naturally considered how it might be used in developing a fundamental approach to predicting fracture strengths. However, the Inglis solution poses a mathematical difficulty: in the limit of a perfectly sharp crack, the stresses approach infinity at the crack tip. This is obviously nonphysical (actually the material generally undergoes some local yielding to blunt the cracktip), and using such a result would predict that materials would have near-zero strength: even for very small applied loads, the stresses near crack tips would become infinite, and the bonds there would rupture. Rather than focusing on the crack-tip stresses directly, Griffith employed an energy-balance approach that has become one of the most famous developments in materials science³.

The strain energy per unit volume of stressed material is

$$U^* = \frac{1}{V} \int f dx = \int \frac{f}{A} \frac{dx}{L} = \int \sigma d\epsilon$$

If the material is linear ($\sigma = E\epsilon$), then the strain energy per unit volume is

$$U^* = \frac{E\epsilon^2}{2} = \frac{\sigma^2}{2E}$$

When a crack has grown into a solid to a depth a , a region of material adjacent to the free surfaces is unloaded, and its strain energy released. Using the Inglis solution, Griffith was able to compute just how much energy this is.

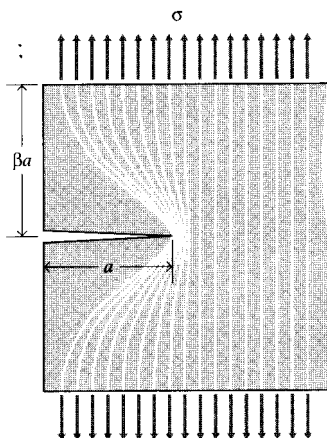


Figure 1: Idealization of unloaded region near crack flanks.

A simple way of visualizing this energy release, illustrated in Fig. 1, is to regard two triangular regions near the crack flanks, of width a and height βa , as being completely unloaded, while the remaining material continues to feel the full stress σ . The parameter β can be selected so as to

²See Module 16.

³A.A. Griffith, *Philosophical Transactions*, Series A, Vol. 221, pp. 163–198, 1920. The importance of Griffith's work in fracture was largely unrecognized until the 1950's. See J.E. Gordon, *The Science of Structures and Materials*, Scientific American Library, 1988, for a personal account of the Griffith story.

agree with the Inglis solution, and it turns out that for plane stress loading $\beta = \pi$. The total strain energy U released is then the strain energy per unit volume times the volume in both triangular regions:

$$U = -\frac{\sigma^2}{2E} \cdot \pi a^2$$

Here the dimension normal to the x - y plane is taken to be unity, so U is the strain energy released per unit thickness of specimen. This strain energy is *liberated* by crack growth. But in forming the crack, bonds must be broken, and the requisite bond energy is in effect *absorbed* by the material. The surface energy S associated with a crack of length a (and unit depth) is:

$$S = 2\gamma a$$

where γ is the surface energy (e.g., Joules/meter²) and the factor 2 is needed since two free surfaces have been formed. As shown in Fig. 2, the total energy associated with the crack is then the sum of the (positive) energy absorbed to create the new surfaces, plus the (negative) strain energy liberated by allowing the regions near the crack flanks to become unloaded.

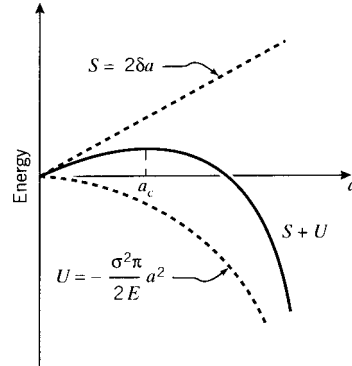


Figure 2: The fracture energy balance.

As the crack grows longer (a increases), the quadratic dependence of strain energy on a eventually dominates the surface energy, and beyond a critical crack length a_c the system can lower its energy by letting the crack grow still longer. Up to the point where $a = a_c$, the crack will grow only if the stress is increased. Beyond that point, crack growth is spontaneous and catastrophic.

The value of the critical crack length can be found by setting the derivative of the total energy $S + U$ to zero:

$$\frac{\partial(S + U)}{\partial a} = 2\gamma - \frac{\sigma_f^2}{E}\pi a = 0$$

Since fast fracture is imminent when this condition is satisfied, we write the stress as σ_f . Solving,

$$\sigma_f = \sqrt{\frac{2E\gamma}{\pi a}}$$

Griffith's original work dealt with very brittle materials, specifically glass rods. When the material exhibits more ductility, consideration of the surface energy alone fails to provide an

accurate model for fracture. This deficiency was later remedied, at least in part, independently by Irwin⁴ and Orowan⁵. They suggested that in a ductile material a good deal – in fact the vast majority – of the released strain energy was absorbed not by creating new surfaces, but by energy dissipation due to plastic flow in the material near the crack tip. They suggested that catastrophic fracture occurs when the strain energy is released at a rate sufficient to satisfy the needs of all these energy “sinks,” and denoted this *critical strain energy release rate* by the parameter \mathcal{G}_c ; the Griffith equation can then be rewritten in the form:

$$\sigma_f = \sqrt{\frac{E\mathcal{G}_c}{\pi a}} \quad (1)$$

This expression describes, in a very succinct way, the interrelation between three important aspects of the fracture process: the *material*, as evidenced in the critical strain energy release rate \mathcal{G}_c ; the *stress level* σ_f ; and the *size*, a , of the flaw. In a design situation, one might choose a value of a based on the smallest crack that could be easily detected. Then for a given material with its associated value of \mathcal{G}_c , the safe level of stress σ_f could be determined. The structure would then be sized so as to keep the working stress comfortably below this critical value.

Example 1

The story of the DeHavilland Comet aircraft of the early 1950’s, in which at least two aircraft disintegrated in flight, provides a tragic but fascinating insight into the importance of fracture theory. It is an eerie story as well, having been all but predicted in a 1948 novel by Nevil Shute named *No Highway*. The book later became a movie starring James Stewart as a perserverant metallurgist convinced that his company’s new aircraft (the “Reindeer”) was fatally prone to metal fatigue. When just a few years later the Comet was determined to have almost exactly this problem, both the book and the movie became rather famous in the materials engineering community.

The postmortem study of the Comet’s problems was one of the most extensive in engineering history⁶. It required salvaging almost the entire aircraft from scattered wreckage on the ocean floor and also involved full-scale pressurization of an aircraft in a giant water tank. Although valuable lessons were learned, it is hard to overstate the damage done to the DeHavilland Company and to the British aircraft industry in general. It is sometimes argued that the long predominance of the United States in commercial aircraft is due at least in part to the Comet’s misfortune.

The Comet aircraft had a fuselage of clad aluminum, with $\mathcal{G}_c \approx 300$ in-psi. The hoop stress due to relative cabin pressurization was 20,000 psi, and at that stress the length of crack that will propagate catastrophically is

$$a = \frac{\mathcal{G}_c E}{\pi \sigma^2} = \frac{(300)(11 \times 10^6)}{\pi(20 \times 10^3)^2} = 2.62''$$

A crack would presumably be detected in routine inspection long before it could grow to this length. But in the case of the Comet, the cracks were propagating from rivet holes near the cabin windows. When the crack reached the window, the size of the window opening was effectively added to the crack length, leading to disaster.

Modern aircraft are built with this failure mode in mind, and have “tear strips” that are supposedly able to stop any rapidly growing crack. But this remedy is not always effective, as was demonstrated in 1988 when a B737 operated by Aloha Airlines had the roof of the first-class cabin tear away.. That aircraft had stress-corrosion damage at a number of rivets in the fuselage lap splices, and this permitted

⁴G.R. Irwin, “Fracture Dynamics,” *Fracturing of Metals*, American Society for Metals, Cleveland, 1948.

⁵E. Orowan, “Fracture and Strength of Solids,” Report of Progress in Physics, Vol. 12, 1949.

⁶T. Bishop, *Metal Progress*, Vol. 67, pp. 79–85, May 1955.

multiple small cracks to link up to form a large crack. A great deal of attention is currently being directed to protection against this sort of “multi-site damage.”

It is important to realize that the critical crack length is an absolute number, not depending on the size of the structure containing it. Each time the crack jumps ahead, say by a small increment δa , an additional quantity of strain energy is released from the newly-unloaded material near the crack. Again using our simplistic picture of a triangular-shaped region that is at zero stress while the rest of the structure continues to feel the overall applied stress, it is easy to see in Fig. 3 that much more more energy is released due to the jump at position 2 than at position 1. This is yet another reason why small things tend to be stronger: they simply aren’t large enough to contain a critical-length crack.

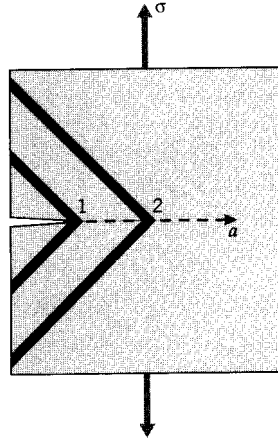


Figure 3: Energy released during an increment of crack growth, for two different crack lengths.

Example 2

Gordon⁷ tells of a ship’s cook who one day noticed a crack in the steel deck of his galley. His superiors assured him that it was nothing to worry about — the crack was certainly small compared with the vast bulk of the ship — but the cook began painting dates on the floor to mark the new length of the crack each time a bout of rough weather would cause it to grow longer. With each advance of the crack, additional decking material was unloaded, and the strain energy formerly contained in it released. But as the amount of energy released grows *quadratically* with the crack length, eventually enough was available to keep the crack growing even with no further increase in the gross load. When this happened, the ship broke into two pieces; this seems amazing but there are a more than a few such occurrences that are very well documented. As it happened, the part of the ship with the marks showing the crack’s growth was salvaged, and this has become one of the very best documented examples of slow crack growth followed by final catastrophic fracture.

Compliance calibration

A number of means are available by which the material property \mathcal{G}_c can be measured. One of these is known as *compliance calibration*, which employs the concept of compliance as a ratio of

⁷J.E. Gordon, *Structures, or Why Things Don't Fall Down*, Plenum, New York, 1978.

deformation to applied load: $C = \delta/P$. The total strain energy U can be written in terms of this compliance as:

$$U = \frac{1}{2}P\delta = \frac{1}{2}CP^2$$

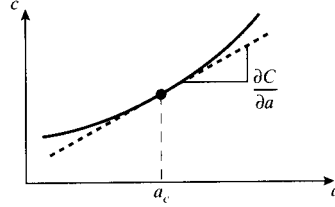


Figure 4: Compliance as a function of crack length.

The compliance of a suitable specimen, for instance a cantilevered beam, could be measured experimentally as a function of the length a of a crack that is grown into the specimen (see Fig. 4). The strain energy release rate can then be determined by differentiating the curve of compliance versus length:

$$\mathcal{G} = \frac{\partial U}{\partial a} = \frac{1}{2}P^2 \frac{\partial C}{\partial a} \quad (2)$$

The *critical* value of \mathcal{G} , \mathcal{G}_c , is then found by measuring the critical load P_c needed to fracture a specimen containing a crack of length a_c , and using the slope of the compliance curve at this same value of a :

$$\mathcal{G}_c = \frac{1}{2}P_c^2 \left. \frac{\partial C}{\partial a} \right|_{a=a_c} \quad (3)$$

Example 3

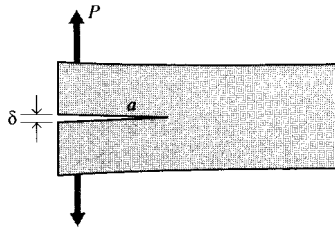


Figure 5: DCB fracture specimen.

For a double-cantilever beam (DCB) specimen such as that shown in Fig. 5, beam theory gives the deflection as

$$\frac{\delta}{2} = \frac{Pa^3}{3EI}$$

where $I = bh^3/12$. The elastic compliance is then

$$C = \frac{\delta}{P} = \frac{2a^3}{3EI}$$

If the crack is observed to jump forward when $P = P_c$, Eqn. 3 can be used to compute the critical strain energy release rate as

$$\mathcal{G}_c = \frac{1}{2}P_c^2 \cdot \frac{2a^2}{EI} = \frac{12P_c^2 a^2}{b^2 h^3 E}$$

The stress intensity approach

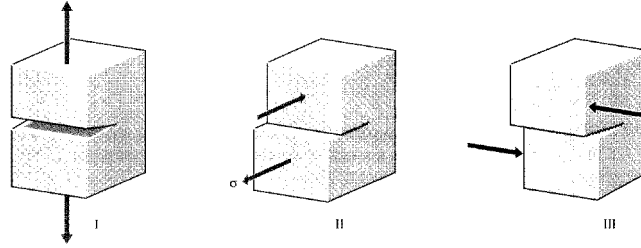


Figure 6: Fracture modes.

While the energy-balance approach provides a great deal of insight to the fracture process, an alternative method that examines the stress state near the tip of a sharp crack directly has proven more useful in engineering practice. The literature treats three types of cracks, termed mode I, II, and III as illustrated in Fig. 6. Mode I is a normal-opening mode and is the one we shall emphasize here, while modes II and III are shear sliding modes. As was outlined in Module 16, the semi-inverse method developed by Westergaard shows the opening-mode stresses to be:

$$\begin{aligned}\sigma_x &= \frac{K_I}{\sqrt{2\pi r}} \cos \frac{\theta}{2} \left(1 - \sin \frac{\theta}{2} \sin \frac{3\theta}{2} \right) + \dots \\ \sigma_y &= \frac{K_I}{\sqrt{2\pi r}} \cos \frac{\theta}{2} \left(1 + \sin \frac{\theta}{2} \sin \frac{3\theta}{2} \right) + \dots \\ \tau_{xy} &= \frac{K_I}{\sqrt{2\pi r}} \cos \frac{\theta}{2} \cos \frac{3\theta}{2} \sin \frac{\theta}{2} \dots\end{aligned}\tag{4}$$

For distances close to the crack tip ($r \leq 0.1a$), the second and higher order terms indicated by dots may be neglected. At large distances from the crack tip, these relations cease to apply and the stresses approach their far-field values that would obtain were the crack not present.

The K_I in Eqns. 4 is a very important parameter known as the *stress intensity factor*. The I subscript is used to denote the crack opening mode, but similar relations apply in modes II and III. The equations show three factors that taken together depict the stress state near the crack tip: the denominator factor $(2\pi r)^{-1/2}$ shows the singular nature of the stress distribution; σ approaches infinity as the crack tip is approached, with a $r^{-1/2}$ dependency. The angular

dependence is separable as another factor; e.g. $f_x = \cos \theta/2 \cdot (1 - \sin \theta/2 \sin 3\theta/2) + \dots$. The factor K_I contains the dependence on applied stress σ_∞ , the crack length a , and the specimen geometry. The K_I factor gives the overall intensity of the stress distribution, hence its name.

For the specific case of a central crack of width $2a$ or an edge crack of length $2a$ in a large sheet, $K_I = \sigma_\infty \sqrt{\pi a}$, and $K_I = 1.12 \sigma_\infty \sqrt{\pi a}$ for an edge crack of length a in the edge of a large sheet. (The factor π could obviously be canceled with the π in the denominator of Eqn. 4, but is commonly retained for consistency with earlier work.) Expressions for K_I for some additional geometries are given in Table 1. The literature contains expressions for K for a large number of crack and loading geometries, and both numerical and experimental procedures exist for determining the stress intensity factor is specific actual geometries.

Table 1: Stress intensity factors for several common geometries.

Type of Crack	Stress Intensity Factor, K_I
Center crack, length $2a$, in an infinite plate	$\sigma_\infty \sqrt{\pi a}$
Edge crack, length a , in a semi-infinite plate	$1.12 \sigma_\infty \sqrt{\pi a}$
Central penny-shaped crack, radius a , in infinite body	$2 \sigma_\infty \sqrt{\frac{a}{\pi}}$
Center crack, length $2a$ in plate of width W	$\sigma_\infty \sqrt{W \tan\left(\frac{\pi a}{W}\right)}$
2 symmetrical edge cracks, each length a , in plate of total width W	$\sigma_\infty \sqrt{W \left[\tan\left(\frac{\pi a}{W}\right) + 0.1 \sin\left(\frac{2\pi a}{W}\right) \right]}$

These stress intensity factors are used in design and analysis by arguing that the material can withstand crack tip stresses up to a critical value of stress intensity, termed K_{Ic} , beyond which the crack propagates rapidly. This *critical stress intensity factor* is then a measure of material toughness. The failure stress σ_f is then related to the crack length a and the fracture toughness by

$$\sigma_f = \frac{K_{Ic}}{\alpha \sqrt{\pi a}} \quad (5)$$

where α is a geometrical parameter equal to 1 for edge cracks and generally on the order of unity for other situations. Expressions for α are tabulated for a wide variety of specimen and crack geometries, and specialty finite element methods are available to compute it for new situations.

The stress intensity and energy viewpoints are interrelated, as can be seen by comparing Eqns. 1 and 5 (with $\alpha = 1$):

$$\sigma_f = \sqrt{\frac{E\mathcal{G}_c}{\pi a}} = \frac{K_{Ic}}{\sqrt{\pi a}} \rightarrow K_{Ic}^2 = E\mathcal{G}_c$$

This relation applies in plane stress; it is slightly different in plane strain:

$$K_{Ic}^2 = E\mathcal{G}_c(1 - \nu^2)$$

For metals with $\nu = .3$, $(1 - \nu^2) = 0.91$. This is not a big change; however, the numerical values of \mathcal{G}_c or K_{Ic} are very different in plane stress or plane strain situations, as will be described below.

Typical values of G_{Ic} and K_{Ic} for various materials are listed in Table 2, and it is seen that they vary over a very wide range from material to material. Some polymers can be very tough, especially when rated on a per-pound bases, but steel alloys are hard to beat in terms of absolute resistance to crack propagation.

Table 2: Fracture toughness of materials.

Material	$G_{Ic}(\text{kJm}^{-2})$	$K_{Ic}(\text{MNm}^2)$	$E(\text{GPa})$
Steel alloy	107	150	210
Aluminum alloy	20	37	69
Polyethylene	20 (J_{Ic})	—	0.15
High-impact polystyrene	15.8 (J_{Ic})	—	2.1
Steel — mild	12	50	210
Rubber	13	—	0.001
Glass-reinforced thermoset	7	7	7
Rubber-toughened epoxy	2	2.2	2.4
PMMA	0.5	1.1	2.5
Polystyrene	0.4	1.1	3
Wood	0.12	0.5	2.1
Glass	0.007	0.7	70

Example 4

Equation 5 provides a design relation among the applied stress σ , the material's toughness K_{Ic} , and the crack length a . Any one of these parameters can be calculated once the other two are known. To illustrate one application of the process, say we wish to determine the safe operating pressure in an aluminum pressure vessel 0.25 m in diameter and with a 5 mm wall thickness. First assuming failure by yield when the hoop stress reaches the yield stress (330 MPa) and using a safety factor of 0.75, we can compute the maximum pressure as

$$p = \frac{0.75\sigma t}{r} = \frac{0.75 \times 330 \times 10^6}{0.25/2} = 9.9 \text{ MPa} = 1400 \text{ psi}$$

To insure against failure by rapid crack growth, we now calculate the maximum crack length permissible at the operating stress, using a toughness value of $K_{Ic} = 41 \text{ MPa}\sqrt{\text{m}}$:

$$a = \frac{K_{Ic}^2}{\pi\sigma^2} = \frac{(41 \times 10^6)^2}{\pi(0.75 \times 330 \times 10^6)^2} = 0.01 \text{ m} = 0.4 \text{ in}$$

Here an edge crack with $\alpha = 1$ has been assumed. An inspection schedule must be implemented that is capable of detecting cracks before they reach this size.

Effect of specimen geometry

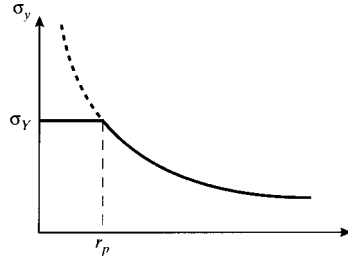


Figure 7: Stress limited by yield within zone r_p .

The toughness, or resistance to crack growth, of a material is governed by the energy absorbed as the crack moves forward. In an extremely brittle material such as window glass, this energy is primarily just that of rupturing the chemical bonds along the crack plane. But as already mentioned, in tougher materials bond rupture plays a relatively small role in resisting crack growth, with by far the largest part of the fracture energy being associated with plastic flow near the crack tip. A “plastic zone” is present near the crack tip within which the stresses as predicted by Eqn. 4 would be above the material’s yield stress σ_Y . Since the stress cannot rise above σ_Y , the stress in this zone is σ_Y rather than that given by Eqn. 4. To a first approximation, the distance r_p this zone extends along the x -axis can be found by using Eqn. 4 with $\theta = 0$ to find the distance at which the crack tip stress reduces to σ_Y :

$$\begin{aligned}\sigma_y = \sigma_Y &= \frac{K_I}{\sqrt{2\pi r_p}} \\ r_p &= \frac{K_I^2}{2\pi\sigma_Y^2}\end{aligned}\tag{6}$$

This relation is illustrated in Fig. 7. As the stress intensity is increased either by raising the imposed stress or by crack lengthening, the plastic zone size will increase as well. But the extent of plastic flow is ultimately limited by the material’s molecular or microstructural mobility, and the zone can become only so large. When the zone can grow no larger, the crack can no longer be constrained and unstable propagation ensues. The value of K_I at which this occurs can then be considered a materials property, named K_{Ic} .

In order for the measured value of K_{Ic} to be valid, the plastic zone size should not be so large as to interact with the specimen’s free boundaries or to destroy the basic nature of the singular stress distribution. The ASTM specification for fracture toughness testing⁸ specifies the specimen geometry to insure that the specimen is large compared to the crack length and the plastic zone size (see Fig. 8):

$$a, B, (W - a) \geq 2.5 \left(\frac{K_I}{\sigma_Y} \right)^2$$

⁸E 399-83, “Standard Test Method for Plane-Strain Fracture Toughness of Metallic Materials,” ASTM, 1983.

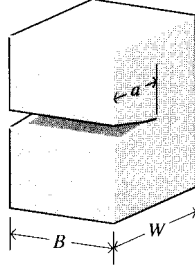


Figure 8: Dimensions of fracture toughness specimen.

A great deal of attention has been paid to the important case in which enough ductility exists to make it impossible to satisfy the above criteria. In these cases the stress intensity view must be abandoned and alternative techniques such as the J-integral or the crack tip opening displacement method used instead. The reader is referred to the references listed at the end of the module for discussion of these approaches.

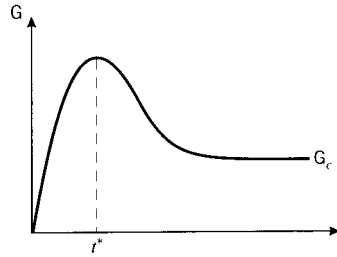


Figure 9: Effect of specimen thickness on toughness.

The fracture toughness as measured by K_c or \mathcal{G}_c is essentially a measure of the extent of plastic deformation associated with crack extension. The quantity of plastic flow would be expected to scale linearly with the specimen thickness, since reducing the thickness by half would naturally cut the volume of plastically deformed material approximately in half as well. The toughness therefore rises linearly, at least initially, with the specimen thickness as seen in Fig. 9. Eventually, however, the toughness is observed to go through a maximum and fall thereafter to a lower value. This loss of toughness beyond a certain critical thickness t^* is extremely important in design against fracture, since using too thin a specimen in measuring toughness will yield an unrealistically optimistic value for \mathcal{G}_C . The specimen size requirements for valid fracture toughness testing are such that the most conservative value is measured.

The critical thickness is that which causes the specimen to be dominated by a state of *plane strain*, as opposed to *plane stress*. The stress in the through-thickness z direction must become zero at the sides of the specimen since no traction is applied there, and in a thin specimen the stress will not have room to rise to appreciable values within the material. The *strain* in the z direction is not zero, of course, and the specimen will experience a Poisson contraction given by $\epsilon_z = \nu(\sigma_x + \sigma_y)$. But when the specimen is thicker, material near the center will be unable to contract laterally due to the constraint of adjacent material. Now the z -direction strain is zero, so a tensile stress will arise as the material tries to contract but is prevented from doing so. The value of σ_z rises from zero at the outer surface and approaches a maximum value given

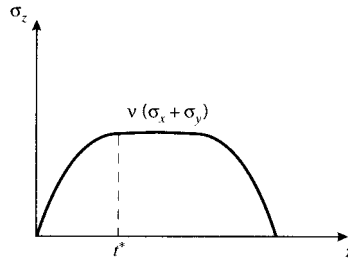


Figure 10: Transverse stress at crack tip.

by $\sigma_z \approx \nu(\sigma_x + \sigma_y)$ in a distance t^* as seen in Fig. 10. To guarantee that plane strain conditions dominate, the specimen thickness t must be such that $t \gg 2t^*$.

The triaxial stress state set up near the center of a thick specimen near the crack tip *reduces* the maximum shear stress available to drive plastic flow, since the maximum shear stress is equal to one half the difference of the largest and smallest principal stress, and the smallest is now greater than zero. Or equivalently, we can state that the mobility of the material is constrained by the inability to contract laterally. From either a stress or a strain viewpoint, the extent of available plasticity is reduced by making the specimen thick.

Example 5

The plastic zone sizes for the plane stress and plane strain cases can be visualized by using a suitable yield criterion along with the expressions for stress near the crack tip. The v. Mises yield criterion was given in terms of principal stresses in Module 20 as

$$2\sigma_Y^2 = (\sigma_1 - \sigma_2)^2 + (\sigma_1 - \sigma_3)^2 + (\sigma_2 - \sigma_3)^2$$

The principal stresses can be obtained from Eqns. 4 as

$$\sigma_1 = \frac{K_I}{\sqrt{2\pi r}} \cos \frac{\theta}{2} \left(1 + \sin \frac{\theta}{2} \right)$$

$$\sigma_2 = \frac{K_I}{\sqrt{2\pi r}} \cos \frac{\theta}{2} \left(1 - \sin \frac{\theta}{2} \right)$$

The third principal stress is

$$\sigma_3 = \begin{cases} 0, & \text{plane stress} \\ \nu(\sigma_1 + \sigma_2), & \text{plane strain} \end{cases}$$

These stresses can be substituted into the yield criterion, which is then solved for the radius r at which yield occurs. It is convenient to normalize this radius by the radius of the plastic zone along the x -axis, given by Eqn. 6. Maple commands to carry out these substitutions and plot the result are:

```
# Radius of plastic zone along x-axis
> rp:=K[I]^2/(2*Pi*sigma[Y]^2):

# v. Mises yield criterion in terms of principal stresses
> v_mises:=2*sigma[Y]^2= (sigma[1]-sigma[2])^2 + (sigma[1]-sigma[3])^2
+ (sigma[2]-sigma[3])^2:

# Principal stresses in crack-tip region
> sigma[1]:=K[I]/sqrt(2*Pi*r))*cos(theta/2)*(1+sin(theta/2)):
```

```

> sigma[2]:= (K[I]/sqrt(2*Pi*r))*cos(theta/2)*(1-sin(theta/2));

# Evaluate v. Mises for plane stress (v_strs) and plane strain (v_strn)
# Take nu = 0.3
> v_strs:=subs(sigma[3]=0,v_mises):
> v_strn:=subs(sigma[3]=.3*(sigma[1]+sigma[2]),v_mises):

# Solve for plastic zone radius, normalize by rp
# pl_strs for plane stress case, pl_strn for plane strain
> pl_strs:=solve(v_strs,r)/rp:
> pl_strn:=solve(v_strn,r)/rp:

# Plot normalized plastic zones for plane stress and plane strain
> plot({pl_strs,pl_strn},theta=0..2*Pi,coords=polar);

```

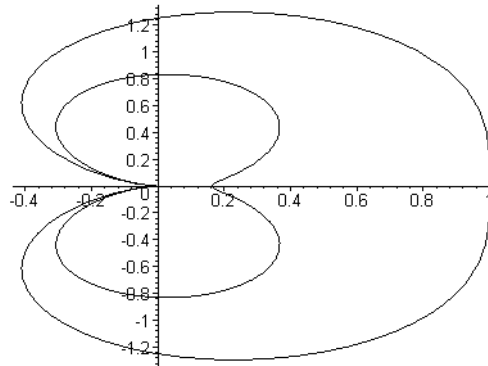


Figure 11: Normalized plastic zone shapes for plane strain (inner contour) and plane stress (outer contour).

Even in a thick specimen, the z -direction stress must approach zero at the side surfaces. Regions near the surface are therefore free of the triaxial stress constraint, and exhibit greater shear-driven plastic flow. After a cracked specimen has been tested to failure, a flat “thumbnail” pattern will often be visible as illustrated in Fig. 12. This is the region of slow crack growth, where the crack is able to maintain its preferred orientation transverse to the y -direction stress. The crack growth near the edges is retarded by the additional plastic flow there, so the crack line bows inward. When the stress is increased enough to cause the crack to grow catastrophically, it typically does so at speeds high enough that the transverse orientation is not always maintained. The region of rapid fracture is thus faceted and rough, leading some backyard mechanics to claim the material failed because it “crystallized.”

Along the edges of the specimen, “shear lips” can often be found on which the crack has developed by shear flow and with intensive plastic deformation. The lips will be near a 45° angle, the orientation of the maximum shear planes.

Grain size and temperature

Steel is such an important and widely used structural material that it is easy to forget that steel is a fairly recent technological innovation. Well into the nineteenth century, wood was the

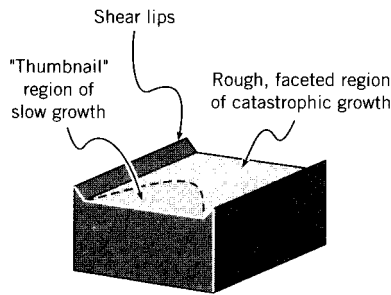


Figure 12: Fracture surface topography.

dominant material for many bridges, buildings, and ships. As the use of iron and steel became more widespread in the latter part of that century and the first part of the present one, a number of disasters took place that can be traced to the then-incomplete state of understanding of these materials, especially concerning their tendency to become brittle at low temperatures. Many of these failures have been described and analyzed in a fascinating book by Parker⁹.

One of these brittle failures is perhaps the most famous disaster of the last several centuries, the sinking of the transatlantic ocean liner *Titanic* on April 15, 1912, with a loss of some 1,500 people and only 705 survivors. Until very recently, the tragedy was thought to be caused by a long gash torn through the ship's hull by an iceberg. However, when the wreckage of the ship was finally discovered in 1985 using undersea robots, no evidence of such a gash was found. Further, the robots were later able to return samples of the ship's steel whose analysis has given rise to an alternative explanation.

It is now well known that lesser grades of steel, especially those having large concentrations of impurities such as interstitial carbon inclusions, are subject to embrittlement at low temperatures. William Garzke, a naval architect with the New York firm of Gibbs & Cox, and his colleagues have argued that the steel in the *Titanic* was indeed brittle in the 31°F waters of the Atlantic that night, and that the 22-knot collision with the iceberg generated not a gash but extensive cracking through which water could enter the hull. Had the steel remained tough at this temperature, these authors feel, the cracking may have been much less extensive. This would have slowed the flooding and allowed more time for rescue vessels to reach the scene, which could have increased greatly the number of survivors.

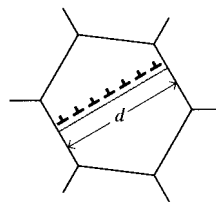


Figure 13: Dislocation pileup within a grain.

In the bcc transition metals such as iron and carbon steel, brittle failure can be initiated by dislocation glide within a crystalline grain. The slip takes place at the yield stress σ_Y , which

⁹E.R. Parker, *Brittle Behavior of Engineering Structures*, John Wiley & Sons, 1957.

varies with grain size according to the Hall-Petch law as described in Module 21:

$$\sigma_Y = \sigma_0 + k_Y d^{-1/2}$$

Dislocations are not able to propagate beyond the boundaries of the grain, since adjoining grains will not in general have their slip planes suitably oriented. The dislocations then “pile up” against the grain boundaries as illustrated in Fig. 13. The dislocation pileup acts similarly to an internal crack with a length that scales with the grain size d , intensifying the stress in the surrounding grains. Replacing a by d in the modified Griffith equation (Eqn. 1), the applied stress needed to cause fracture in adjacent grains is related to the grain size as

$$\sigma_f = k_f d^{-1/2}, \quad k_f \propto \sqrt{\frac{E\mathcal{G}_c}{\pi}}$$

The above two relations for yielding and fracture are plotted in Fig. 14 against inverse root grain size (so grain size increases to the left), with the slopes being k_Y and k_f respectively. When $k_f > k_Y$, fracture will not occur until $\sigma = \sigma_Y$ for values of d to the left of point A , since yielding and slip is a prerequisite for cleavage. In this region the yielding and fracture stresses are the same, and the failure appears brittle since large-scale yielding will not have a chance to occur. To the right of point A , yielding takes place prior to fracture and the material appears ductile. The point A therefore defines a critical grain size d^* at which a “nil-ductility” transition from ductile (grains smaller than d^*) to brittle failure will take place.

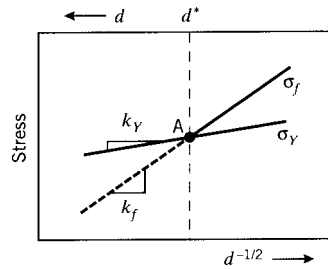


Figure 14: Effect of grain size on yield and fracture stress.

As the temperature is lowered, the yield stress σ_Y will increase as described in Module 20, and the fracture stress σ_f will decrease (since atomic mobility and thus \mathcal{G}_C decrease). Therefore, point A shifts to the right as temperature is lowered. The critical grain size for nil ductility now occurs at a smaller value; i.e. the grains must be smaller to avoid embrittling the material. Equivalently, refining the grain size has the effect of lowering the ductile-brittle transition temperature. Hence grain-size refinement raises both the yield and fracture stress, lowers the ductile-brittle transition temperature, and promotes toughness as well. This is a singularly useful strengthening mechanism, since other techniques such as strain hardening and solid-solution hardening tend to achieve strengthening at the expense of toughness.

Factors other than temperature can also embrittle steel. Inclusions such as carbon and phosphorus act to immobilize slip systems that might otherwise relieve the stresses associated with dislocation pileups, and these inclusions can raise the yield stress and thus the ductile-brittle transition temperature markedly. Similar effects can be induced by damage from high-energy radiation, so embrittlement of nuclear reactor components is of great concern. Embrittlement is also facilitated by the presence of notches, since they generate triaxial stresses that constrain

plastic flow. High strain rates promote brittleness because the flow stress needed to accommodate the strain rate is higher, and improper welding can lead to brittleness both by altering the steel's microstructure and by generating residual internal stresses.

General References

1. Anderson, T.L., *Fracture Mechanics: Fundamentals and Applications*, CRC Press, Boca Raton, 1991.
2. Barsom, J.M., ed., *Fracture Mechanics Retrospective*, American Society for Testing and Materials, Philadelphia, 1987.
3. Collins, J.A., *Failure of Materials in Mechanical Design*, Wiley, 1981.
4. Courtney, T.H., *Mechanical Behavior of Materials*, McGraw-Hill, New York, 1990.
5. Gordon, J.E., *The New Science of Strong Materials, or Why You Don't Fall Through the Floor*, Princeton University Press, 1976.
6. Hertzberg, R.W., *Deformation and Fracture Mechanics of Engineering Materials*, Wiley, New York, 1976.
7. Knott, J.F., *Fundamentals of Fracture Mechanics*, John Wiley – Halsted Press, New York, 1973.
8. Mendenhall, W., R.L. Scheaffer and D.D. Wackerly, *Mathematical Statistics with Applications*, Duxbury Press, Boston, 1986.
9. Strawley, J.E., and W.F. Brown, *Fracture Toughness Testing*, *ASTM STP 381*, 133, 1965.
10. Tetelman, A.S., and A.J. McEvily, Jr., *Fracture of Structural Materials*, Wiley, New York, 1967.

Problems

1. Using a development analogous to that employed in Module 21 for the theoretical yield stress, show that the theoretical ultimate tensile strength is $\sigma_{th} \approx E/10$ (much larger than that observed experimentally). Assume a harmonic atomic force function $\sigma = \sigma_{th} \sin(2\pi x/\lambda)$, where x is the displacement of an atom from its equilibrium position and $\lambda \approx a_0$ is the interatomic spacing. The maximum stress σ_{th} can then be found by using

$$E = \left(\frac{d\sigma}{d\epsilon} \right)_{x \rightarrow 0} \quad \text{and} \quad \epsilon = \frac{x}{a_0}$$

2. Using a safety factor of 2, find the safe operating pressure in a closed-end steel pressure vessel 1' in diameter and 0.2'' wall thickness.
3. A pressure vessel is constructed with a diameter of $d = 18''$ and a length of $L = 6'$. The vessel is to be capable of withstanding an internal pressure of $p = 1000$ psi, and the wall thickness is such as to keep the nominal hoop stress under 2500 psi. However, the vessel bursts at an internal pressure of only 500 psi, and a micrographic investigation reveals the

fracture to have been initiated by an internal crack 0.1" in length. Calculate the fracture toughness (K_{Ic}) of the material.

4. A highly cross-linked epoxy resin has a coefficient of linear thermal expansion $\alpha = 5 \times 10^{-5} \text{ K}^{-1}$, $G_{IC} = 120 \text{ J/m}^2$, $E = 3.2 \text{ GPa}$, and $\nu = 0.35$. A thick layer of resin is cured and is firmly bonded to an aluminum part ($\alpha = 2.5 \times 10^{-5} \text{ K}^{-1}$) at 180°C. Calculate the minimum defect size needed to initiate cracking in the resin on cooling to 20°C. Take α in Eqn. 5 to be $2/\pi$ for penny-shaped cracks of radius a in a wide sheet.
5. (a) A thick plate of aluminum alloy, 175 mm wide, contains a centrally-located crack 75 mm in length. The plate experiences brittle fracture at an applied stress (uniaxial, transverse to the crack) of 110 MPa. Determine the fracture toughness of the material.
(b) What would the fracture stress be if the plate were wide enough to permit an assumption of infinite width?
6. In order to obtain valid plane-strain fracture toughnesses, the plastic zone size must be small with respect to the specimen thickness B , the crack length a , and the "ligament" width $W - a$. The established criterion is

$$(W - a), B, a \geq \left(\frac{K_{Ic}}{\sigma_Y} \right)^2$$

Rank the materials in the database in terms of the parameter given on the right-hand side of this expression.

7. When a 150 kN load is applied to a tensile specimen containing a 35 mm crack, the overall displacement between the specimen ends is 0.5 mm. When the crack has grown to 37 mm, the displacement for this same load is 0.505 mm. The specimen is 40 mm thick. The fracture load of an identical specimen, but with a crack length of 36 mm, is 175 kN. Find the fracture toughness K_{Ic} of the material.

Fatigue

David Roylance
Department of Materials Science and Engineering
Massachusetts Institute of Technology
Cambridge, MA 02139

May 1, 2001

Introduction

The concept of “fatigue” arose several times in the Module on Fracture (Module 23), as in the growth of cracks in the Comet aircraft that led to disaster when they became large enough to propagate catastrophically as predicted by the Griffith criterion. Fatigue, as understood by materials technologists, is a process in which damage accumulates due to the repetitive application of loads that may be well below the yield point. The process is dangerous because a single application of the load would not produce any ill effects, and a conventional stress analysis might lead to a assumption of safety that does not exist.

In one popular view of fatigue in metals, the fatigue process is thought to begin at an internal or surface flaw where the stresses are concentrated, and consists initially of shear flow along slip planes. Over a number of cycles, this slip generates intrusions and extrusions that begin to resemble a crack. A true crack running inward from an intrusion region may propagate initially along one of the original slip planes, but eventually turns to propagate transversely to the principal normal stress as seen in Fig. 1.

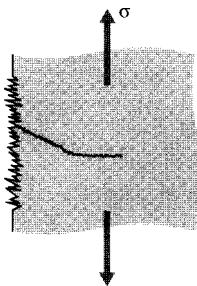


Figure 1: Intrusion-extrusion model of fatigue crack initiation.

When the failure surface of a fatigued specimen is examined, a region of slow crack growth is usually evident in the form of a “clamshell” concentric around the location of the initial flaw. (See Fig. 2.) The clamshell region often contains concentric “beach marks” at which the crack was arrested for some number of cycles before resuming its growth. Eventually, the crack may become large enough to satisfy the energy or stress intensity criteria for rapid propagation, following the previous expressions for fracture mechanics. This final phase produces the rough surface typical of fast fracture. In postmortem examination of failed parts, it is often possible to

correlate the beach marks with specific instances of overstress, and to estimate the applied stress at failure from the size of the crack just before rapid propagation and the fracture toughness of the material.



Figure 2: Typical fatigue-failure surfaces. From B. Chalmers, *Physical Metallurgy*, Wiley, p. 212, 1959.

The modern study of fatigue is generally dated from the work of A. Wöhler, a technologist in the German railroad system in the mid-nineteenth century. Wohler was concerned by the failure of axles after various times in service, at loads considerably less than expected. A railcar axle is essentially a round beam in four-point bending, which produces a compressive stress along the top surface and a tensile stress along the bottom (see Fig. 3). After the axle has rotated a half turn, the bottom becomes the top and vice versa, so the stresses on a particular region of material at the surface varies sinusoidally from tension to compression and back again. This is now known as *fully reversed* fatigue loading.

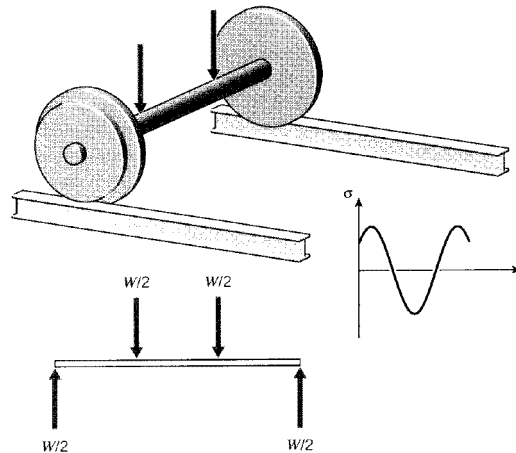


Figure 3: Fatigue in a railcar axle.

S-N curves

Well before a microstructural understanding of fatigue processes was developed, engineers had developed empirical means of quantifying the fatigue process and designing against it. Perhaps the most important concept is the $S-N$ diagram, such as those shown in Fig. 4¹, in which a constant cyclic stress amplitude S is applied to a specimen and the number of loading cycles N until the specimen fails is determined. Millions of cycles might be required to cause failure at lower loading levels, so the abscissa is usually plotted logarithmically.

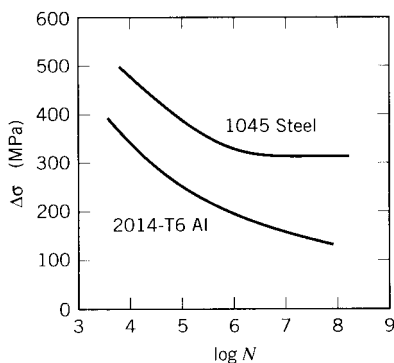


Figure 4: $S - N$ curves for aluminum and low-carbon steel.

In some materials, notably ferrous alloys, the $S - N$ curve flattens out eventually, so that below a certain *endurance limit* σ_e failure does not occur no matter how long the loads are cycled. Obviously, the designer will size the structure to keep the stresses below σ_e by a suitable safety factor if cyclic loads are to be withstood. For some other materials such as aluminum, no endurance limit exists and the designer must arrange for the planned lifetime of the structure to be less than the failure point on the $S - N$ curve.

Statistical variability is troublesome in fatigue testing; it is necessary to measure the lifetimes of perhaps twenty specimens at each of ten or so load levels to define the $S - N$ curve with statistical confidence². It is generally impossible to cycle the specimen at more than approximately 10Hz (inertia in components of the testing machine and heating of the specimen often become problematic at higher speeds) and at that speed it takes 11.6 days to reach 10^7 cycles of loading. Obtaining a full $S - N$ curve is obviously a tedious and expensive procedure.

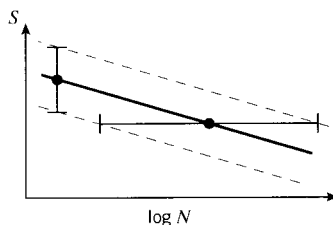


Figure 5: Variability in fatigue lifetimes and fracture strengths.

¹H.W. Hayden, W.G. Moffatt, and J. Wulff, *The Structure and Properties of Materials*, Vol. III, John Wiley & Sons, 1965.

²*A Guide for Fatigue Testing and the Statistical Analysis of Fatigue Data*, ASTM STP-91-A, 1963.

At first glance, the scatter in measured lifetimes seems enormous, especially given the logarithmic scale of the abscissa. If the coefficient of variability in conventional tensile testing is usually only a few percent, why do the fatigue lifetimes vary over orders of magnitude? It must be remembered that in tensile testing, we are measuring the variability in stress at a given number of *cycles* (one), while in fatigue we are measuring the variability in cycles at a given *stress*. Stated differently, in tensile testing we are generating vertical scatter bars, but in fatigue they are horizontal (see Fig. 5). Note that we must expect more variability in the lifetimes as the $S - N$ curve becomes flatter, so that materials that are less prone to fatigue damage require more specimens to provide a given confidence limit on lifetime.

Effect of mean load

Of course, not all actual loading applications involve fully reversed stress cycling. A more general sort of fatigue testing adds a *mean stress* σ_m on which a sinusoidal cycle is superimposed, as shown in Fig. 6. Such a cycle can be phrased in several ways, a common one being to state the alternating stress σ_{alt} and the *stress ratio* $R = \sigma_{min}/\sigma_{max}$. For fully reversed loading, $R = -1$. A stress cycle of $R = 0.1$ is often used in aircraft component testing, and corresponds to a tension-tension cycle in which $\sigma_{min} = 0.1\sigma_{max}$.

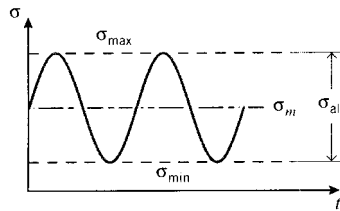


Figure 6: Simultaneous mean and cyclic loading.

A very substantial amount of testing is required to obtain an $S - N$ curve for the simple case of fully reversed loading, and it will usually be impractical to determine whole families of curves for every combination of mean and alternating stress. There are a number of stratagems for finessing this difficulty, one common one being the *Goodman diagram*, shown in Fig. 7. Here a graph is constructed with mean stress as the abscissa and alternating stress as the ordinate, and a straight “lifeline” is drawn from σ_e on the σ_{alt} axis to the ultimate tensile stress σ_f on the σ_m axis. Then for any given mean stress, the endurance limit — the value of alternating stress at which fatigue fracture never occurs — can be read directly as the ordinate of the lifeline at that value of σ_m . Alternatively, if the design application dictates a given ratio of σ_e to σ_{alt} , a line is drawn from the origin with a slope equal to that ratio. Its intersection with the lifeline then gives the effective endurance limit for that combination of σ_f and σ_m .

Miner’s law for cumulative damage

When the cyclic load level varies during the fatigue process, a *cumulative damage* model is often hypothesized. To illustrate, take the lifetime to be N_1 cycles at a stress level σ_1 and N_2 at σ_2 . If damage is assumed to accumulate at a constant rate during fatigue and a number of cycles n_1 is applied at stress σ_1 , where $n_1 < N_1$ as shown in Fig. 8, then the fraction of lifetime consumed

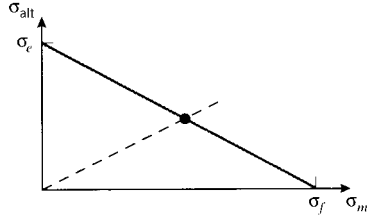


Figure 7: The Goodman diagram.

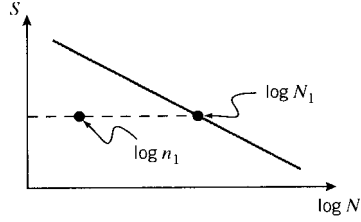


Figure 8: The concept of fractional lifetime.

will be n_1/N_1 . To determine how many additional cycles the specimen will survive at stress σ_2 , an additional fraction of life will be available such that the sum of the two fractions equals one:

$$\frac{n_1}{N_1} + \frac{n_2}{N_2} = 1$$

Note that absolute cycles and not log cycles are used here. Solving for the remaining cycles permissible at σ_2 :

$$n_2 = N_2 \left(1 - \frac{n_1}{N_1} \right)$$

The generalization of this approach is called *Miner's Law*, and can be written

$$\boxed{\sum \frac{n_j}{N_j} = 1} \quad (1)$$

where n_j is the number of cycles applied at a load corresponding to a lifetime of N_j .

Example 1

Consider a hypothetical material in which the S - N curve is linear from a value equal to the fracture stress σ_f at one cycle ($\log N = 0$), falling to a value of $\sigma_f/2$ at $\log N = 7$ as shown in Fig. 9. This behavior can be described by the relation

$$\log N = 14 \left(1 - \frac{S}{\sigma_f} \right)$$

The material has been subjected to $n_1 = 10^5$ load cycles at a level $S = 0.6\sigma_f$, and we wish to estimate how many cycles n_2 the material can now withstand if we raise the load to $S = 0.7\sigma_f$. From the S - N relationship, we know the lifetime at $S = 0.6\sigma_f = \text{constant}$ would be $N_1 = 3.98 \times 10^5$ and the lifetime at $S = 0.7\sigma_f = \text{constant}$ would be $N_2 = 1.58 \times 10^4$. Now applying Eqn. 1:

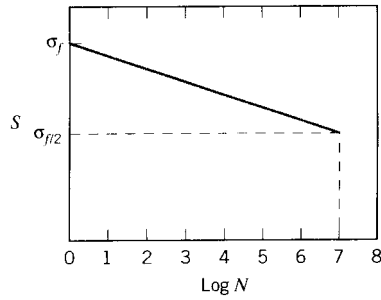


Figure 9: Linear S - N curve.

$$\frac{n_1}{N_1} + \frac{n_2}{N_2} = \frac{1 \times 10^5}{3.98 \times 10^5} + \frac{n_2}{1.58 \times 10^4} = 1$$

$$n_2 = 1.18 \times 10^4$$

Miner’s “law” should be viewed like many other material “laws,” a useful approximation, quite easy to apply, that *might* be accurate enough to use in design. But damage accumulation in fatigue is usually a complicated mixture of several different mechanisms, and the assumption of linear damage accumulation inherent in Miner’s law should be viewed skeptically. If portions of the material’s microstructure become unable to bear load as fatigue progresses, the stress must be carried by the surviving microstructural elements. The rate of damage accumulation in these elements then increases, so that the material suffers damage much more rapidly in the last portions of its fatigue lifetime. If on the other hand cyclic loads induce strengthening mechanisms such as molecular orientation or crack blunting, the rate of damage accumulation could drop during some part of the material’s lifetime. Miner’s law ignores such effects, and often fails to capture the essential physics of the fatigue process.

Crack growth rates

Certainly in aircraft, but also in other structures as well, it is vital that engineers be able to predict the rate of crack growth during load cycling, so that the part in question be replaced or repaired before the crack reaches a critical length. A great deal of experimental evidence supports the view that the crack growth rate can be correlated with the cyclic variation in the stress intensity factor³:

$$\boxed{\frac{da}{dN} = A \Delta K^m} \quad (2)$$

where da/dN is the fatigue crack growth rate per cycle, $\Delta K = K_{max} - K_{min}$ is the stress intensity factor range during the cycle, and A and m are parameters that depend the material, environment, frequency, temperature and stress ratio. This is sometimes known as the “Paris law,” and leads to plots similar to that shown in Fig. 10.

³See Module 23.

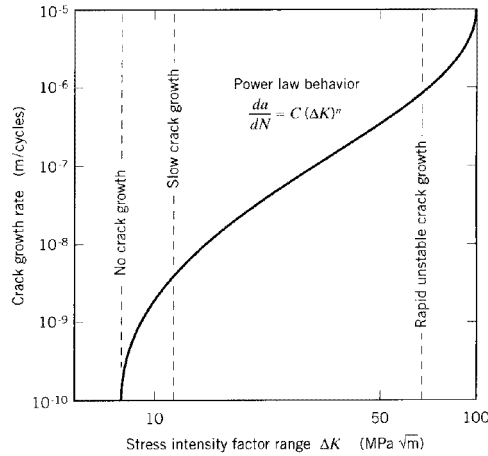


Figure 10: The Paris law for fatigue crack growth rates.

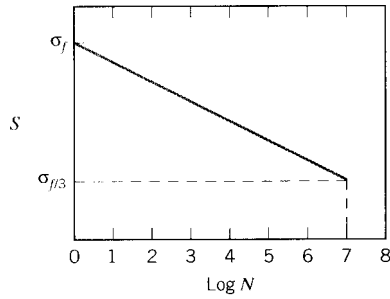
The exponent m is often near 4 for metallic systems, which might be rationalized as the damage accumulation being related to the volume V_p of the plastic zone: since the volume V_p of the zone scales with r_p^2 and $r_p \propto K_I^2$, then $da/dn \propto \Delta K^4$. Some specific values of the constants m and A for various alloys are given in Table 1.

Table 1: Numerical parameters in the Paris equation.

alloy	m	A
Steel	3	10^{-11}
Aluminum	3	10^{-12}
Nickel	3.3	4×10^{-12}
Titanium	5	10^{-11}

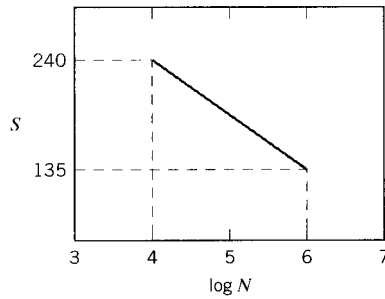
Problems

1. A steel has an ultimate tensile strength of 110 kpsi and a fatigue endurance limit of 50 kpsi. The load is such that the alternating stress is 0.4 of the mean stress. Using the Goodman method with a safety factor of 1.5, find the magnitude of alternating stress that gives safe operation.
2. A titanium alloy has an ultimate tensile strength of 120 kpsi and a fatigue endurance limit of 60 kpsi. The alternating stress is 20 kpsi. Find the allowable mean stress, using a safety factor of 2.
3. A material has an S - N curve that is linear from a value equal to the fracture stress σ_f at one cycle ($\log N = 0$), falling to a value of $\sigma_f/3$ at $\log N = 7$. The material has been subjected to $n_1 = 1000$ load cycles at a level $S = 0.7\sigma_f$. Estimate how many cycles n_2 the material can withstand if the stress amplitude is now raised to $S = 0.8\sigma_f$.



Prob. 3

4. A steel alloy has an S-N curve that falls linearly from 240 kpsi at 10^4 cycles to 135 kpsi at 10^6 cycles. A specimen is loaded at 160 kpsi alternating stress for 10^5 cycles, after which the alternating stress is raised to 180 kpsi. How many additional cycles at this higher stress would the specimen be expected to survive?



Prob. 4

5. Consider a body, large enough to be considered infinite in lateral dimension, containing a central through-thickness crack initially of length $2a_0$ and subjected to a cyclic stress of amplitude $\Delta\sigma$. Using the Paris Law (Eqn. 2), show that the number of cycles N_f needed for the crack to grow to a length $2a_f$ is given by the relation

$$\ln\left(\frac{a_f}{a_0}\right) = A(\Delta\sigma)^2\pi N_f$$

when $m = 2$, and for other values of m

$$\left|a_f^{1-m/2} - a_0^{1-m/2}\right| = \frac{2-m}{2m} A(\Delta\sigma)^m \pi^{m/2} N_f$$

6. Use the expression obtained in Prob. 5 to compute the number of cycles a steel component can sustain before failure, where the initial crack halflength is 0.1 mm and the critical crack halflength to cause fracture is 2.5 mm. The stress amplitude per cycle is 950 MPa. Take the crack to be that of a central crack in an infinite plate.
7. Use the expression developed in Prob. 5 to investigate whether it is better to limit the size a_0 of initial flaws or to extend the size a_f of the flaw at which fast fracture occurs. Limiting a_0 might be done with improved manufacturing or better inspection methods,

and increasing a_f could be done by selecting a material with greater fracture toughness. For the “baseline” case, take $m = 3.5$, $a_0 = 2$ mm, $a_f =$ mm. Compute the percentage increase in N_f by letting (a) the initial flaw size to be reduced to $a_0 = 1$ mm, and (b) increasing the final flaw size to $N_f = 10$ mm.

MATERIAL	Type	Cost (\$/kg)	Density (ρ , Mg/m ³)	Young's Modulus (E , GPa)	Shear Modulus (G , GPa)	Poisson's Ratio (ν)	Yield Stress (s_y , MPa)	UTS (s_f , MPa)	Breaking strain (ϵ_f , %)	Fracture Toughness (K_{Ic} , MN m ^{3/2})	Thermal Expansion (α , 10 ⁻⁶ /C)
Alumina (Al ₂ O ₃)	ceramic	1.90	3.9	390	125	0.26	4800	35	0.0	4.4	8.1
Aluminum alloy (7075-T6)	metal	1.80	2.7	70	28	0.34	500	570	12	28	33
Beryllium alloy	metal	315.00	2.9	245	110	0.12	360	500	6.0	5.0	14
Bone (compact)	natural	1.90	2.0	14	3.5	0.43	100	100	9.0	5.0	20
Brass (70Cu30Zn, annealed)	metal	2.20	8.4	130	39	0.33	75	325	70.0	80	20
Cermets (Co/WC)	composite	78.60	11.5	470	200	0.30	650	1200	2.5	13	5.8
CFRP Laminate (graphite)	composite	110.00	1.5	1.5	53	0.28	200	550	2.0	38	12
Concrete	ceramic	0.05	2.5	48	20	0.20	25	3.0	0.0	0.75	11
Copper alloys	metal	2.25	8.3	135	50	0.35	510	720	0.3	94	18
Cork	natural	9.95	0.18	0.032	0.005	0.25	1.4	1.5	80	0.074	180
Epoxy thermoset	polymer	5.50	1.2	3.5	1.4	0.25	45	45	4.0	0.50	60
GFRP Laminate (glass)	composite	3.90	1.8	26	10	0.28	125	530	2.0	40	19
Glass (soda)	ceramic	1.35	2.5	65	26	0.23	3500	35	0.0	0.71	8.8
Granite	ceramic	3.15	2.6	66	26	0.25	2500	60	0.1	1.5	6.5
Ice (H ₂ O)	ceramic	0.23	0.92	9.1	3.6	0.28	85	6.5	0.0	0.11	55
Lead alloys	metal	1.20	11.1	16	5.5	0.45	33	42	60	40	29
Nickel alloys	metal	6.10	8.5	180	70	0.31	900	1200	30	93	13
Polyamide (nylon)	polymer	4.30	1.1	3.0	0.76	0.42	40	55	5.0	3.0	103
Polybutadiene elastomer	polymer	1.20	0.91	0.0016	0.0005	0.50	2.1	2.1	500	0.087	140
Polycarbonate	polymer	4.90	1.2	2.7	0.97	0.42	70	77	60	2.6	70
Polyester thermoset	polymer	3.00	1.3	3.5	1.4	0.25	50	0.7	2.0	0.70	150
Polyethylene (HDPE)	polymer	1.00	0.95	0.7	0.31	0.42	25	33	90	3.5	225
Polypropylene	polymer	1.10	0.89	0.9	0.42	0.42	35	45	90	3.0	85
Polyurethane elastomer	polymer	4.00	1.2	0.025	0.0086	0.50	30	30	500	0.30	125
Polyvinyl chloride (rigid PVC)	polymer	1.50	1.4	1.5	0.6	0.42	53	60	50	0.54	75
Silicon	ceramic	2.35	2.3	110	44	0.24	3200	35	0.0	1.5	6
Silicon Carbide (SiC)	ceramic	36.00	2.8	450	190	0.15	9800	35	0.0	4.2	4.2
Spruce (parallel to grain)	natural	1.00	0.60	9	0.8	0.30	48	50	10	2.5	4
Steel, high strength 4340	metal	0.25	7.8	210	76	0.29	1240	1550	2.5	100	14
Steel, mild 1020	metal	0.50	7.8	210	76	0.29	200	380	25	140	14
Steel, stainless austenitic 304	metal	2.70	7.8	210	76	0.28	240	590	60	50	17
Titanium alloy (6Al4V)	metal	16.25	4.5	100	39	0.36	910	950	15	85	9.4
Tungsten Carbide (WC)	ceramic	50.00	15.5	550	270	0.21	6800	35	0.0	3.7	5.8

Matrix and Index Notation

David Roylance
Department of Materials Science and Engineering
Massachusetts Institute of Technology
Cambridge, MA 02139

September 18, 2000

A *vector* can be described by listing its components along the *xyz* cartesian axes; for instance the displacement vector \mathbf{u} can be denoted as u_x, u_y, u_z , using letter subscripts to indicate the individual components. The subscripts can employ numerical indices as well, with 1, 2, and 3 indicating the *x*, *y*, and *z* directions; the displacement vector can therefore be written equivalently as u_1, u_2, u_3 .

A common and useful shorthand is simply to write the displacement vector as u_i , where the *i* subscript is an *index* that is assumed to range over 1,2,3 (or simply 1 and 2 if the problem is a two-dimensional one). This is called the *range convention* for index notation. Using the range convention, the vector equation $u_i = a$ implies three separate scalar equations:

$$u_1 = a$$

$$u_2 = a$$

$$u_3 = a$$

We will often find it convenient to denote a vector by listing its components in a vertical list enclosed in braces, and this form will help us keep track of matrix-vector multiplications a bit more easily. We therefore have the following equivalent forms of vector notation:

$$\mathbf{u} = u_i = \left\{ \begin{array}{c} u_1 \\ u_2 \\ u_3 \end{array} \right\} = \left\{ \begin{array}{c} u_x \\ u_y \\ u_z \end{array} \right\}$$

Second-rank quantities such as stress, strain, moment of inertia, and curvature can be denoted as 3×3 matrix arrays; for instance the stress can be written using numerical indices as

$$[\sigma] = \left[\begin{array}{ccc} \sigma_{11} & \sigma_{12} & \sigma_{13} \\ \sigma_{21} & \sigma_{22} & \sigma_{23} \\ \sigma_{31} & \sigma_{32} & \sigma_{33} \end{array} \right]$$

Here the first subscript index denotes the row and the second the column. The indices also have a physical meaning, for instance σ_{23} indicates the stress on the 2 face (the plane whose normal is in the 2, or *y*, direction) and acting in the 3, or *z*, direction. To help distinguish them, we'll use brackets for second-rank tensors and braces for vectors.

Using the range convention for index notation, the stress can also be written as σ_{ij} , where both the *i* and the *j* range from 1 to 3; this gives the nine components listed explicitly above.

(Since the stress matrix is symmetric, i.e. $\sigma_{ij} = \sigma_{ji}$, only six of these nine components are independent.)

A subscript that is repeated in a given term is understood to imply summation over the range of the repeated subscript; this is the *summation convention* for index notation. For instance, to indicate the sum of the diagonal elements of the stress matrix we can write:

$$\sigma_{kk} = \sum_{k=1}^3 \sigma_{kk} = \sigma_{11} + \sigma_{22} + \sigma_{33}$$

The multiplication rule for matrices can be stated formally by taking $\mathbf{A} = (a_{ij})$ to be an $(M \times N)$ matrix and $\mathbf{B} = (b_{ij})$ to be an $(R \times P)$ matrix. The matrix product \mathbf{AB} is defined only when $R = N$, and is the $(M \times P)$ matrix $\mathbf{C} = (c_{ij})$ given by

$$c_{ij} = \sum_{k=1}^N a_{ik}b_{kj} = a_{i1}b_{1j} + a_{i2}b_{2j} + \cdots + a_{iN}b_{Nj}$$

Using the summation convention, this can be written simply

$$c_{ij} = a_{ik}b_{kj}$$

where the summation is understood to be over the repeated index k . In the case of a 3×3 matrix multiplying a 3×1 column vector we have

$$\begin{bmatrix} a_{11} & a_{12} & a_{13} \\ a_{21} & a_{22} & a_{23} \\ a_{31} & a_{32} & a_{33} \end{bmatrix} \begin{Bmatrix} b_1 \\ b_2 \\ b_3 \end{Bmatrix} = \begin{Bmatrix} a_{11}b_1 + a_{12}b_2 + a_{13}b_3 \\ a_{21}b_1 + a_{22}b_2 + a_{23}b_3 \\ a_{31}b_1 + a_{32}b_2 + a_{33}b_3 \end{Bmatrix} = a_{ij}b_j$$

The *comma convention* uses a subscript comma to imply differentiation with respect to the variable following, so $f_{,2} = \partial f / \partial y$ and $u_{i,j} = \partial u_i / \partial x_j$. For instance, the expression $\sigma_{ij,j} = 0$ uses all of the three previously defined index conventions: range on i , sum on j , and differentiate:

$$\begin{aligned} \frac{\partial \sigma_{xx}}{\partial x} + \frac{\partial \sigma_{xy}}{\partial y} + \frac{\partial \sigma_{xz}}{\partial z} &= 0 \\ \frac{\partial \sigma_{yx}}{\partial x} + \frac{\partial \sigma_{yy}}{\partial y} + \frac{\partial \sigma_{yz}}{\partial z} &= 0 \\ \frac{\partial \sigma_{zx}}{\partial x} + \frac{\partial \sigma_{zy}}{\partial y} + \frac{\partial \sigma_{zz}}{\partial z} &= 0 \end{aligned}$$

The *Kronecker delta* is a useful entity is defined as

$$\delta_{ij} = \begin{cases} 0, & i \neq j \\ 1, & i = j \end{cases}$$

This is the index form of the *unit matrix* \mathbf{I} :

$$\delta_{ij} = \mathbf{I} = \begin{bmatrix} 1 & 0 & 0 \\ 0 & 1 & 0 \\ 0 & 0 & 1 \end{bmatrix}$$

So, for instance

$$\sigma_{kk}\delta_{ij} = \begin{bmatrix} \sigma_{kk} & 0 & 0 \\ 0 & \sigma_{kk} & 0 \\ 0 & 0 & \sigma_{kk} \end{bmatrix}$$

where $\sigma_{kk} = \sigma_{11} + \sigma_{22} + \sigma_{33}$.

Modules in Mechanics of Materials

List of Symbols

A	area, free energy, Madelung constant
\mathbf{A}	transformation matrix
\mathcal{A}	plate extensional stiffness
a	length, transformation matrix, crack length
a_T	time-temperature shifting factor
B	design allowable for strength
\mathbf{B}	matrix of derivatives of interpolation functions
\mathcal{B}	plate coupling stiffness
b	width, thickness
C	stress optical coefficient, compliance
\mathcal{C}	viscoelastic compliance operator
c	numerical constant, length, speed of light
C.V.	coefficient of variation
\mathbf{D}	stiffness matrix, flexural rigidity of plate
\mathcal{D}	plate bending stiffness
d	diameter, distance, grain size
E	modulus of elasticity, electric field
E^*	activation energy
\mathcal{E}	viscoelastic stiffness operator
e	electronic charge
e_{ij}	deviatoric strain
F	force
f_s	form factor for shear
G	shear modulus
\mathcal{G}	viscoelastic shear stiffness operator
\mathcal{G}_c	critical strain energy release rate
g	acceleration of gravity
GF	gage factor for strain gages
H	Brinell hardness
h	depth of beam
I	moment of inertia, stress invariant
\mathbf{I}	identity matrix
J	polar moment of inertia
K	bulk modulus, global stiffness matrix, stress intensity factor
\mathcal{K}	viscoelastic bulk stiffness operator
k	spring stiffness, element stiffness, shear yield stress, Boltzman's constant
L	length, beam span
\mathbf{L}	matrix of differential operators

M	bending moment
N	crosslink or segment density, moire fringe number, interpolation function, cycles to failure
\mathbf{N}	traction per unit width on plate
N_A	Avogadro's number
\mathcal{N}	viscoelastic Poisson operator
n	refractive index, number of fatigue cycles
$\hat{\mathbf{n}}$	unit normal vector
P	concentrated force
P_f	fracture load, probability of failure
P_s	probability of survival
p	pressure, moire gridline spacing
Q	force resultant, first moment of area
q	distributed load
R	radius, reaction force, strain or stress rate, gas constant, electrical resistance
\mathbf{R}	Reuter's matrix
r	radius, area reduction ratio
S	entropy, moire fringe spacing, total surface energy, alternating stress
\mathbf{S}	compliance matrix
s	Laplace variable, standard deviation
SCF	stress concentration factor
T	temperature, tensile force, stress vector, torque
T_g	glass transition temperature
t	time, thickness
t_f	time to failure
U	strain energy
U^*	strain energy per unit volume
UTS	ultimate tensile stress
\tilde{u}	approximate displacement function
V	shearing force, volume, voltage
V^*	activation volume
v	velocity
W	weight, work
u, v, w	components of displacement
x, y, z	rectangular coordinates
X	standard normal variable
α, β	curvilinear coordinates
α_L	coefficient of linear thermal expansion
γ	shear strain, surface energy per unit area, weight density
δ	deflection
δ_{ij}	Kronecker delta
ϵ	normal strain
$\boldsymbol{\epsilon}$	strain pseudovector
ϵ_{ij}	strain tensor
ϵ_T	thermal strain
η	viscosity
θ	angle, angle of twist per unit length
κ	curvature
λ	extension ratio, wavelength

ν	Poisson's ratio
ρ	density, electrical resistivity
Σ_{ij}	distortional stress
σ	normal stress
$\boldsymbol{\sigma}$	stress pseudovector
σ_{ij}	stress tensor
σ_e	endurance limit
σ_f	failure stress
σ_m	mean stress
σ_M	Mises stress
σ_t	true stress
σ_Y	yield stress
τ	shear stress, relaxation time
ϕ	Airy stress function
ξ	dummy length or time variable
Ω	configurational probability
ω	angular frequency
∇	gradient operator

Modules in Mechanics of Materials

Unit Conversion Factors

Density	1 Mg/m ³ =	1	gm/cm ³
	=	62.42	lb/ft ³
	=	0.03613	lb/in ³
	=	102.0	N/m ³
Energy	1 J =	0.2390	calorie
	=	9.45×10^{-4}	Btu
	=	10^7	erg
	=	0.7376	ft-lb
	=	6.250×10^{18}	ev
Force	1 N =	10^5	d (dyne)
	=	0.2248	lbf
	=	0.1020	kg
	=	3.597	oz
	=	1.124×10^{-4}	ton (2000lb)
Length	1 m =	39.37	in
	=	3.281	ft
	=	10^{10}	Å
Mass	1 kg =	2.205	lb
	=	35.27	oz
	=	1.102×10^{-3}	ton (2000lb)
Power	1 W =	1	J/s
	=	0.7378	ft-lb/s
	=	1.341×10^{-3}	hp
Stress	1 Pa =	1	N/m ²
	=	10	d/cm ²
	=	1.449×10^{-4}	psi
	=	1.020×10^{-7}	kg/mm ²
Toughness	1 MPa√m =	0.910	ksi√in

Physical constants:

Boltzman constant $k = 1.381 \times 10^{-23}$ J/K

Gas constant $R = 8.314$ J/mol-K

Avogadro constant $N_A = 6.022 \times 10^{23}$ /mol

Acceleration of gravity $g = 9.805$ m/s²